Εθνικό Μετσόβιο Πολυτεχνείο
Σχολή Πολιτικών Μηχανικών
Εργαστήριο Εδαφομηχανικής

National Technical University of Athens
School of Civil Engineering
Soil Mechanics Laboratory

Διπλωματική Εργασία
Rasha Zakkak

Diploma thesis by
Rasha Zakkak

Επιβλέποντες:
Καθηγητής Γ.Γκαζέτας
Καθηγητής. Ι.Αναστασόπουλος

Supervised by:
Professor G.Gazetas
Professor. I.Anastasopoulos

Δυναμική Σεισμική Απόκριση Τοίχων Βαρύτητας : Αριθμητική και Προσεγγιστική Θεώρηση

Seismic Response of Gravity Retaining Walls: Numerical and Pseudo-Static Analysis

Οκτώβριος 2013

October 2013

Ευχαριστίες

Φτάνοντας στο τέλος, Θα ήθελα να ευχαριστήσω όλους αυτούς που ήταν δίπλα μου και με βοήθησαν να φτάσω στον στόχο μου.

Πρώτα και σημαντικότερα τους καθηγητές μου, στον κ. Γ.Γκαζέτα καθώς και στον κ. Ι.Αναστασόπουλο για την πολύτιμη βοήθεια και καθοδήγηση που μου παρείχαν κατά την εκπόνηση αυτής της διπλωματικής εργασίας, καθώς και στις διδάκτορες Ευαγγέλια Γαρίνη και Νάντια Παπαδοπούλου.

Ευχαριστώ τους γονείς μου για τη στήριξη τους και για όλα όσα μου προσφέρουν και και τις φίλες μου Μ. Δακορώνια και Κ.Δεντάκη που ήταν σαν οικογένεια μου εδώ.

Contents

Περίληψη

Οι κατασκευές αντιστηρίξεως εδαφών ,όπως τοίχοι αντιστηρίξεως, ακρόβαθρα γεφυρών, κρηπιδότοιχοι και αγκυρωμένοι πασσαλότοιχοι, χρισμποιούνται ευρέως σε σεισμογενείς περιοχές. Συχνά αποτελούν στοιχεία <κλειδιά> λιμένων, συγκοινωνιακών συστημάτων και άλλων κατασκευών. Οι σεισμοί προκαλούν μόνιμες παραμορφώσεις στις κατασκευές αντιστηρίξεων, όπως είχαμε την ευκαιρία να διαπιστώσουμε σε πολλά ιστορικά περιστατικά. Σε μερικές περιπτώσεις, αυτές οι παραμορφώσεις ήταν αμελητέες. Σε άλλες προκάλεσαν σημαντικές βλάβες ή παρατηρήθηκε και κατάρευση της ίδιας της κατασκευής αντιστηρίξεως, με καταστροφικές υλικές και οικονομικές συνέπειες. Η δυναμική απόκριση ακόμα και του πιο απλού τοίχου αντιστηρίξεως είναι αρκετά περίπλοκη. Οι μετακινήσεις του τοίχου και οι πιέσεις που ασκούνται σαύτόν εξαρτώνται από την απόκριση του εδάφους κάτω από τον τοίχου, την απόκριση του εδάφους επιχώσεως, την αδρανειακή και καμπτική απόκριση του ίδιου του τοίχου, και τν φύση της επιβαλλόμενης κίνησης.

Το αντικείμενο της διπλωματικής αυτής εργασίας είναι η αναλύση της δυναμικής απόκρισης τοίχων αντιστηρίξεως υπό σεισμική διέγερση, με στόχο αφ' ενός μεν τον υπολογισμό των αναπτυσσομένων εδαφικών ωθήσεων, αφ' ετέτρου δε την εκτίμηση των μετατοπίσεων. Για την προσομοίωση του φαινομένου χρησιμοποιείται η μέθοδος των πεπαρσμένων στοιχείων. Τρία συστήματα εδάφους-τοίχων εξετάζονται, στην πρώτη περίπτωση είχαμε πιο σκληρό το

αντιστηριζόμενο έδαφος , στην δεύτερη πιο σκληρό έδαφος θεμελίωσης και στην τρίτη ακόμα πιο σκληρό έδαφος θεμελίωσης. τα αποτελέσματα της αριθμητικα προσομοιωσης συγκρίνεται με την αναλυτική λύση Mononobe-Okabe. Διερευνάται παραμετρικά η επιρροη της δυσκαμψία του εδάφους θεμελίωσης, του συντελεστή τριβής και του μέτρο ελαστικότητας του εδάφους. Επιπλέον, πραγματοποιήθηκε μια πρώτη απόπειρα δημιουργίας ενός απλοποιημένου μοντέλου.

SYNOPSIS

An evaluation is made of the seismic response of gravity retaining walls supported on deformable foundation soil layer. To obtain lateral earth pressures against the wall, horizontal and vertical displacements ,finite element analyses were performed, taking into account the non-linearities in the response of the wall-soil system. Three wall-soil systems were examined, one consisting of a stiffer retained soil, the second one consisting of a very stiff foundation soil and the third one of an even stiffer foundation soil. The numerical results are compared to the analytical solution of Mononobe-Okabe. A parametric investigation is made in order to assess the effect of factors such as stiffness of the foundation soil, friction coefficient and elasticity moduli of the soil layers. Additionally, a first attempt for a simplified and efficient model.

Chapter 1

LITERATURE REVIEW

1.1 Introduction

A retaining wall is a wall constructed for the purpose of supporting a vertical or nearly vertical earth bank which, inturn, may support vertical loads. Gravity retaining walls are the type of retaining walls that rely on their huge weight to retain the material behind it and achieve stability against failures. They can be constructed from concrete, stone or even brick masonry. The weight of the wall has two roles: resisting the overturning of the wall and causing frictional sliding resistance at the base of the wall --- hence the name. Retaining walls must be designed so that foundation pressures do not exceed allowable bearing values, wall settlements are tolerable, safety factors against sliding and overturning are adequate, and the wall possesses adequate structural strength. Retaining walls shall be designed for a safety factor of 1.5 against lateral sliding and overturning.

The Seismic response of even the simplest retaining wall is a complicated soil-structure interaction problem. The displacements of the wall and the dynamic earth pressures depend on the response of the retained soil, the inertia of the wall itself, the foundation soil and the nature of the input motions. Throughout the years, different approaches were used to study the dynamic earth pressures. These approaches can be divided into analytical, numerical and experimental methods.

The MO method (1926) is the earliest and most widely used analytical method. It gives the total active thrust acting on the wall by applying pseudostatic equilibrium to the forces acting of the soil wedge with the point of application of the thrust at 1/3 the height of the wall above its base.This method modified and simplified by Seed and Whitman (1970), whoperformed a parametric study to evaluate the effects of changing the angle of wall friction.Richards and Elms(1979) determined permanent (inelastic)outward displacements, using the Newmark sliding block concept. Mylonakis (2007)is a recent alternative method to the MO method for plastic soils.

Chapter 2

MODEL,STATIC AND DYNAMIC ANALYSES

2.1 Introduction

The aim of this chapter is to understand the seismic response of the gravity retaining walls, in the case of stiffer retained soil. For this end, numerical analyses of two typical gravity retaining walls were developed and subjected to a series of seismic excitations. The results are presented along with an effort to interpret the predominant phenomena.

2.2 Geometry of the case studied

The 2-D plane strain finite elements model was constructed using the ABAQUS FE code.The discretization of the retained soil is made by two dimensional,four-noded quadrilateral, plane-strain elements.In

As shown in **Fig.2.1**,the model consists of two identical walls, one on each side of the retained wall, in order to render the model symmetrical, which is important to minimize boundary effects. This way for each excitation, the model will also yield results for two directions of loading. This is important since the response of the gravity walls is unsymmetrical.The height and the width of each wall were 12 m and 8 m respectively. The geometrical limits of the model are 100 m behind each wall. In order to avoid any interaction between the two walls, they were placed at a distance of 100 m.

The properties of the retained and foundation soil layer are shown in **table 2.1**.The properties of the concrete were $\boldsymbol{\rho}$= 2.5 Mgr/m^3, $\mathbf{E_{conc}}$= 25000 MPa, **v** = 0.2. The behavior of the concrete is presumed to be elastic. As for the soil-wall interface, small sliding is allowed and the friction coefficient is calculated as follows: $\boldsymbol{\mu}=\phi$ for the retained soil and $\boldsymbol{\mu}= (2/3)\ \phi$ for the foundation soil. The damping ratio $\boldsymbol{\xi}$=2% but the equivalent damping ratio will be greater because of the hysteretic behavior of the soil and the wall-soil interfaces, that is allowed to develop in the plastic analysis.

Horizontal and vertical viscous dashpots with free field boundarieswere added to the model to absorb the radiated energy from the P and S waves, respectively.The free field boundaries are

highly rigid, so they won't be affected by the model and to improve the accuracy of the simulation. The finite elements' dimensions were 0.5m x 0.5m for a distance of 18 m on the side of the retained soil and 16 m on the other side. For the remaining mesh, the dimensions were 1m x 1m.

Non-linear analysis of the soil-wall system where the soil behavior was described by Mohr-Coulomb theory.

	Retained Soil	Foundation Soil
Elasticity Modulus**E** (MPa)	100	50
Poisson's ratio **v**	0.25	0.25
Cohesion **c** (kPa)	5	5
Friction angle **ϕ** (degrees)	37.5	35
Dilation angle **ψ** (degrees)	7.5	5
Density **ρ** (Mgr/m^3)	1.9	1.7
Viscous damping ratio **ξ**	2%	2%
Friction coefficient **μ**	0.77	0.43

Table 2.1: The properties of the retained and foundation soil layer.

2.3 Input Earthquake Motions

Five shaking events were applied to the model. The acceleration time histories are directly applied to the base nodes of the grid and not to the base of the wall. This helps understanding the effect of the compliance of the foundation soil and simulating the presence of infinitely rigid bedrock.Since the seismic response depends on the intensity, frequency, duration and number of the cycles of the earthquake, the peak acceleration of each shaking event was

normalized from 0.1g to 1g.This way a wider range of results are obtained ,therefore we get a better understanding of the seismic response of a retaining wall.

The input acceleration time series and their characteristics can be found in Appendix A

2.4 Static analysis

Static earth pressure calculated using the Rankine theory

$$\sigma_h = K_A \sigma_v = K_A \rho g H$$

Where $K_A = \tan^2 (45^o - \phi/2)$

The distribution of static lateral earth pressure on the retaining wall is shown in**Fig.2.2.**

It can be noticed that they are in reasonably good agreement. The static earth pressure increases with the depth, but shows a reduction of the earth pressure close to the top of the wall. This happens when the wall tries to rotate because of the static pressure; the soil due to its cohesion loses contact with the wall, which is called the height of free cut in clay. This height can be calculated from the equation:

$$h_{cr} = \frac{2\,Su}{\gamma}$$

This observation refers to all cases examined in this chapter,as the initial conditions are always the same for every analysis.

Note:

Time in all diagrams refers to the whole time and not seismic step time, except for the acceleration-Time diagrams.

Step 1 that lasts for one second includes the geostatic load of the underlying soil and the weight of both walls.

Step 2 that also has duration of one second and has the static load of the retained soil.

Step 3 is the dynamic step where the model is subjected to the seismic excitation.

2.5 Dynamic analyses

2.5.1 AEGION SEISMIC EXCITATION

Left wall

Dynamic earth pressures, horizontal forces and acceleration

Figures 2.3-2.7 show the distribution of the earth pressures on the left wall at the time of : Maximum pressure, maximum horizontal displacement, maximum differential settlement and residual pressure after the earthquake. Earth pressure increases with the depth. Again a reduction of the earth pressure is noticed close to the top of the wall. This happens when the wall tries to rotate because of the static pressure; the soil due to its cohesion loses contact with the wall. As observed for peak accelerations from 0.2g until 0.6g, the maximum horizontal displacement and differential settlement occur at the same time and so the distributions of the earth pressures at these moments are very close.For other peak accelerations the maximum differential settlements happens at the end of the earthquake.

As can be seen from horizontal force-time diagrams for all the peak accelerations (**Figures 2.8, 2.10, 2.12, 2.14, 2.16**),it is noticed that the left and right wall are completely out of phase for all the peak accelerations.. A prove that it is not a symmetrical problem.In opposition to the observations of Al-Homoud and Whitman (1999),the highest location of the resultant force above the bottom of the wall doesn't occur at the same time of the maximum lateral pressure on the wall **(Figures 2.8-2.17)**.Neither does the maximum inward movement occur at the same time of the maximum lateral pressure**(Figures 2.31-2.35)**.

Corresponding though to Al-Homoud and Whitman (1999),the peak acceleration at the top of the far field and at the top of the wall lag those at the base **(Figures 2.23-2.25)**.

Comparison to MO:

The Mononobe-Okabe was implemented in the present study to calculate the expected lateral thrust, mostly to use it as a yardstick to compare the result from the analyses. The lateral earth pressure employing the empirical methods that were based on the M-O method is calculated by the relationship:

$$P_{MO} = (K_A + \Delta Kae\ a_h)\ \gamma\ z$$

Where:

z = height of the wall (m)

γ= specific weight of the retained wall (kN/m^3)

$K_A = \tan^2 (45^o - \phi/2)$

andΔKae= 0.75 oρ1.

$a_h = \frac{A}{g}$ = Peak ground acceleration

Right Wall

Dynamic earth pressures, horizontal forces and acceleration

Earth pressure increases with the depth. A reduction of the earth pressure is noticed close to the top of the wall for the same reason it happens in the left wall **(Figures 2.36-2.40)**.Again in opposition to the observations of Al-Homoud and Whitman (1999),the highest location of the resultant force above the bottom of the wall doesn't occur at the same time of the maximum lateral pressure on the wall **(Figures 2.8-2.17)**.On the other hand for the right wall the maximum inward movement occurs at the same time of the maximum lateral pressure,where the displacement at the moment of the maximum pressure is at its local minimum **(Figures 2.51-2.55)**.

Comparison to MO:

Same approximations as with the left wall were used to estimate the expected lateral thrust using two dynamic earth pressure coefficients **(Figures 2.41-2.45).**

Peak ground acceleration 0.2g:

The maximum earth pressure behind the left wall is at t=4.36 while at the same time as observed from **figure 2.31** the wall is moving outwards.The distribution of the maximum earth pressure is in good agreement with the estimated M-O computed with a dynamic pressure coefficient 0.75**(figure 2.18)**.Maximum and residual horizontal forces on the wall are 448 kN and 311 kN respectively**(figure 2.8)**. The highest point of application of the resultant force is observed to be equal to 6.5 m at t=3.88 sec while the residual point of application is 3.9 m above the bottom of the wall. And again as noticed from **figure 2.31** The permanent displacement due to rotation is 0.033 m,permanent displacement due to sliding is 0.02 m and the overall horizontal permanent displacement is 0.05 m which is almost equal to the maximum overall displacement (0.06 m).The average settlement is 0.08 m and the differential settlement is 0.05 m **(figure 2.26).**

The maximum earth pressure behind the right wall is at t=4.7 while at the same time as observed from **figure 2.51** the wall is at its local minimum (maximum inward movement). The distribution of the maximum earth pressure is in good agreement with the estimated M-O computed with a dynamic pressure coefficient 0.75**(figure 2.41)**. Maximum and residual horizontal forces on the wall are 420 kN and 358 kN respectively **(figure 2.8)**. The highest point of application of the resultant force is observed to be equal to 5.85 m at t=3.64 sec while the residual point of application is 3.9 m above the bottom of the wall. And again as noticed from **figure 2.51** The permanent displacement due to rotation is 0.04 m,permanent displacement due to sliding is 0.03 m and the overall horizontal permanent displacement is 0.07 m which is almost equal to the maximum overall displacement (0.08 m).The average settlement is 0.08 m and the differential settlement is 0.06 m **(figure 2.46).**

Peak ground acceleration 0.4g:

The maximum earth pressure behind the left wall is at t=4.34 while at the same time as observed from **figure 2.32** the wall is moving outwards. The distribution of the maximum earth pressure is in good agreement with the estimated M-O computed with a dynamic pressure coefficient 0.75**(figure 2.19)**. Maximum and residual horizontal forces on the wall are610kN and 362 kN respectively **(figure 2.10)**. The highest point of application of the resultant force is

observed to be equal to 7.55 m at t=3.9 sec while the residual point of application of the resultant force is 3.9 m above the bottom of the wall. And again as noticed from **figure 2.32** the permanent displacement due to rotation is 0.08 m,permanent displacement due to sliding is 0.03 m and the overall horizontal permanent displacement is 0.11 m and the maximum overall displacement is 0.14 m.The average settlement is 0.1 m and the differential settlement is 0.11 m **(figure 2.27).**

The maximum earth pressure behind the right wall is at t=4.7 while at the same time as observed from **figure 2.52** the wall is at its local minimum (maximum inward movement). The distribution of the maximum earth pressure is in good agreement with the estimated M-O computed with a dynamic pressure coefficient 0.75 (**figure 2.42)**. Maximum and residual horizontal forces on the wall are 545 kN and 433 kN respectively **(figure 2.10)**. The highest point of application of the resultant force is observed to be equal to 7.0 m at t=3.64 sec while the residual point of application of the resultant force is 3.9 m above the bottom of the wall. And again as noticed from **figure 2.52** the permanent displacement due to rotation is 0.08 m,permanent displacement due to sliding is 0.06 m and the overall horizontal permanent displacement is 0.14 m which is almost equal to the maximum overall displacement 0.15 m.The average settlement is 0.1 m and the differential settlement is 0.11 m **(figure 2.47).**

Peak ground acceleration 0.6g:

The maximum earth pressure behind the left wall is at t=4.34 while at the same time as observed from **figure 2.33** the wall is moving outwards. The distribution of the maximum earth pressure is in good agreement with the estimated M-O computed with a dynamic pressure coefficient 0.75 (**figure 2.20)**. Maximum and residual horizontal forces on the wall are776kN and 409 kN respectively **(figure 2.12)**. The highest point of application of the resultant force is observed to be equal to 7.85 m at t=3.96 sec while the residual point of application of the resultant force is 4.3 m above the bottom of the wall. And again as noticed from **figure 2.33**the permanent displacement due to rotation is 0.12 m,permanent displacement due to sliding is 0.05 m and the overall horizontal permanent displacement is 0.17 m and the maximum overall

displacement is 0.22 m.The average settlement is 0.12 m and the differential settlement is 0.16 m **(figure 2.28).**

The maximum earth pressure behind the right wall is at t=4.18while at the same time as observed from **figure 2.53** the wall is at its local minimum (maximum inward movement). The distribution of the maximum earth pressure is in good agreement with the estimated M-O computed with a dynamic pressure coefficient 0.75 (**figure 2.43)**. Maximum and residual horizontal forces on the wall are 683 kN and 490 kN respectively **(figure 2.12)**. The highest point of application of the resultant force is observed to be equal to 7.6 m at t=3.68 sec while the residual point of application of the resultant force is 3.5 m above the bottom of the wall. And again as noticed from **figure 2.53** the permanent displacement due to rotation is 0.12 m,permanent displacement due to sliding is 0.10 m and the overall horizontal permanent displacement is 0.22 m which is almost equal to the maximum overall displacement 0.23 m.The average settlement is 0.12 m and the differential settlement is 0.17 m **(figure 2.48).**

Peak ground acceleration 0.8g:

The maximum earth pressure behind the left wall is at t=4.34 while at the same time as observed from **figure 2.34** the wall is moving outwards. The distribution of the maximum earth pressure is in good agreement with the estimated M-O computed with a dynamic pressure coefficient 0.75 (**figure 2.21)**. Maximum and residual horizontal forces on the wall are910kN and 440 kN respectively **(figure 2.14)**. The highest point of application of the resultant force is observed to be equal to 7.91 m at t=3.96 sec while the residual point of application of the resultant force is 4.4 m above the bottom of the wall. And again as noticed from **figure 2.34**the permanent displacement due to rotation is 0.15 m,permanent displacement due to sliding is 0.08 m and the overall horizontal permanent displacement is 0.23 m and the maximum overall displacement is 0.3 m.The average settlement is 0.3 m and the differential settlement is 0.2 m **(figure 2.29).**

The maximum earth pressure behind the right wall is at t=4.68 while at the same time as observed from **figure 2.54** the wall is at its local minimum (maximum inward movement). The distribution of the maximum earth pressure is in good agreement with the estimated M-O

computed with a dynamic pressure coefficient 0.75 (**figure 2.43)**. Maximum and residual horizontal forces on the wall are782kN and 517 kN respectively **(figure 2.14)**. The highest point of application of the resultant force is observed to be equal to 8.03 m at t=3.68 sec while the residual point of application of the resultant force is 3.6 m above the bottom of the wall. And again as noticed from **figure 2.54** the permanent displacement due to rotation is 0.14 m,permanent displacement due to sliding is 0.14 m and the overall horizontal permanent displacement is 0.28 m which is equal to the maximum overall displacement.The average settlement is 0.14 m and the differential settlement is 0.21 m **(figure 2.49).**

Peak ground acceleration 1g:

The maximum earth pressure behind the left wall is at t=4.32 while at the same time as observed from **figure 2.35** the wall is moving outwards. The distribution of the maximum earth pressure is in good agreement with the estimated M-O computed with a dynamic pressure coefficient 0.75 (**figure 2.22)**. Maximum and residual horizontal forces on the wall are 1023 kN and 459 kN respectively **(figure 2.16)**. The highest point of application of the resultant force is observed to be equal to 7.97 m at t=3.96 sec while the residual point of application of the resultant force is 4.4 m above the bottom of the wall. And again as noticed from **figure 2.35** the permanent displacement due to rotation is 0.18 m,permanent displacement due to sliding is 0.1 m and the overall horizontal permanent displacement is 0.28 m and the maximum overall displacement is 0.36 m.The average settlement is 0.15 m and the differential settlement is 0.25 m **(figure 2.30).**

The maximum earth pressure behind the right wall is at t=4.66 sec while at the same time as observed from **figure 2.55** the wall is at its local minimum (maximum inward movement). The distribution of the maximum earth pressure is in good agreement with the estimated M-O computed with a dynamic pressure coefficient 0.75 (**figure 2.44)**. Maximum and residual horizontal forces on the wall are 861 kN and 517 kN respectively **(figure 2.14)**. The highest point of application of the resultant force is observed to be equal to 8.17 m at t=3.7 sec while the residual point of application of the resultant force is 3.9 m above the bottom of the wall. And again as noticed from **figure 2.55** the permanent displacement due to rotation is 0.17

m,permanent displacement due to sliding is 0.19 m and the overall horizontal permanent displacement is 0.35 m which is equal to the maximum overall displacement.The average settlement is 0.14 m and the differential settlement is 0.25 m **(figure 2.50).**

2.5.2 LEFKADA SEISMIC EXCITATION

Left wall

Dynamic earth pressures, horizontal forces and acceleration

Figures 2.71-2.73 show the distribution of the earth pressures on the left wall at the time of : Maximum pressure, maximum horizontal displacement, maximum differential settlement and residual pressure after the earthquake. Earth pressure increases with the depth at all times except for the maximum pressure. Again a reduction of the earth pressure is noticed close to the top of the wall. This happens when the wall tries to rotate because of the static pressure; the soil due to its cohesion loses contact with the wall. As observedthe distributions of the earth pressures at maximum horizontal displacement and differential settlement are very close.

As can be seen from horizontal force-time diagrams for all the peak accelerations (**Figures 2.77, 2.79, 2.81**),it is noticed that the left and right wall are again completely out of phase for all the peak accelerations.. A prove that it is not a symmetrical problem. In opposition to the observations of Al-Homoud and Whitman (1999),the highest location of the resultant force above the bottom of the wall doesn't occur at the same time of the maximum lateral pressure on the wall **(Figures 2.77-2.82)**,while the maximum inward movement occurs at the same time of the maximum lateral pressure**(Figures 2.89-2.91)**.

Comparison to MO:

Same approximations as with the Aegion seismic excitation were used to estimate the expected lateral thrust using two dynamic earth pressure coefficients **(Figures 2.74-2.76).**One can notice that the distribution of the maximum earth pressures are more like trapezoidal shape than the triangular one estimated by MO.

Right Wall

Dynamic earth pressures, horizontal forces and acceleration

Earth pressure increases with the depth at all times except for the maximum pressure. A reduction of the earth pressure is noticed close to the top of the wall for the same reason it happens in the left wall **(Figures 2.92-2.94)**.Again in opposition to the observations of Al-Homoud and Whitman (1999),the highest location of the resultant force above the bottom of the wall doesn't occur at the same time of the maximum lateral pressure on the wall **(Figures 2.77-2.82)**.On the other hand, the maximum inward movement occurs at the same time of the maximum lateral pressure, where the displacement at the moment of the maximum pressure is at its local minimum **(Figures 2.101-2.103)**.

Comparison to MO:

Same approximations as with the left wall were used to estimate the expected lateral thrust using two dynamic earth pressure coefficients **(Figures 2.95-2.97).**Again it is noticed that the distribution of the maximum earth pressures are more like trapezoidal shape than the triangular one estimated by MO.

Peak ground acceleration 0.3g:

The maximum earth pressure behind the left wall is at t=9.94 while at the same time as observed from **figure 2.89**the horizontal displacement is at its local minimum (moving inwards). The distribution of the maximum earth pressure as mentioned before has the shape of a trapezoid (**figure 2.74)**, and an increased height of the resultant earth force can be observed that can be attributed to the rotation and sliding of the wall that reduces the penetration of the wall heel in the backfill. Maximum and residual horizontal forces on the wall are 610kN and 402 kN respectively **(figure 2.71)**. The highest point of application of the resultant force is observed to be equal to 7.56 m at t=8.92 sec while the residual point of application of the resultant force is 3.85 m above the bottom of the wall. And again as noticed from **figure 2.89**the permanent displacement due to rotation is 0.16 m,permanent displacement due to sliding is 0.06 m and the overall horizontal permanent displacement is 0.22m and the maximum overall

displacement is 0.25m.The average settlement is 0.11 m and the differential settlement is 0.21 m **(figure 2.86).**

The maximum earth pressure behind the right wall is at t=10.86 sec while at the same time as observed from **figure 2.101** the wall is at its local minimum (maximum inward movement).The distribution of the maximum earth pressure as mentioned before has the shape of a trapezoid (**figure 2.95)**. Maximum and residual horizontal forces on the wall are 600kN and 370 kN respectively **(figure 2.71)**. The highest point of application of the resultant force is observed to be equal to 7.12 m at t=8.64 sec while the residual point of application of the resultant force is 4.24 m above the bottom of the wall. And again as noticed from **figure 2.101**the permanent displacement due to rotation is 0.15m,permanent displacement due to sliding is 0.06 m and the overall horizontal permanent displacement is 0.21 m which is close to the maximum overall displacement(0.23 m).The average settlement is 0.11 m and the differential settlement is 0.19 m **(figure 2.98).**

Peak ground acceleration 0.6g:

The maximum earth pressure behind the left wall is at t=9.94sec while at the same time as observed from **figure 2.90**the horizontal displacement is at its local minimum (moving inwards). The distribution of the maximum earth pressure as mentioned before has the shape of a trapezoid (**figure 2.75)**, and an increased height of the resultant earth force can be observed that can be attributed to the rotation and sliding of the wall that reduces the penetration of the wall heel in the backfill. Maximum and residual horizontal forces on the wall are 829kN and 400 kN respectively **(figure 2.73)**. The highest point of application of the resultant force is observed to be equal to 8.56 m at t=7.02 sec while the residual point of application of the resultant force is 3.85 m above the bottom of the wall. And again as noticed from **figure 2.90**the permanent displacement due to rotation is 0.43 m,permanent displacement due to sliding is 0.17m and the overall horizontal permanent displacement is 0.60 m which is close to the maximum overall displacement(0.63 m).The average settlement is 0.18 m and the differential settlement is 0.54 m **(figure 2.87).**

The maximum earth pressure behind the right wall is at t=10.88 sec while at the same time as observed from **figure 2.102** the wall is at its local minimum (maximum inward movement). The distribution of the maximum earth pressure as mentioned before has the shape of a trapezoid (**figure 2.96)**. Maximum and residual horizontal forces on the wall are 737kN and 377 kN respectively **(figure 2.73)**. The highest point of application of the resultant force is observed to be equal to 8.06 m at t=8.66 sec while the residual point of application of the resultant force is 4.60 m above the bottom of the wall. And again as noticed from **figure 2.102**the permanent displacement due to rotation is 0.44 m,permanent displacement due to sliding is 0.18 m and the overall horizontal permanent displacement is 0.63 m which is close to the maximum overall displacement(0.66 m).The average settlement is 0.19m and the differential settlement is 0.55 m **(figure 2.99).**

Peak ground acceleration 0.9g:

The maximum earth pressure behind the left wall is at t=9.38 sec while at the same time as observed from **figure 2.91**the horizontal displacement is at its local minimum (moving inwards). The distribution of the maximum earth pressure as mentioned before has the shape of a trapezoid (**figure 2.76)**, and an increased height of the resultant earth force can be observed that can be attributed to the rotation and sliding of the wall that reduces the penetration of the wall heel in the backfill. Maximum and residual horizontal forces on the wall are 911 kN and 388 kN respectively **(figure 2.75)**. The highest point of application of the resultant force is observed to be equal to 9.38 m at t=7.04 sec while the residual point of application of the resultant force is 4.29 m above the bottom of the wall. And again as noticed from **figure 2.91** the permanent displacement due to rotation is 0.76 m,permanent displacement due to sliding is 0.39 m and the overall horizontal permanent displacement is 1.14 m which is close to the maximum overall displacement (1.19 m).The average settlement is 0.28 m and the differential settlement is 0.99 m **(figure 2.88).**

The maximum earth pressure behind the right wall is at t=7.64 sec while at the same time as observed from **figure 2.103** the wall is at its local minimum (maximum inward movement). The distribution of the maximum earth pressure as mentioned before has the shape of a trapezoid

(**figure 2.97)**. Maximum and residual horizontal forces on the wall are 815 kN and 409 kN respectively **(figure 2.75)**. The highest point of application of the resultant force is observed to be equal to 8.64 m at t=8.7 sec while the residual point of application of the resultant force is 4.45 m above the bottom of the wall. And again as noticed from **figure 2.103**the permanent displacement due to rotation is 0.80m,permanent displacement due to sliding is 0.40 m and the overall horizontal permanent displacement is 1.2 m which is equal to the maximum overall displacement. The average settlement is 0.29m and the differential settlement is 0.98 m **(figure 2.100).**

2.5.3 TAKATORI SEISMIC EXCITATION

Left wall

Dynamic earth pressures, horizontal forces and acceleration

Figures 2.118-2.120 show the distribution of the earth pressures on the left wall at the time of : Maximum pressure, maximum horizontal displacement, maximum differential settlement and residual pressure after the earthquake. Earth pressure increases with the depth at all times except for the maximum pressure. Again a reduction of the earth pressure is noticed close to the top of the wall,this happens for the same reason mentioned above.

As can be seen from horizontal force-time diagrams for all the peak accelerations (**Figures 2.124, 2.126, 2.128**),it is noticed that the left and right wall are again completely out of phase for all the peak accelerations.. A prove that it is not a symmetrical problem. In opposition to the observations of Al-Homoud and Whitman (1999),the highest location of the resultant force above the bottom of the wall doesn't occur at the same time of the maximum lateral pressure on the wall **(Figures 2.124-2.129)**.At the time of the maximum horizontal force the horizontal displacement is almost at its local minimum (inward movement)**(Figures 2.136-2.138)**.

Comparison to MO:

Same approximations as with the Aegion seismic excitation were used to estimate the expected lateral thrust using two dynamic earth pressure coefficients **(Figures 2.121-2.123).**

Right Wall

Dynamic earth pressures, horizontal forces and acceleration

Earth pressure increases with the depth at all times except for the maximum pressure. A reduction of the earth pressure is noticed close to the top of the wall for the same reason it happens in the left wall **(Figures 2.139-2.141)**.Again in opposition to the observations of Al-Homoud and Whitman (1999),the highest location of the resultant force above the bottom of the wall doesn't occur at the same time of the maximum lateral pressure on the wall **(Figures 2.124-2.129)**.On the other hand, at the time of the maximum horizontal force the horizontal displacement is almost at its local minimum (inward movement)**(Figures 2.148-2.150)**.

Comparison to MO:

Same approximations as with the left wall were used to estimate the expected lateral thrust using two dynamic earth pressure coefficients **(Figures 2.142-2.144).**One can notice that the distribution of the maximum earth pressures are more like trapezoidal shape than the triangular one estimated by MO.

Peak ground acceleration 0.3g:

The maximum earth pressure behind the left wall is at t=9.16 sec while at the same time as observed from **figure 2.136** the wall is moving inwards. The distribution of the maximum earth pressure is in good agreement with the estimated M-O computed with a dynamic pressure coefficient 1 (**figure 2.121)**, and an increased height of the resultant earth force can be observed that can be attributed to the rotation and sliding of the wall that reduces the penetration of the wall heel in the backfill. Maximum and residual horizontal forces on the wall are 724 kN and 462 kN respectively **(figure 2.124)**. The highest point of application of the resultant force is observed to be equal to 7.5 m at t=5.9 sec while the residual point of application of the resultant force is 4.4 m above the bottom of the wall. And again as noticed from **figure 2.136** the permanent displacement due to rotation is 0.29m,permanent displacement due to sliding is 0.12 m and the overall horizontal permanent displacement is 0.41

m and the maximum overall displacement is 0.48m.The average settlement is 0.13 m and the differential settlement is 0.37 m **(figure 2.133).**

The maximum earth pressure behind the right wall is at t=8.8 sec while at the same time as observed from **figure 2.148** the wall is moving inwards. The distribution of the maximum earth pressure as mentioned before has the shape of a trapezoid (**figure 2.142)**. Maximum and residual horizontal forces on the wall are 600 kN and 370 kN respectively **(figure 2.124)**. The highest point of application of the resultant force is observed to be equal to 7.7 m at t=7.6 sec while the residual point of application of the resultant force is 3.8 m above the bottom of the wall. And again as noticed from **figure 2.148**the permanent displacement due to rotation is 0.30 m,permanent displacement due to sliding is 0.11 m and the overall horizontal permanent displacement is 0.41 m and the maximum overall displacement is 0.48 m.The average settlement is 0.13 m and the differential settlement is 0.38 m **(figure 2.145).**

Peak ground acceleration 0.6g:

The maximum earth pressure behind the left wall is at t=6.14 sec while at the same time as observed from **figure 2.137**the wall is moving outwards. The distribution of the maximum earth pressure is in good agreement with the estimated M-O computed with a dynamic pressure coefficient 1 (**figure 2.122)**, and an increased height of the resultant earth force can be observed that can be attributed to the rotation and sliding of the wall that reduces the penetration of the wall heel in the backfill. Maximum and residual horizontal forces on the wall are 1049kN and 473 kN respectively **(figure 2.126)**. The highest point of application of the resultant force is observed to be equal to 8.0 m at t=5.8 sec while the residual point of application of the resultant force is 4.2 m above the bottom of the wall. And again as noticed from **figure 2.137**the permanent displacement due to rotation is 0.97 m,permanent displacement due to sliding is 0.50 m and the overall horizontal permanent displacement is 1.47 m and the maximum overall displacement is 1.52 m.The average settlement is 0.22m and the differential settlement is 1.22 m **(figure 2.134).**

The maximum earth pressure behind the right wall is at t=9.16 sec while at the same time as observed from **figure 2.149** the wall is moving inwards. The distribution of the maximum earth

pressure as mentioned before has the shape of a trapezoid (**figure 2.143)**. Maximum and residual horizontal forces on the wall are 600 kN and 370 kN respectively **(figure 2.142)**. The highest point of application of the resultant force is observed to be equal to 8.34 m at t=5.4 sec while the residual point of application of the resultant force is 4.7 m above the bottom of the wall. And again as noticed from **figure 2.149**the permanent displacement due to rotation is 1.03m,permanent displacement due to sliding is 0.46 m and the overall horizontal permanent displacement is 1.48 m and the maximum overall displacement is 1.55 m. The average settlement is 0.25 m and the differential settlement is 1.21 m **(figure 2.146).**

Peak ground acceleration 0.9g:

The maximum earth pressure behind the left wall is at t=6.16 sec while at the same time as observed from **figure 2.138**the wall is moving outwards. The distribution of the maximum earth pressure is in good agreement with the estimated M-O computed with a dynamic pressure coefficient 1 (**figure 2.123)**, and an increased height of the resultant earth force can be observed that can be attributed to the rotation and sliding of the wall that reduces the penetration of the wall heel in the backfill. Maximum and residual horizontal forces on the wall are 1274kN and 450 kN respectively **(figure 2.128)**. The highest point of application of the resultant force is observed to be equal to 8.19 m at t=5.84 sec while the residual point of application of the resultant force is 4.42 m above the bottom of the wall. And again as noticed from **figure 2.138** the permanent displacement due to rotation is 1.82m,permanent displacement due to sliding is 0.99 m and the overall horizontal permanent displacement is 2.82 m which is equal to the maximum overall displacement.The average settlement is 0.30m and the differential settlement is 2.13 m **(figure 2.135).**

The maximum earth pressure behind the right wall is at t=10.12 sec while at the same time as observed from **figure 2.150** the wall is moving inwards and it's at its local minimum. The distribution of the maximum earth pressure as mentioned before has the shape of a trapezoid (**figure 2.144)**. Maximum and residual horizontal forces on the wall are 1257kN and 460 kN respectively **(figure 2.143)**. The highest point of application of the resultant force is observed to be equal to 8.7 m at t=5.4 sec while the residual point of application of the resultant force is

4.53 m above the bottom of the wall. And again as noticed from **figure 2.150** the permanent displacement due to rotation is 1.89m,permanent displacement due to sliding is 0.98 m and the overall horizontal permanent displacement is 2.87 m and the maximum overall displacement is 2.97m. The average settlement is 0.36 m and the differential settlement is 2.15 m **(figure 2.147).**

2.5.4 Kalamata Seismic excitation

Left wall

Dynamic earth pressures, horizontal forces and acceleration

Figures 2.165-2.167show the distribution of the earth pressures on the left wall at the time of : Maximum pressure, maximum horizontal displacement, maximum differential settlement and residual pressure after the earthquake. Earth pressure increases with the depth. Again a reduction of the earth pressure is noticed close to the top of the wall.

As can be seen from horizontal force-time diagrams for all the peak accelerations (**Figures 2.171, 2.173, 2.175**),it is noticed that the left and right wall are again completely out of phase for all the peak accelerations.. A prove that it is not a symmetrical problem. In opposition to the observations of Al-Homoud and Whitman (1999),the highest location of the resultant force above the bottom of the wall doesn't occur at the same time of the maximum lateral pressure on the wall **(Figures 2.171-2.176)**,while the maximum inward movement occurs at the same time of the maximum lateral pressure **(Figures 2.183-2.185)**.

Comparison to MO

Same approximations as with the Aegion seismic excitation were used to estimate the expected lateral thrust using two dynamic earth pressure coefficients **(Figures 2.189-2.191).**

Right Wall

Dynamic earth pressures, horizontal forces and acceleration

Earth pressure increases with the depth. A reduction of the earth pressure is noticed close to the top of the wall for the same reason it happens in the left wall **(Figures 2.186-2.188)**.Again in

opposition to the observations of Al-Homoud and Whitman (1999),the highest location of the resultant force above the bottom of the wall doesn't occur at the same time of the maximum lateral pressure on the wall **(Figures 2.171-2.176)**.On the other hand, the maximum lateral pressure occurs when the wall is moving inwards**(Figures 2.195-2.197)**.

Comparison to MO:

Same approximations as with the left wall were used to estimate the expected lateral thrust using two dynamic earth pressure coefficients **(Figures 2.189-2.191).**

Peak acceleration 0.3g

The maximum earth pressure behind the left wall is at t=7.2 sec while at the same time as observed from **figure 2.183** the wall is moving inwards. The distribution of the maximum earth pressure is in good agreement with the estimated M-O computed with a dynamic pressure coefficient 1 **(figure 2.168)**. Maximum and residual horizontal forces on the wall are 586 kN and 366 kN respectively **(figure 2.171)**. The highest point of application of the resultant force is observed to be equal to 6.6 m at t=5.48 sec while the residual point of application is 4.1 m above the bottom of the wall. And again as noticed from **figure 2.183** the permanent displacement due to rotation is 0.11 m,permanent displacement due to sliding is 0.08 m and the overall horizontal permanent displacement is 0.18 m which is almost equal to the maximum overall displacement (0.20 m).The average settlement is 0.11 m and the differential settlement is 0.13 m **(figure 2.180).**

The maximum earth pressure behind the right wall is at t=6.8 while at the same time as observed from **figure 2.195** the wall is moving inwards. The distribution of the maximum earth pressure is in good agreement with the estimated M-O computed with a dynamic pressure coefficient 1 **(figure 2.189)**. Maximum and residual horizontal forces on the wall are 512 kN and 385 kN respectively **(figure 2.171)**. The highest point of application of the resultant force is observed to be equal to 7.02 m at t=6.38 sec while the residual point of application is 4.2 m above the bottom of the wall. And again as noticed from **figure 2.195** the permanent displacement due to rotation is 0.11 m,permanent displacement due to sliding is 0.018 m and

the overall horizontal permanent displacement is 0.12 m and the maximum overall displacement is 0.17 m.The average settlement is 0.11 m and the differential settlement is 0.14m**(figure2.192).**

Peak acceleration 0.6g

The maximum earth pressure behind the left wall is at t=7.2 sec while at the same time as observed from **figure 2.184** the wall is moving inwards. The distribution of the maximum earth pressure is in good agreement with the estimated M-O computed with a dynamic pressure coefficient 1 **(figure 2.169)**. Maximum and residual horizontal forces on the wall are 917 kN and 381 kN respectively **(figure 2.173)**. The highest point of application of the resultant force is observed to be equal to 7.4 m at t=5.5 sec while the residual point of application is 4.2 m above the bottom of the wall. And again as noticed from **figure 2.184** the permanent displacement due to rotation is 0.28 m,permanent displacement due to sliding is 0.18 m and the overall horizontal permanent displacement is 0.46 m which is equal to the maximum overall displacement.The average settlement is 0.16 m and the differential settlement is 0.33 m **(figure 2.181).**

The maximum earth pressure behind the right wall is at t=6.8 while at the same time as observed from **figure 2.196** the wall is moving inwards. The distribution of the maximum earth pressure is in good agreement with the estimated M-O computed with a dynamic pressure coefficient 1 **(figure 2.190)**. Maximum and residual horizontal forces on the wall are 785 kN and 430 kN respectively **(figure 2.173)**. The highest point of application of the resultant force is observed to be equal to 7.9 m at t=6.46 sec while the residual point of application is 4.1 m above the bottom of the wall. And again as noticed from **figure 2.196** the permanent displacement due to rotation is 0.24 m,permanent displacement due to sliding is 0.05 m and the overall horizontal permanent displacement is 0.30 m and the maximum overall displacement is 0.37 m.The average settlement is 0.16 m and the differential settlement is 0.30 m **(figure 2.193).**

Peak acceleration 0.9g

The maximum earth pressure behind the left wall is at t=7.14 sec while at the same time as observed from **figure 2.185** the wall is moving inwards. The distribution of the maximum earth pressure is in good agreement with the estimated M-O computed with a dynamic pressure coefficient 1 **(figure 2.170)**. Maximum and residual horizontal forces on the wall are 1080 kN and 380 kN respectively **(figure 2.175)**. The highest point of application of the resultant force is observed to be equal to 8.17 m at t=6.74 sec while the residual point of application is 4.5 m above the bottom of the wall. And again as noticed from **figure 2.185** the permanent displacement due to rotation is 0.48 m,permanent displacement due to sliding is 0.37 m and the overall horizontal permanent displacement is 0.85 m which is equal to the maximum overall displacement.The average settlement is 0.22 m and the differential settlement is 0.56m **(figure 2.182).**

The maximum earth pressure behind the right wall is at t=6.8 while at the same time as observed from **figure 2.197** the wall is moving inwards. The distribution of the maximum earth pressure is in good agreement with the estimated M-O computed with a dynamic pressure coefficient 1 **(figure 2.191)**. Maximum and residual horizontal forces on the wall are 991 kN and 447 kN respectively **(figure 2.175)**. The highest point of application of the resultant force is observed to be equal to 8.05 m at t=5.12 sec while the residual point of application is 4.2 m above the bottom of the wall. And again as noticed from **figure 2.197** the permanent displacement due to rotation is 0.36 m,permanent displacement due to sliding is 0.07 m and the overall horizontal permanent displacement is 0.42 m and the maximum overall displacement is 0.54 m.The average settlement is 0.20 m and the differential settlement is 0.47 m **(figure 2.194).**

2.5.5 Sakarya Seismic excitation

Left wall

Dynamic earth pressures, horizontal forces and acceleration

Figures 2.212-2.214show the distribution of the earth pressures on the left wall at the time of : Maximum pressure, maximum horizontal displacement, maximum differential

settlement and residual pressure after the earthquake. Earth pressure increases with the depth. Again a reduction of the earth pressure is noticed close to the top of the wall.

As can be seen from horizontal force-time diagrams for all the peak accelerations (**Figures 2.218, 2.220, 2.222**),it is noticed that the left and right wall are again completely out of phase for all the peak accelerations.. A prove that it is not a symmetrical problem. In opposition to the observations of Al-Homoud and Whitman (1999),the highest location of the resultant force above the bottom of the wall doesn't occur at the same time of the maximum lateral pressure on the wall **(Figures 2.218-2.223)**,while the maximum inward movement occurs at the same time of the maximum lateral pressure **(Figures 2.183-2.185)**.

Comparison to MO

Same approximations as with the Aegion seismic excitation were used to estimate the expected lateral thrust using two dynamic earth pressure coefficients **(Figures 2.189-2.191).**

Right Wall

Dynamic earth pressures, horizontal forces and acceleration

Earth pressure increases with the depth. A reduction of the earth pressure is noticed close to the top of the wall for the same reason it happens in the left wall **(Figures 2.186-2.188)**.Again in opposition to the observations of Al-Homoud and Whitman (1999),the highest location of the resultant force above the bottom of the wall doesn't occur at the same time of the maximum lateral pressure on the wall **(Figures 2.171-2.176)**.On the other hand, the maximum lateral pressure occurs when the wall is moving inwards **(Figures 2.195-2.197)**.

Comparison to MO:

Same approximations as with the left wall were used to estimate the expected lateral thrust using two dynamic earth pressure coefficients **(Figures 2.189-2.191).**

Peak ground acceleration 0.3g:

The maximum earth pressure behind the left wall is at t=8.96 while at the same time as observed from **figure 2.230**the wall is moving inwards. The distribution of the maximum earth

pressure as mentioned before has the shape of a trapezoid (**figure 2.215)**, and an increased height of the resultant earth force can be observed that can be attributed to the rotation and sliding of the wall that reduces the penetration of the wall heel in the backfill. Maximum and residual horizontal forces on the wall are 482kN and 368 kN respectively **(figure 2.218)**. The highest point of application of the resultant force is observed to be equal to 6.7 m at t=9.5 sec while the residual point of application of the resultant force is 4.6 m above the bottom of the wall. And again as noticed from **figure 2.230**the permanent displacement due to rotation is +0.084 m,permanent displacement due to sliding is -0.12 m and the overall horizontal permanent displacement is -0.04 m and the maximum overall displacement is -0.2 m.The average settlement is 0.09 m and the differential settlement is 0.12 m **(figure 2.227).**
The maximum earth pressure behind the right wall is at t=10.26 sec while at the same time as observed from **figure 2.233** the wall is moving inwards. The distribution of the maximum earth pressure as mentioned before has the shape of a trapezoid (**figure 2.236)**. Maximum and residual horizontal forces on the wall are 524kN and 400 kN respectively **(figure 2.218)**. The highest point of application of the resultant force is observed to be equal to 6.9 m at t=9.8 sec while the residual point of application of the resultant force is 4.0 m above the bottom of the wall. And again as noticed from **figure 2.233**the permanent displacement due to rotation is 0.097 m,permanent displacement due to sliding is 0.206 m and the overall horizontal permanent displacement is 0.30 m which is close to the maximum overall displacement is 0.36 m.The average settlement is 0.097 m and the differential settlement is 0.13 m **(figure 2.239).**

Peak ground acceleration 0.6g:

The maximum earth pressure behind the left wall is at t=8.92 while at the same time as observed from **figure 2.231**the wall is moving inwards. The distribution of the maximum earth pressure as mentioned before has the shape of a trapezoid (**figure 2.216)**, and an increased height of the resultant earth force can be observed that can be attributed to the rotation and sliding of the wall that reduces the penetration of the wall heel in the backfill. Maximum and residual horizontal forces on the wall are 711 kN and 423 kN respectively **(figure 2.220)**. The highest point of application of the resultant force is observed to be equal to 7.6 m at t=7.4 sec

while the residual point of application of the resultant force is 4.1 m above the bottom of the wall. And again as noticed from **figure 2.231** the permanent displacement due to rotation is +0.27 m,permanent displacement due to sliding is -0.19 m and the overall horizontal permanent displacement is -0.073 m and the maximum overall displacement is -0.362 m.The average settlement is 0.14 m and the differential settlement is 0.32 m **(figure 2.228).**

The maximum earth pressure behind the right wall is at t=10.22 sec while at the same time as observed from **figure 2.234** the wall is moving inwards. The distribution of the maximum earth pressure as mentioned before has the shape of a trapezoid (**figure 2.237)**. Maximum and residual horizontal forces on the wall are 826kN and 440 kN respectively **(figure 2.220)**. The highest point of application of the resultant force is observed to be equal to 7.1 m at t=8.12 sec while the residual point of application of the resultant force is 3.8 m above the bottom of the wall. And again as noticed from **figure 2.234** the permanent displacement due to rotation is 0.31m,permanent displacement due to sliding is 0.42 m and the overall horizontal permanent displacement is 0.73 m and the maximum overall displacement is 0.80 m.The average settlement is 0.15 m and the differential settlement is 0.37 m **(figure 2.240).**

Peak ground acceleration 0.9g:

The maximum earth pressure behind the left wall is at t=8.8 while at the same time as observed from **figure 2.232**the wall is moving inwards. The distribution of the maximum earth pressure as mentioned before has the shape of a trapezoid (**figure 2.217)**, and an increased height of the resultant earth force can be observed that can be attributed to the rotation and sliding of the wall that reduces the penetration of the wall heel in the backfill. Maximum and residual horizontal forces on the wall are 822kN and 467 kN respectively **(figure 2.222)**. The highest point of application of the resultant force is observed to be equal to 8.04 m at t=7.4 sec while the residual point of application of the resultant force is 3.7 m above the bottom of the wall. And again as noticed from **figure 2.232**the permanent displacement due to rotation is +0.52 m,permanent displacement due to sliding is -0.24 m and the overall horizontal permanent displacement is -0.28 m and the maximum overall displacement is -0.56 m.The average settlement is 0.19 m and the differential settlement is 0.60 m **(figure 2.229).**

The maximum earth pressure behind the right wall is at t=10.24 sec while at the same time as observed from **figure 2.235** the wall is moving inwards. The distribution of the maximum earth pressure as mentioned before has the shape of a trapezoid (**figure 2.238)**. Maximum and residual horizontal forces on the wall are 1180kN and 412 kN respectively **(figure 2.222)**. The highest point of application of the resultant force is observed to be equal to 7.4 m at t=11.16 sec while the residual point of application of the resultant force is 4.3 m above the bottom of the wall. And again as noticed from **figure 2.235**the permanent displacement due to rotation is 0.65m,permanent displacement due to sliding is 0.79 m and the overall horizontal permanent displacement is 1.44 m which is equal to the maximum overall displacement .The average settlement is 0.21 m and the differential settlement is 0.80 m **(figure 2.241).**

2.6 SUMMARY AND OBSERVATIONS

Based on the aboveanalyses the main points are the following:

- The distribution of the earth pressures for the left and right wall is completely different. The response of the wall-soil system is that its behavior is, naturally, strongly asymmetrical. The residual horizontal force on the wall, which was approximately 400 kN for all the earthquakes, is always smaller than the maximum horizontal one.A thing that reassures that the peak ground acceleration occurs for only one instant of time.
- Takatori was the most harmful earthquake for the walls ,where the horizontal displacement for a PGA 1g was 2.87 m and the differential settlement was 2.15 m**(figures 2.163-2.164)**. This can be appertaining to the intensity, duration and frequency content.
- Kalamata earthquake with a peak ground acceleration greater than 0.4g caused greater horizontal displacements on the left wall **(figure 2.210)**.This can be attributed to the negative peak accelerations in the input acceleration time history.Due to this characteristic, the left wall,which develops an outward inertia force at the negative accelerations,displays increased outward displacement and tilt compared to the right one.

- There is a linear relationship between the ground peak acceleration and the overall permanent horizontal displacement and the differential settlement as noticed from
- As for the point of application of the maximum dynamic force is at two thirds the wall height above its base, in agreement with the observations if Seed and Whitman (1970). On the other hand, the point of application of the residual force is at one thirds the wall height which reassures that the peak ground acceleration occurs for only one instant of time and doesn't have sufficient duration **(figure 2.68)**.
- The maximum horizontal force on the wall occurs when the wall is moving inwards or almost at its local minimum (maximum inward movement) ,except for the left wall when subjected to the Aegion seismic excitation.

Chapter 2

FIGURES

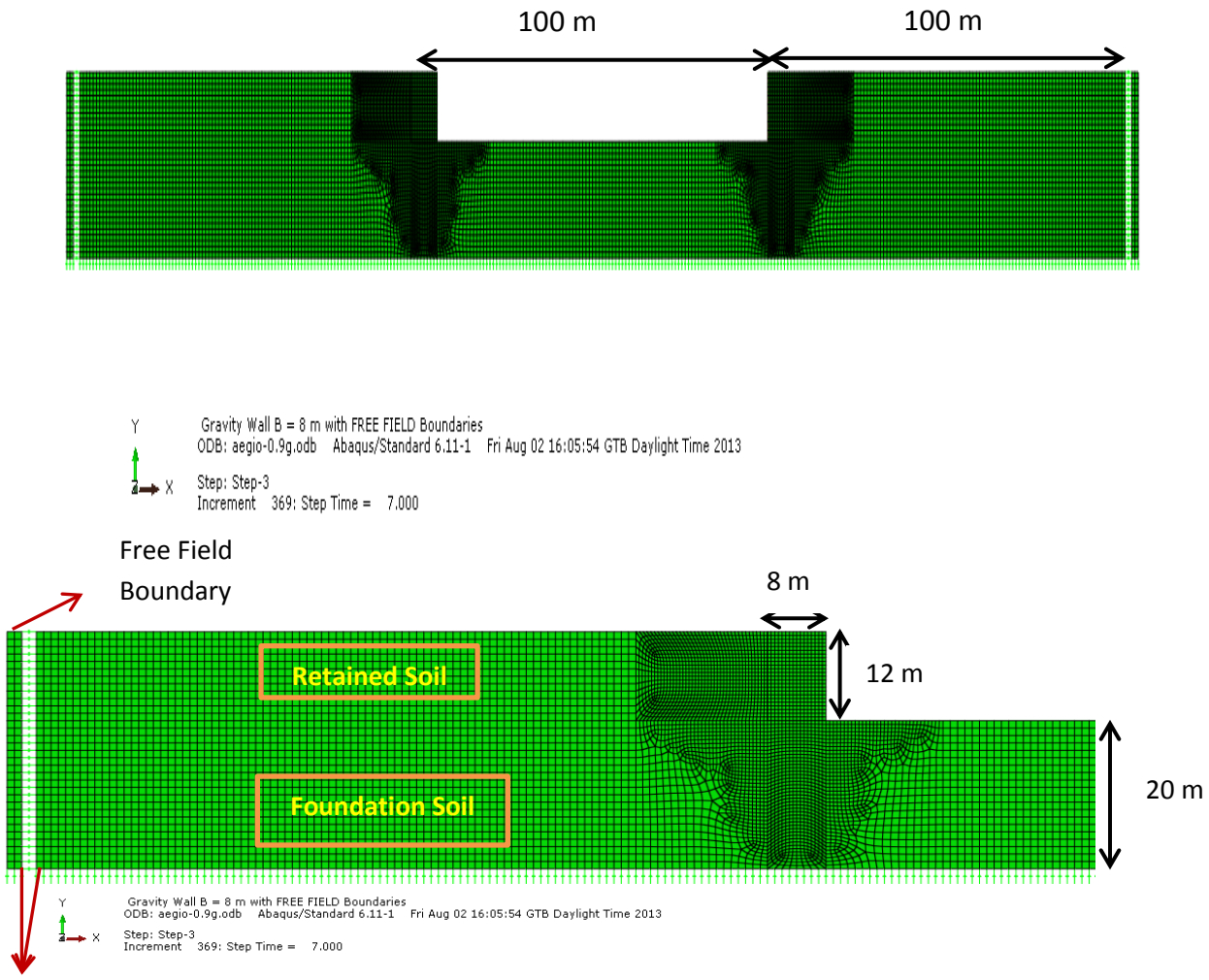

Fig. 2.1. Two-dimensional finite element mesh (ABAQUS) of the problem (soil-structure system)

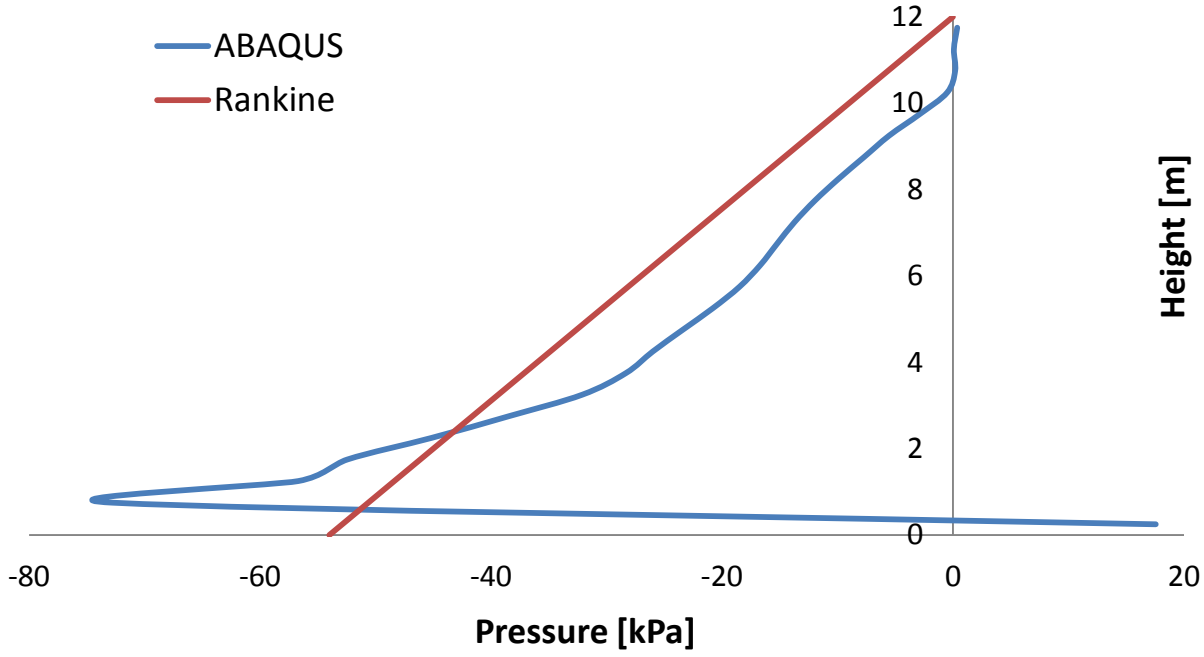

Fig. 2.2. Distribution of static earth pressure computed using the rankine theory and ABAQUS

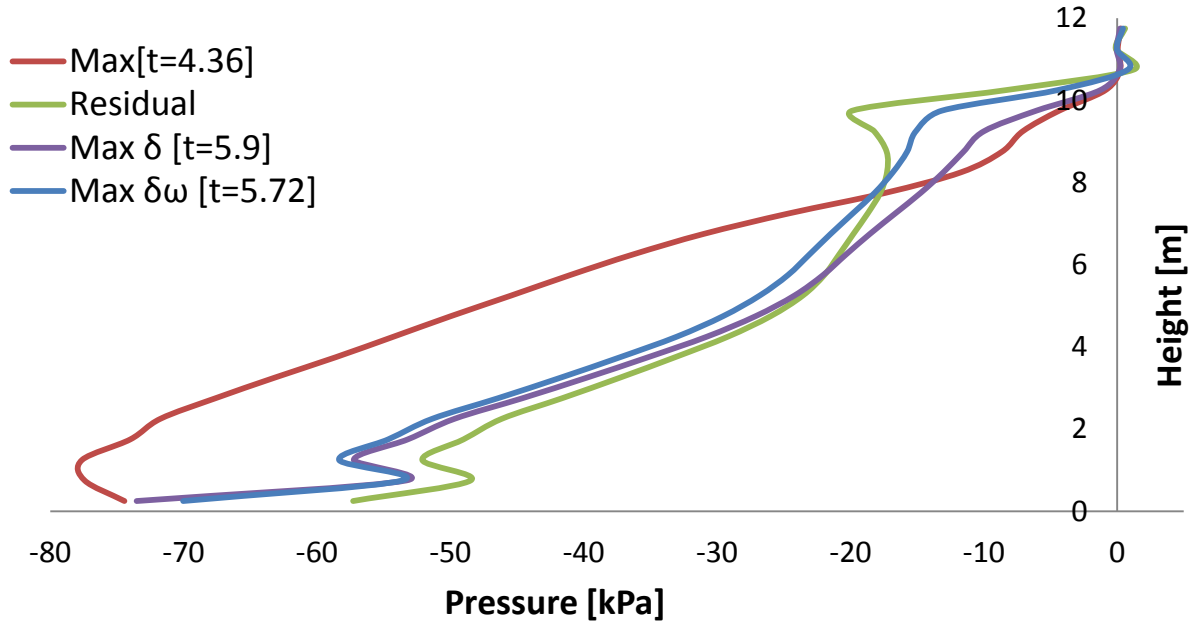

Fig. 2.3. Earth pressures profiles on the left wall at different moments when subjected to Aegion Seismic excitation with peak ground acceleration 0.2g.

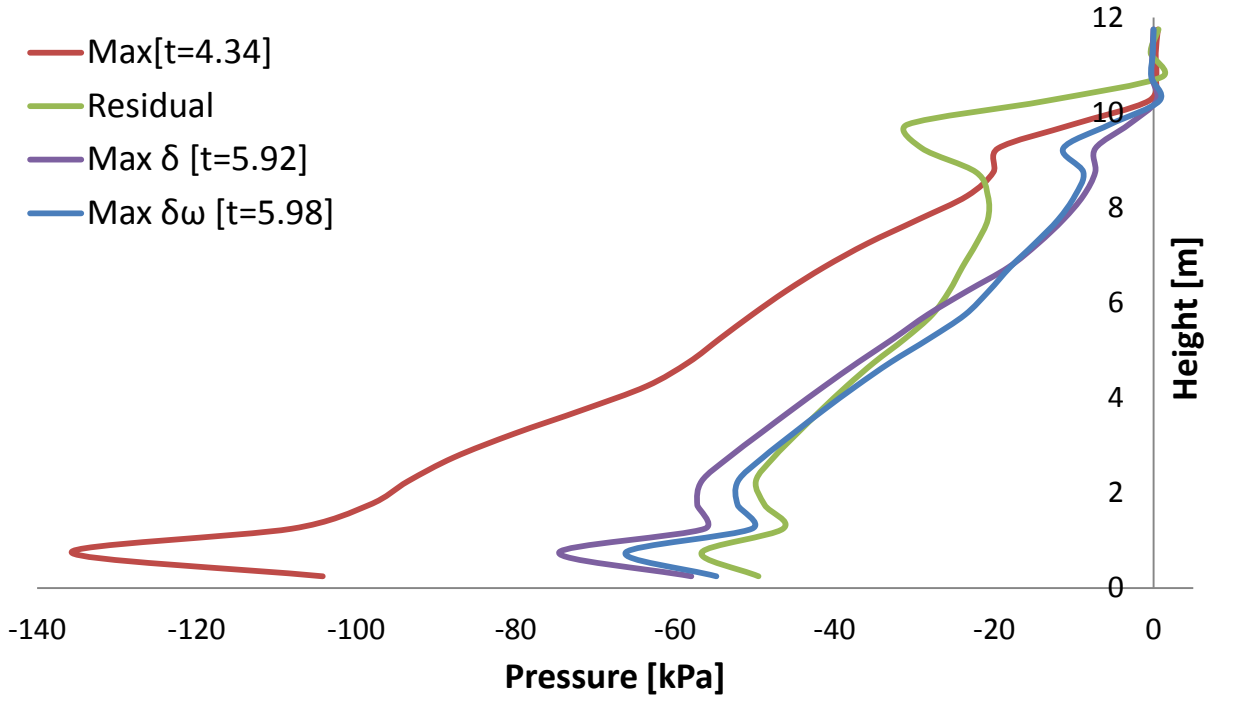

Fig. 2.4. Earth pressures profiles on the left wall at different moments when subjected to Aegion Seismic excitation with peak ground acceleration 0.4g.

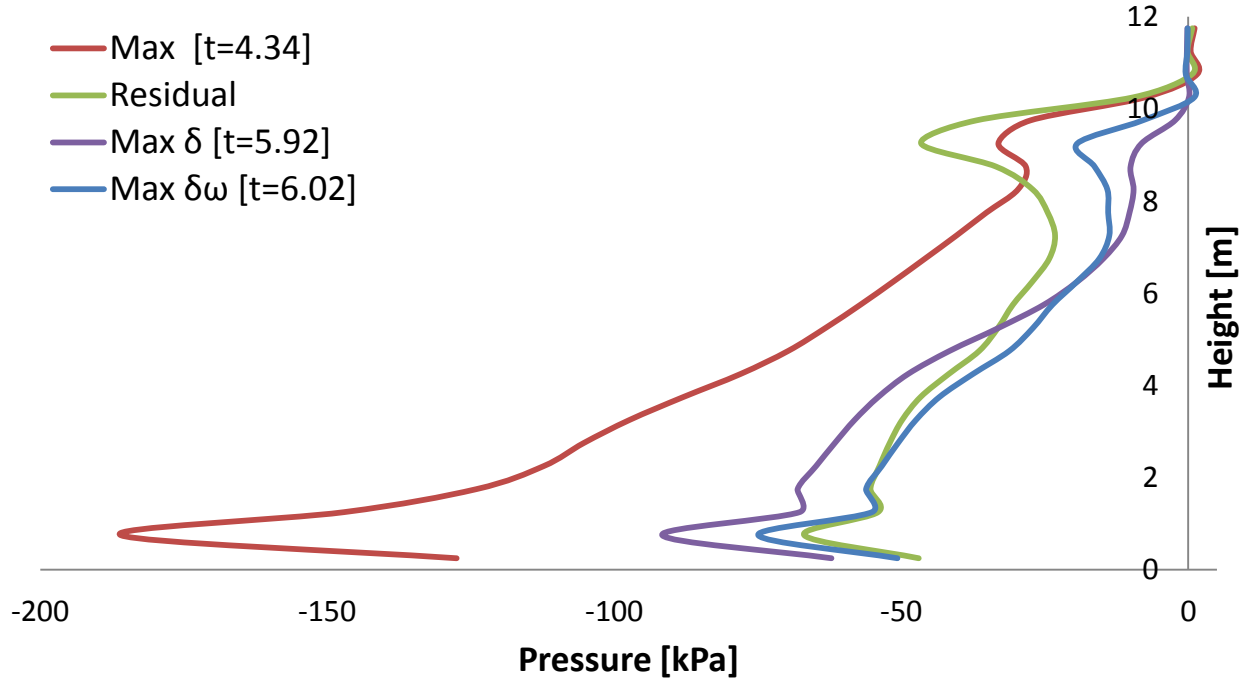

Fig. 2.5. Earth pressures profiles on the left wall at different moments when subjected to Aegion Seismic excitation with peak ground acceleration 0.6g.

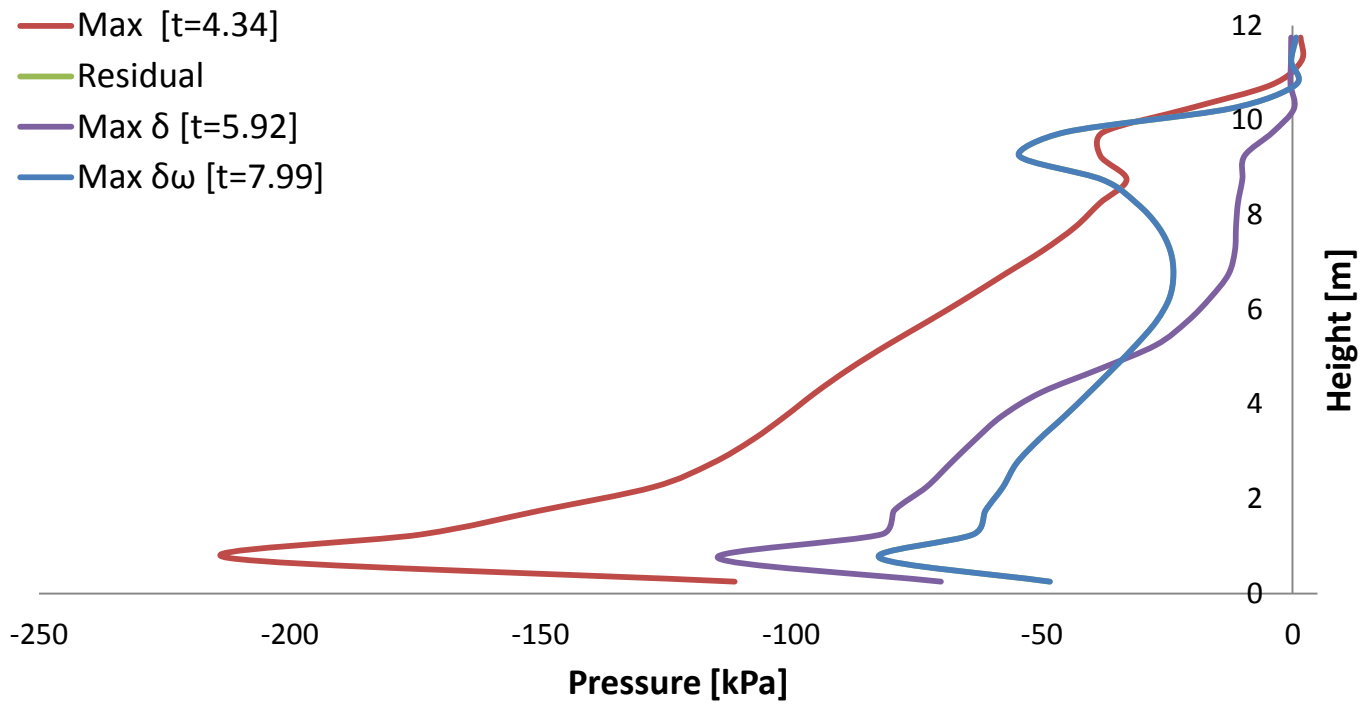

Fig. 2.6. Earth pressures profiles on the left wall at different moments when subjected to Aegion Seismic excitation with peak ground acceleration 0.8g.

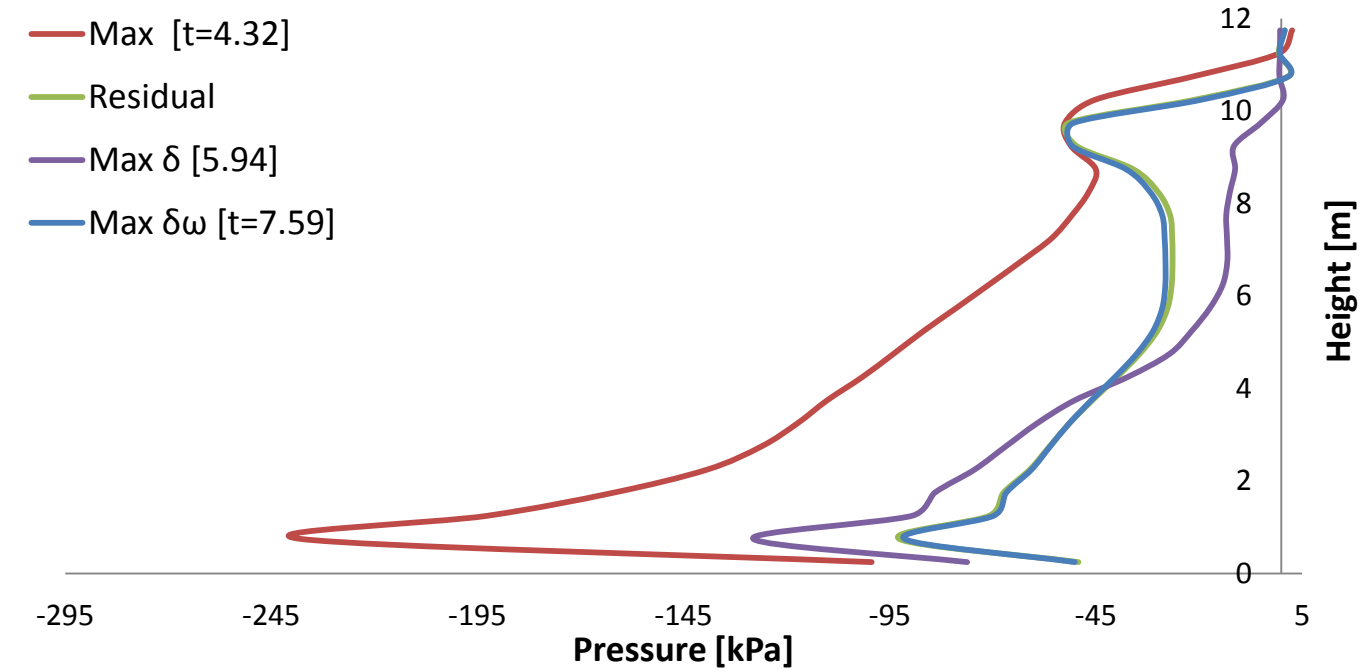

Fig. 2.7. Earth pressures profiles on the left wall at different moments when subjected to Aegion Seismic excitation with peak ground acceleration 1g.

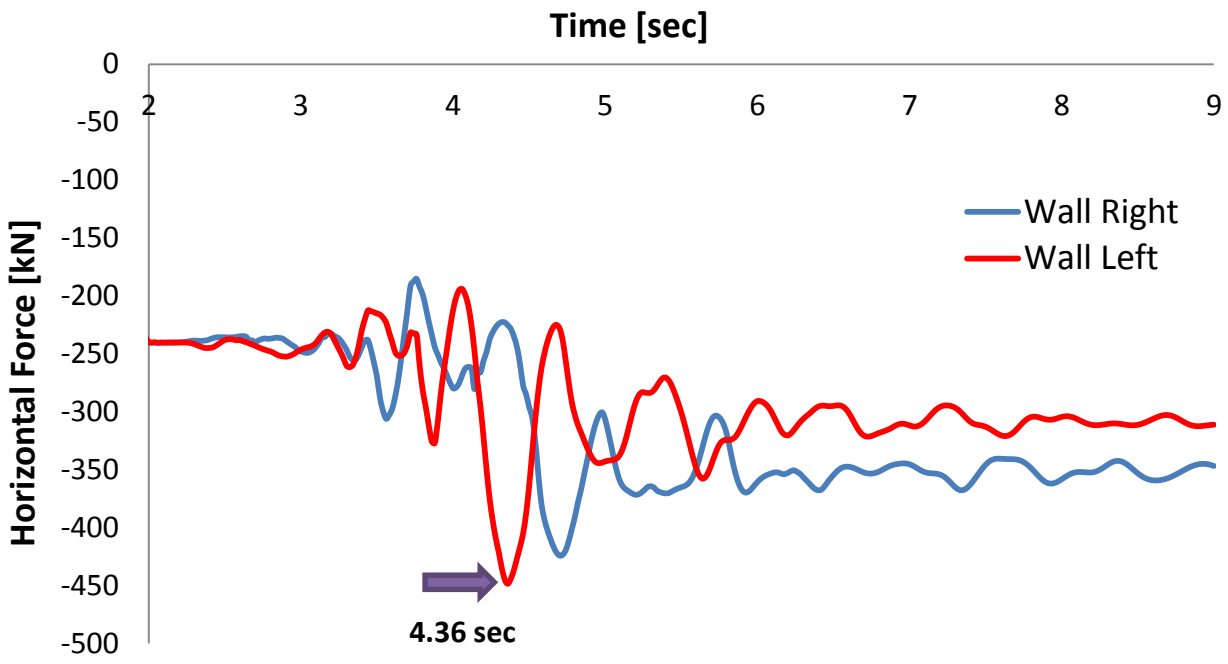

Fig. 2.8. Horizontal force-time history of the left wall when subjected to Aegion Seismic excitation with peak ground acceleration 0.2g

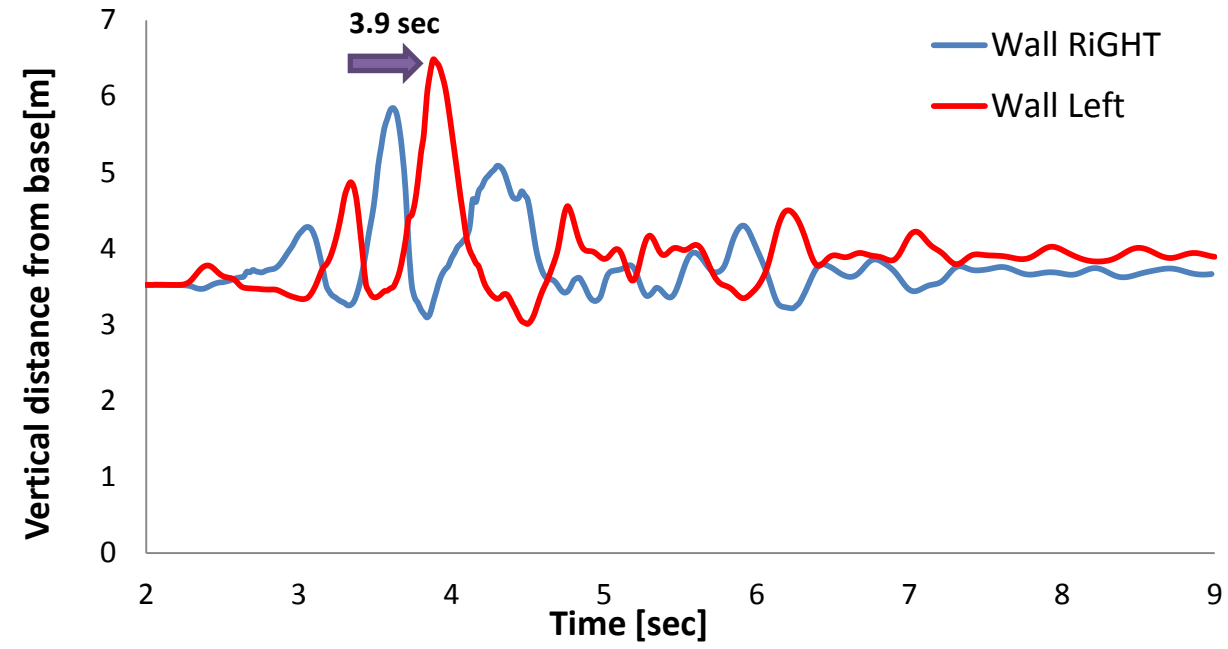

Fig. 2.9. Point of application of dynamic increment on the left wall when subjected to Aegion Seismic excitation with peak ground acceleration 0.2g

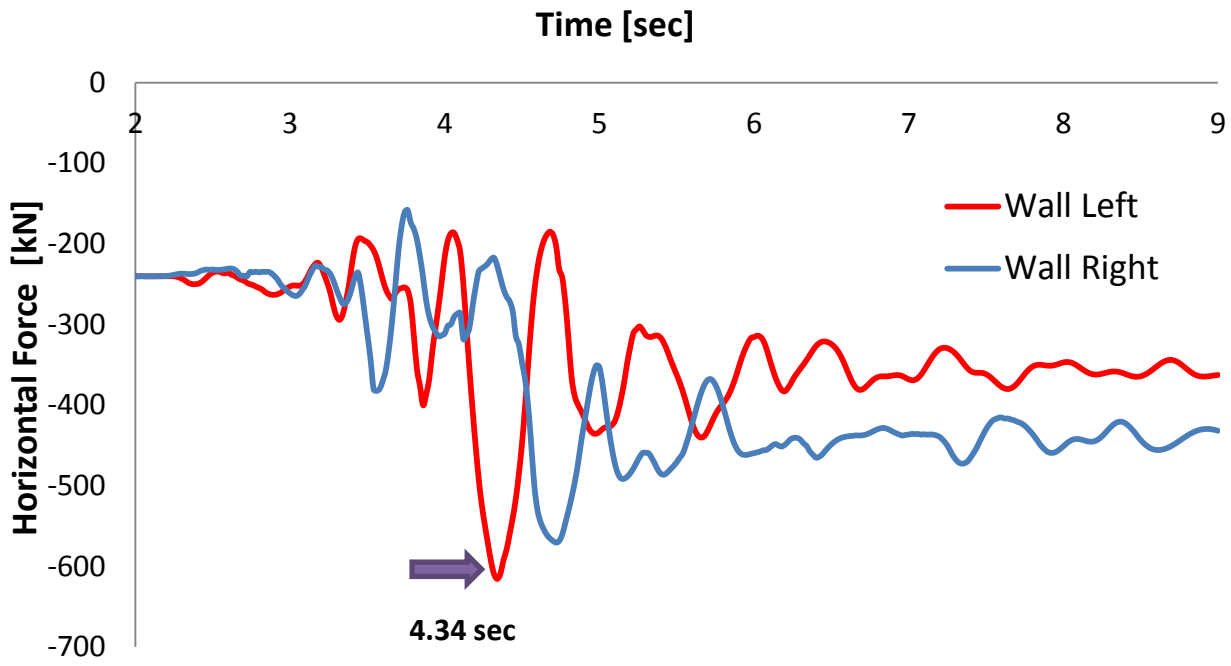

Fig. 2.10. Horizontal force-time history of the left and right wall when subjected to Aegion Seismic excitation with peak ground acceleration 0.4g.

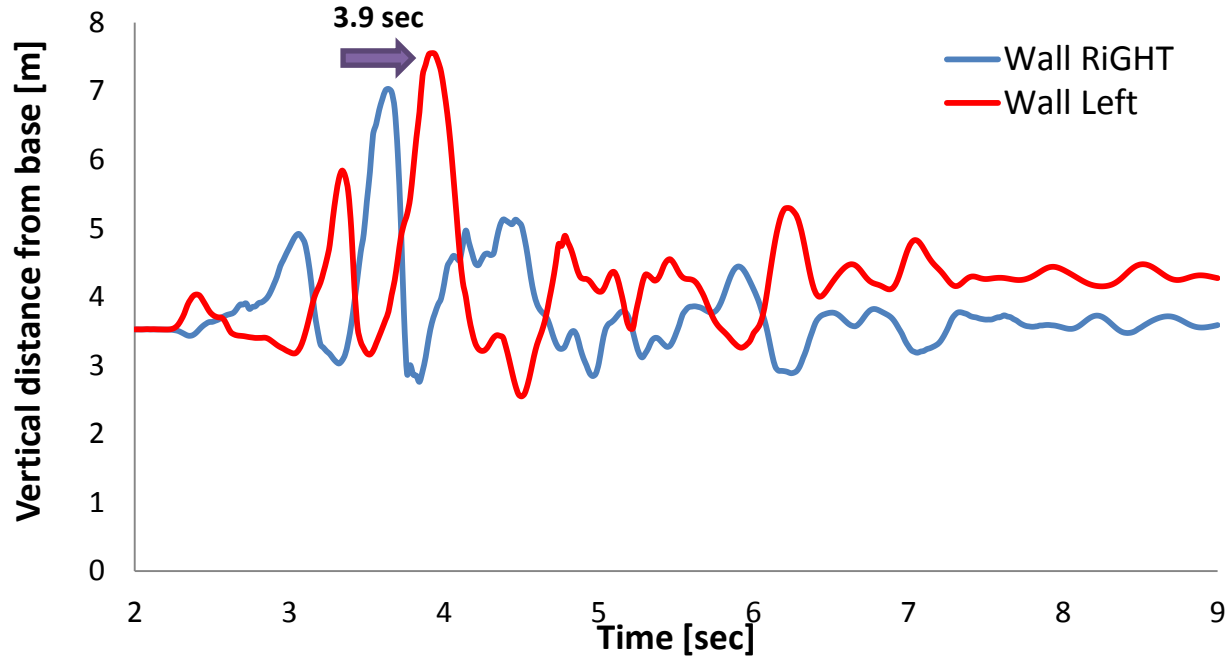

Fig. 2.11. Point of application of dynamic increment on the left and right wall when subjected to Aegion Seismic excitation with peak ground acceleration 0.4g

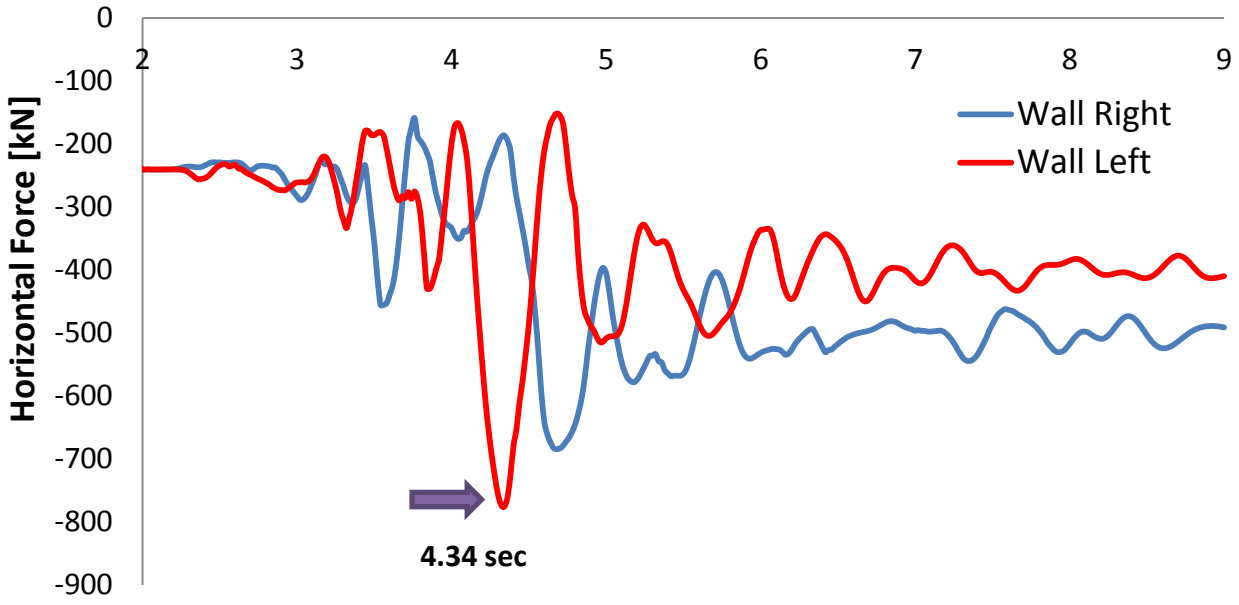

Fig. 2.12. Horizontal force-time history of the left wall when subjected to Aegion Seismic excitation with peak ground acceleration 0.6g.

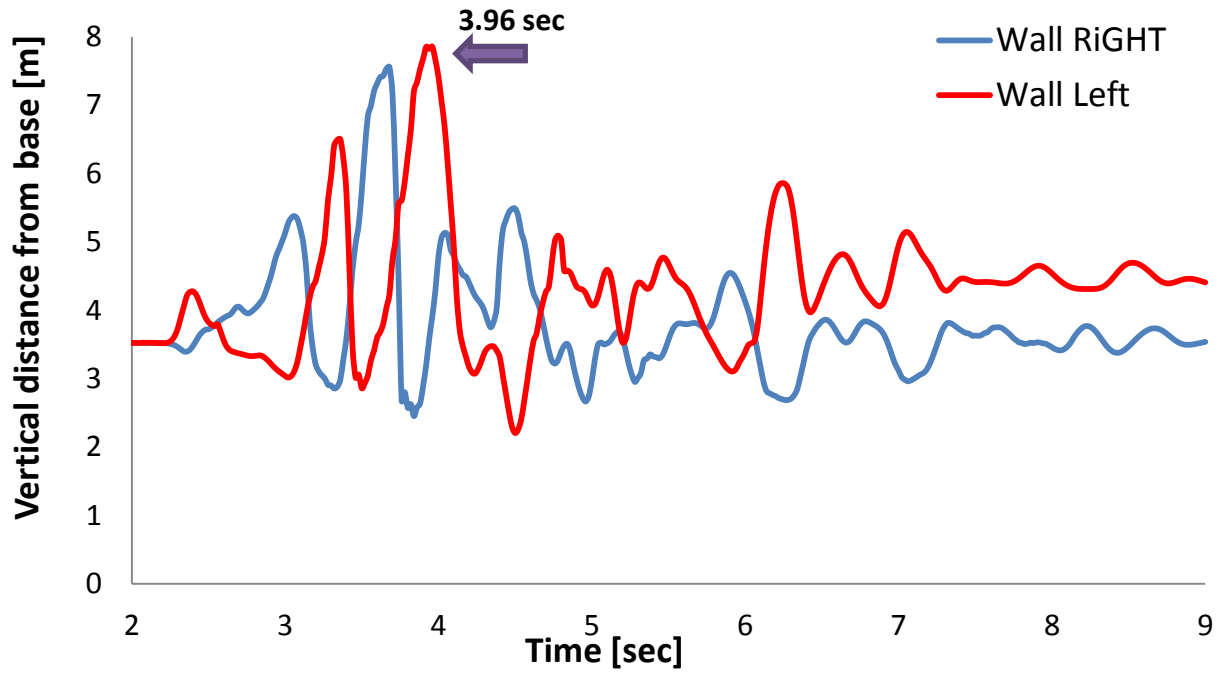

Fig. 2.13. Point of application of dynamic increment on the left and right wall when subjected to Aegion Seismic excitation with peak ground acceleration 0.6g.

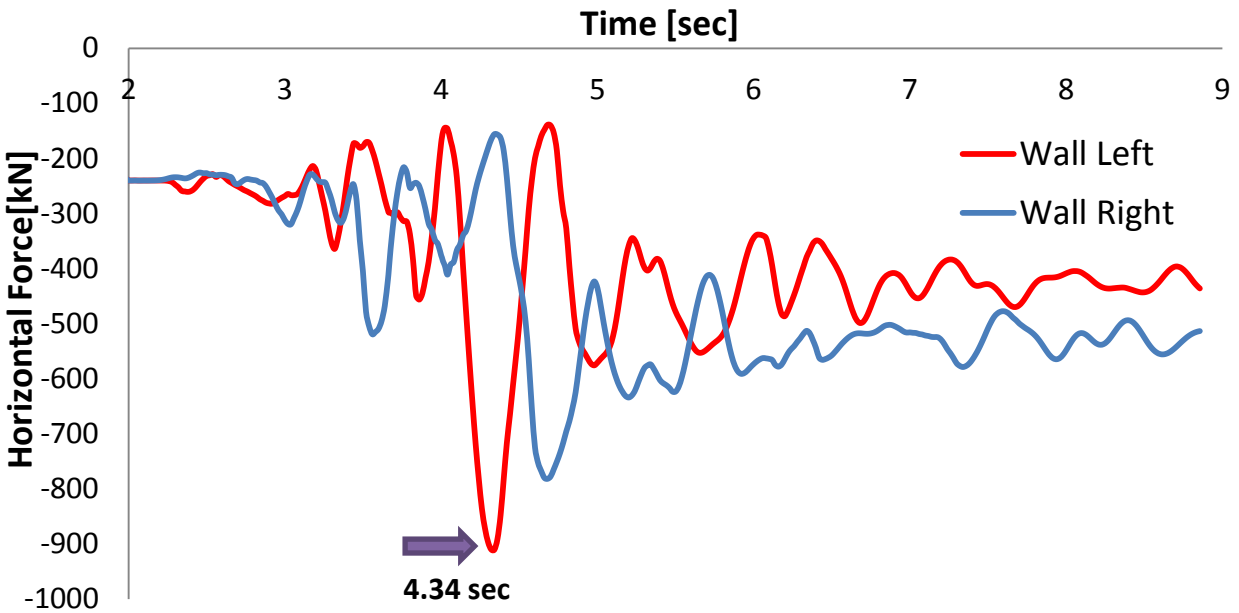

Fig. 2.14. Horizontal force-time history of the left wall when subjected to Aegion Seismic excitation with peak ground acceleration 0.8g.

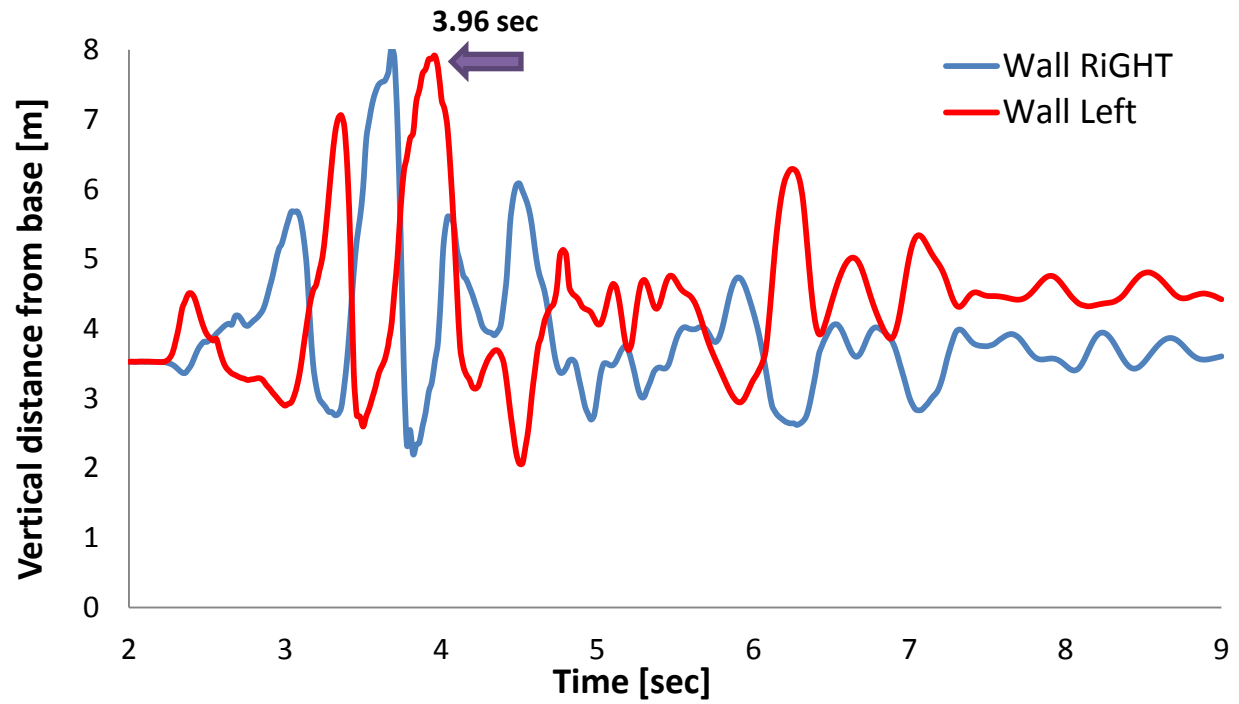

Fig. 2.15. Point of application of dynamic increment on the left and right wall when subjected to Aegion Seismic excitation with peak ground acceleration 0.8g.

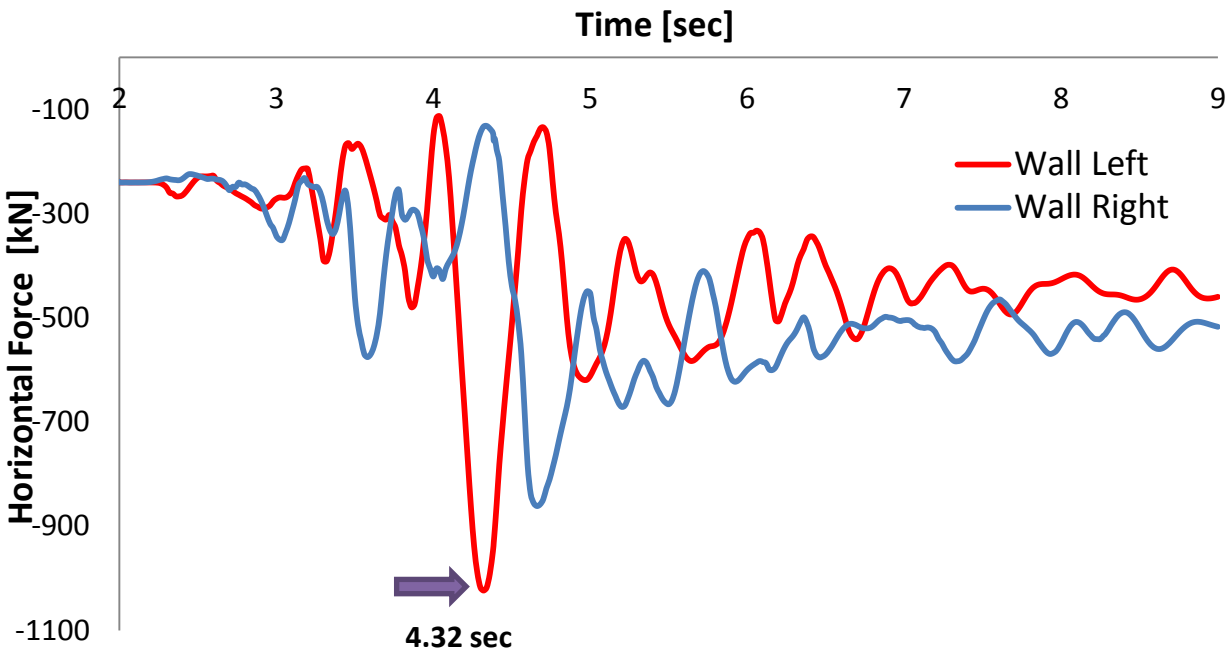

Fig. 2.16. Horizontal force-time history of the left wall when subjected to Aegion Seismic excitation with peak ground acceleration 1g.

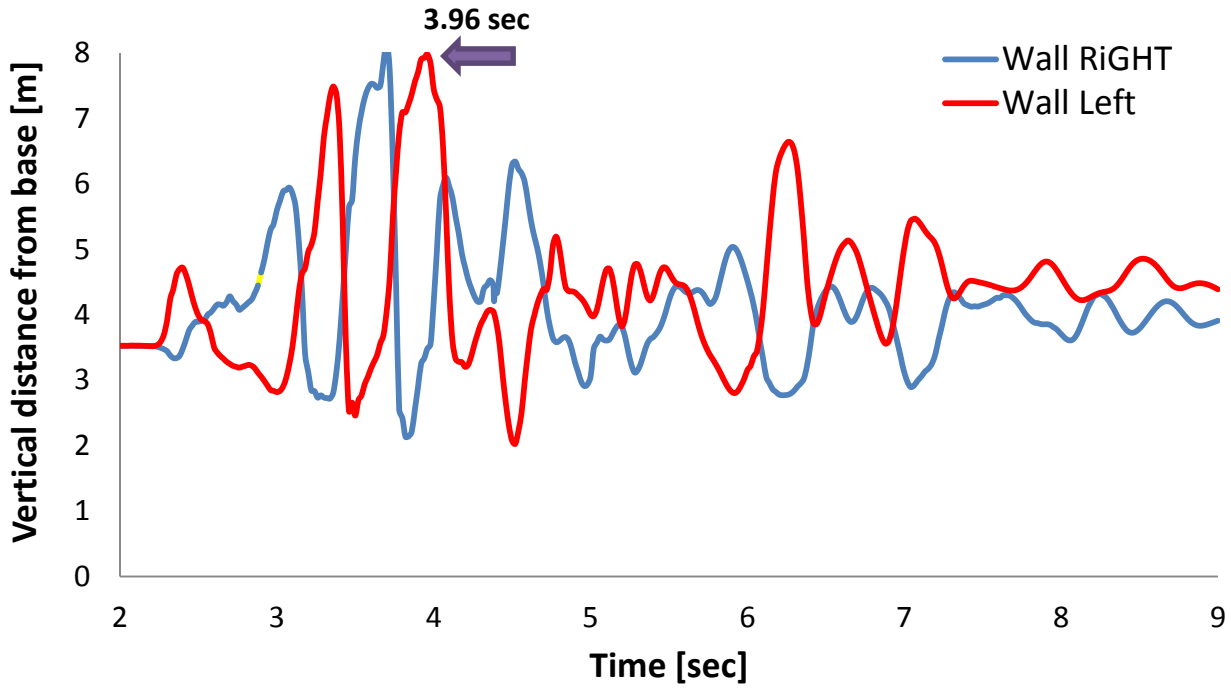

Fig. 2.17. Point of application of dynamic increment on the left and right wall when subjected to Aegion Seismic excitation with peak ground acceleration 1g.

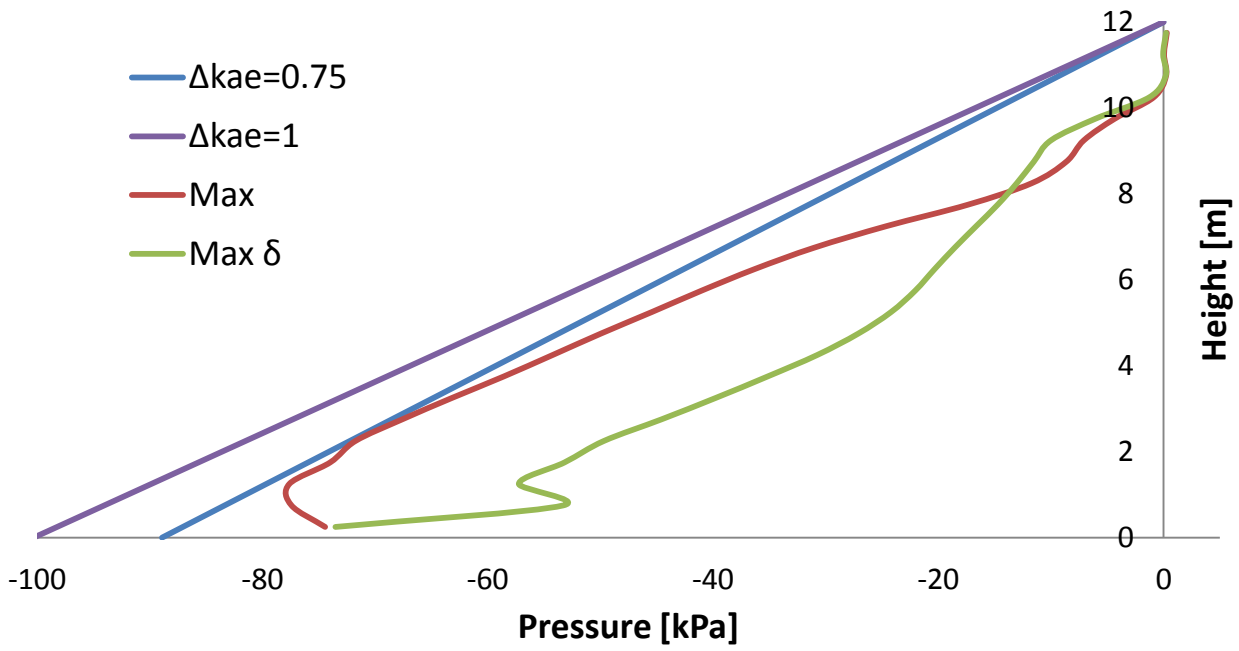

Fig. 2.18. Earth pressure profiles computed in ABAQUS and estimated using the M-O when the wall is subjected to the Aegion Seismic excitation with peak acceleration 0.2g.

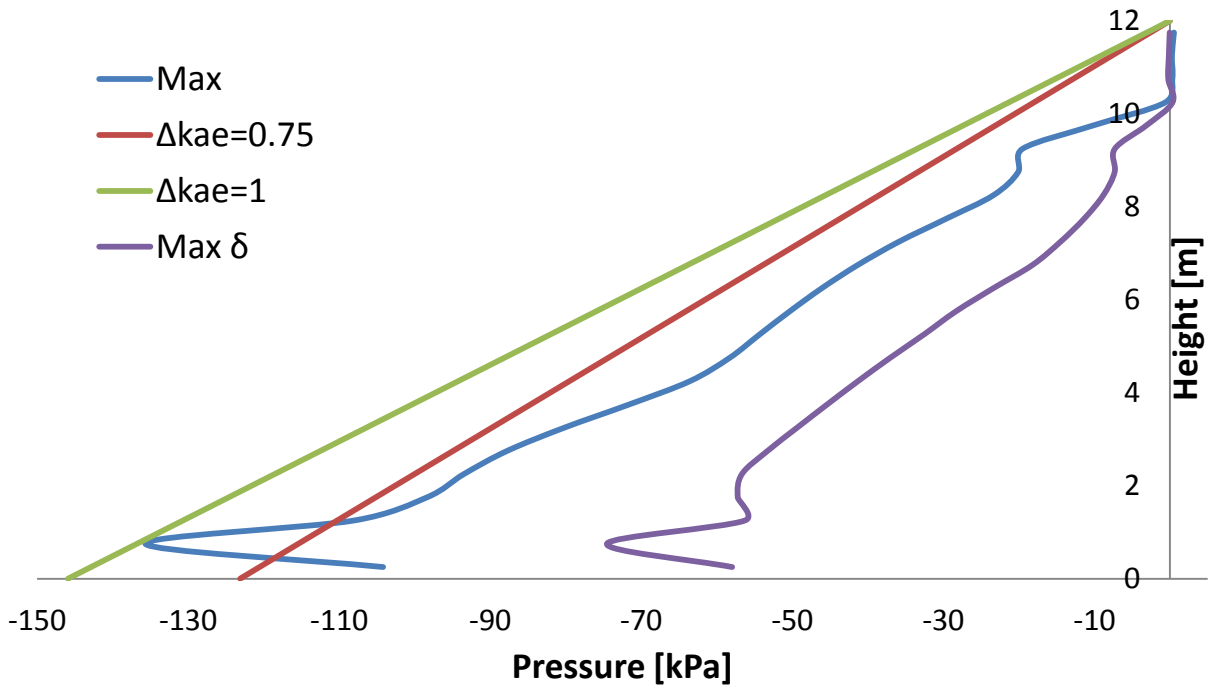

Fig. 2.19. Earth pressure profiles computed in ABAQUS and estimated using the M-O when the wall is subjected to the Aegion Seismic excitation with peak acceleration 0.4g.

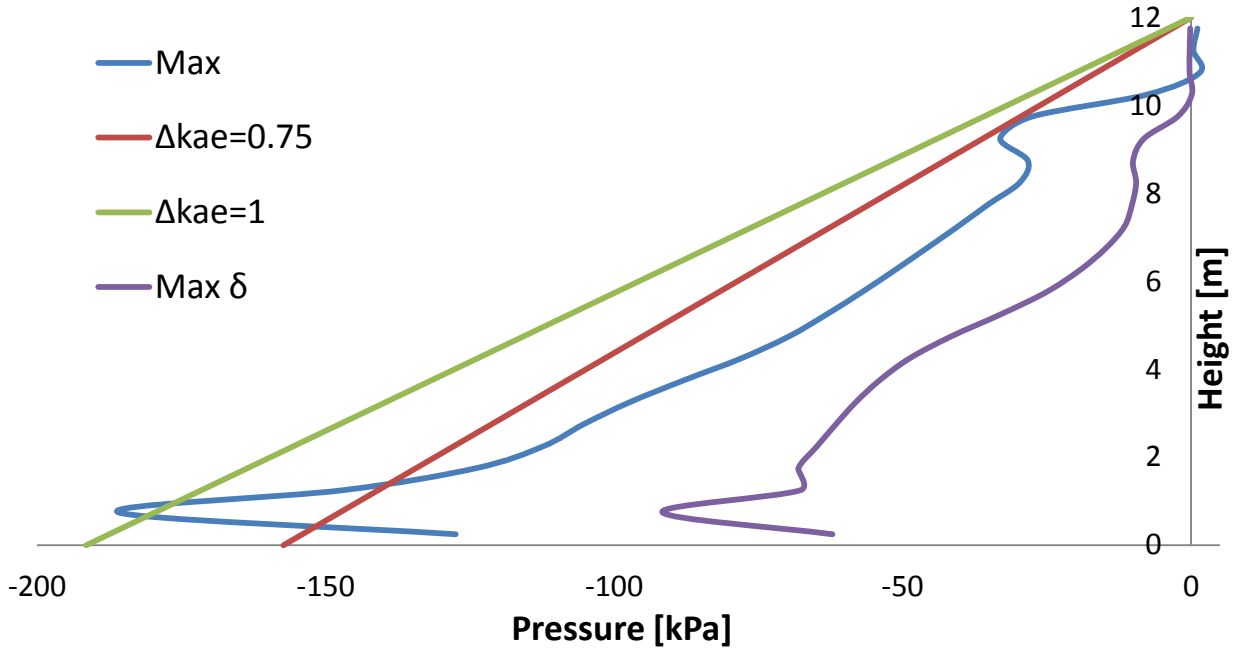

Fig. 2.20. Earth pressure profiles computed in ABAQUS and estimated using the M-O when the wall is subjected to the Aegion Seismic excitation with peak acceleration 0.6g.

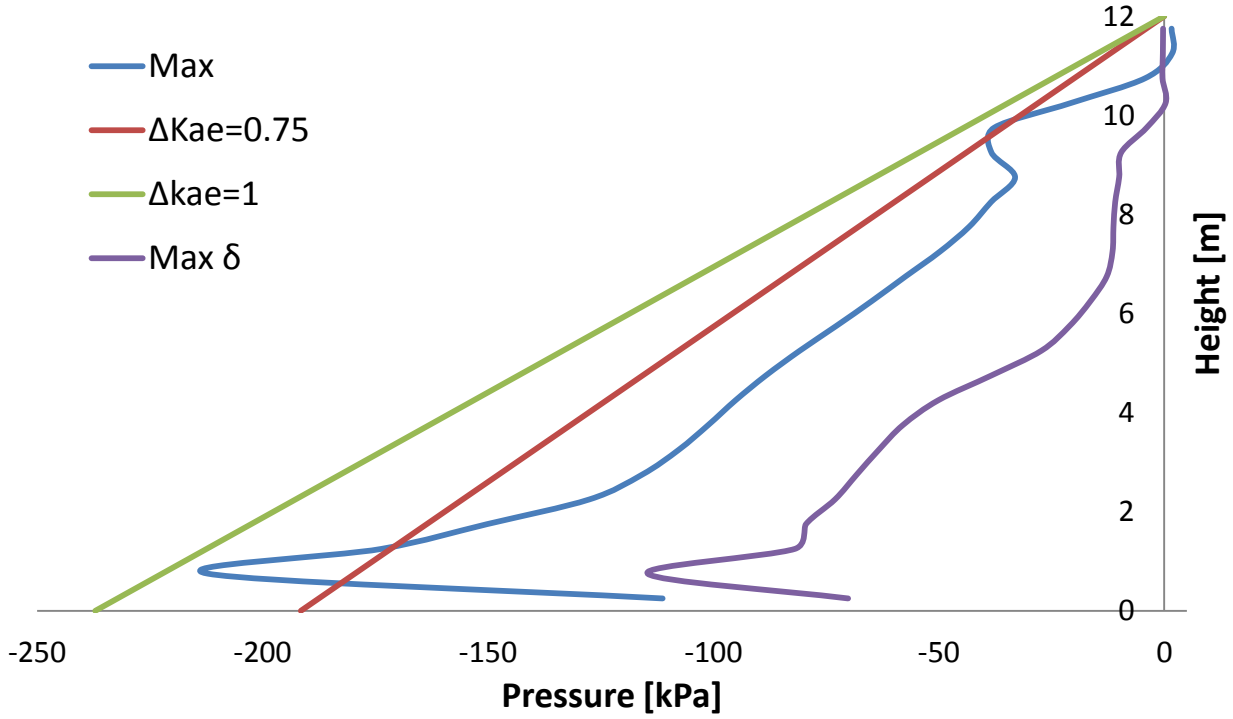

Fig. 2.21. Earth pressure profiles computed in ABAQUS and estimated using the M-O when the wall is subjected to the Aegion Seismic excitation with peak acceleration 0.8g.

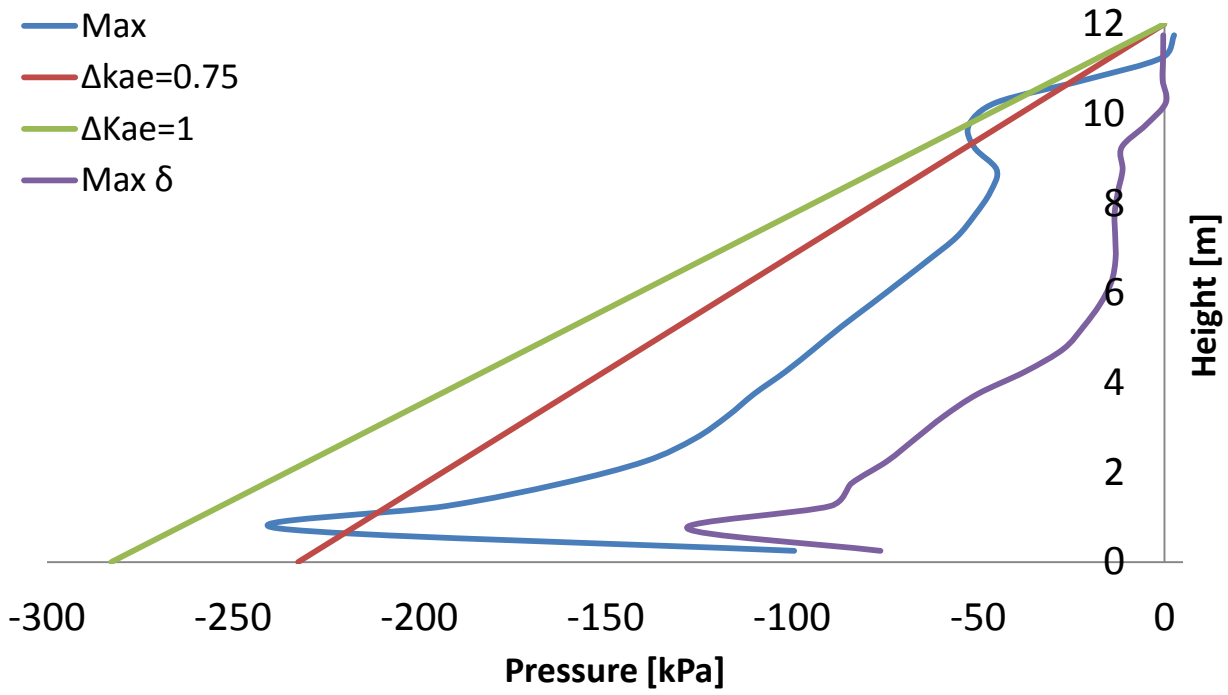

Fig. 2.22. Earth pressure profiles computed in ABAQUS and estimated using the M-O when the wall is subjected to the Aegion Seismic excitation with peak acceleration 1g.

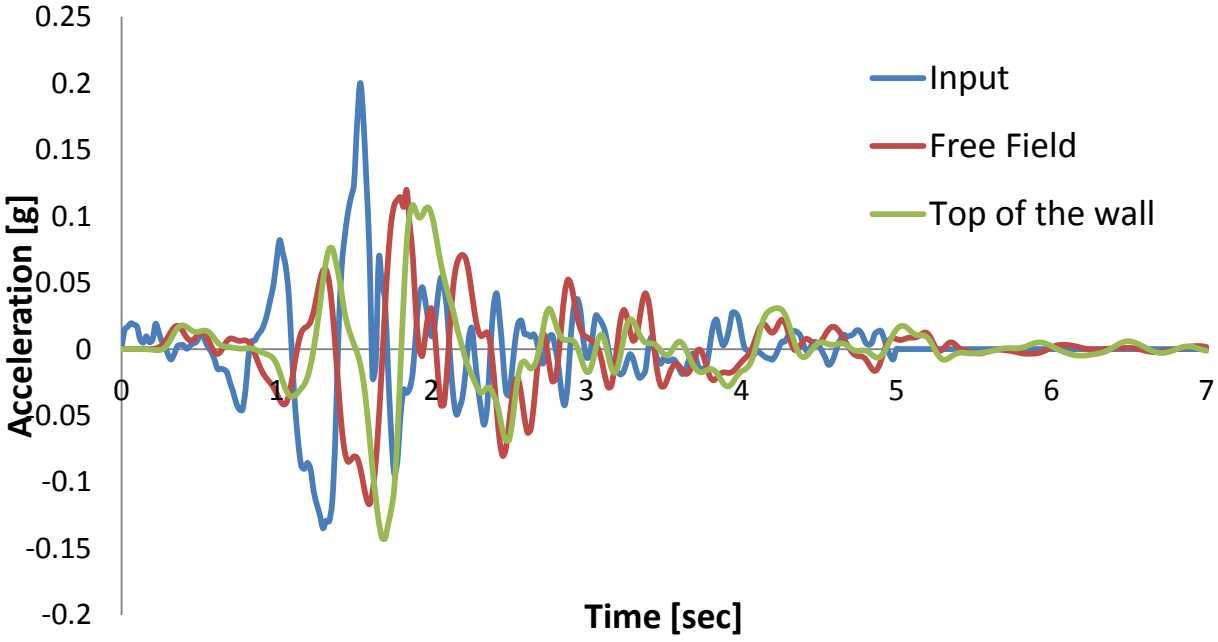

Fig. 2.23. Comparison of input acceleration and computed at the top of the wall and top of the free field when subjected to Ageio Seismic excitation with peak acceleration 0.2g.

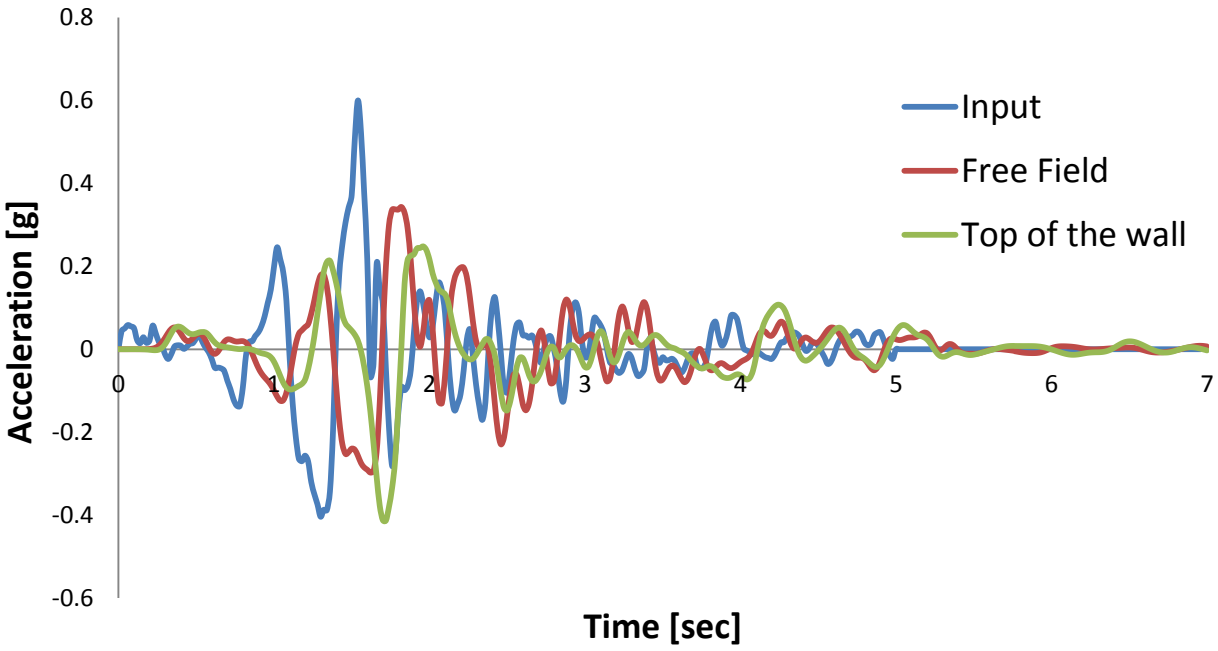

Fig. 2.24. Comparison of input acceleration and computed at the top of the left wall and top of the free field when subjected to Ageio Seismic excitation with peak acceleration 0.6g.

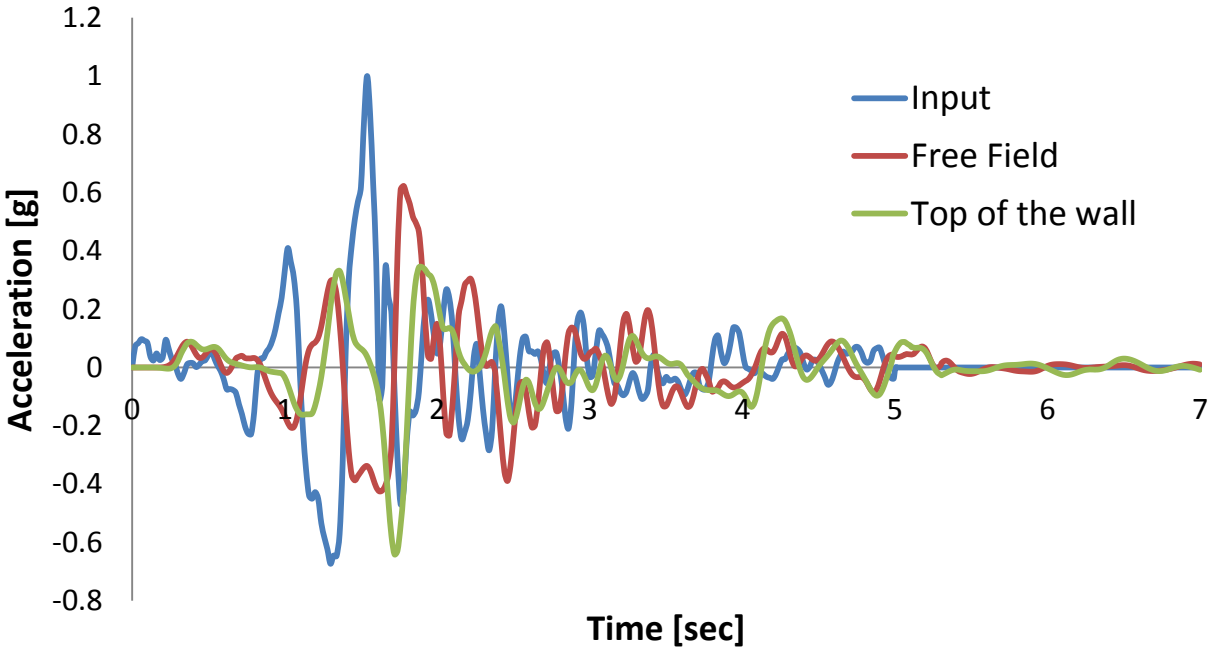

Fig. 2.25. Comparison of input acceleration and computed at the top of the left wall and top of the free field when subjected to Ageio Seismic excitation with peak acceleration 1g.

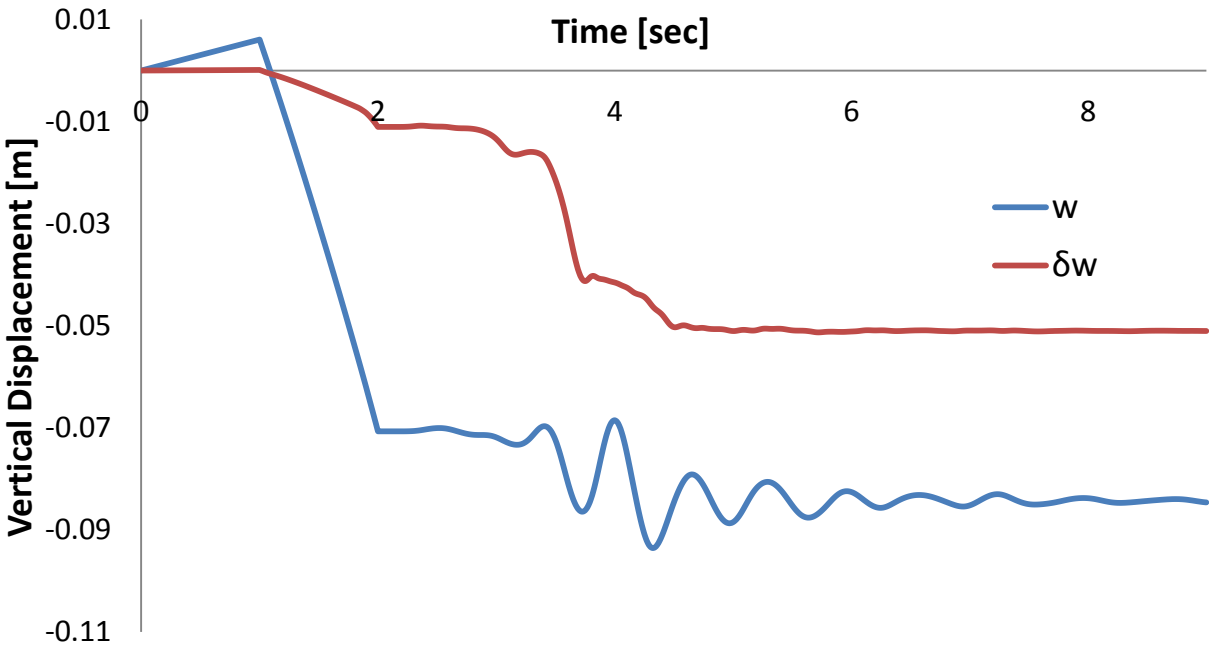

Fig. 2.26. Vertical displacement-time history of the left wall when subjected to Ageion Seismic excitation with peak acceleration 0.2g.

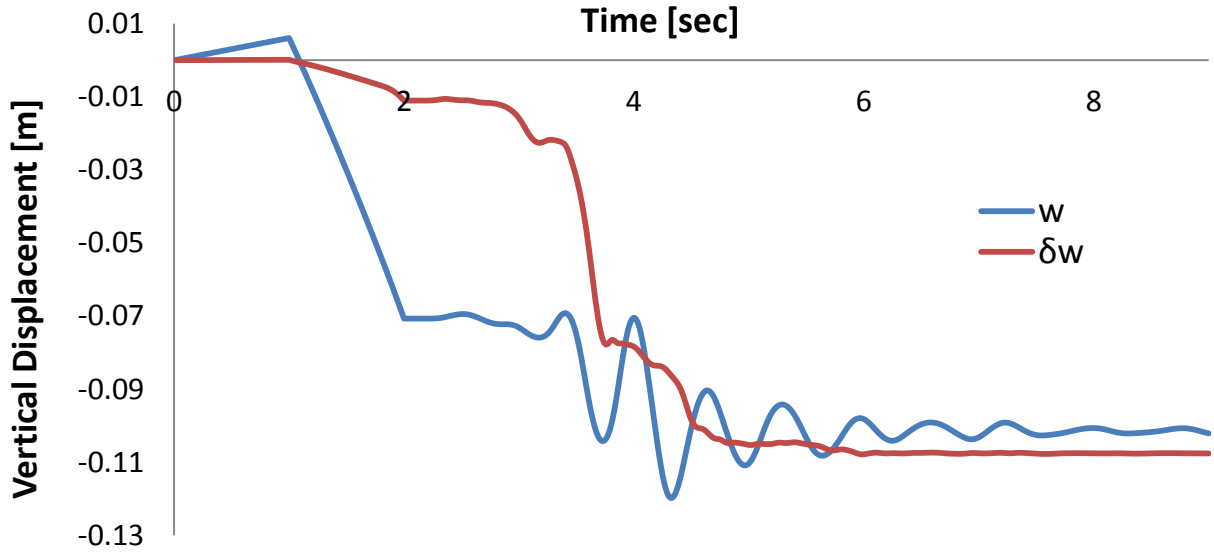

Fig. 2.27. Vertical displacement-time history of the left wall when subjected to Ageion Seismic excitation with peak acceleration 0.4g.

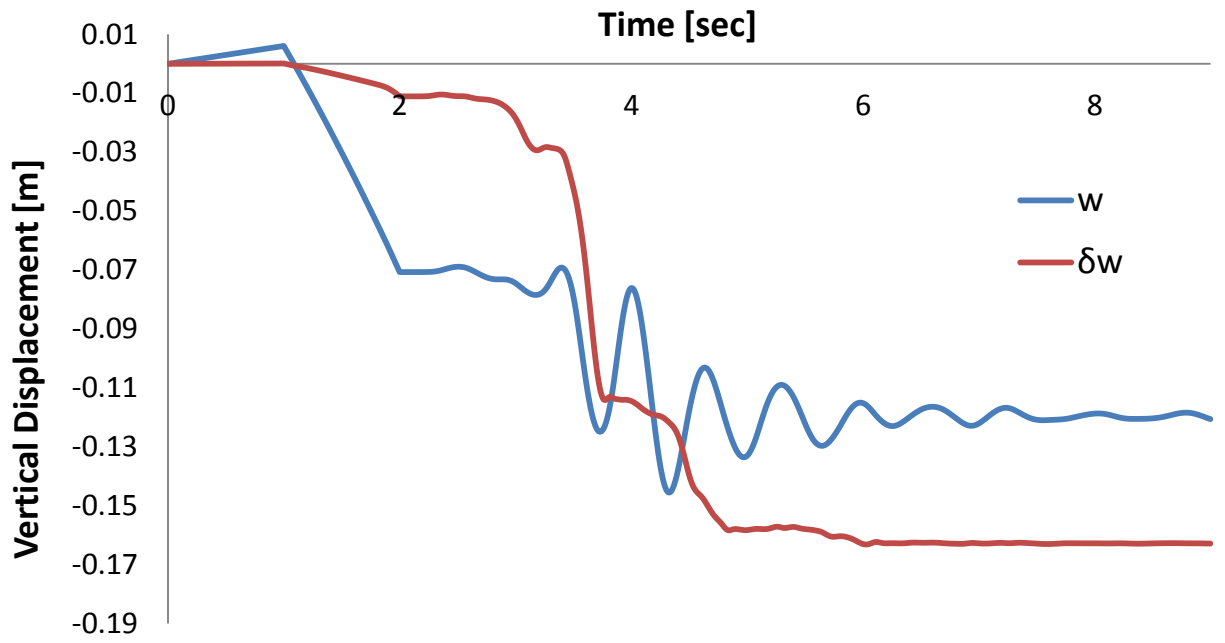

Fig. 2.28. Vertical displacement-time history of the left wall when subjected to Ageion Seismic excitation with peak acceleration 0.6g.

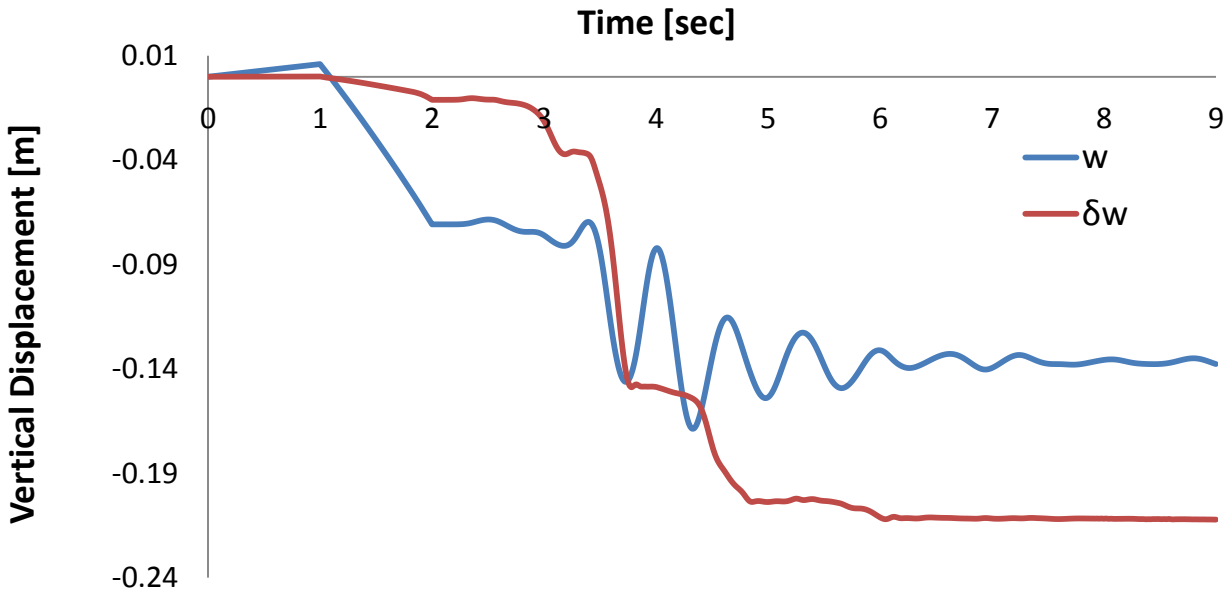

Fig. 2.29. Vertical displacement-time history of the left wall when subjected to Ageion Seismic excitation with peak acceleration 0.8g.

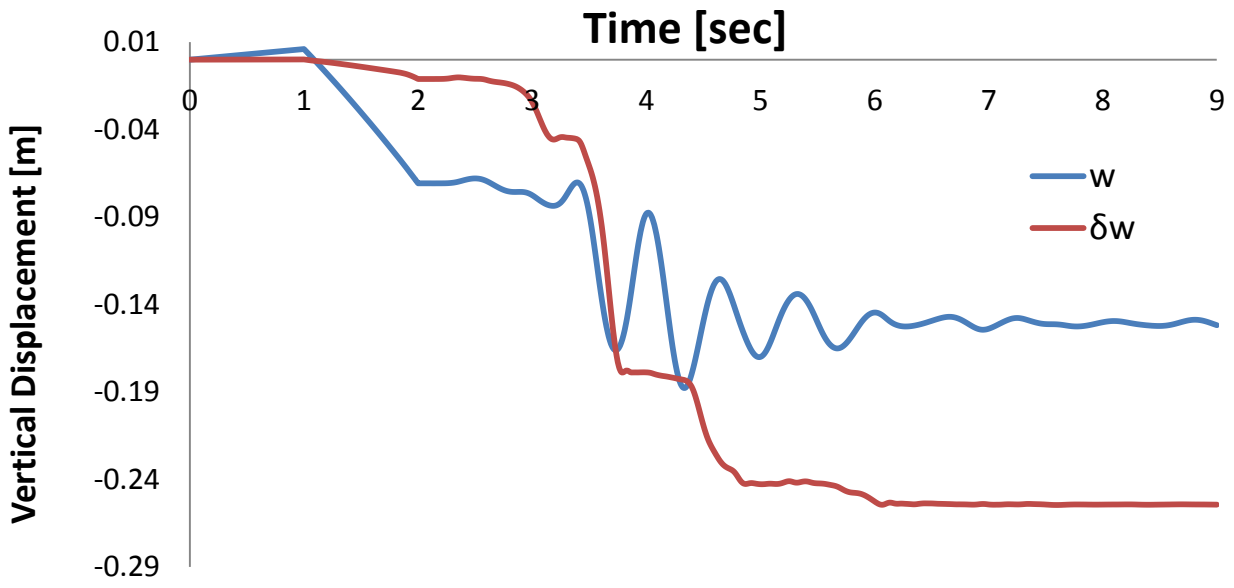

Fig. 2.30. Vertical displacement-time history of the left wall when subjected to Ageion Seismic excitation with peak acceleration 1g.

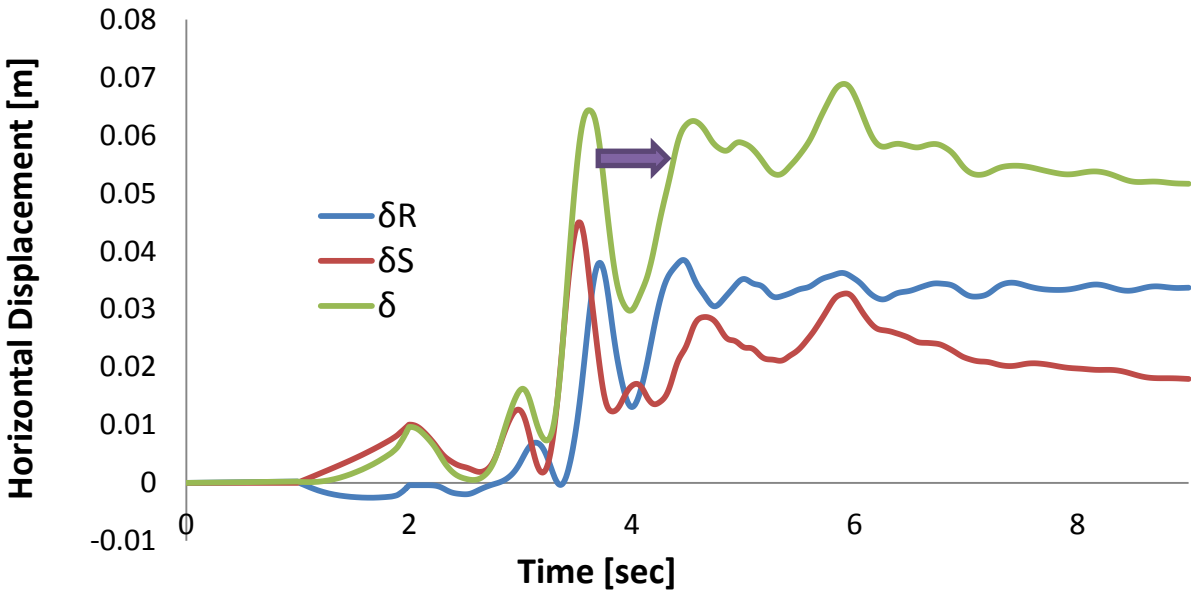

Fig. 2.31. Horizontal displacement-time history of the left wall when subjected to Ageion Seismic excitation with peak acceleration 0.2g.

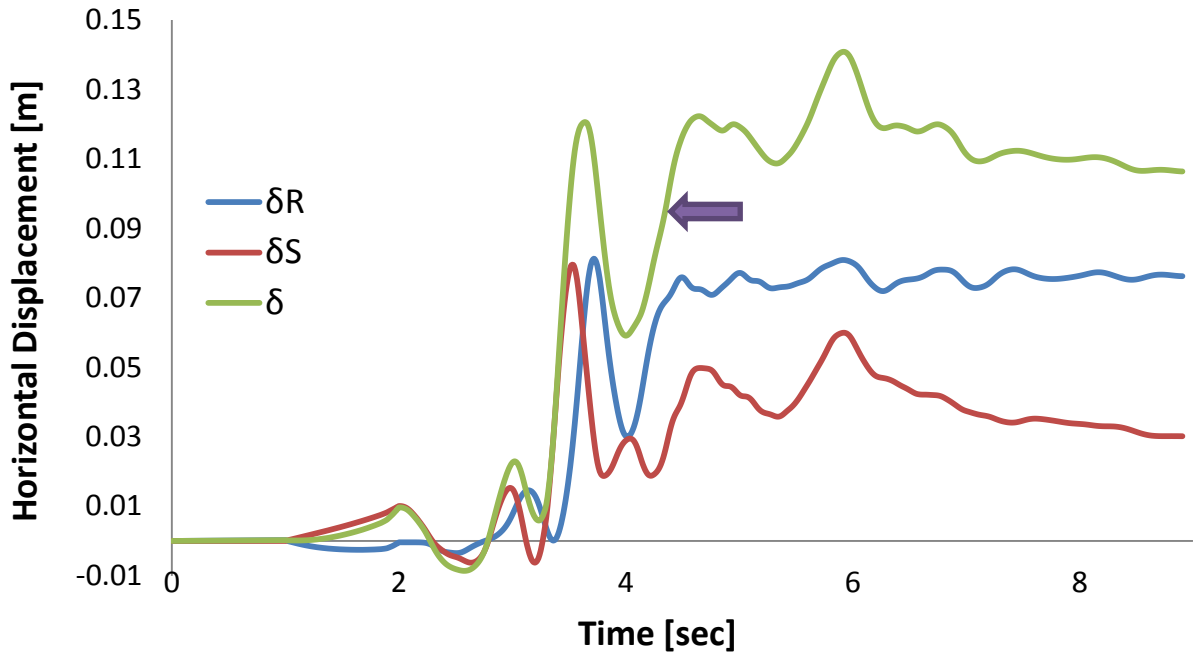

Fig. 2.32. Horizontal displacement-time history of the left wall when subjected to Ageion Seismic excitation with peak acceleration 0.4g.

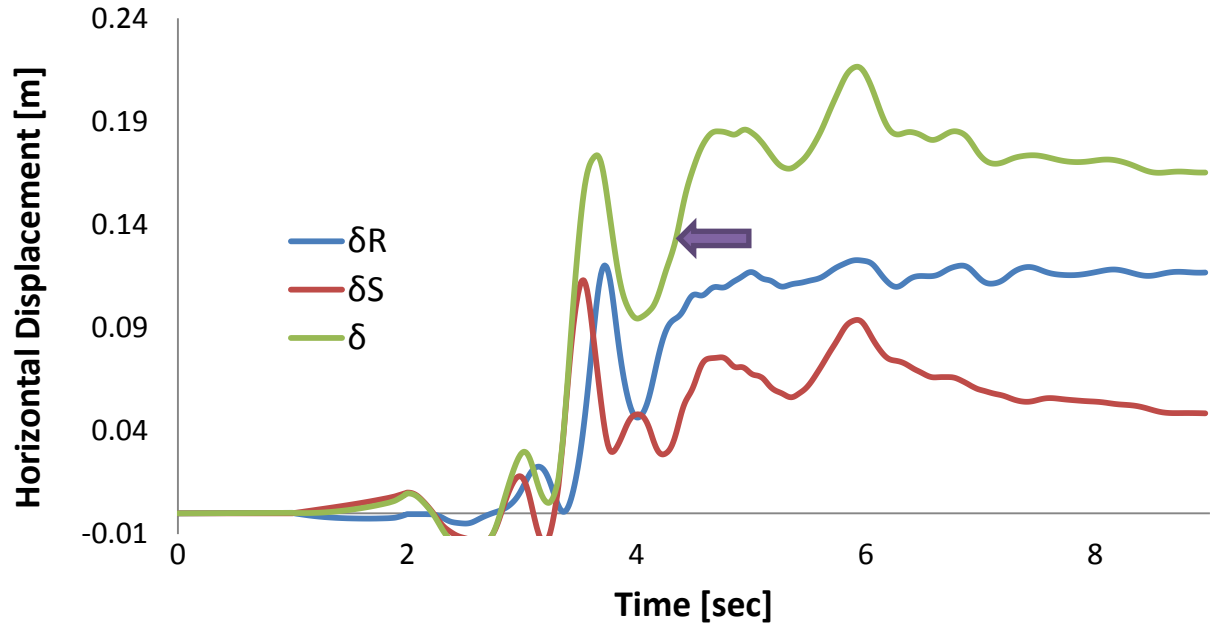

Fig. 2.33. Horizontal displacement-time history of the left wall when subjected to Ageion Seismic excitation with peak acceleration 0.6g.

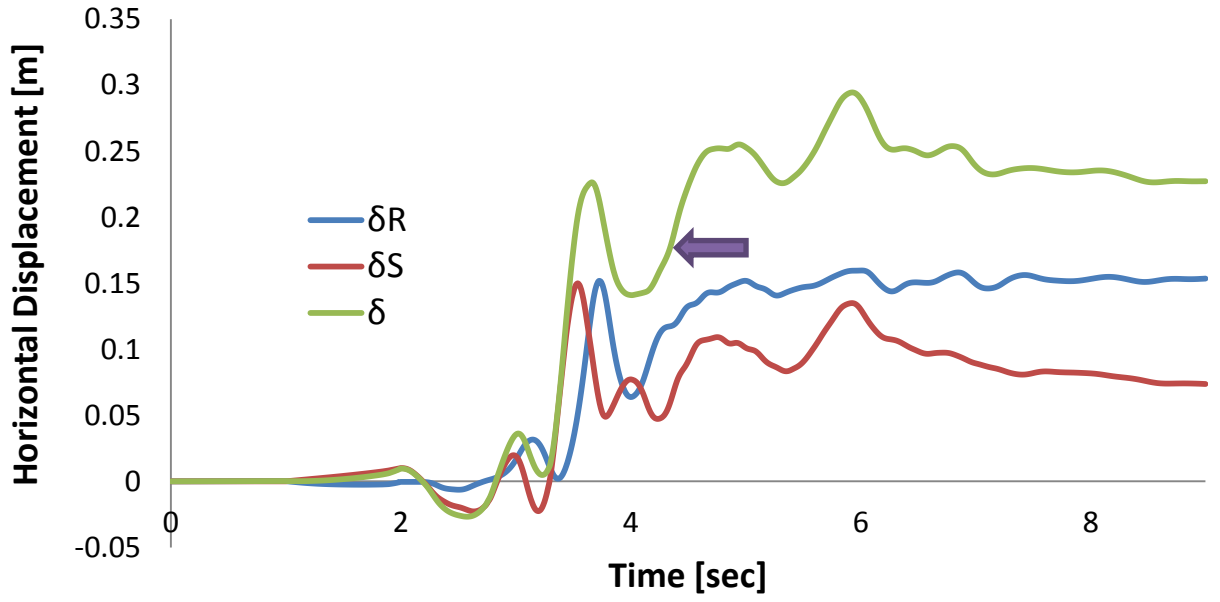

Fig. 2.34. Horizontal displacement-time history of the left wall when subjected to Ageion Seismic excitation with peak acceleration 0.8g.

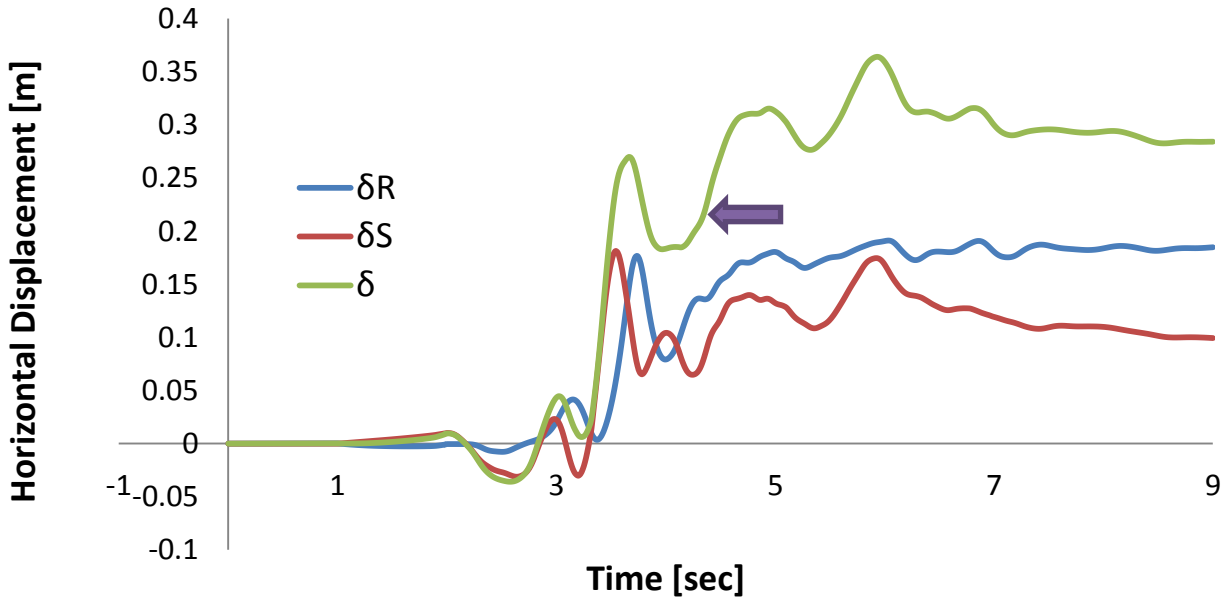

Fig. 2.35. Horizontal displacement-time history of the left wall when subjected to Ageion Seismic excitation with peak acceleration 1g.

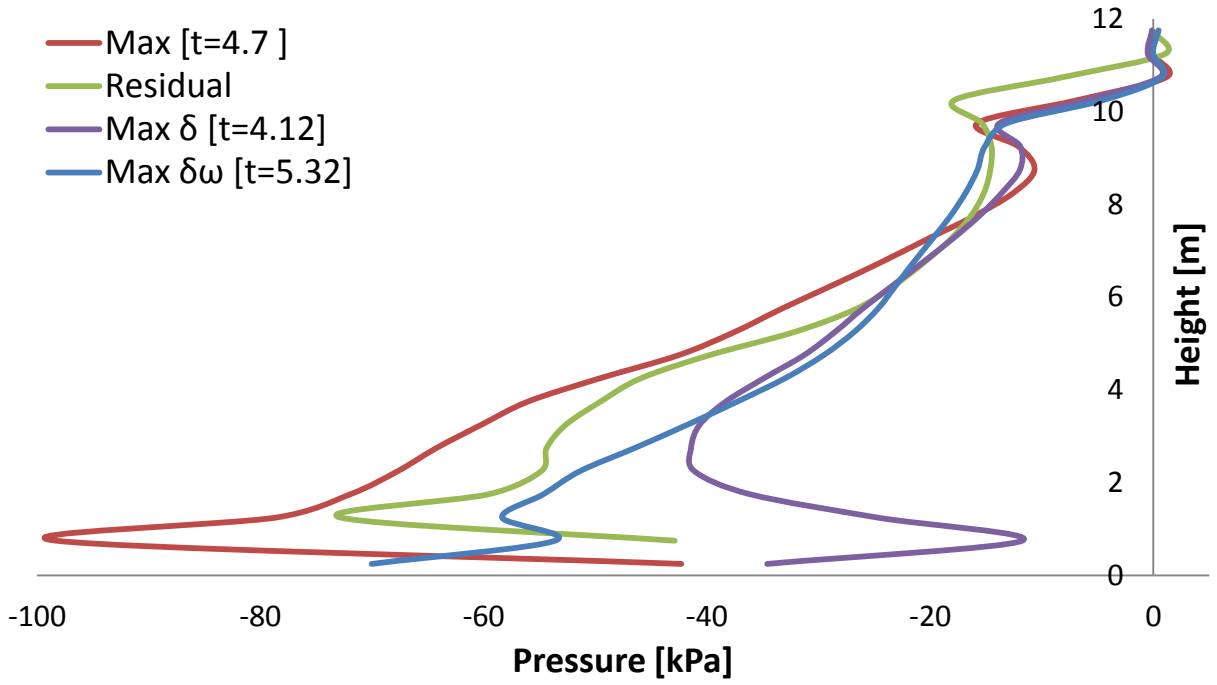

Fig. 2.36. Earth pressures profiles on the right wall at different moments when subjected to Aegion Seismic excitation with peak ground acceleration 0.2g.

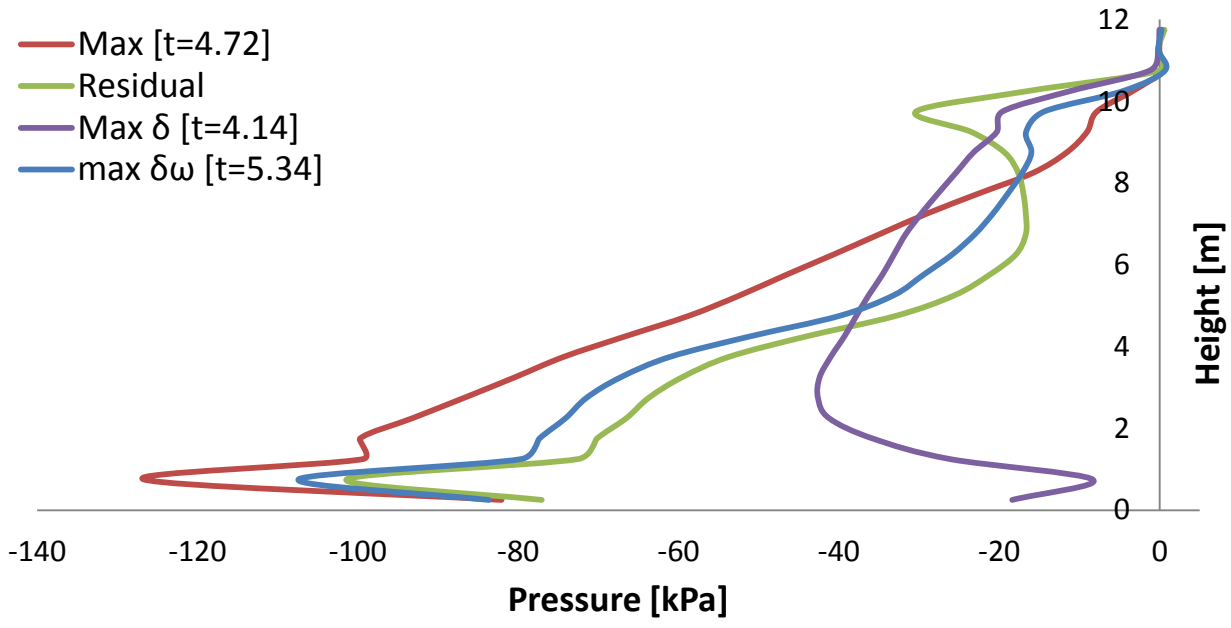

Fig. 2.37. Earth pressures profiles on the right wall at different moments when subjected to Aegion Seismic excitation with peak ground acceleration 0.4g.

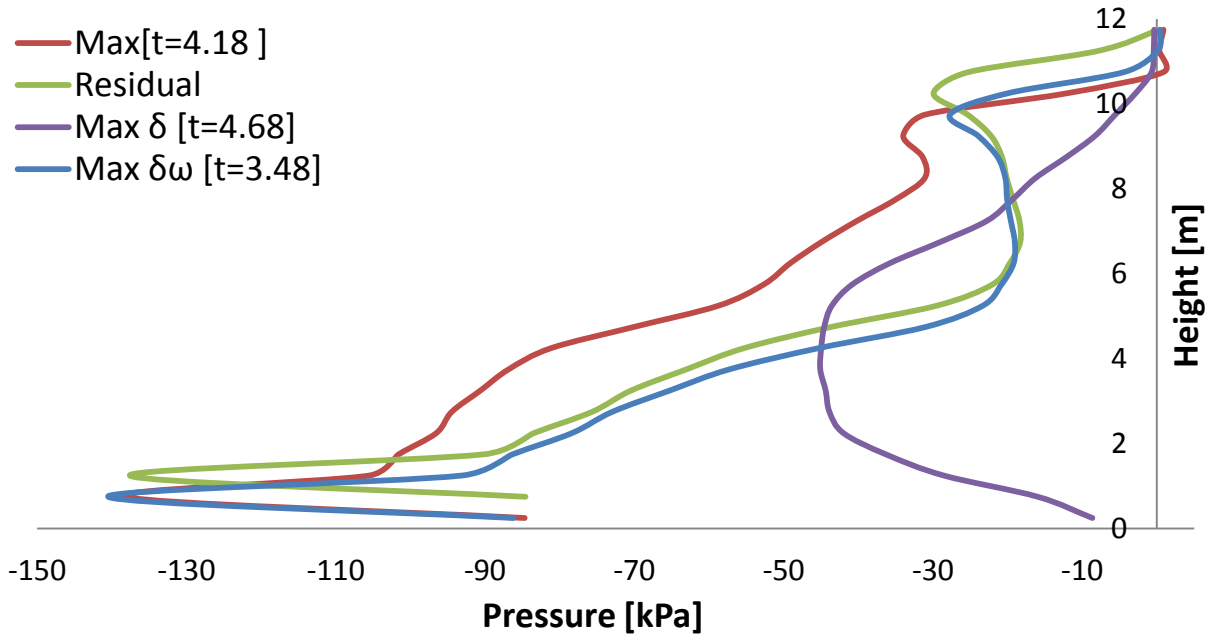

Fig. 2.38. Earth pressures profiles on the right wall at different moments when subjected to Aegion Seismic excitation with peak ground acceleration 0.6g.

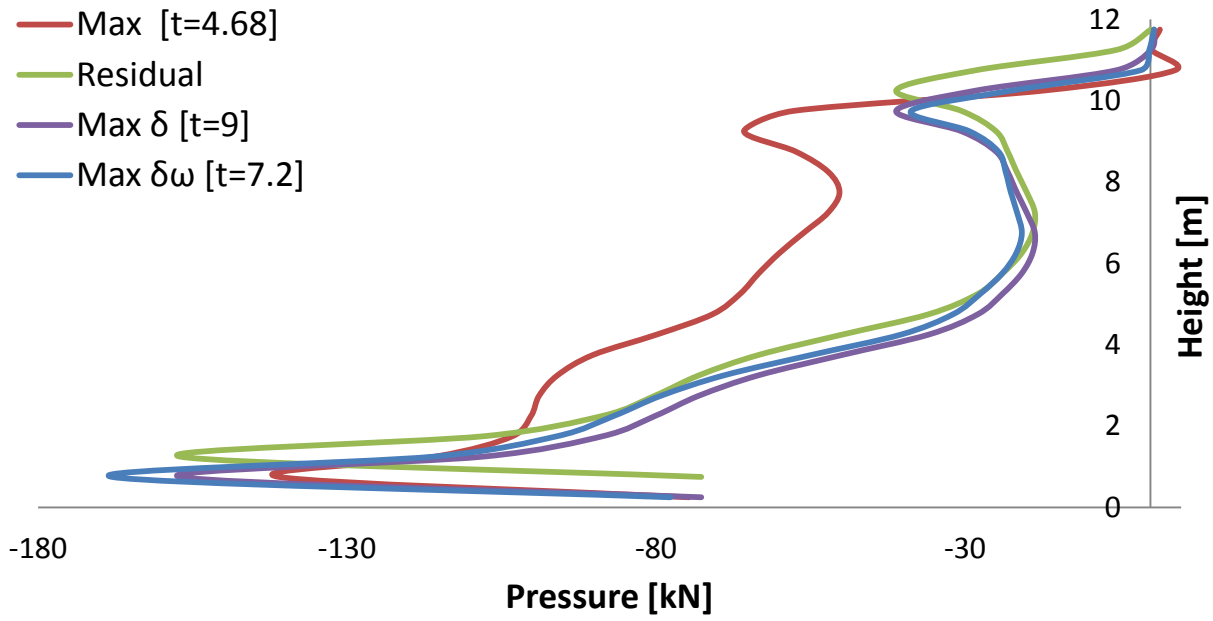

Fig. 2.39. Earth pressures profiles on the right wall at different moments when subjected to Aegion Seismic excitation with peak ground acceleration 0.8g.

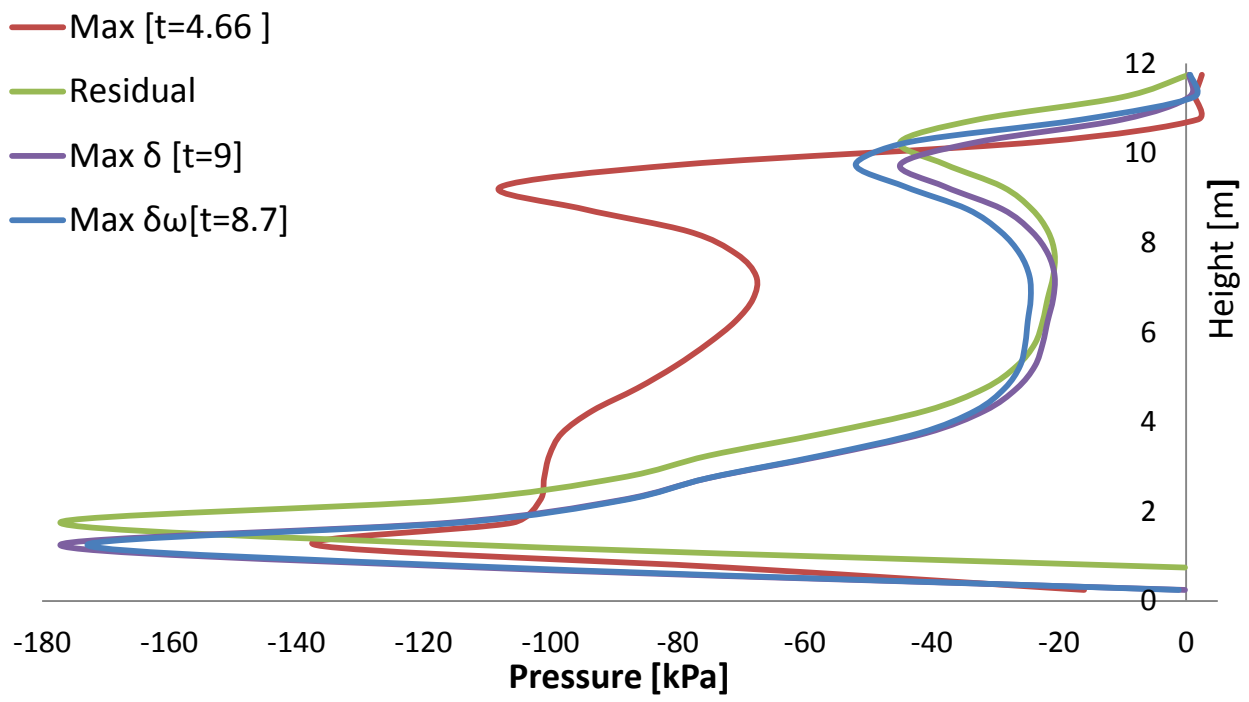

Fig. 2.40. Earth pressures profiles on the right wall at different moments when subjected to Aegion Seismic excitation with peak ground acceleration 1g.

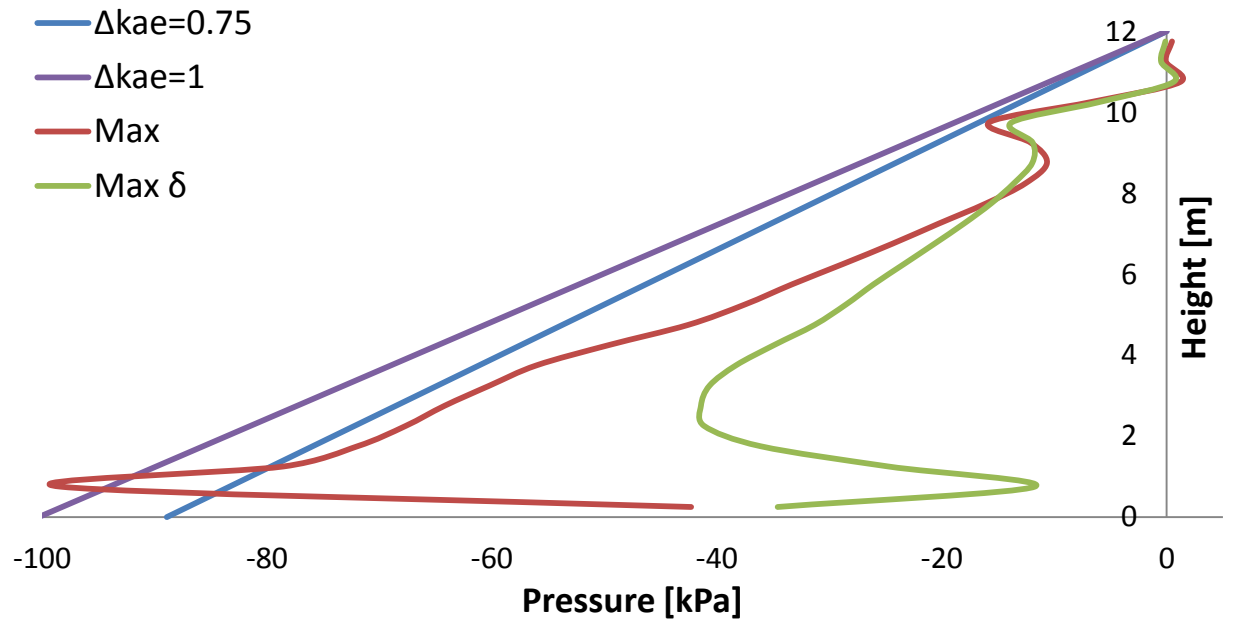

Fig. 2.41. Earth pressure profiles computed in ABAQUS and estimated using the M-O when the wall is subjected to the Aegion Seismic excitation with peak acceleration 0.2g.

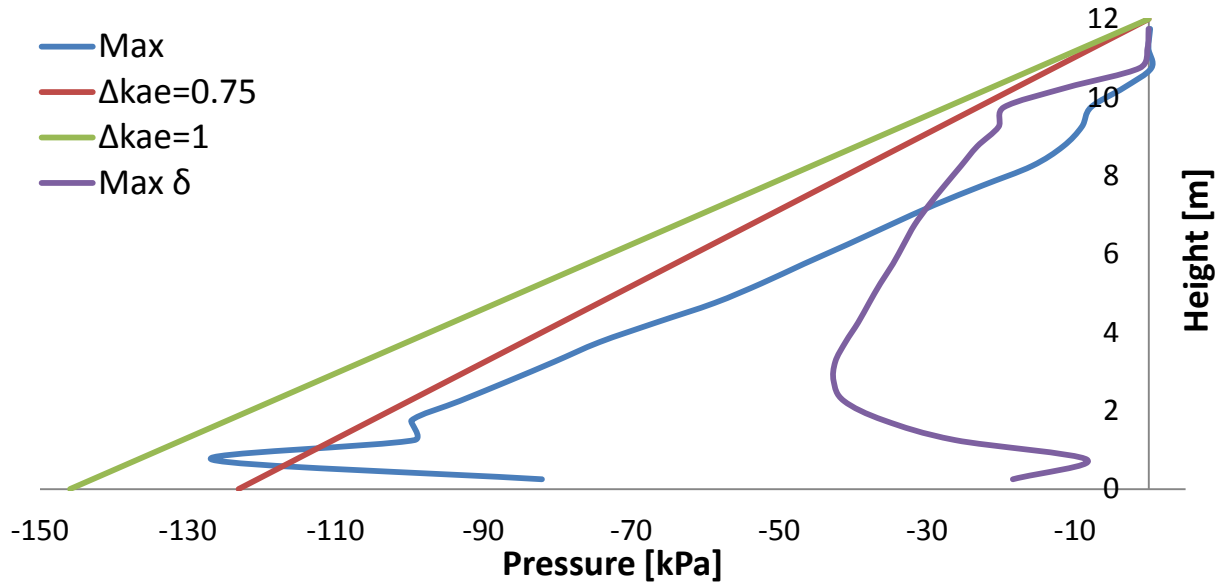

Fig. 2.42. Earth pressure profiles computed in ABAQUS and estimated using the M-O when the wall is subjected to the Aegion Seismic excitation with peak acceleration 0.4g.

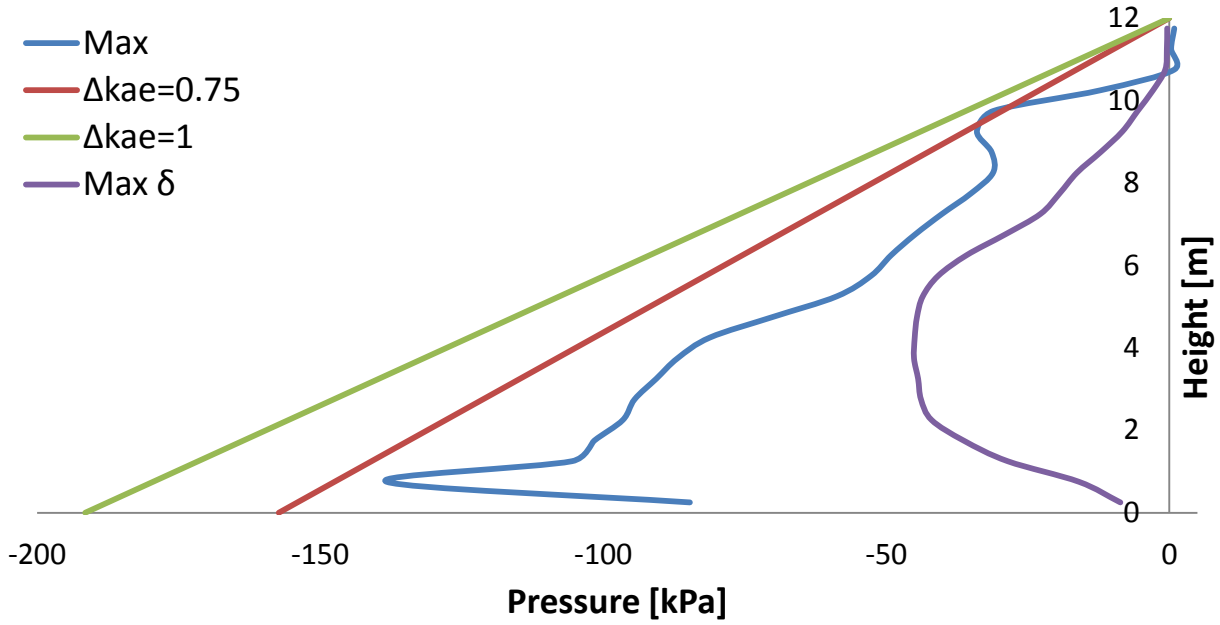

Fig. 2.43. Earth pressure profiles computed in ABAQUS and estimated using the M-O when the wall is subjected to the Aegion Seismic excitation with peak acceleration 0.6g.

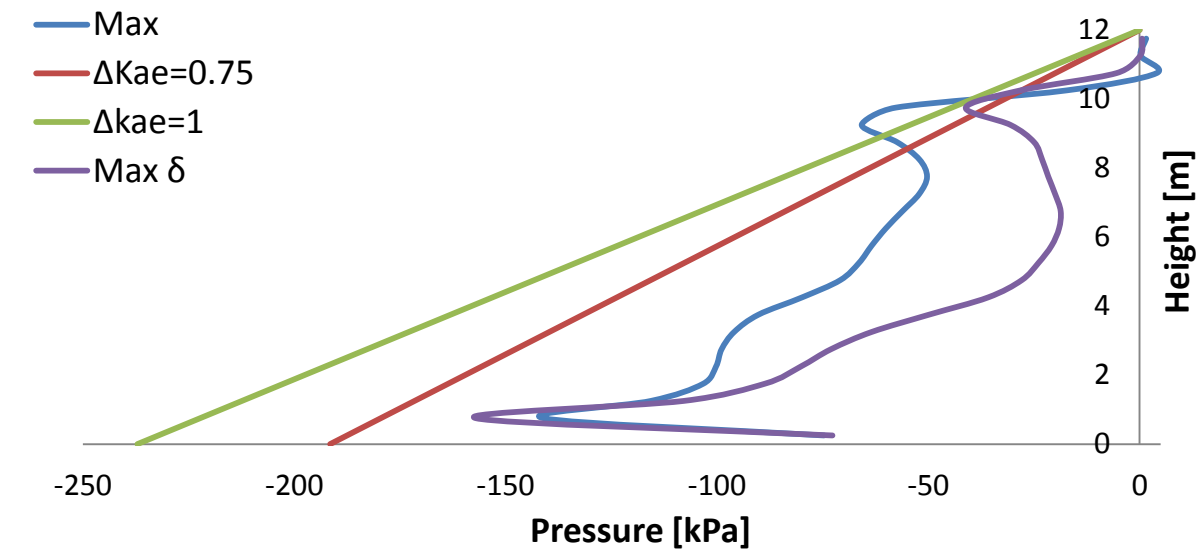

Fig. 2.44. Earth pressure profiles computed in ABAQUS and estimated using the M-O when the wall is subjected to the Aegion Seismic excitation with peak acceleration 0.8g.

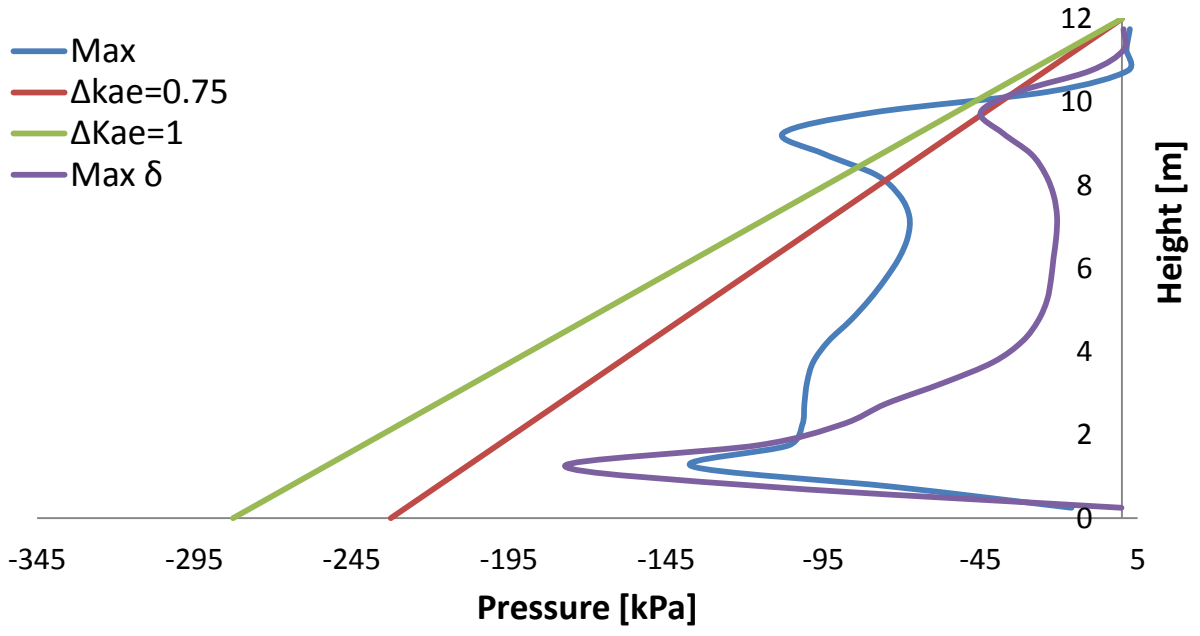

Fig. 2.45. Earth pressure profiles computed in ABAQUS and estimated using the M-O when the wall is subjected to the Aegion Seismic excitation with peak acceleration 1g.

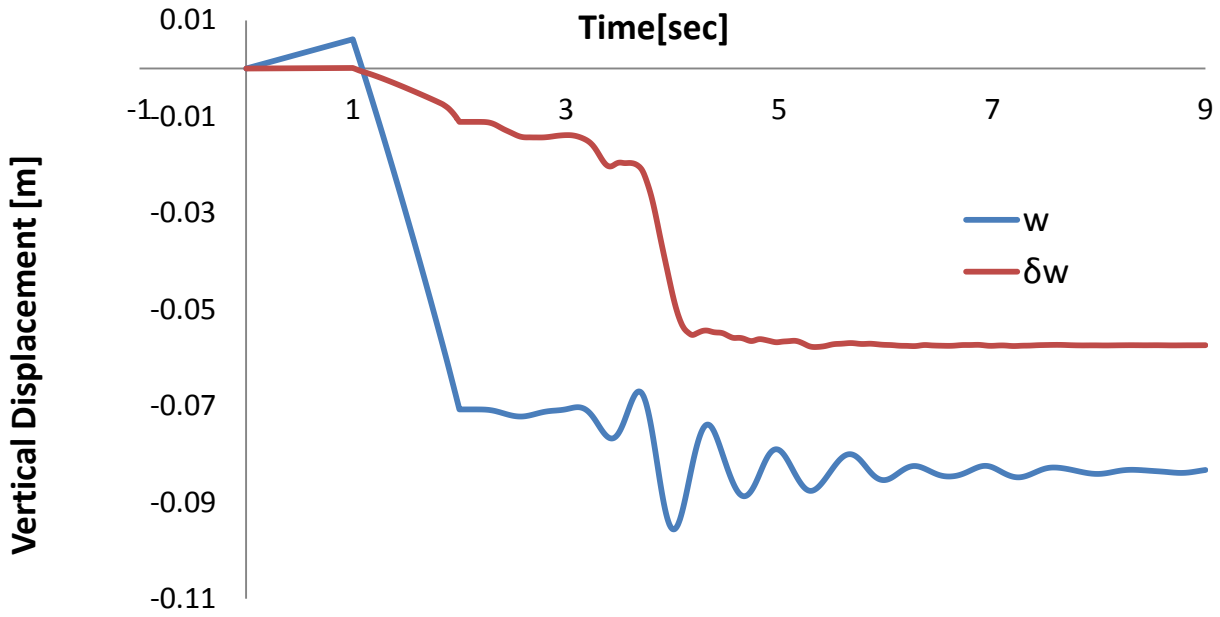

Fig. 2.46. Vertical displacement-time history of the left wall when subjected to Ageion Seismic excitation with peak acceleration 0.2g.

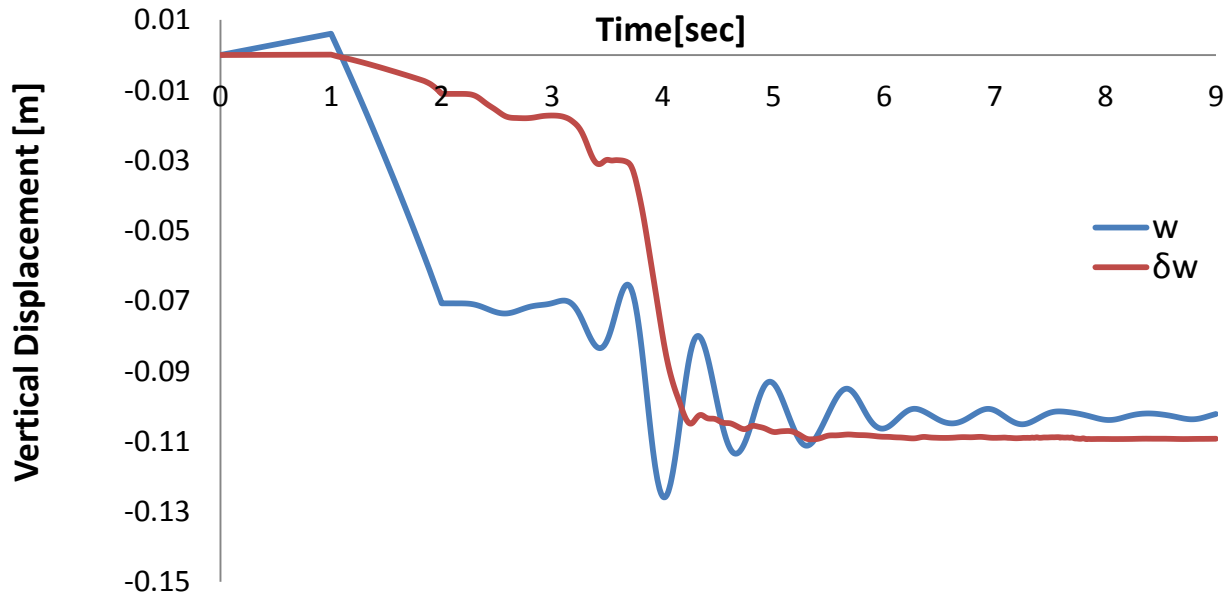

Fig. 2.47. Vertical displacement-time history of the left wall when subjected to Ageion Seismic excitation with peak acceleration 0.4g.

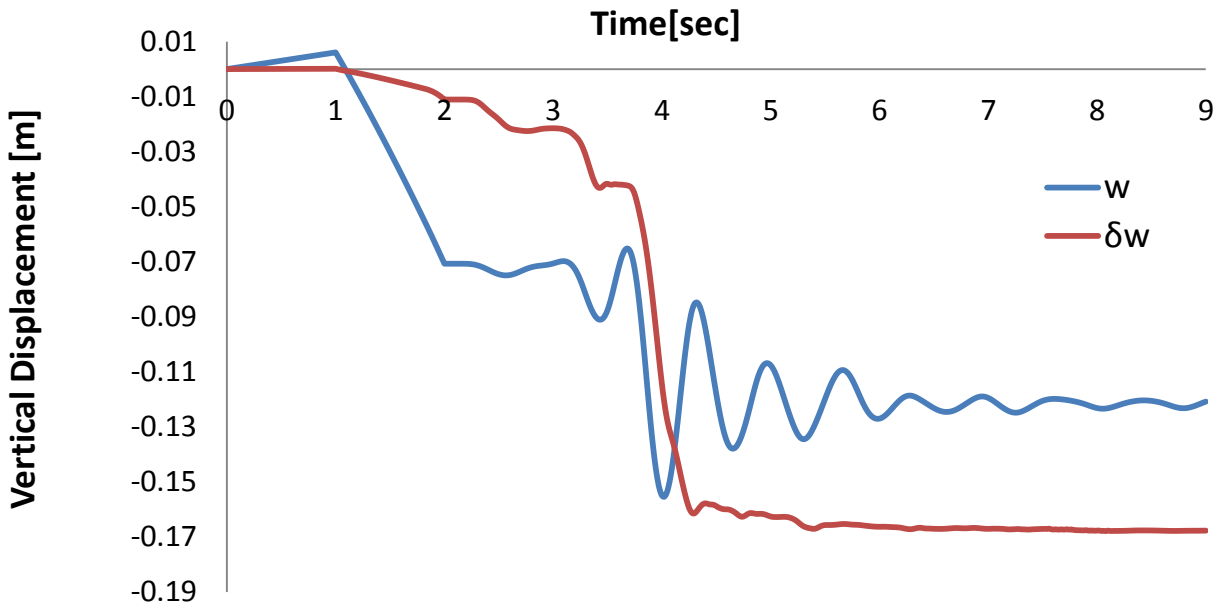

Fig. 2.48. Vertical displacement-time history of the left wall when subjected to Ageion Seismic excitation with peak acceleration 0.6g.

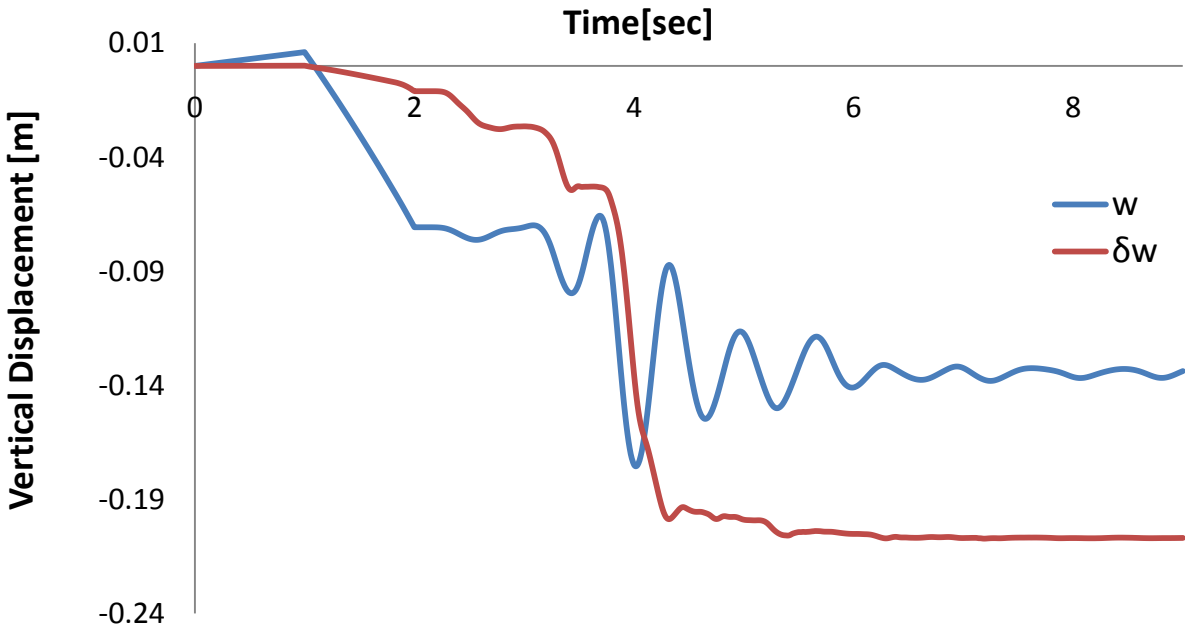

Fig. 2.49. Vertical displacement-time history of the left wall when subjected to Ageion Seismic excitation with peak acceleration 0.8g.

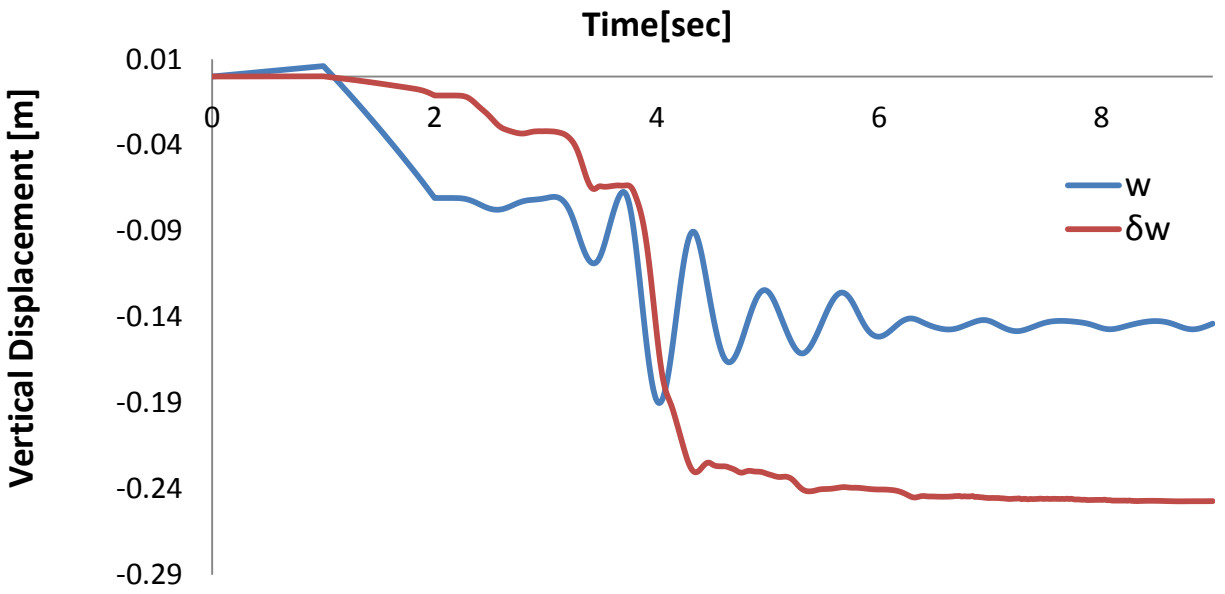

Fig. 2.50. Vertical displacement-time history of the left wall when subjected to Ageion Seismic excitation with peak acceleration 1g.

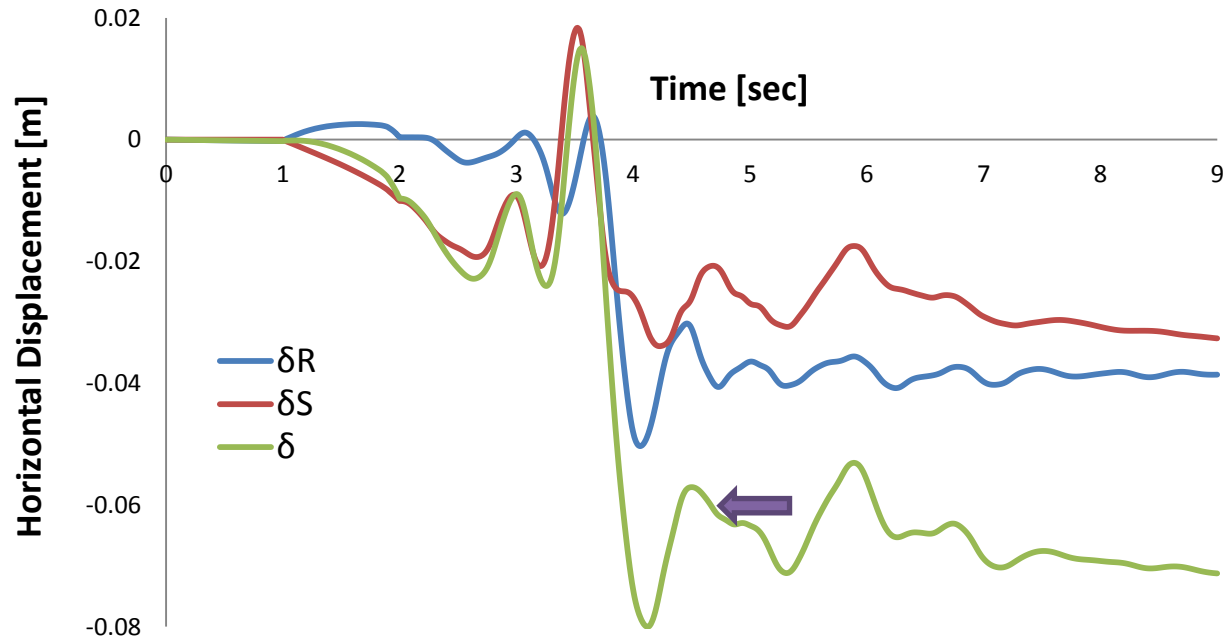

Fig. 2.51. Horizontal displacement-time history of the left wall when subjected to Ageion Seismic excitation with peak acceleration 0.2g.

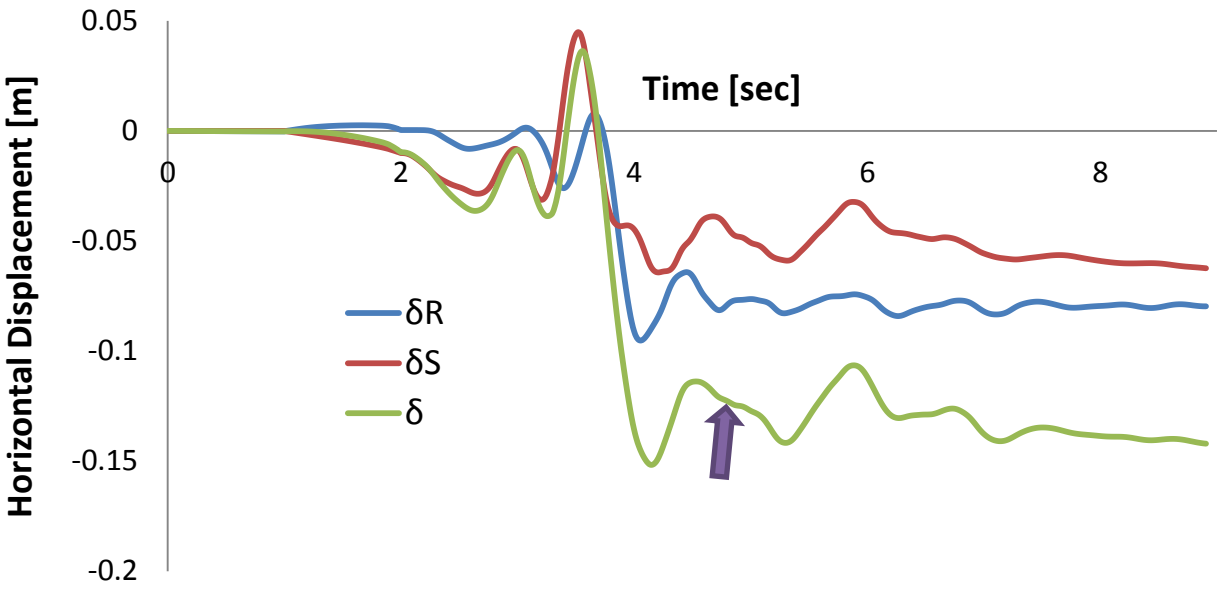

Fig. 2.52. Horizontal displacement-time history of the left wall when subjected to Ageion Seismic excitation with peak acceleration 0.4g.

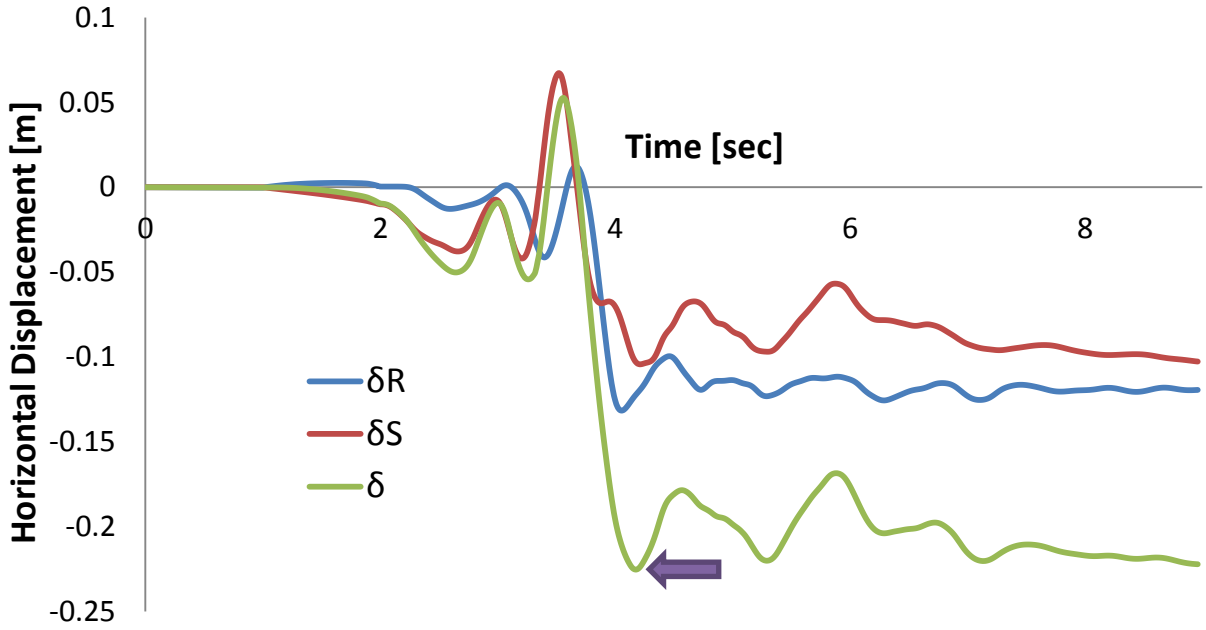

Fig. 2.53. Horizontal displacement-time history of the left wall when subjected to Ageion Seismic excitation with peak acceleration 0.6g.

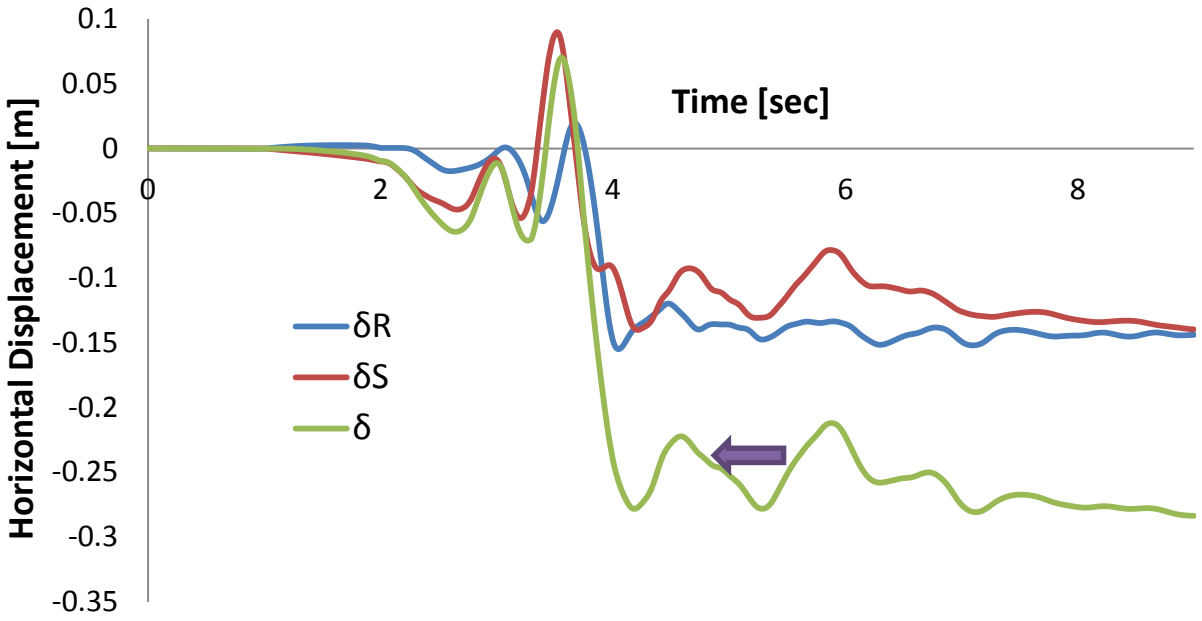

Fig. 2.54. Horizontal displacement-time history of the left wall when subjected to Ageion Seismic excitation with peak acceleration 0.8g.

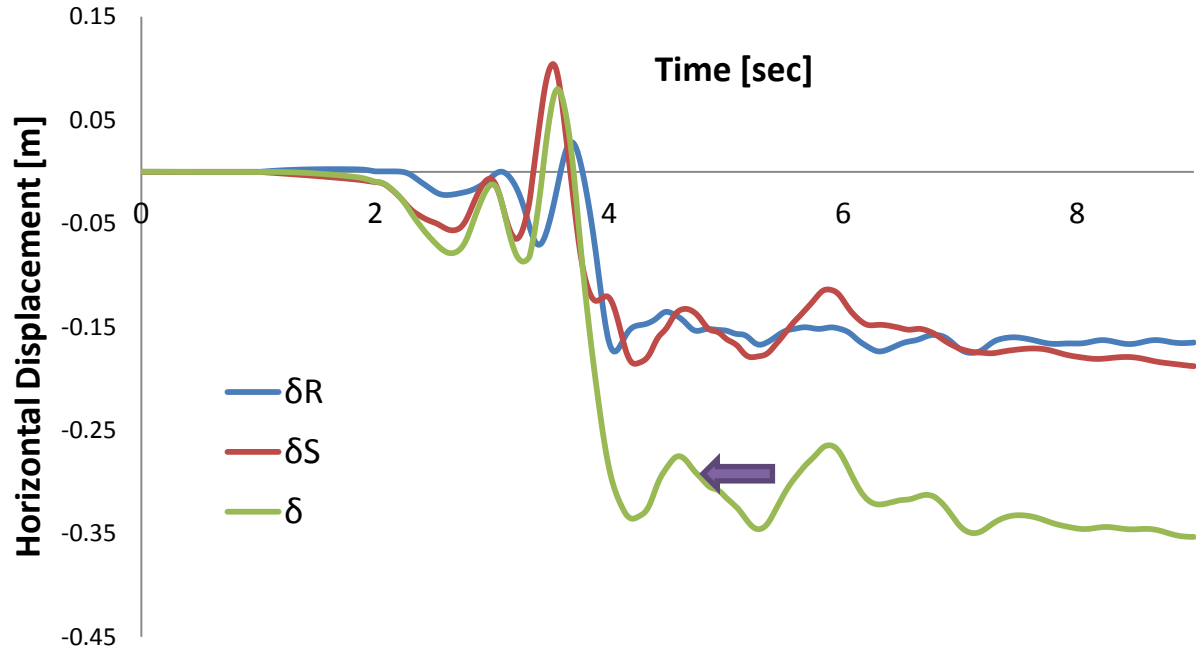

Fig. 2.55. Horizontal displacement-time history of the left wall when subjected to Ageion Seismic excitation with peak acceleration 1g.

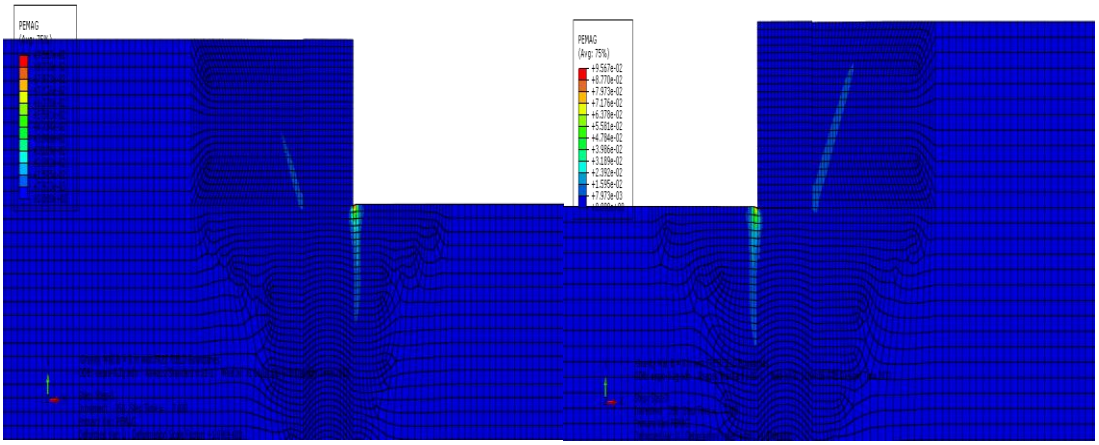

Fig. 2.56. Plastic strain contours at the end of seismic shaking (a)Left wall (b)Right wall when subjected to Aegion seismic excitation with peak acceleration 0.2g

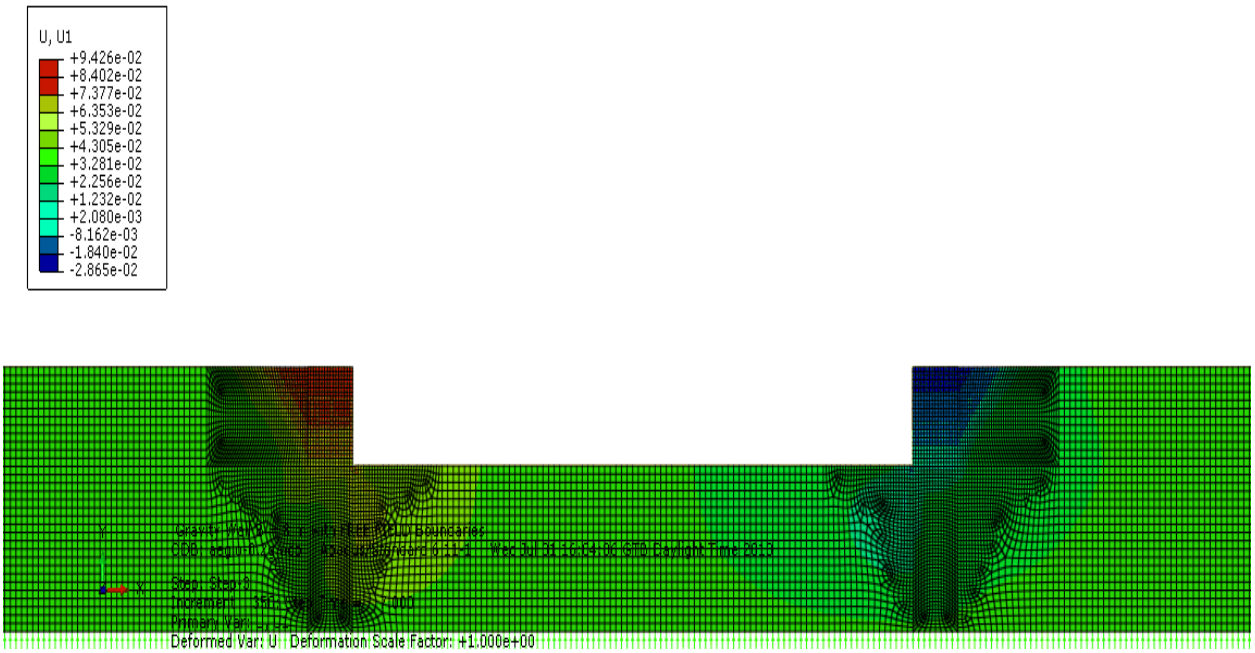

Fig. 2.57. Horizontal displacement contours at the end of the seismic excitation Aegion PGA 0.2g.

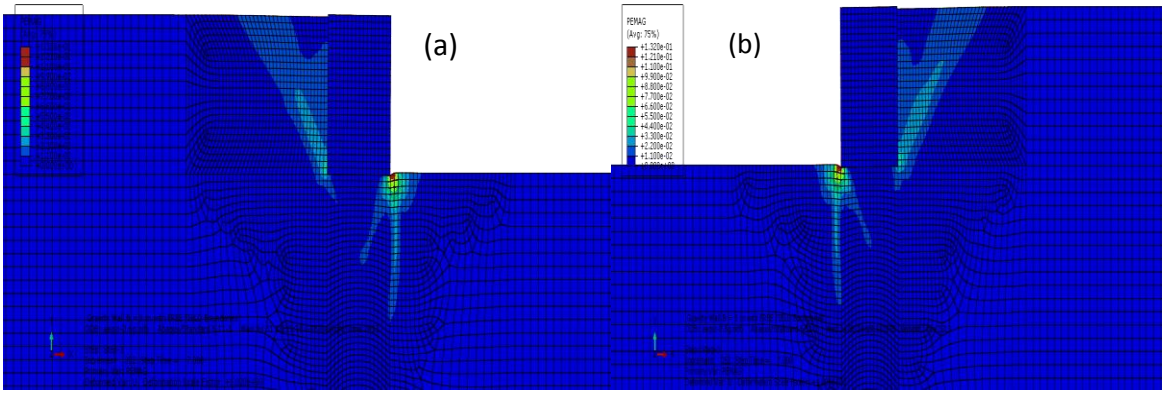

Fig. 2.58. Plastic strain contours at the end of seismic shaking (a)Left wall (b)Right wall when subjected to Aegion seismic excitation with peak acceleration 0.6g

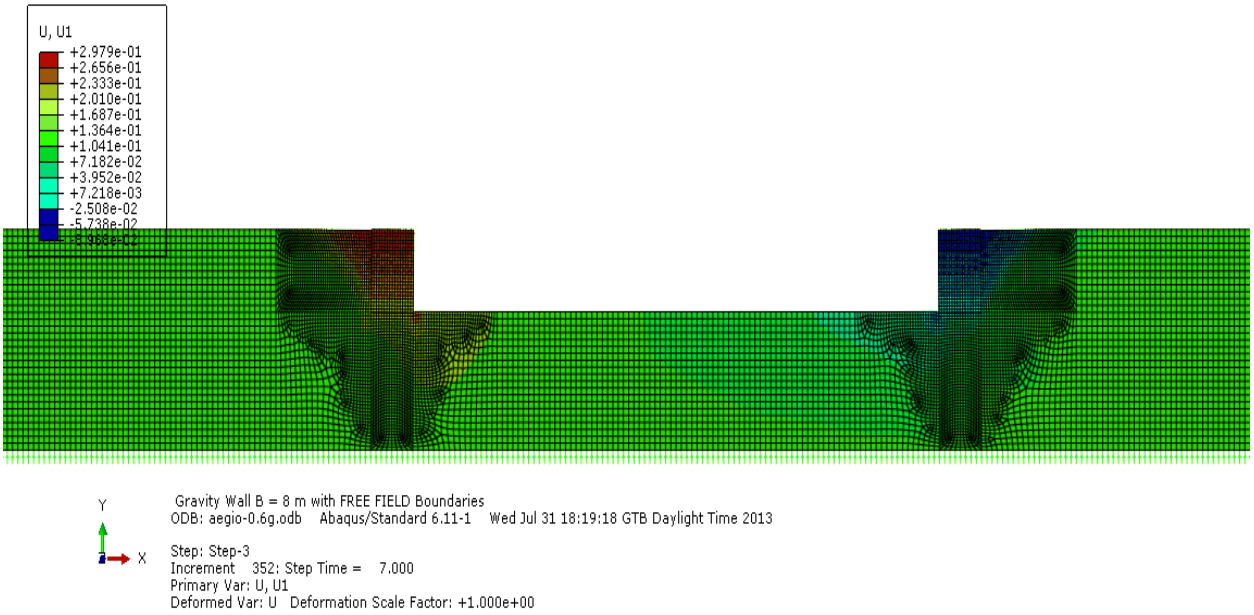

Fig. 2.59. Horizontal displacement contours at the end of the seismic excitation Aegion PGA 0.6g.

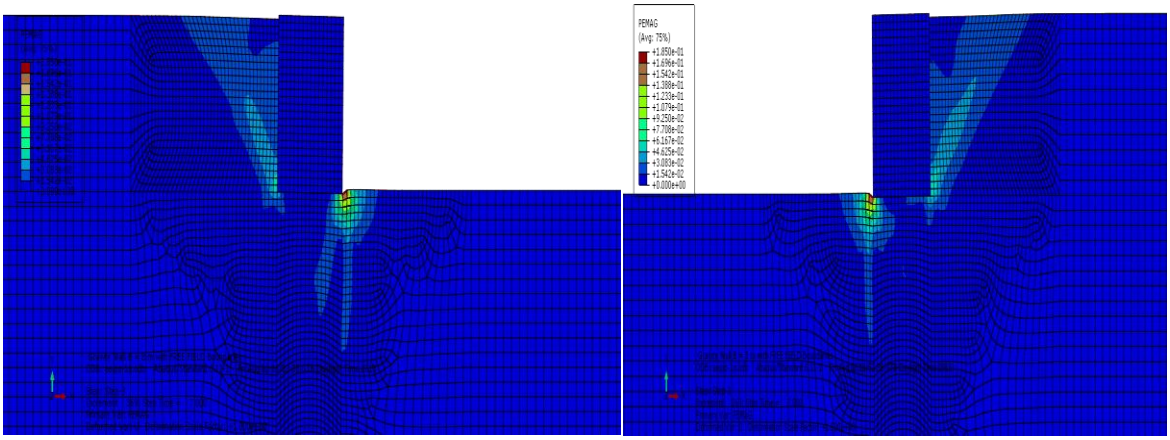

Fig. 2.60. Plastic strain contours at the end of seismic shaking (a)Left wall (b)Right wall when subjected to Aegion seismic excitation with peak acceleration 1g.

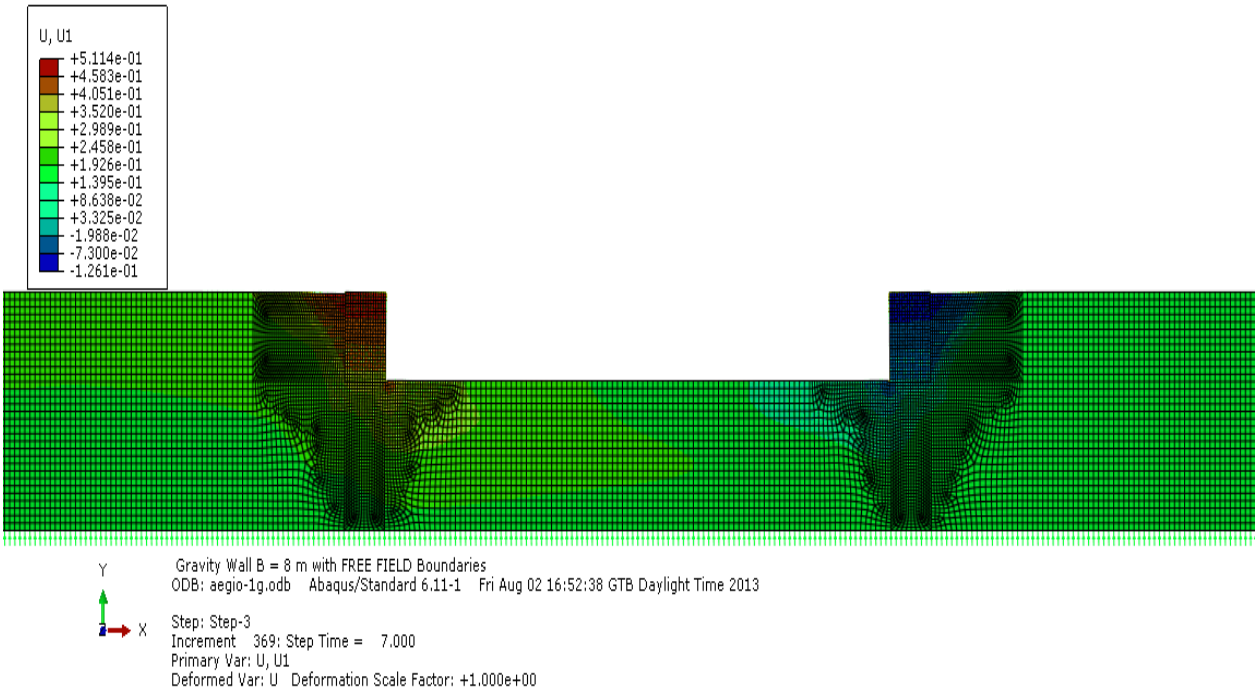

Fig. 2.61. Horizontal displacement contours at the end of the seismic excitation Aegion PGA 1g.

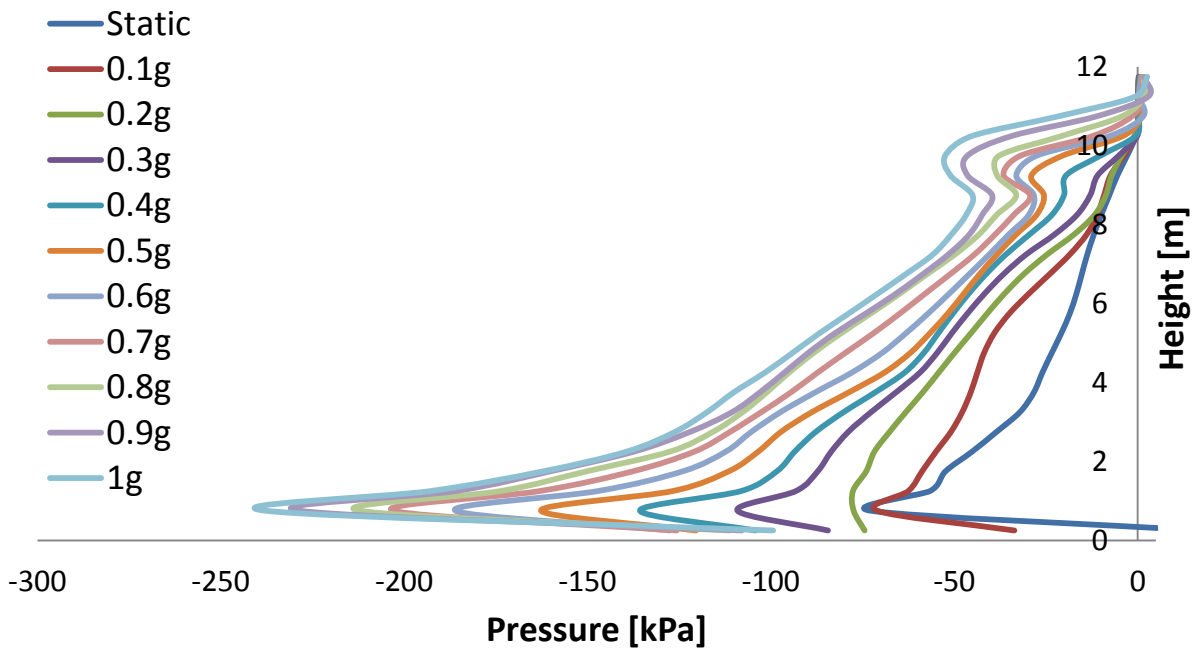

Fig. 2.62. Static and maximum earth pressure profiles for different peak accelerations on the left wall when subjected to Aegion Seismic excitation.

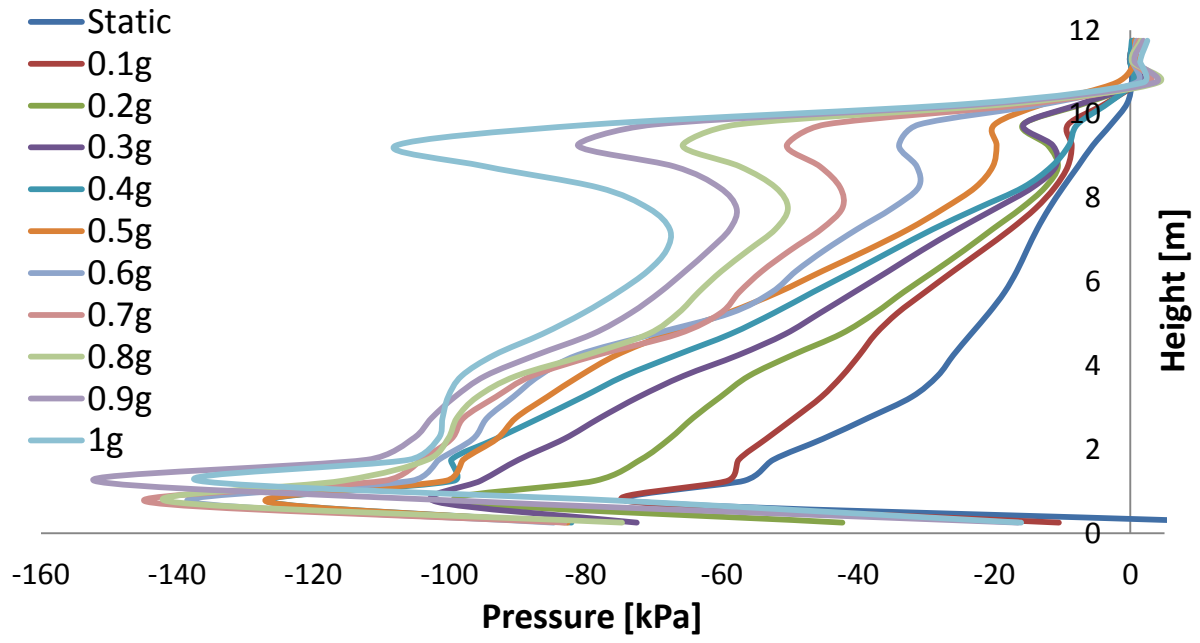

Fig. 2.63. Static and maximum earth pressure profiles for different peak accelerations on the right wall when subjected to Ageion Seismic excitation.

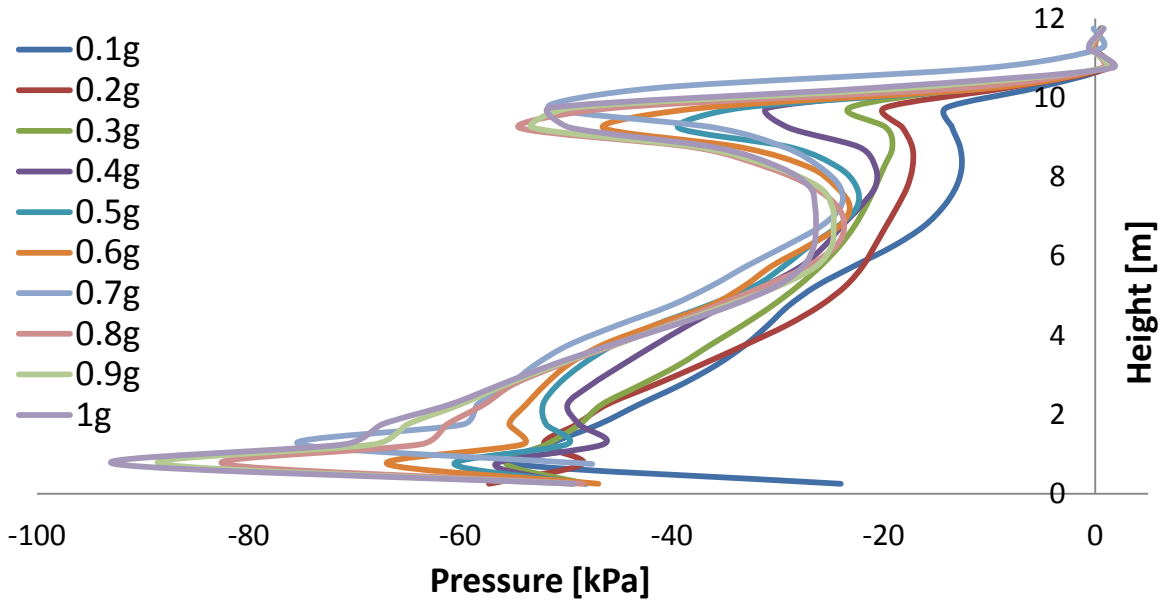

Fig. 2.64. Residual earth pressure profiles for different peak accelerations on the left wall when subjected to Ageion Seismic excitation.

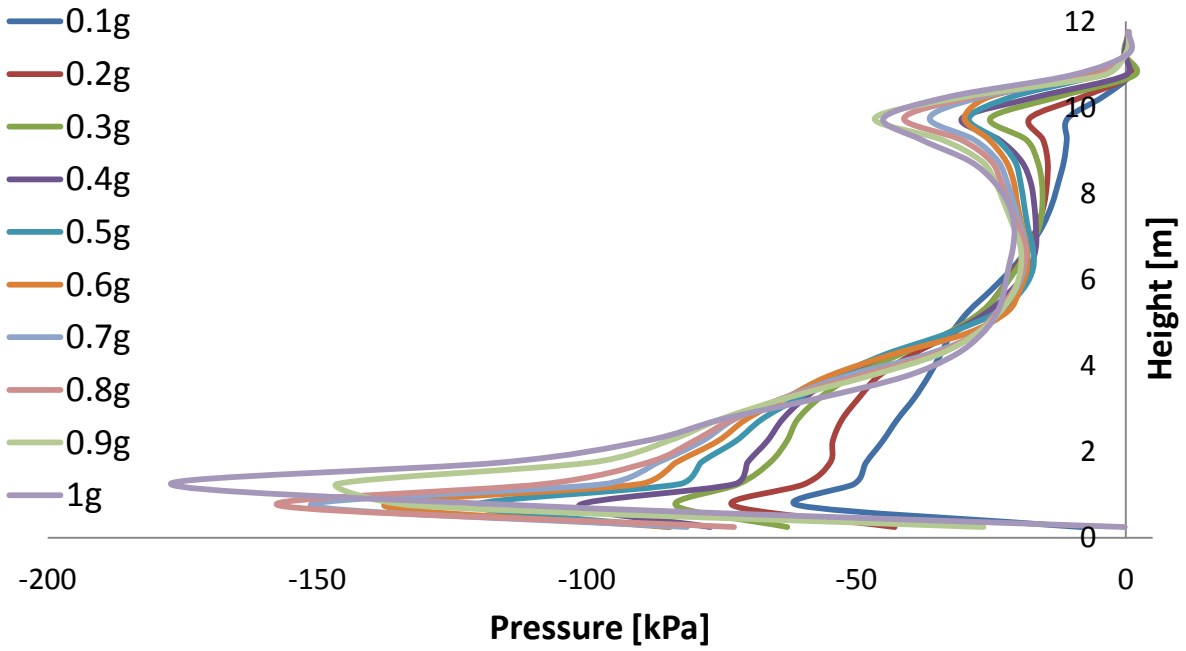

Fig. 2.65. Residual earth pressure profiles for different peak accelerations on the right wall when subjected to Ageion Seismic excitation.

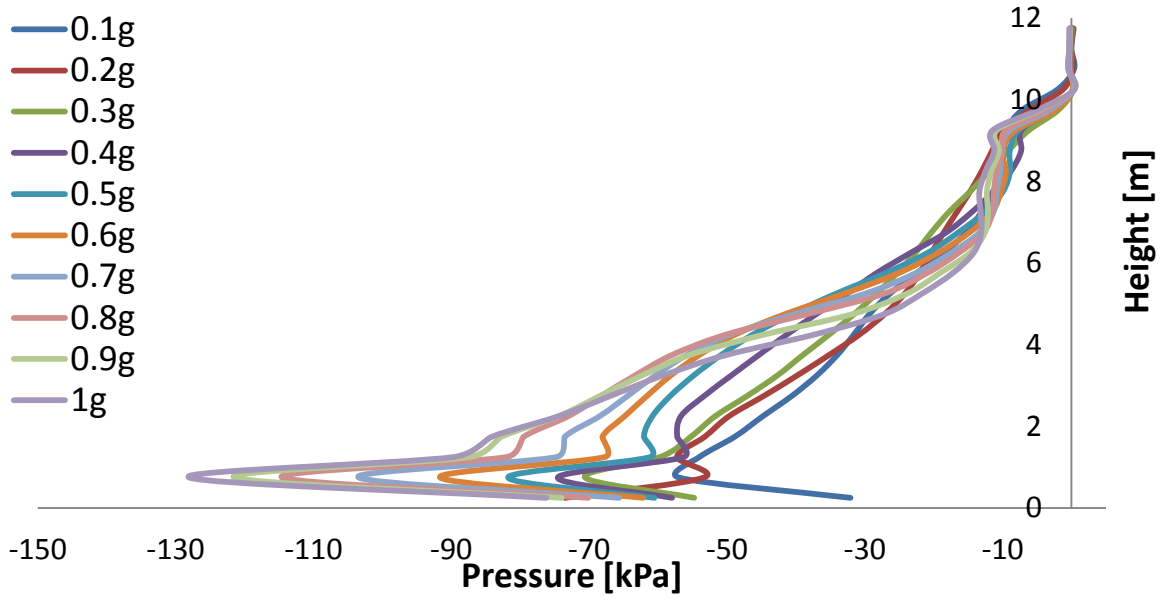

Fig. 2.66. Earth pressure profiles at maximum displacement for different peak accelerations on the left wall when subjected to Ageion Seismic excitation.

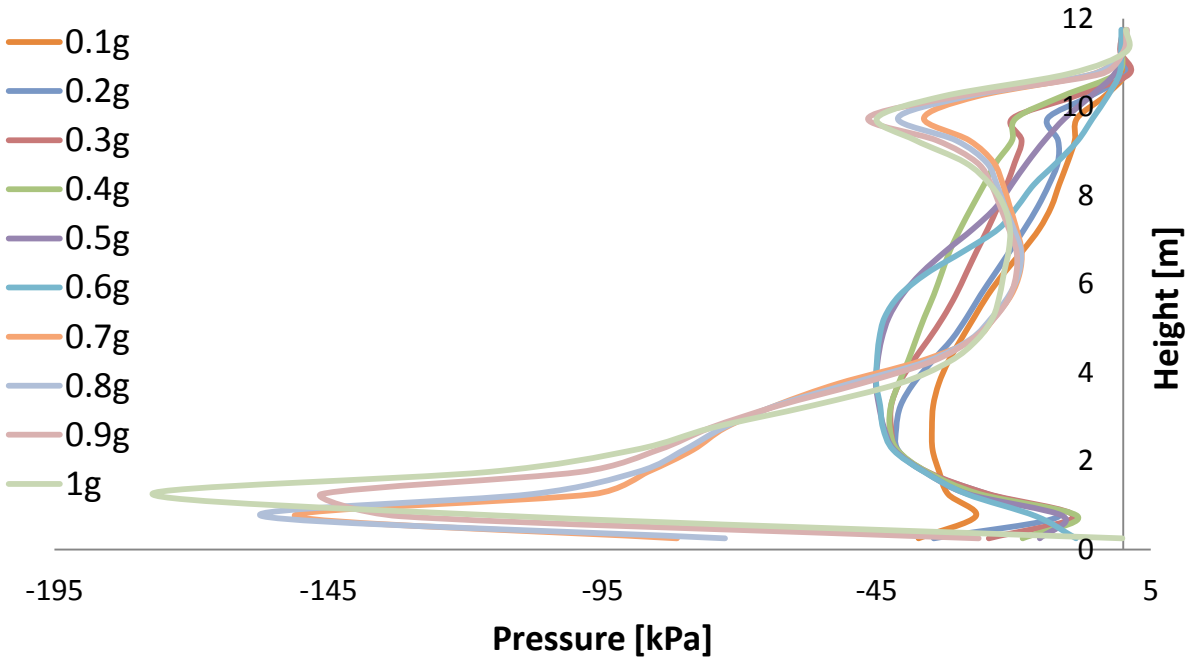

Fig. 2.67. Earth pressure profiles at maximum displacement for different peak accelerations on the right wall when subjected to Aegion Seismic excitation.

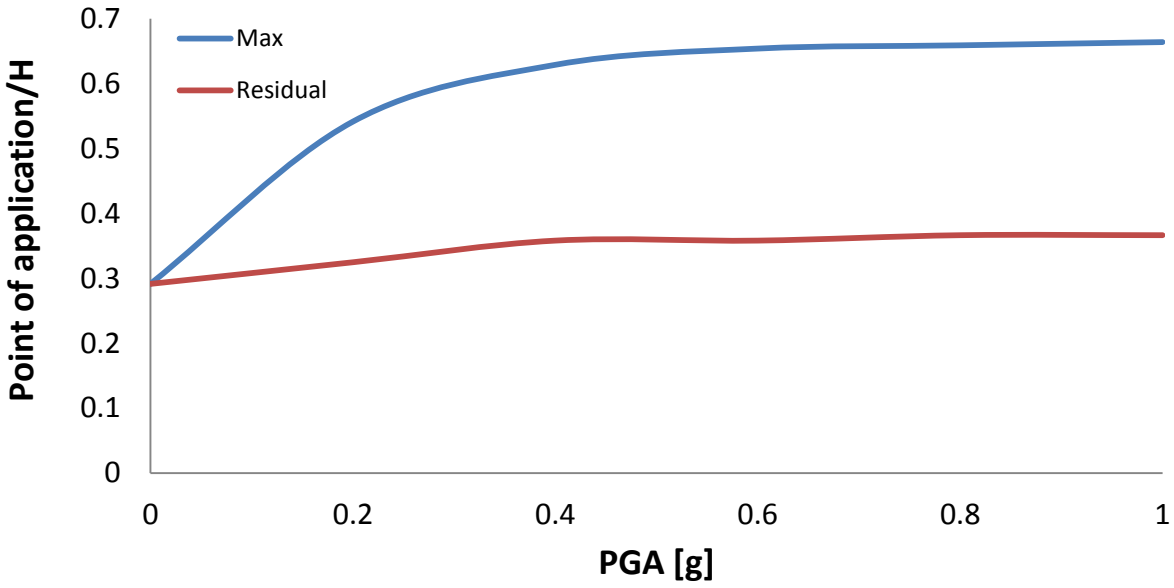

Fig. 2.68. Normalized point of application of dynamic force as a function of PGA.

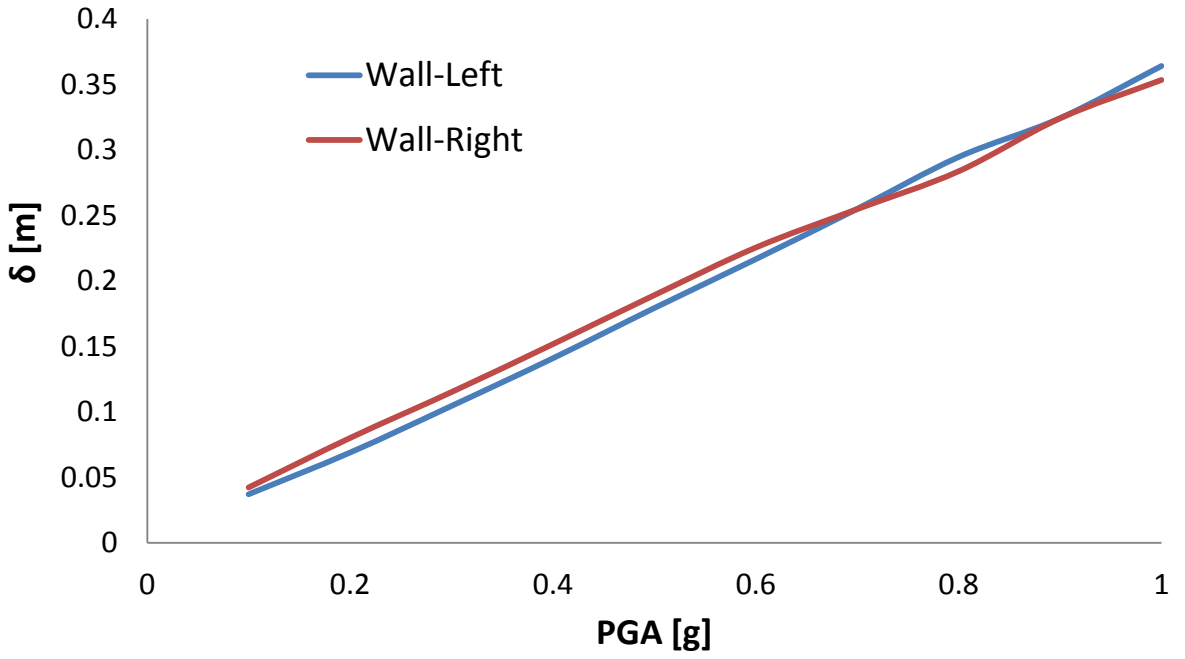

Fig. 2.69. Horizontal displacement as a function of PGA for the left and right wall when subjected to Ageion Seismic excitation.

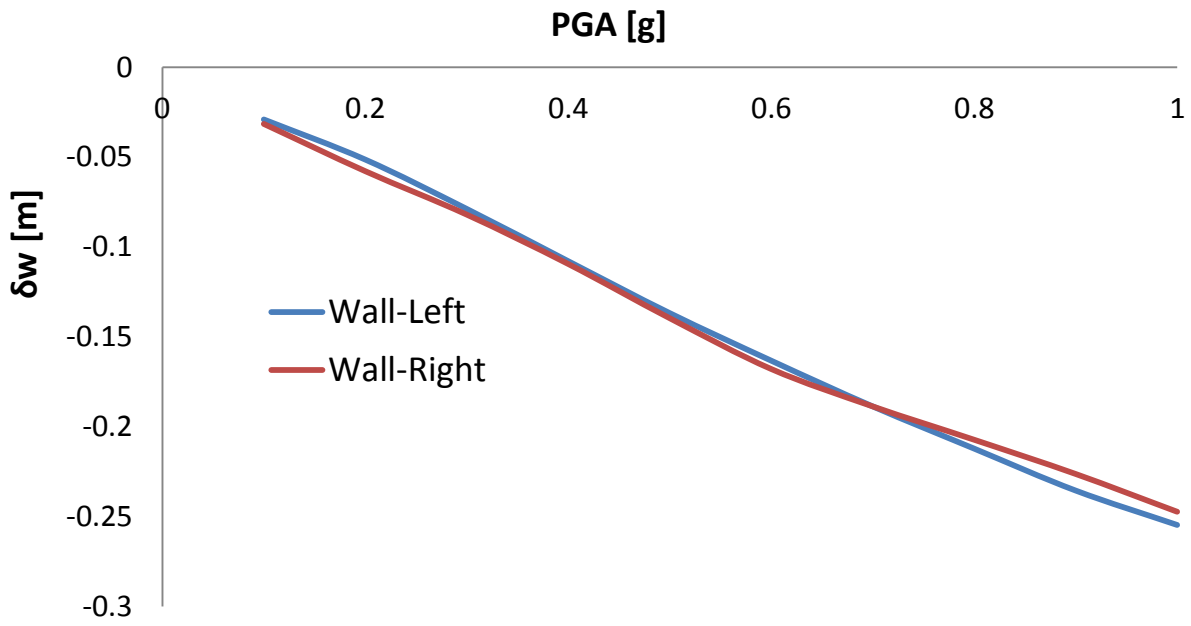

Fig. 2.70. Differential settelement as a function of PGA for the left and right wall when subjected to Ageion Seismic excitation.

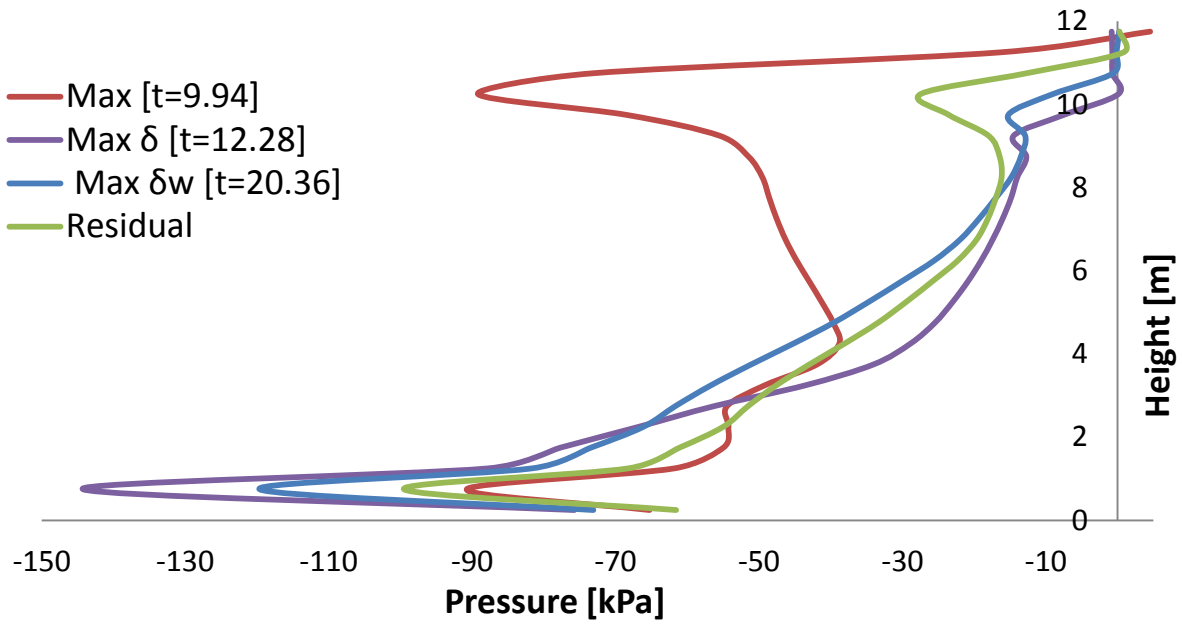

Fig. 2.71 . Earth pressures profiles on the left wall at different moments when subjected to Lefkada Seismic excitation with peak ground acceleration 0.3 g.

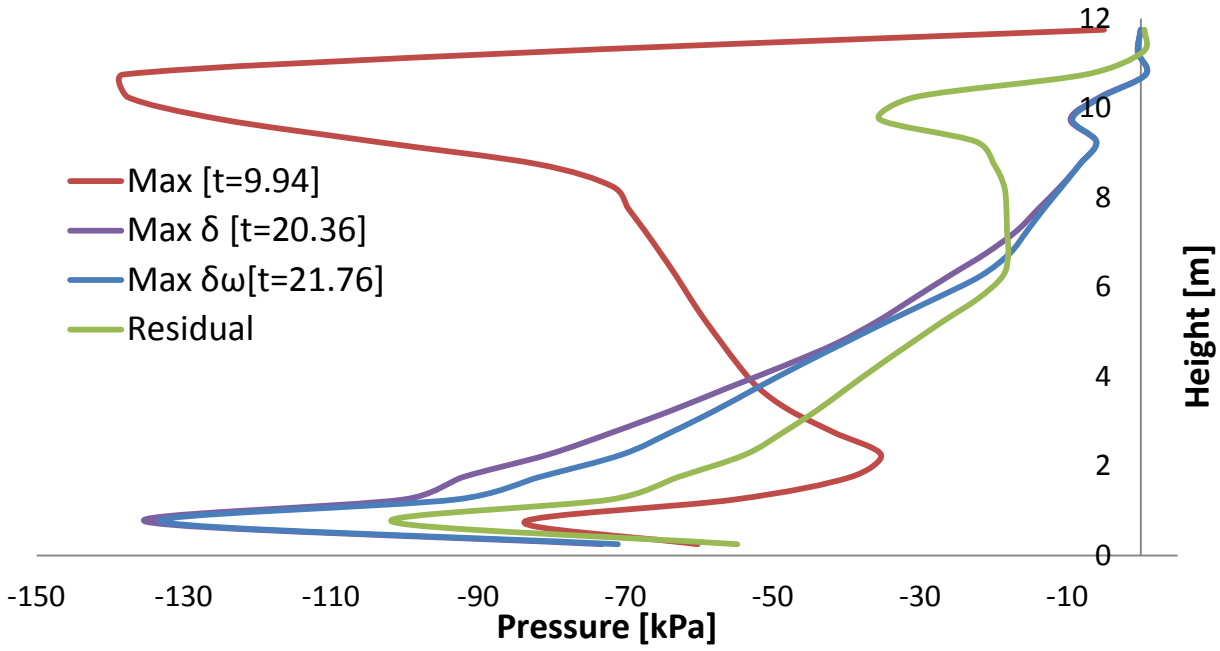

Fig. 2.72 . Earth pressures profiles on the left wall at different moments when subjected to Lefkada Seismic excitation with peak ground acceleration 0.6 g.

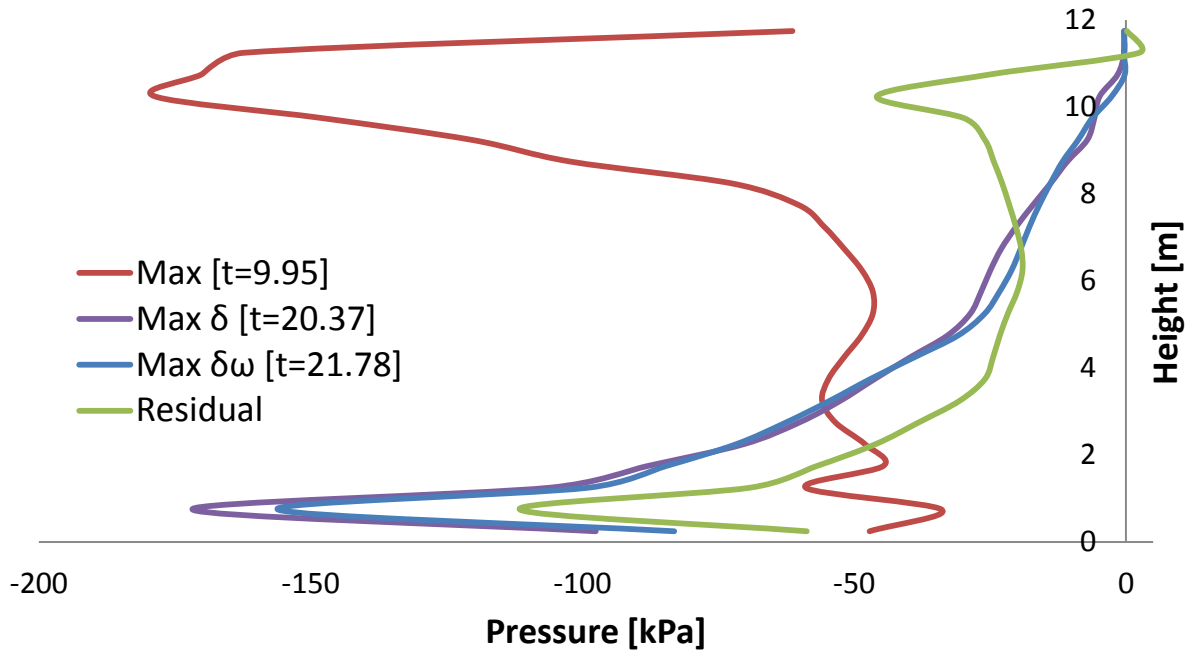

Fig. 2.73 . Earth pressures profiles on the left wall at different moments when subjected to Lefkada Seismic excitation with peak ground acceleration 0.9g.

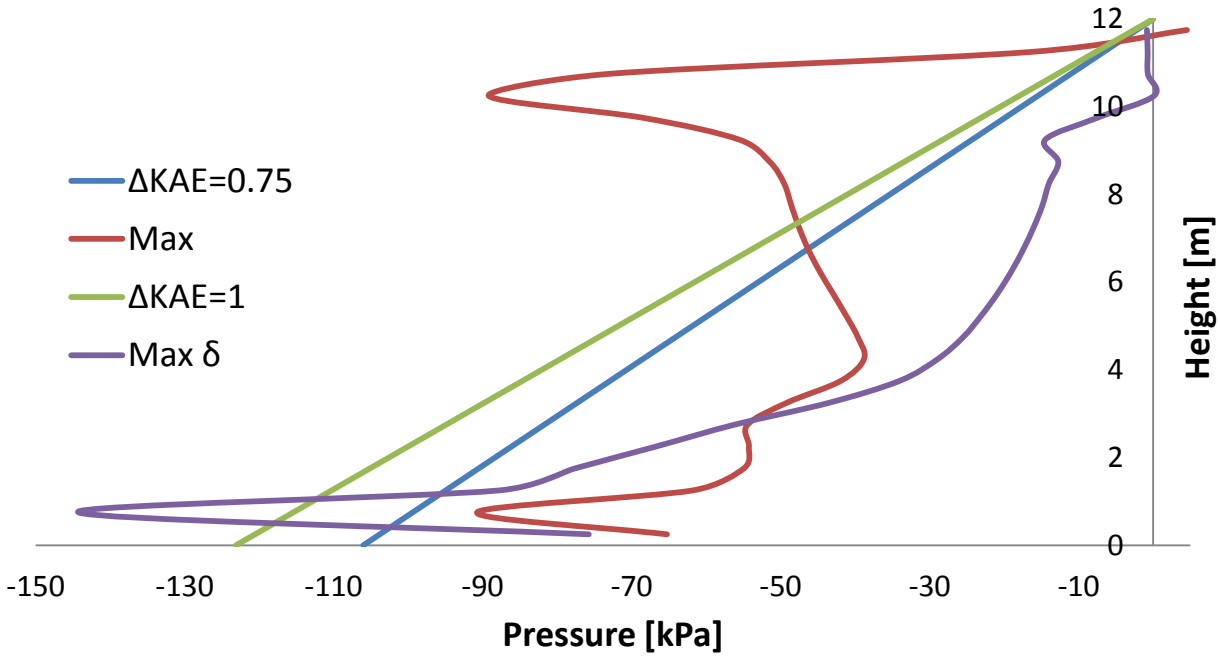

Fig. 2.74. Earth pressure profiles computed in ABAQUS and estimated using the M-O when the left wall is subjected to the Lefkada Seismic excitation with peak acceleration 0.3g.

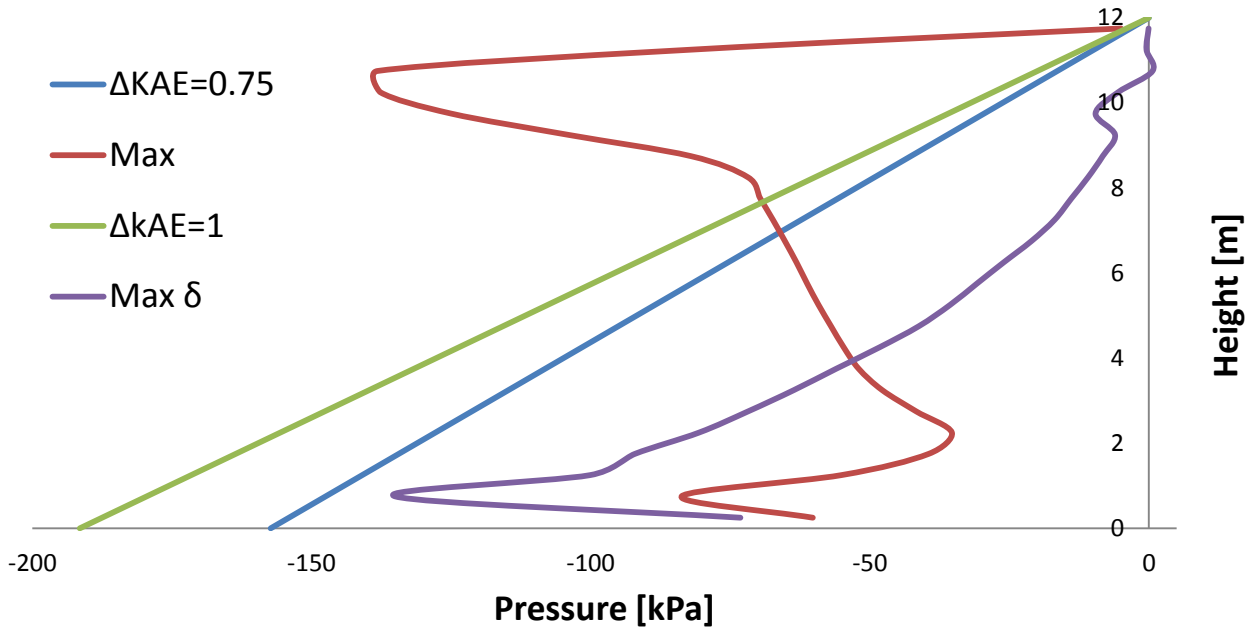

Fig. 2.75. Earth pressure profiles computed in ABAQUS and estimated using the M-O when the left wall is subjected to the Lefkada Seismic excitation with peak acceleration 0.6g.

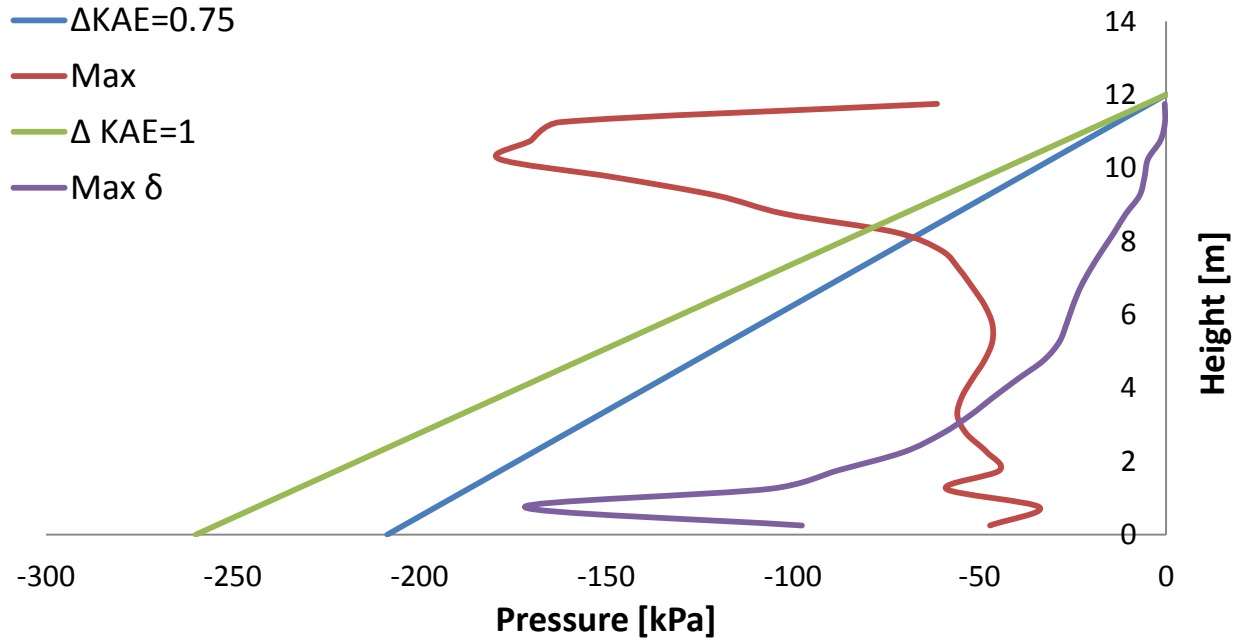

Fig. 2.76. Earth pressure profiles computed in ABAQUS and estimated using the M-O when the left wall is subjected to the Lefkada Seismic excitation with peak acceleration 0.9g.

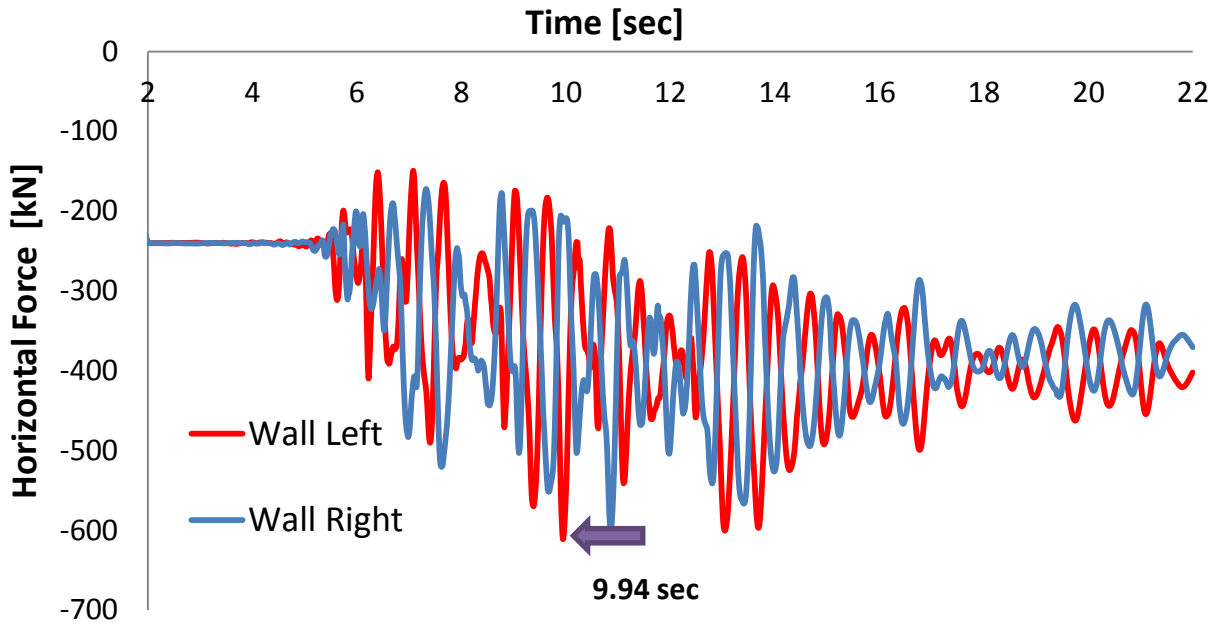

Fig. 2.77. Horizontal force-time history of the left and right wall when subjected to Lefkada Seismic excitation with peak ground acceleration 0.3g.

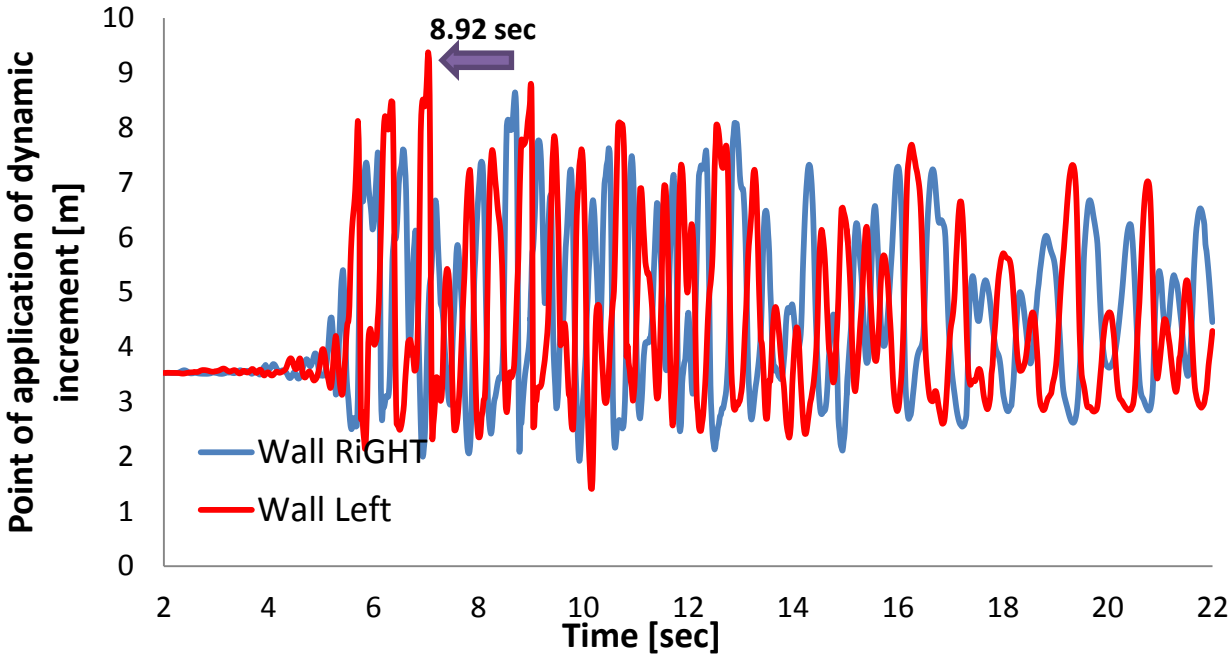

Fig. 2.78. Point of application of dynamic increment on the left wall when subjected to Lefkada Seismic excitation with peak ground acceleration 0.3g.

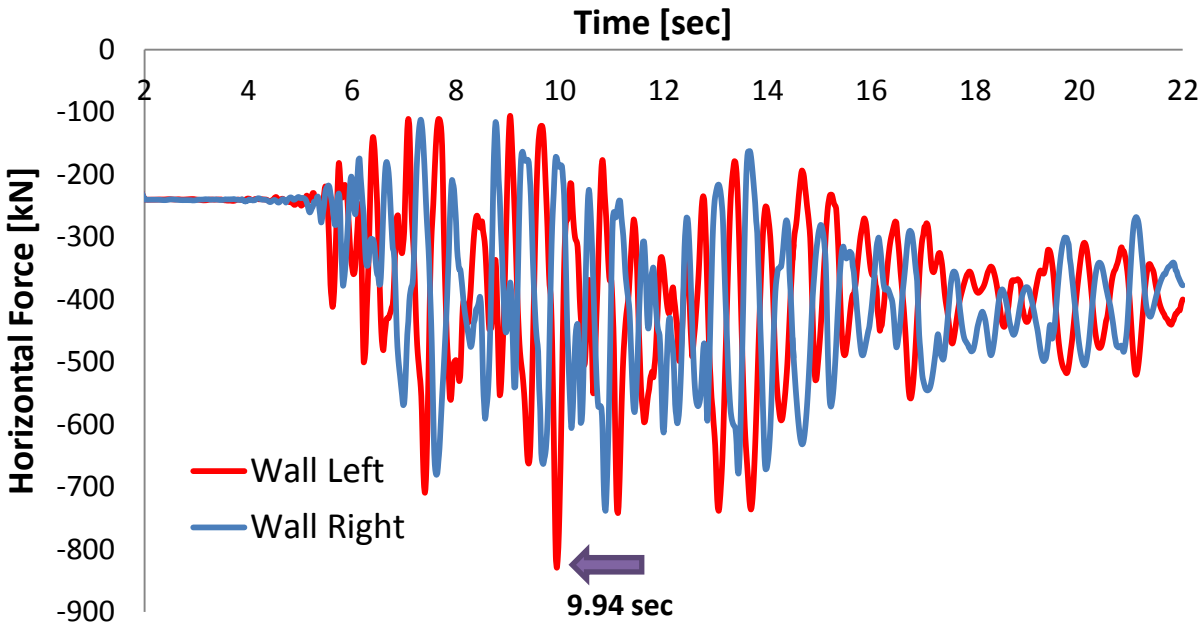

Fig. 2.79. Horizontal force-time history of the left and right wall when subjected to Lefkada Seismic excitation with peak ground acceleration 0.6g

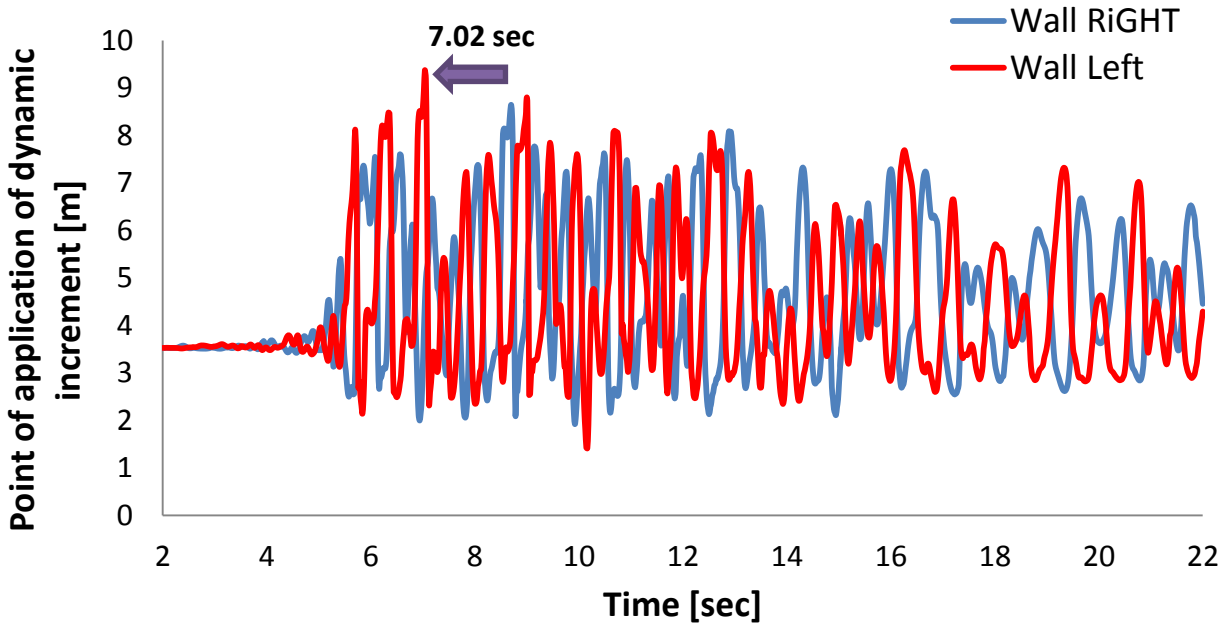

Fig. 2.80. Point of application of dynamic increment on the left wall when subjected to Lefkada Seismic excitation with peak ground acceleration 0.6g

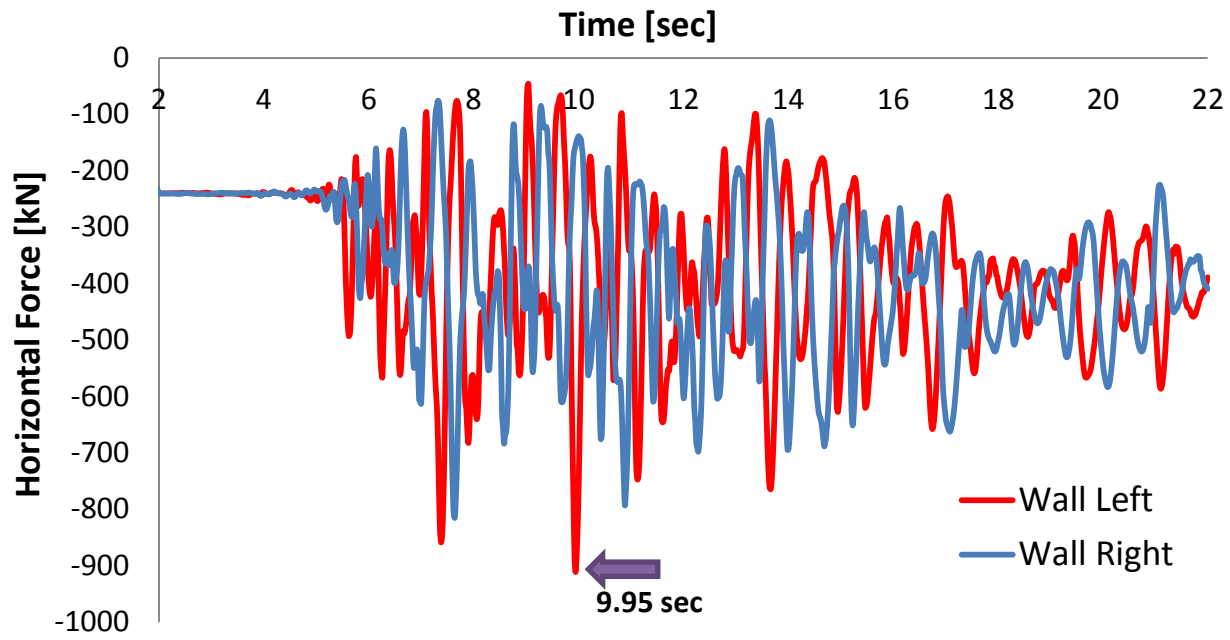

Fig. 2.81. Horizontal force-time history of the left and right wall when subjected to Lefkada Seismic excitation with peak ground acceleration 0.9g

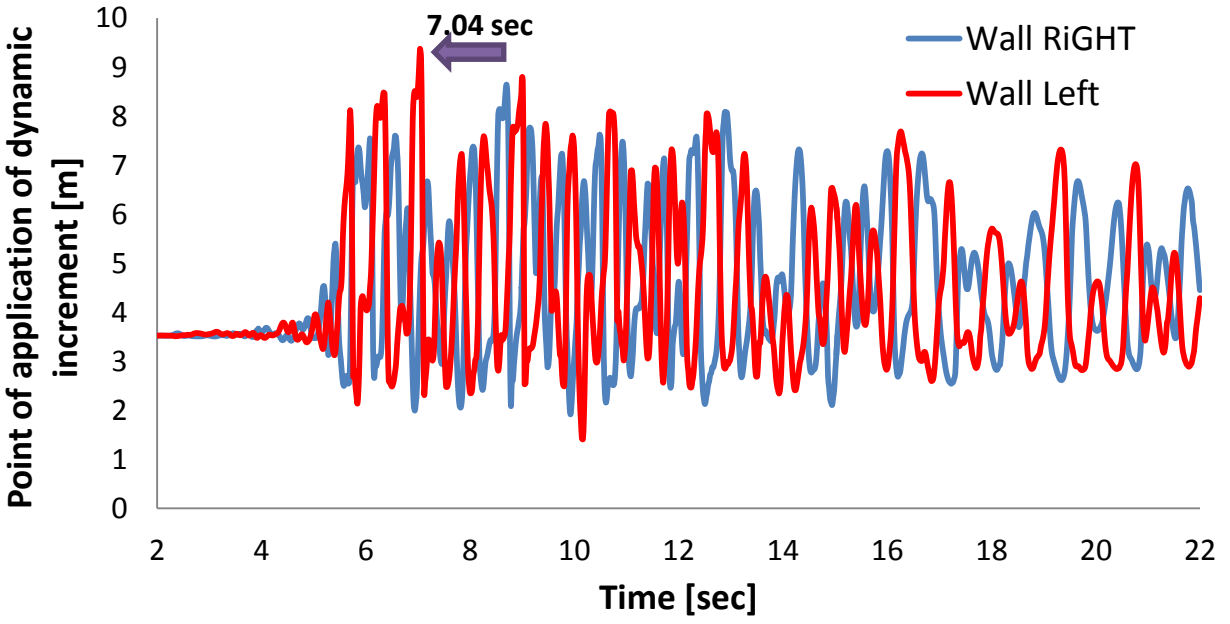

Fig. 2.82. Point of application of dynamic increment on the left wall when subjected to Lefkada Seismic excitation with peak ground acceleration 0.9g.

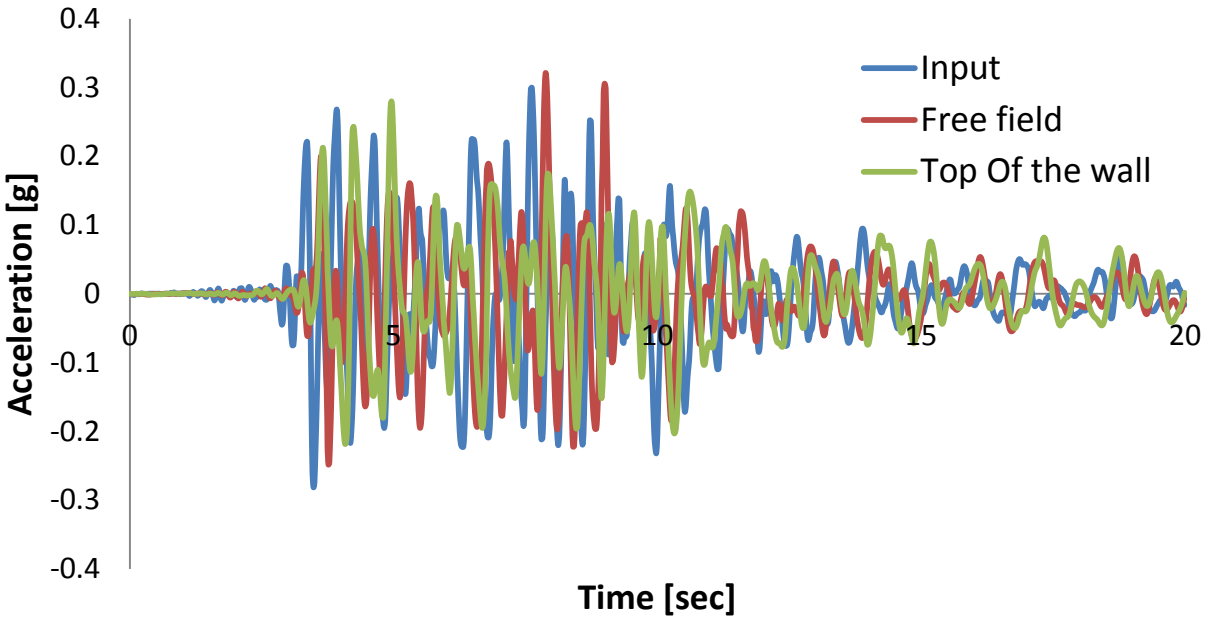

Fig. 2.83. Comparison of input acceleration and computed at the top of the left wall and top of the free field when subjected to Lefkada Seismic excitation with peak acceleration 0.3g.

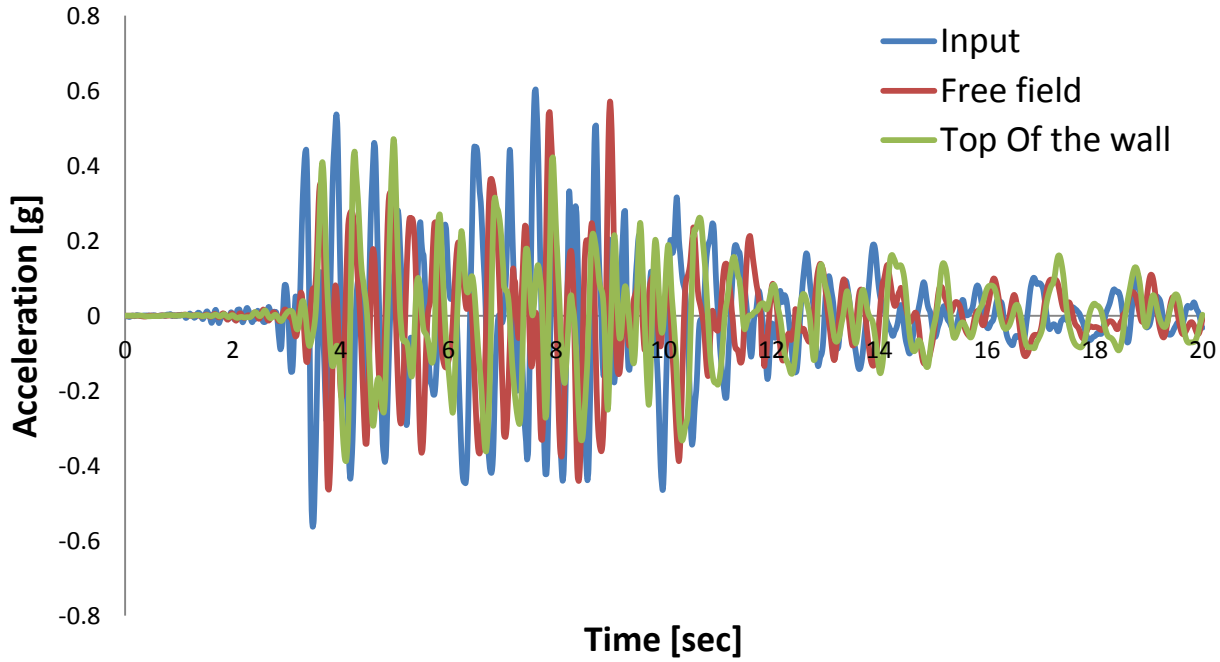

Fig. 2.84. Comparison of input acceleration and computed at the top of the left wall and top of the free field when subjected to Lefkada Seismic excitation with peak acceleration 0.6g.

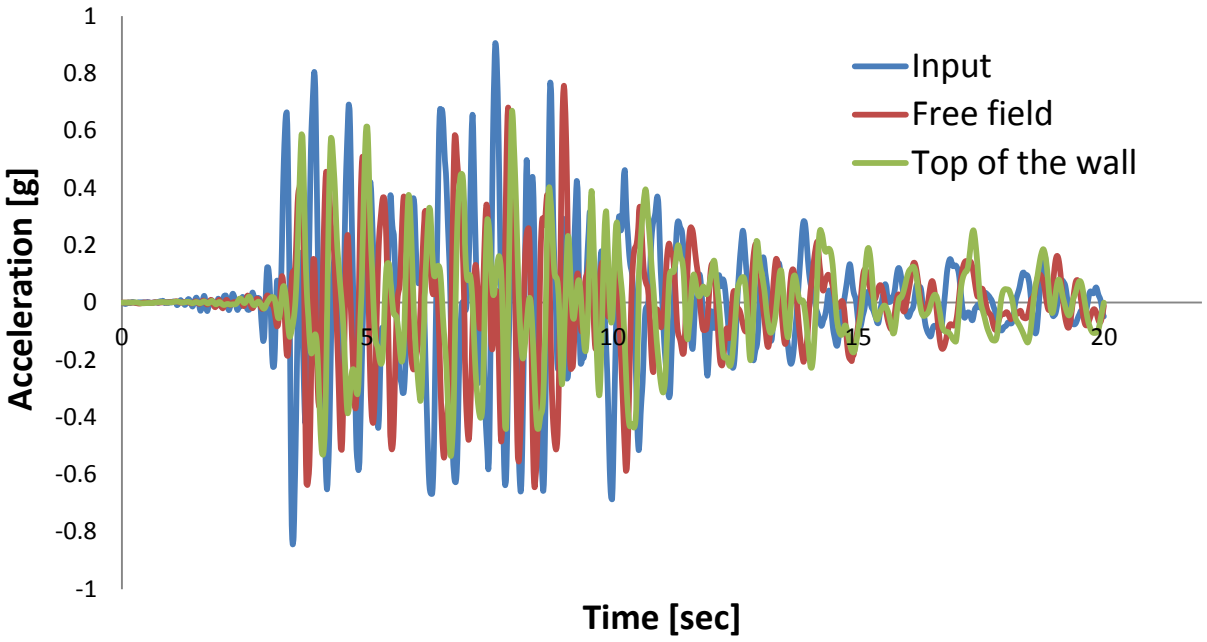

Fig. 2.85. Comparison of input acceleration and computed at the top of the left wall and top of the free field when subjected to Lefkada Seismic excitation with peak acceleration 0.9g

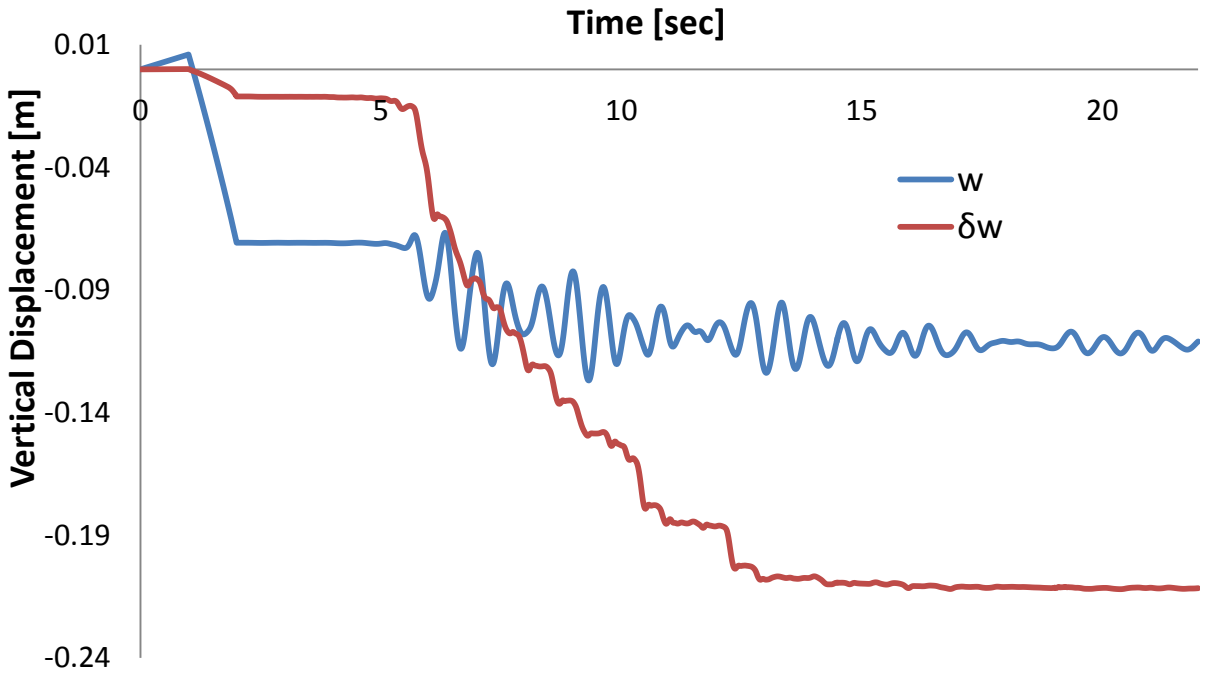

Fig. 2.86. Vertical displacement-time history of the left wall when subjected to Lefkada Seismic excitation with peak acceleration 0.3g.

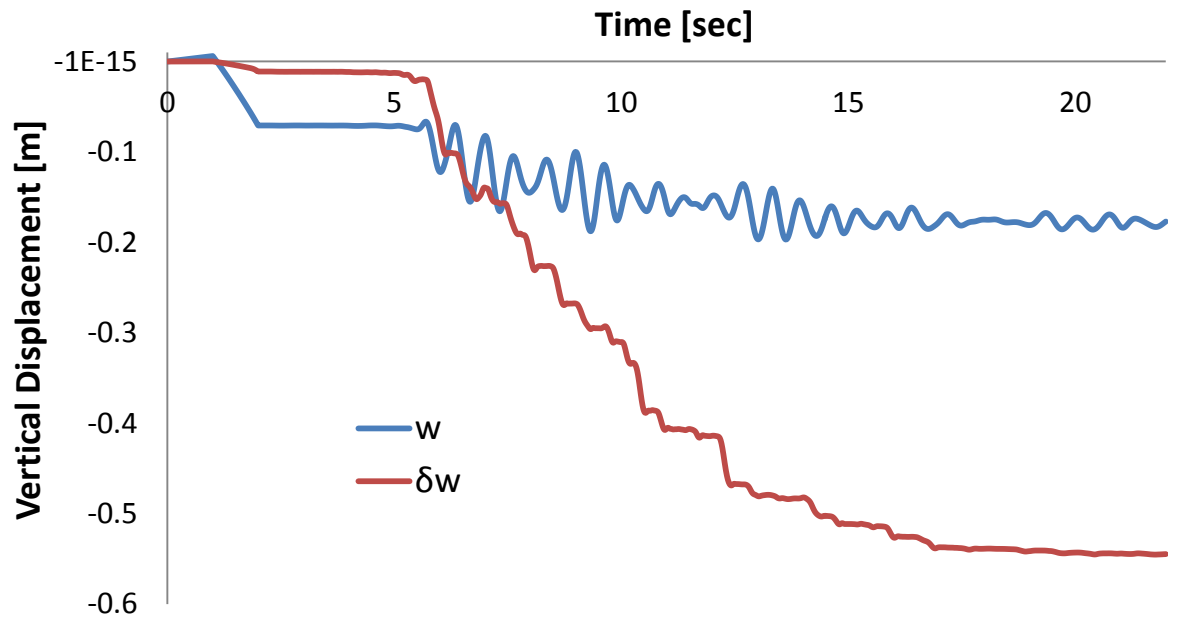

Fig. 2.87. Vertical displacement-time history of the left wall when subjected to Lefkada Seismic excitation with peak acceleration 0.6g.

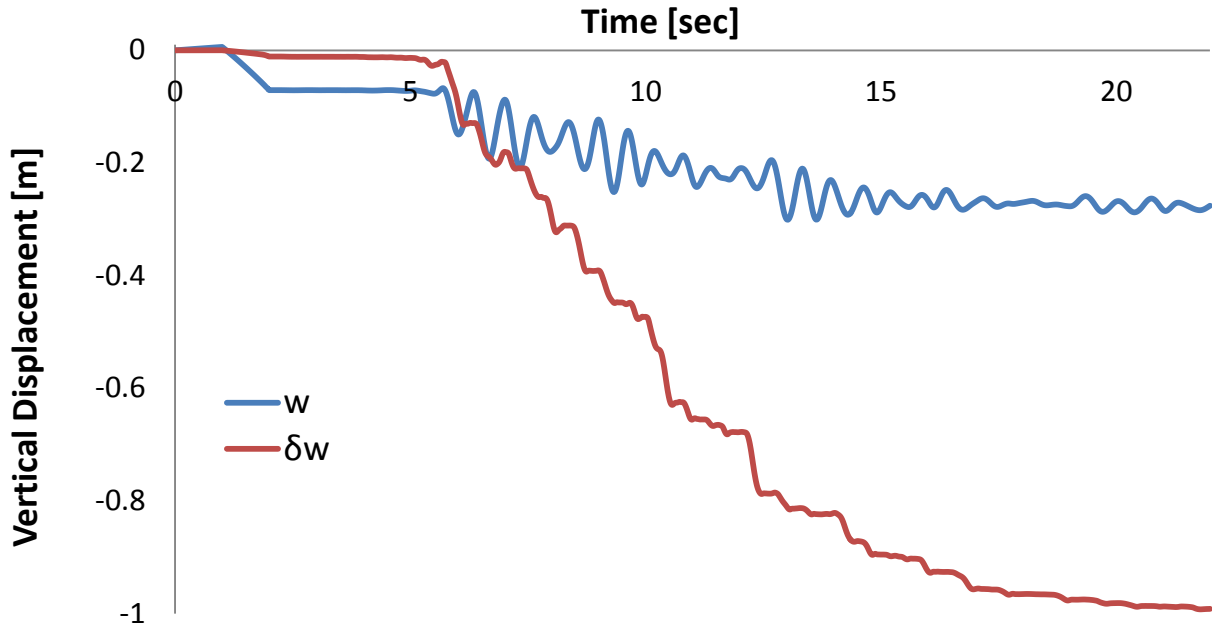

Fig. 2.88. Vertical displacement-time history of the left wall when subjected to Lefkada Seismic excitation with peak acceleration 0.9g.

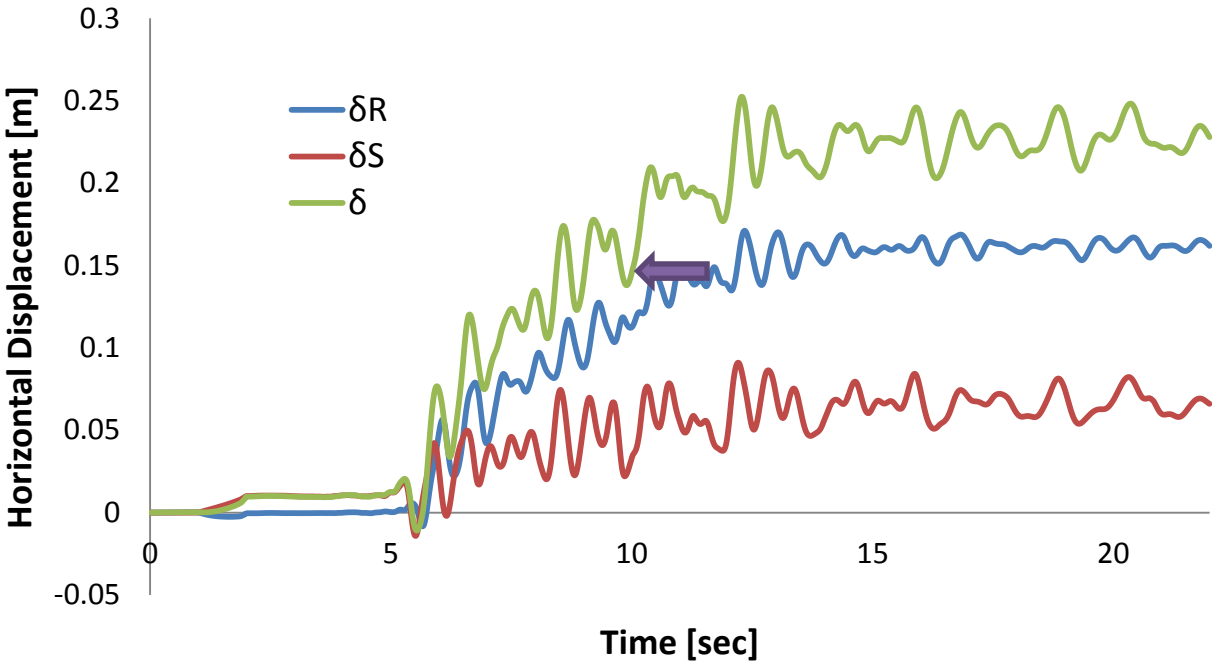

Fig. 2.89. Horizontal displacement-time history of the left wall when subjected to Lefkada Seismic excitation with peak acceleration 0.3g.

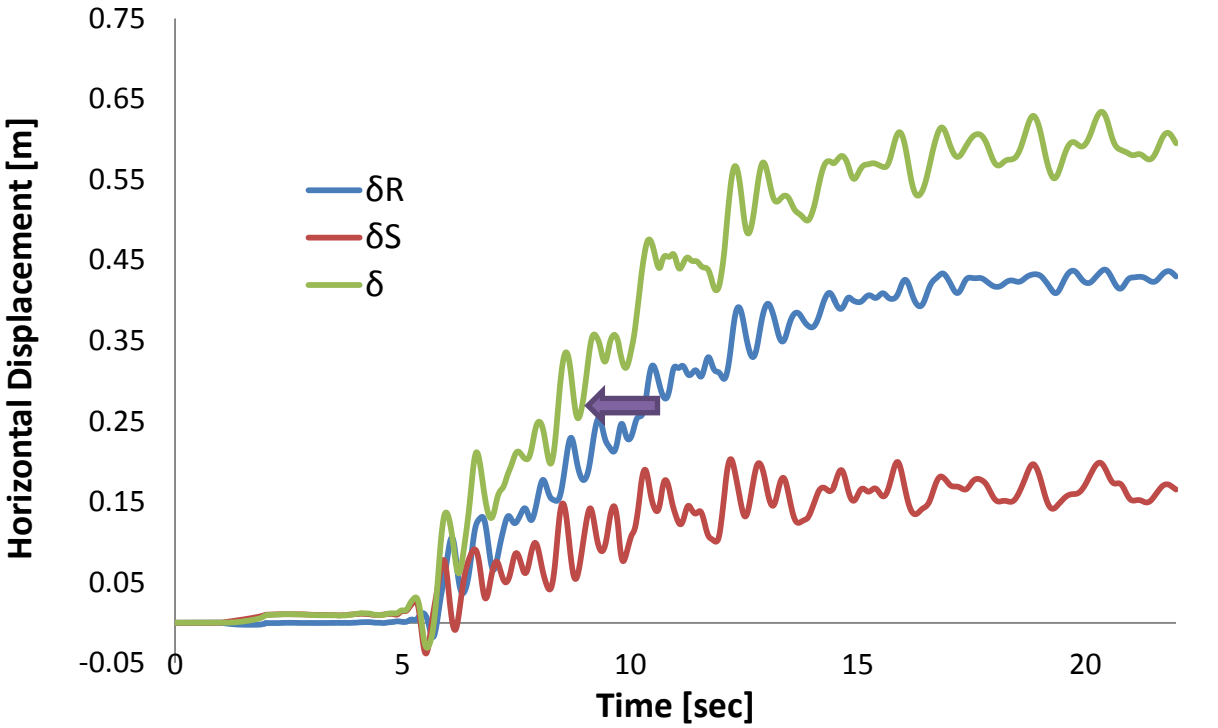

Fig. 2.90. Horizontal displacement-time history of the left wall when subjected to Lefkada Seismic excitation with peak acceleration 0.6g.

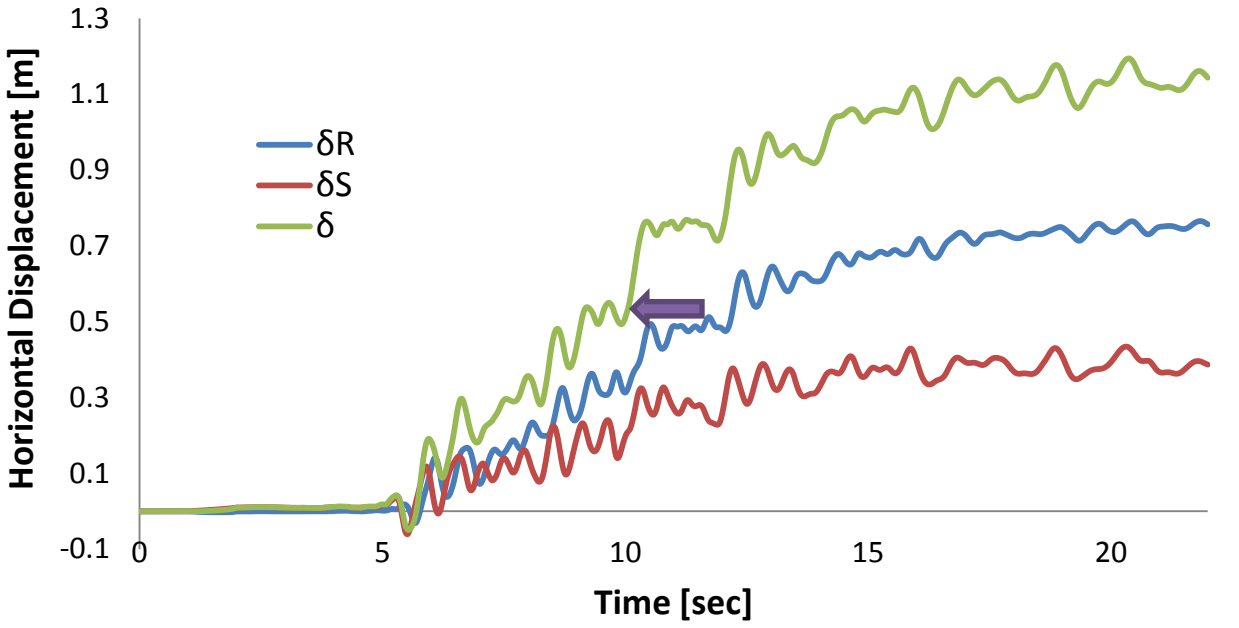

Fig. 2.91. Horizontal displacement-time history of the left wall when subjected to Lefkada Seismic excitation with peak acceleration 0.9g.

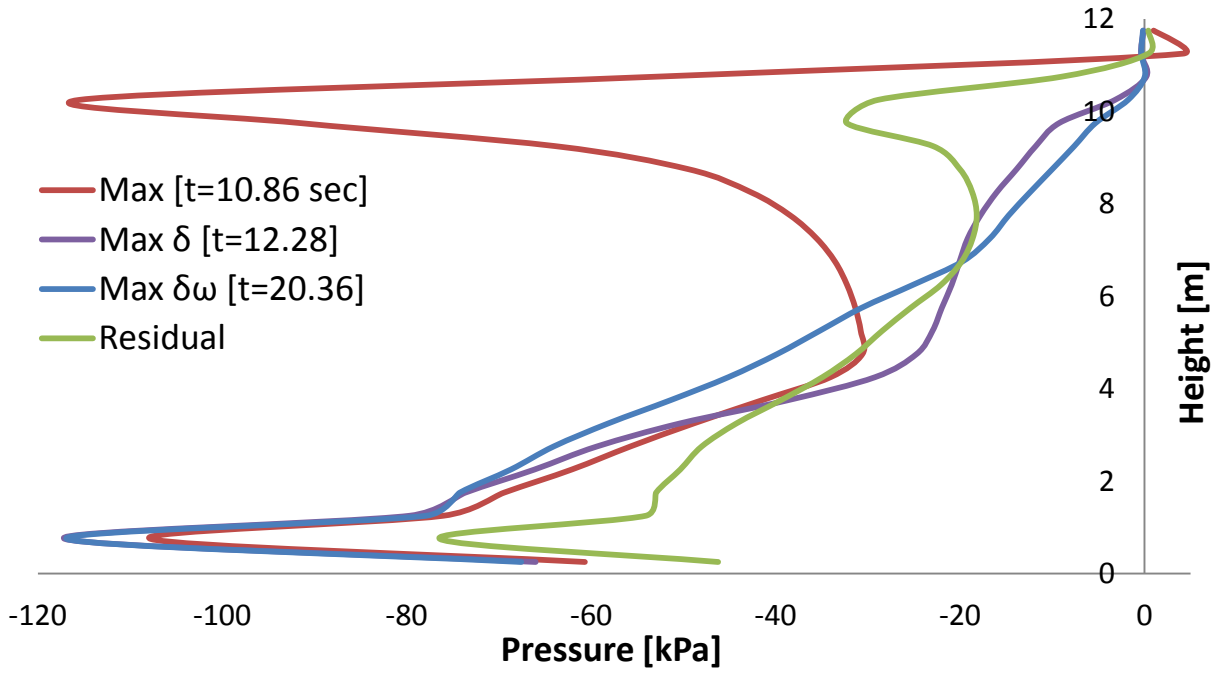

Fig. 2.92. Earth pressures profiles on the right wall at different moments when subjected to Lefkada Seismic excitation with peak ground acceleration 0.3 g.

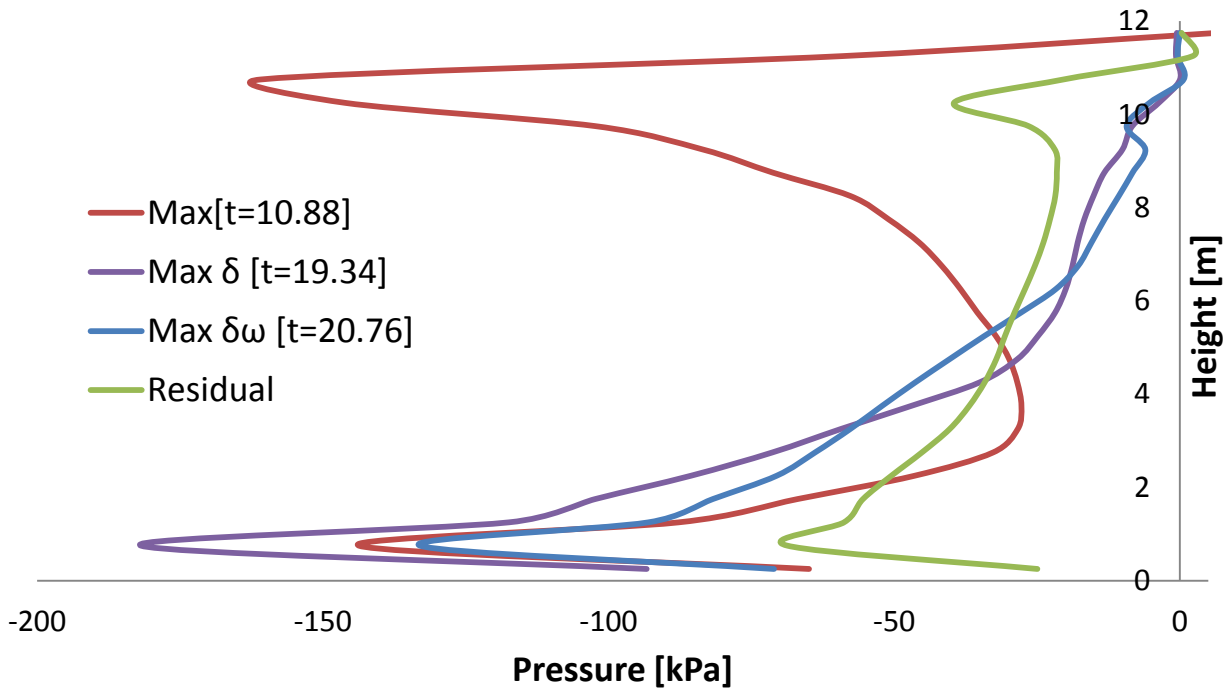

Fig. 2.93 . Earth pressures profiles on the right wall at different moments when subjected to Lefkada Seismic excitation with peak ground acceleration 0.6 g.

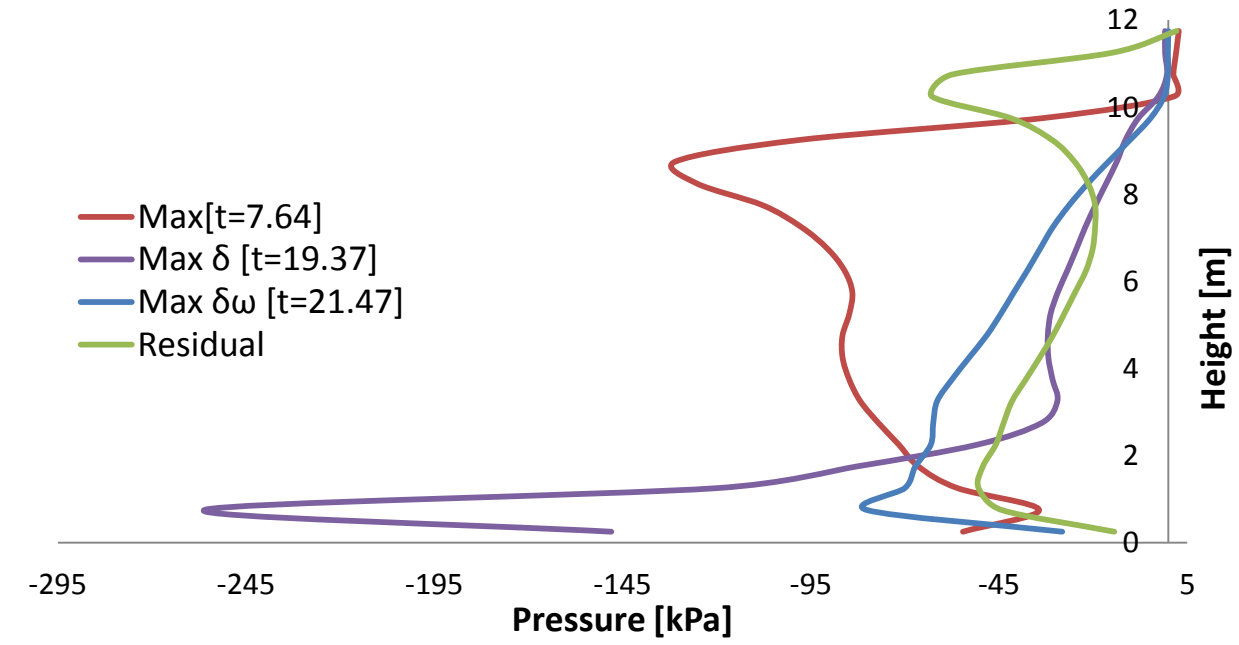

Fig. 2.94 . Earth pressures profiles on the right wall at different moments when subjected to Lefkada Seismic excitation with peak ground acceleration 0.9 g.

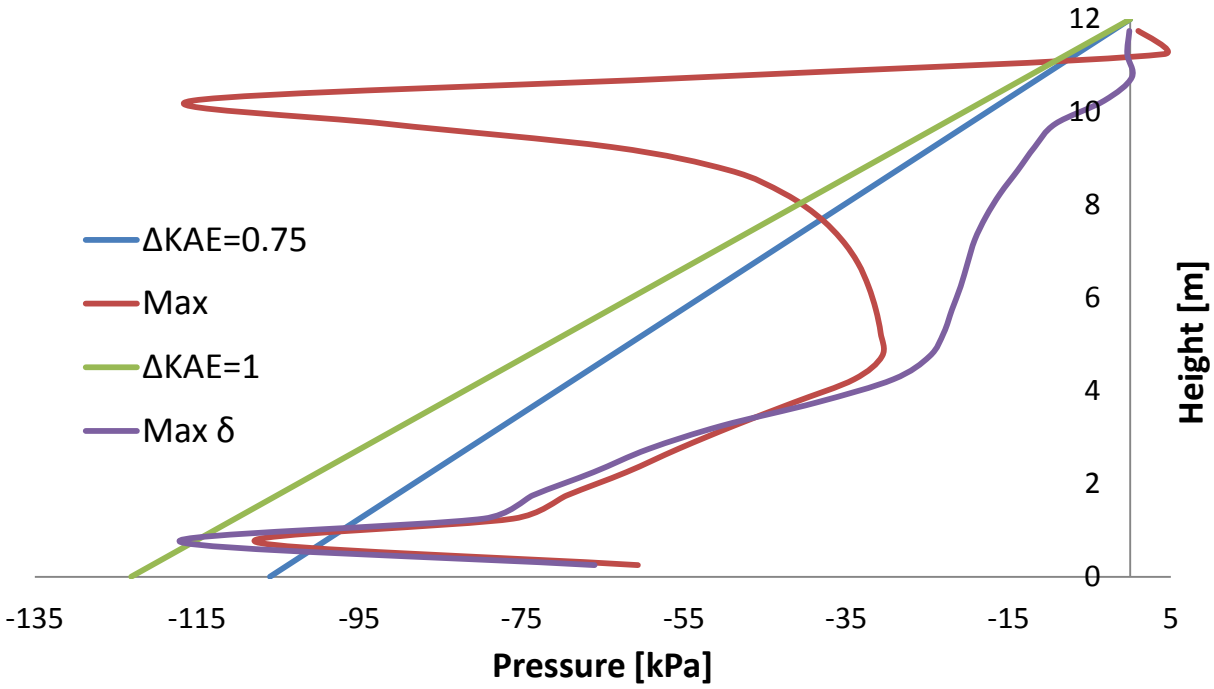

Fig. 2.95. Earth pressure profiles computed in ABAQUS and estimated using the M-O when the right wall is subjected to the Lefkada Seismic excitation with peak acceleration 0.3g.

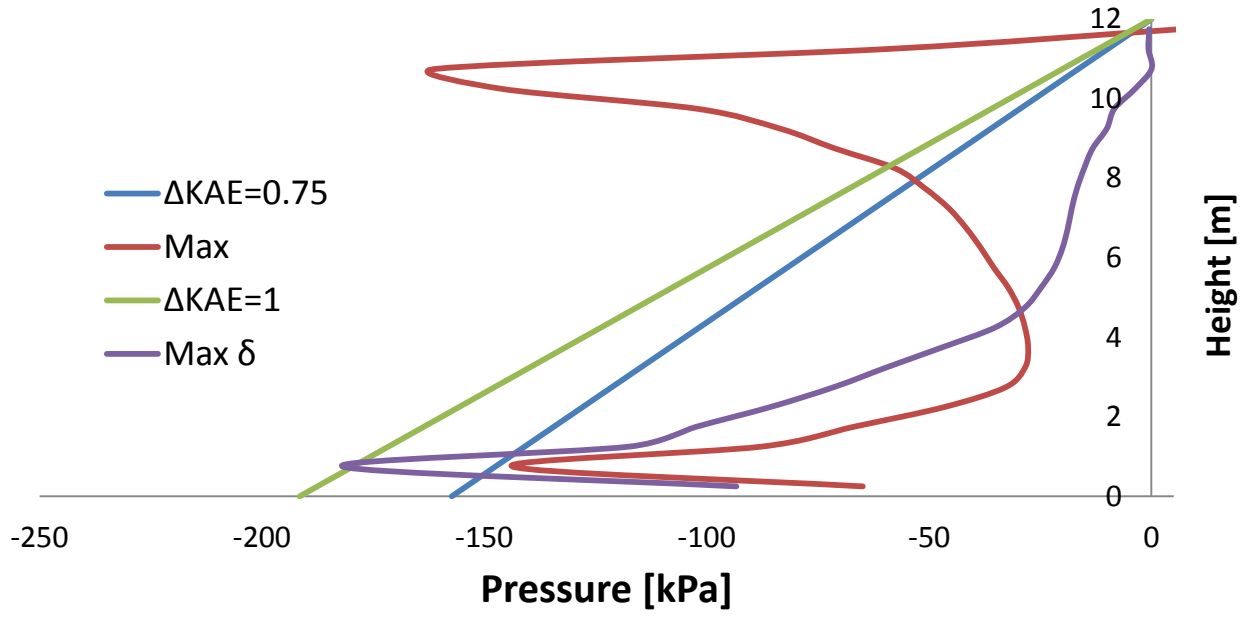

Fig. 2.96. Earth pressure profiles computed in ABAQUS and estimated using the M-O when the right wall is subjected to the Lefkada Seismic excitation with peak acceleration 0.6g.

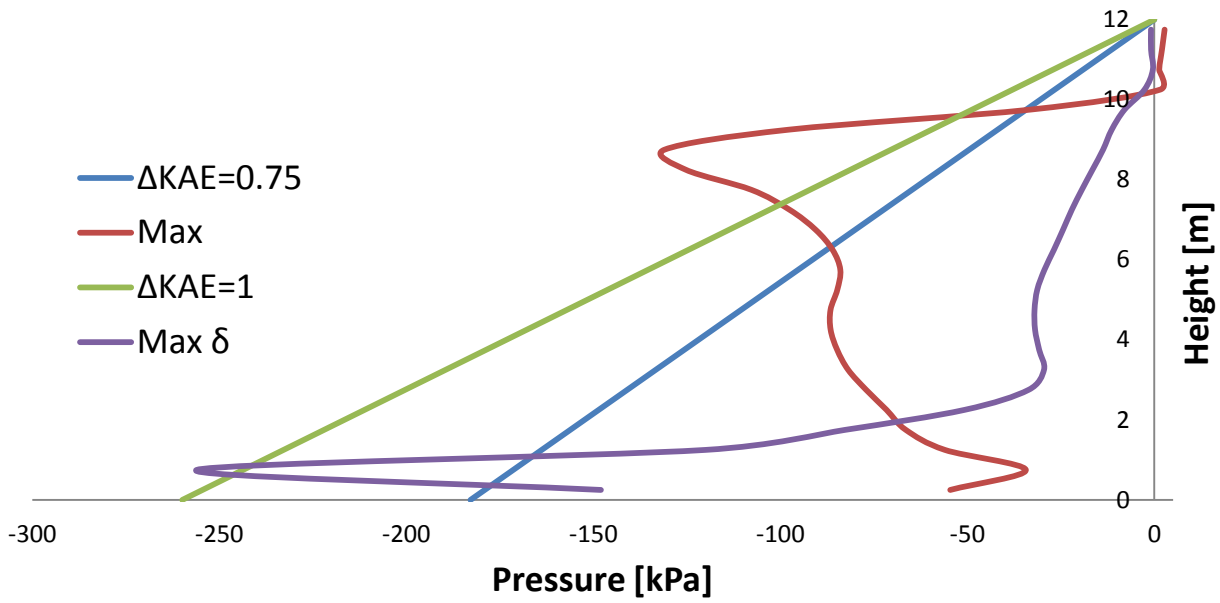

Fig. 2.97. Earth pressure profiles computed in ABAQUS and estimated using the M-O when the right wall is subjected to the Lefkada Seismic excitation with peak acceleration 0.9g.

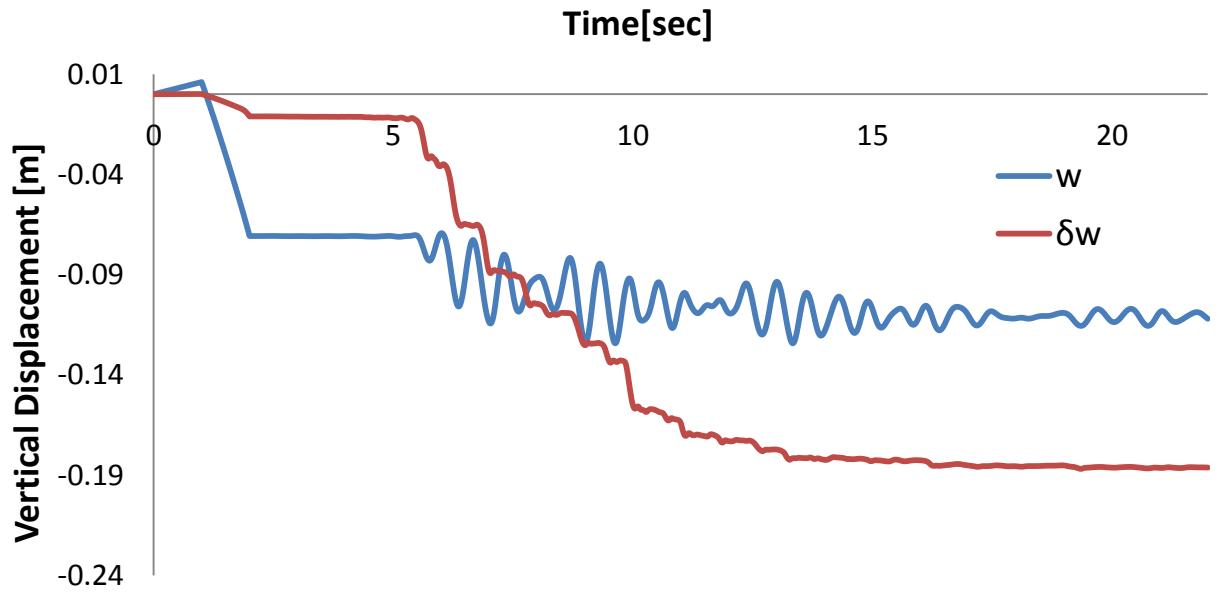

Fig. 2.98. Vertical displacement-time history of the right wall when subjected to Lefkada Seismic excitation with peak acceleration 0.3g.

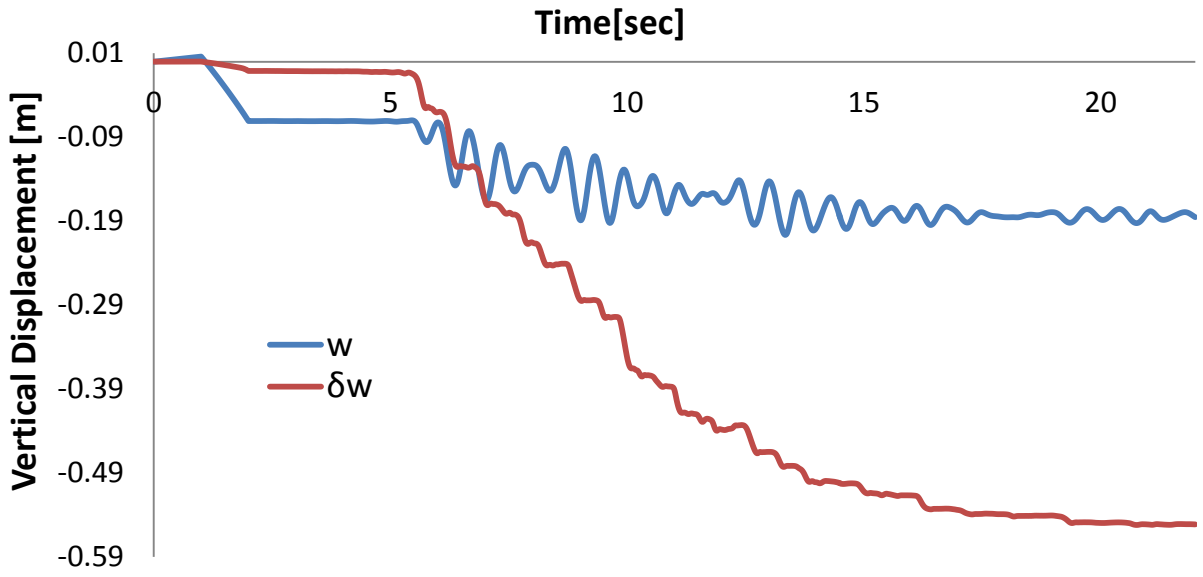

Fig. 2.99. Vertical displacement-time history of the right wall when subjected to Lefkada Seismic excitation with peak acceleration 0.6g.

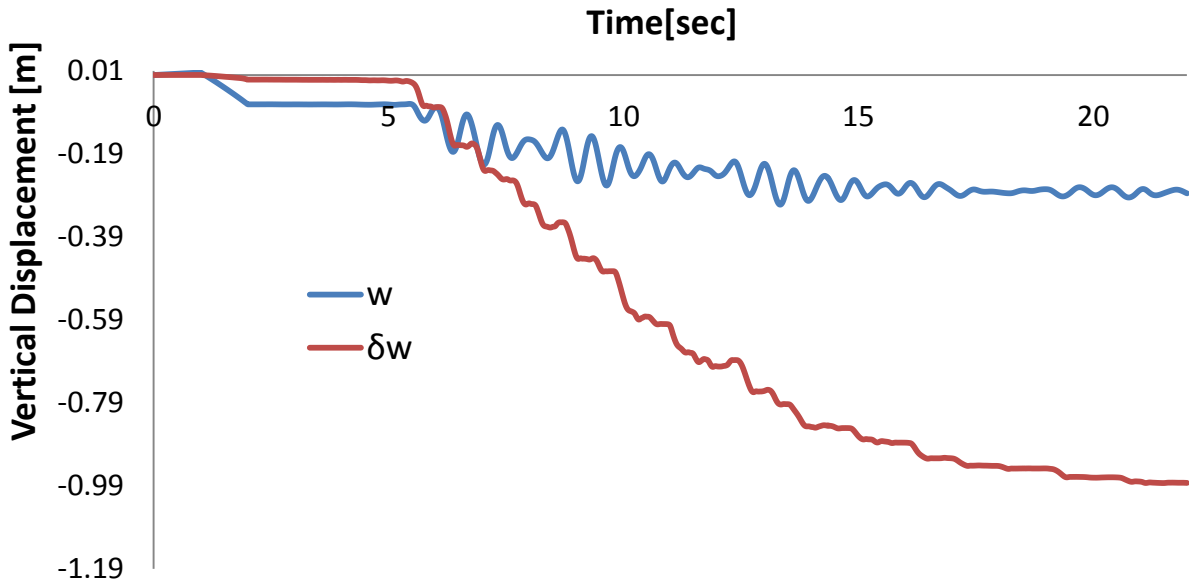

Fig. 2.100. Vertical displacement-time history of the right wall when subjected to Lefkada Seismic excitation with peak acceleration 0.9g.

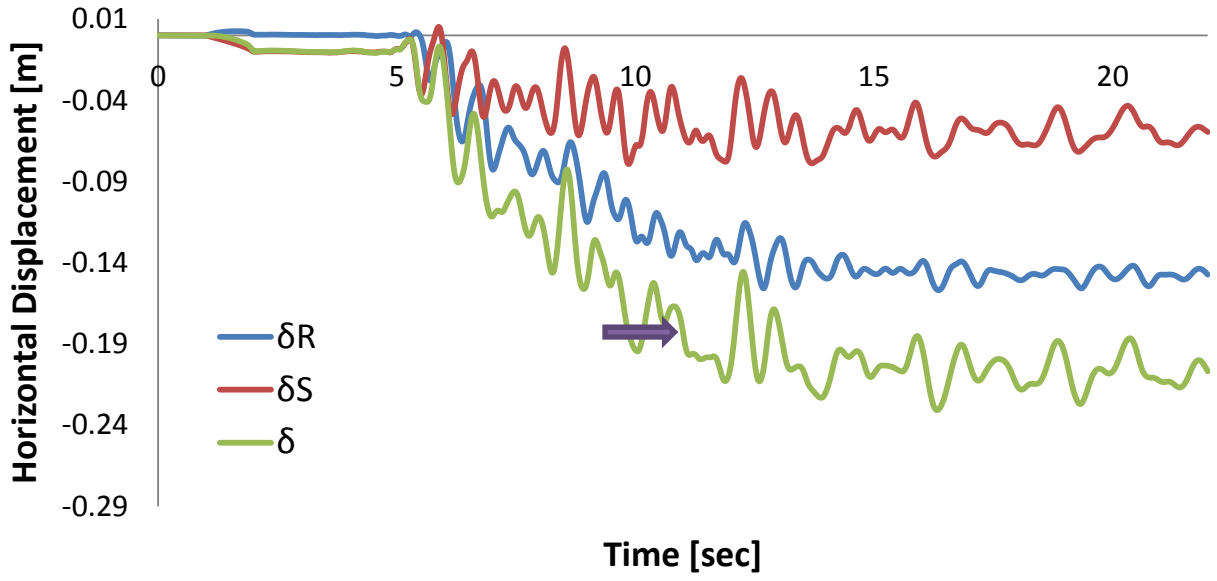

Fig. 2.101. Horizontal displacement-time history of the right wall when subjected to Lefkada Seismic excitation with peak acceleration 0.3g.

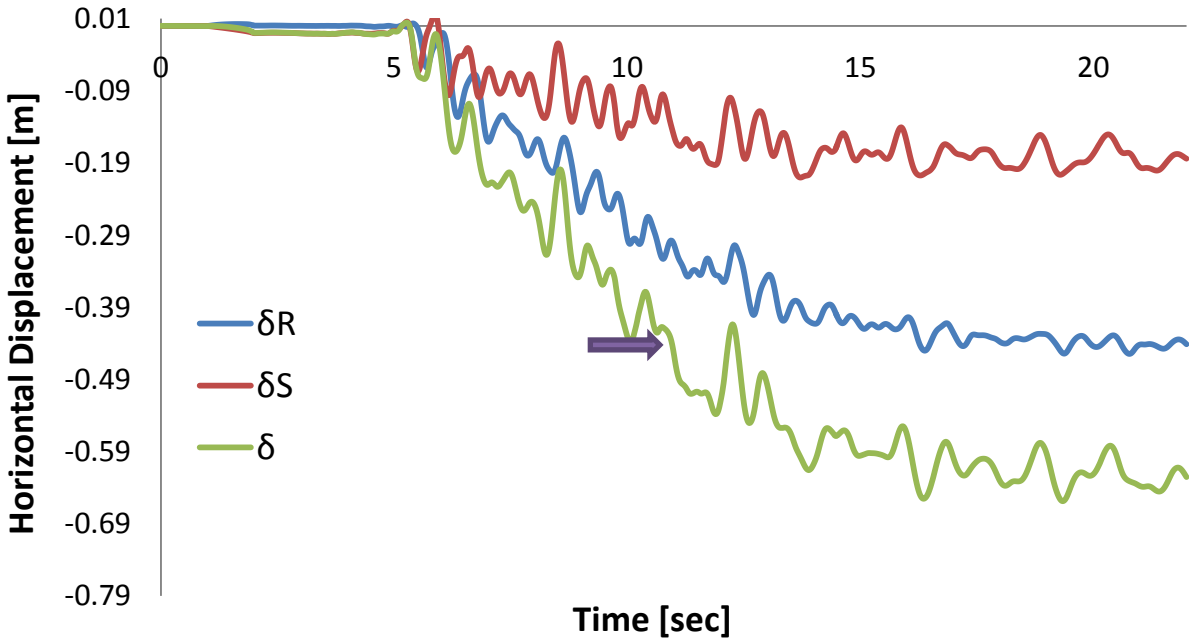

Fig. 2.102. Horizontal displacement-time history of the right wall when subjected to Lefkada Seismic excitation with peak acceleration 0.6g.

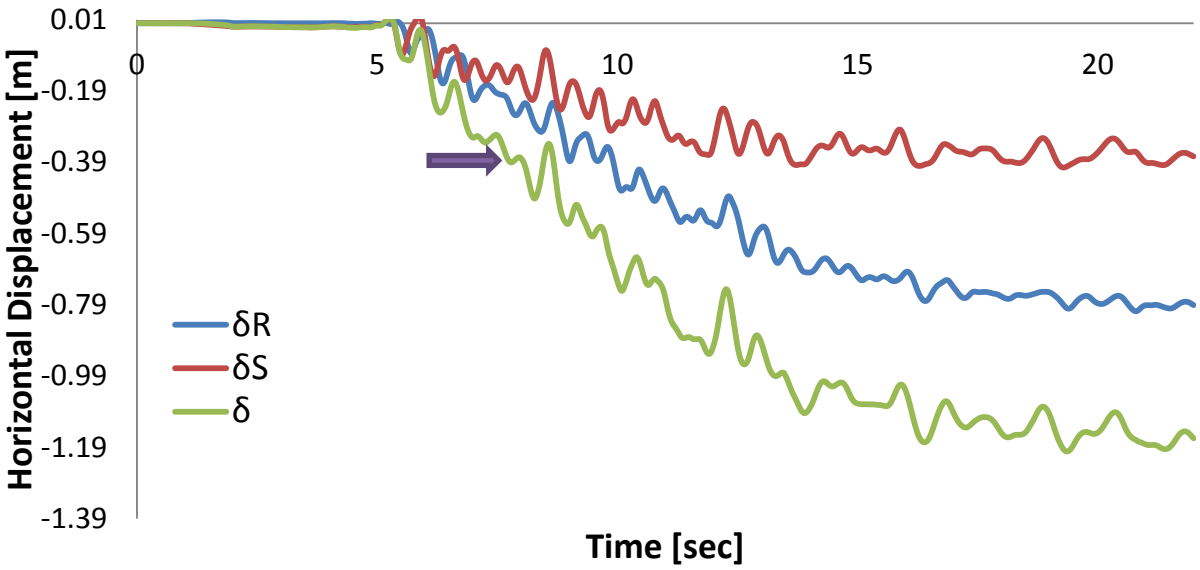

Fig. 2.103. Horizontal displacement-time history of the right wall when subjected to Lefkada Seismic excitation with peak acceleration 0.9g.

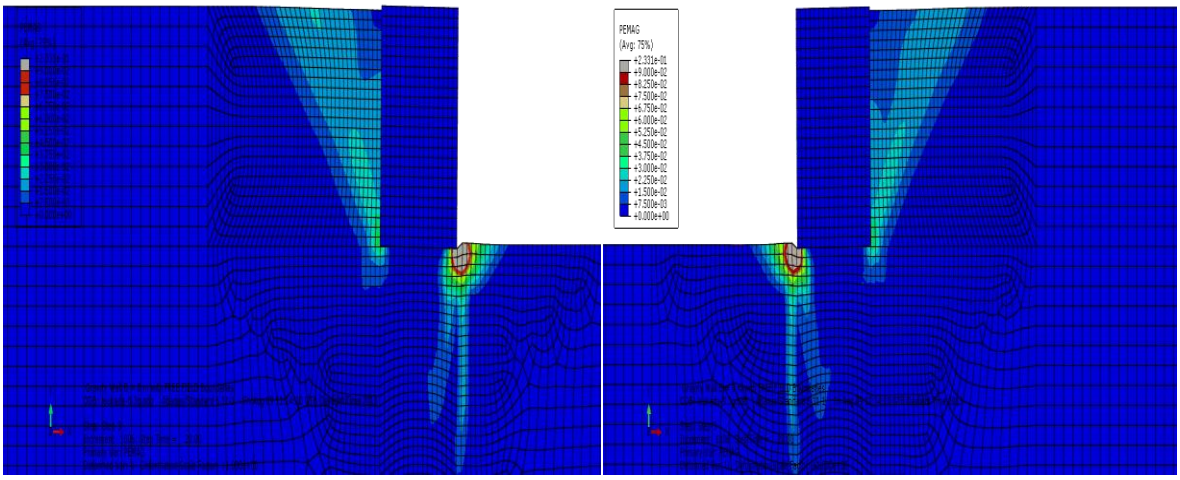

Fig. 2.104. Plastic strain contours at the end of seismic shaking (a)Left wall (b)Right wall when subjected to Lefkada seismic excitation with peak acceleration 0.3g

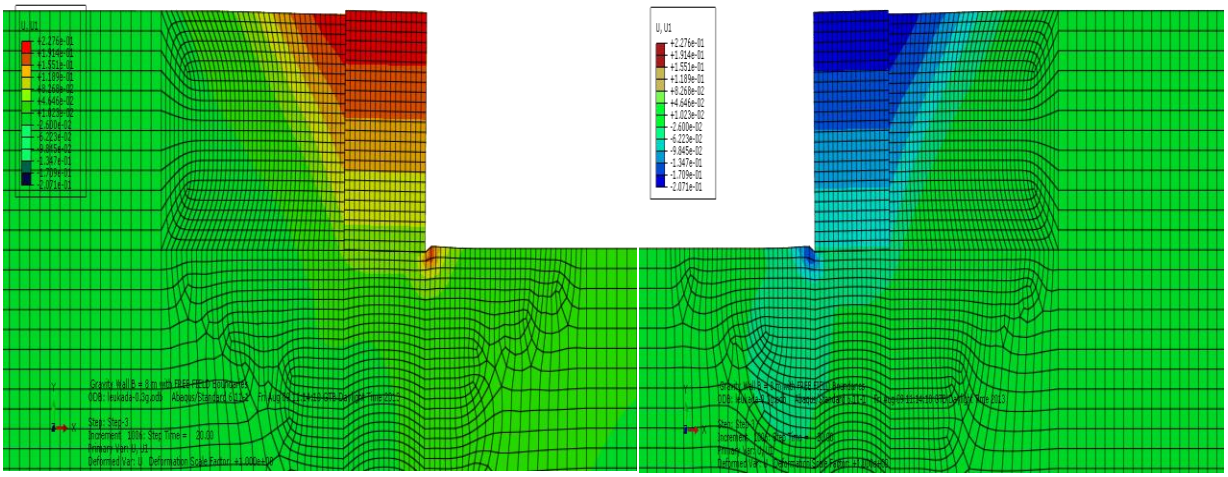

Fig. 2.105. Horizontal displacement contours at the end of the seismic excitation Lefkada PGA 0.3g.

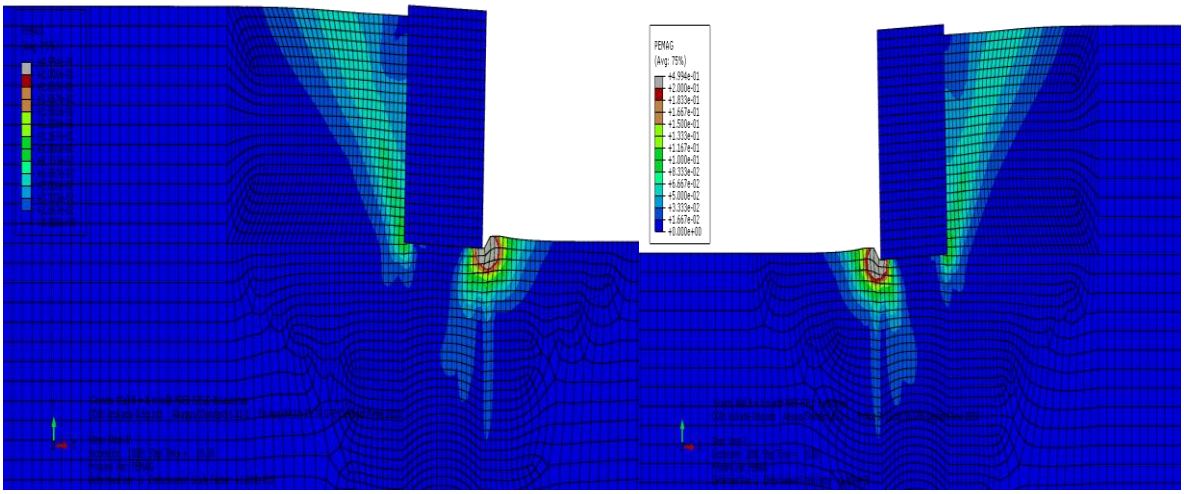

Fig. 2.106. Plastic strain contours at the end of seismic shaking (a)Left wall (b)Right wall when subjected to Lefkada seismic excitation with peak acceleration 0.6g

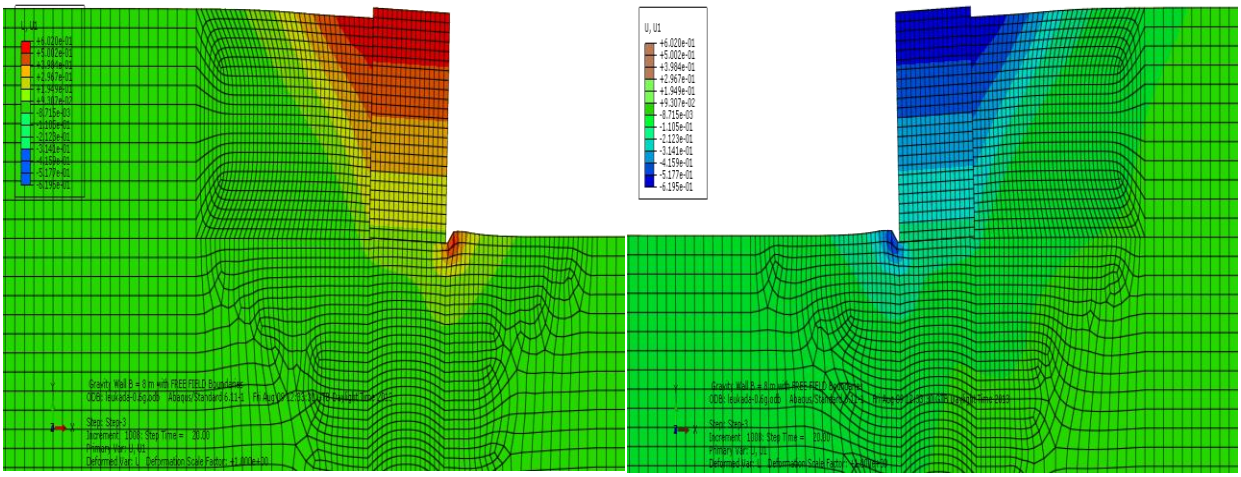

Fig. 2.107. Horizontal displacement contours at the end of the seismic excitation Lefkada PGA 0.6g.

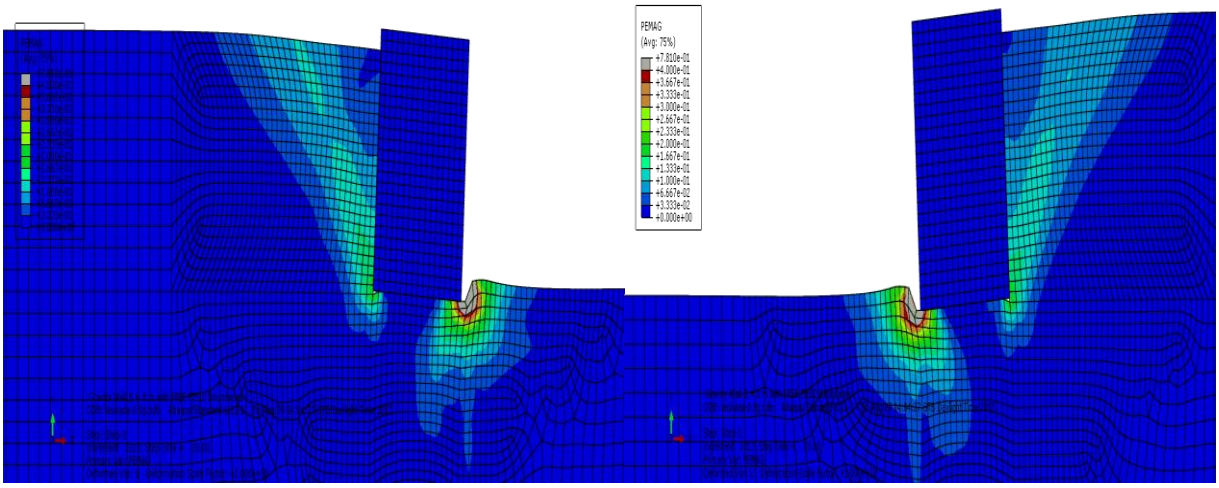

Fig. 2.108. Plastic strain contours at the end of seismic shaking (a)Left wall (b)Right wall when subjected to Lefkada seismic excitation with peak acceleration 0.9g

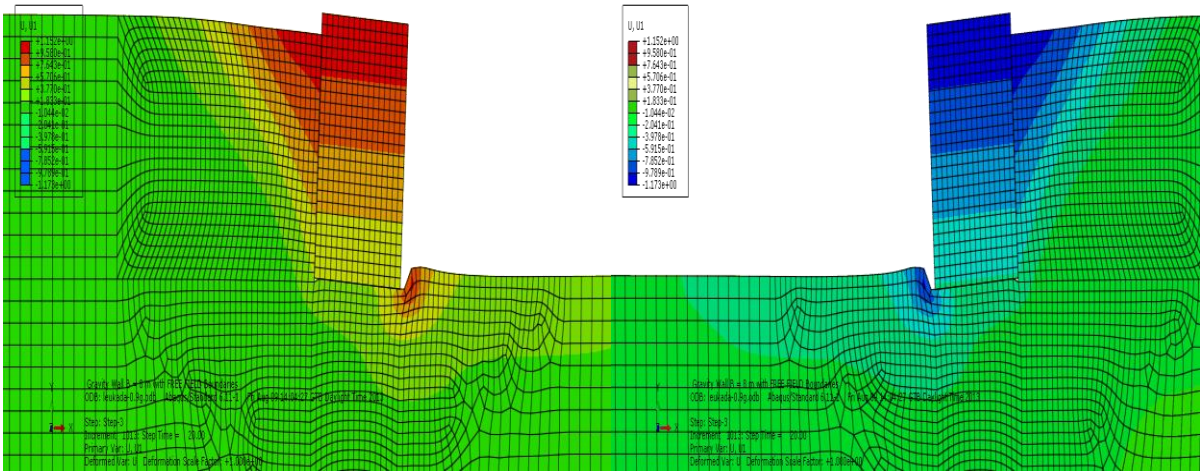

Fig. 2.109. Horizontal displacement contours at the end of the seismic excitation Lefkada PGA 0.9

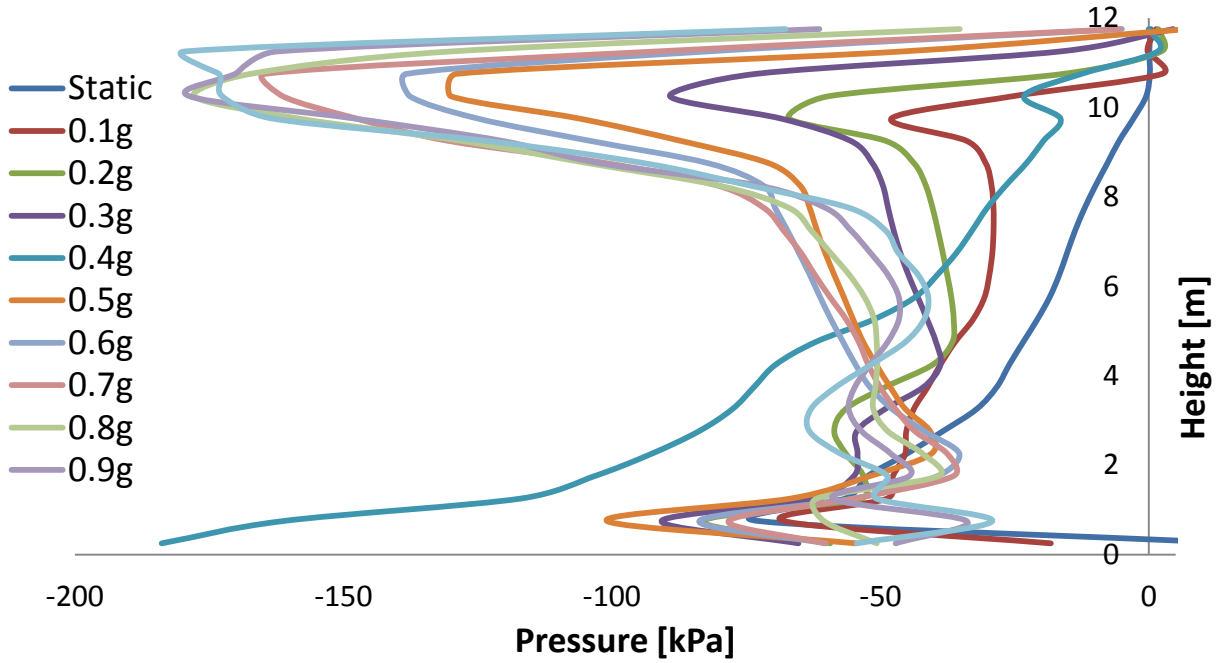

Fig. 2.110. Static and maximum earth pressure profiles for different peak accelerations on the left wall when subjected to Lefkada Seismic excitation.

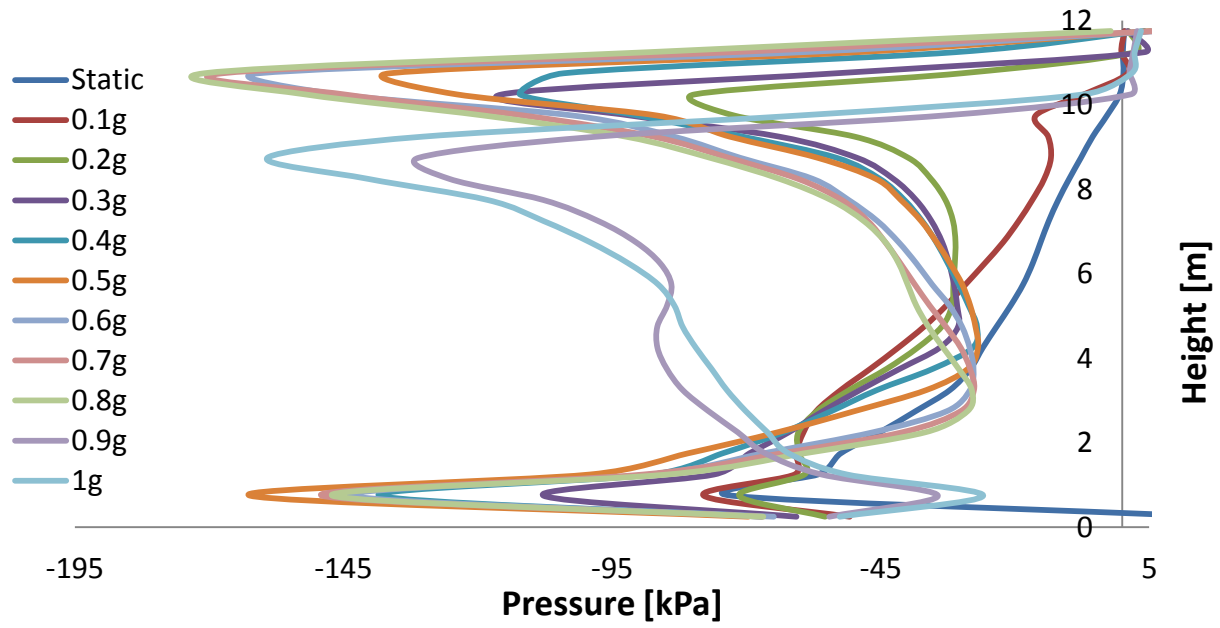

Fig. 2.111. Static and maximum earth pressure profiles for different peak accelerations on the right wall when subjected to Lefkada Seismic excitation.

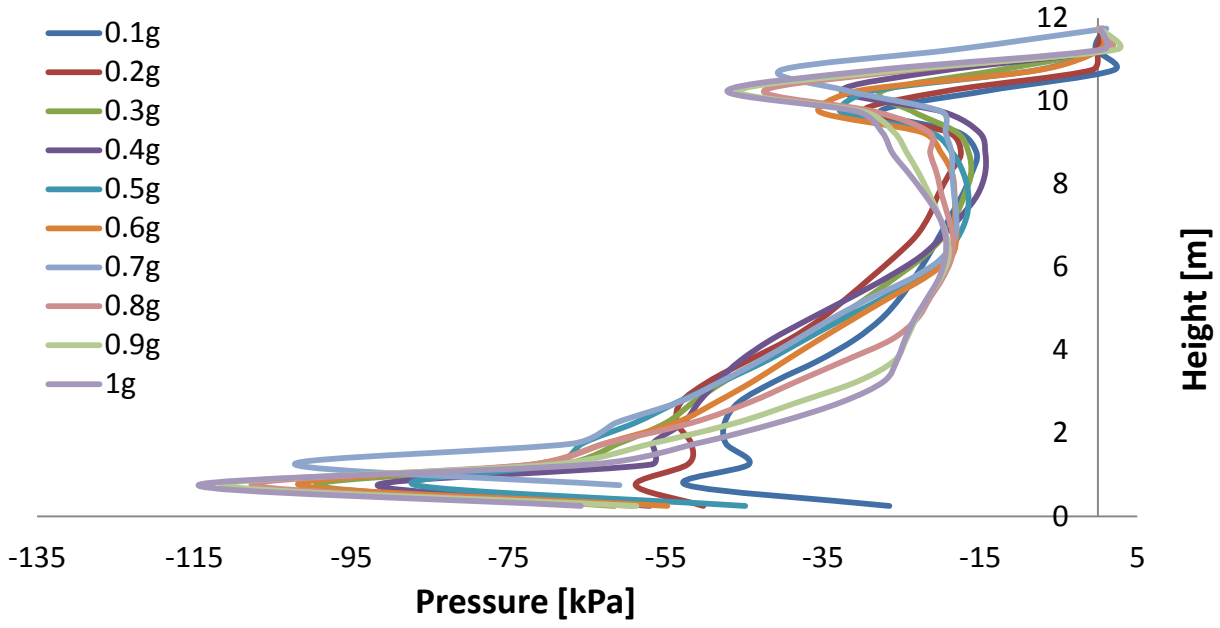

Fig. 2.112. Residual earth pressure profiles for different peak accelerations on the left wall when subjected to Lefkada Seismic excitation.

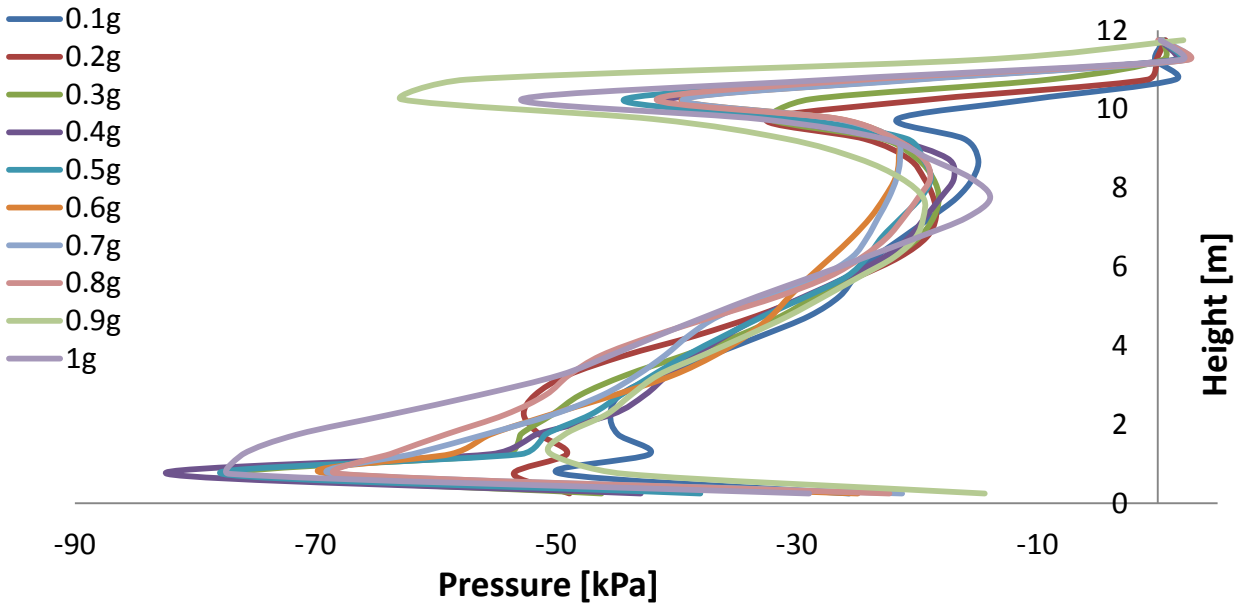

Fig. 2.113. Residual earth pressure profiles for different peak accelerations on the right wall when subjected to Lefkada Seismic excitation.

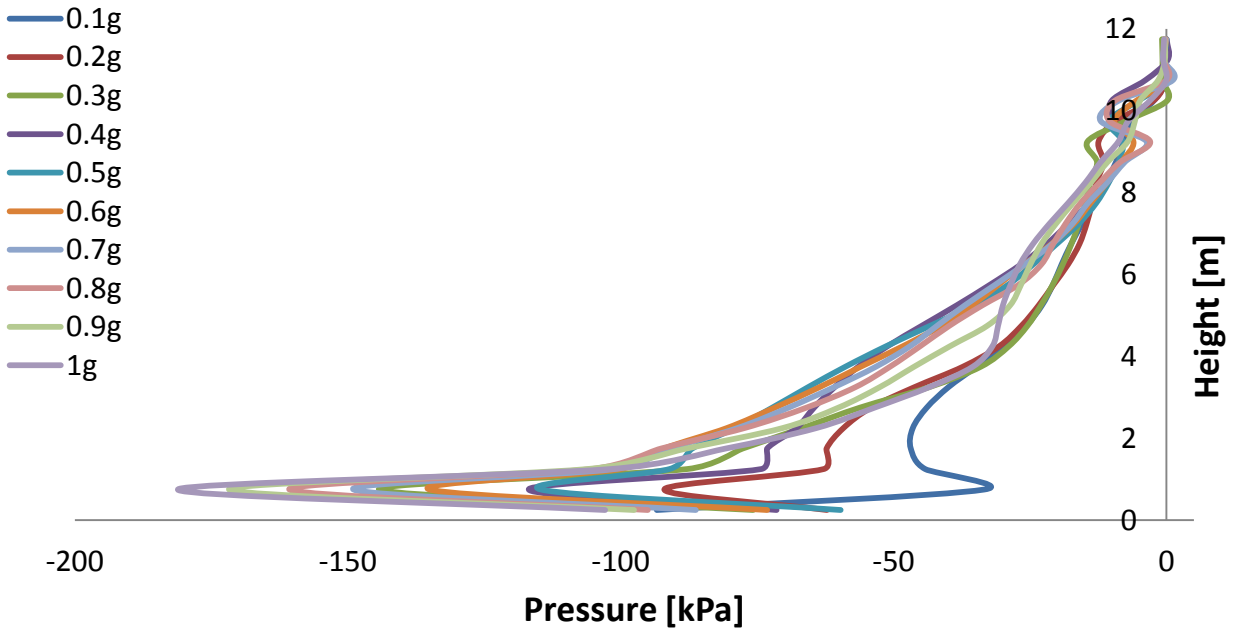

Fig. 2.114. Earth pressure profiles at maximum displacement for different peak accelerations on the left wall when subjected to Lefkada Seismic excitation.

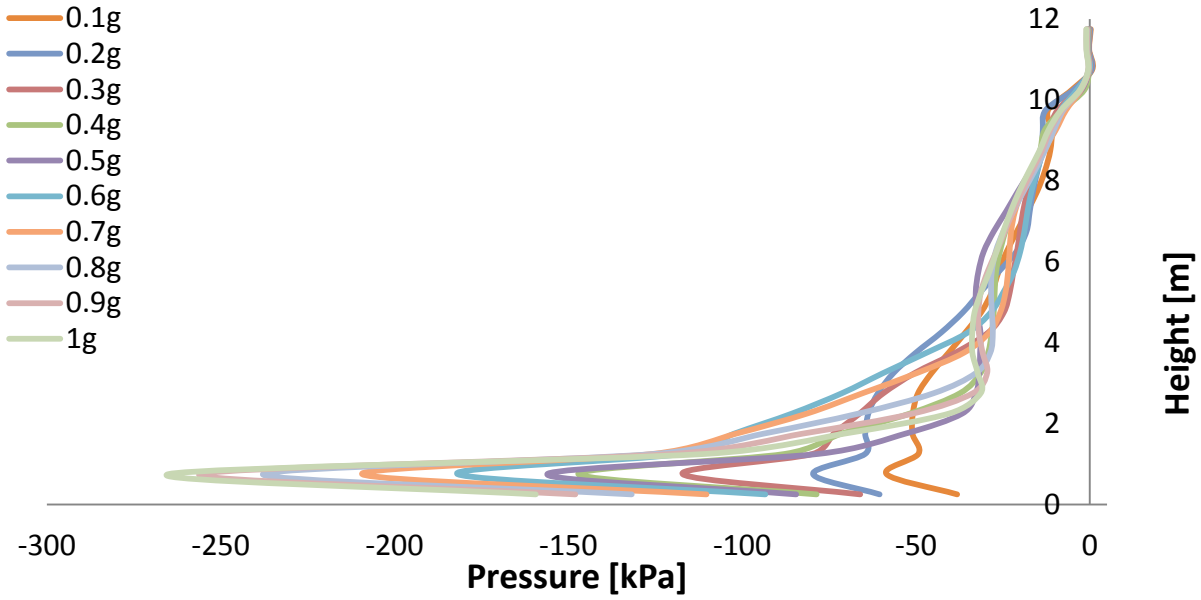

Fig. 2.115. Earth pressure profiles at maximum displacement for different peak accelerations on the right wall when subjected to Lefkada Seismic excitation.

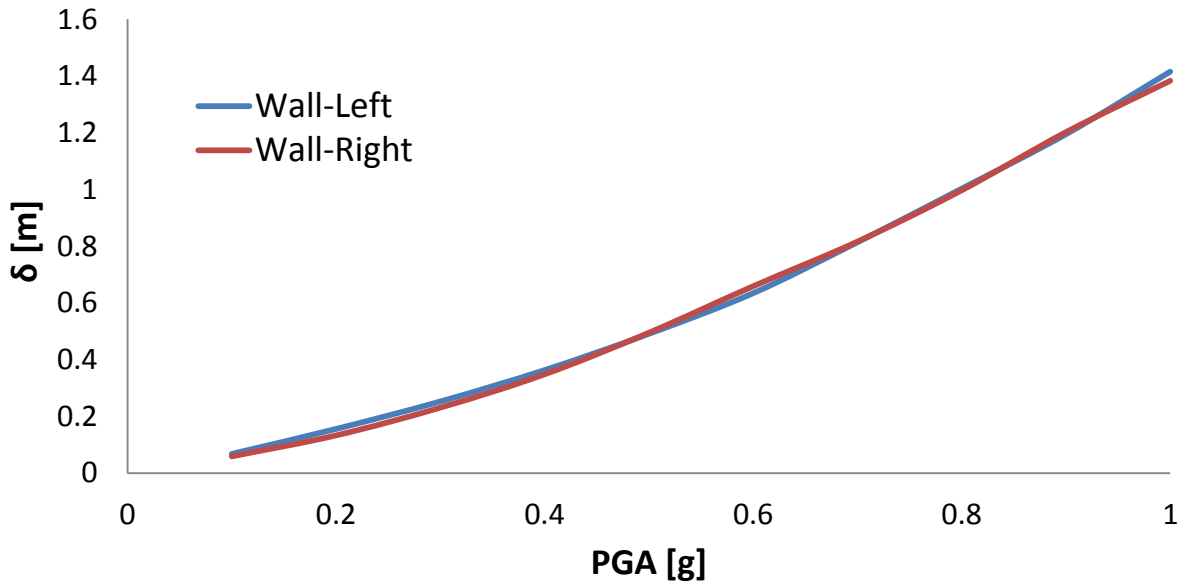

Fig. 2.116. Horizontal displacement as a function of PGA for the left and right wall when subjected to Lefkada Seismic excitation.

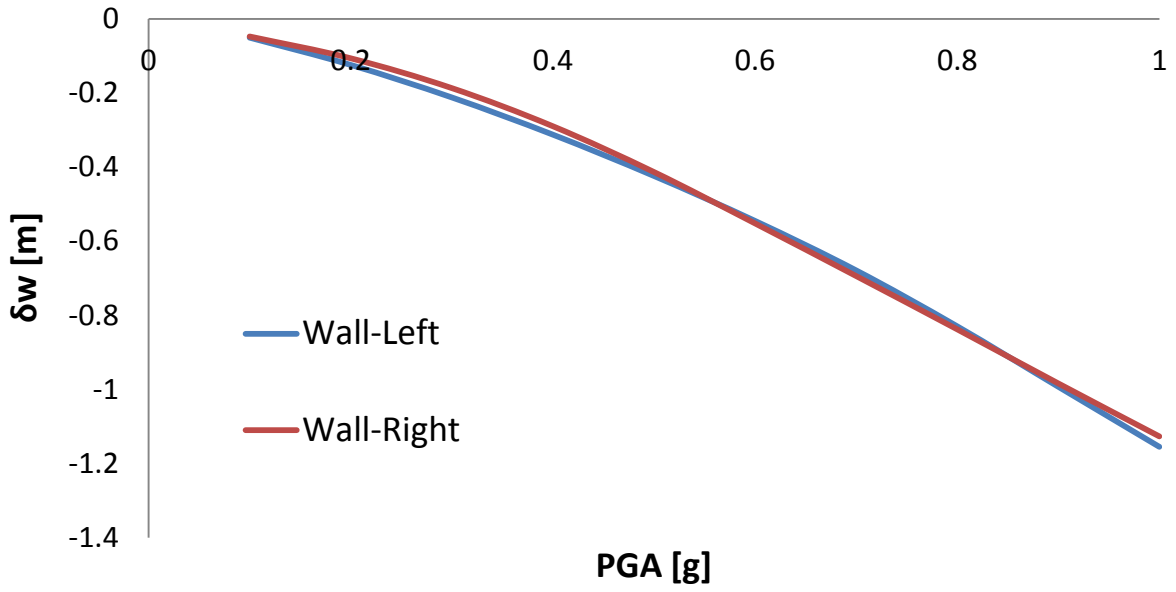

Fig. 2.117. Differential settlement as a function of PGA for the left and right wall when subjected to Lefkada Seismic excitation.

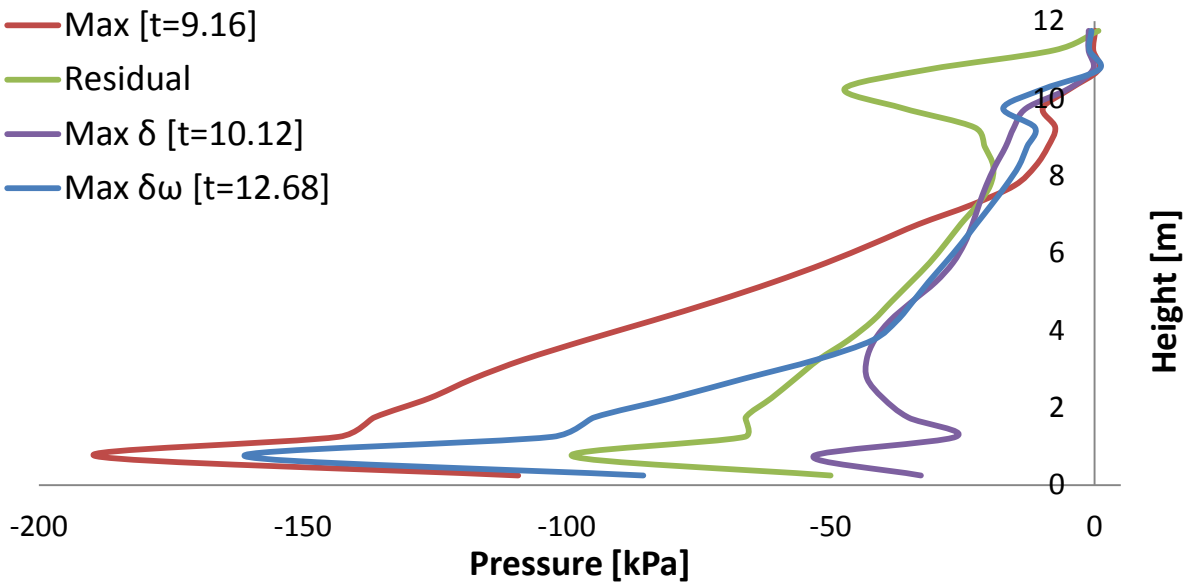

Fig. 2.118. Earth pressures profiles on the left wall at different moments when subjected to Takatori Seismic excitation with peak ground acceleration 0.3 g.

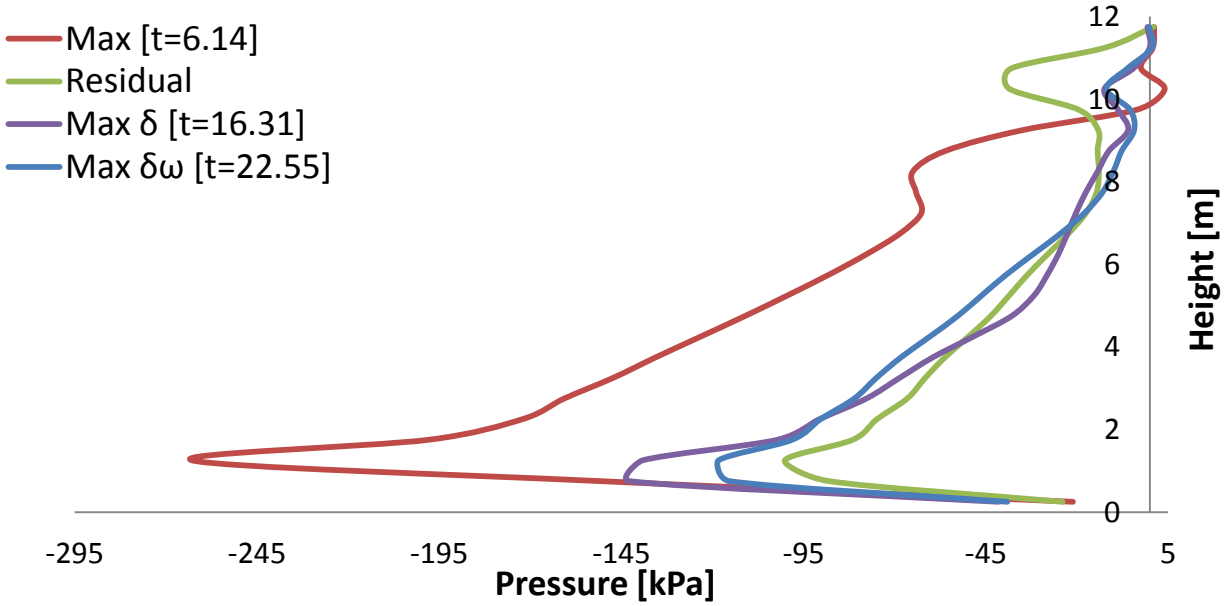

Fig. 2.119. Earth pressures profiles on the left wall at different moments when subjected to Takatori Seismic excitation with peak ground acceleration 0.6 g.

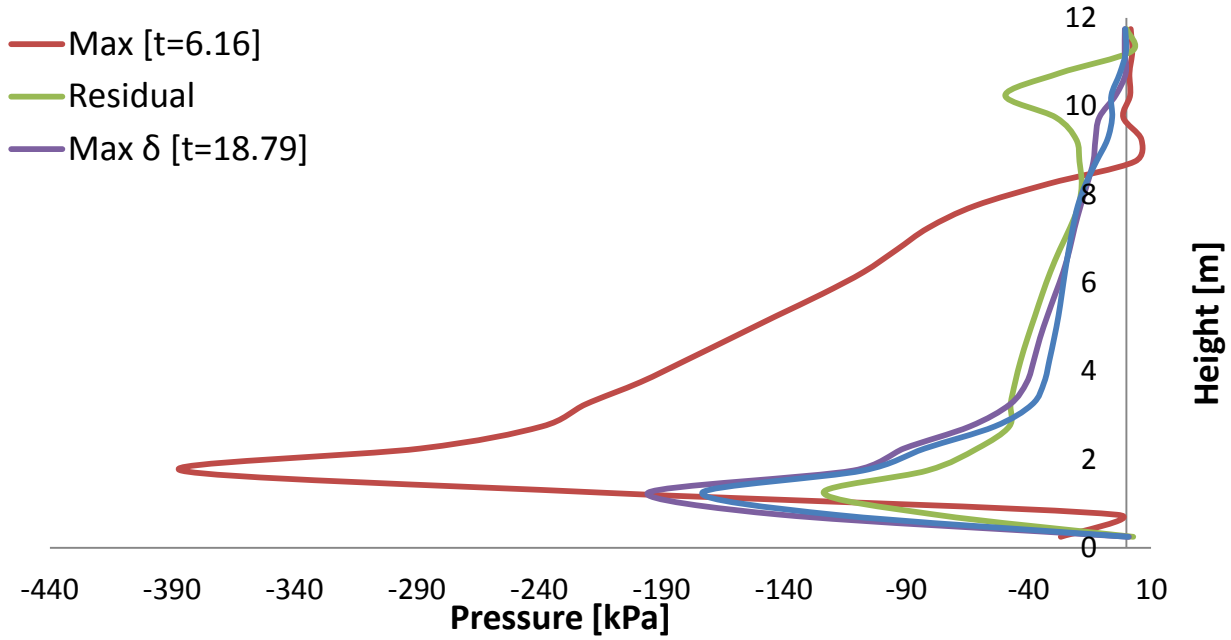

Fig. 2.120. Earth pressures profiles on the left wall at different moments when subjected to Takatori Seismic excitation with peak ground acceleration 0.9 g.

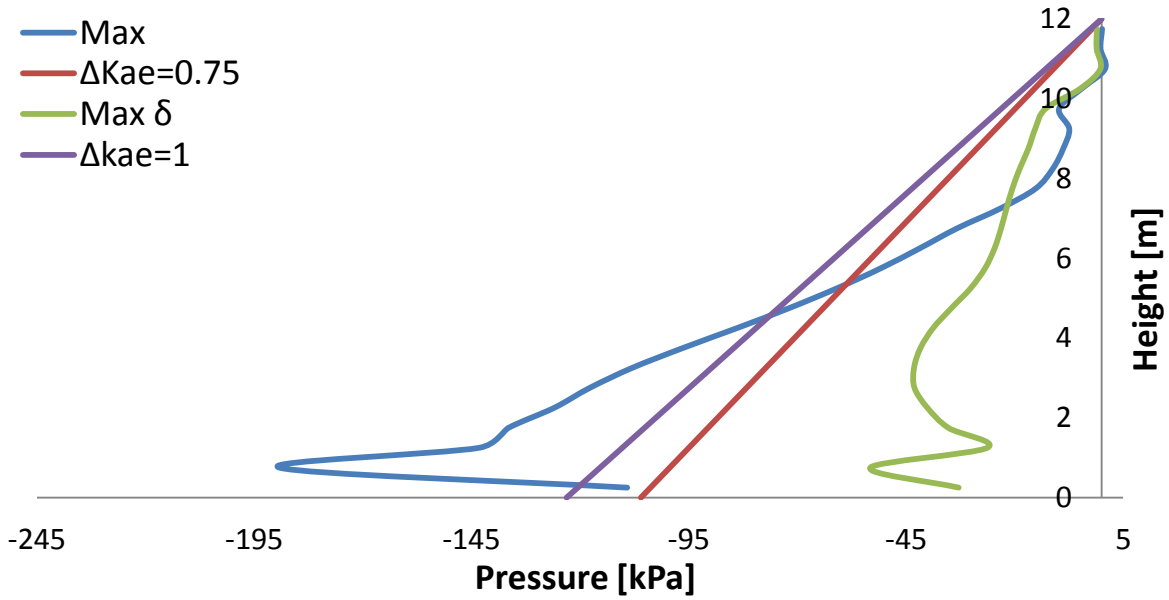

Fig. 2.121. Earth pressure profiles computed in ABAQUS and estimated using the M-O when the left wall is subjected to the Takatori Seismic excitation with peak acceleration 0.3g.

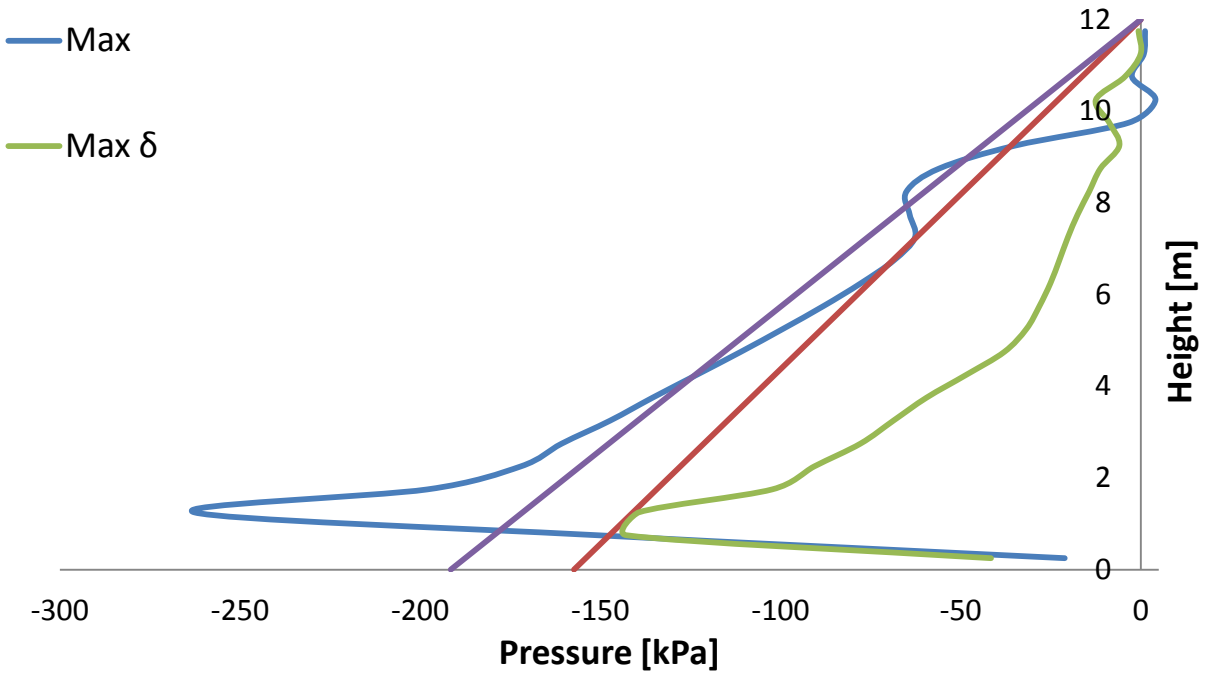

Fig. 2.122. Earth pressure profiles computed in ABAQUS and estimated using the M-O when the left wall is subjected to the Takatori Seismic excitation with peak acceleration 0.6g.

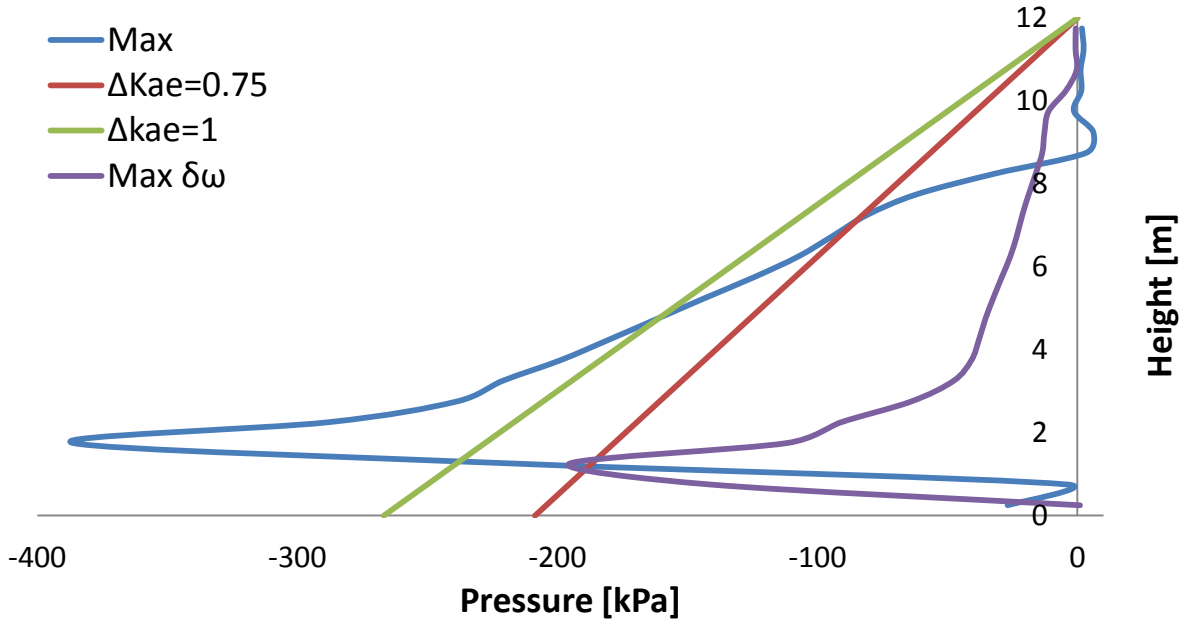

Fig. 2.123. Earth pressure profiles computed in ABAQUS and estimated using the M-O when the left wall is subjected to the Takatori Seismic excitation with peak acceleration 0.9.

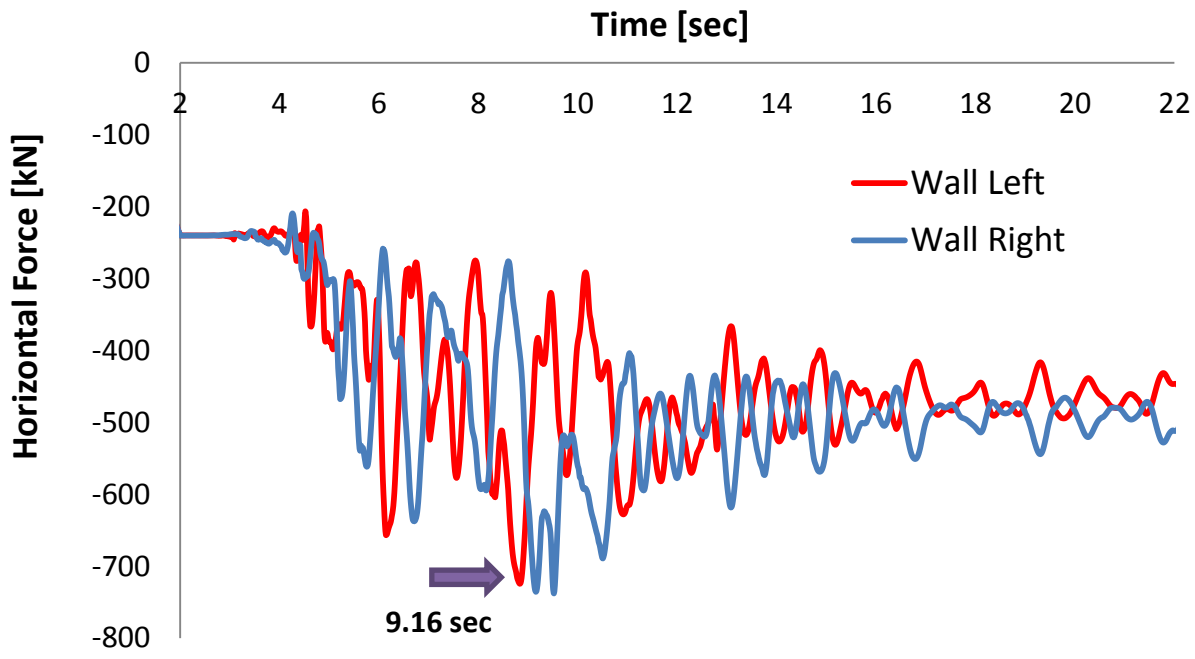

Fig. 2.124. Horizontal force-time history of the left and right wall when subjected to Takatori Seismic excitation with peak ground acceleration 0.3g.

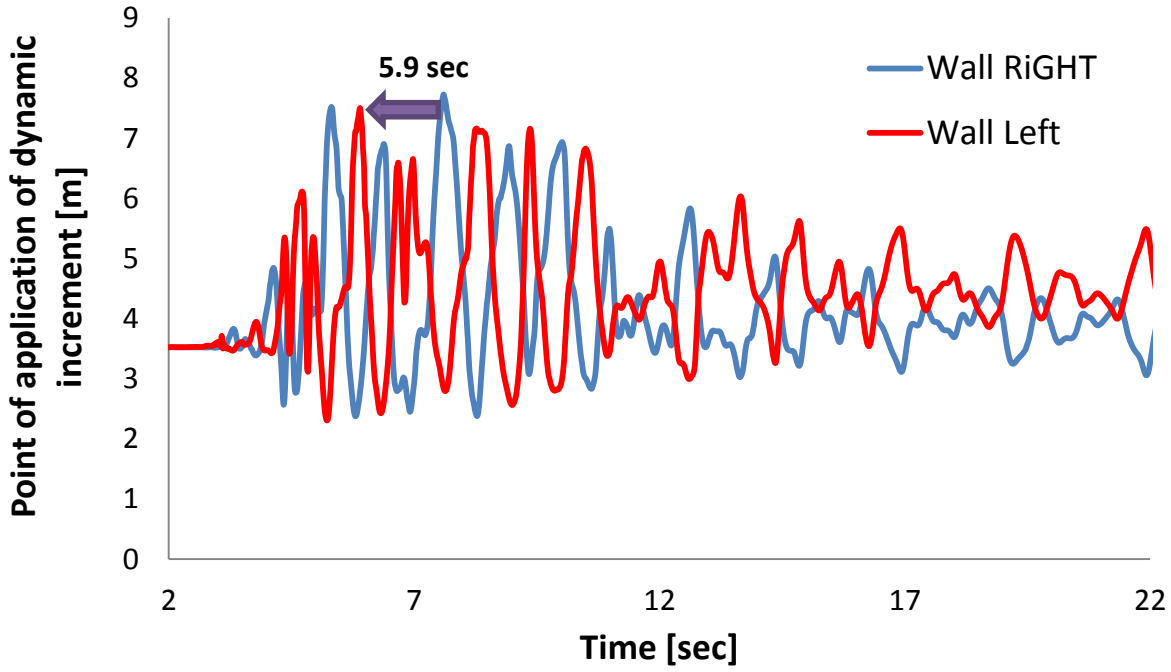

Fig. 2.125. Point of application of dynamic increment on the left wall when subjected to Lefkada Seismic excitation with peak ground acceleration 0.3g.

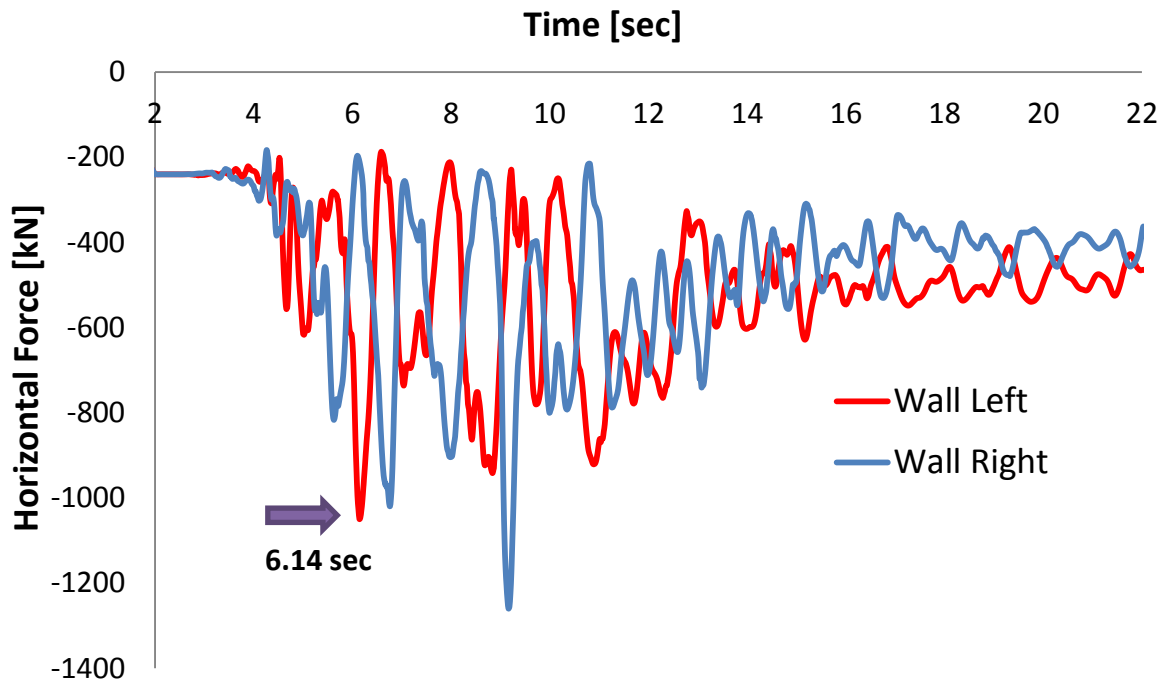

Fig. 2.126. Horizontal force-time history of the left and right wall when subjected to Takatori Seismic excitation with peak ground acceleration 0.6g.

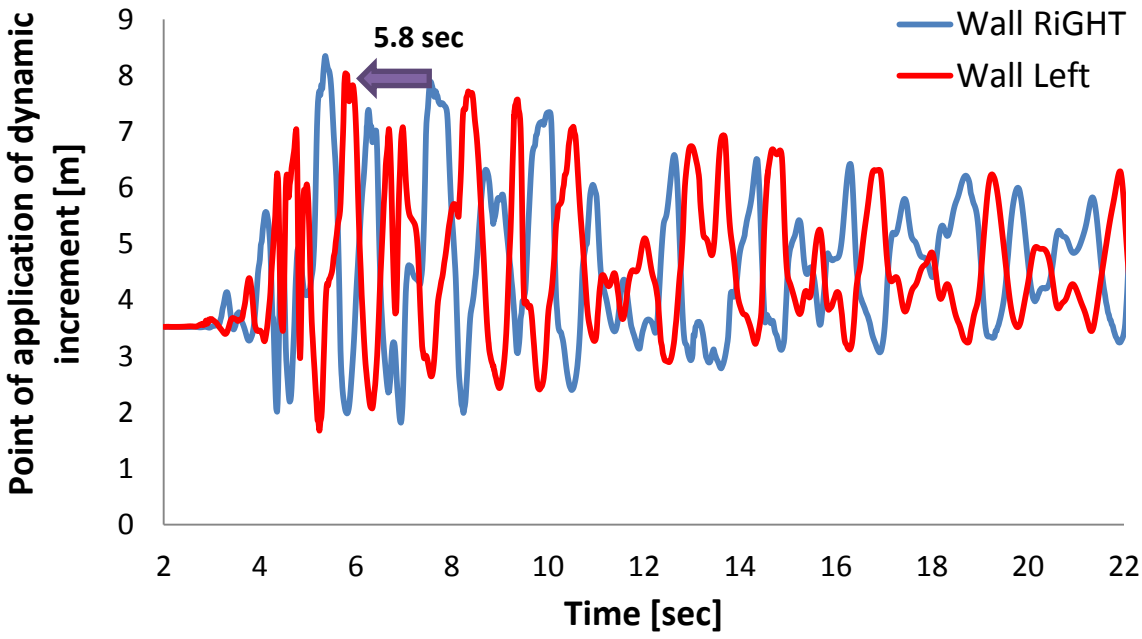

Fig. 2.127. Point of application of dynamic increment on the left wall when subjected to Lefkada Seismic excitation with peak ground acceleration 0.6g.

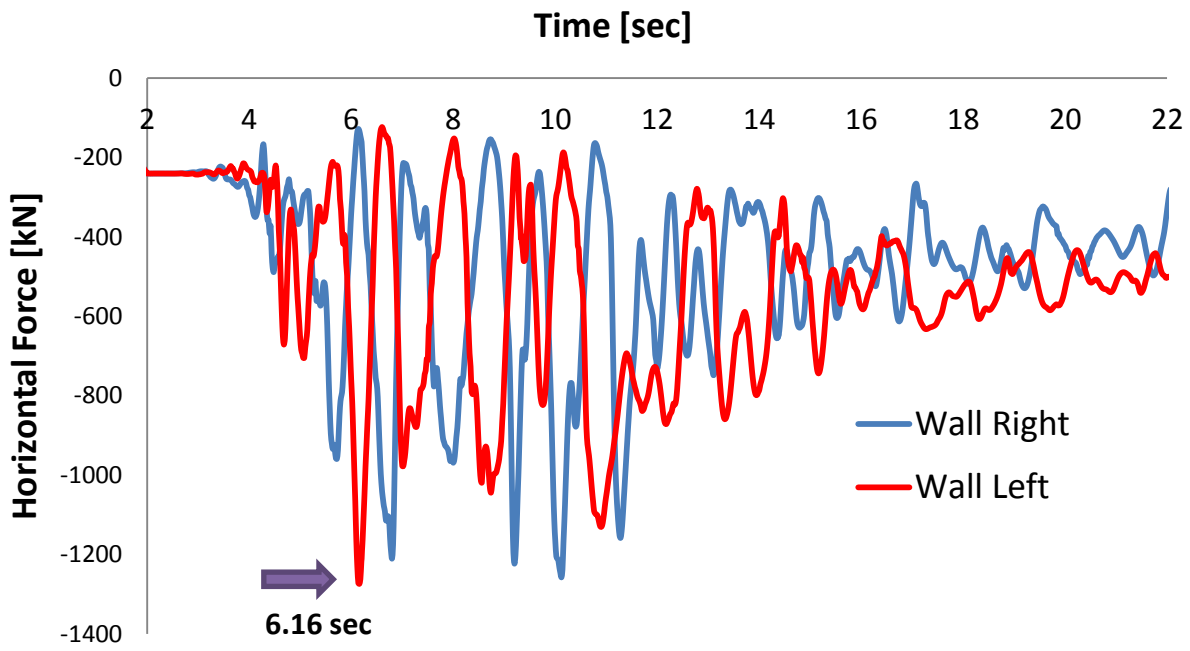

Fig. 2.128. Horizontal force-time history of the left and right wall when subjected to Takatori Seismic excitation with peak ground acceleration 0.9g.

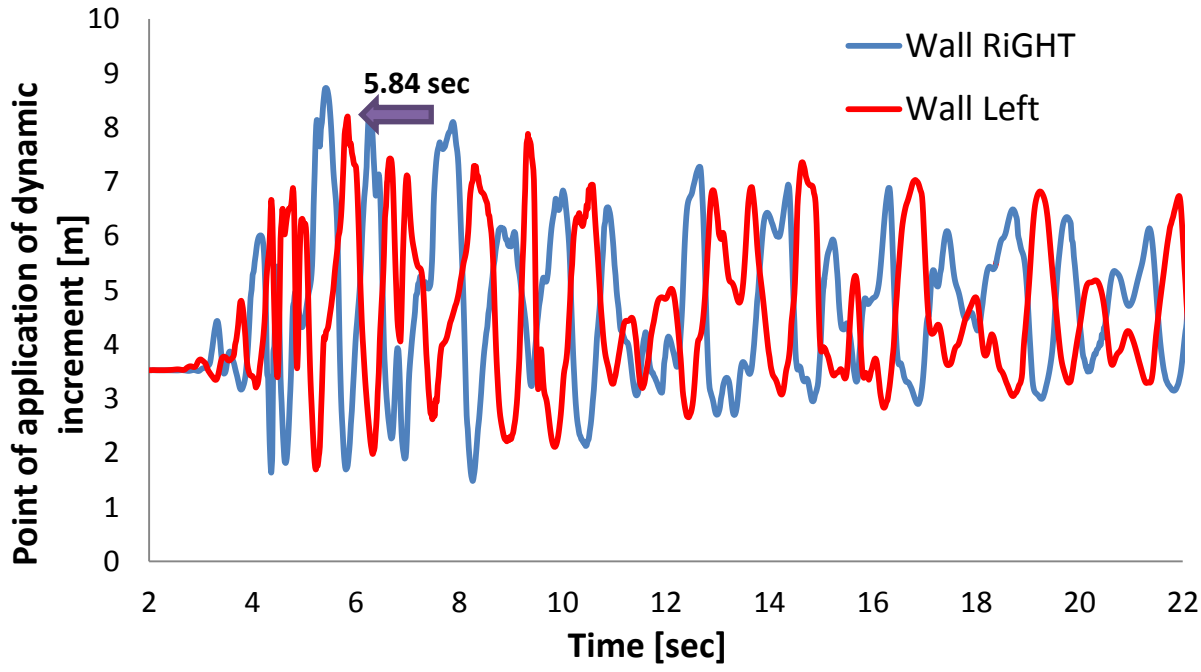

Fig. 2.129. Point of application of dynamic increment on the left wall when subjected to Lefkada Seismic excitation with peak ground acceleration 0.9g.

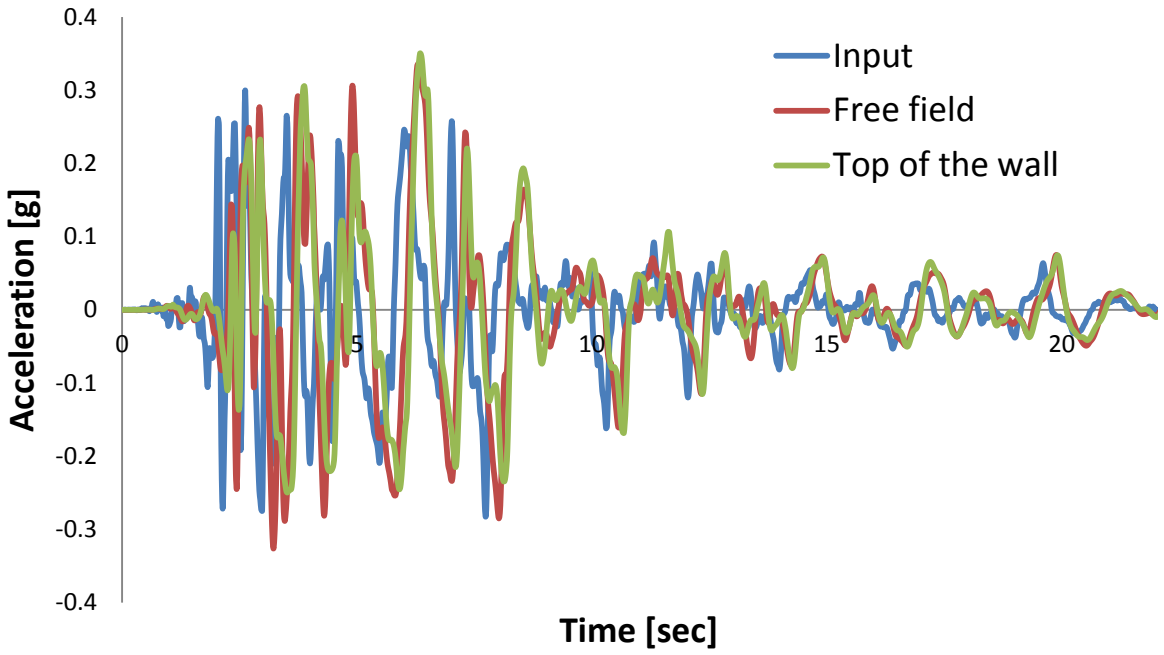

Fig. 2.130. Comparison of input acceleration and computed at the top of the left wall and top of the free field when subjected to Takatori Seismic excitation with peak acceleration 0.3g.

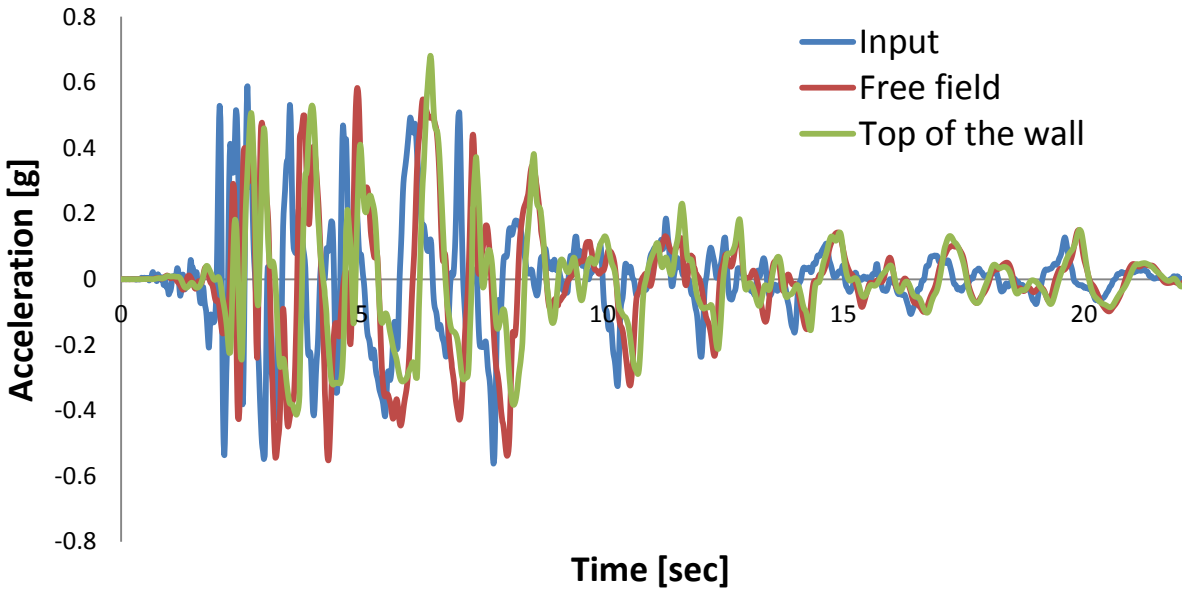

Fig. 2.131. Comparison of input acceleration and computed at the top of the left wall and top of the free field when subjected to Takatori Seismic excitation with peak acceleration 0.6g.

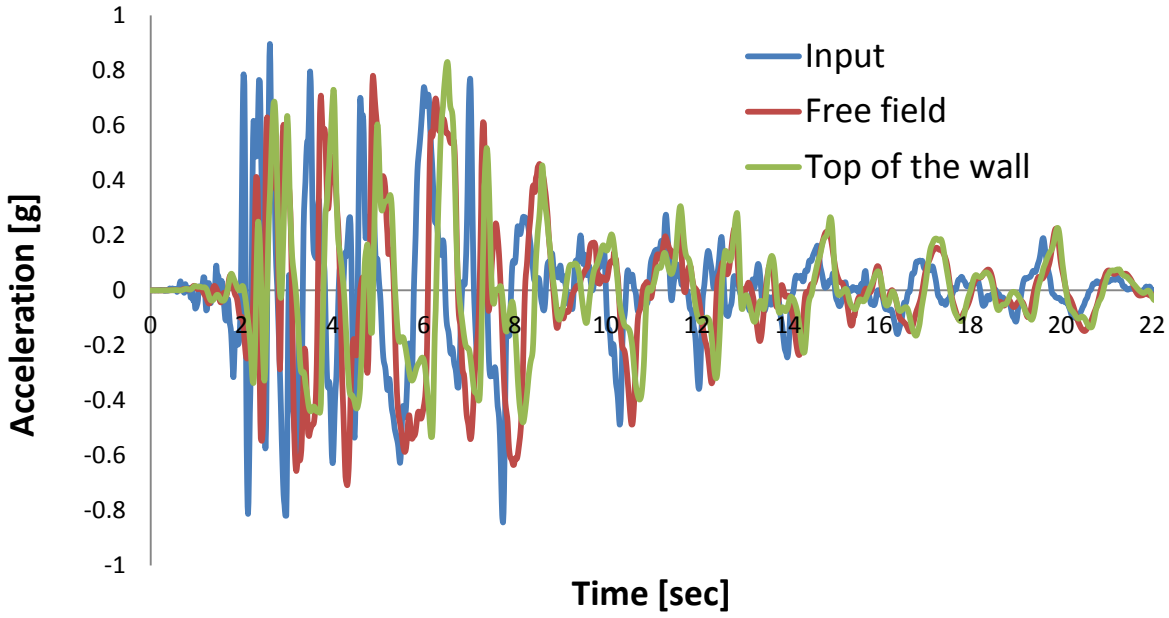

Fig. 2.132. Comparison of input acceleration and computed at the top of the left wall and top of the free field when subjected to Takatori Seismic excitation with peak acceleration 0.9g.

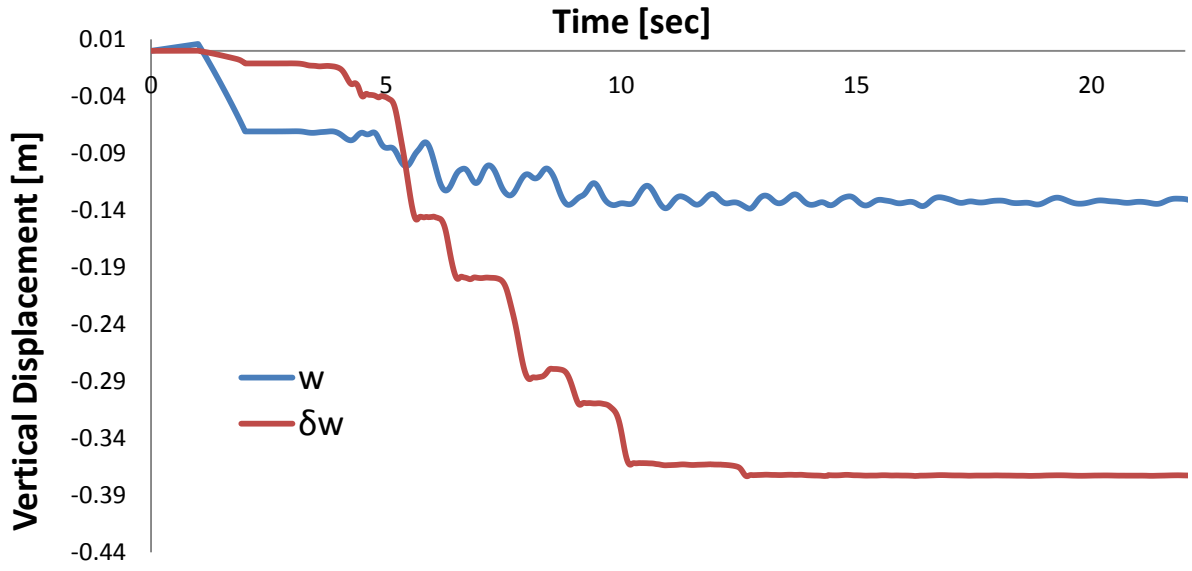

Fig. 2.133. Vertical displacement-time history of the left wall when subjected to Takatori Seismicexcitation with peak acceleration 0.3g.

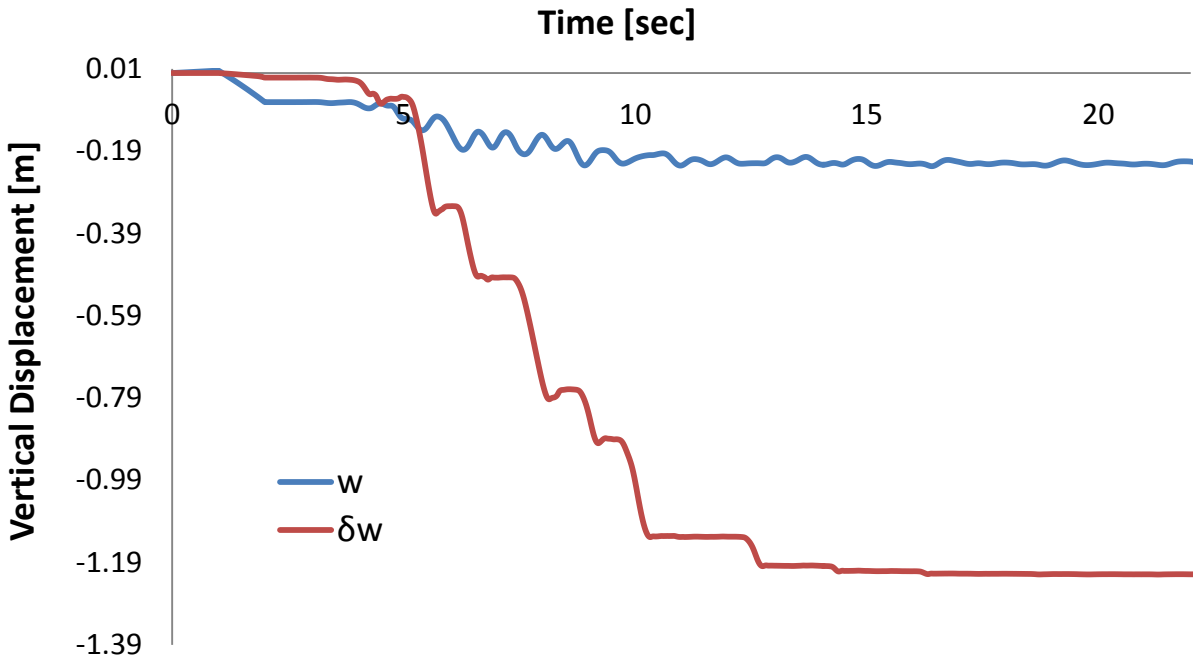

Fig. 2.134. Vertical displacement-time history of the left wall when subjected to Takatori Seismic excitation with peak acceleration 0.6 g.

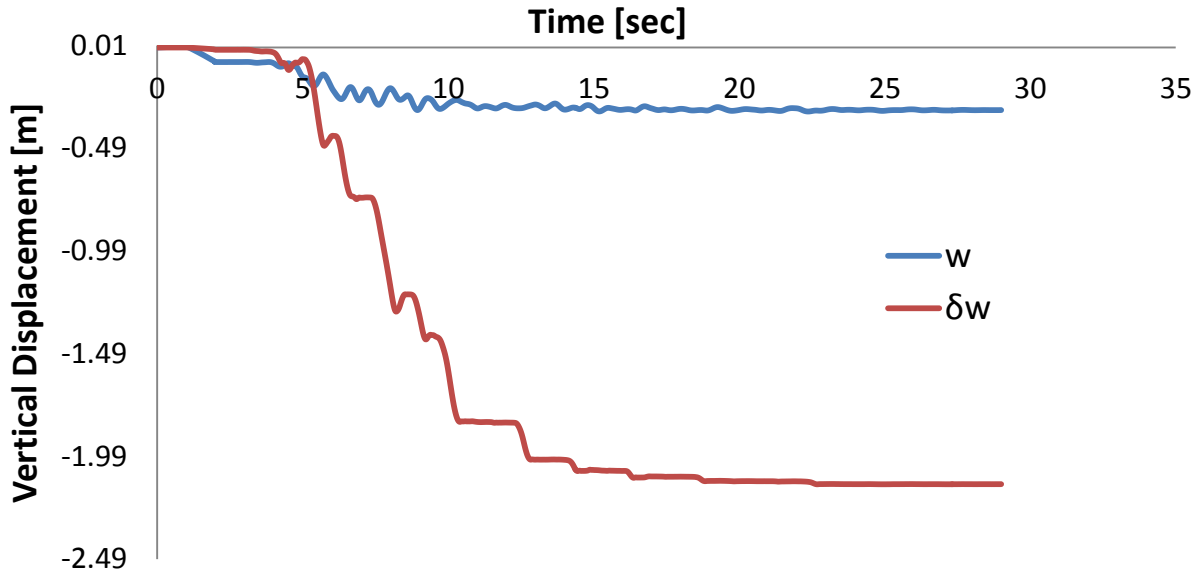

Fig. 2.135. Vertical displacement-time history of the left wall when subjected to Takatori Seismic excitation with peak acceleration 0.9g.

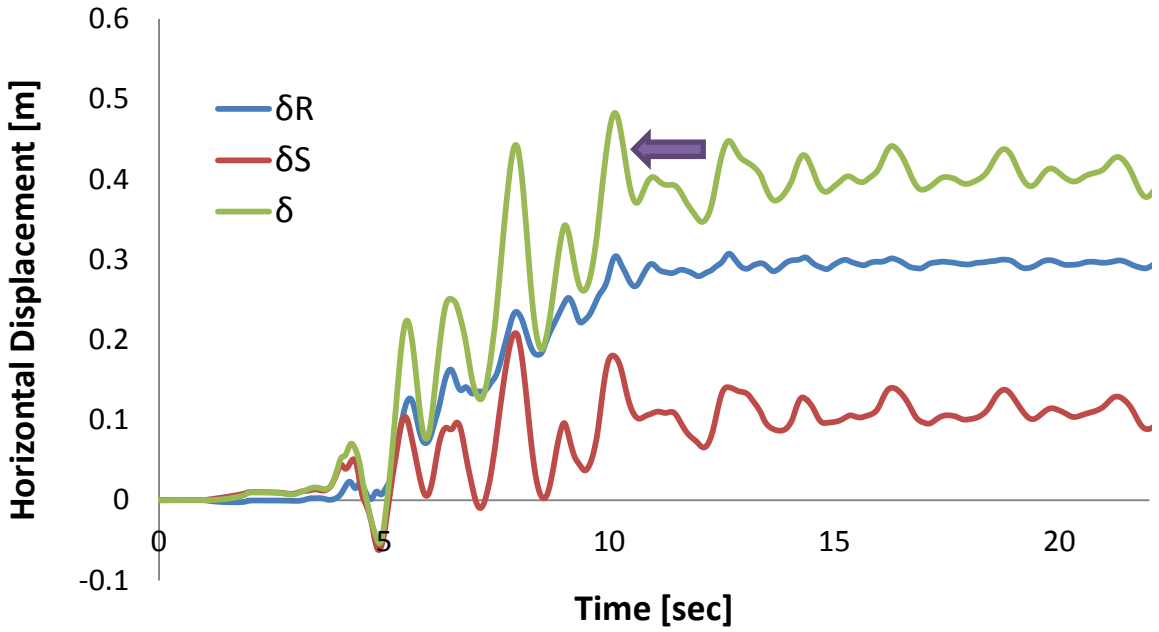

Fig. 2.136. Horizontal displacement-time history of the left wall when subjected to Takatori Seismic excitation with peak acceleration 0.3g.

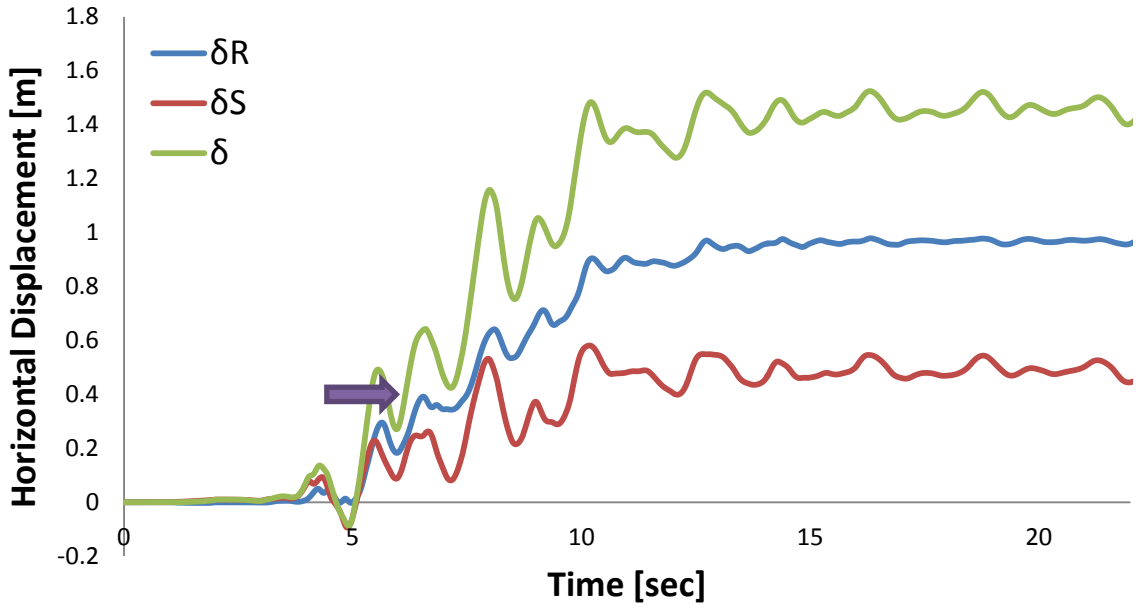

Fig. 2.137. Horizontal displacement-time history of the left wall when subjected to Takatori Seismic excitation with peak acceleration 0.6g.

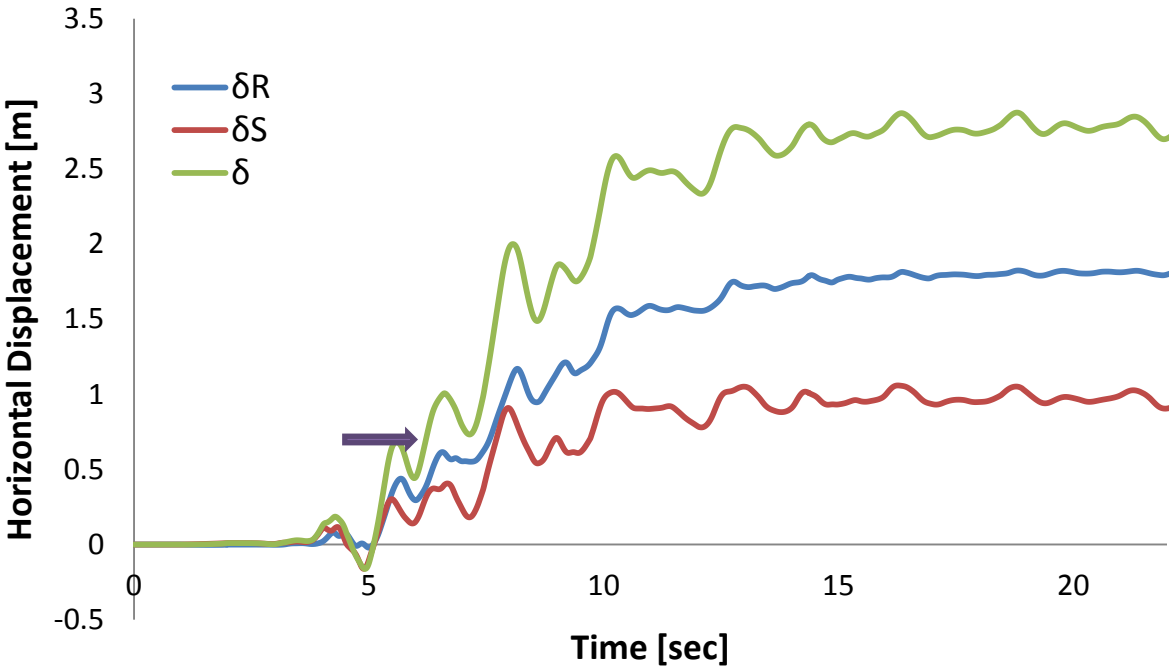

Fig. 2.138. Horizontal displacement-time history of the left wall when subjected to Takatori Seismic excitation with peak acceleration 0.9g.

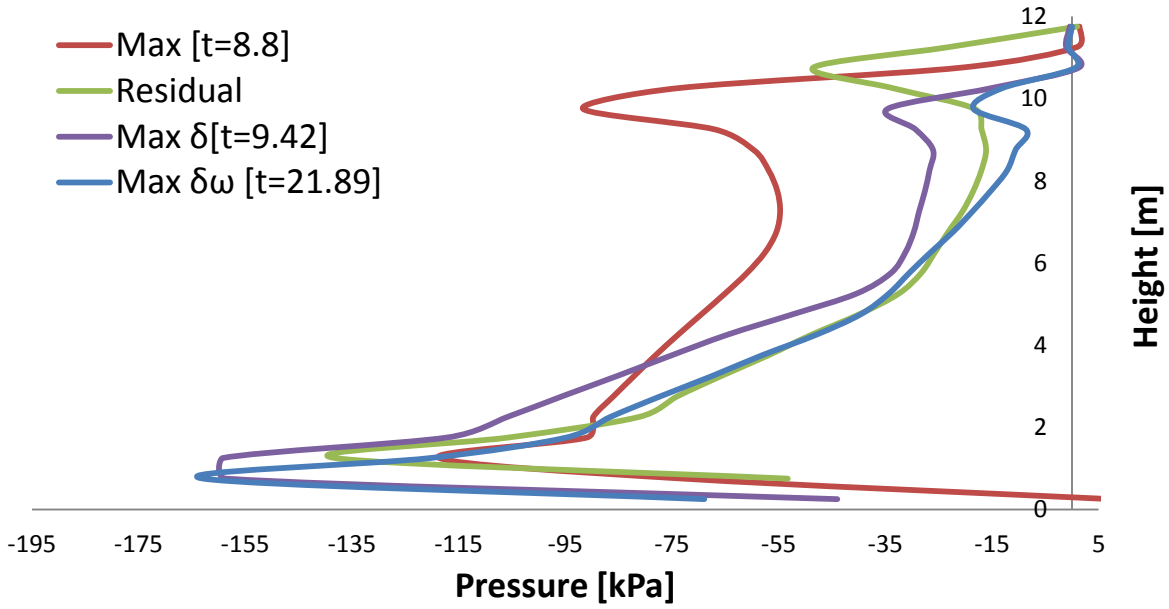

Fig. 2.139. Earth pressures profiles on the right wall at different moments when subjected to Takatori Seismic excitation with peak ground acceleration 0.3g.

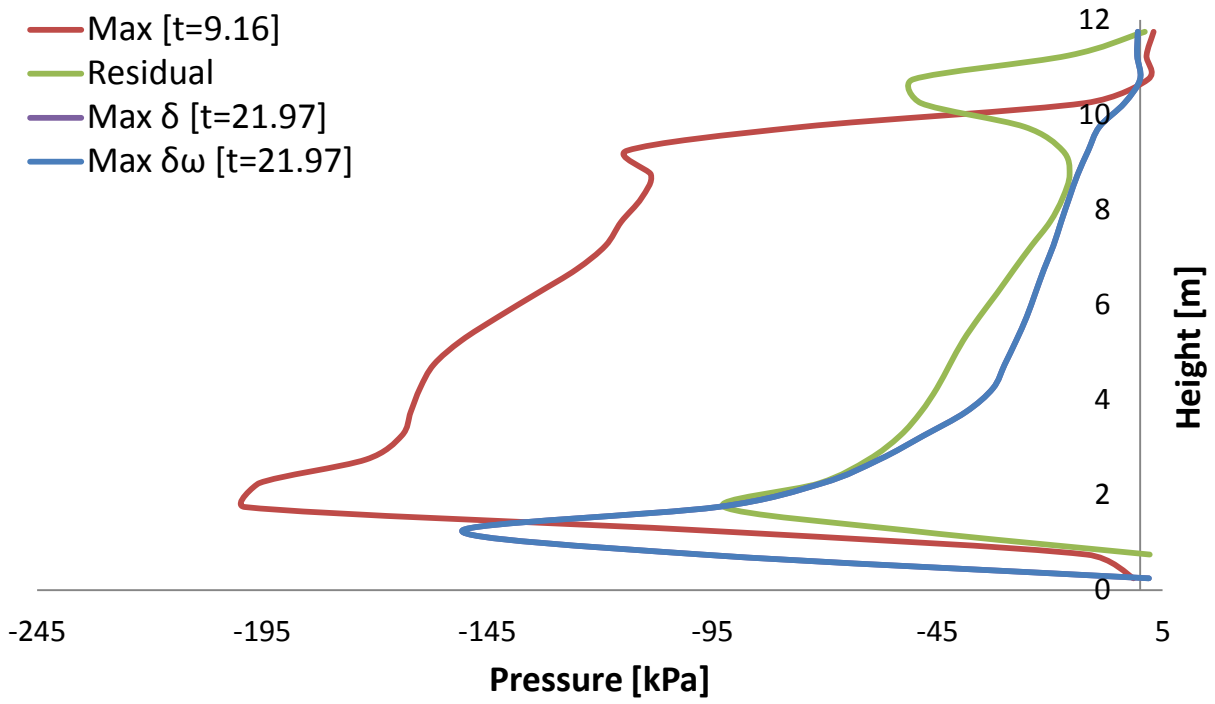

Fig. 2.140. Earth pressures profiles on the right wall at different moments when subjected to Takatori Seismic excitation with peak ground acceleration 0.3g.

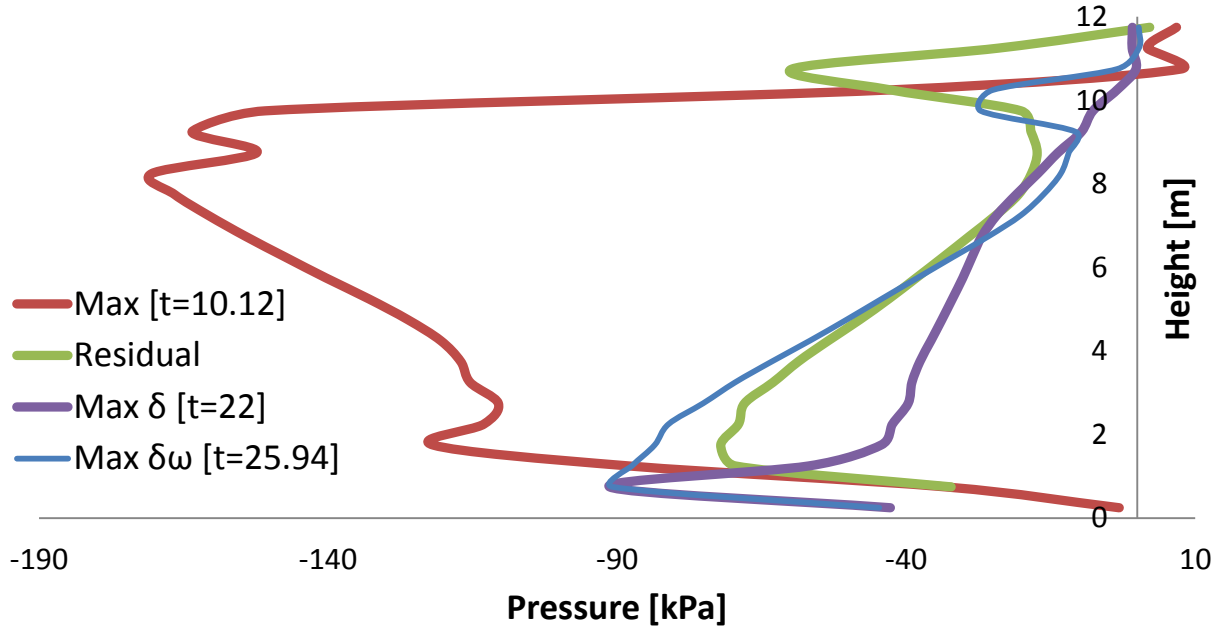

Fig. 2.141. Earth pressures profiles on the right wall at different moments when subjected to Takatori Seismic excitation with peak ground acceleration 0.9.

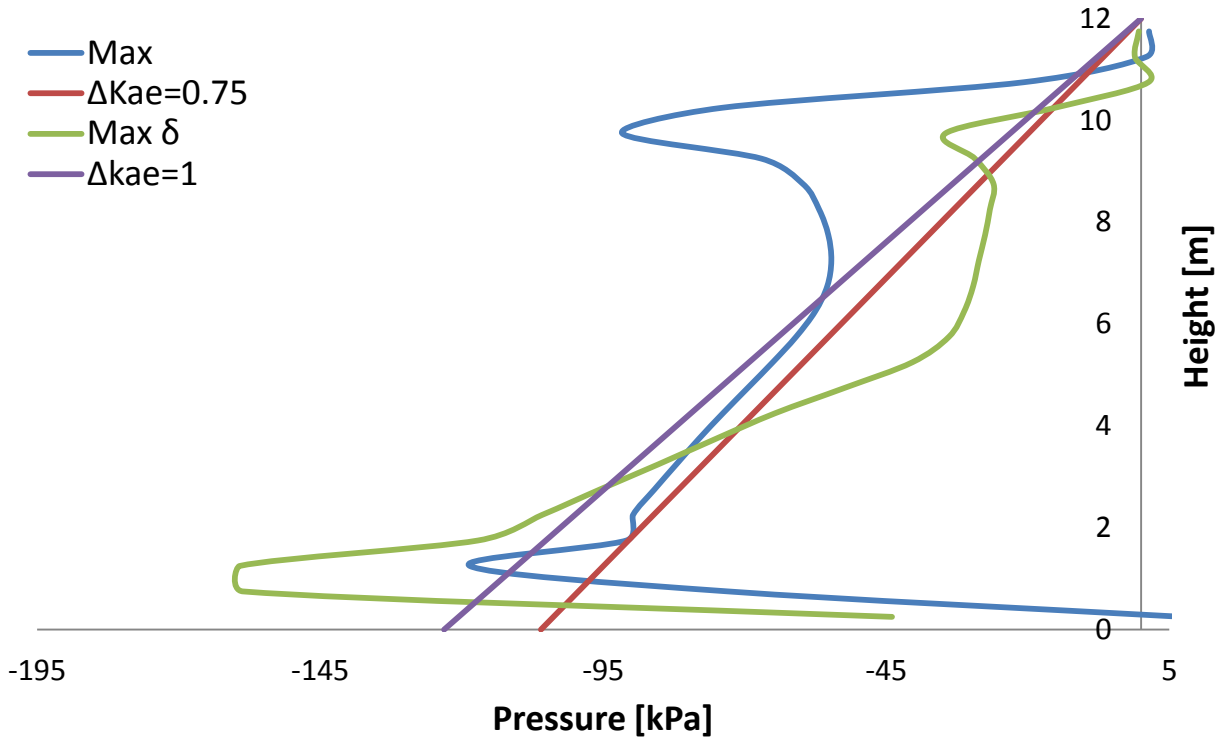

Fig. 2.142. Earth pressure profiles computed in ABAQUS and estimated using the M-O when the right wall is subjected to the Takatori Seismic excitation with peak acceleration 0.3g.

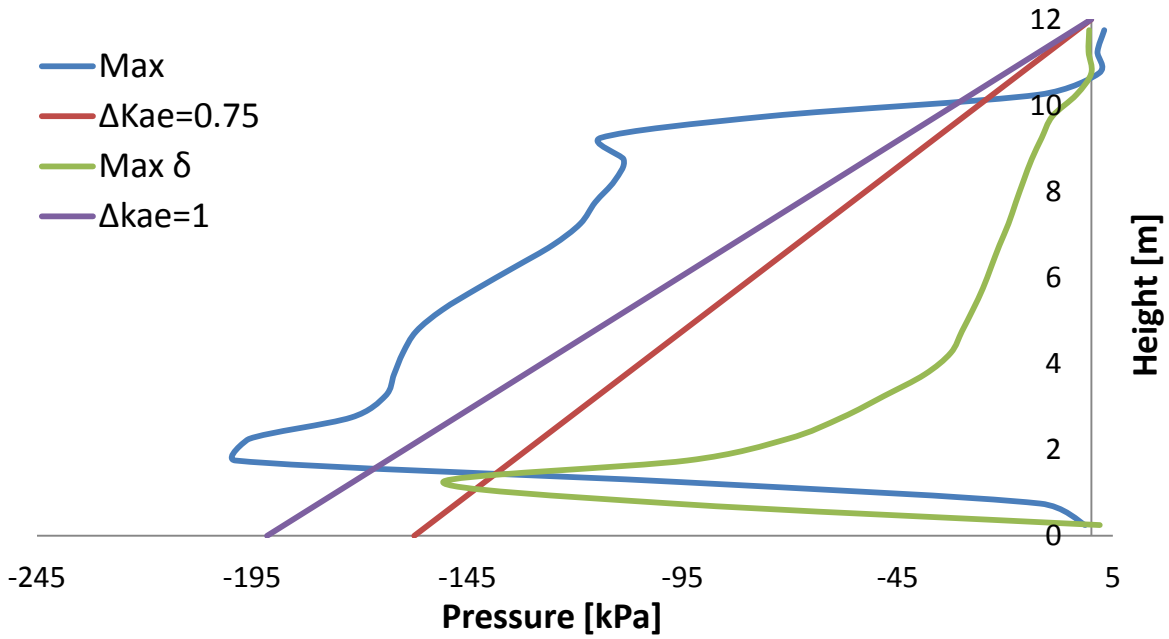

Fig. 2.143. Earth pressure profiles computed in ABAQUS and estimated using the M-O when the right wall is subjected to the Takatori Seismic excitation with peak acceleration 0.6g.

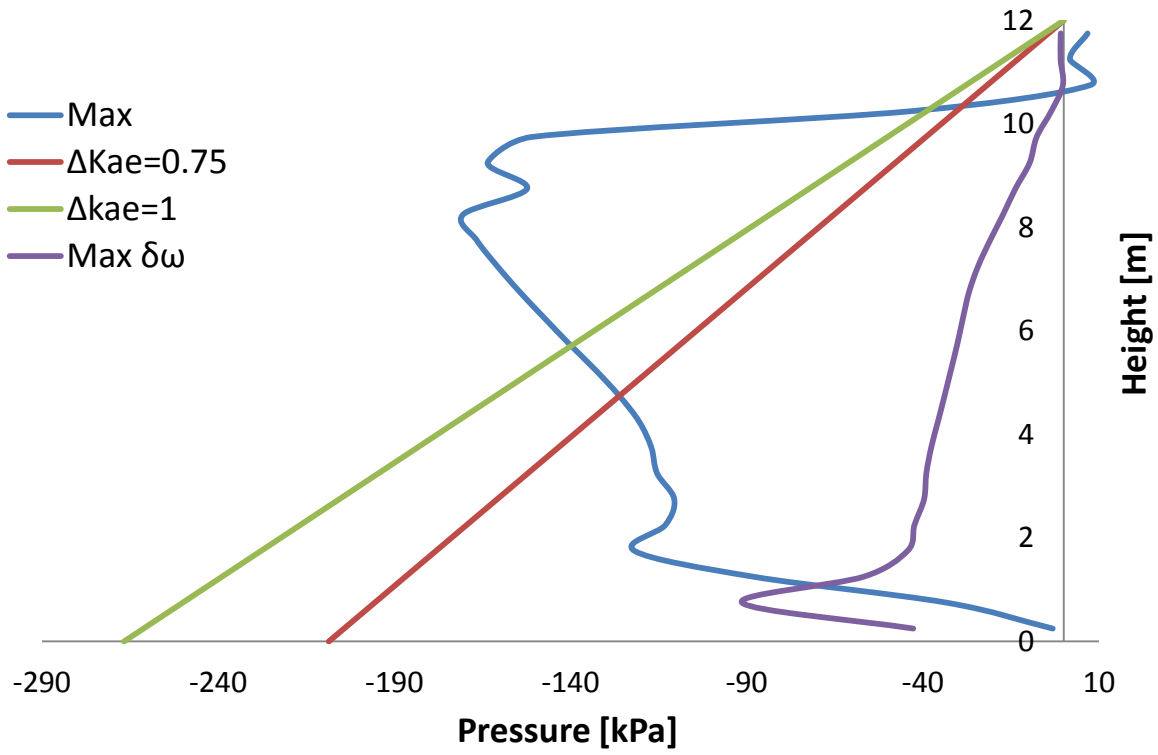

Fig. 2.144. Earth pressure profiles computed in ABAQUS and estimated using the M-O when the right wall is subjected to the Takatori Seismic excitation with peak acceleration 0.9g

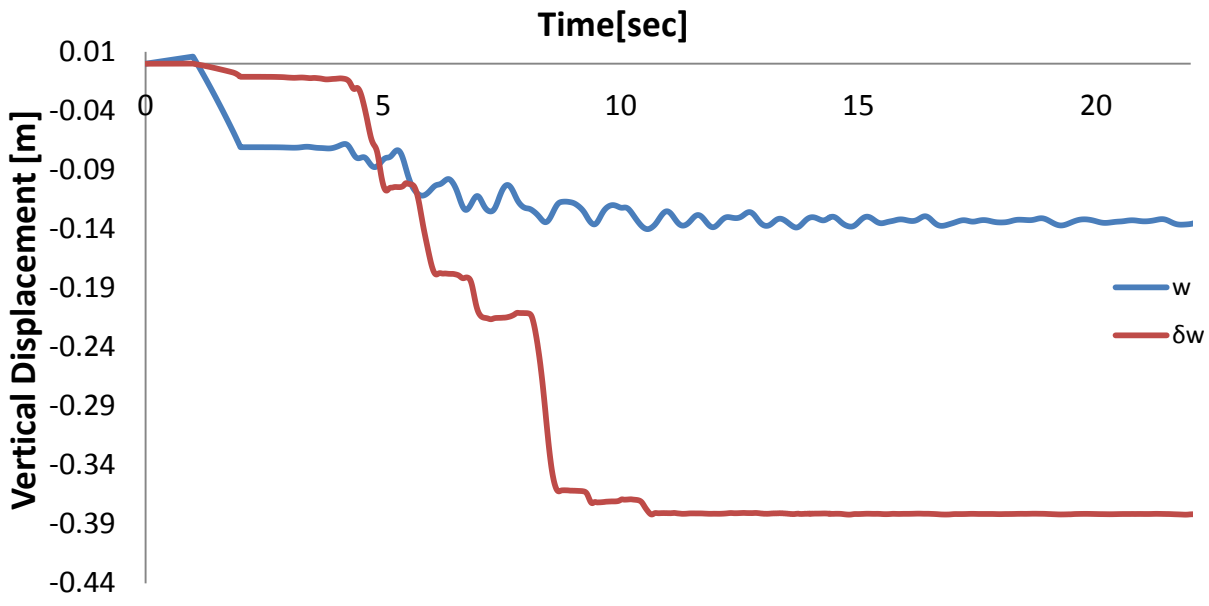

Fig. 2.145. Vertical displacement-time history of the right wall when subjected to Takatori Seismic excitation with peak acceleration 0.3g.

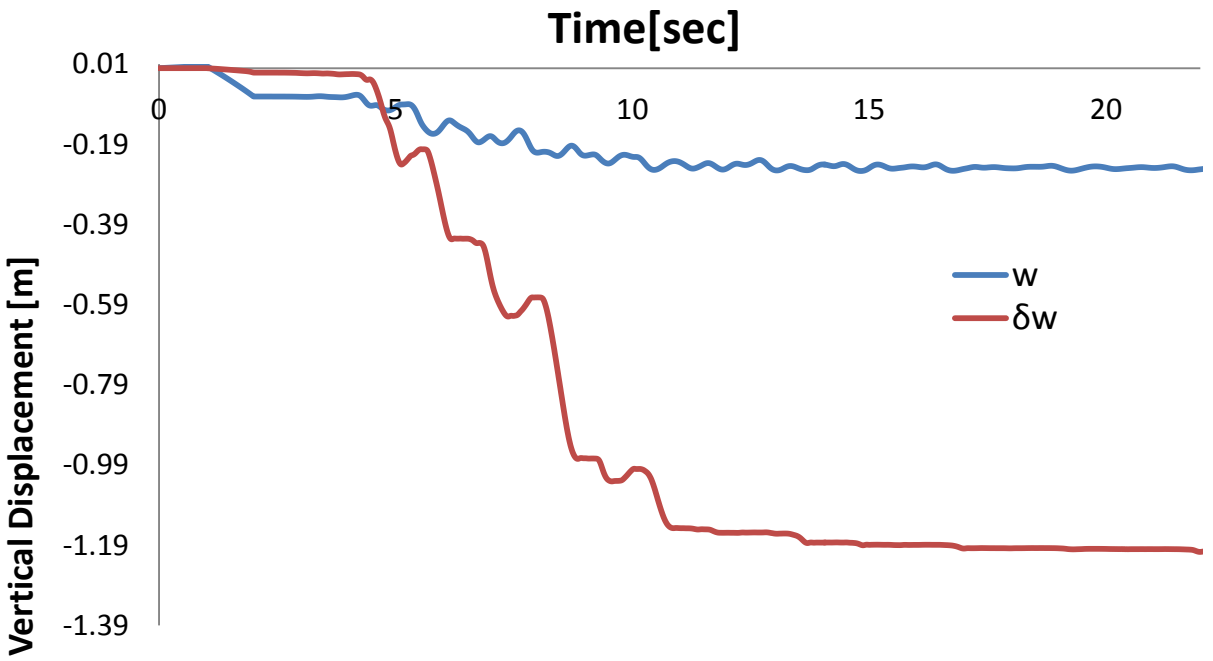

Fig. 2.146. Vertical displacement-time history of the right wall when subjected to Takatori Seismic excitation with peak acceleration 0.6g.

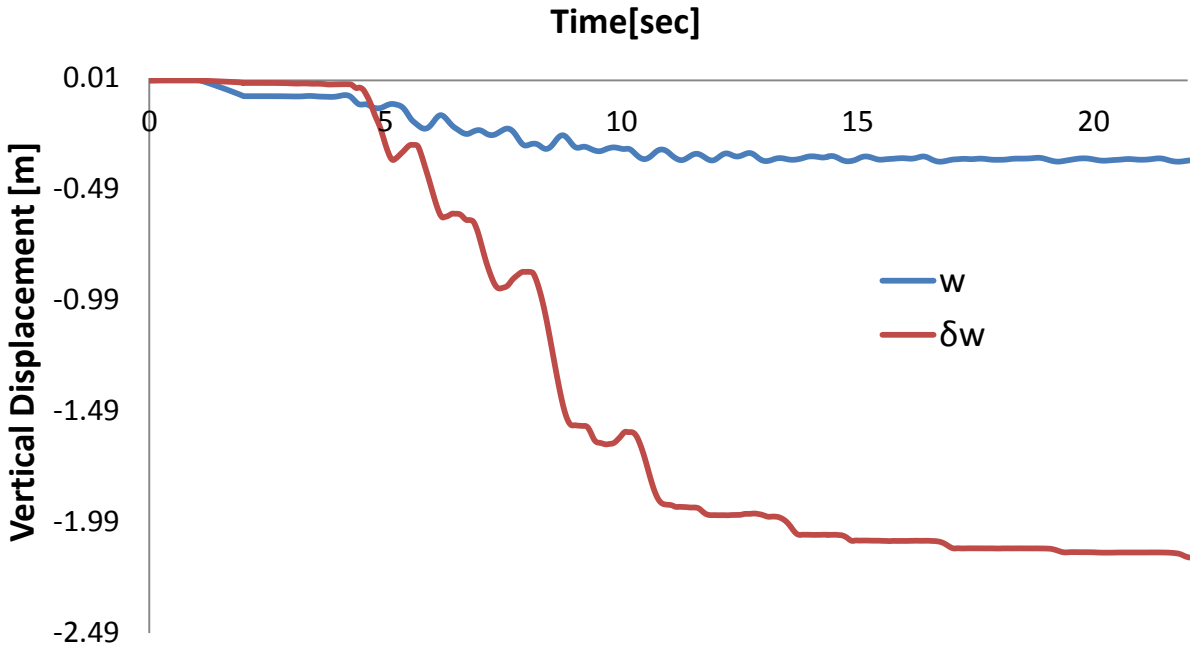

Fig. 2.147. Vertical displacement-time history of the right wall when subjected to Takatori Seismic excitation with peak acceleration 0.9g.

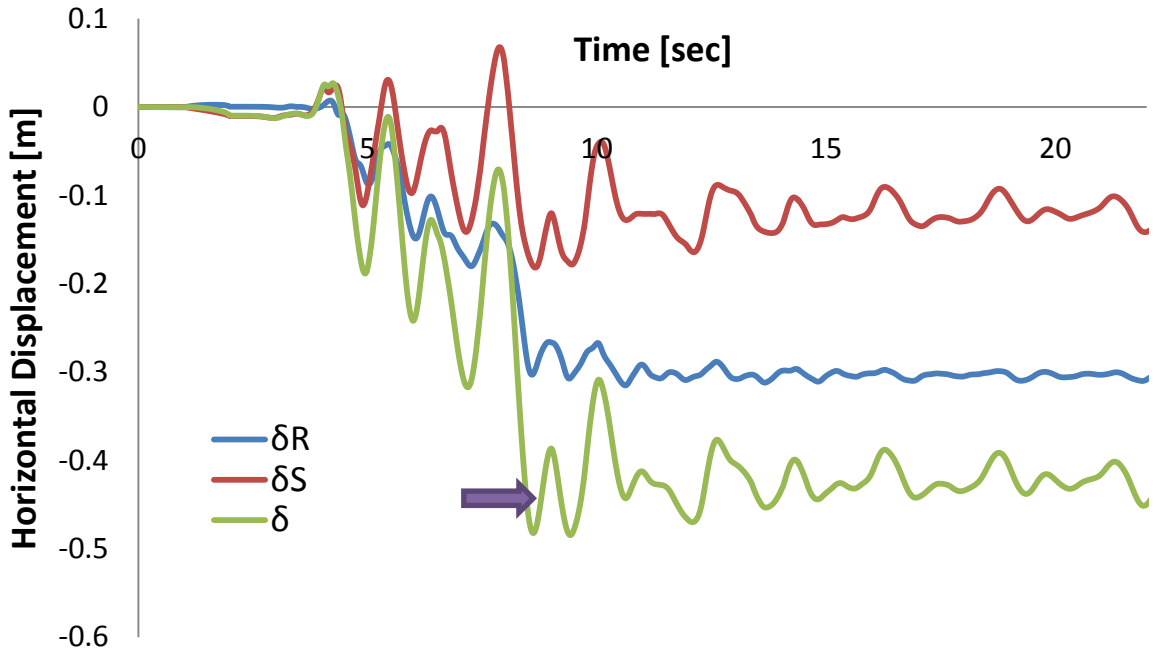

Fig. 2.148. Horizontal displacement-time history of the right wall when subjected to Takatori Seismic excitation with peak acceleration 0.3g.

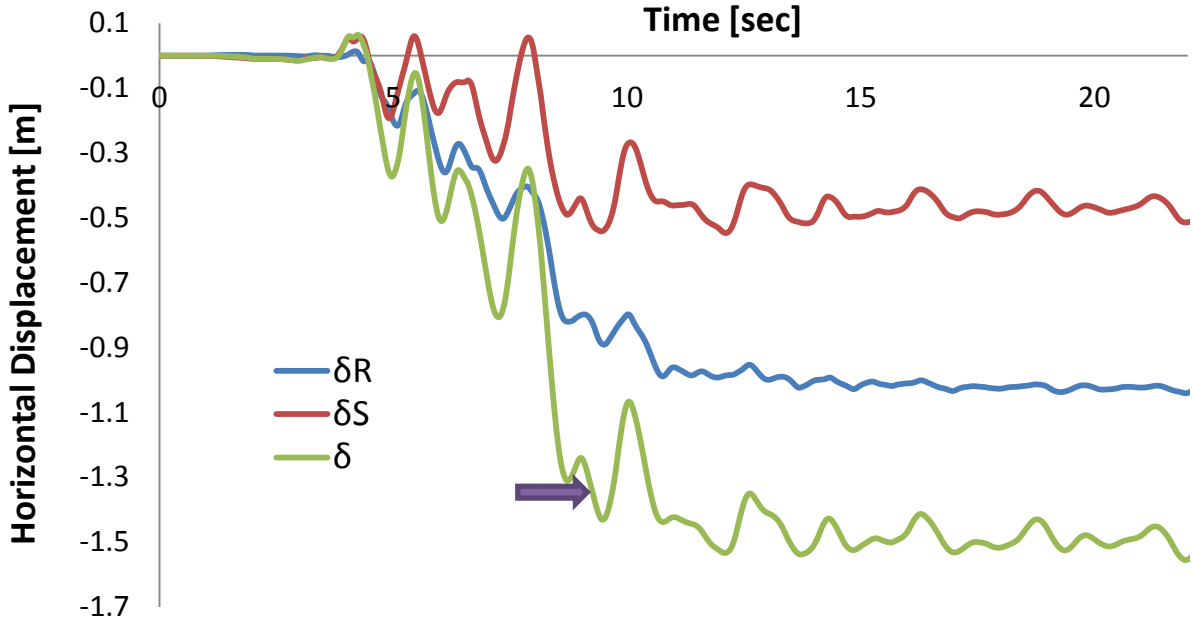

Fig. 2.149. Horizontal displacement-time history of the right wall when subjected to Takatori Seismic excitation with peak acceleration 0.6g.

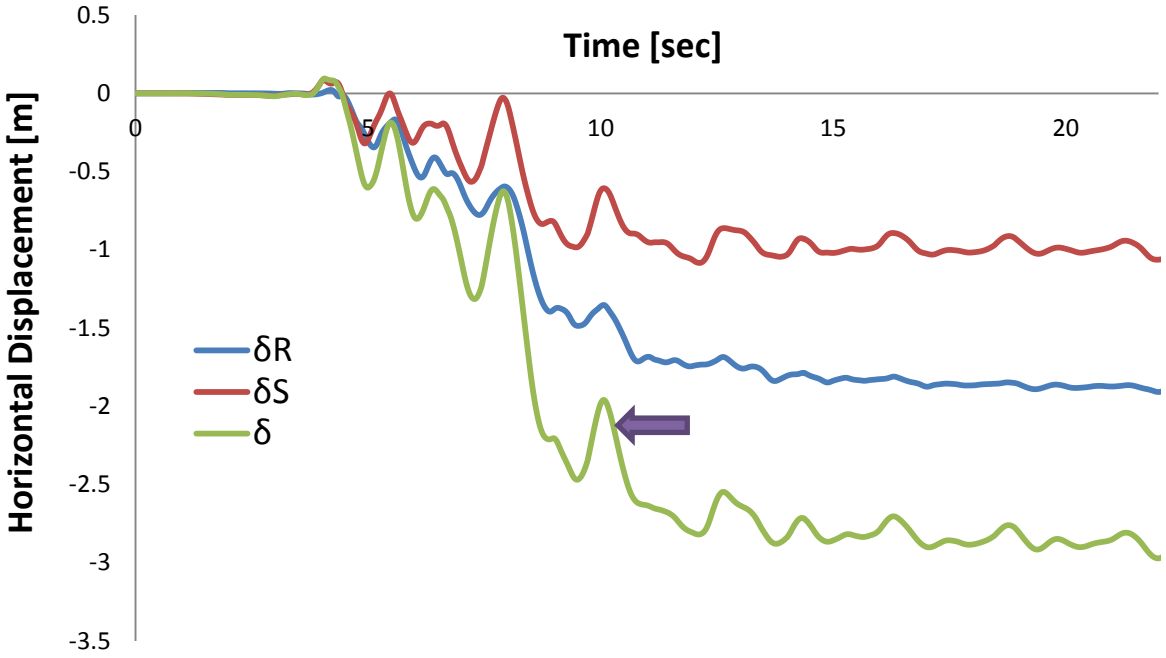

Fig. 2.150. Horizontal displacement-time history of the right wall when subjected to Takatori Seismic excitation with peak acceleration 0.9g.

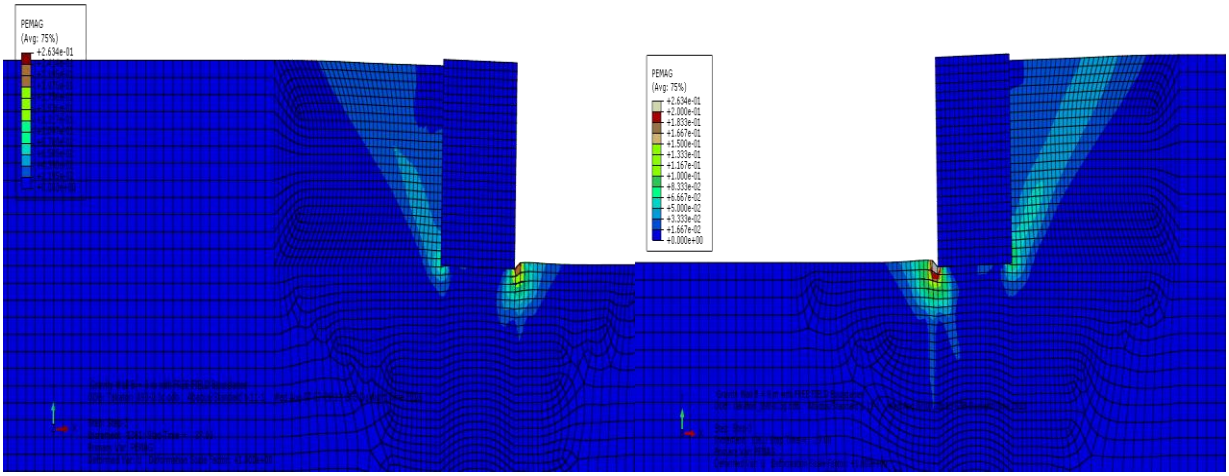

Fig. 2.151. Plastic strain contours at the end of seismic shaking (a)Left wall (b)Right wall when subjected to Takatori seismic excitation with peak acceleration 0.3g.

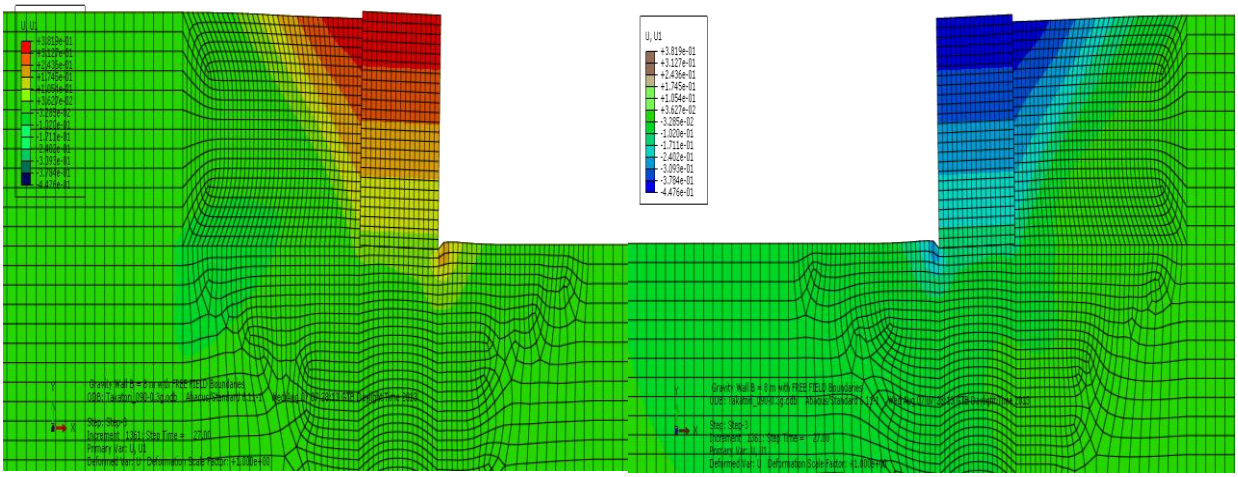

Fig. 2.152. Horizontal displacement contours at the end of the seismic excitation Takatori PGA 0.3g.

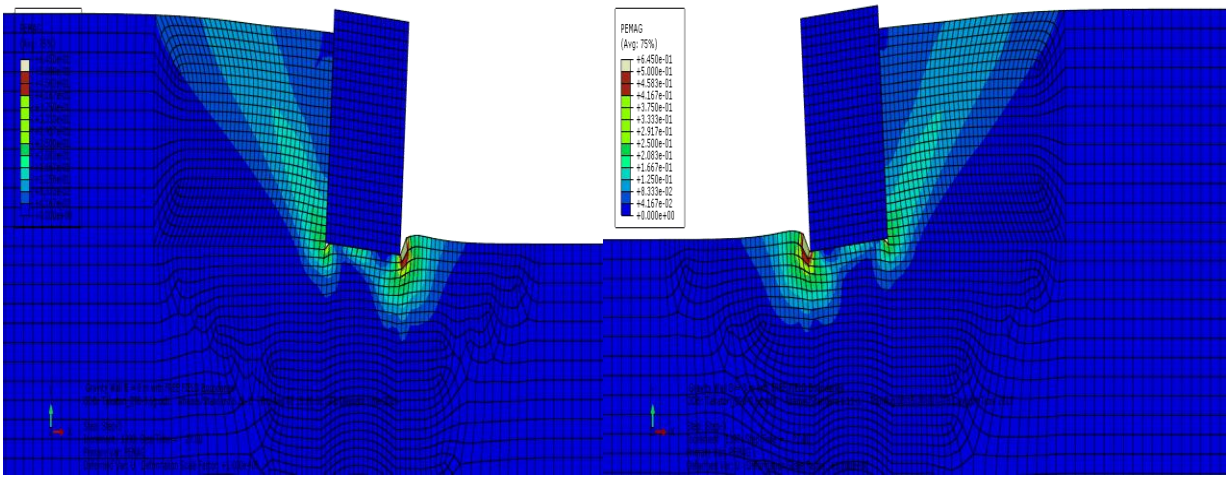

Fig. 2.153. Plastic strain contours at the end of seismic shaking (a)Left wall (b)Right wall when subjected to Takatori seismic excitation with peak acceleration 0.6g.

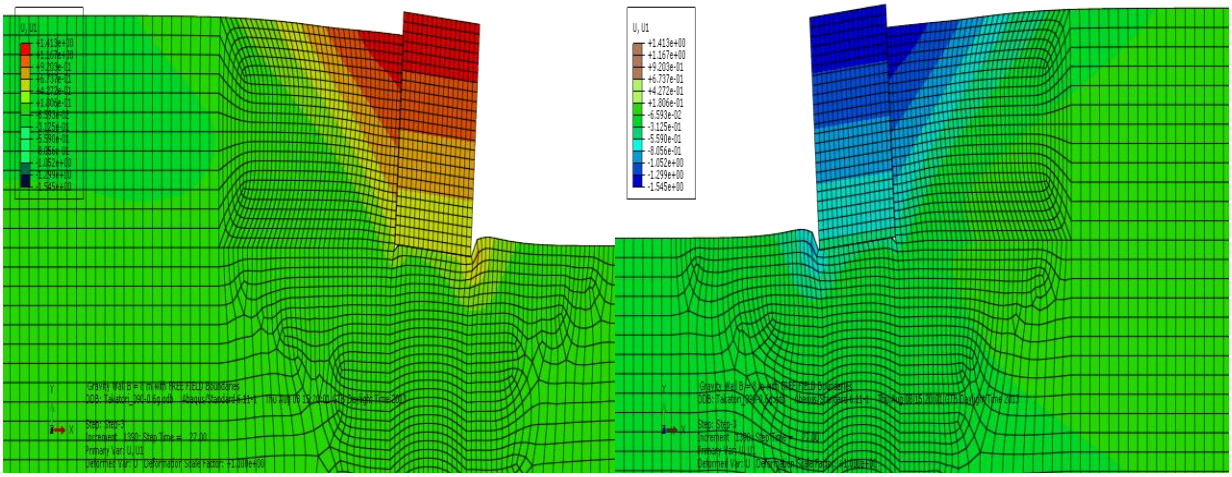

Fig. 2.154. Horizontal displacement contours at the end of the seismic excitation Takatori PGA 0.6g.

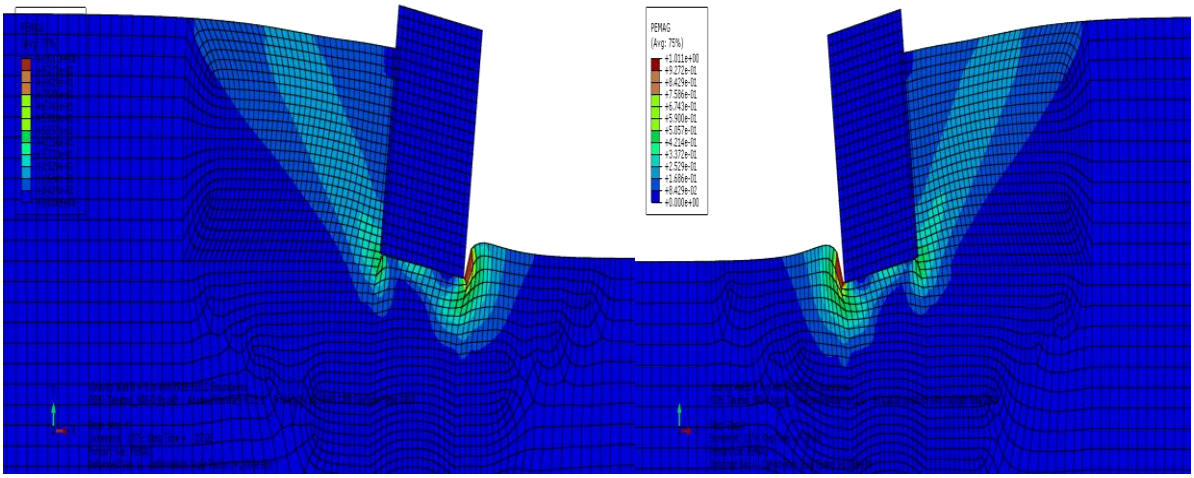

Fig. 2.155. Plastic strain contours at the end of seismic shaking (a)Left wall (b)Right wall when subjected to Takatori seismic excitation with peak acceleration 0.9g.

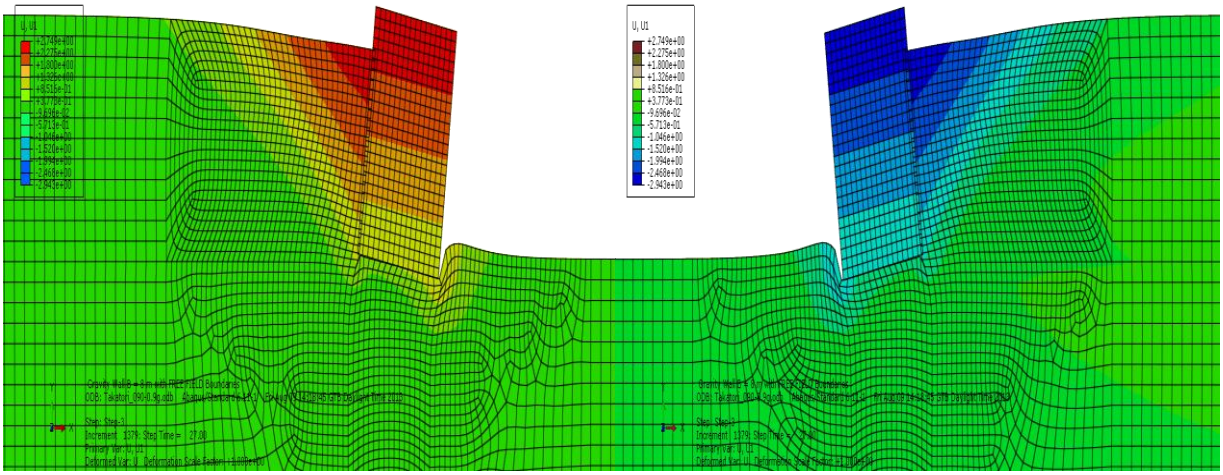

Fig. 2.156. Horizontal displacement contours at the end of the seismic excitation Takatori PGA 0.9g.

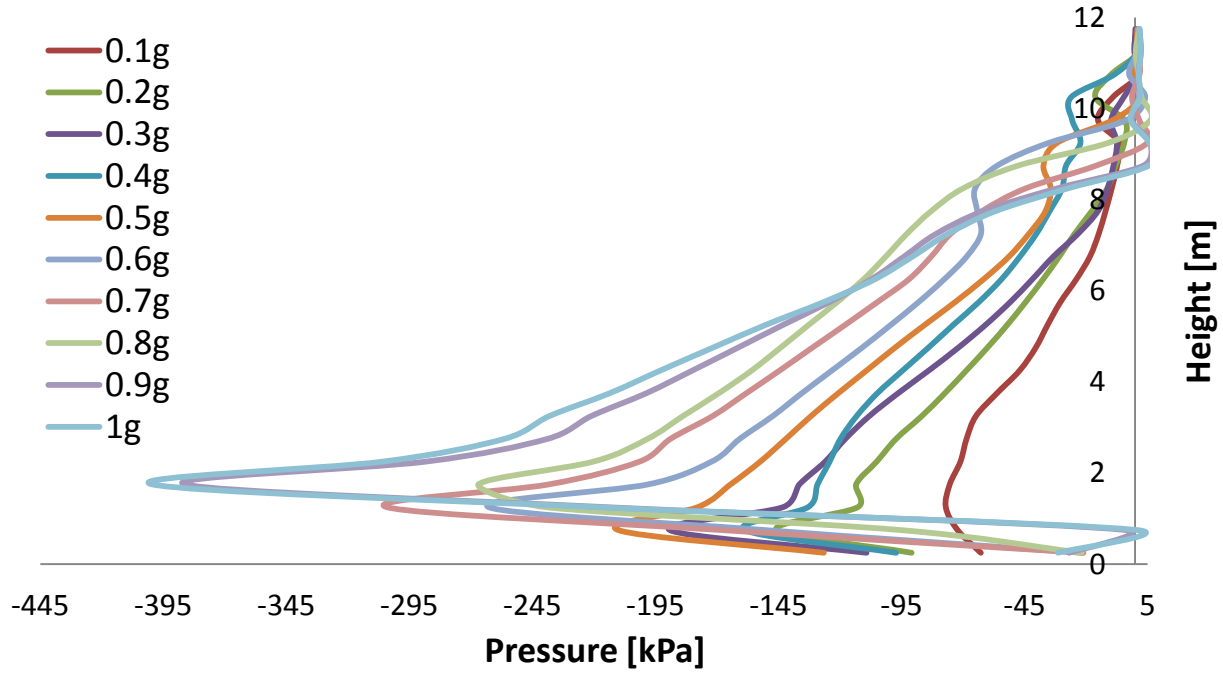

Fig. 2.157. Maximum earth pressure profiles for different peak accelerations on the left wall when subjected to Takatori Seismic excitation.

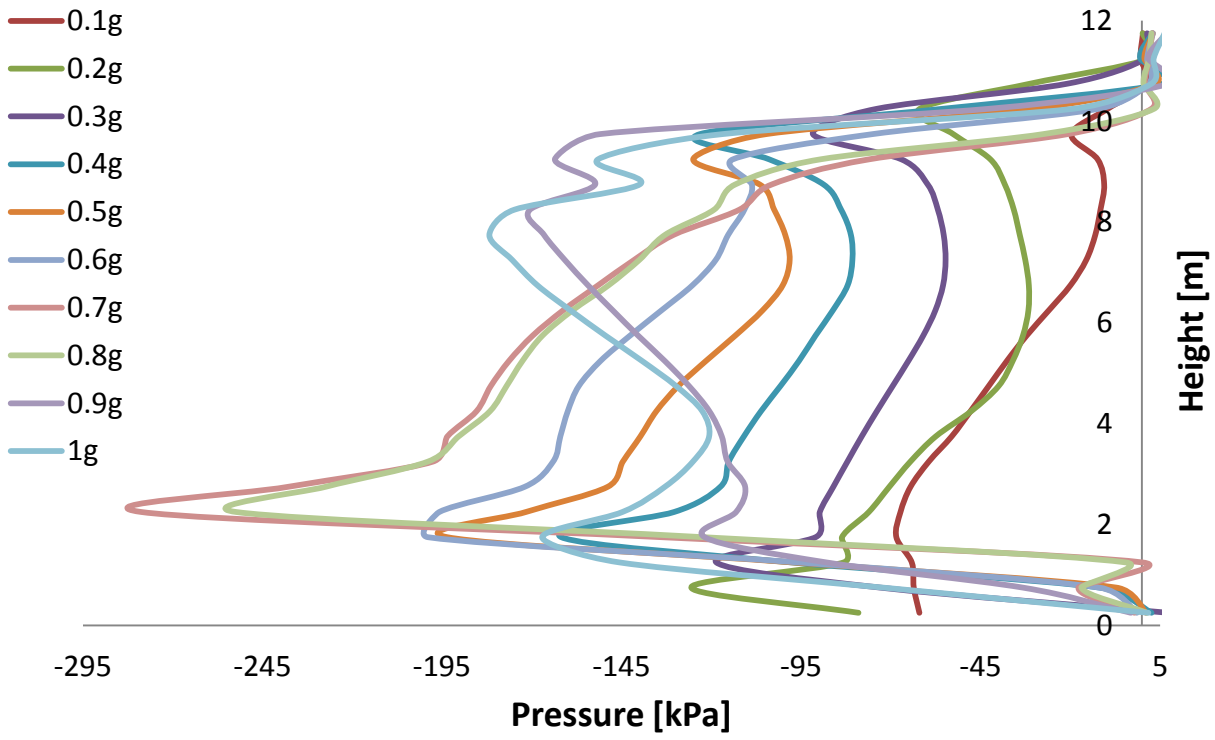

Fig. 2.158. Maximum earth pressure profiles for different peak accelerations on the right wall when subjected to Takatori Seismic excitation.

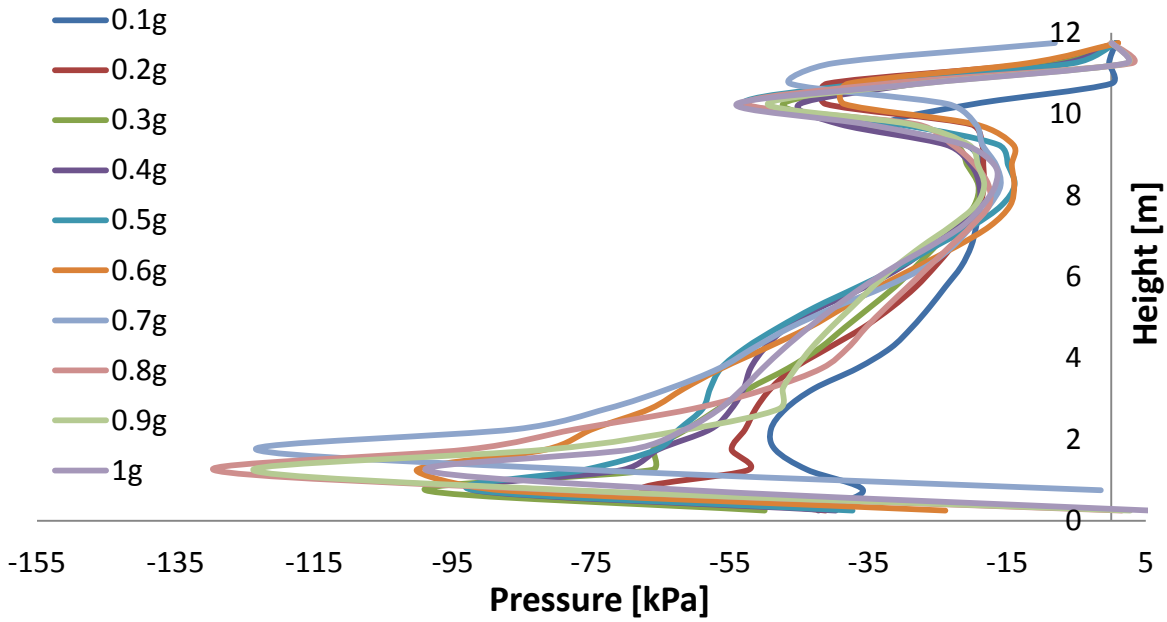

Fig. 2.159. Residual earth pressure profiles for different peak accelerations on the left wall when subjected to Takatori Seismic excitation.

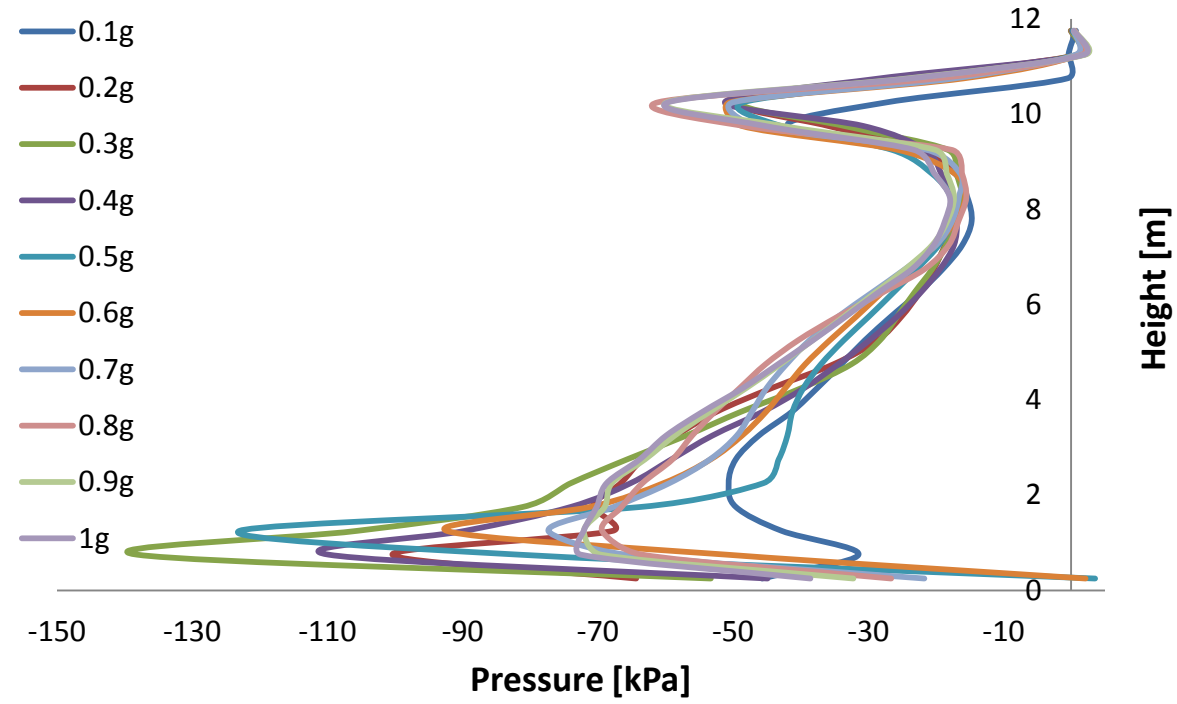

Fig. 2.160. Residual earth pressure profiles for different peak accelerations on the left wall when subjected to Takatori Seismic excitation

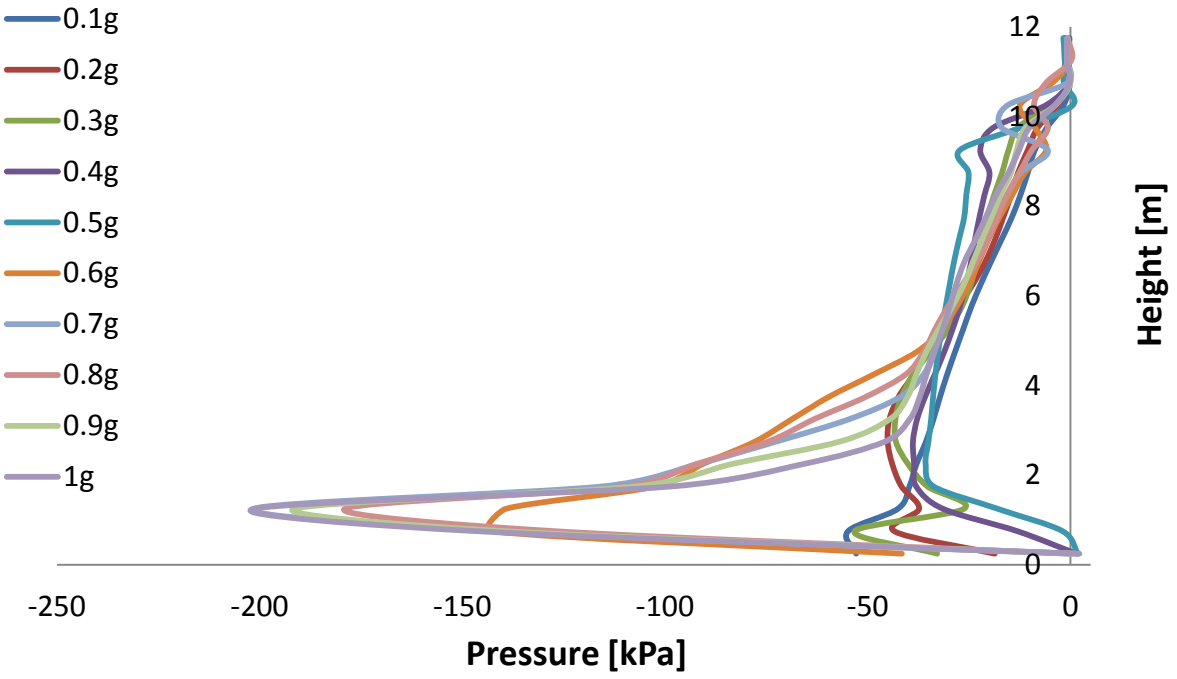

Fig. 2.161. Earth pressure profiles at maximum displacement for different peak accelerations on the left wall when subjected to Takatori Seismic excitation.

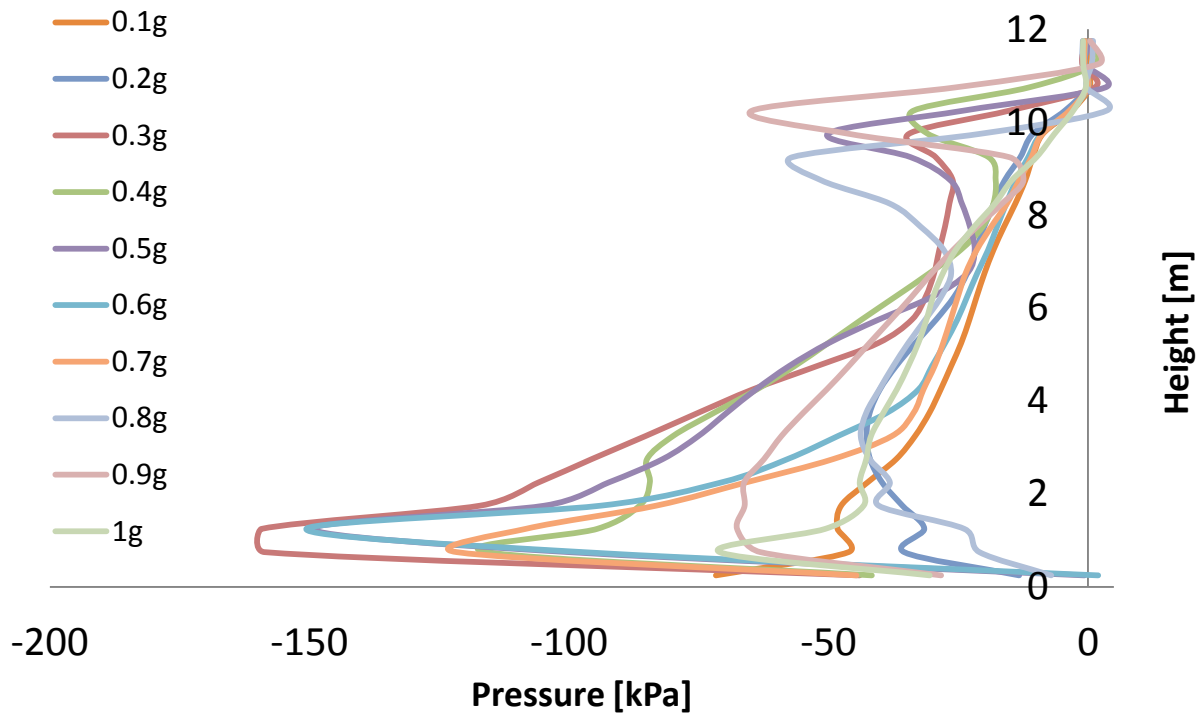

Fig. 2.162. Earth pressure profiles at maximum displacement for different peak accelerations on the right wall when subjected to Takatori Seismic excitation.

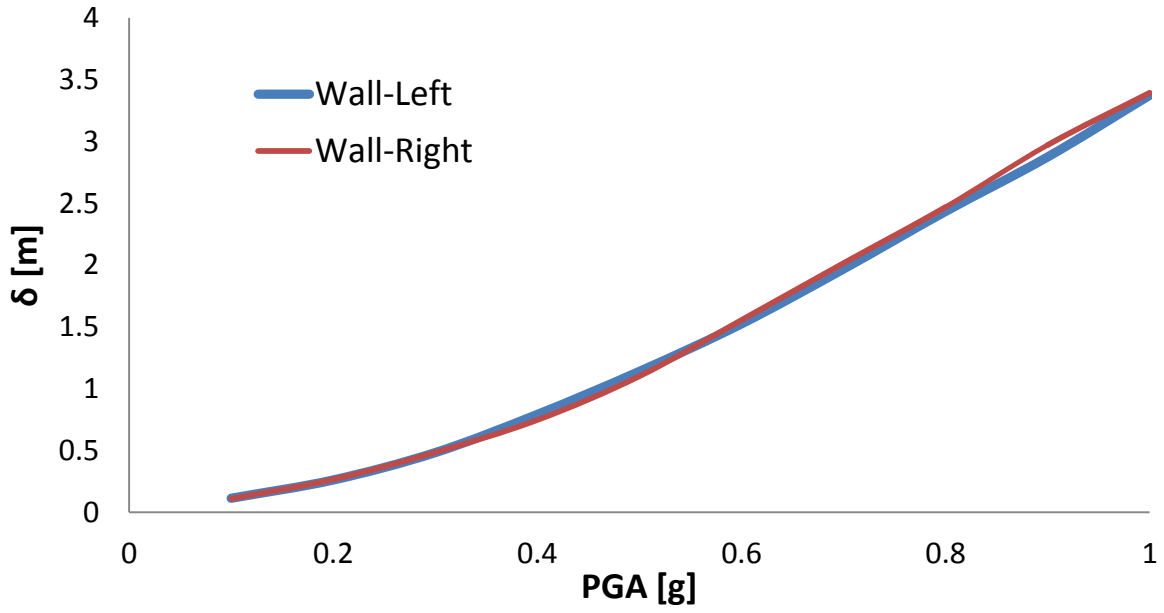

Fig. 2.163. Horizontal displacement as a function of PGA for the left and right wall when subjected to Ageion Seismic excitation.

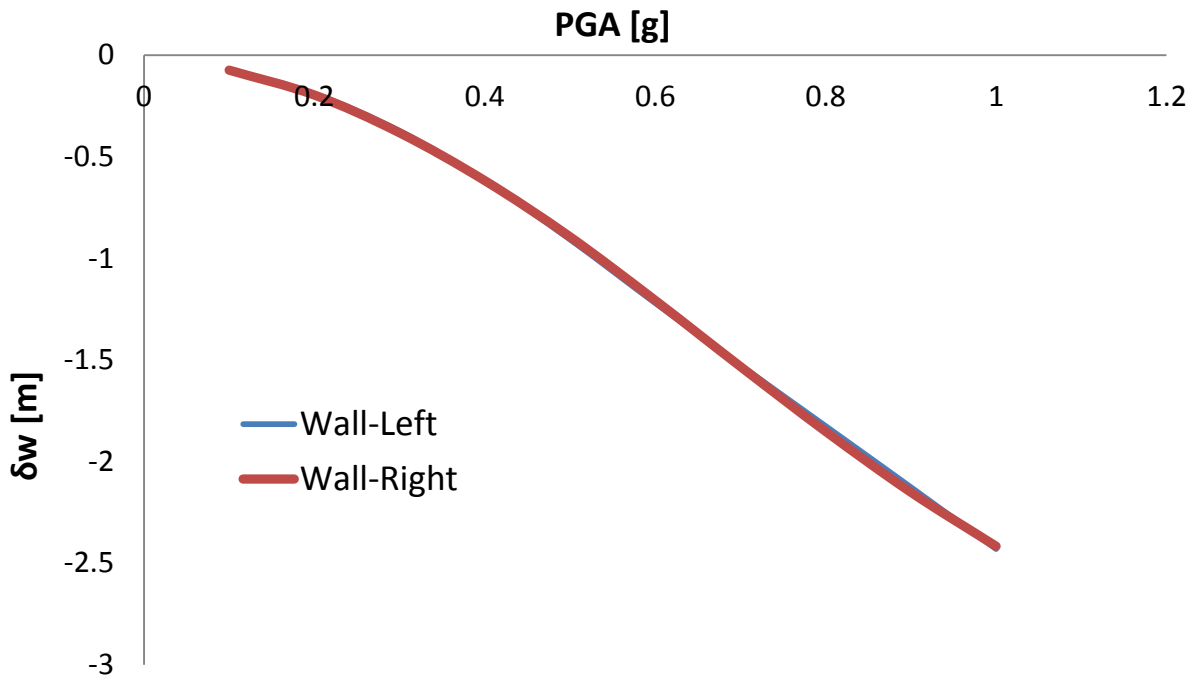

Fig. 2.164. Differential settlement as a function of PGA for the left and right wall when subjected to Lefkada Seismic excitation.

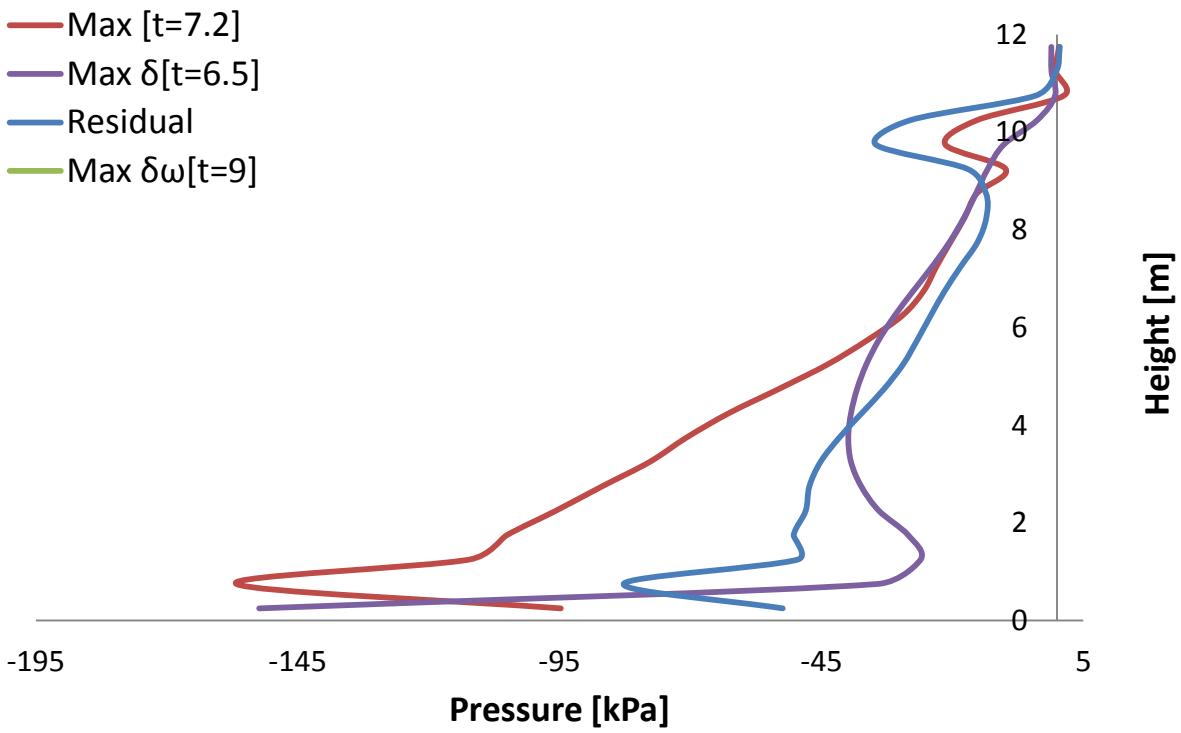

Fig. 2.165. Earth pressures profiles on the left wall at different moments when subjected to Kalamata Seismic excitation with peak ground acceleration 0.3g.

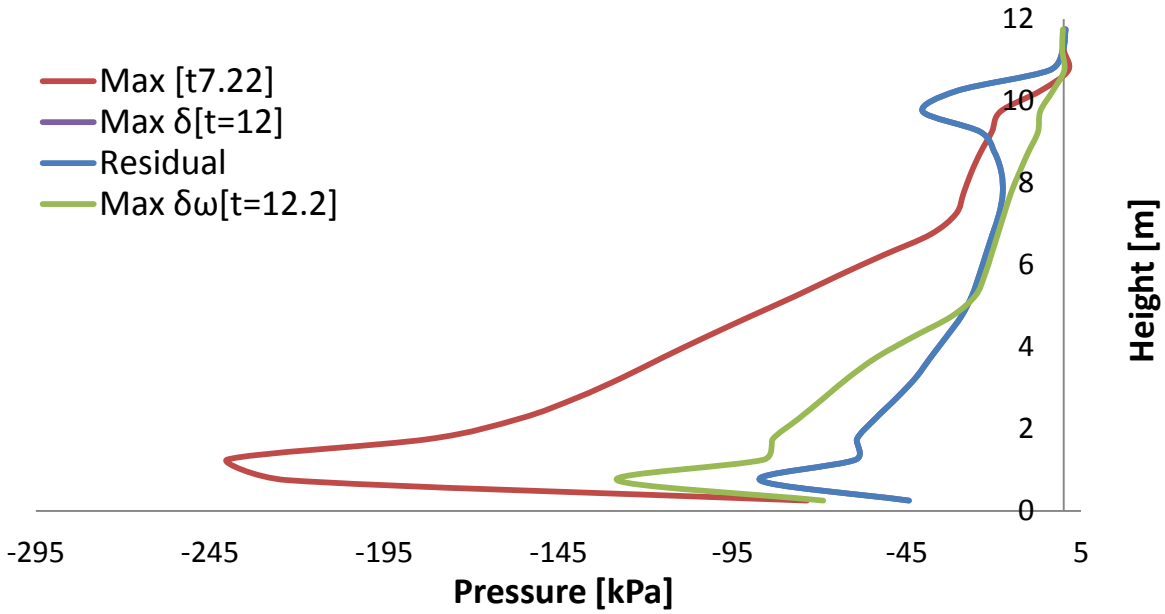

Fig. 2.166. Earth pressures profiles on the left wall at different moments when subjected to Kalamata Seismic excitation with peak ground acceleration 0.6g.

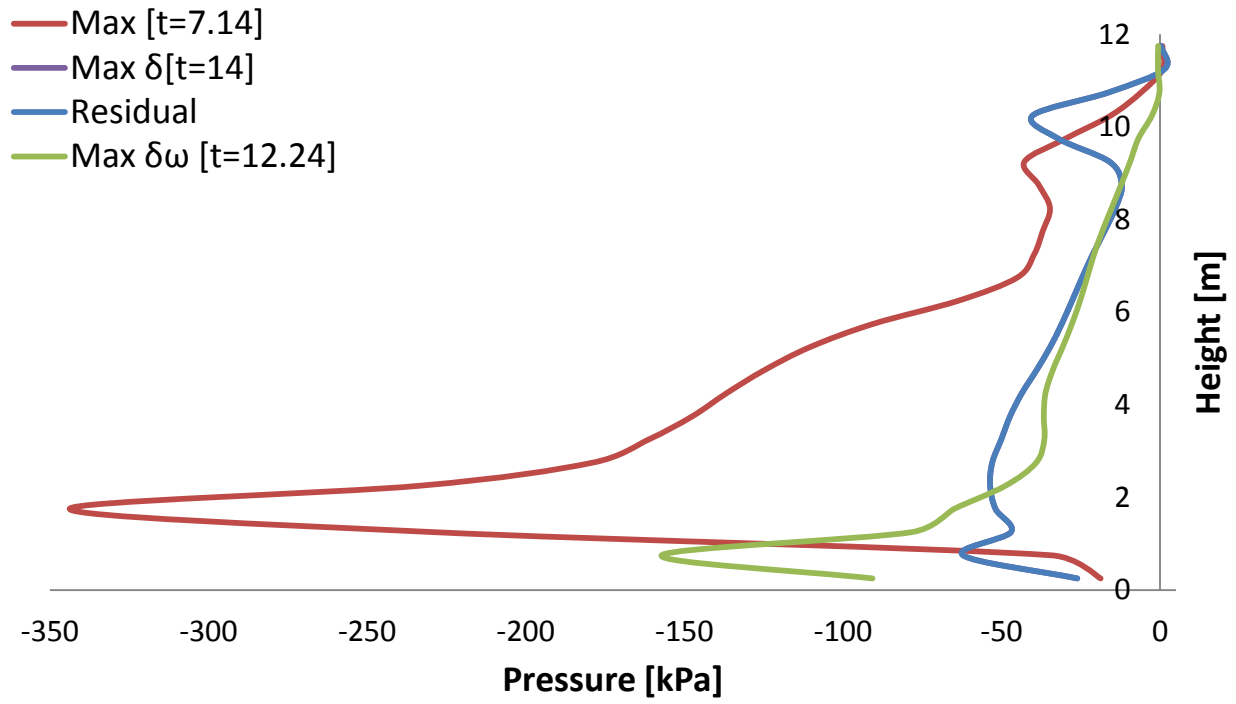

Fig. 2.167. Earth pressures profiles on the left wall at different moments when subjected to Kalamata Seismic excitation with peak ground acceleration 0.9g.

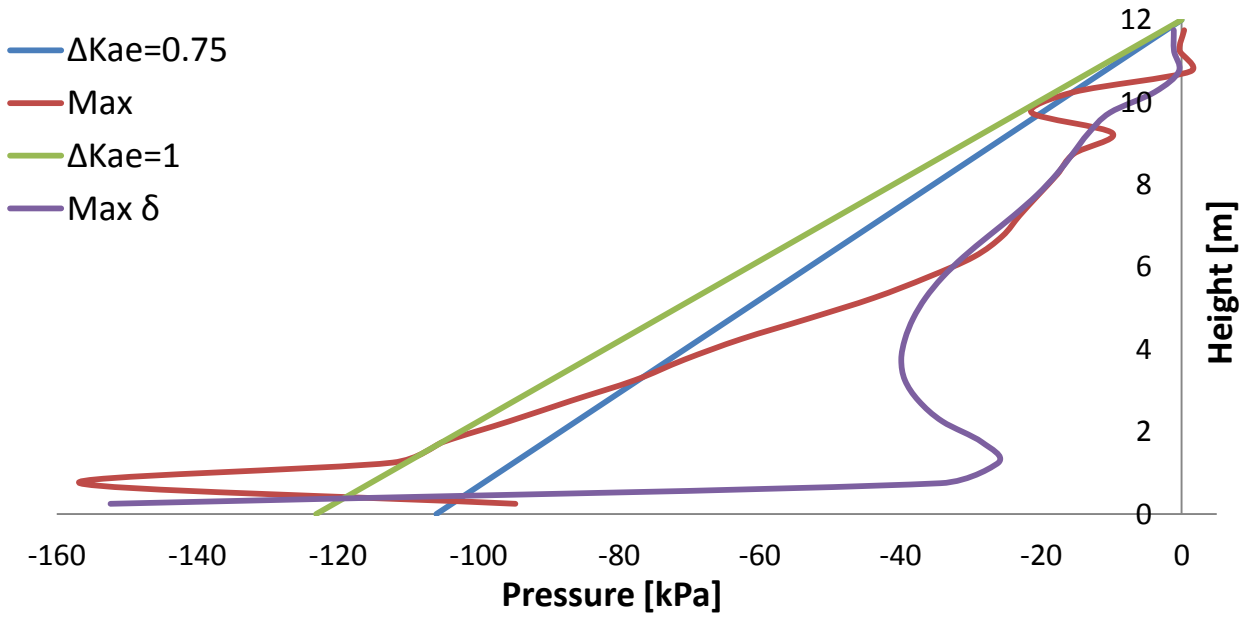

Fig. 2.168. Earth pressure profiles computed in ABAQUS and estimated using the M-O when the left wall is subjected to the Kalamata Seismic excitation with peak acceleration 0.3g.

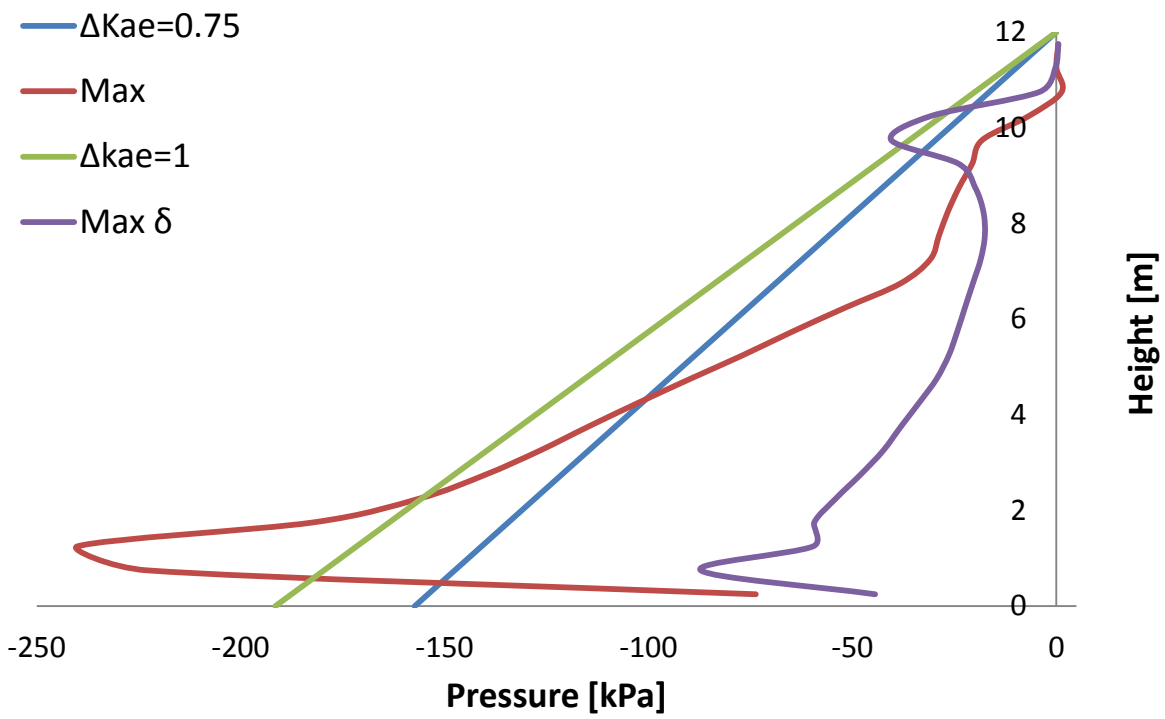

Fig. 2.169. Earth pressure profiles computed in ABAQUS and estimated using the M-O when the leftwall is subjected to the Kalamata Seismic excitation with peak acceleration 0.6g.

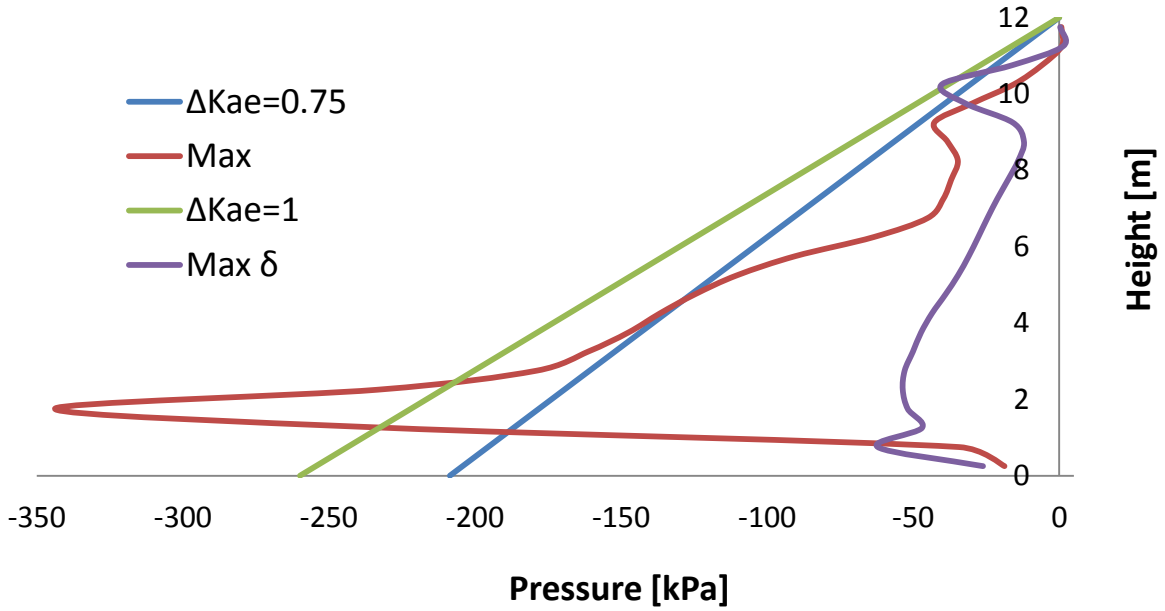

Fig. 2.170. Earth pressure profiles computed in ABAQUS and estimated using the M-O when the left wall is subjected to the Kalamata Seismic excitation with peak acceleration 0.9g.

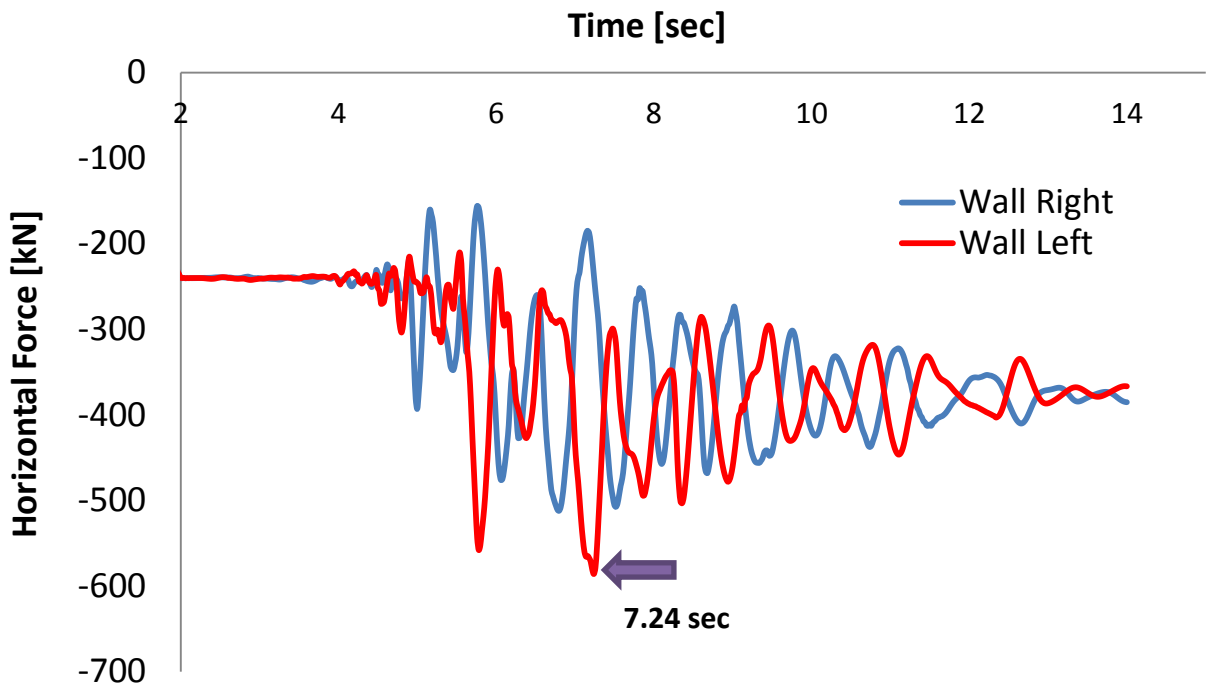

Fig. 2.171. Horizontal force-time history of the left and right wall when subjected to Kalamata Seismic excitation with peak ground acceleration 0.3 g.

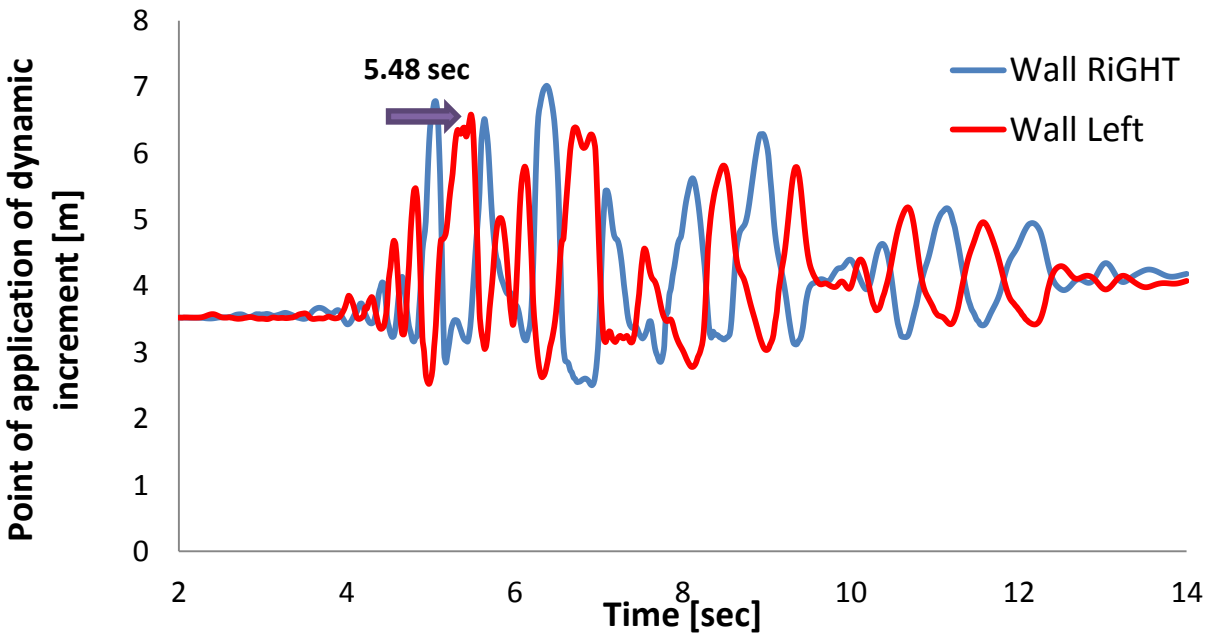

Fig. 2.172. Point of application of dynamic increment on the left and right wall when subjected to Kalamata Seismic excitation with peak ground acceleration 0.3g

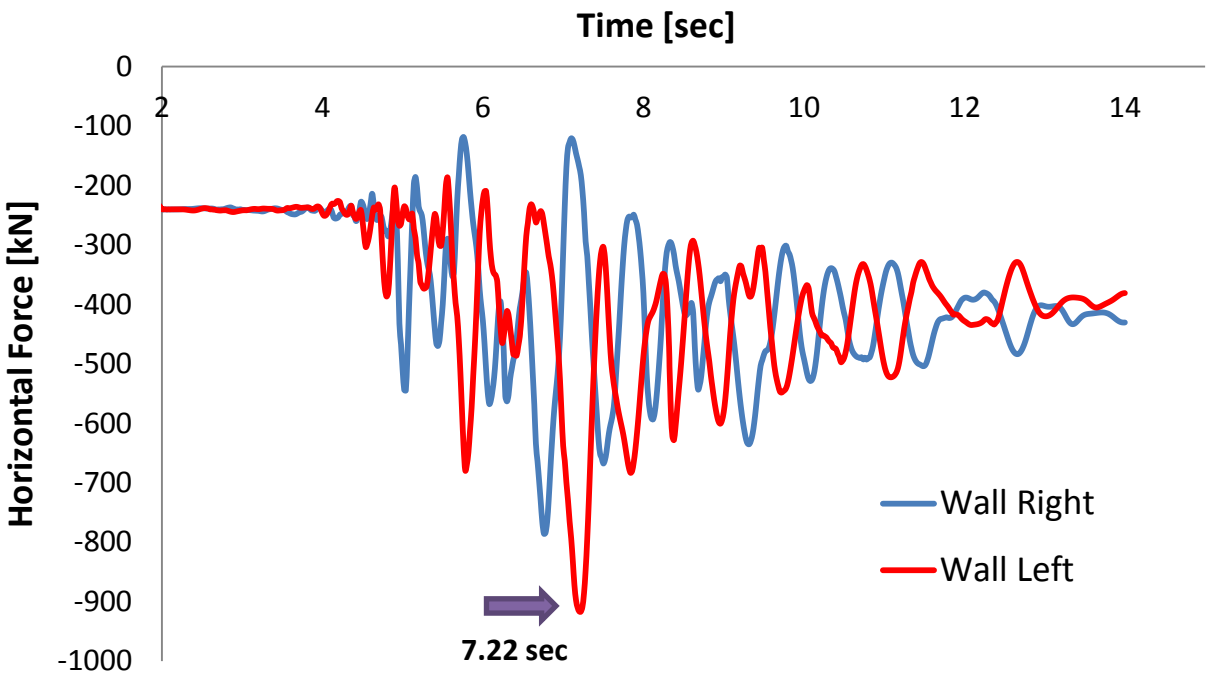

Fig. 2.173. Horizontal force-time history of the left and right wall when subjected to Kalamata Seismic excitation with peak ground acceleration 0.6 g.

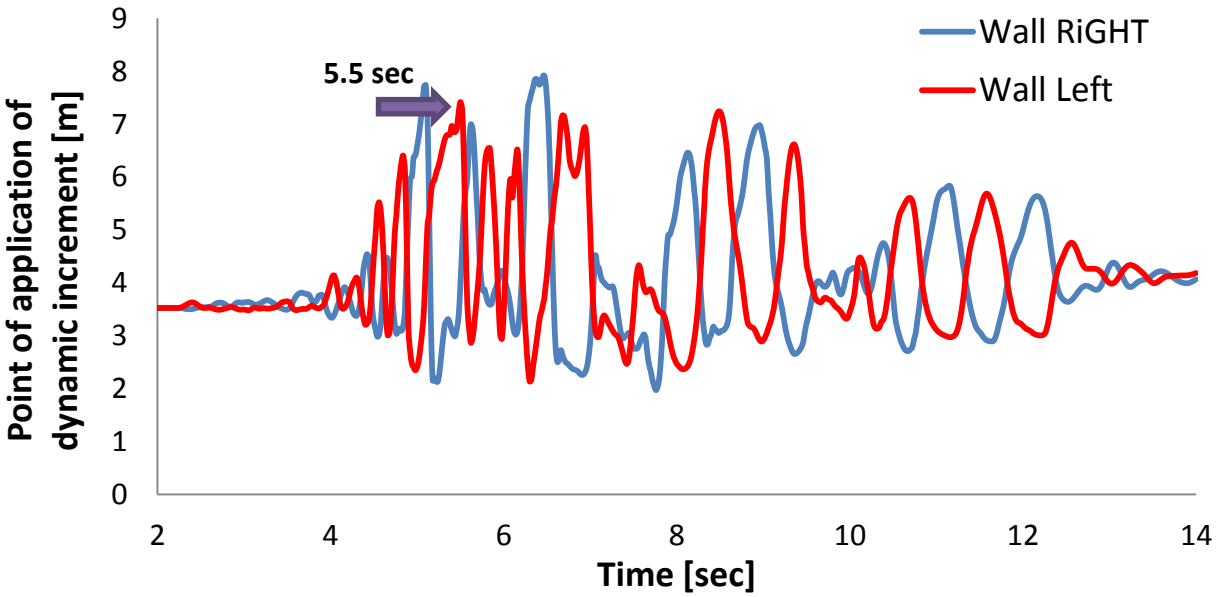

Fig. 2.174. Point of application of dynamic increment on the left and right wall when subjected to Kalamata Seismic excitation with peak ground acceleration 0.6g

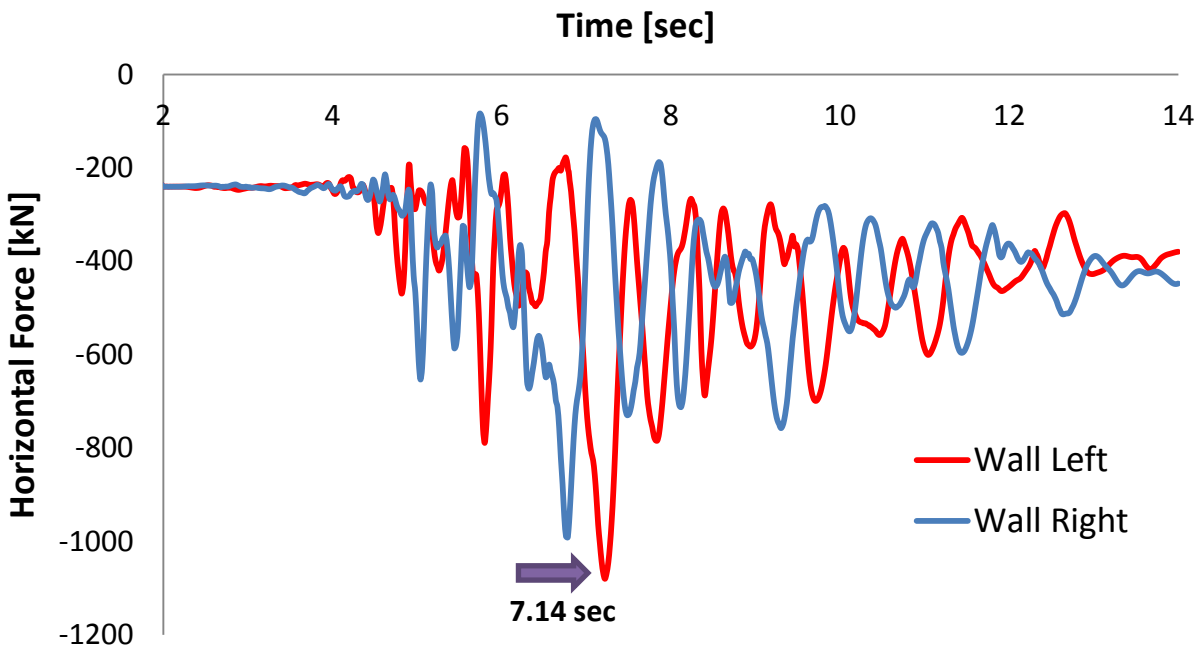

Fig. 2.175. Horizontal force-time history of the left and right wall when subjected to Kalamata Seismic excitation with peak ground acceleration 0.9 g.

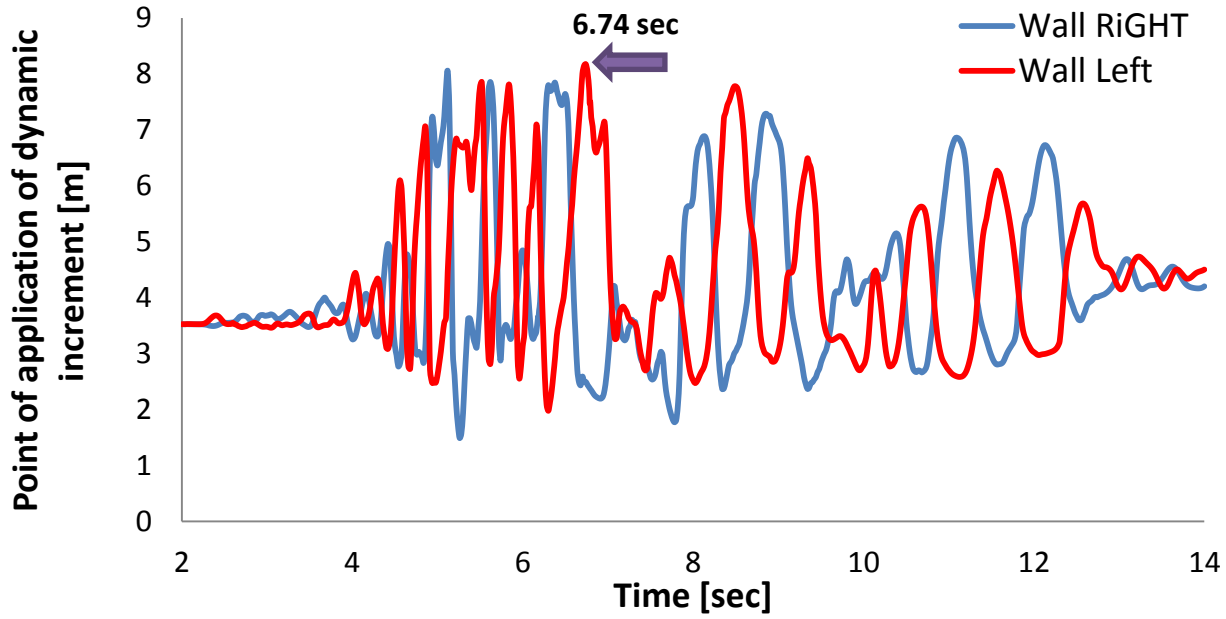

Fig. 2.176. Point of application of dynamic increment on the left and right wall when subjected to Kalamata Seismic excitation with peak ground acceleration 0.9 g.

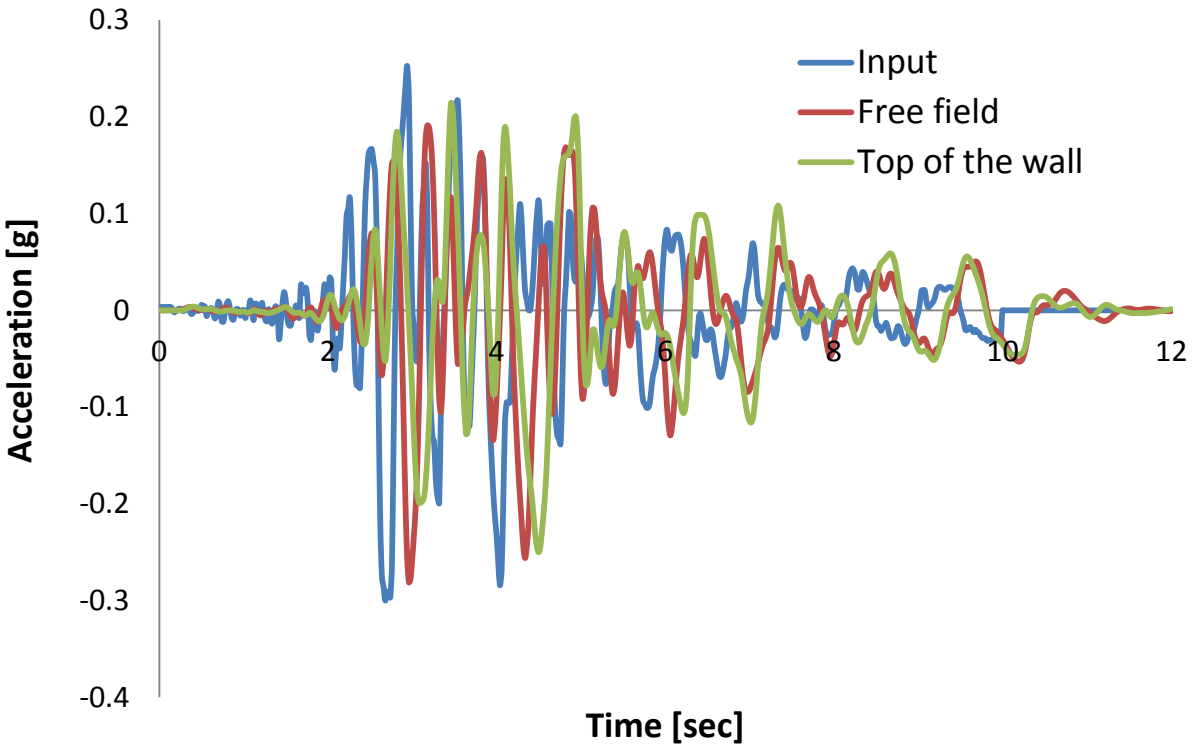

Fig. 2.177. Comparison of input acceleration and computed at the top of the left wall and top of the free field when subjected to Kalamata Seismic excitation with peak acceleration 0.3g.

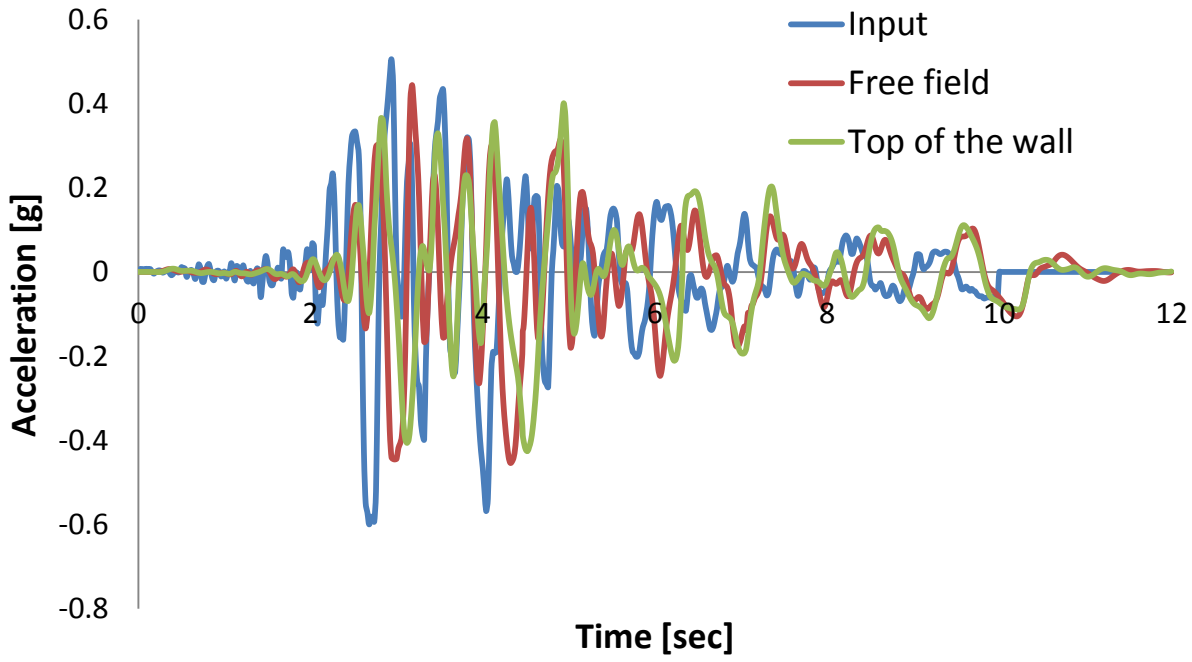

Fig. 2.178. Comparison of input acceleration and computed at the top of the left wall and top of the free field when subjected to Kalamata Seismic excitation with peak acceleration 0.6 g.

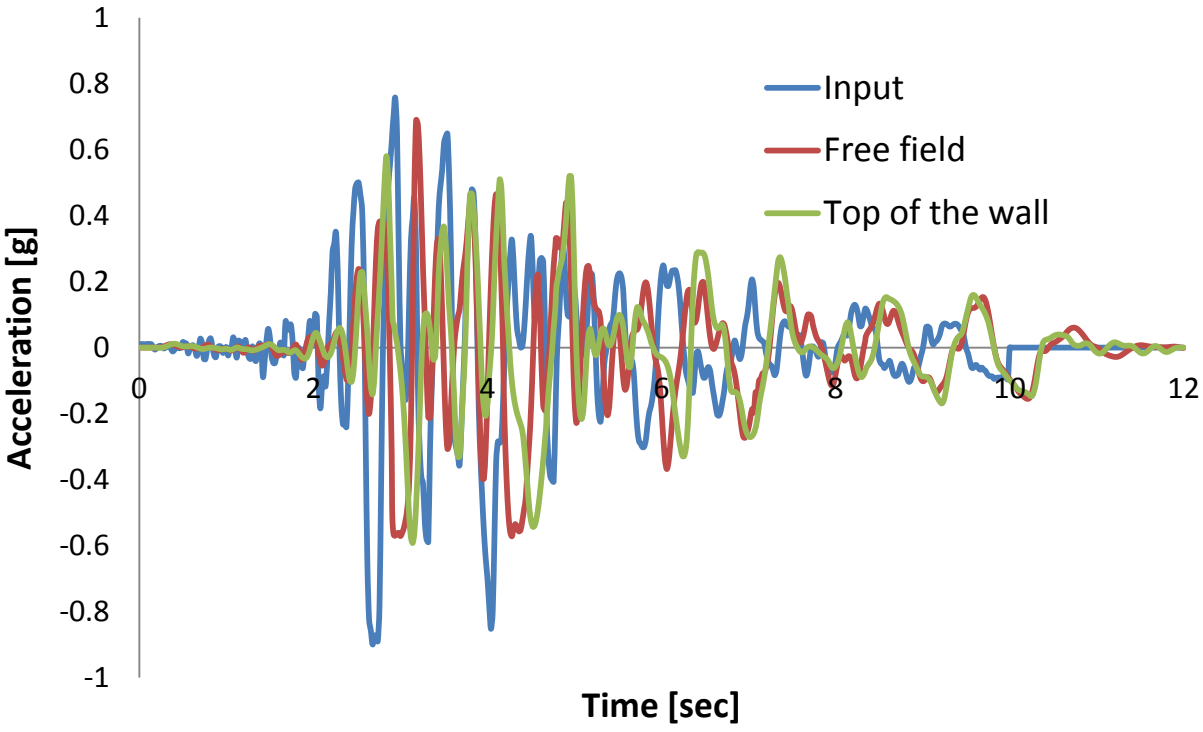

Fig. 2.179. Comparison of input acceleration and computed at the top of the left wall and top of the free field when subjected to Kalamata Seismic excitation with peak acceleration 0.9g.

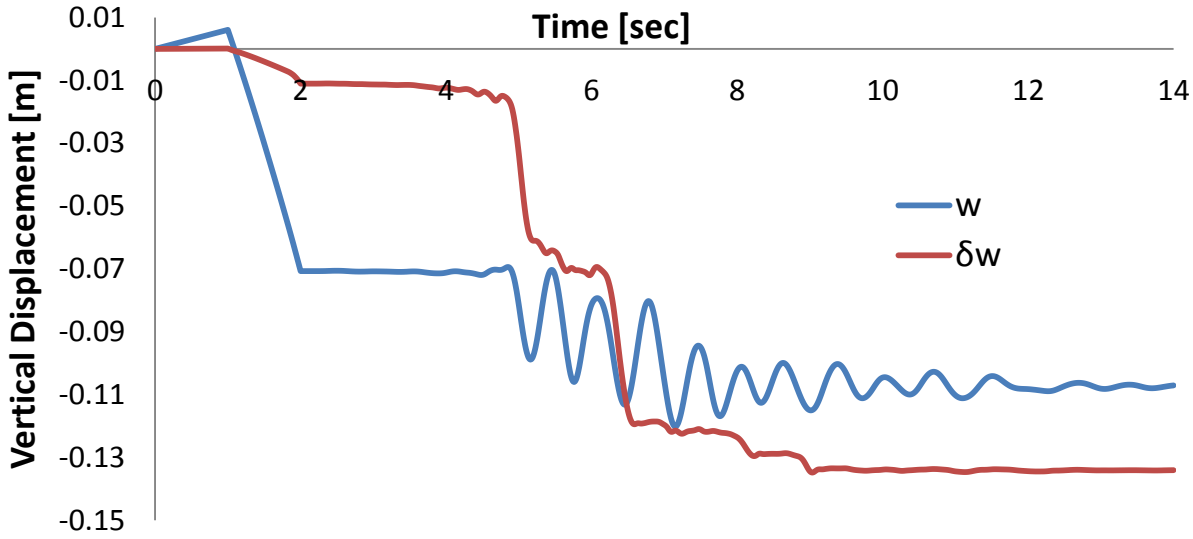

Fig. 2.180. Vertical displacement-time history of the left wall when subjected to Kalamata Seismic excitation with peak acceleration 0.3g.

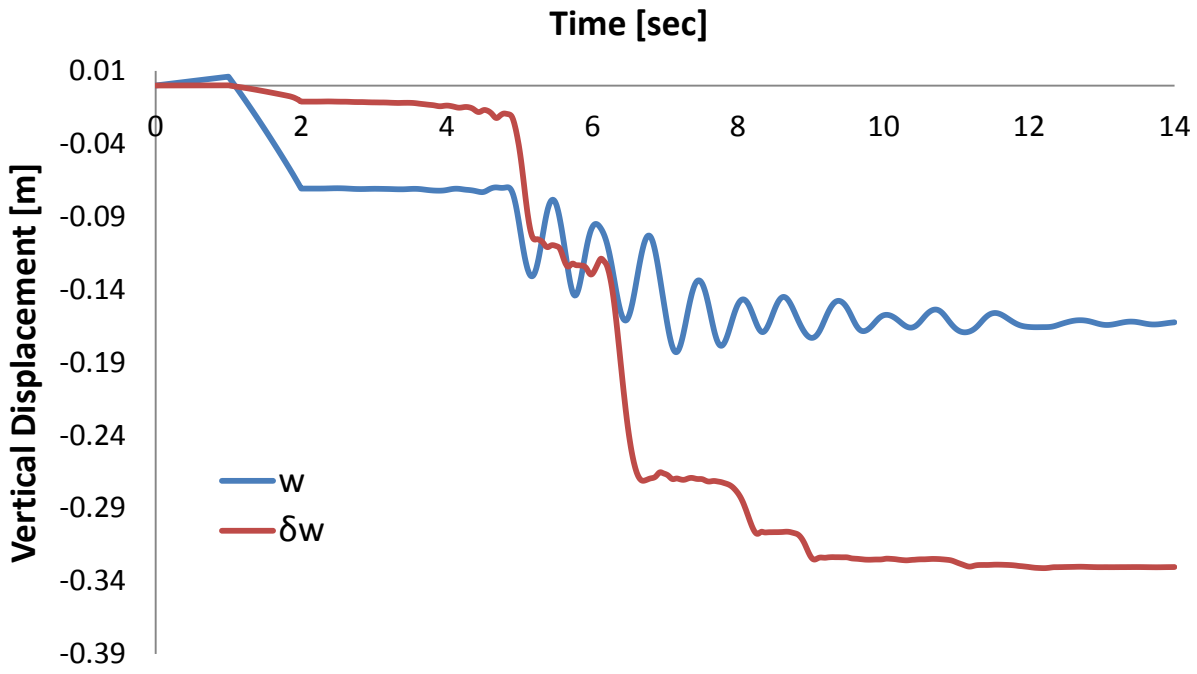

Fig. 2.181. Vertical displacement-time history of the left wall when subjected to Kalamata Seismic excitation with peak acceleration 0.6g.

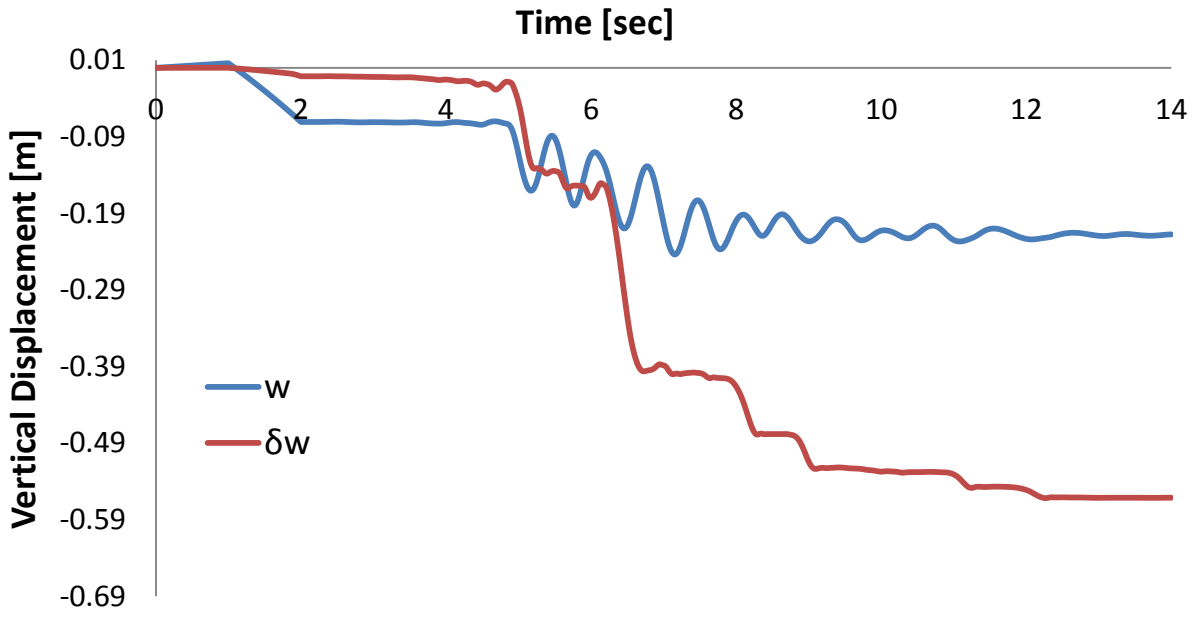

Fig. 2.182. Vertical displacement-time history of the left wall when subjected to Kalamata Seismic excitation with peak acceleration 0.9g.

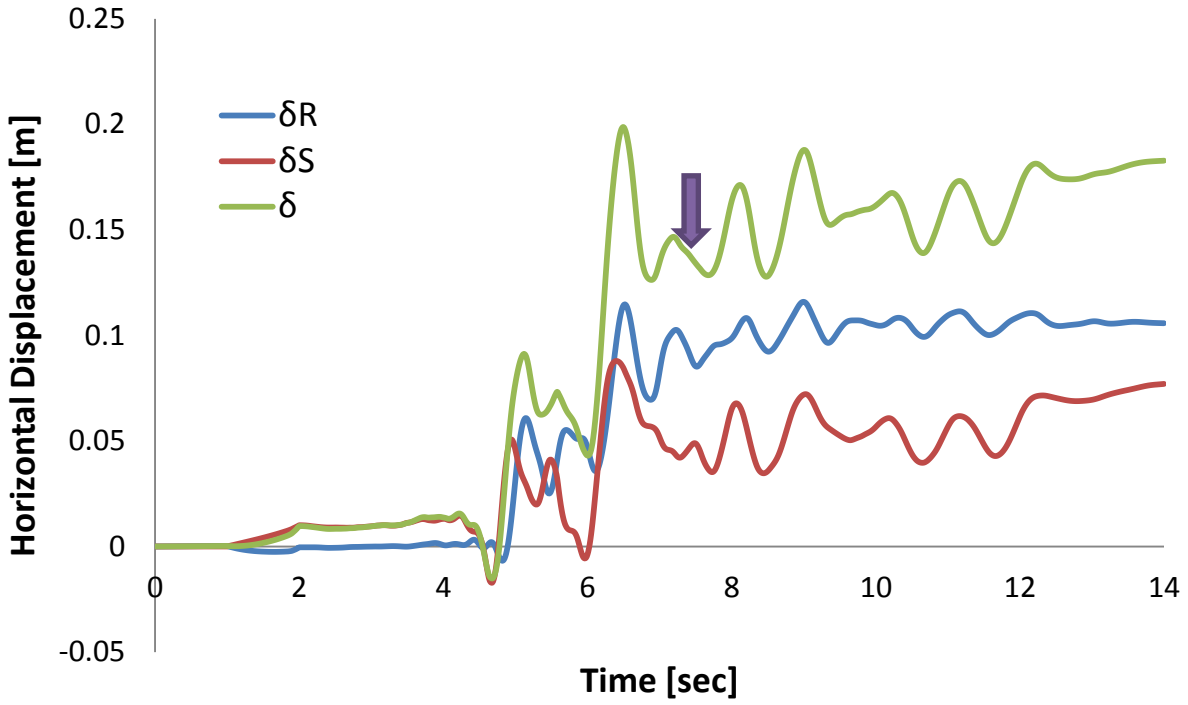

Fig. 2.183. Horizontal displacement-time history of the left wall when subjected to Kalamata Seismic excitation with peak acceleration 0.3g.

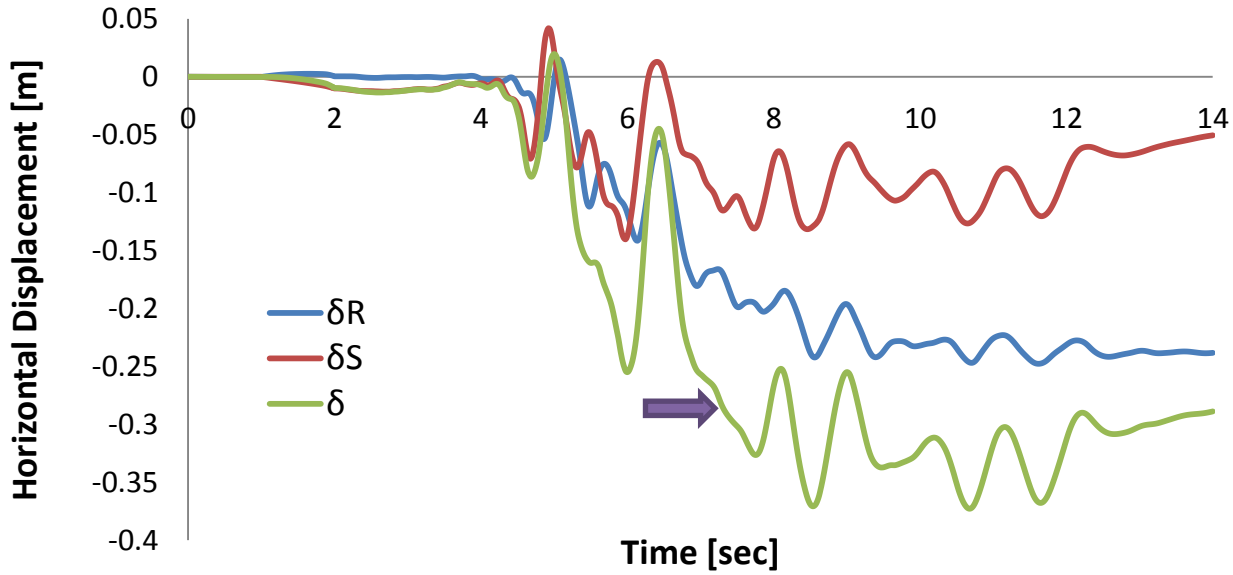

Fig. 2.184. Horizontal displacement-time history of the left wall when subjected to Kalamata Seismic excitation with peak acceleration 0.6g.

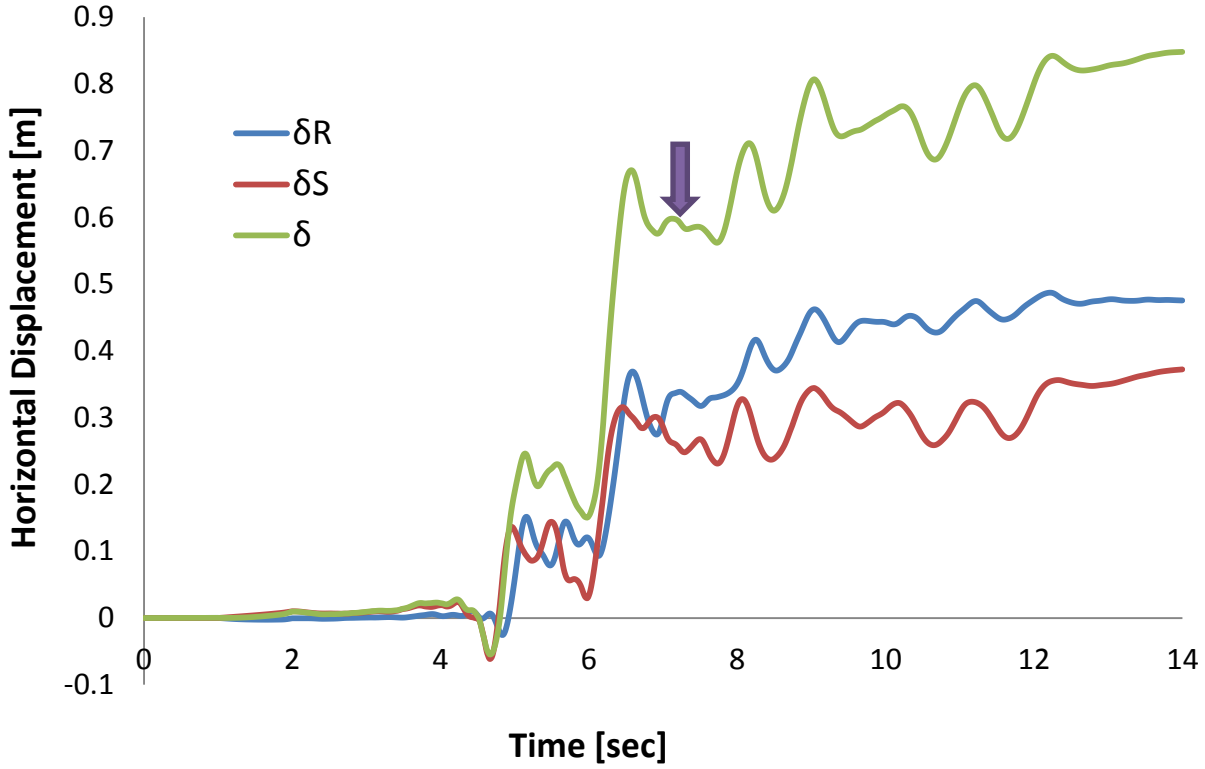

Fig. 2.185. Horizontal displacement-time history of the left wall when subjected to Kalamata Seismic excitation with peak acceleration 0.9g.

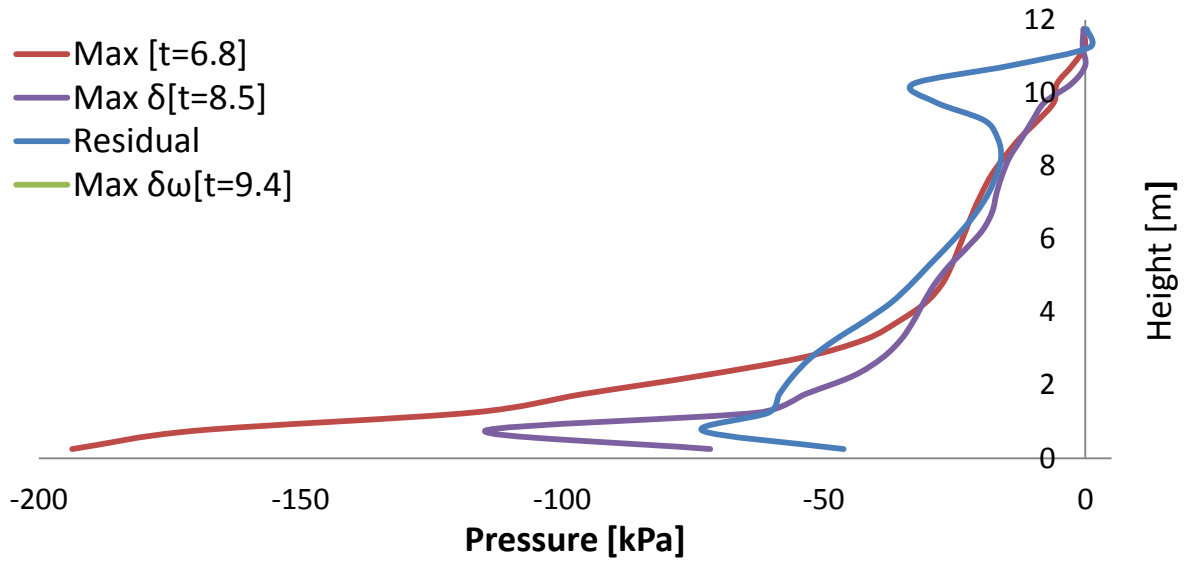

Fig. 2.186. Earth pressures profiles on the right wall at different moments when subjected to Kalamata Seismic excitation with peak ground acceleration 0.3g.

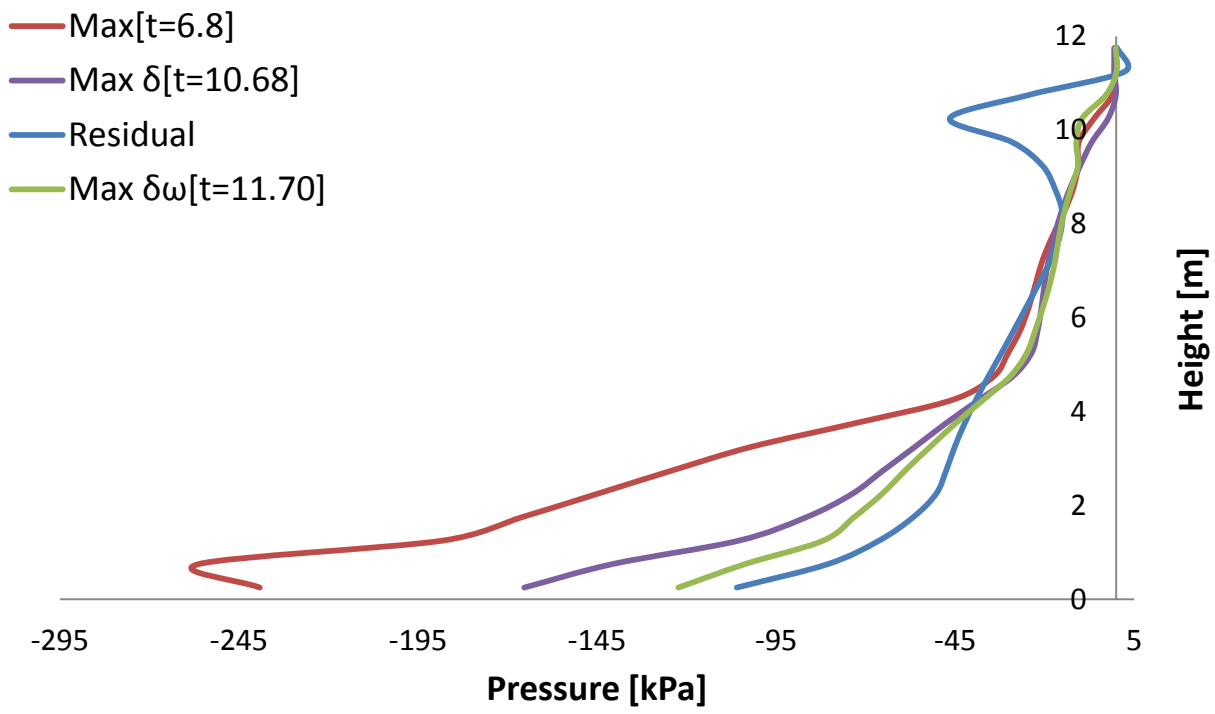

Fig. 2.187. Earth pressures profiles on the right wall at different moments when subjected to Kalamata Seismic excitation with peak ground acceleration 0.6g.

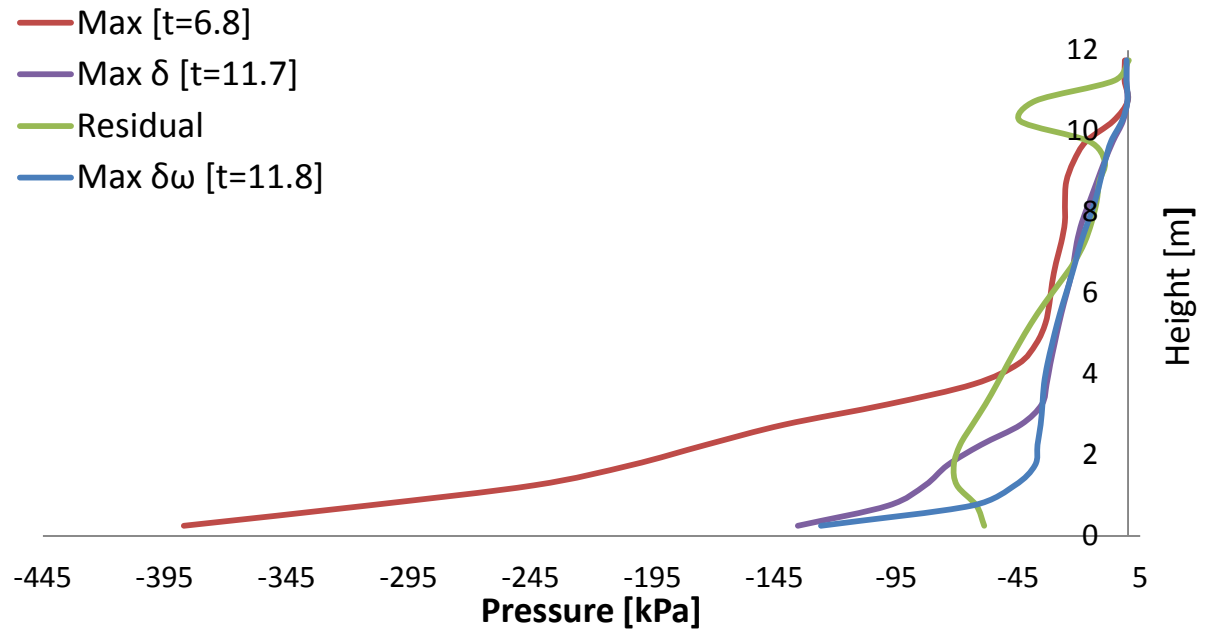

Fig. 2.188. Earth pressures profiles on the right wall at different moments when subjected to Kalamata Seismic excitation with peak ground acceleration 0.9g.

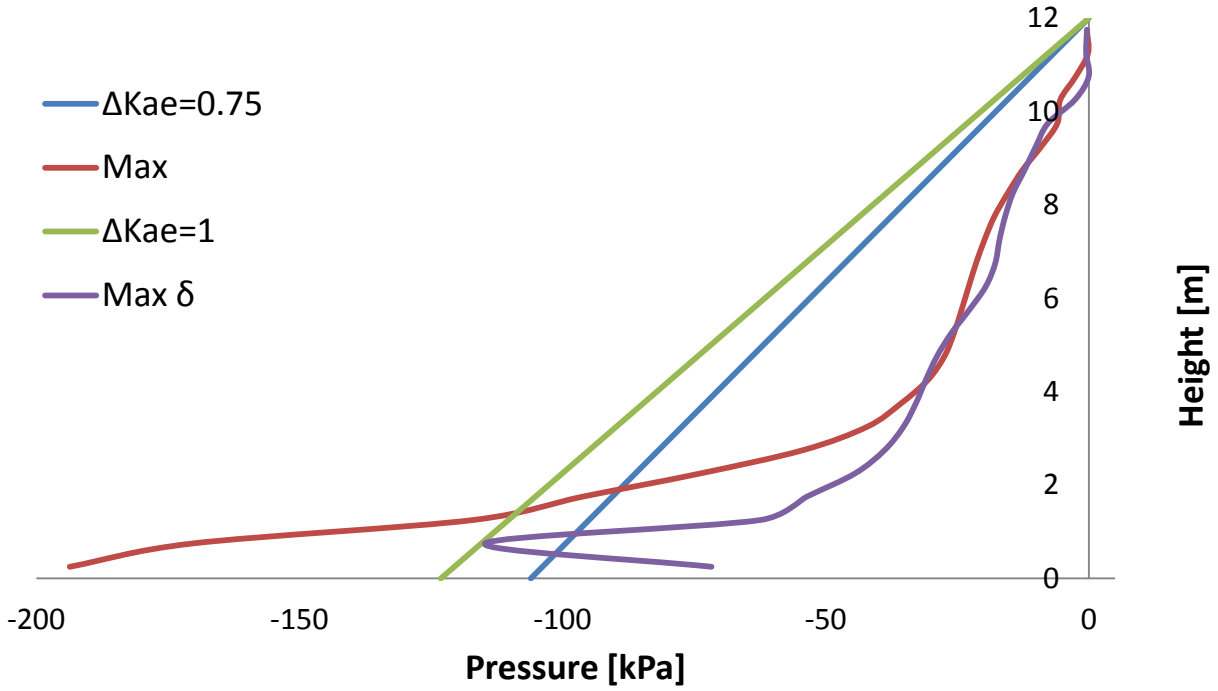

Fig. 2.189. Earth pressure profiles computed in ABAQUS and estimated using the M-O when the right wall is subjected to the Kalamata Seismic excitation with peak acceleration 0.3g.

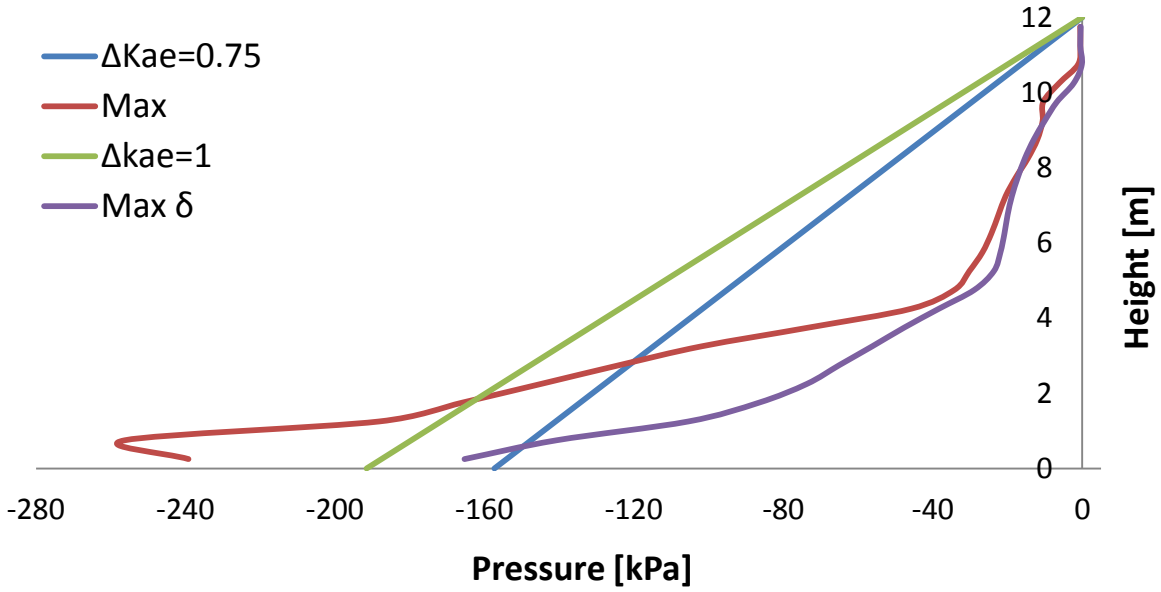

Fig. 2.190. Earth pressure profiles computed in ABAQUS and estimated using the M-O when the right wall is subjected to the Kalamata Seismic excitation with peak acceleration 0.6g.

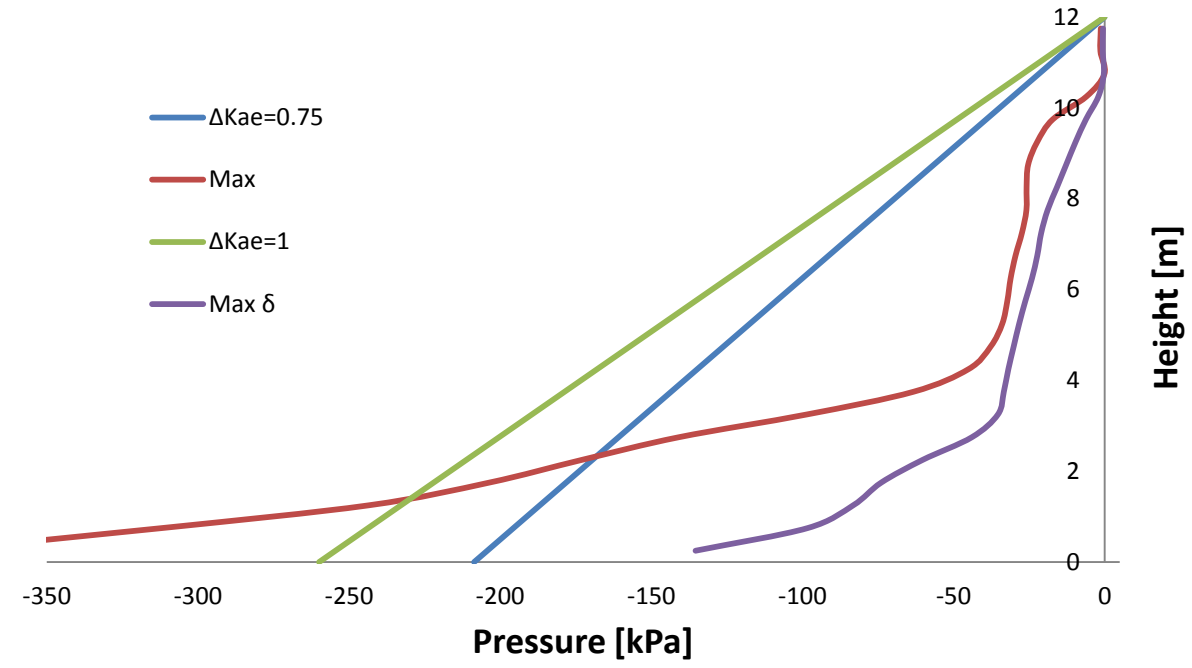

Fig. 2.191. Earth pressure profiles computed in ABAQUS and estimated using the M-O when the right wall is subjected to the Kalamata Seismic excitation with peak acceleration 0.9g.

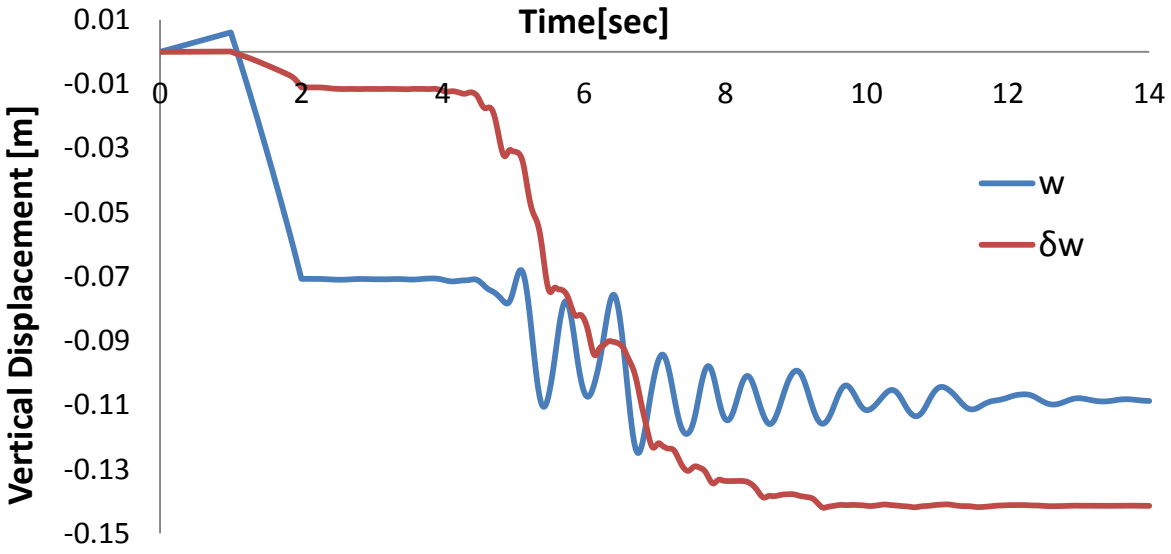

Fig. 2.192. Vertical displacement-time history of the right wall when subjected to Kalamata seismic excitation with peak acceleration 0.3g.

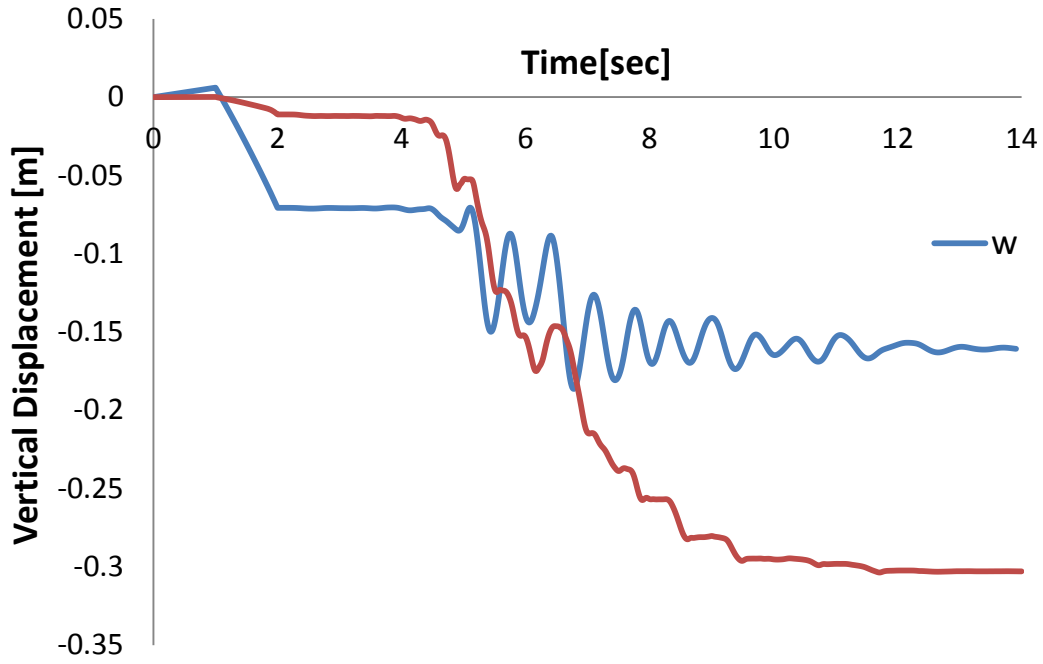

Fig. 2.193. Vertical displacement-time history of the right wall when subjected to Kalamata Seismic excitation with peak acceleration 0.6g.

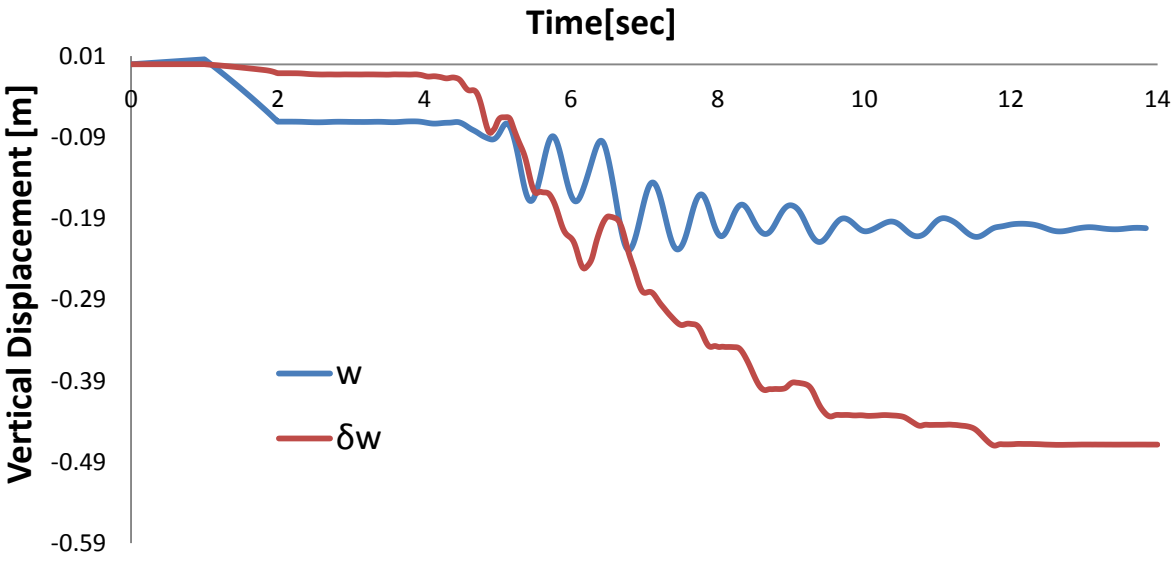

Fig. 2.194. Vertical displacement-time history of the right wall when subjected to Kalamata Seismic excitation with peak acceleration 0.9g.

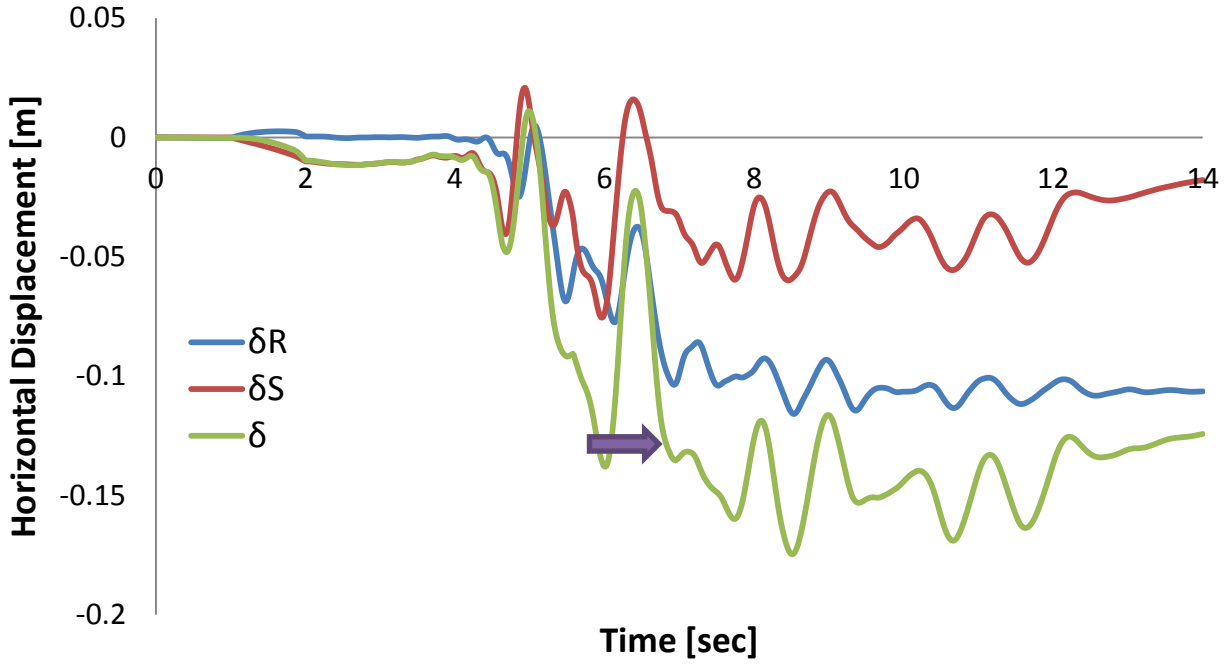

Fig. 2.195. Horizontal displacement-time history of the right wall when subjected to Kalamata Seismic excitation with peak acceleration 0.3g.

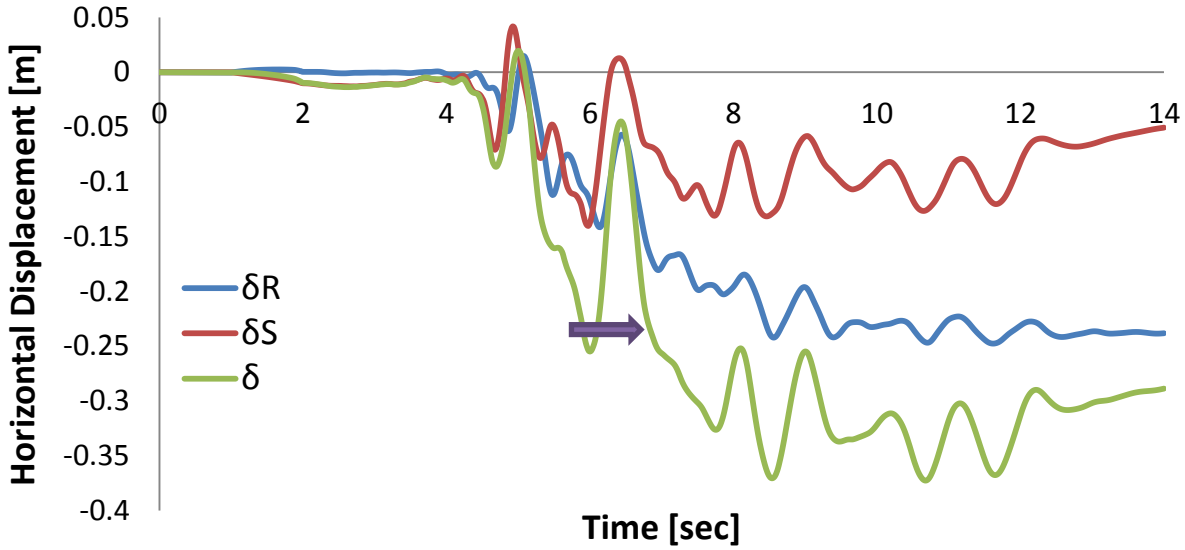

Fig. 2.196. Horizontal displacement-time history of the right wall when subjected to Kalamata Seismic excitation with peak acceleration 0.6g.

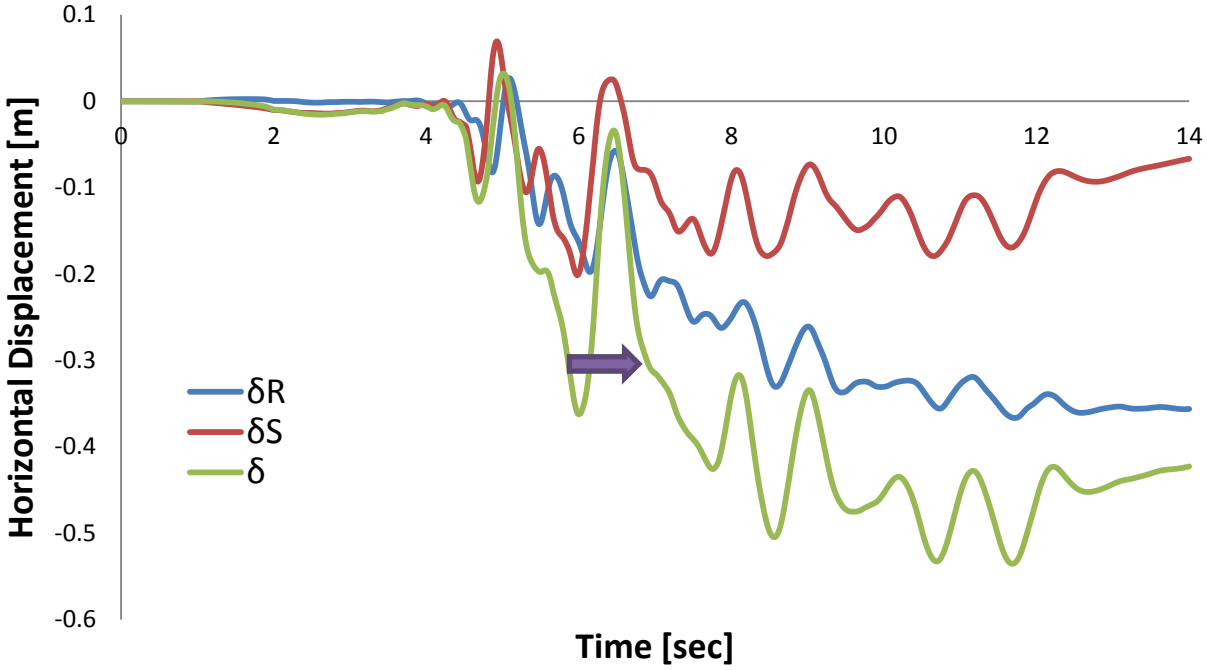

Fig. 2.197. Horizontal displacement-time history of the right wall when subjected to Kalamata Seismic excitation with peak acceleration 0.9g.

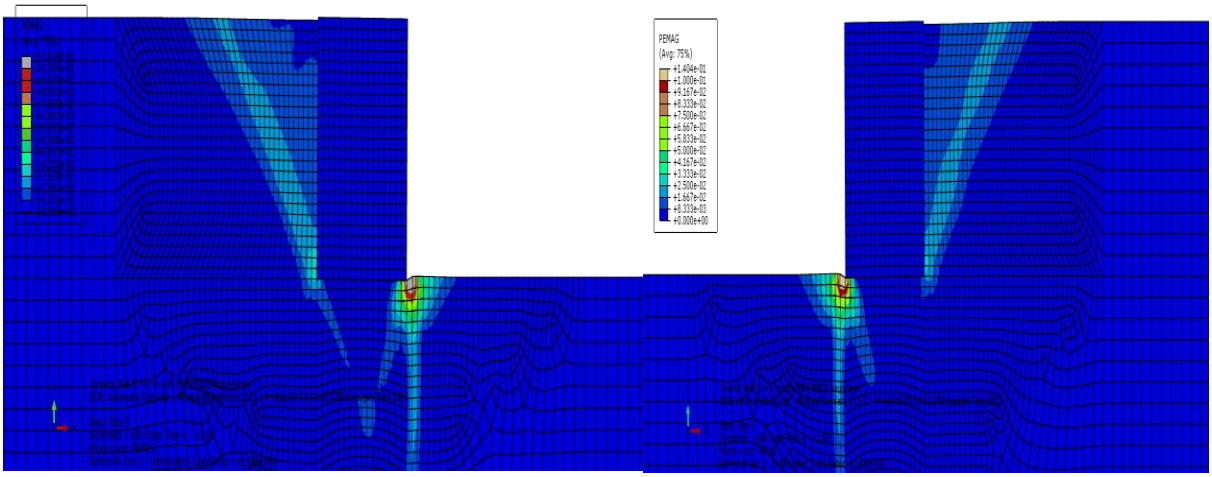

Fig. 2.198. Plastic strain contours at the end of seismic shaking (a)Left wall (b)Right wall when subjected to Kalamata seismic excitation with peak acceleration 0.3g

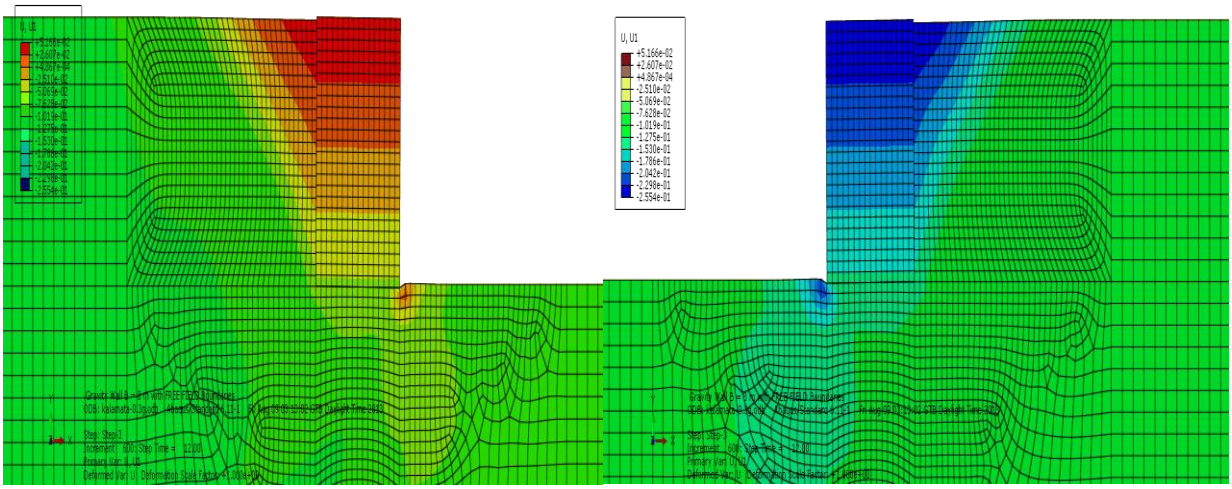

Fig. 2.199. Horizontal displacement contours at the end of the seismic excitation Kalamata PGA 0.3g.

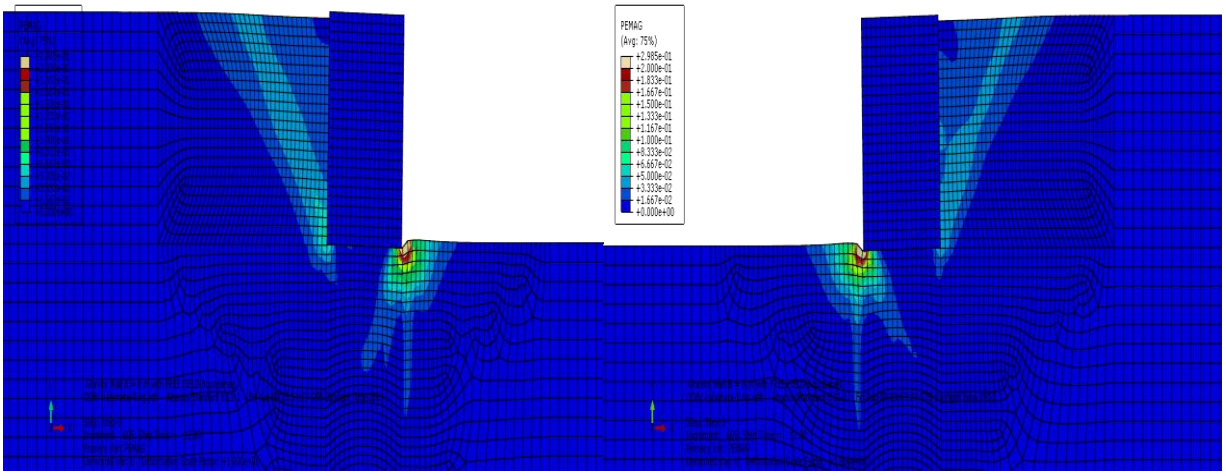

Fig. 2.200. Plastic strain contours at the end of seismic shaking (a)Left wall (b)Right wall when subjected to Kalamata seismic excitation with peak acceleration 0.6g.

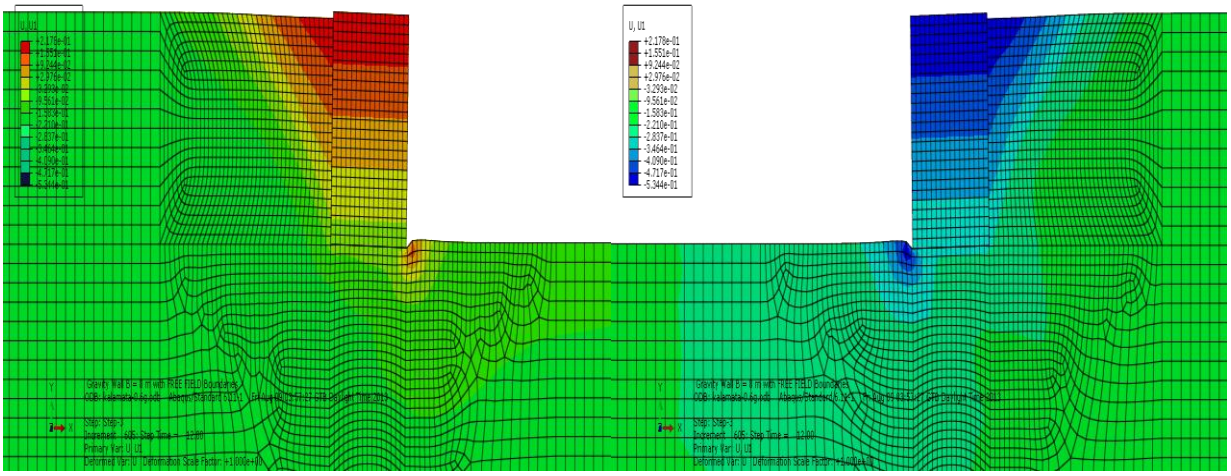

Fig. 2.201. Horizontal displacement contours at the end of the seismic excitation Kalamata PGA 0.6g.

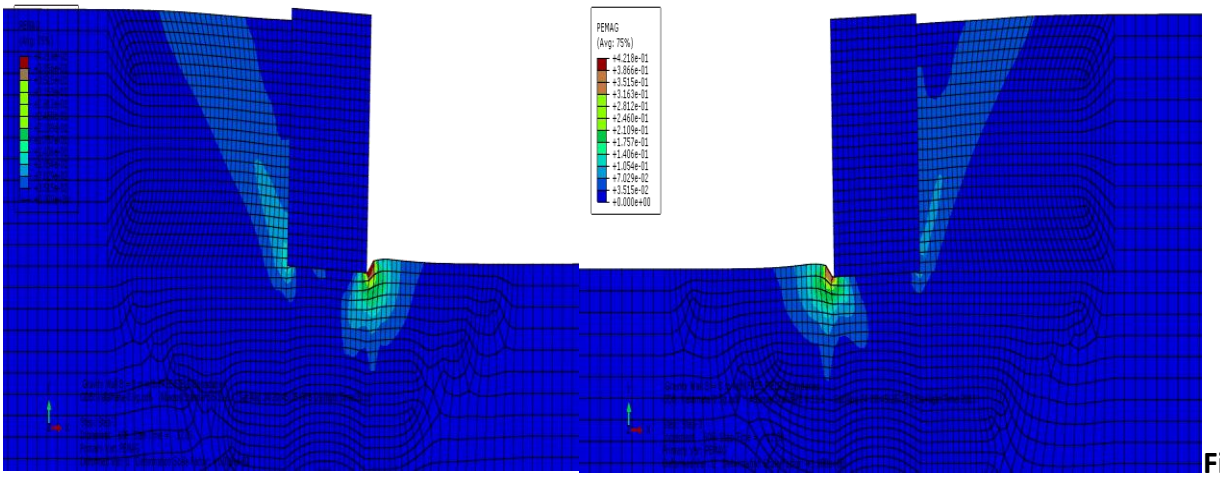

Fig. 2.202. Plastic strain contours at the end of seismic shaking (a)Left wall (b)Right wall when subjected to Kalamata seismic excitation with peak acceleration 0.9g

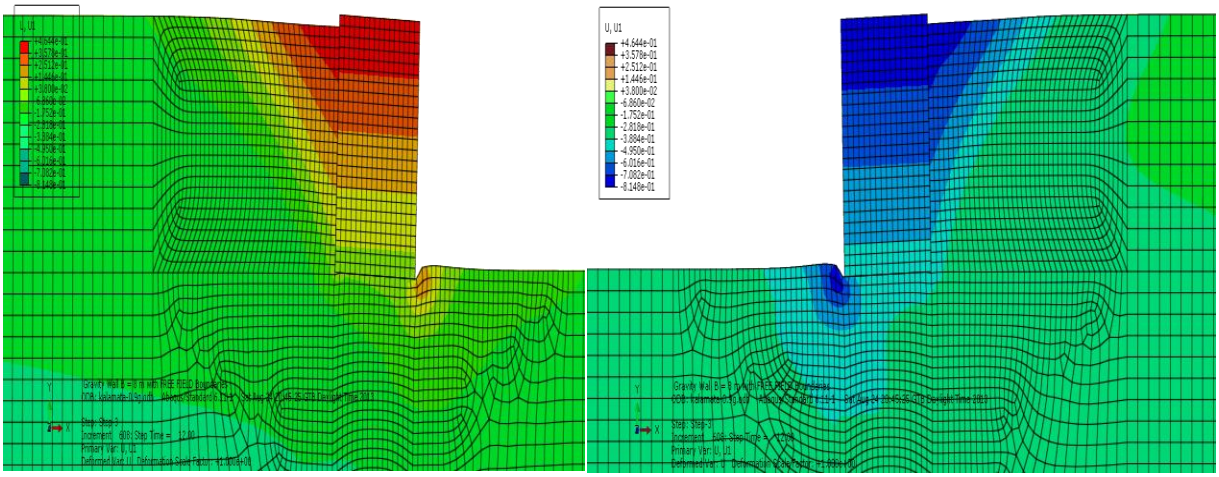

Fig. 2.203. Horizontal displacement contours at the end of the seismic excitation Kalamata PGA 0.9g.

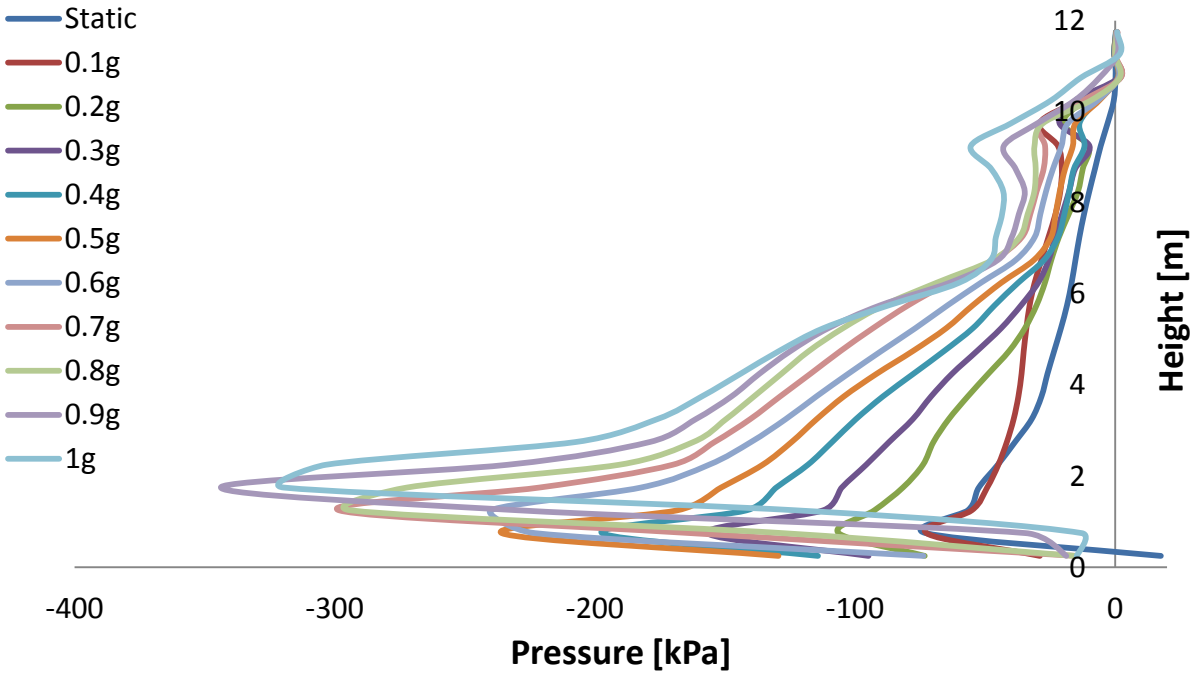

Fig. 2.204. Static and maximum earth pressure profiles for different peak accelerations on the left wall when subjected to Kalamata Seismic excitation.

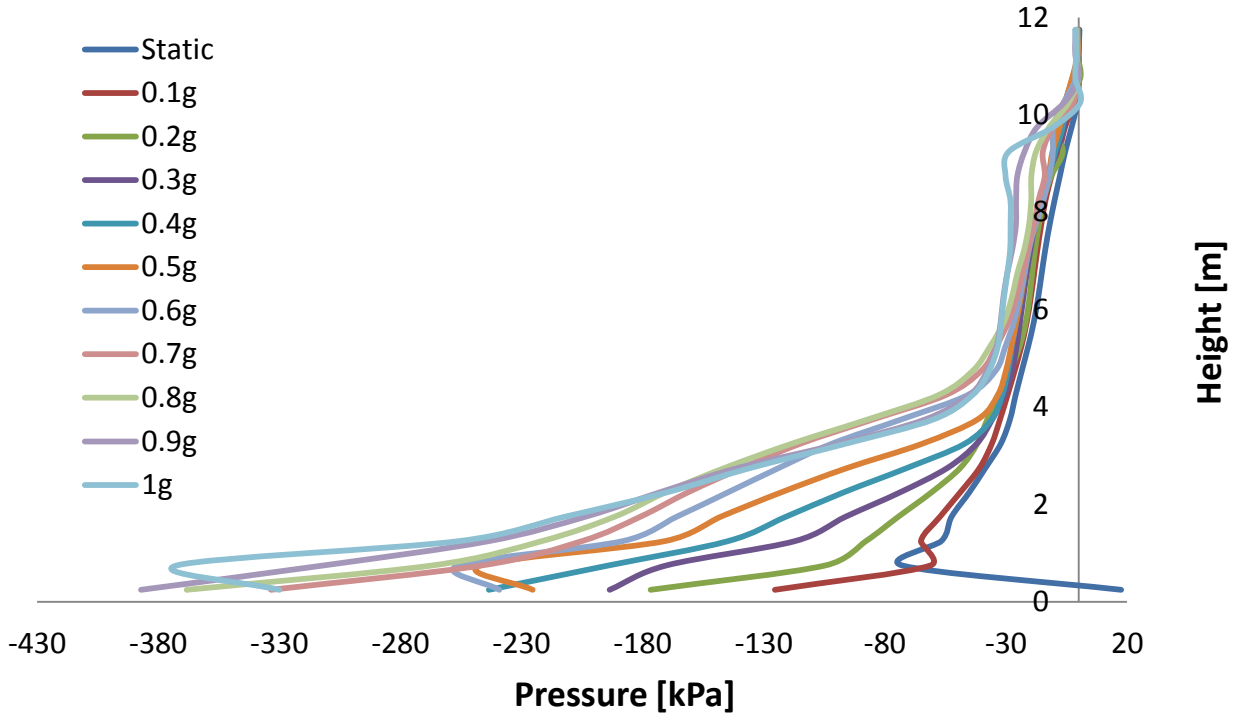

Fig. 2.205. Static and maximum earth pressure profiles for different peak accelerations on the right wall when subjected to Kalamata Seismic excitation.

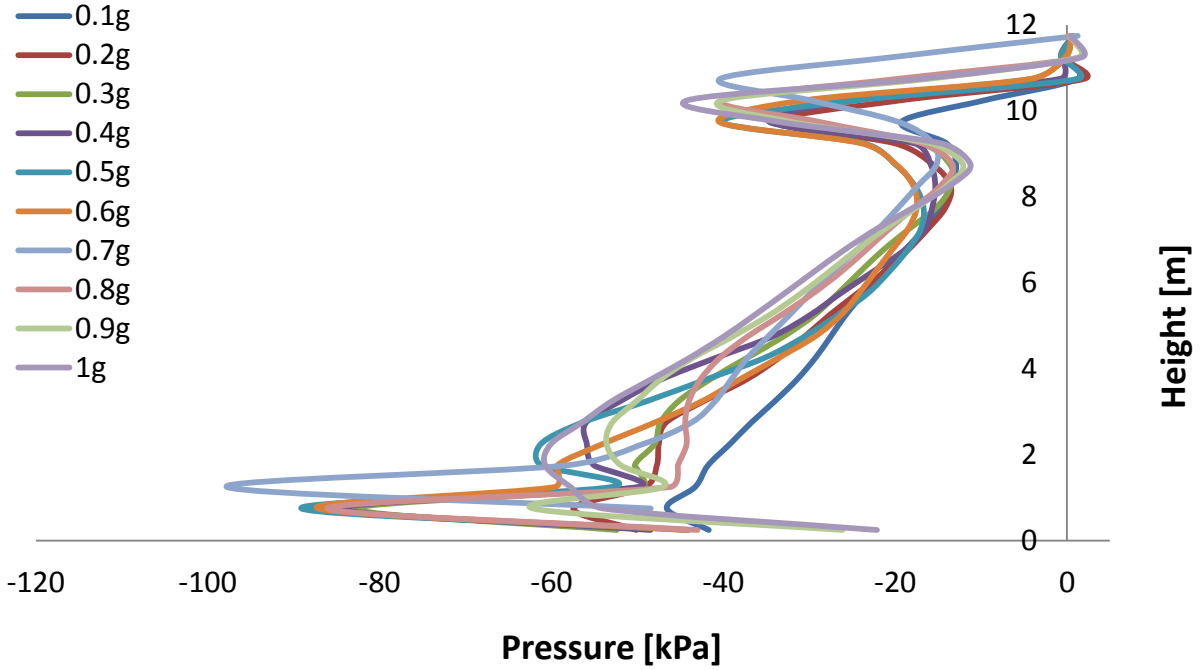

Fig. 2.206. Residual earth pressure profiles for different peak accelerations on the left wall when subjected to Kalamata seismic excitation.

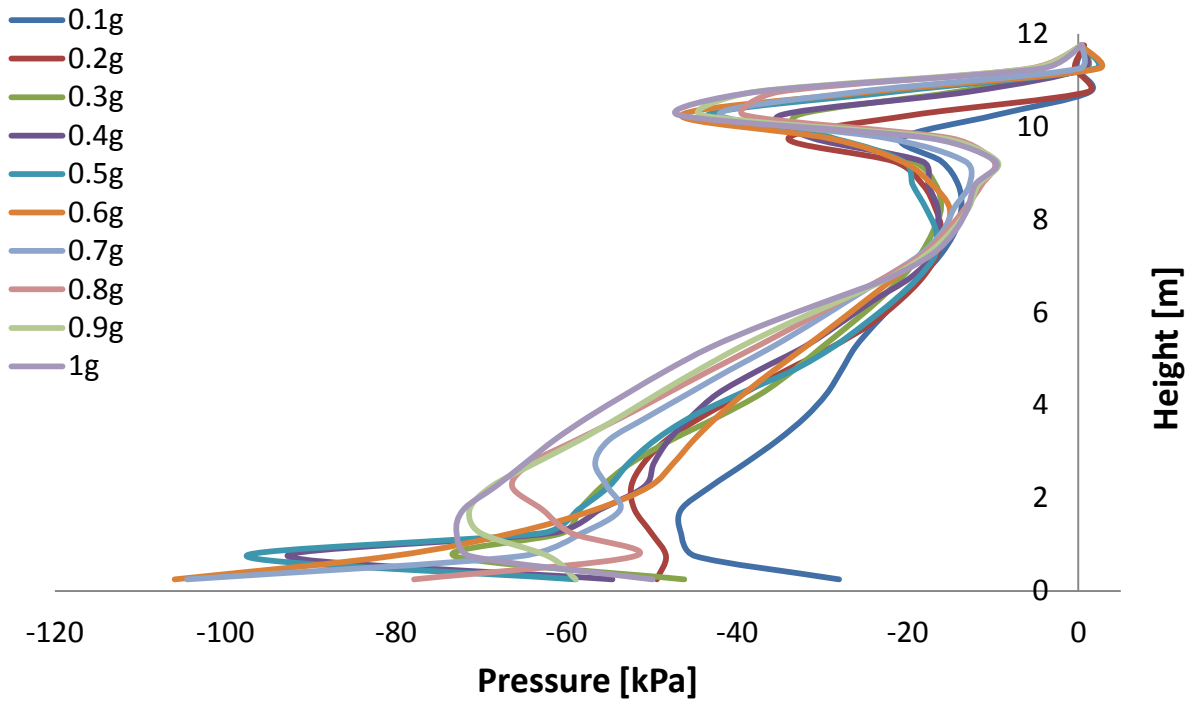

Fig. 2.207. Residual earth pressure profiles for different peak accelerations on the right wall when subjected to Kalamata Seismic excitation.

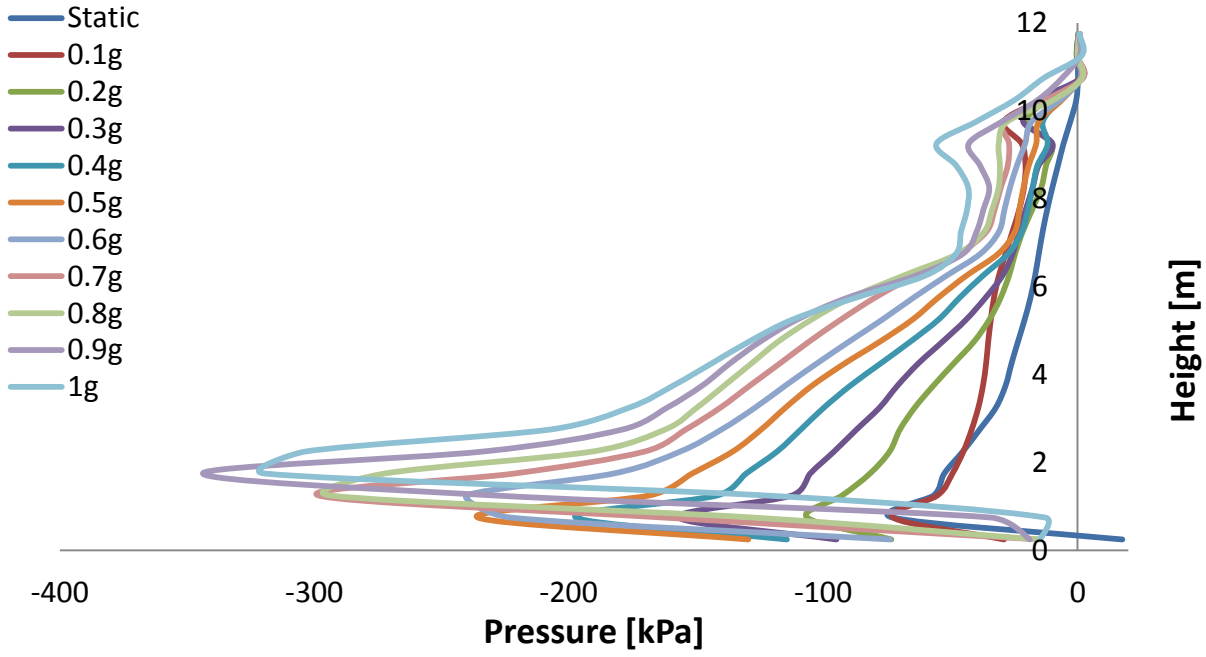

Fig. 2.208. Earth pressure profiles at maximum displacement for different peak accelerations on the left wall when subjected to Kalamata Seismic excitation.

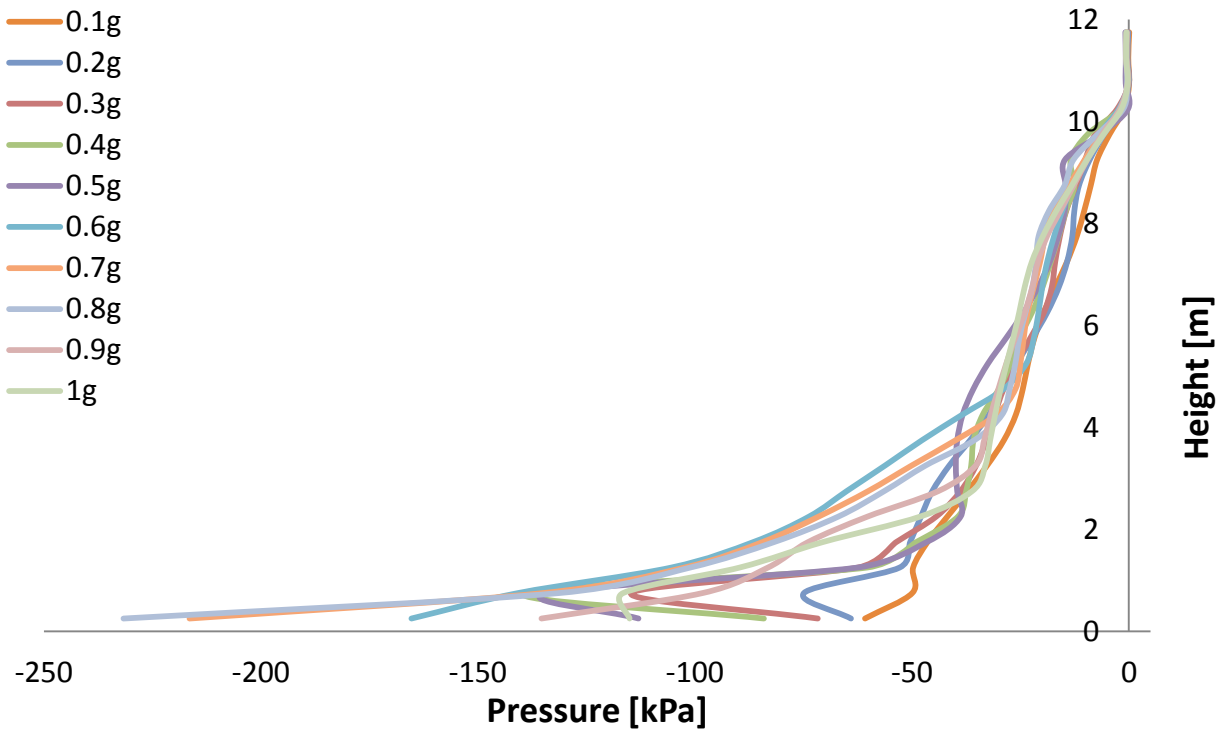

Fig. 2.209. Earth pressure profiles at maximum displacement for different peak accelerations on the right wall when subjected to Kalamata Seismic excitation.

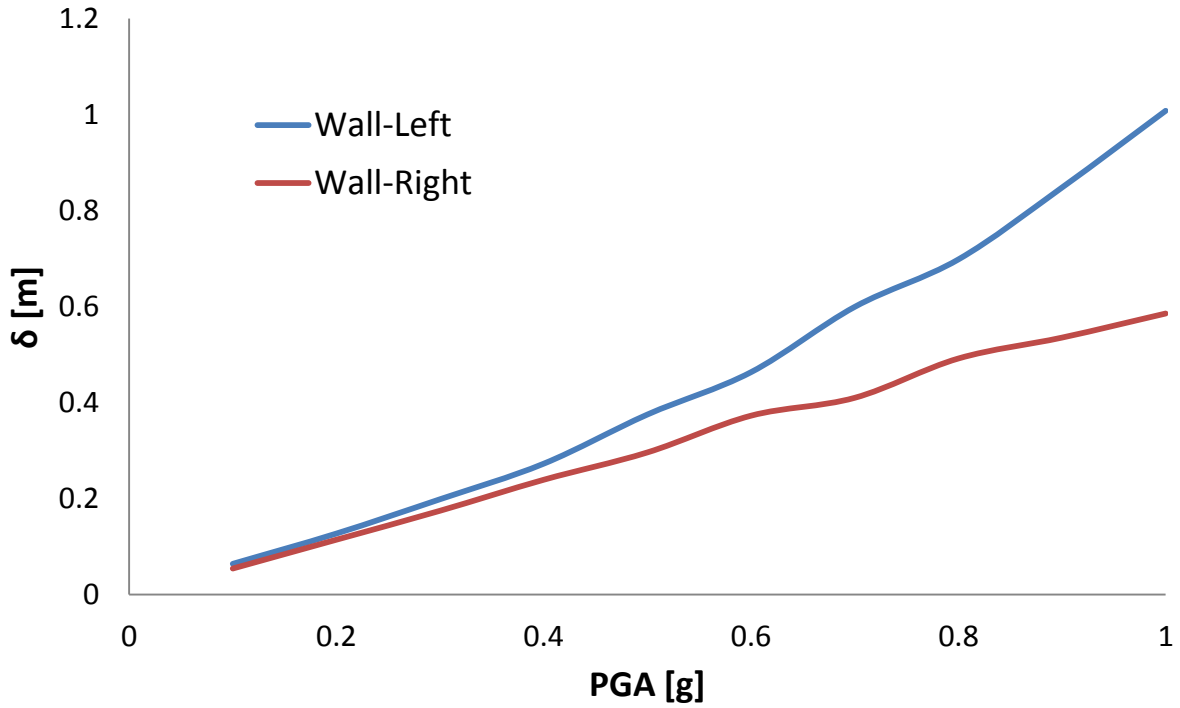

Fig. 2.210. Horizontal displacement as a function of PGA for the left and right wall when subjected to Kalamata Seismic excitation.

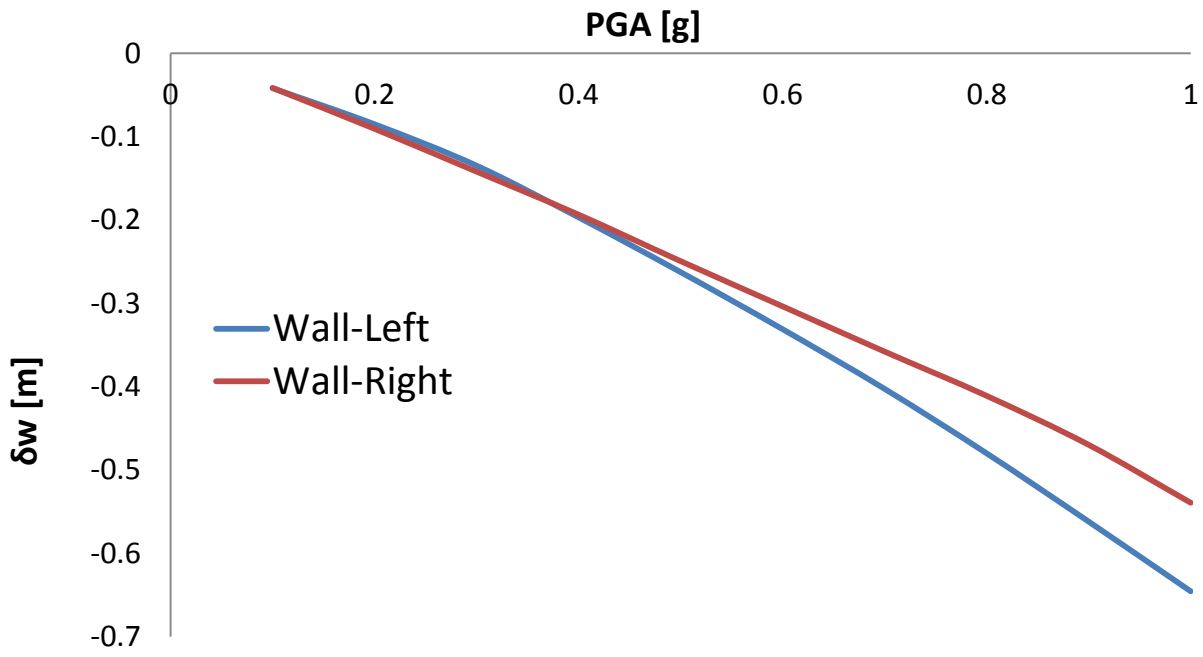

Fig. 2.211. Vertical displacement as a function of PGA for the left and right wall when subjected to Kalamata Seismic excitation.

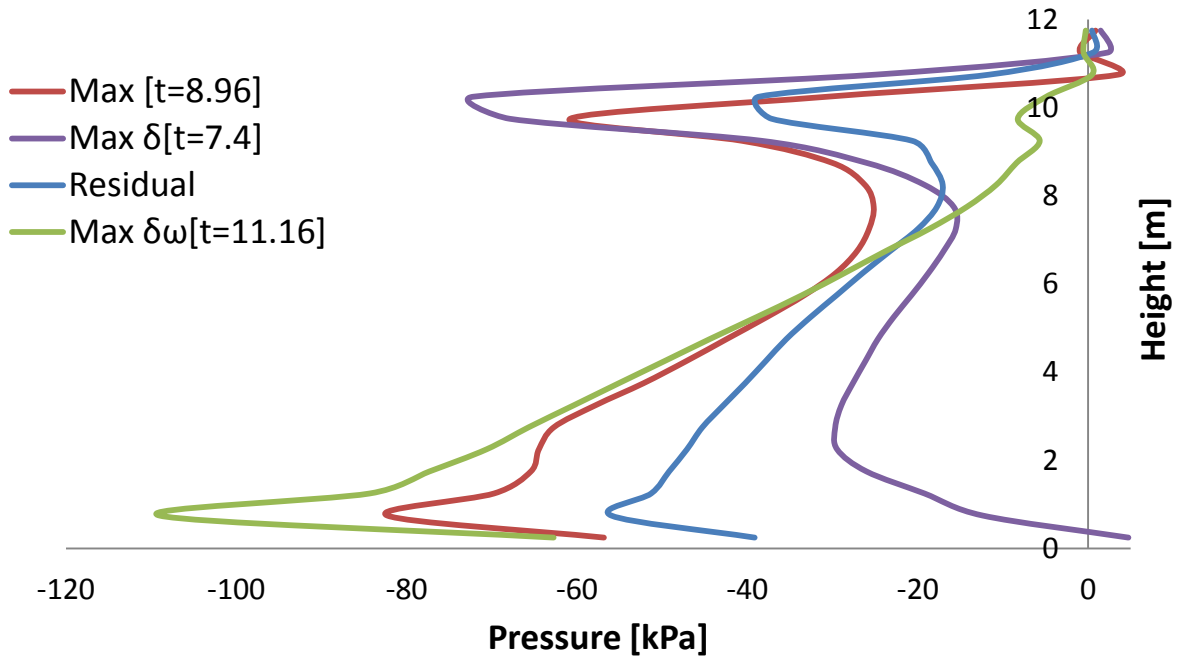

Fig. 2.212. Earth pressures profiles on the left wall at different moments when subjected to Sakarya Seismic excitation with peak ground acceleration 0.3g.

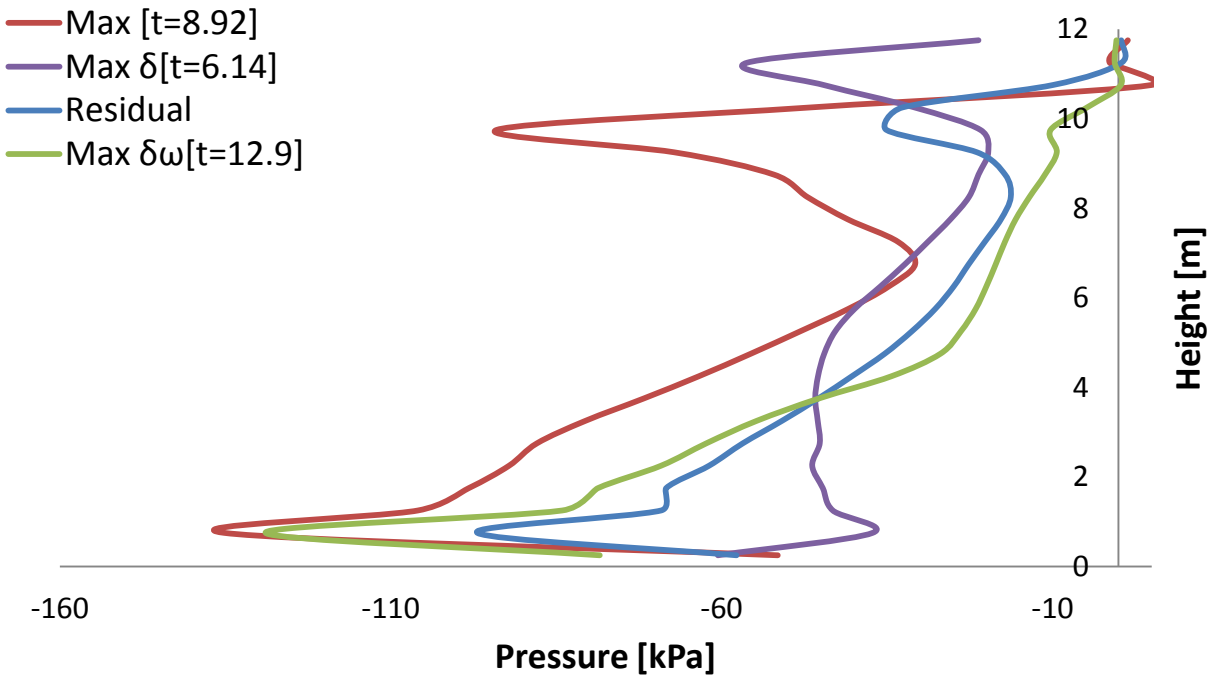

Fig. 2.213. Earth pressures profiles on the left wall at different moments when subjected to Sakarya Seismic excitation with peak ground acceleration 0.6g.

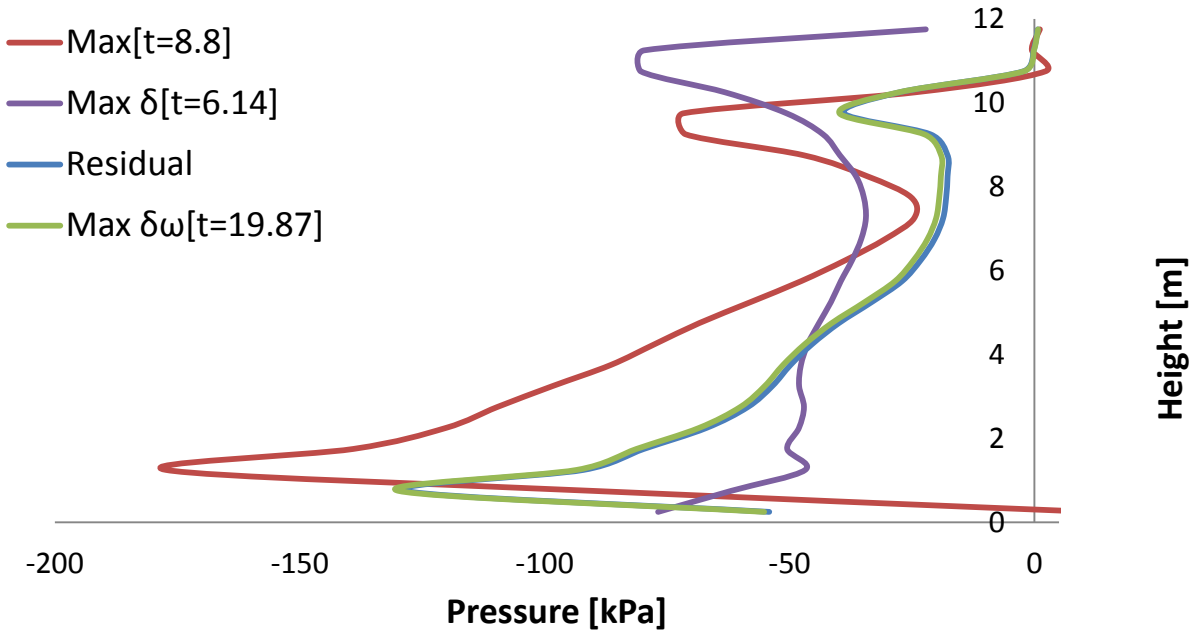

Fig. 2.214. Earth pressures profiles on the left wall at different moments when subjected to Sakarya Seismic excitation with peak ground acceleration 0.3g.

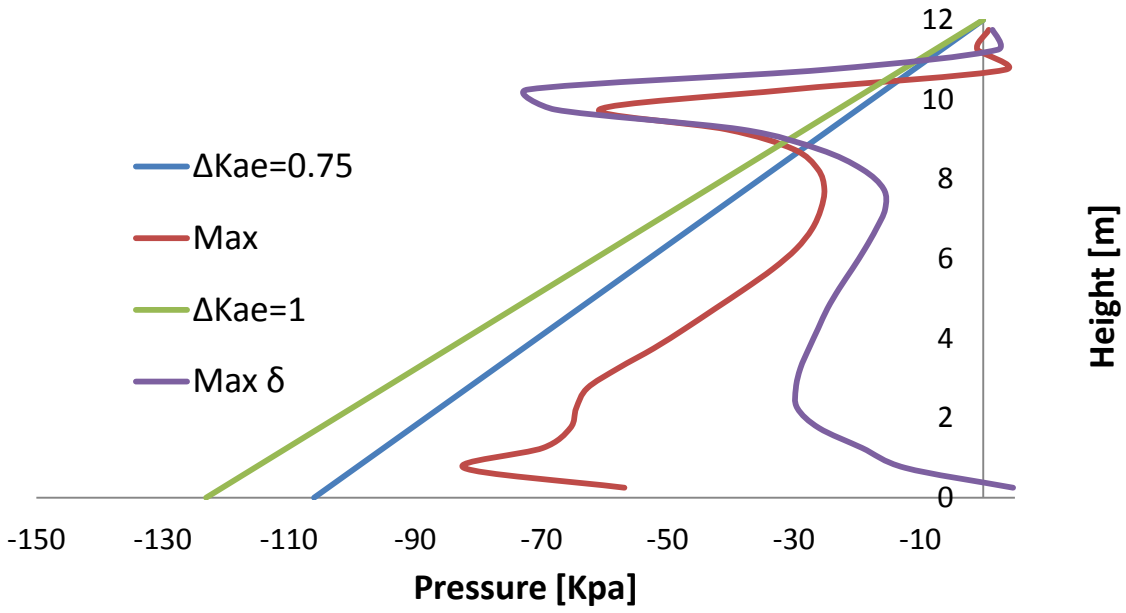

Fig. 2.215. Earth pressure profiles computed in ABAQUS and estimated using the M-O when the left wall is subjected to the Sakarya Seismic excitation with peak acceleration 0.3g.

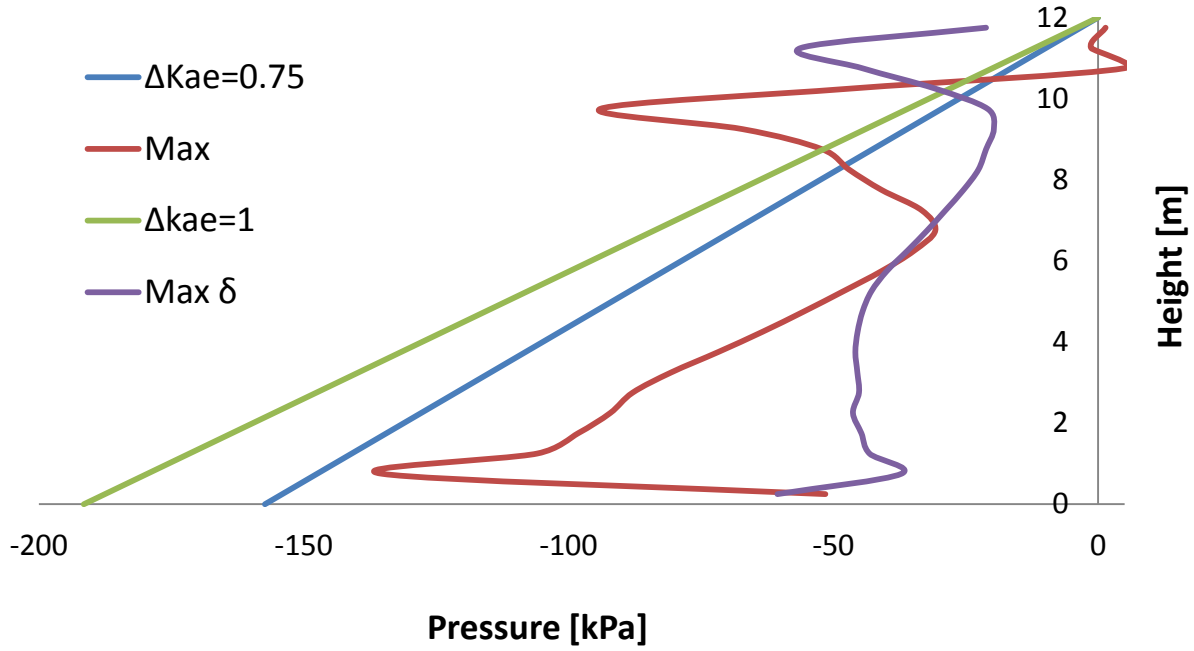

Fig. 2.216. Earth pressure profiles computed in ABAQUS and estimated using the M-O when the left wall is subjected to the Sakarya Seismic excitation with peak acceleration 0.6g.

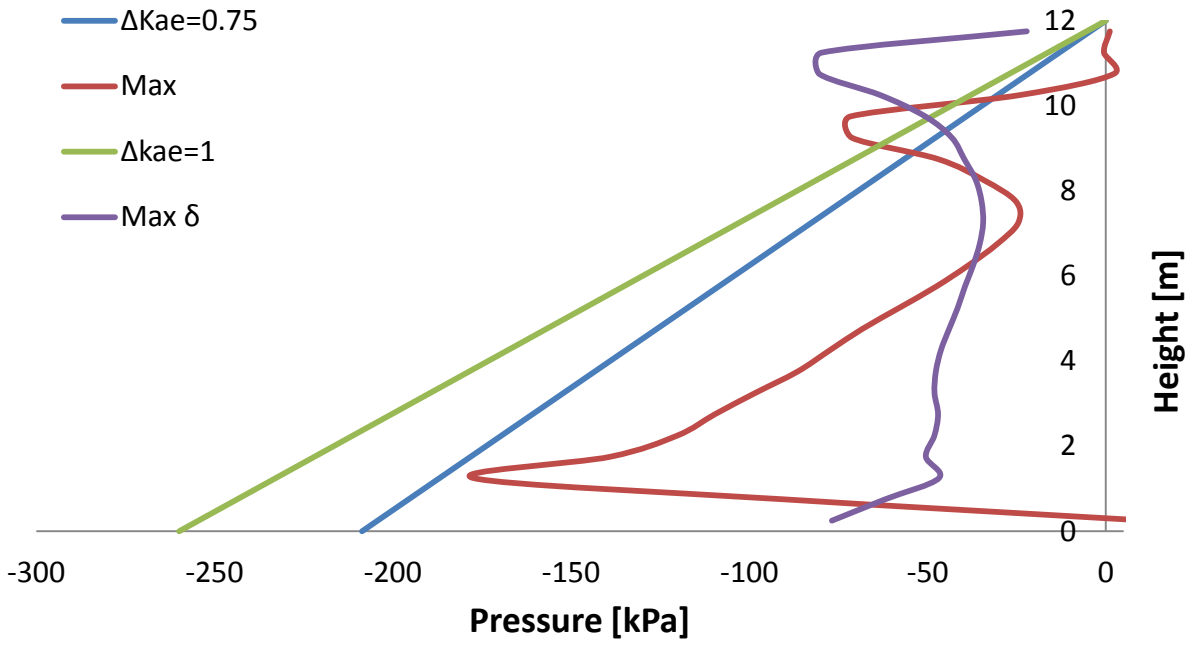

Fig. 2.217. Earth pressure profiles computed in ABAQUS and estimated using the M-O when the left wall is subjected to the Sakarya Seismic excitation with peak acceleration 0.9g.

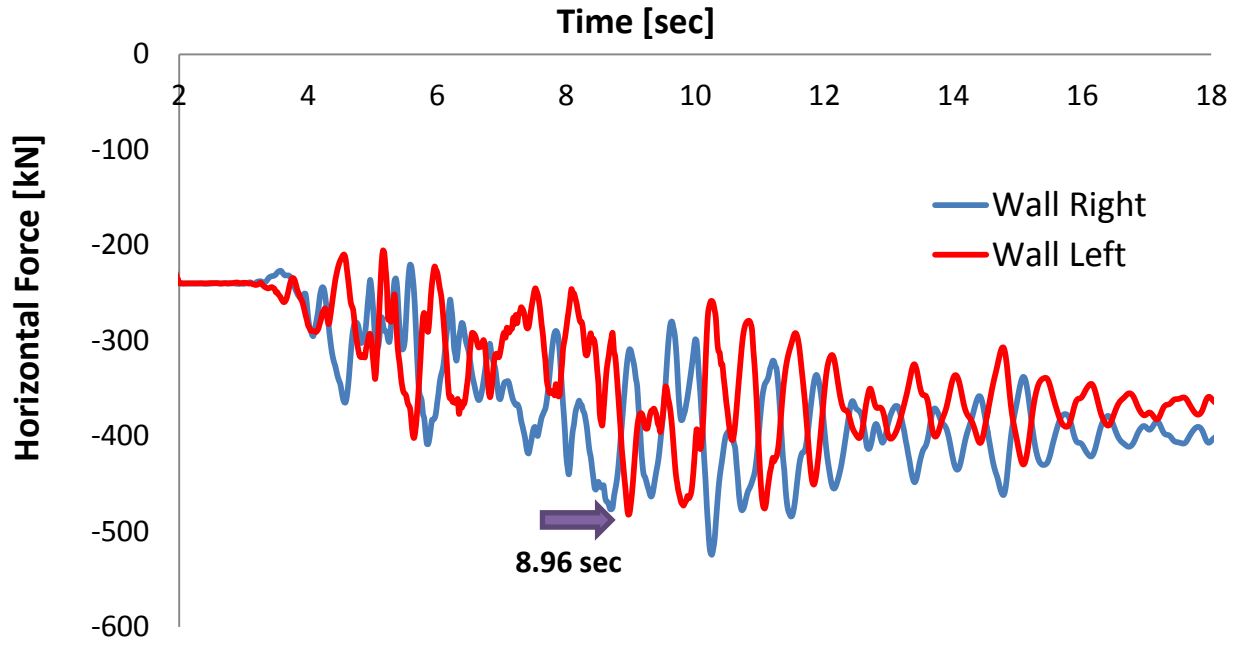

Fig. 2.218. Horizontal force-time history of the left wall when subjected to Sakarya Seismic excitation with peak ground acceleration 0.3g.

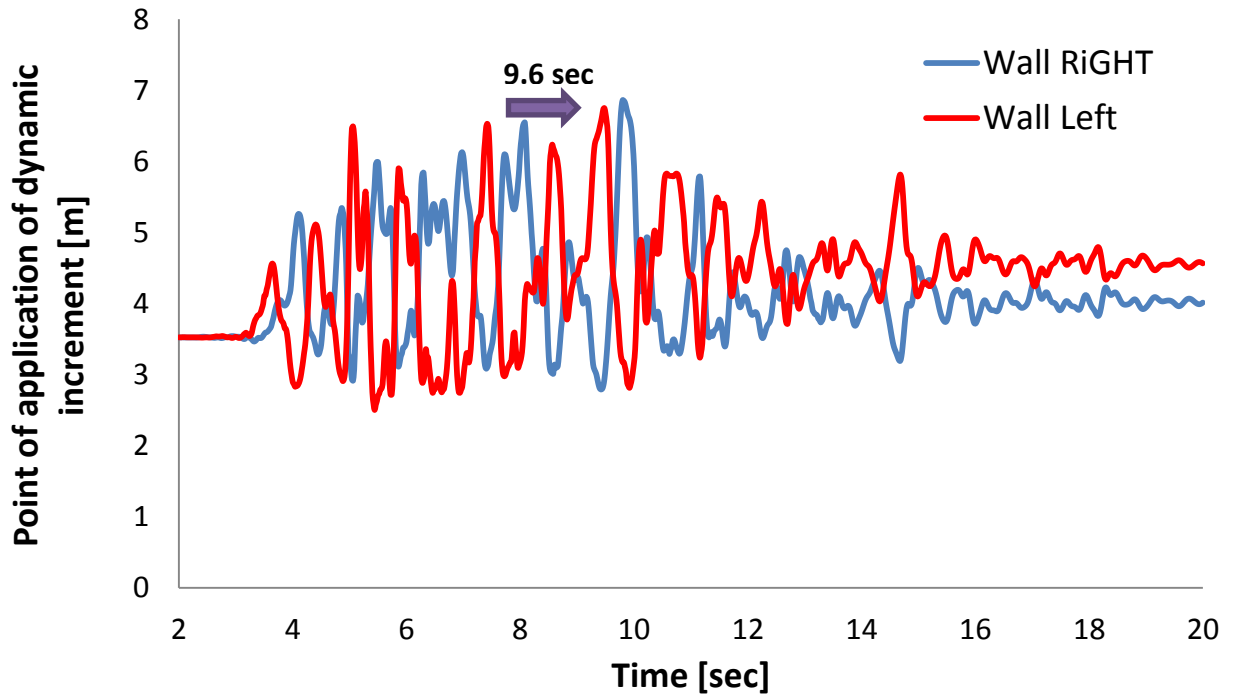

Fig. 2.219. Point of application of dynamic force on the left and right wall when subjected to Sakarya Seismic excitation with peak ground acceleration 0.3g.

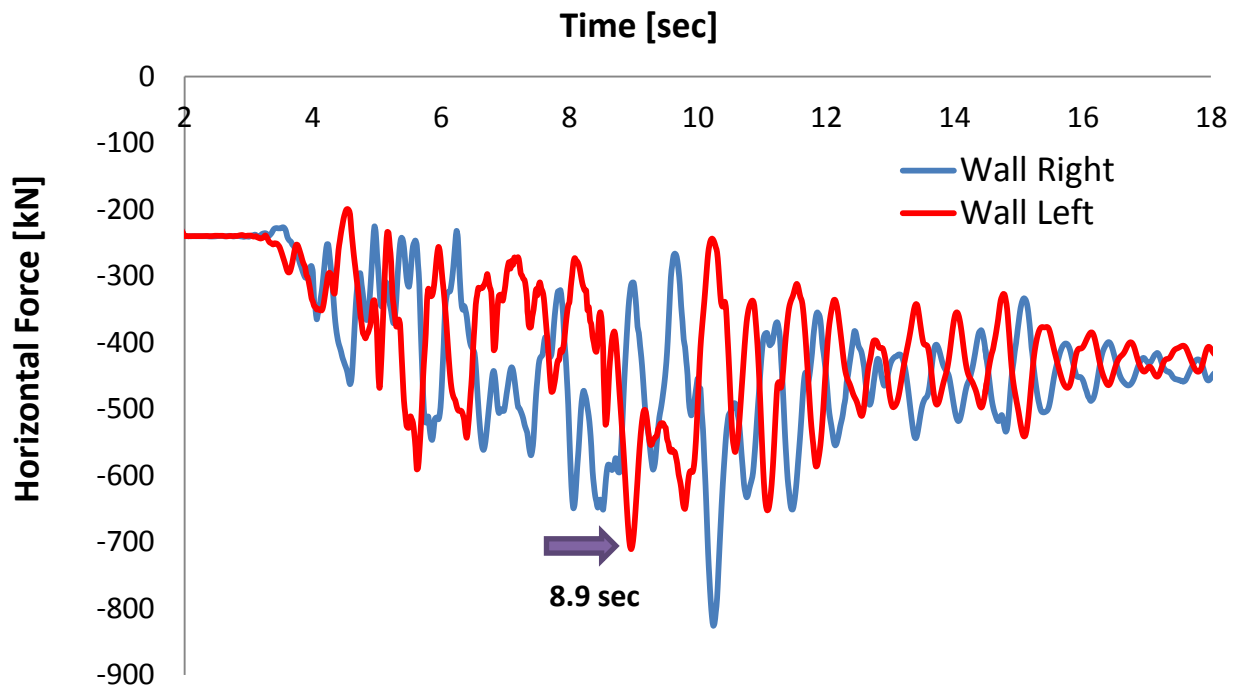

Fig. 2.220. Horizontal force-time history of the left wall when subjected to Sakarya Seismic excitation with peak ground acceleration 0.6g.

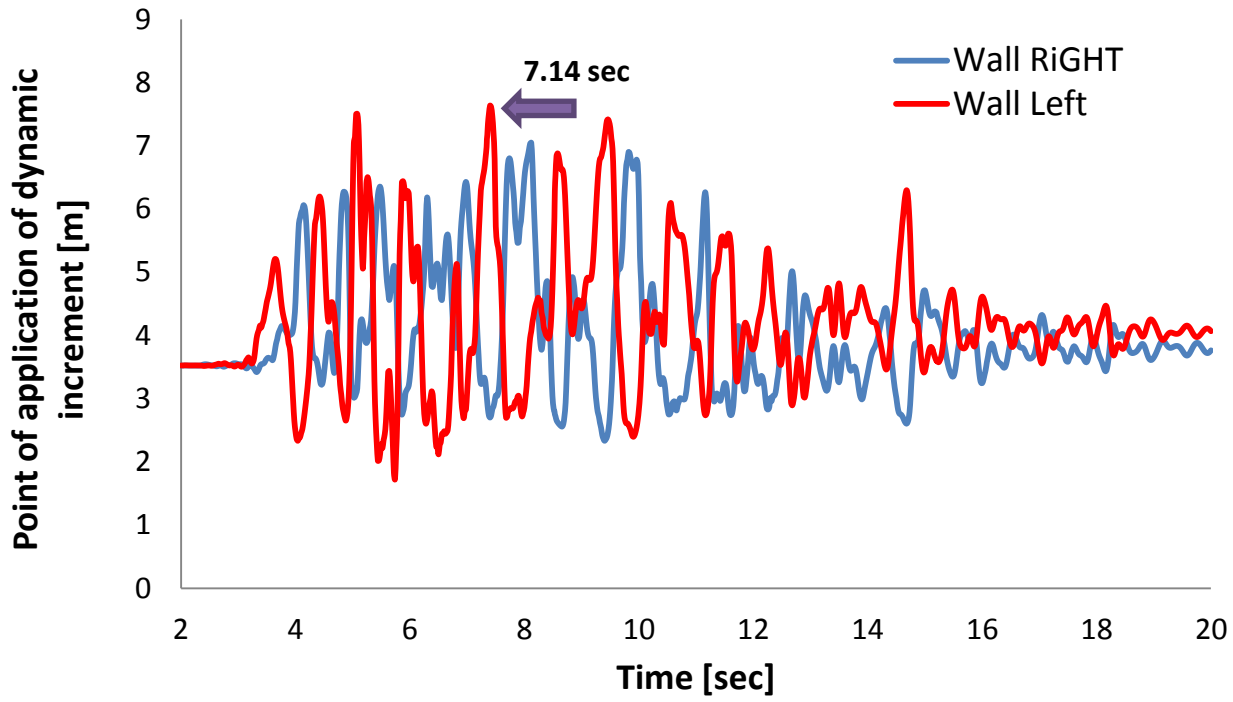

Fig. 2.221. Point of application of dynamic force on the left and right wall when subjected to Sakarya Seismic excitation with peak ground acceleration 0.6g.

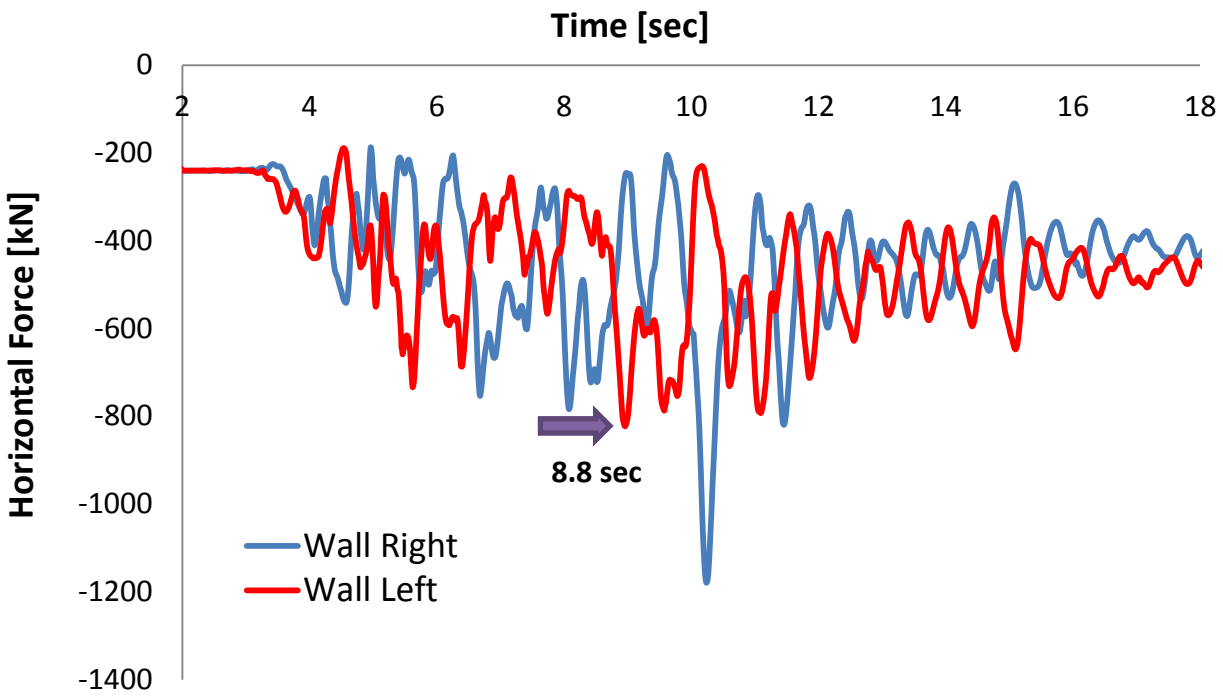

Fig. 2.222. Horizontal force-time history of the left wall when subjected to Sakarya Seismic excitation with peak ground acceleration 0.9g.

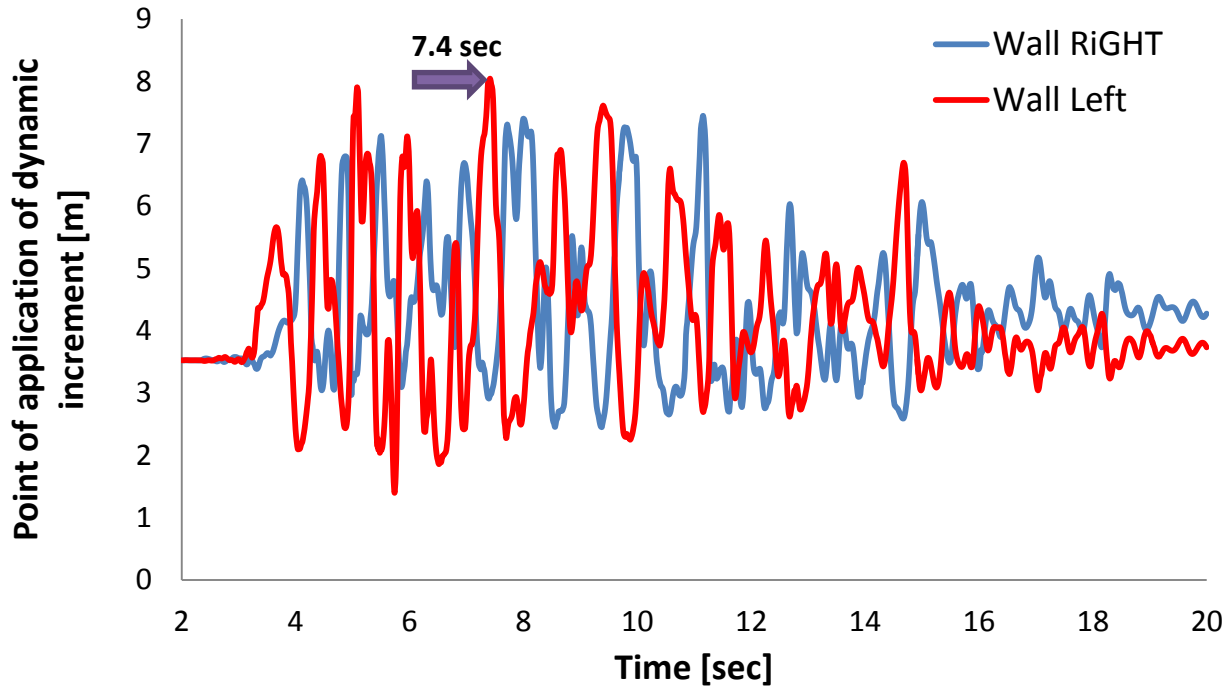

Fig. 2.223. Point of application of dynamic force on the left and right wall when subjected to Sakarya Seismic excitation with peak ground acceleration 0.9g.

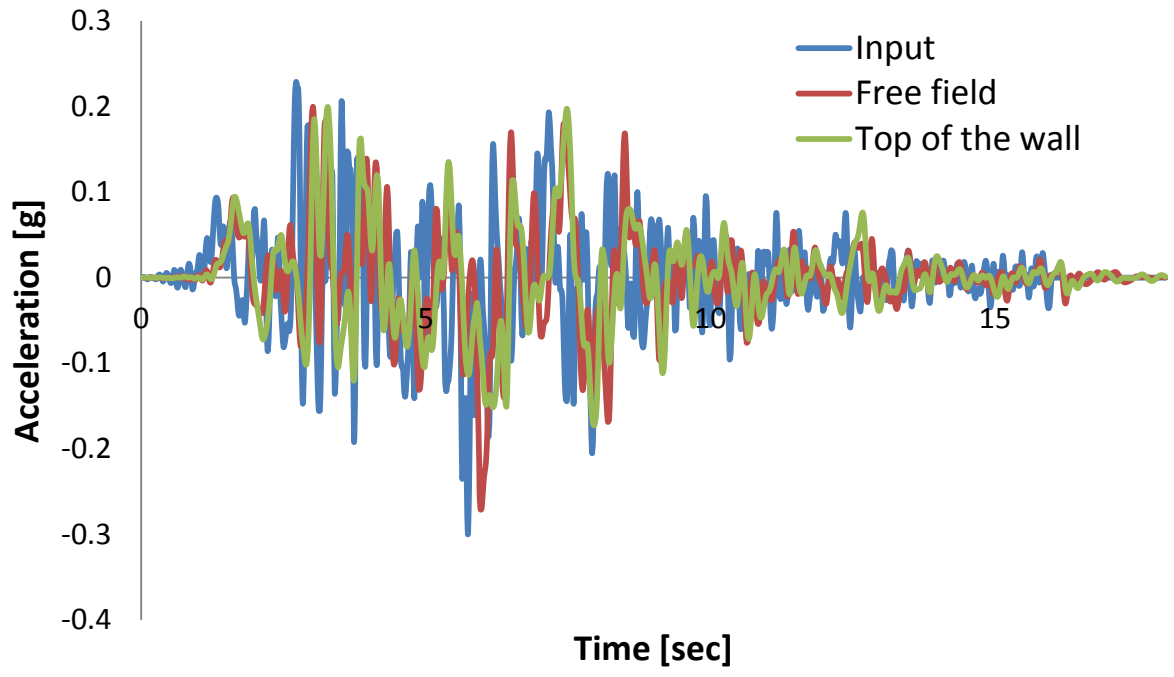

Fig. 2.224. Comparison of input acceleration and computed at the top of the left wall and top of the free field when subjected to Sakarya Seismic excitation with peak acceleration 0.3g.

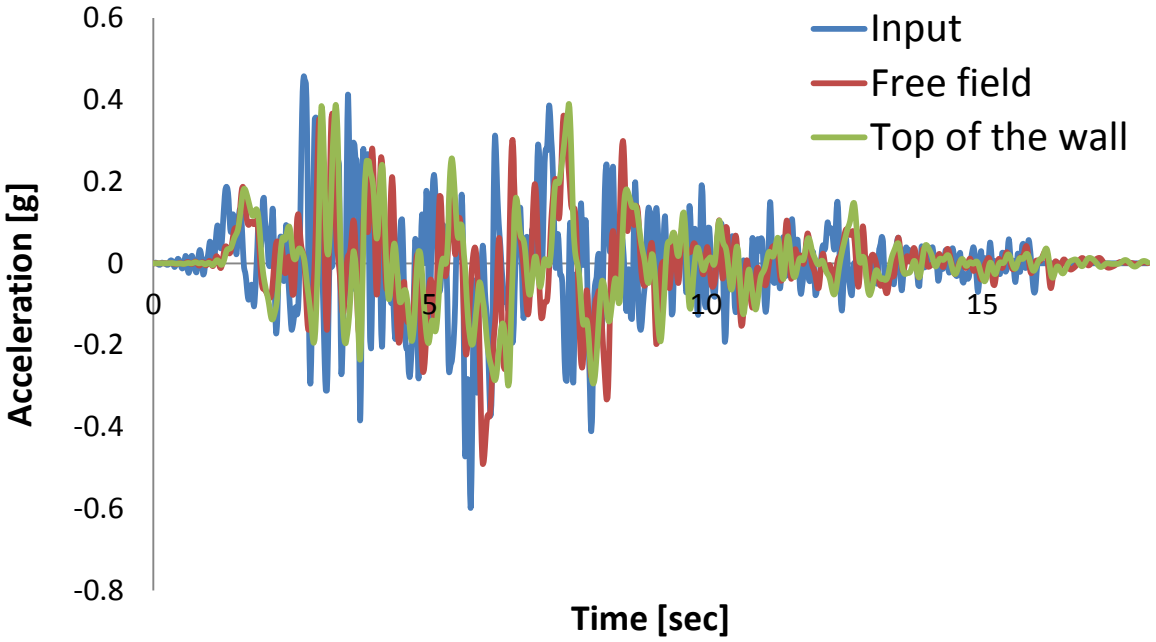

Fig. 2.225. Comparison of input acceleration and computed at the top of the left wall and top of the free field when subjected to Sakarya Seismic excitation with peak acceleration 0.6g.

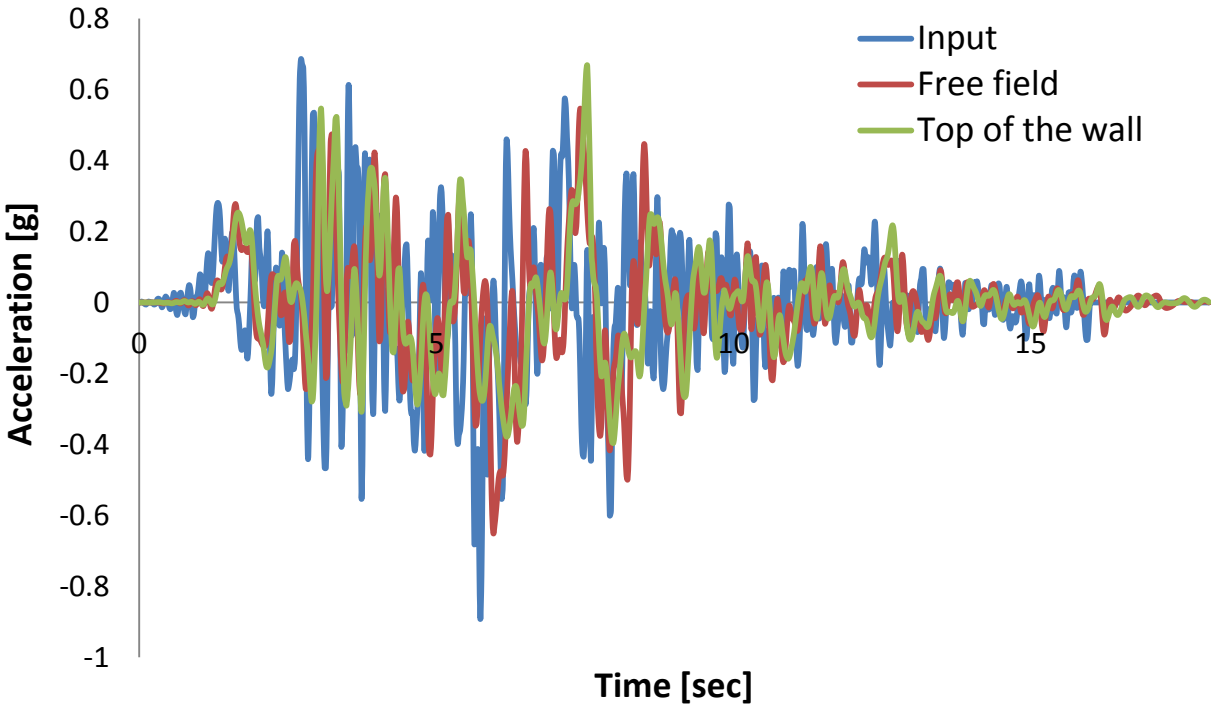

Fig. 2.226. Comparison of input acceleration and computed at the top of the left wall and top of the free field when subjected to Sakarya Seismic excitation with peak acceleration 0.9g.

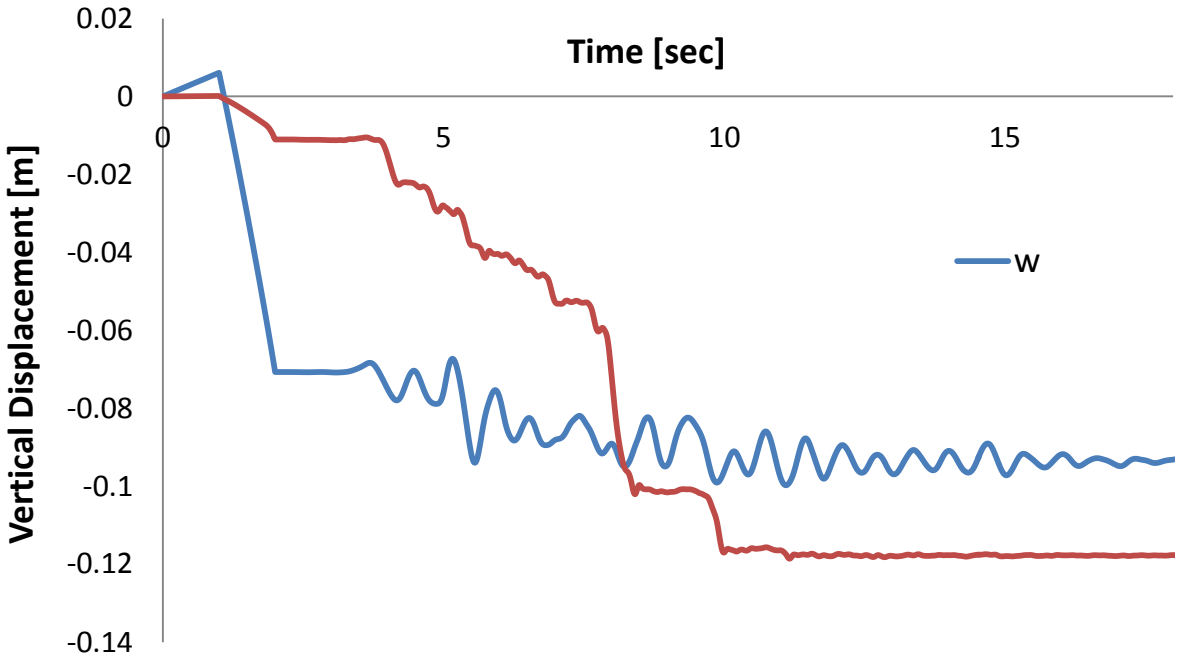

Fig. 2.227. Vertical displacement-time history of the left wall when subjected to Sakarya Seismic excitation with peak acceleration 0.3g.

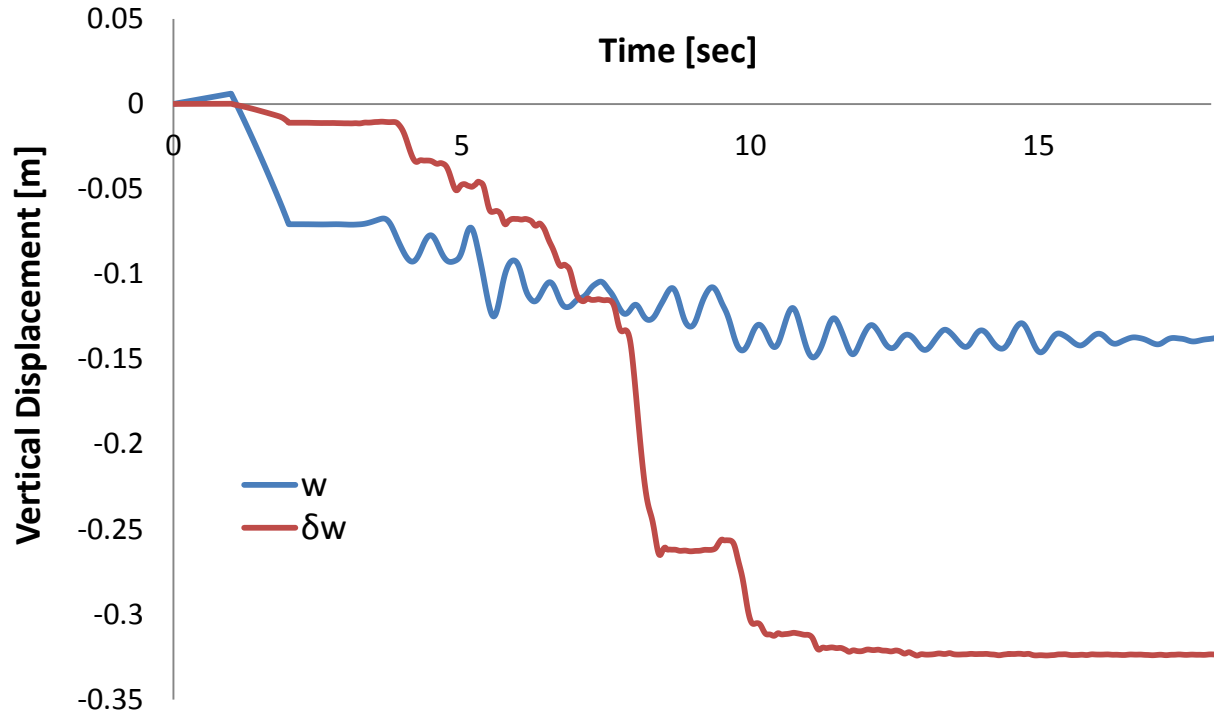

Fig. 2.228. Vertical displacement-time history of the left wall when subjected to Sakarya Seismic excitation with peak acceleration 0.6g.

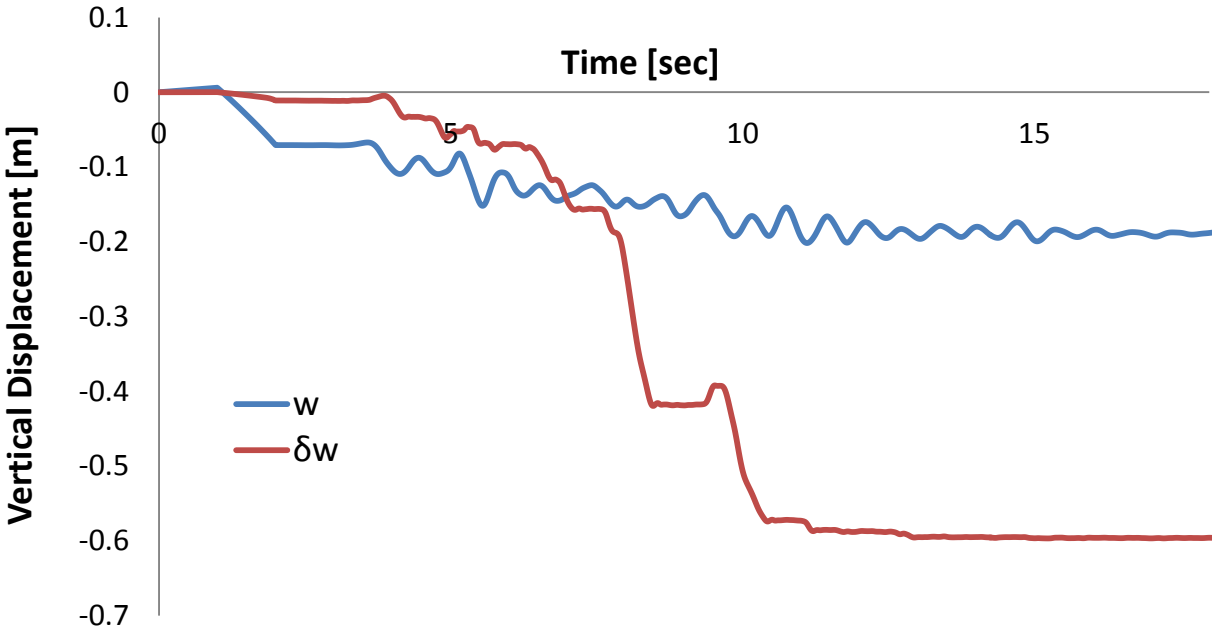

Fig. 2.229. Vertical displacement-time history of the left wall when subjected to Sakarya Seismic excitation with peak acceleration 0.9g.

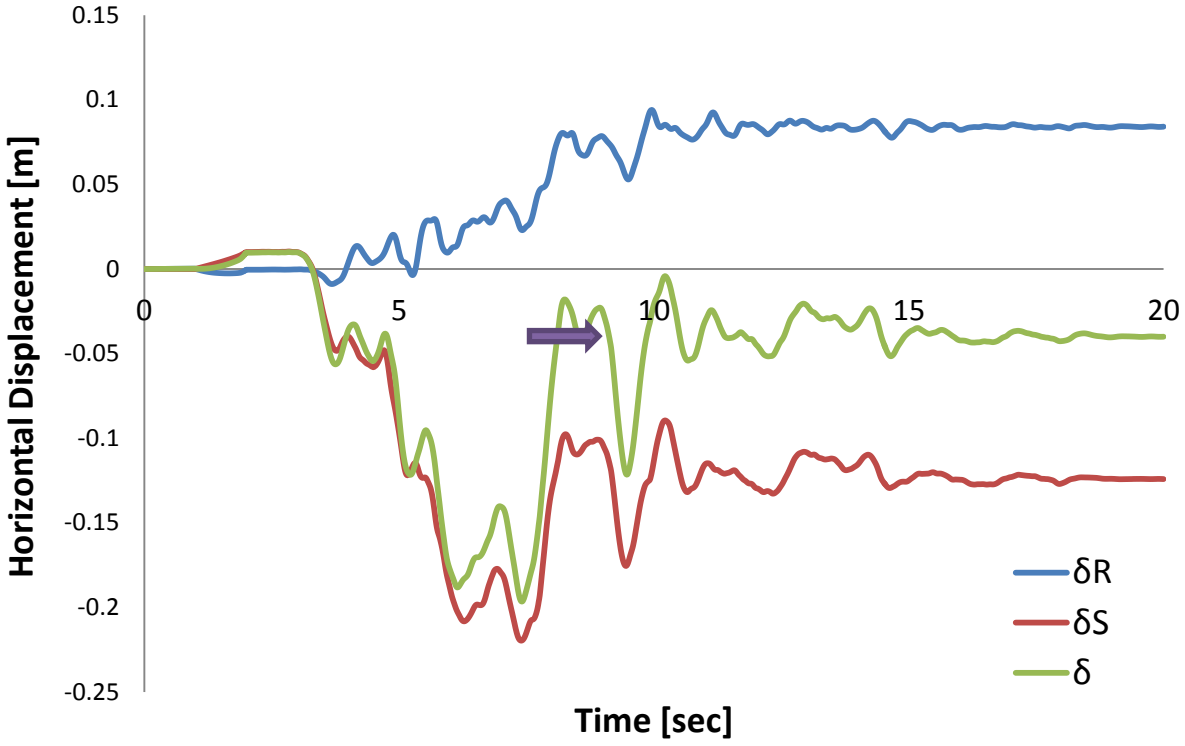

Fig. 2.230. Horizontal displacement-time history of the left wall when subjected to Sakarya Seismic excitation with peak acceleration 0.3g.

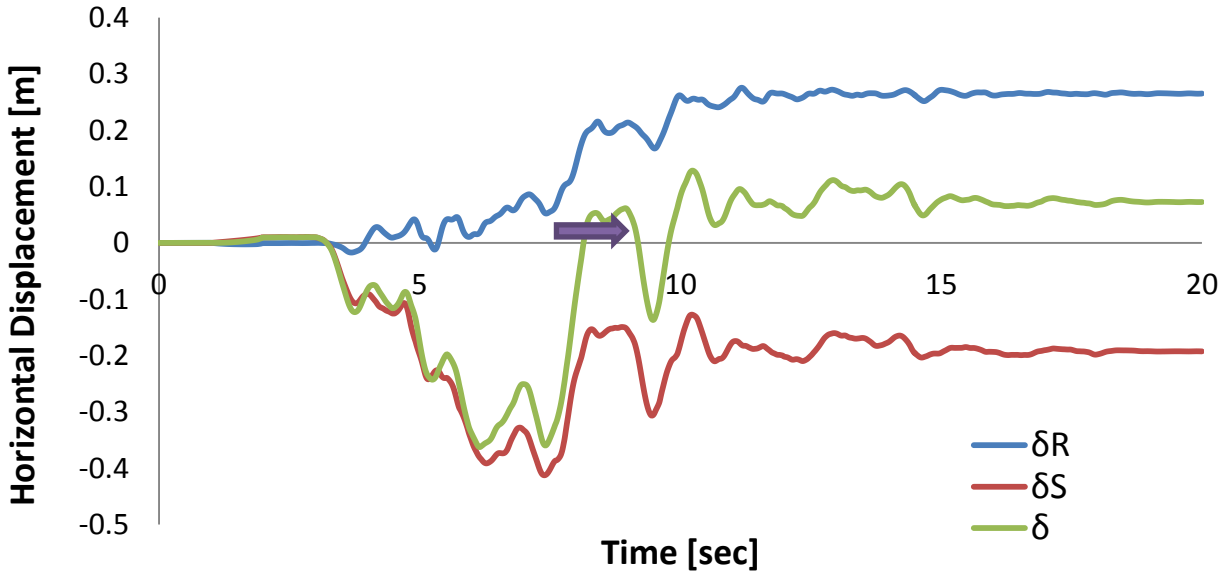

Fig. 2.231. Horizontal displacement-time history of the left wall when subjected to Sakarya Seismic excitation with peak acceleration 0.6g.

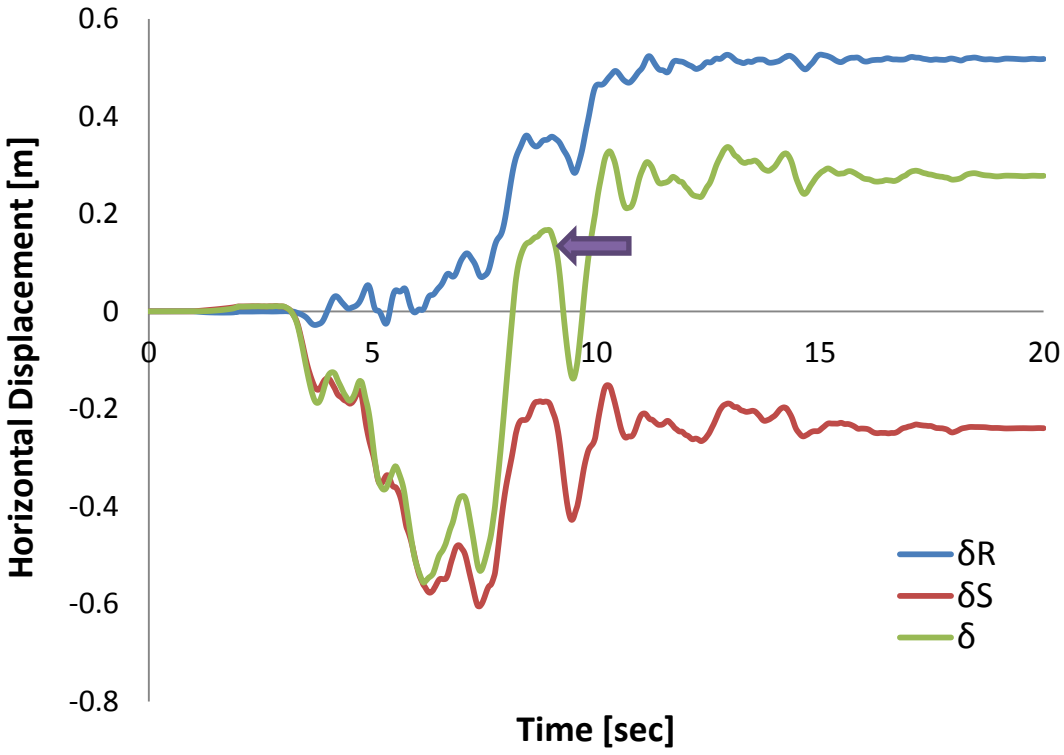

Fig. 2.232. Horizontal displacement-time history of the left wall when subjected to Sakarya Seismic excitation with peak acceleration 0.9g.

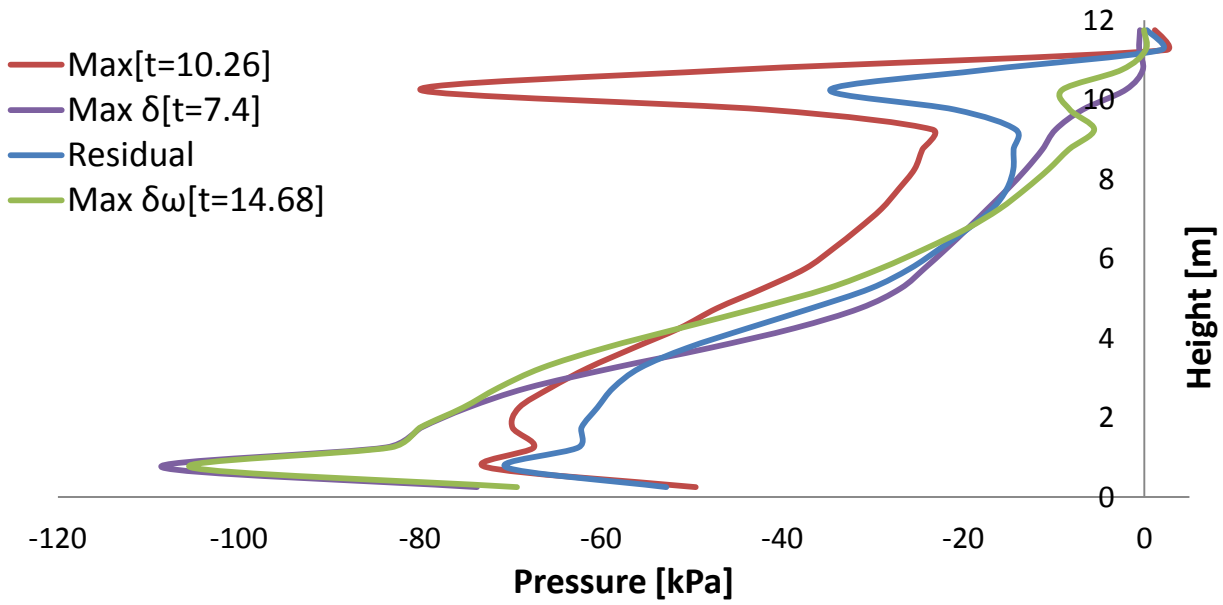

Fig. 2.233. Earth pressures profiles on the right wall at different moments when subjected to Sakarya Seismic excitation with peak ground acceleration 0.3g.

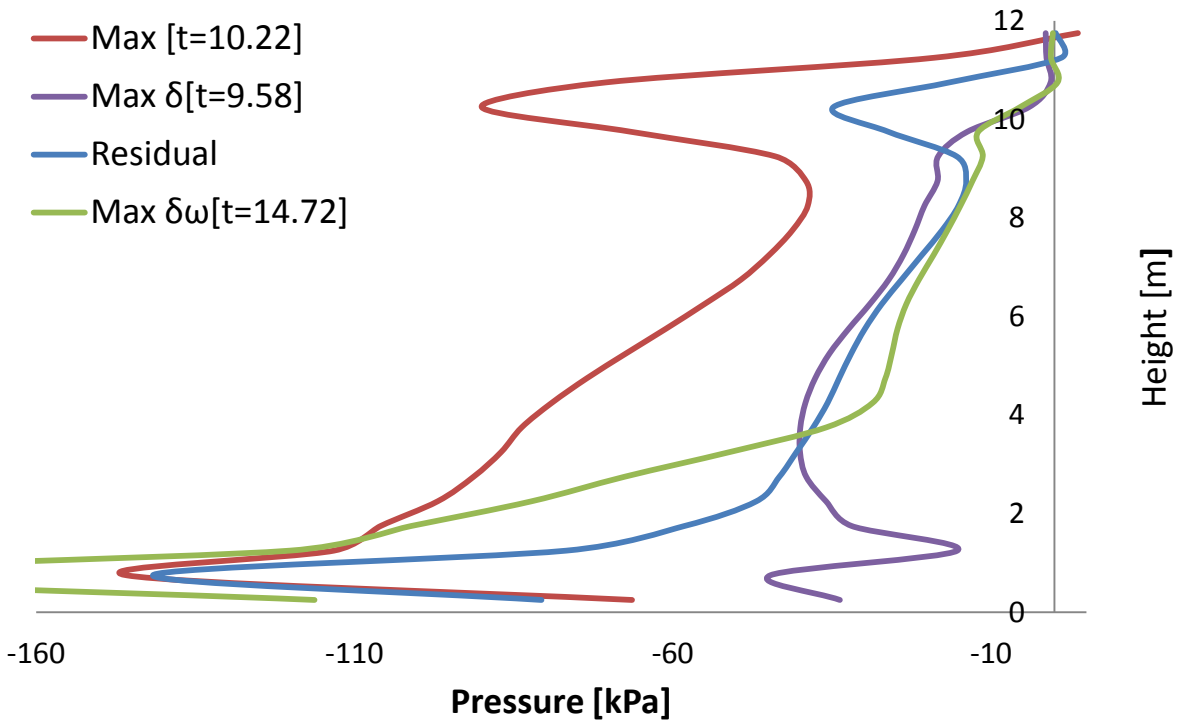

Fig. 2.234. Earth pressures profiles on the right wall at different moments when subjected to Sakarya Seismic excitation with peak ground acceleration 0.6g.

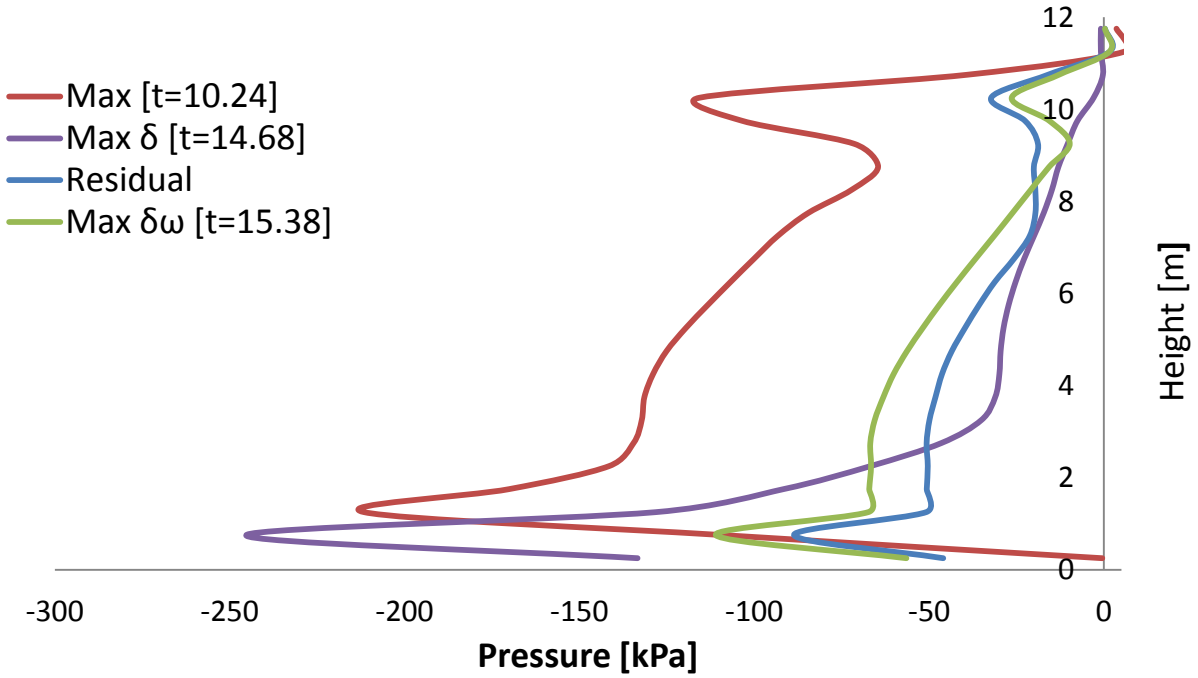

Fig. 2.235. Earth pressures profiles on the right wall at different moments when subjected to Sakarya Seismic excitation with peak ground acceleration 0.9g.

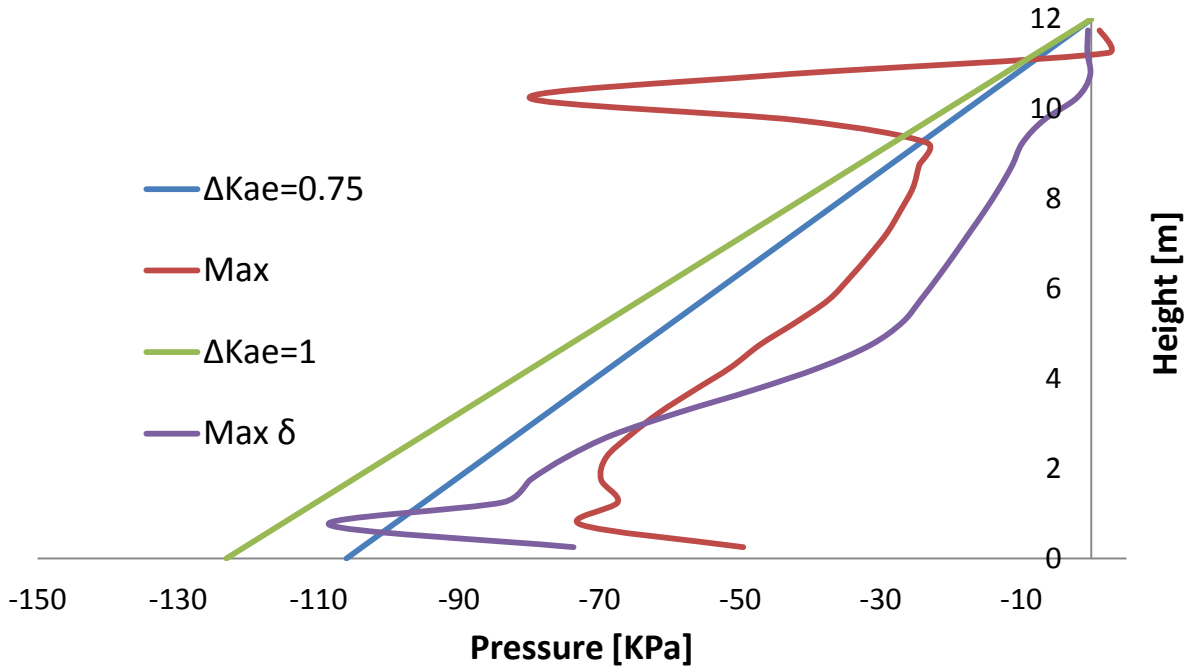

Fig. 2.236. Earth pressure profiles computed in ABAQUS and estimated using the M-O when the right wall is subjected to the Sakarya Seismic excitation with peak acceleration 0.3g.

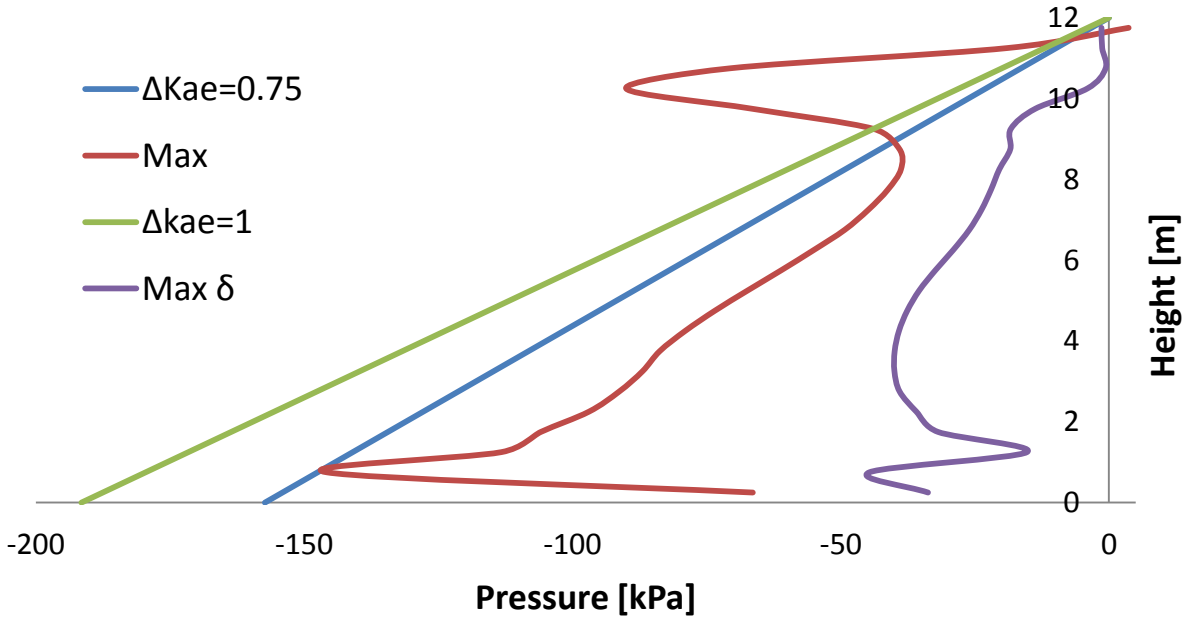

Fig. 2.237. Earth pressure profiles computed in ABAQUS and estimated using the M-O when the right wall is subjected to the Sakarya Seismic excitation with peak acceleration 0.6g.

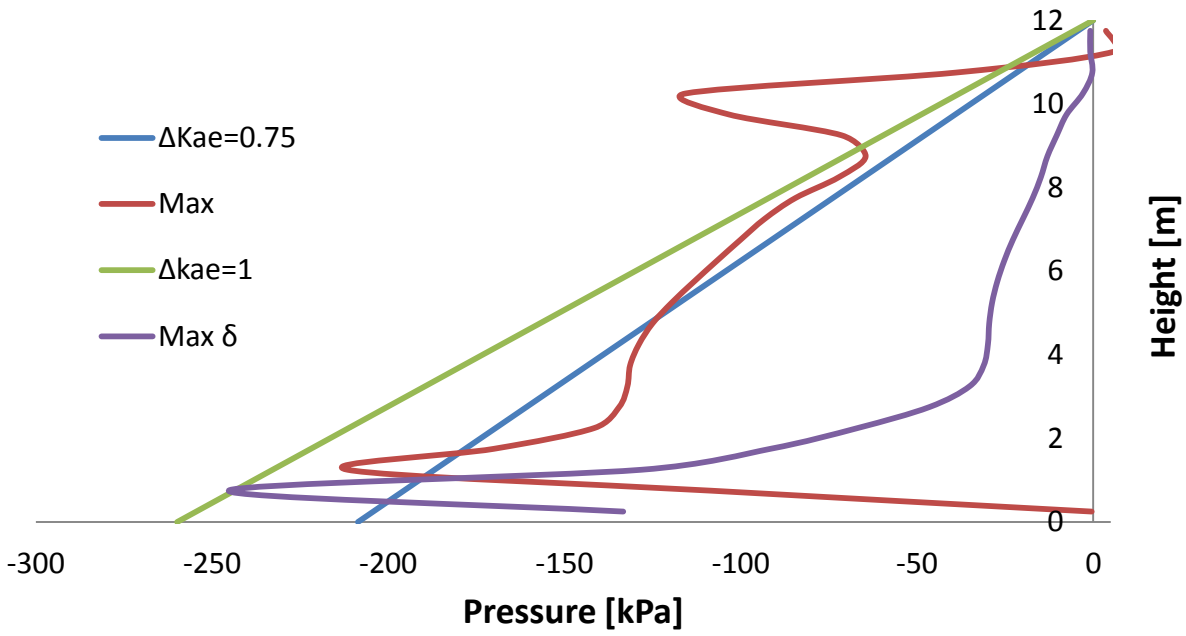

Fig. 2.238. Earth pressure profiles computed in ABAQUS and estimated using the M-O when the right wall is subjected to the Sakarya Seismic excitation with peak acceleration 0.9g.

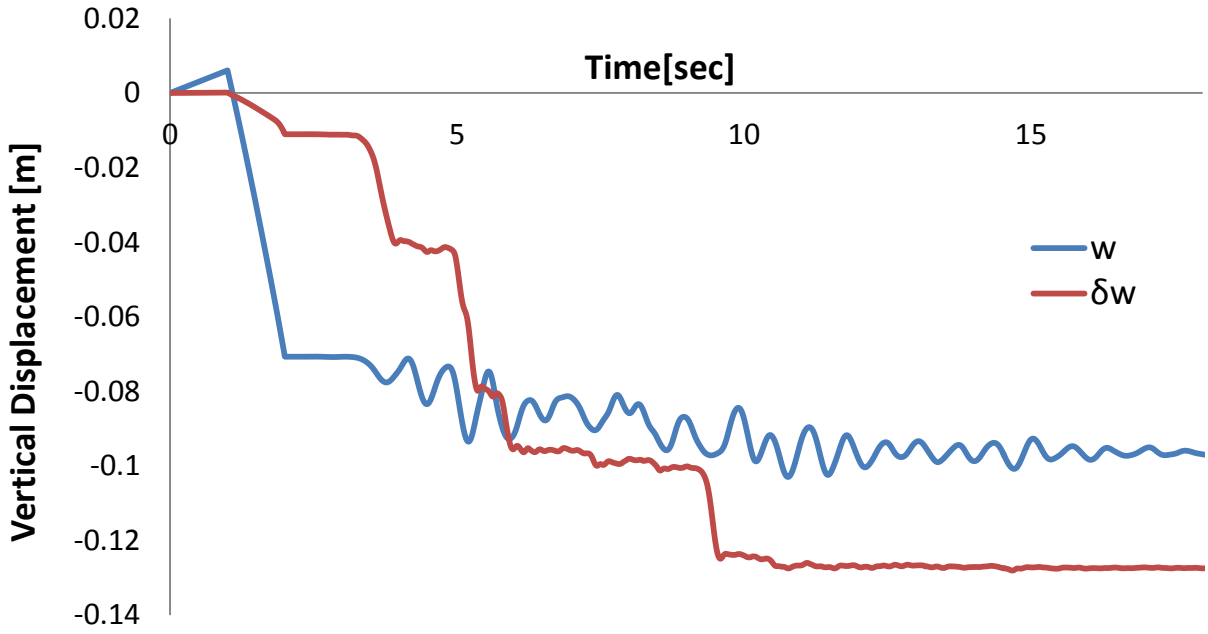

Fig. 2.239. Vertical displacement-time history of the right wall when subjected to Sakarya Seismic excitation with peak acceleration 0.3g.

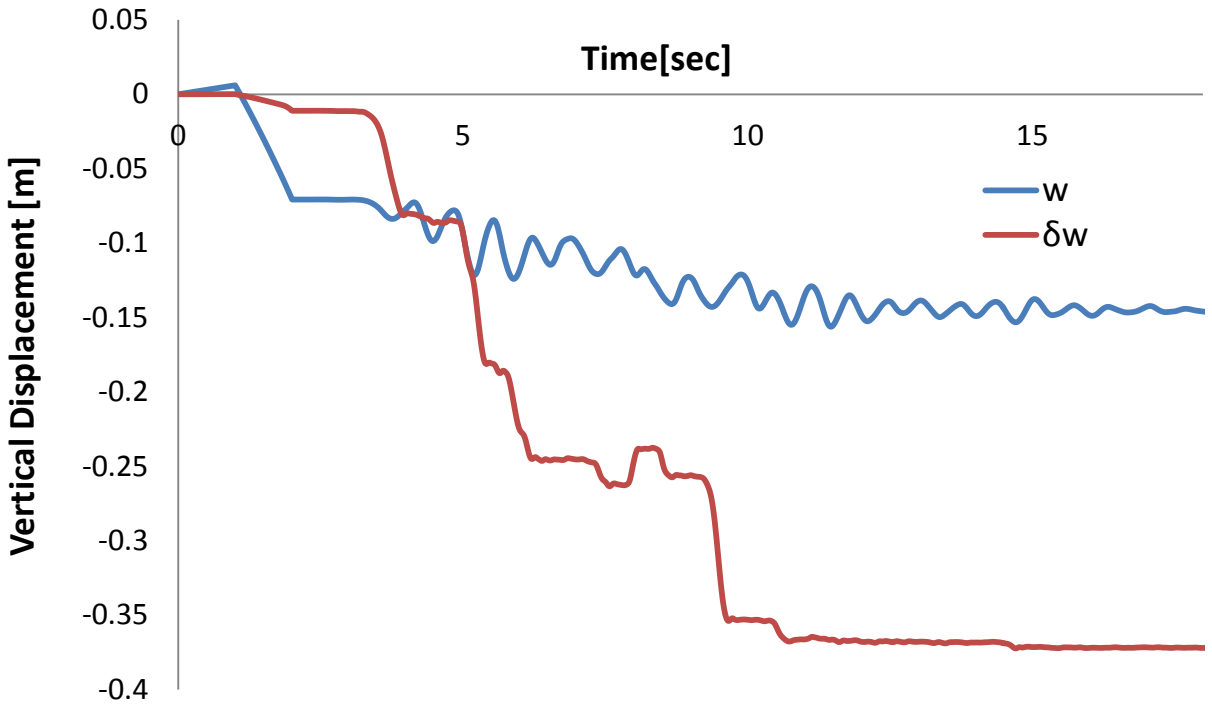

Fig. 2.240. Vertical displacement-time history of the right wall when subjected to Sakarya Seismic excitation with peak acceleration 0.6g.

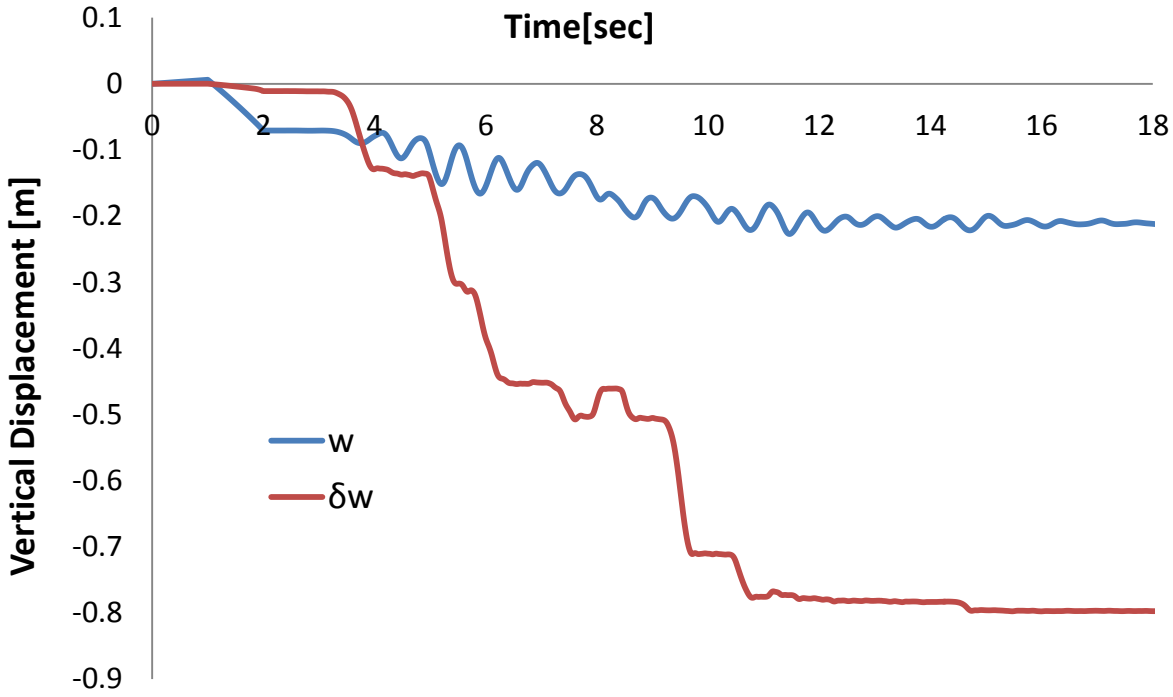

Fig. 2.241. Vertical displacement-time history of the right wall when subjected to Sakarya Seismic excitation with peak acceleration 0.9g.

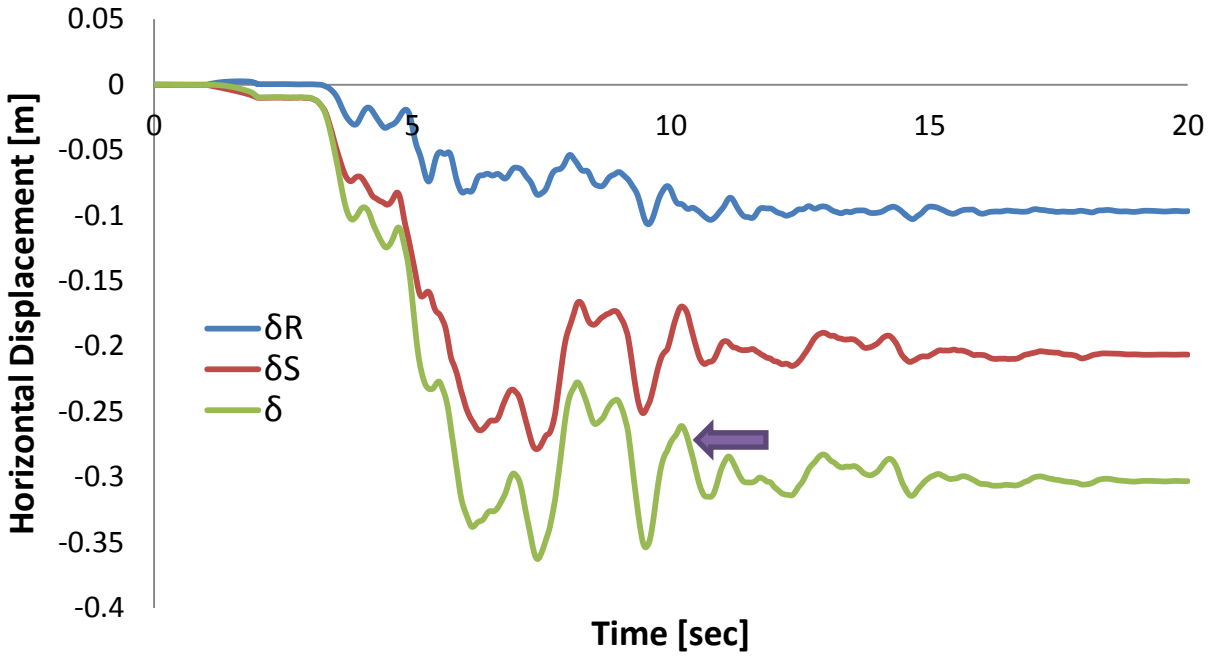

Fig. 2.242. Horizontal displacement-time history of the right wall when subjected to Sakarya Seismic excitation with peak acceleration 0.3g.

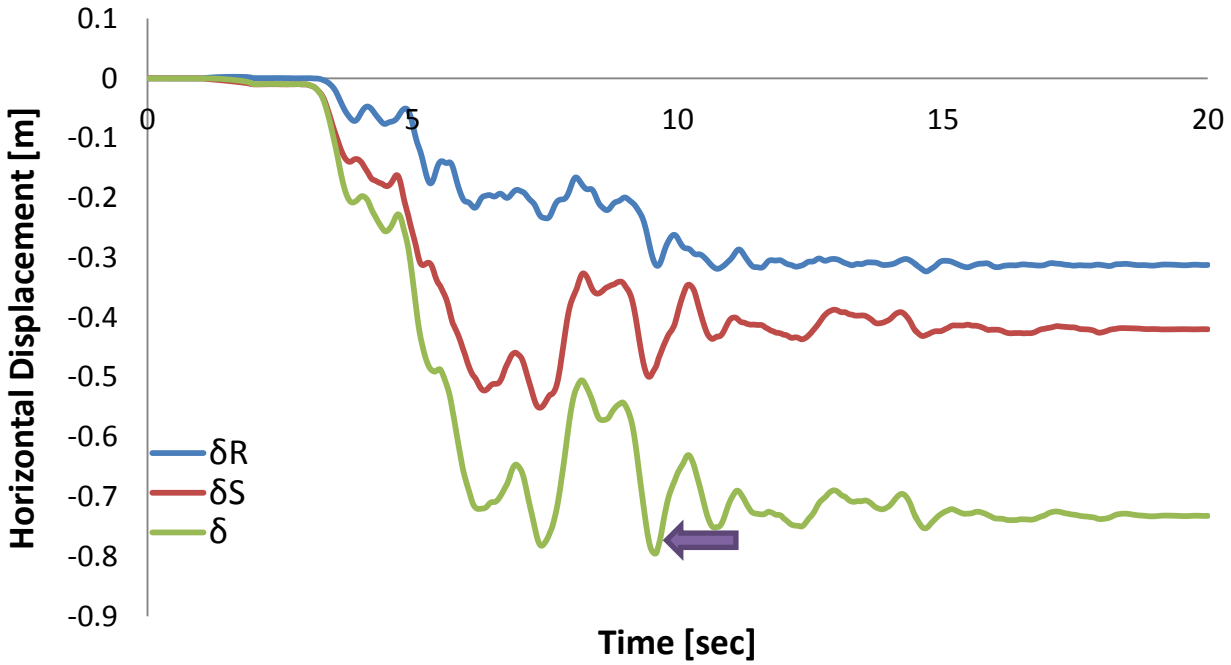

Fig. 2.243. Horizontal displacement-time history of the right wall when subjected to Sakarya Seismic excitation with peak acceleration 0.6g.

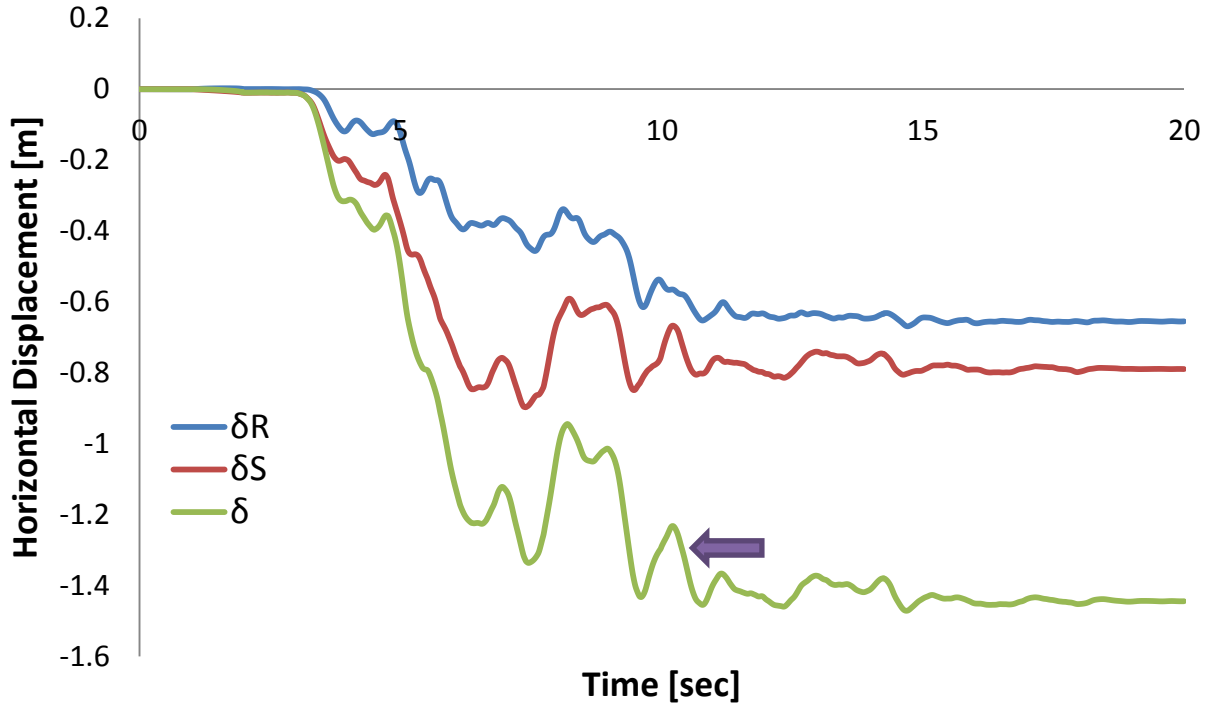

Fig. 2.244. Horizontal displacement-time history of the right wall when subjected to Sakarya Seismic excitation with peak acceleration 0.9g.

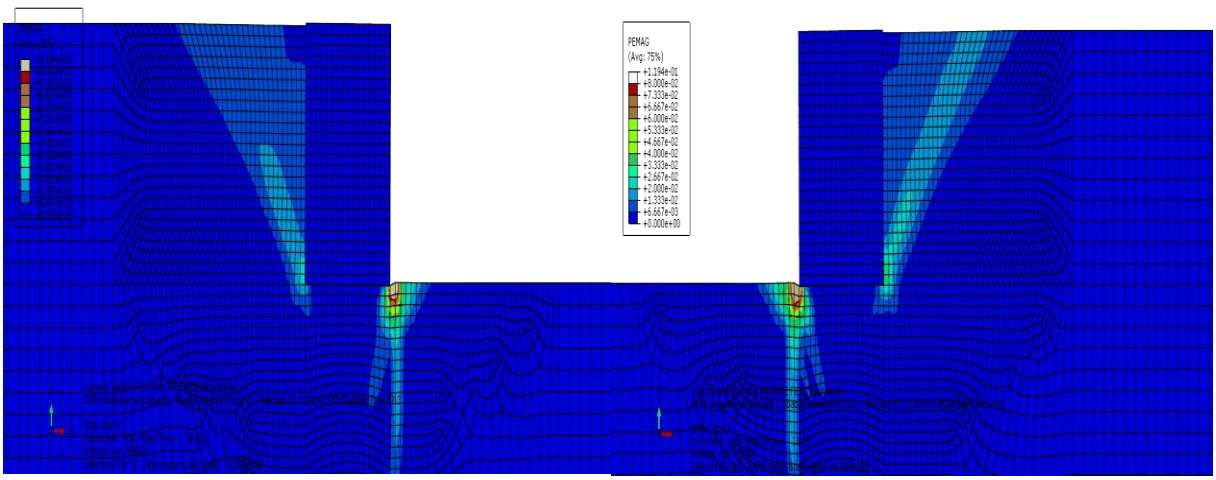

Fig. 2.245. Plastic strain contours at the end of seismic shaking (a)Left wall (b)Right wall when subjected to Sakarya seismic excitation with peak acceleration 0.3g.

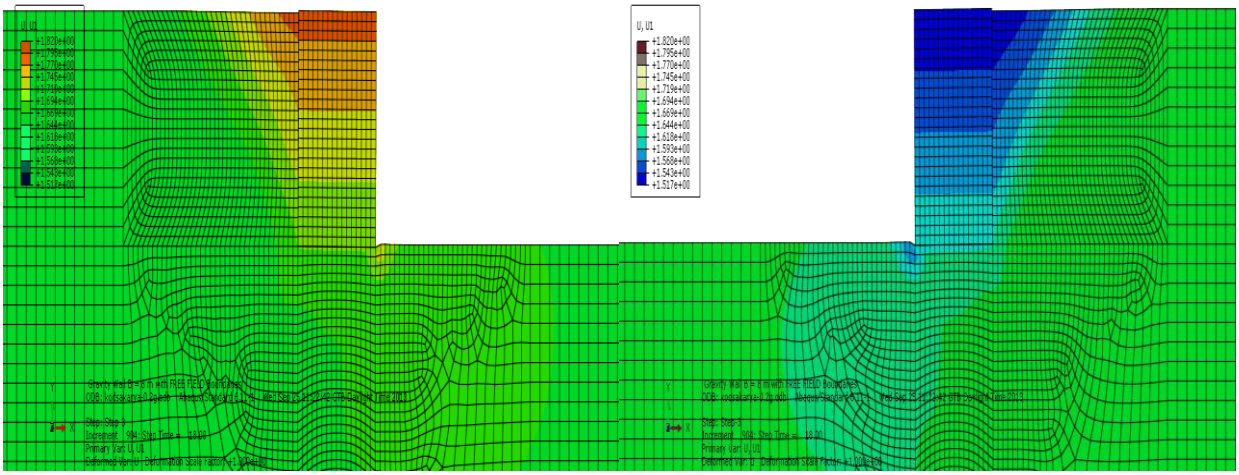

Fig. 2.246. Horizontal displacement contours at the end of the seismic excitation Sakarya PGA 0.3g.

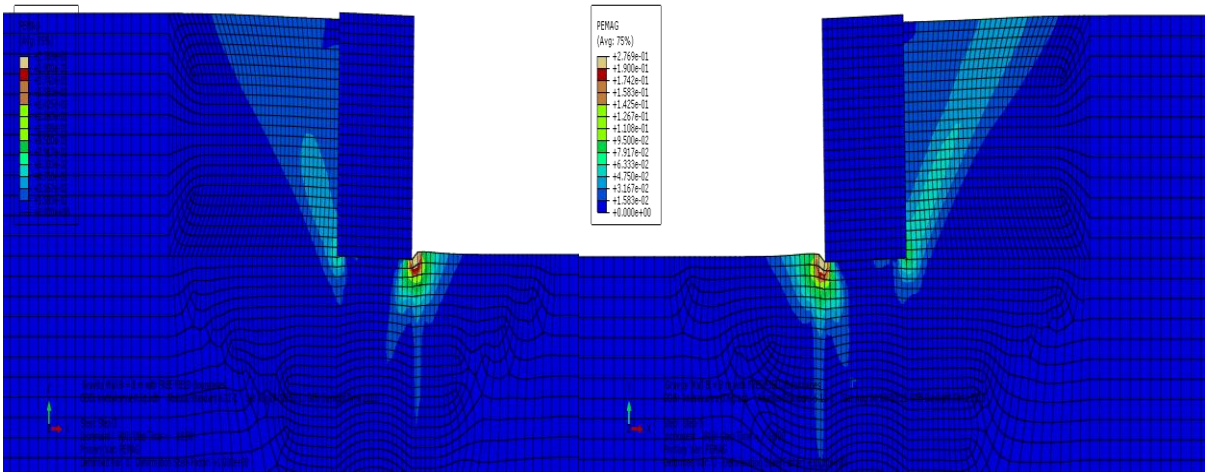

Fig. 2.247. Plastic strain contours at the end of seismic shaking (a)Left wall (b)Right wall when subjected to Sakarya seismic excitation with peak acceleration 0.6g.

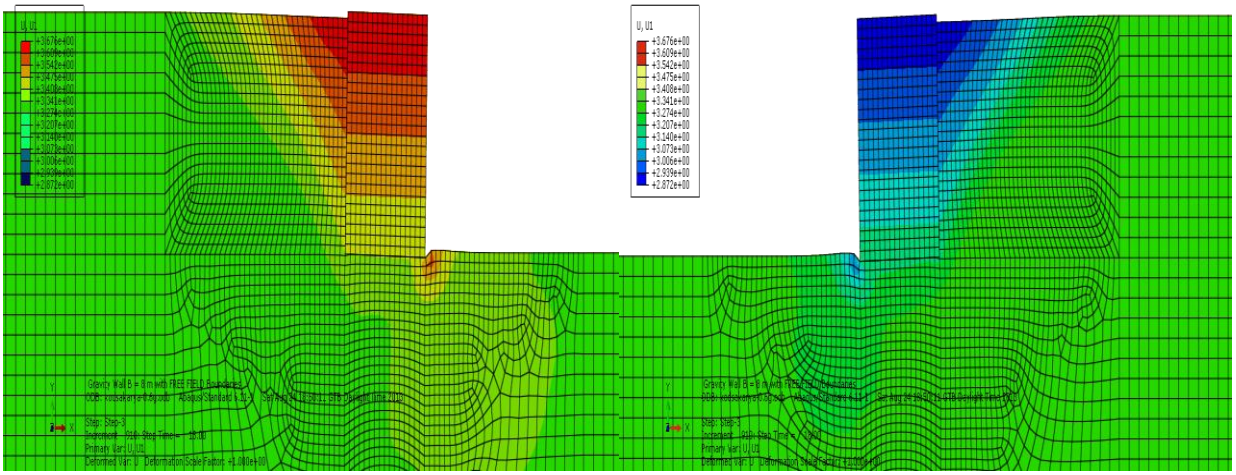

Fig. 2.248. Horizontal displacement contours at the end of the seismic excitation Sakarya PGA 0.6g.

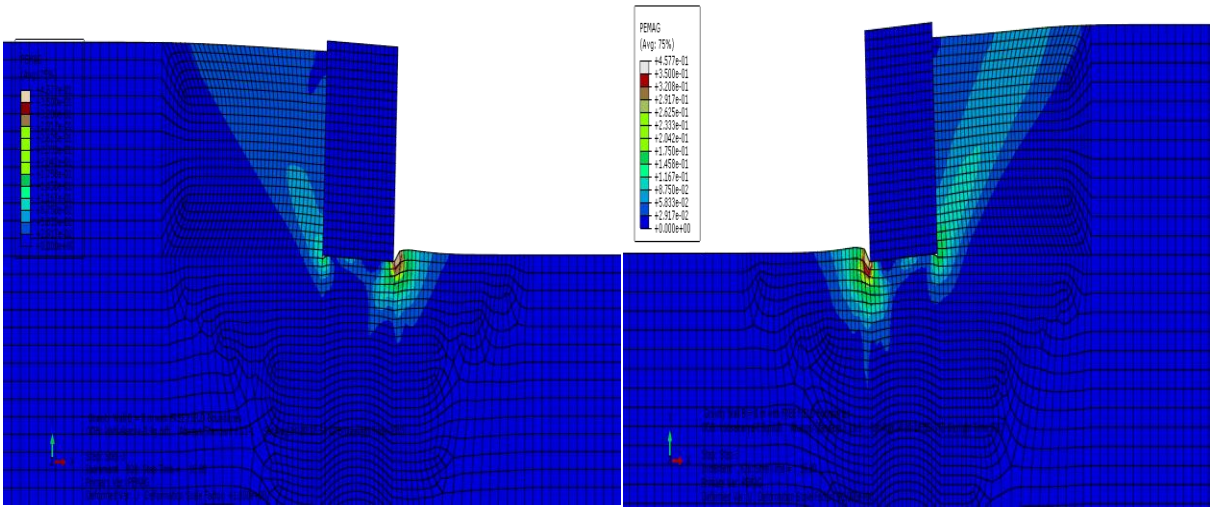

Fig. 2.249. Plastic strain contours at the end of seismic shaking (a)Left wall (b)Right wall when subjected to Sakarya seismic excitation with peak acceleration 0.9g.

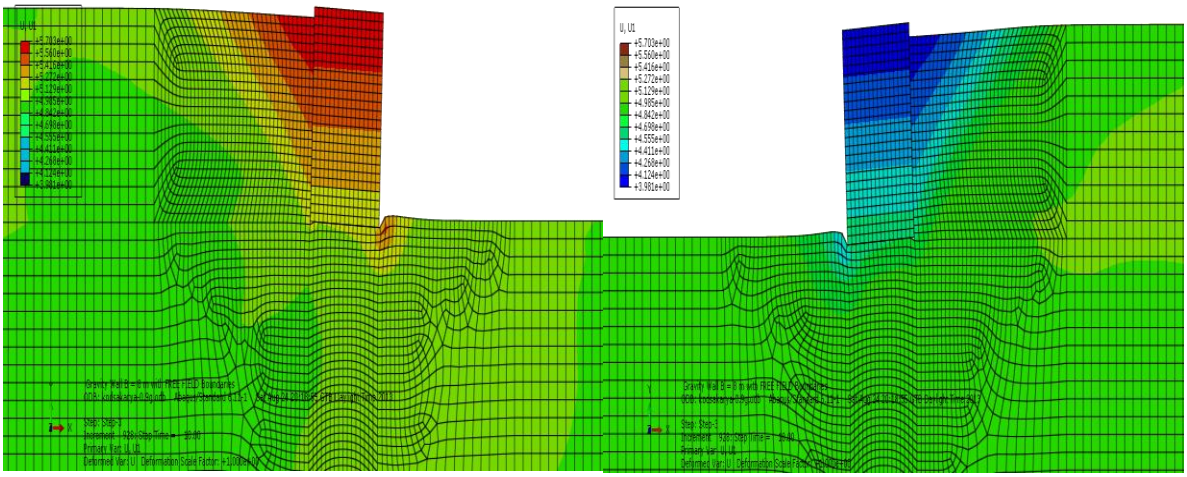

Fig. 2.250. Horizontal displacement contours at the end of the seismic excitation Sakarya PGA 0.9g.

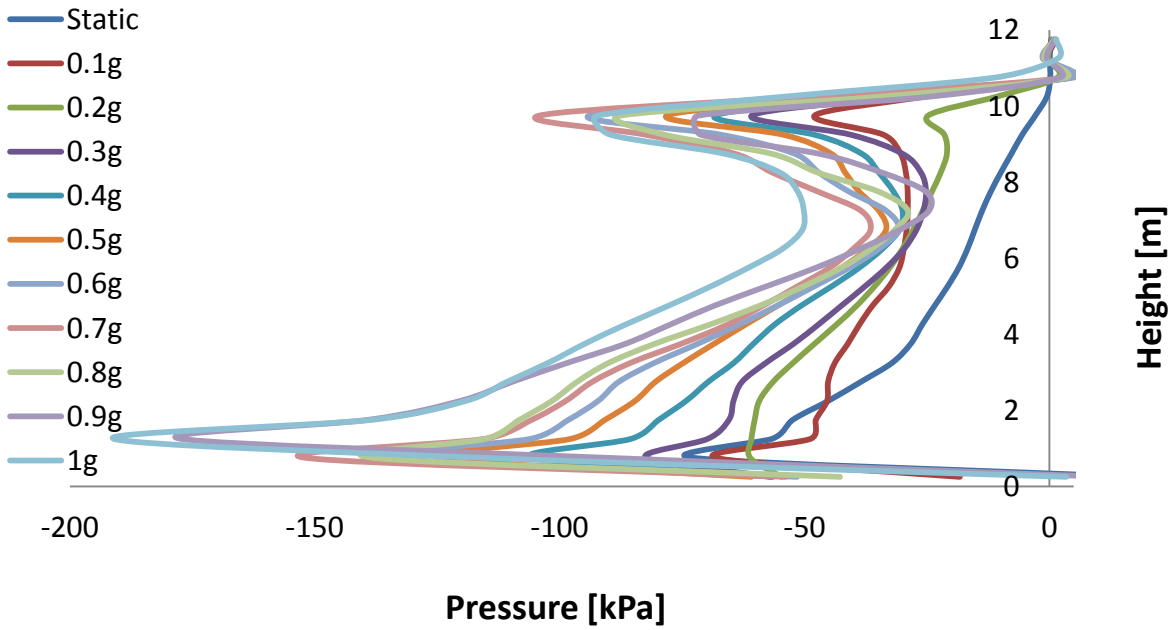

Fig. 2.251. Static and maximum earth pressure profiles for different peak accelerations on the left wall when subjected to Sakarya Seismic excitation.

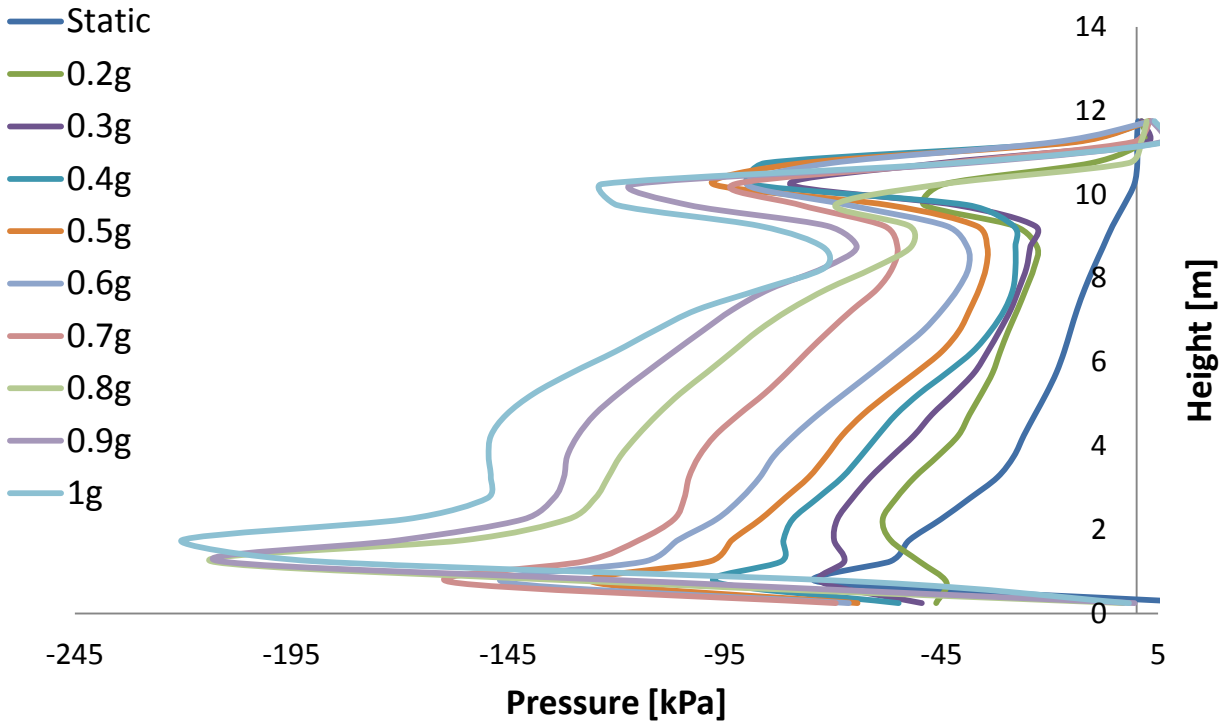

Fig. 2.252. Static and maximum earth pressure profiles for different peak accelerations on the right wall when subjected to Sakarya Seismic excitation.

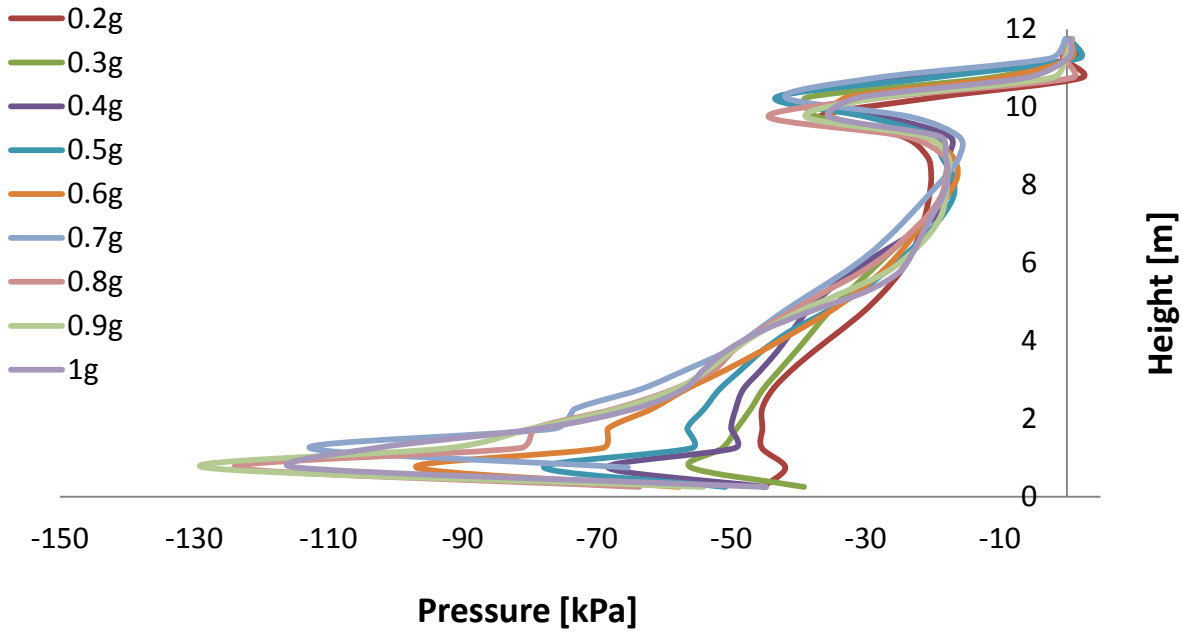

Fig. 2.253. Residual earth pressure profiles for different peak accelerations on the left wall when subjected to Sakarya Seismic excitation.

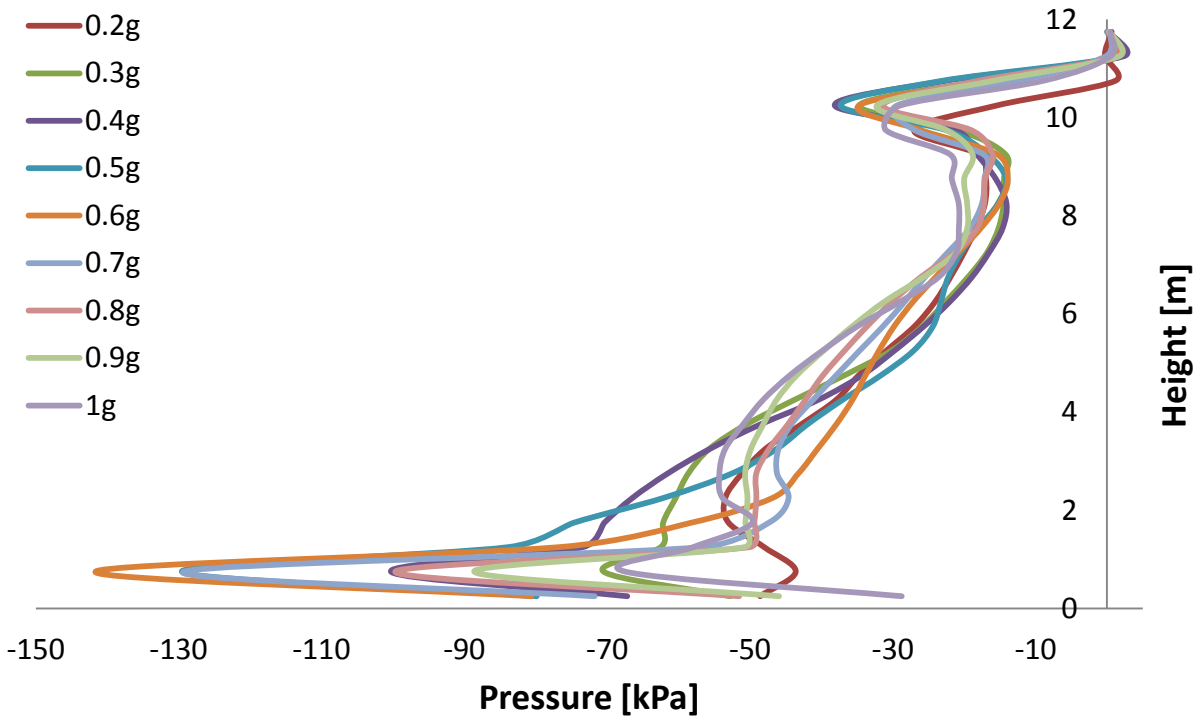

Fig. 2.254. Residual earth pressure profiles for different peak accelerations on the right wall when subjected to Sakarya Seismic excitation.

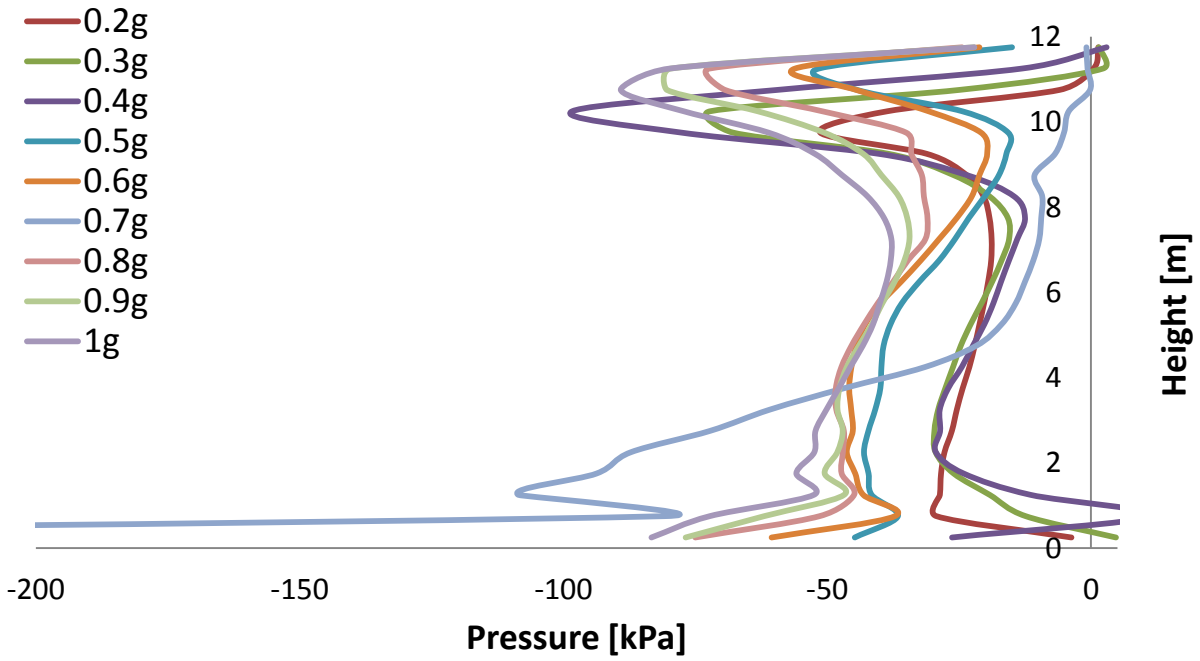

Fig. 2.255. Earth pressure profiles at maximum displacement for different peak accelerations on the left wall when subjected to Sakarya Seismic excitation.

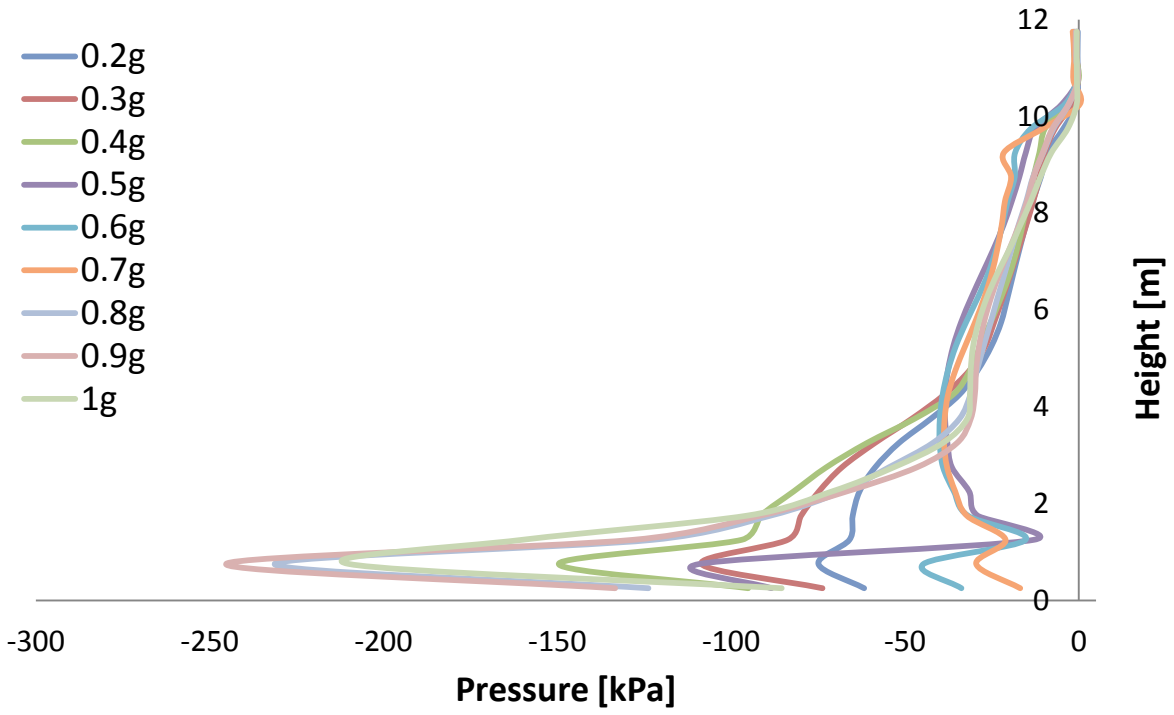

Fig. 2.256. Earth pressure profiles at maximum displacement for different peak accelerations on the right wall when subjected to Sakarya Seismic excitation.

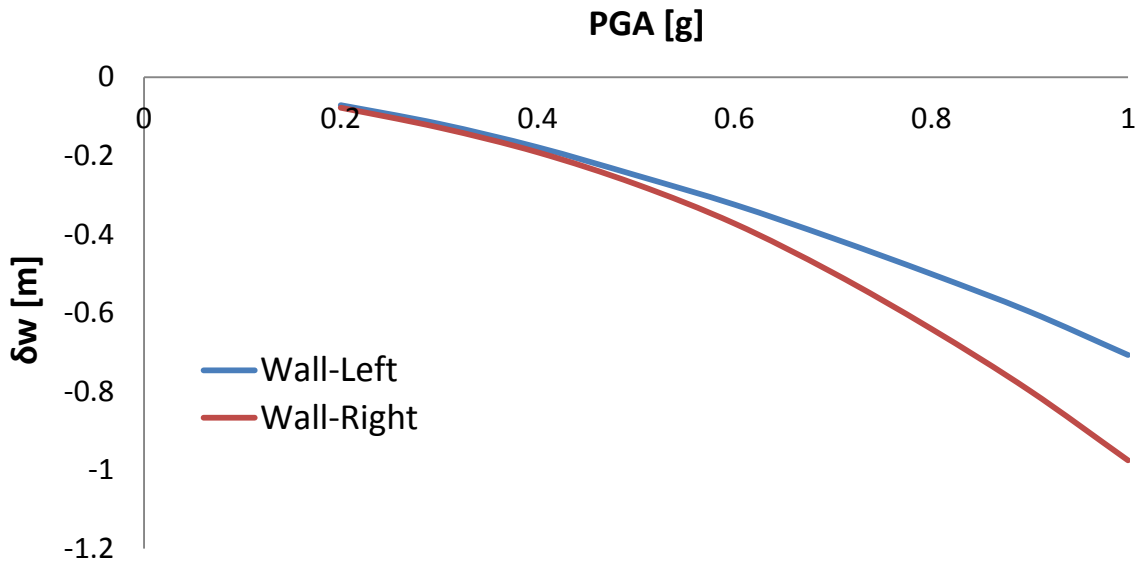

Fig. 2.257. Vertical displacement as a function of PGA for the left and right wall when subjected to Sakarya Seismic excitation.

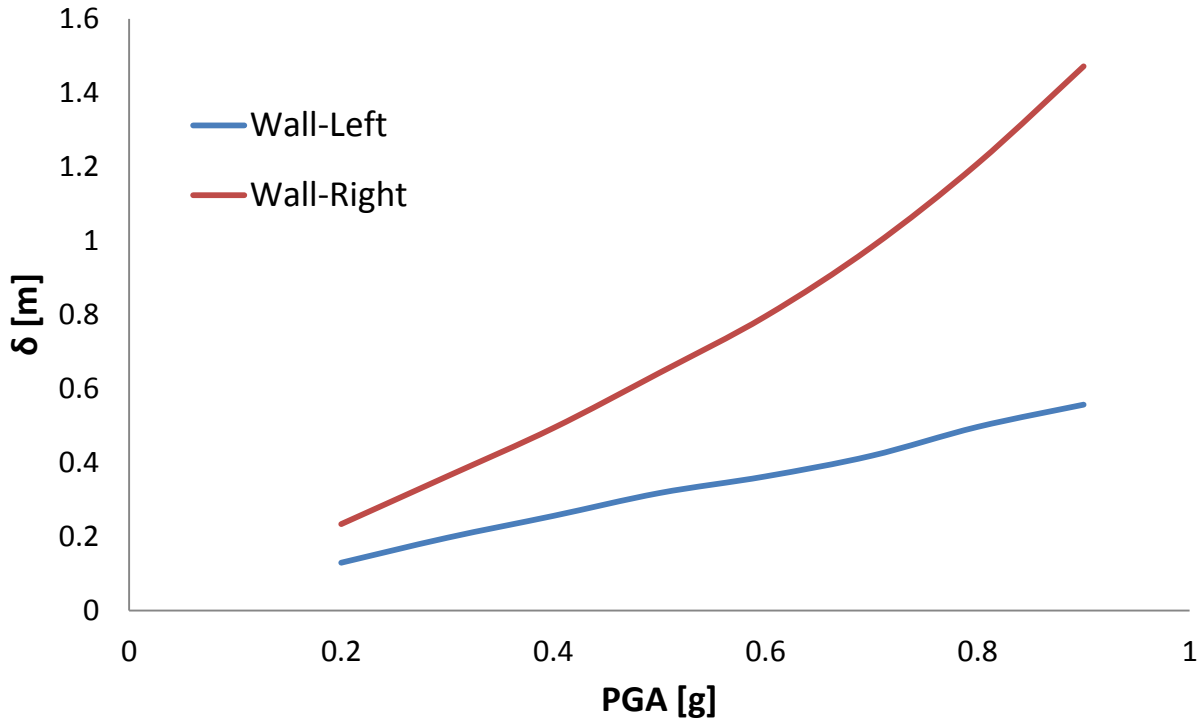

Fig. 2.258. Horizontal displacement as a function of PGA for the left and right wall when subjected to Sakarya Seismic excitation.

Chapter 3

THE ROLE OF THE FOUNDATION SOIL

3.1 Introduction

In this chapter the properties of the foundation soil were changed, in order to obtain a comprehensive evaluation of its effect on the performance of the retaining walls.To this end ,the same numerical model as in chapter 2 was subjected to the same five earthquakes.

The properties of the foundation soil in this chapter were :Elasticity Modulus **E**=300 MPa, Poisson's ratio **v**=0.25, cohesion **c**=15 kPa, friction angle **ϕ**=45^{o}, dilation angle **ψ**=15^{o}, density **ρ**=1.9 Mgr/m^{3} and friction coefficient **μ**=1.The results of the analyses of three of these earthquakes of the wall-soil system are presented below.

3.2 Static analysis

The distribution of the static lateral earth pressure on the retaining wall with the stiffer foundation soil is shown in**fig.3.1.**As observed, the static earth pressure is estimated as 105 kPa while as seen from **fig. 2.2, the** static earth pressure was estimated as 70 kPa.The fact that the static earth pressure is **greater** with the stiffer foundation soilcan be attributed to the soil compliance, where the wall doesn't rotate as in the previous case, and thus greater static earth pressure is applied on the wall.

3.3 Dynamic analyses

3.3.1 Aegion Seismic excitation

Peak ground acceleration 0.2g:

The maximum earth pressure behind the left wall is at t=3.92 sec while at the same time as observed from **figure 3.20**the wall is at its local maximum which means it is moving outwards. The distribution of the maximum earth pressure is in good agreement with the estimated M-O computed with a dynamic pressure coefficient 0.75 (**figure 3.5)**. Maximum and residual horizontal forces on the wall are 500kN and 401 kN respectively **(figure 3.8)**. The highest point of application of the resultant force is observed to be equal to 4.4 m at t=3.94 sec while the

residual point of application of the resultant force is 4.1 m above the bottom of the wall. And again as noticed from **figure 3.20**the permanent displacement due to rotation is 0.0013m,permanent displacement due to sliding is 0.0033 m and the overall horizontal permanent displacement is 0.0046 m and the maximum overall displacement is 0.024 m.The average settlement is 0.0122m and the differential settlement is 0.011 m **(figure 3.17).**

The maximum earth pressure behind the right wall is at t=3.68 sec while at the same time as observed from **figure 3.32** the wall is at its local minimum.. The distribution of the maximum earth pressure is in good agreement with the estimated M-O computed with a dynamic pressure coefficient 0.75 (**figure 3.26)**. Maximum and residual horizontal forces on the wall are 502 kN and 388 kN respectively **(figure 3.8)**. The highest point of application of the resultant force is observed to be equal to 4.4 m at t=4.12 sec while the residual point of application of the resultant force is 4.12 m above the bottom of the wall. And again as noticed from **figure 3.32**the permanent displacement due to rotation is 0.0008m,permanent displacement due to sliding is 0.0068 m and the overall horizontal permanent displacement is 0.006 m and the maximum overall displacement is 0.025 m. The average settlement is 0.0121 m and the differential settlement is 0.011 m **(figure 3.29).**

Peak ground acceleration 0.6g:

The maximum earth pressure behind the left wall is at t=3.92 sec while at the same time as observed from **figure 3.21** the wall is at its local maximum which means it is moving outwards. The distribution of the maximum earth pressure is in good agreement with the estimated M-O computed with a dynamic pressure coefficient 1 (**figure 3.6)**. Maximum and residual horizontal forces on the wall are 500 kN and 401 kN respectively **(figure 3.10)**. The highest point of application of the resultant force is observed to be equal to 5.9 m at t=3.62 sec while the residual point of application of the resultant force is 3.92 m above the bottom of the wall. And again as noticed from **figure 3.21**the permanent displacement due to rotation is 0.00017m,permanent displacement due to sliding is 0.0115 m and the overall horizontal permanent displacement is 0.012 m and the maximum overall displacement is 0.071 m.The average settlement is 0.016m and the differential settlement is 0.032 m **(figure 3.18).**

The maximum earth pressure behind the right wall is at t=3.68 sec while at the same time as observed from **figure 3.33** the wall is at its local minimum.. The distribution of the maximum earth pressure is in good agreement with the estimated M-O computed with a dynamic pressure coefficient 1 (**figure 3.27)**. Maximum and residual horizontal forces on the wall are 992kN and 773 kN respectively **(figure 3.10)**. The highest point of application of the resultant force is observed to be equal to 6.5 m at t=3.9 sec while the residual point of application of the resultant force is 5.13 m above the bottom of the wall. And again as noticed from **figure 3.33**the permanent displacement due to rotation is 0.011m,permanent displacement due to sliding is 0.024 m and the overall horizontal permanent displacement is 0.035 m and the maximum overall displacement is 0.06 m. The average settlement is 0.0139 m and the differential settlement is 0.03903 m **(figure 3.30).**

Peak ground acceleration 1g:

The maximum earth pressure behind the left wall is at t=3.8 sec while at the same time as observed from **figure 3.22**the wall is at its local minimum which means it is moving inwards. The distribution of the maximum earth pressure is in good agreement with the estimated M-O computed with a dynamic pressure coefficient 1 (**figure 3.7)**. Maximum and residual horizontal forces on the wall are 1251kN and 897 kN respectively **(figure 3.12)**. The highest point of application of the resultant force is observed to be equal to 6.63 m at t=3.66 sec while the residual point of application of the resultant force is 3.9 m above the bottom of the wall. And again as noticed from **figure 3.22**the permanent displacement due to rotation is 0.02m,permanent displacement due to sliding is 0.0163 m and the overall horizontal permanent displacement is 0.0077 m and the maximum overall displacement is 0.132 m.The average settlement is 0.0164m and the differential settlement is 0.06 m **(figure 3.19).**

The maximum earth pressure behind the right wall is at t=3.94 sec while at the same time as observed from **figure 3.34** the wall is moving inwards. The distribution of the maximum earth pressure is in good agreement with the estimated M-O computed with a dynamic pressure coefficient 1 (**figure 3.28)**. Maximum and residual horizontal forces on the wall are 1294kN and 1020kN respectively **(figure 3.12)**. The highest point of application of the resultant force is observed to be equal to 7.1 m at t=3.94 sec while the residual point of application of the

resultant force is 5.6 m above the bottom of the wall. And again as noticed from **figure 3.34**the permanent displacement due to rotation is 0.045m,permanent displacement due to sliding is 0.065 m and the overall horizontal permanent displacement is 0.11 m and the maximum overall displacement is 0.12 m. The average settlement is 0.012 m and the differential settlement is 0.089 m **(figure 3.31).**

As noticed, the dynamic earth pressures on the retaining walls in the second model are greater than that in the first one, especially the residual force for great peak ground accelerations, where it is twice the value.For PGA 0.6g, the residual forces on the left and right wall in the first model are 409 kN and 490 kN respectively **(fig. 2.12)**,while in the second one they are equal to 814 kN and 773 kN **(fig. 3.8)**.One can also notice that the permanent horizontal displacement is much smaller when the foundation soil is stiffer ,furthermore this permanent displacementis also smaller than the maximum displacement that happens instantly. This can explain the greater earth pressures on the walls. Concerning the vertical displacement, as the PGA increases, the maximum differential settlement also increases. The permanent differential settlement is significantly smaller in the second model. Contrary to the first model ,acceleration amplification for both walls can be seen in **fig. 3.14-3.16.**

3.3.2 LEFKADA SEISMIC EXCITATION

Peak ground acceleration 0.3g:

The maximum earth pressure behind the left wall is at t=11.17 sec while at the same time as observed from **figure 3.67** the wall is moving outwards. The distribution of the maximum earth pressure is in good agreement with the estimated M-O computed with a dynamic pressure coefficient 0.75 (**figure 3.52)**. Maximum and residual horizontal forces on the wall are 719 kN and 519 kN respectively **(figure 3.55)**. The highest point of application of the resultant force is observed to be equal to 5.8 m at t=7.14 sec while the residual point of application of the resultant force is 4.8 m above the bottom of the wall. And again as noticed from **figure 3.67** the permanent displacement due to rotation is 0.0081 m,permanent displacement due to sliding is 0.0087 m and the overall horizontal permanent displacement is 0.017 m and the

maximum overall displacement is 0.047 m.The average settlement is 0.014m and the differential settlement is 0.04 m **(figure 3.64).**

The maximum earth pressure behind the right wall is at t=10.99 sec while at the same time as observed from **figure 3.79** the wall is moving outwards. The distribution of the maximum earth pressure is in good agreement with the estimated M-O computed with a dynamic pressure coefficient 0.75 (**figure 3.73)**. Maximum and residual horizontal forces on the wall are 700kN and 530 kN respectively **(figure 3.55)**. The highest point of application of the resultant force is observed to be equal to 5.9 m at t=12.17 sec while the residual point of application of the resultant force is 5.1 m above the bottom of the wall. And again as noticed from **figure 3.79** the permanent displacement due to rotation is 0.0097m,permanent displacement due to sliding is 0.0006 m and the overall horizontal permanent displacement is 0.0102 m and the maximum overall displacement is 0.040 m. The average settlement is 0.014 m and the differential settlement is 0.05 m **(figure 3.76).**

Peak ground acceleration 0.6g:

The maximum earth pressure behind the left wall is at t=11.18 sec while at the same time as observed from **figure 3.68** the wall is moving inwards. The distribution of the maximum earth pressure is in good agreement with the estimated M-O computed with a dynamic pressure coefficient 1.0 (**figure 3.53)**. Maximum and residual horizontal forces on the wall are 1200 kN and 845 kN respectively **(figure 3.57)**. The highest point of application of the resultant force is observed to be equal to 6.8 m at t=7.17 sec while the residual point of application of the resultant force is 4.5 m above the bottom of the wall. And again as noticed from **figure 3.68**the permanent displacement due to rotation is 0.04m,permanent displacement due to sliding is 0.072 m and the overall horizontal permanent displacement is 0.11 m and the maximum overall displacement is 0.14 m.The average settlement is 0.02m and the differential settlement is 0.11 m **(figure 3.65).**

The maximum earth pressure behind the right wall is at t=9.25 sec while at the same time as observed from **figure 3.80** the wall isat its local minimum. The distribution of the maximum earth pressure is in good agreement with the estimated M-O computed with a dynamic pressure coefficient 1.0 (**figure 3.74)**. Maximum and residual horizontal forces on the wall are

1284kN and 813 kN respectively **(figure 3.57)**. The highest point of application of the resultant force is observed to be equal to 6.85 m at t=6.3 sec while the residual point of application of the resultant force is 4.8 m above the bottom of the wall. And again as noticed from **figure 3.80**the permanent displacement due to rotation is 0.05m,permanent displacement due to sliding is 0.009 m and the overall horizontal permanent displacement is 0.040 m and the maximum overall displacement is 0.08 m. The average settlement is 0.018 m and the differential settlement is 0.09 m **(figure 3.77).**

Peak ground acceleration 0.9g:

The maximum earth pressure behind the left wall is at t=12.51 sec while at the same time as observed from **figure 3.69** the wall is at its local minimum. The distribution of the maximum earth pressure is in good agreement with the estimated M-O computed with a dynamic pressure coefficient 1.0 (**figure 3.54)**. Maximum and residual horizontal forces on the wall are 1519 kN and 917 kN respectively **(figure 3.59)**. The highest point of application of the resultant force is observed to be equal to 7.4 m at t=7.19 sec while the residual point of application of the resultant force is 4.6 m above the bottom of the wall. And again as noticed from **figure 3.69** the permanent displacement due to rotation is 0.113 m,permanent displacement due to sliding is 0.0.93 m and the overall horizontal permanent displacement is 0.21 m and the maximum overall displacement is 0.28 m.The average settlement is 0.008 m and the differential settlement is 0.15 m **(figure 3.66).**

The maximum earth pressure behind the right wall is at t=10.12 sec while at the same time as observed from **figure 3.81** the wall is at its local minimum . The distribution of the maximum earth pressure is in good agreement with the estimated M-O computed with a dynamic pressure coefficient 1.0 (**figure 3.75)**. Maximum and residual horizontal forces on the wall are 1583 kN and 784 kN respectively **(figure 3.59)**. The highest point of application of the resultant force is observed to be equal to 7.4 m at t=8.9 sec while the residual point of application of the resultant force is 4.7 m above the bottom of the wall. And again as noticed from **figure 3.81** the permanent displacement due to rotation is 0.13 m,permanent displacement due to sliding is 0.133 m and the overall horizontal permanent displacement is 0.27 m and the maximum

overall displacement is 0.31 m. The average settlement is 0.011 m and the differential settlement is 0.089 m **(figure 3.78).**

We can notice again as in the Aegion seismic excitation, the dynamic earth pressures on the retaining walls in the second model are greater than that in the first one, especially the residual force for great peak ground accelerations, where it is twice the value. For PGA 0.6g, the residual forces on the left and right wall in the first model are 400 kN and 377 kN respectively **(fig. 2.79)**, while in the second one they are equal to 845 kN and 813 kN **(fig. 3.57)**.One can also notice that the permanent horizontal displacement is much smaller when the foundation soil is stiffer,but in this case the permanent displacement is almost equal to the maximum displacement. This can explain the greater earth pressures on the walls.The relationship between the PGA and the horizontal displacement is not linear anymore **(fig. 3.94).** Concerning the vertical displacement, as the PGA increases, the maximum differential settlement of the left wall also increases,while the right wall has almost the same differential settlement for peak ground accelerations greater than 0.4 g **(fig. 3.95).**. The permanent differential settlement is significantly smaller in the second model.

3.3.3 TAKATORI SEISMIC EXCITATION

Peak ground acceleration 0.3g:

The maximum earth pressure behind the left wall is at t=5.88 sec while at the same time as observed from **figure 3.114**the wall is as its local minimum. The distribution of the maximum earth pressure is in good agreement with the estimated M-O computed with a dynamic pressure coefficient 0.75 (**figure 3.99)**. Maximum and residual horizontal forces on the wall are 707kN and 512 kN respectively **(figure 3.102)**. The highest point of application of the resultant force is observed to be equal to 5.5 m at t=5.6 sec while the residual point of application of the resultant force is 4.6 m above the bottom of the wall. And again as noticed from **figure 3.114**the permanent displacement due to rotation is 0.005m,permanent displacement due to sliding is 0.017 m and the overall horizontal permanent displacement is 0.023 m and the

maximum overall displacement is 0.085 m.The average settlement is 0.014 m and the differential settlement is 0.031 m **(figure 3.111).**

The maximum earth pressure behind the right wall is at t=6.88 sec while at the same time as observed from **figure 3.126** the wall is moving inwards. The distribution of the maximum earth pressure is in good agreement with the estimated M-O computed with a dynamic pressure coefficient 0.75 (**figure 3.120)**. Maximum and residual horizontal forces on the wall are 683kN and 520 kN respectively **(figure 3.102)**. The highest point of application of the resultant force is observed to be equal to 5.8 m at t=5.02 sec while the residual point of application of the resultant force is 4.8 m above the bottom of the wall. And again as noticed from **figure 3.126**the permanent displacement due to rotation is 0.0071m,permanent displacement due to sliding is 0.0098 m and the overall horizontal permanent displacement is 0.0027 m and the maximum overall displacement is 0.066 m. The average settlement is 0.014 m and the differential settlement is 0.04 m **(figure 3.123).**

Peak ground acceleration 0.6g:

The maximum earth pressure behind the left wall is at t=5.9 sec while at the same time as observed from **figure 3.115**the wall is as its local minimum. The distribution of the maximum earth pressure is in good agreement with the estimated M-O computed with a dynamic pressure coefficient 1 and has more a trapezoid shape (**figure 3.100)**. Maximum and residual horizontal forces on the wall are 1359kN and 789 kN respectively **(figure 3.104)**. The highest point of application of the resultant force is observed to be equal to 6.8 m at t=5.6 sec while the residual point of application of the resultant force is 4.5 m above the bottom of the wall. And again as noticed from **figure 3.115**the permanent displacement due to rotation is 0.03m,permanent displacement due to sliding is 0.0015 m and the overall horizontal permanent displacement is 0.023 m and the maximum overall displacement is 0.028 m.The average settlement is 0.014 m and the differential settlement is 0.082 m **(figure 3.112).**

The maximum earth pressure behind the right wall is at t=6.42 sec while at the same time as observed from **figure 3.127** the wall isits local minimum. The distribution of the maximum earth pressure is in good agreement with the estimated M-O computed with a dynamic pressure

coefficient 1 (**figure 3.121)**. Maximum and residual horizontal forces on the wall are 1162kN and 894 kN respectively **(figure 3.102)**. The highest point of application of the resultant force is observed to be equal to 6.8 m at t=4.7 sec while the residual point of application of the resultant force is 4.9 m above the bottom of the wall. And again as noticed from **figure 3.127**the permanent displacement due to rotation is 0.05m,permanent displacement due to sliding is 0.052 m and the overall horizontal permanent displacement is 0.104 m and the maximum overall displacement is 0.17 m. The average settlement is 0.19 m and the differential settlement is 0.12 m **(figure 3.124).**

Peak ground acceleration 0.9g:

The maximum earth pressure behind the left wall is at t=5.94 sec while at the same time as observed from **figure 3.116**the wall is as its local minimum. The distribution of the maximum earth pressure is in good agreement with the estimated M-O computed with a dynamic pressure coefficient 1 (**figure 3.101)**. Maximum and residual horizontal forces on the wall are 1698kN and 851 kN respectively **(figure 3.106)**. The highest point of application of the resultant force is observed to be equal to 6.8 m at t=10.19 sec while the residual point of application of the resultant force is 5.4 m above the bottom of the wall. And again as noticed from **figure 3.116**the permanent displacement due to rotation is 0.10m,permanent displacement due to sliding is 0.11 m and the overall horizontal permanent displacement is 0.21 m and the maximum overall displacement is 0.36 m.The average settlement is 0.003m and the differential settlement is 0.19 m **(figure 3.113).**

The maximum earth pressure behind the right wall is at t=6.44 sec while at the same time as observed from **figure 3.128** the wall is its local minimum . The distribution of the maximum earth pressure is in good agreement with the estimated M-O computed with a dynamic pressure coefficient 1 (**figure 3.122)**. Maximum and residual horizontal forces on the wall are 1615kN and 1093 kN respectively **(figure 3.106)**. The highest point of application of the resultant force is observed to be equal to 7.9 m at t=4.7 sec while the residual point of application of the resultant force is 4.0 m above the bottom of the wall. And again as noticed from **figure 3.128**the permanent displacement due to rotation is 0.15 m,permanent

displacement due to sliding is 0.052 m and the overall horizontal permanent displacement is 0.15 m and the maximum overall displacement is 0.30 m. The average settlement is 0.01 m and the differential settlement is 0.19 m **(figure 3.125).**

Chapter 3

FIGURES

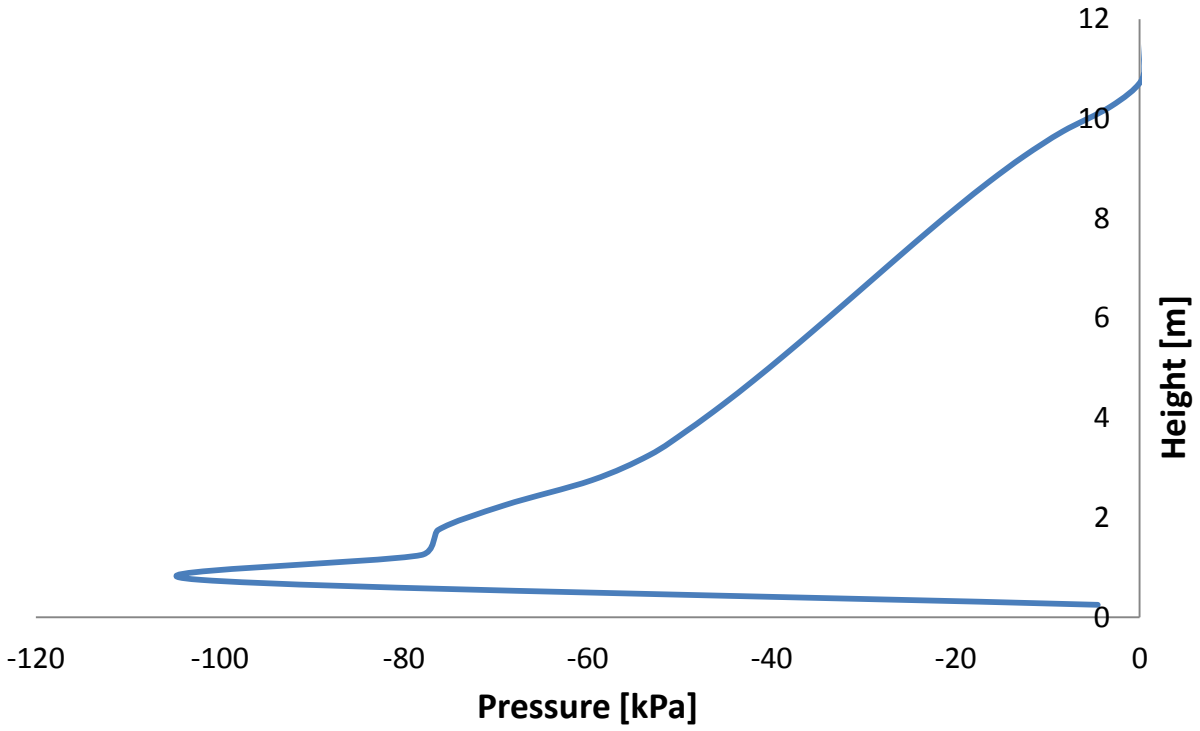

Fig. 3.1. Distribution of static earth pressure computed using the ABAQUS.

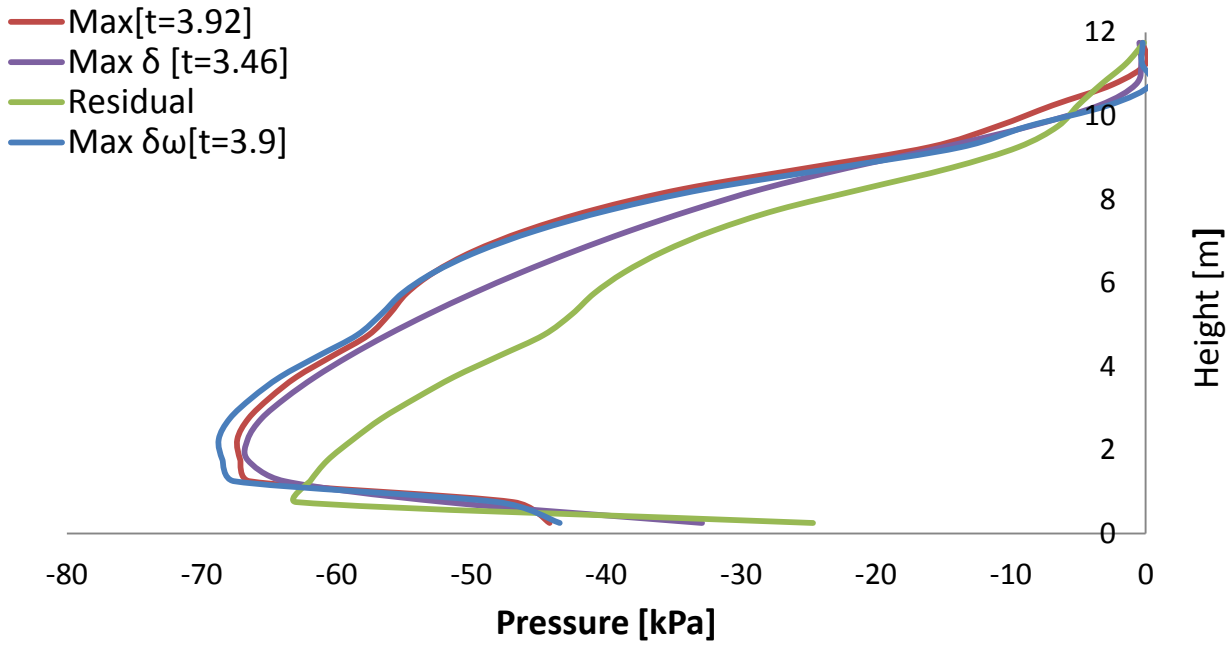

Fig. 3.2. Earth pressures profiles on the left wall at different moments when subjected to Aegion Seismic excitation with peak ground acceleration 0.2g.

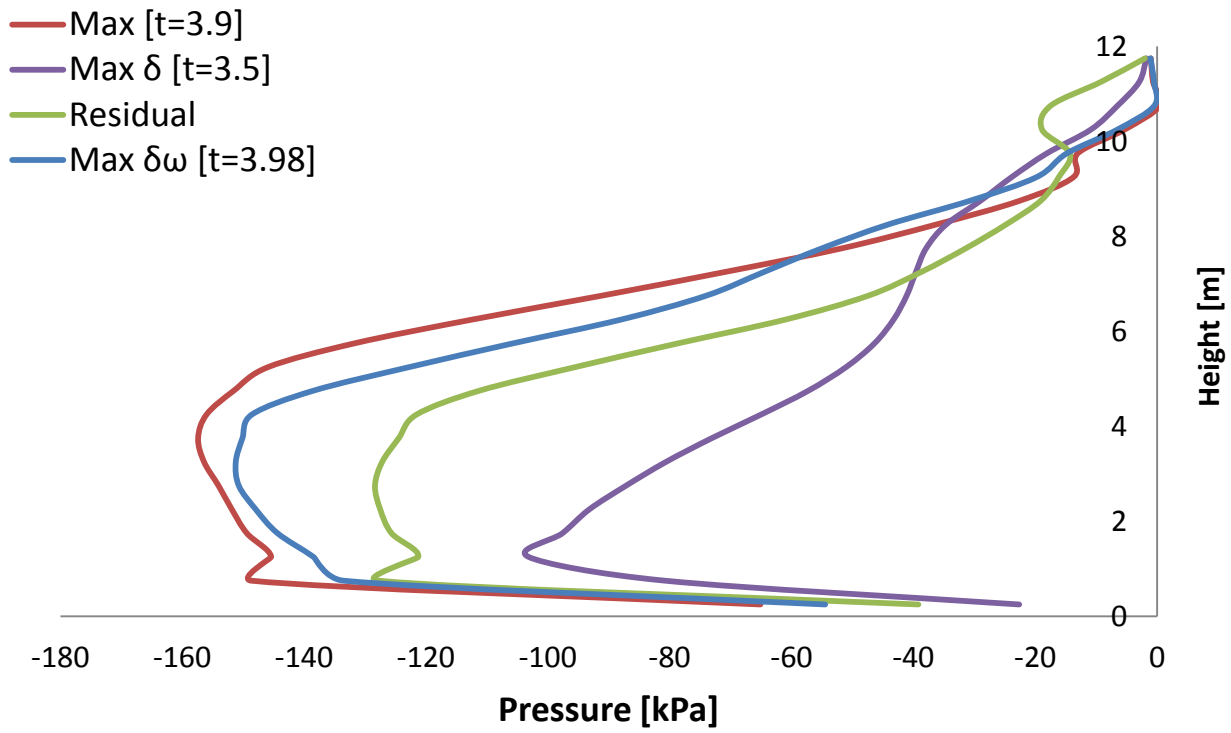

Fig. 3.3. Earth pressures profiles on the left wall at different moments when subjected to Aegion Seismic excitation with peak ground acceleration 0.6g.

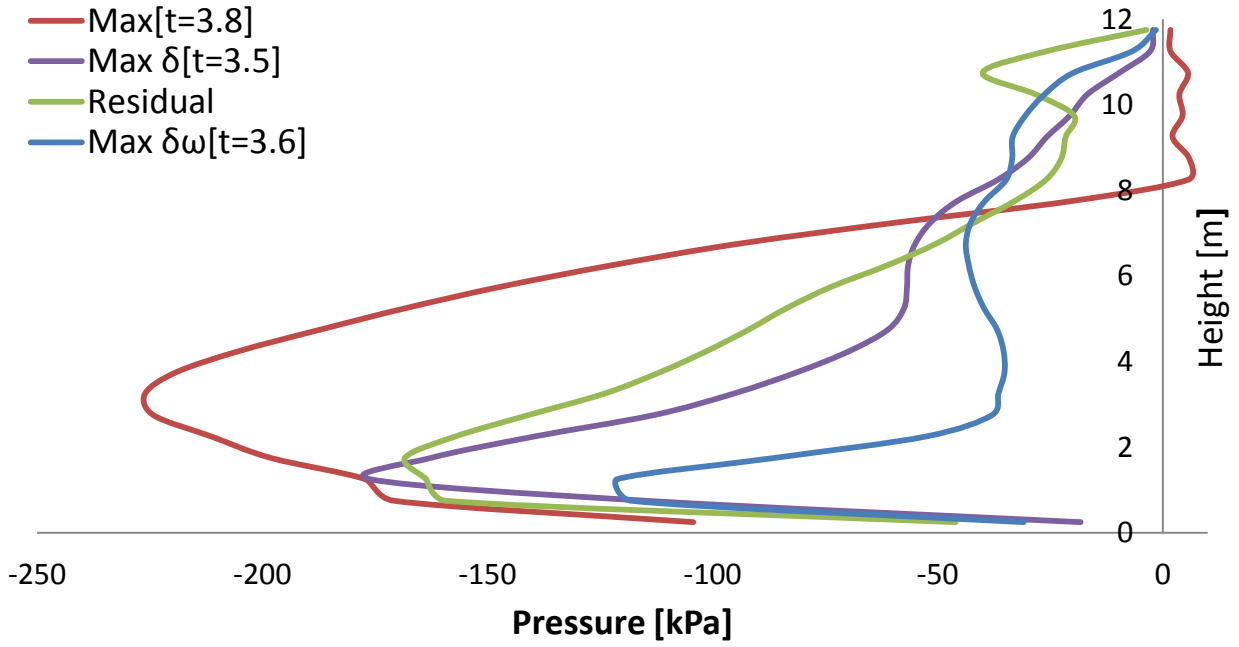

Fig. 3.4. Earth pressures profiles on the left wall at different moments when subjected to Aegion Seismic excitation with peak ground acceleration 1g..

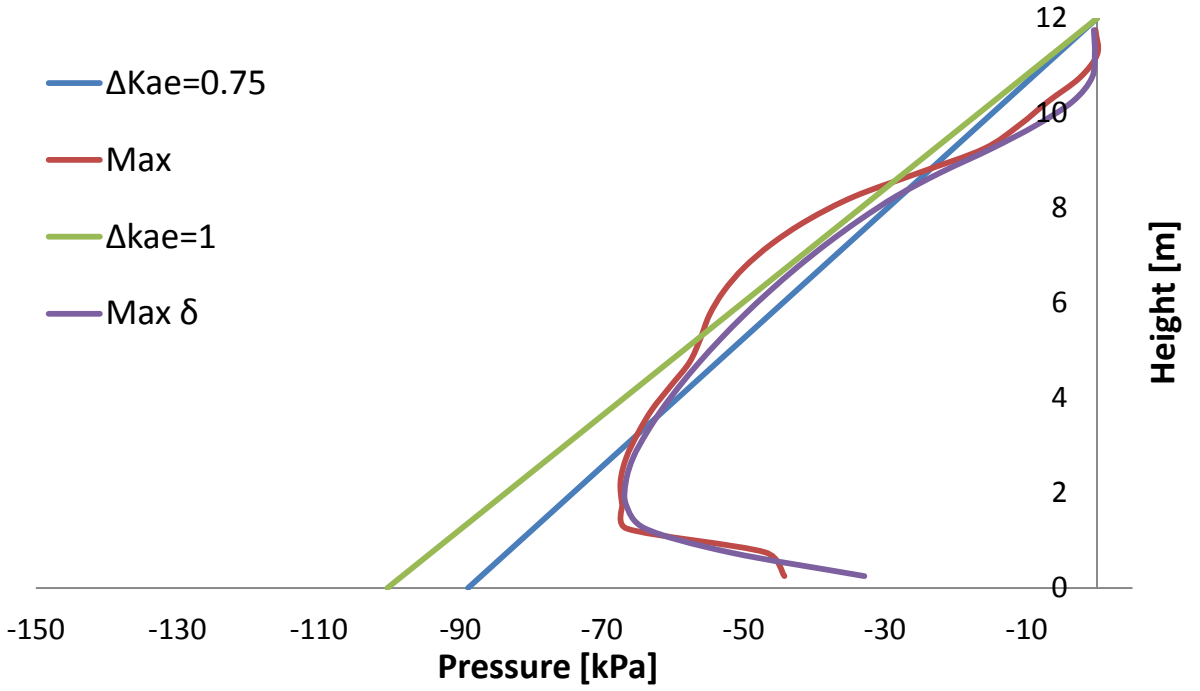

Fig. 3.5. Earth pressure profiles computed in ABAQUS and estimated using the M-O when the left wall is subjected to the Aegion Seismic excitation with peak acceleration 0.2g.

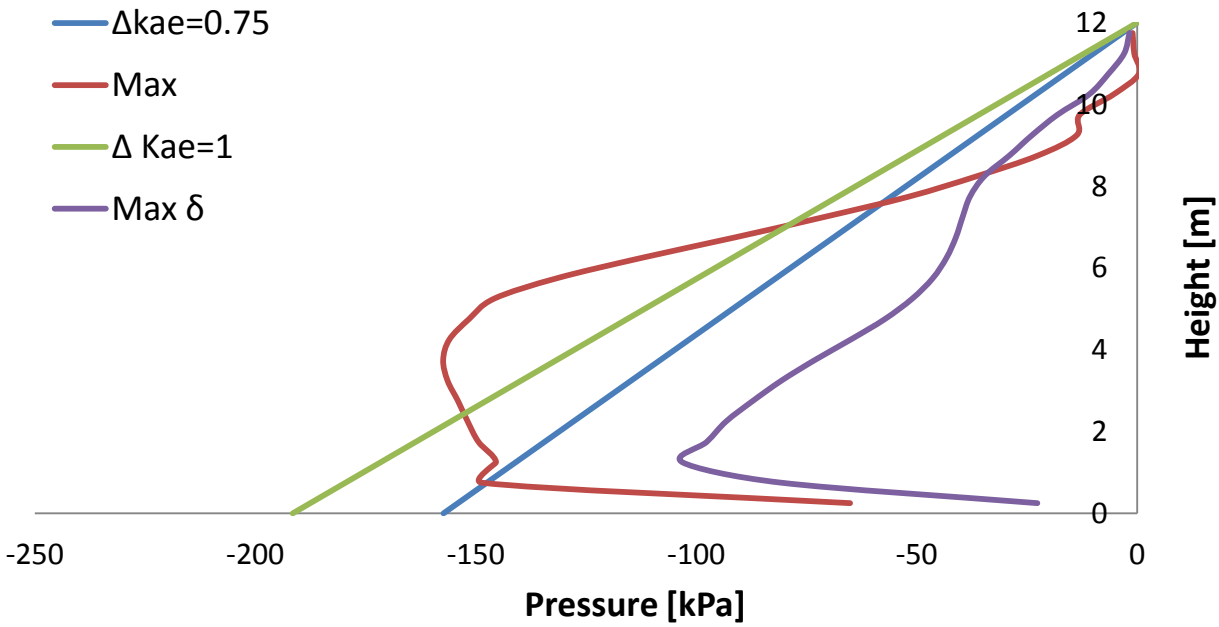

Fig. 3.6. Earth pressure profiles computed in ABAQUS and estimated using the M-O when the left wall is subjected to the Aegion Seismic excitation with peak acceleration 0.6g.

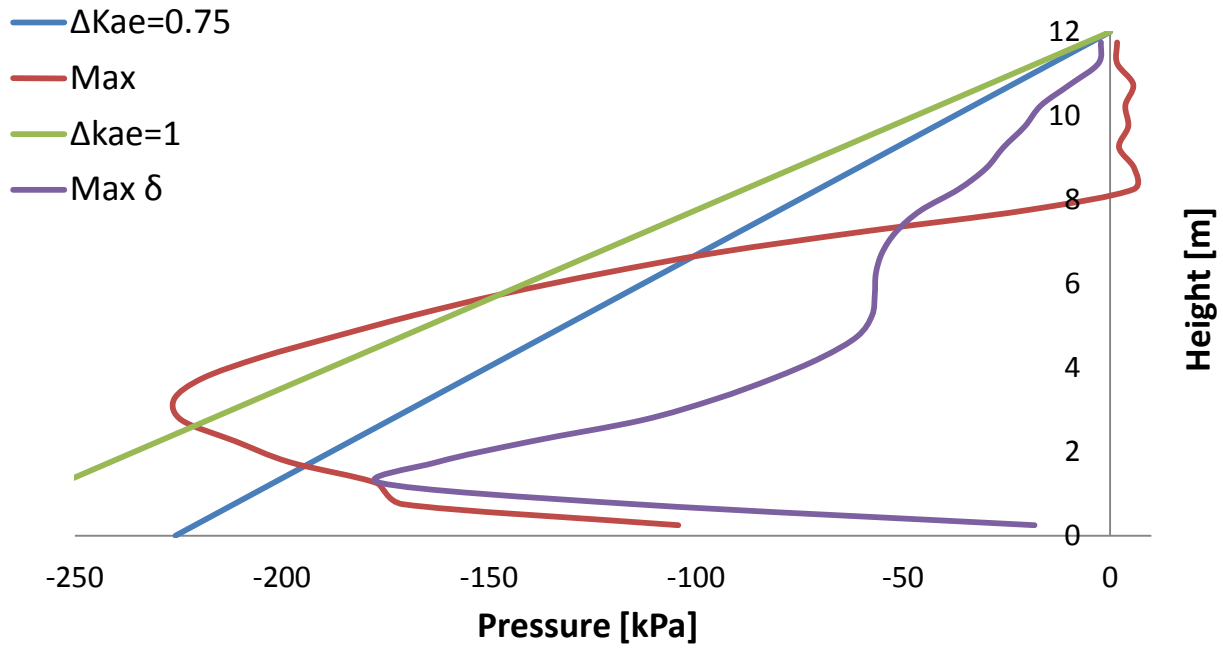

Fig. 3.7. Earth pressure profiles computed in ABAQUS and estimated using the M-O when the left wall is subjected to the Aegion Seismic excitation with peak acceleration 1g.

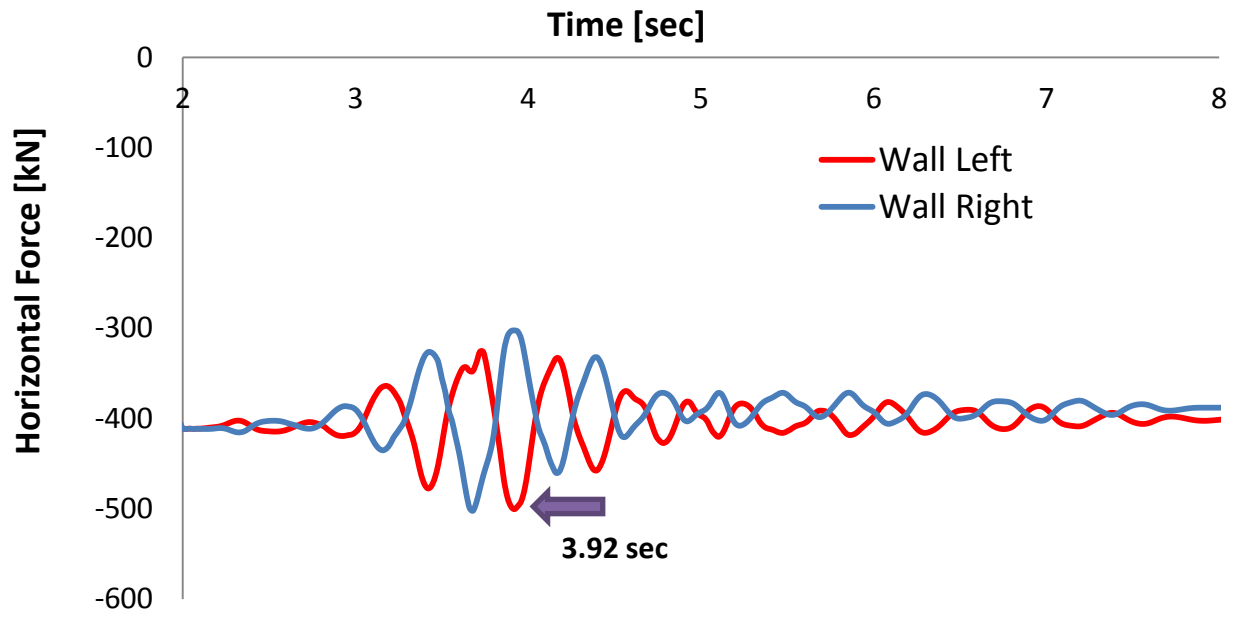

Fig. 3.8. Horizontal force-time history of the left wall when subjected to Aegion Seismic excitation with peak ground acceleration 0.2g.

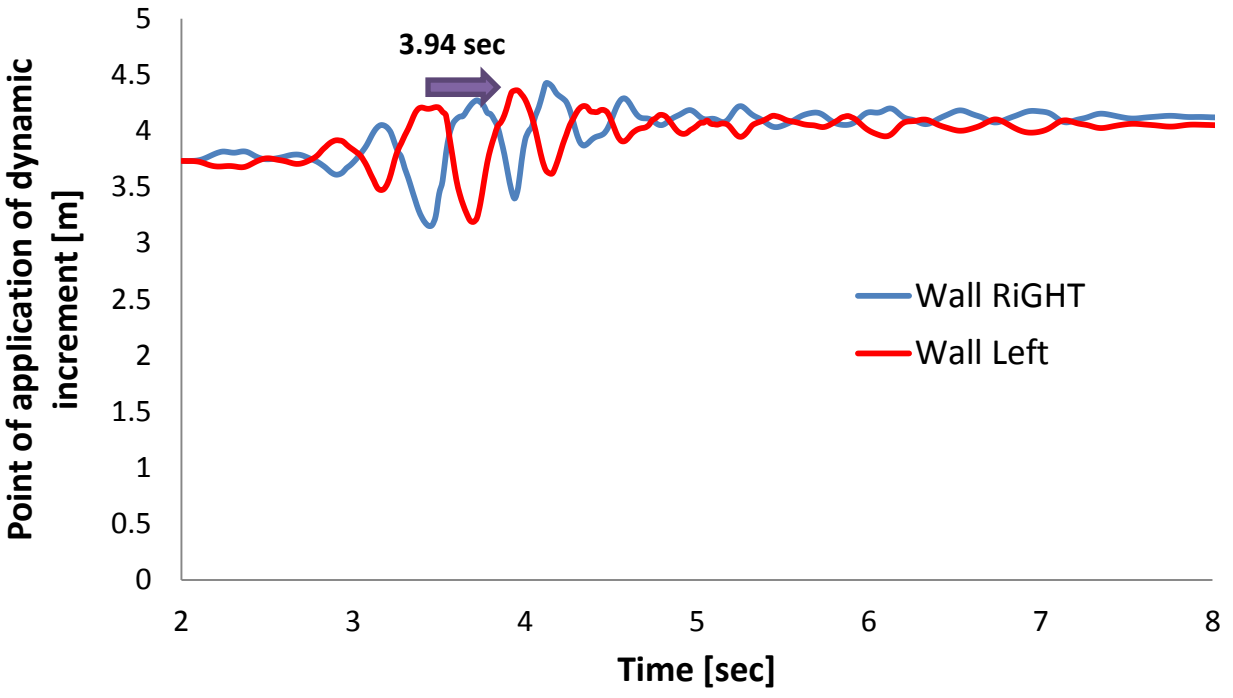

Fig. 3.9. Point of application of dynamic force on the left and right wall when subjected to Aegion Seismic excitation with peak ground acceleration 0.2g.

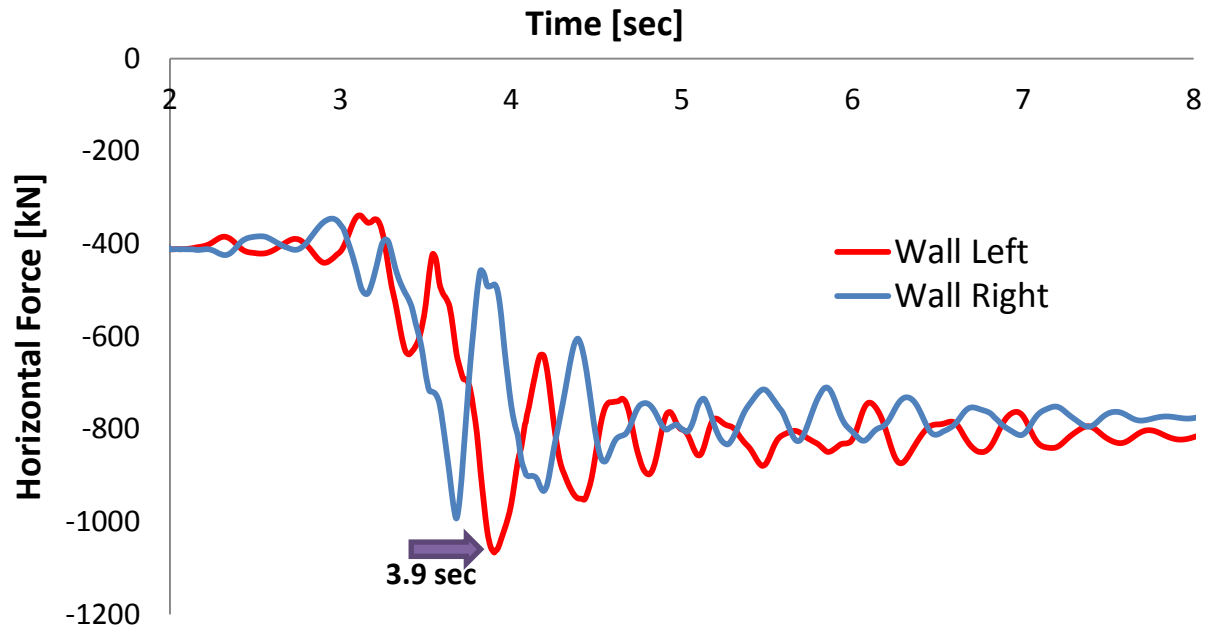

Fig. 3.10. Horizontal force-time history of the left wall when subjected to Aegion Seismic excitation with peak ground acceleration 0.6g.

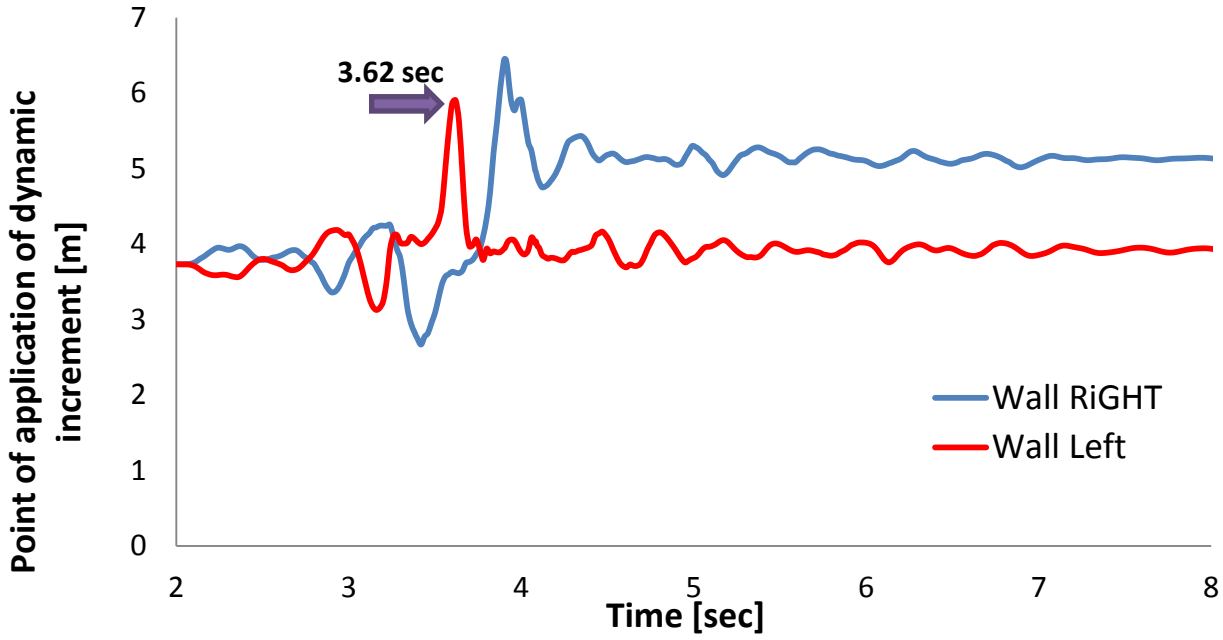

Fig. 3.11. Point of application of dynamic force on the left and right wall when subjected to Aegion Seismic excitation with peak ground acceleration 0.6g.

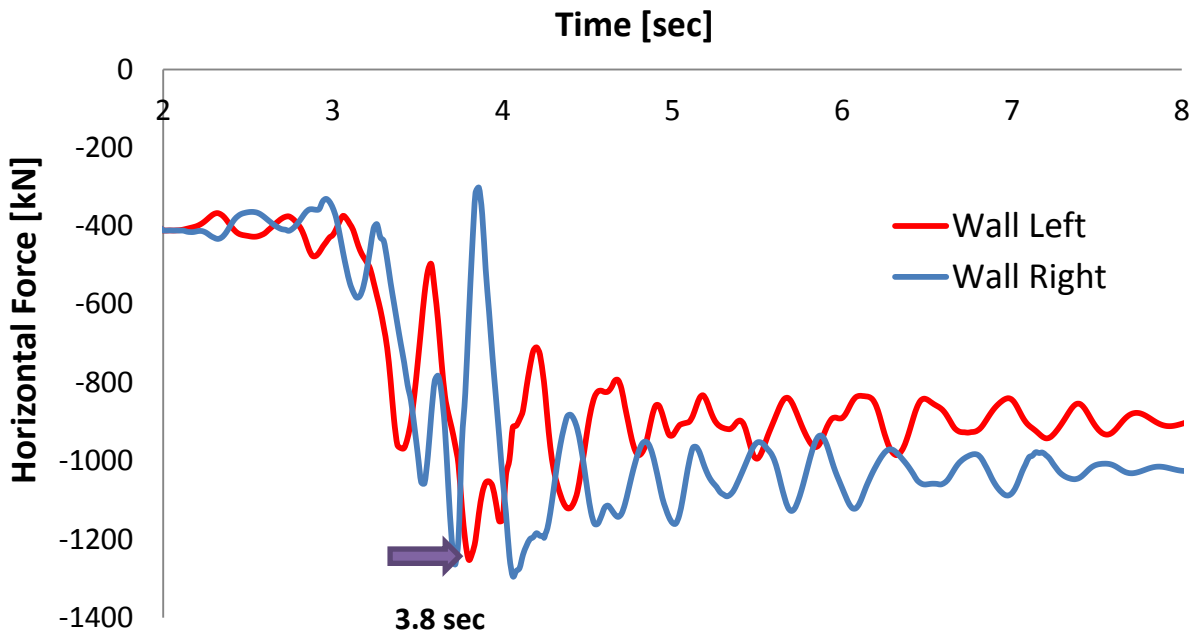

Fig. 3.12. Horizontal force-time history of the left wall when subjected to Aegion Seismic excitation with peak ground acceleration 1g.

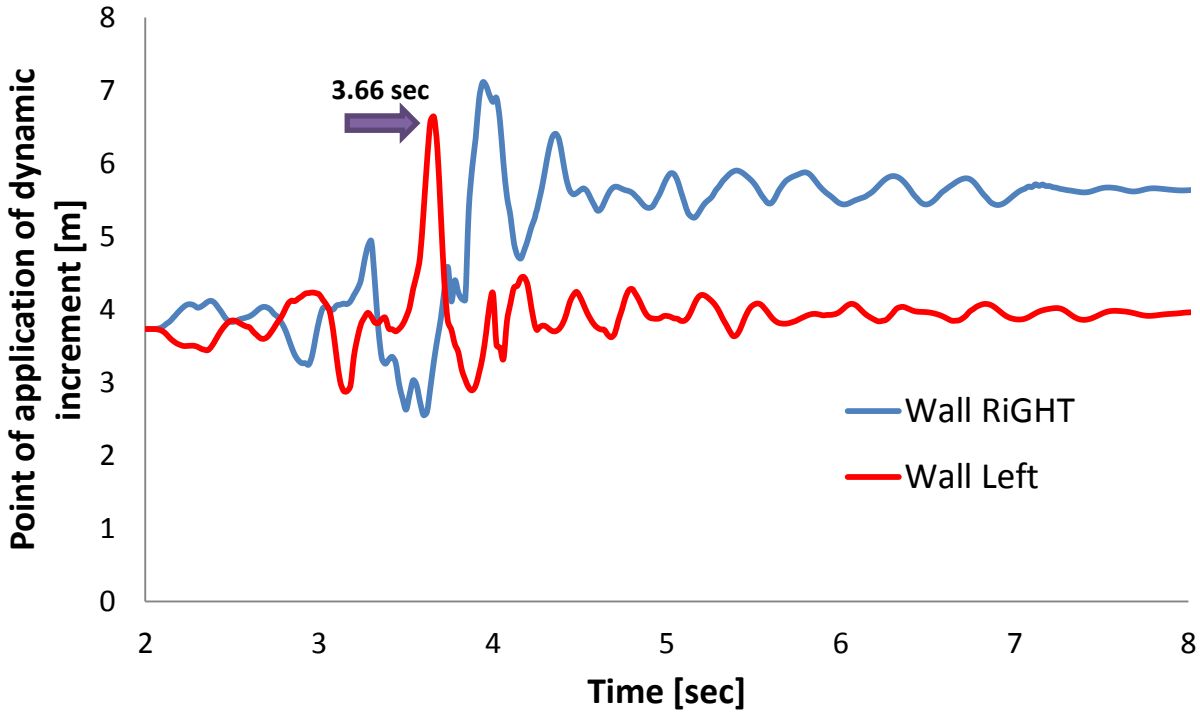

Fig. 3.13. Point of application of dynamic force on the left and right wall when subjected to Aegion Seismic excitation with peak ground acceleration 1g.

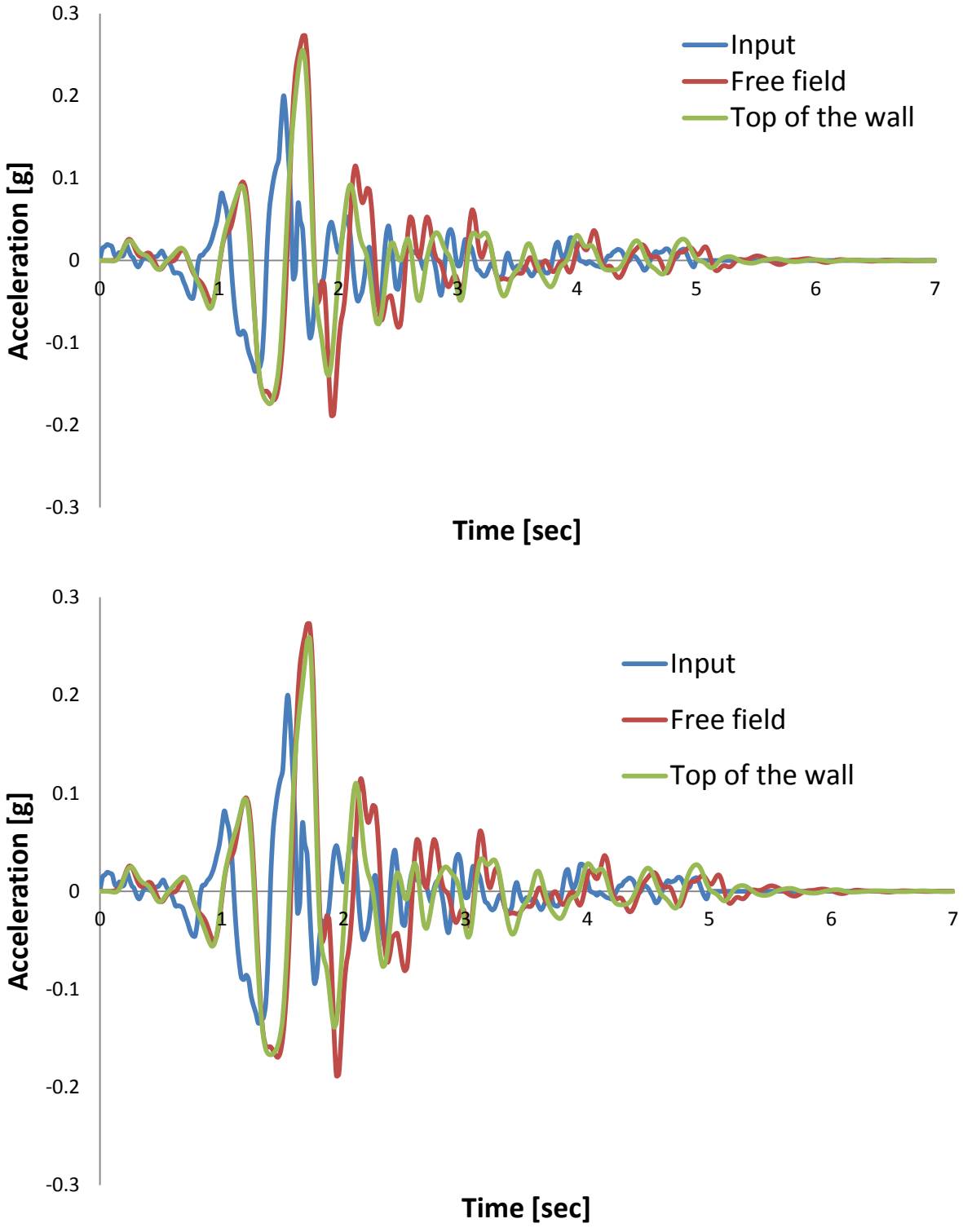

Fig. 3.14. Comparison of input acceleration and computed at the top of the a)left wall b)right wall and top of the free field when subjected to Aegion Seismic excitation with peak acceleration 0.2g.

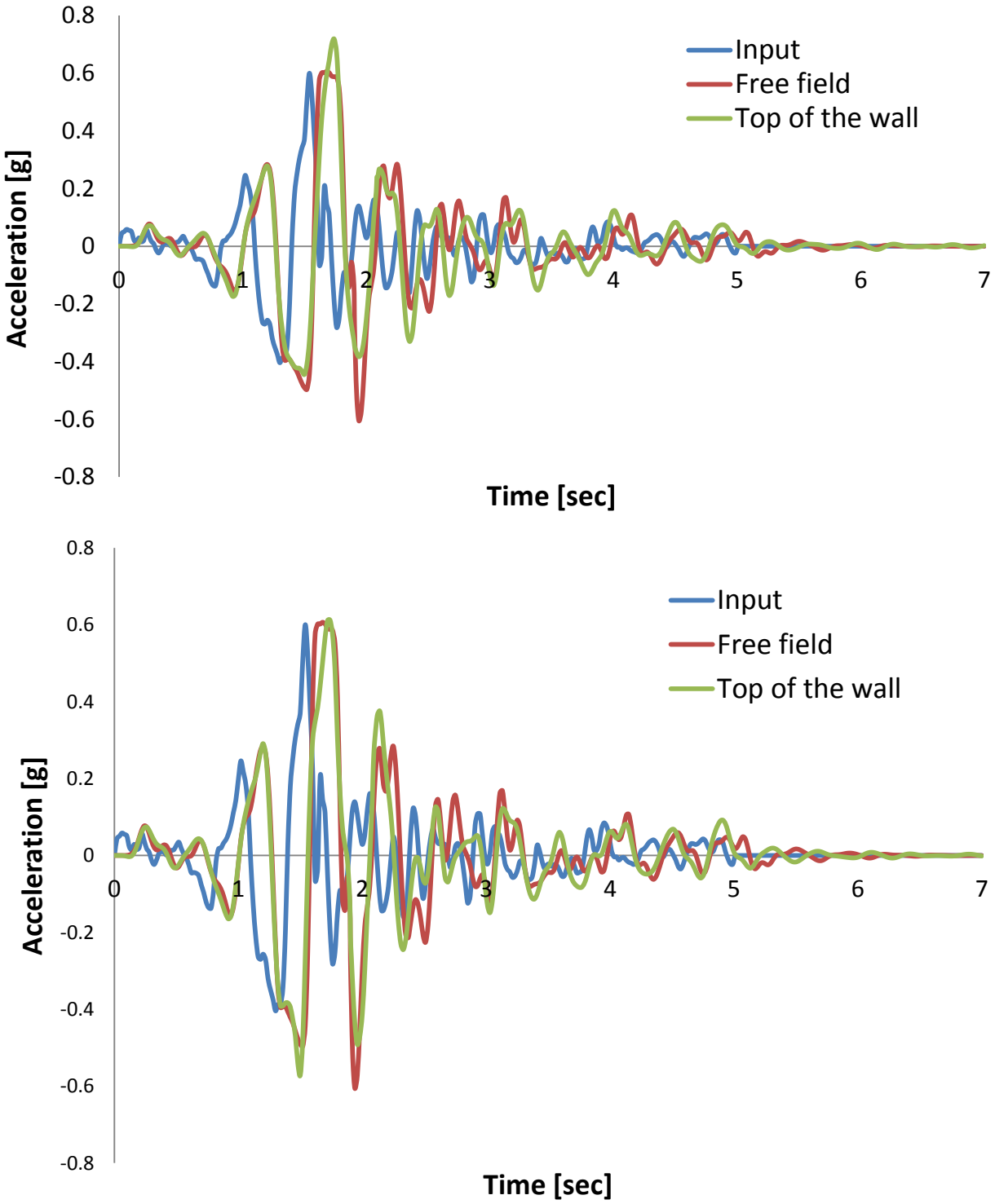

Fig. 3.15. Comparison of input acceleration and computed at the top of the a)left wall b)right wall and top of the free field when subjected to Aegion Seismic excitation with peak acceleration 0.6g.

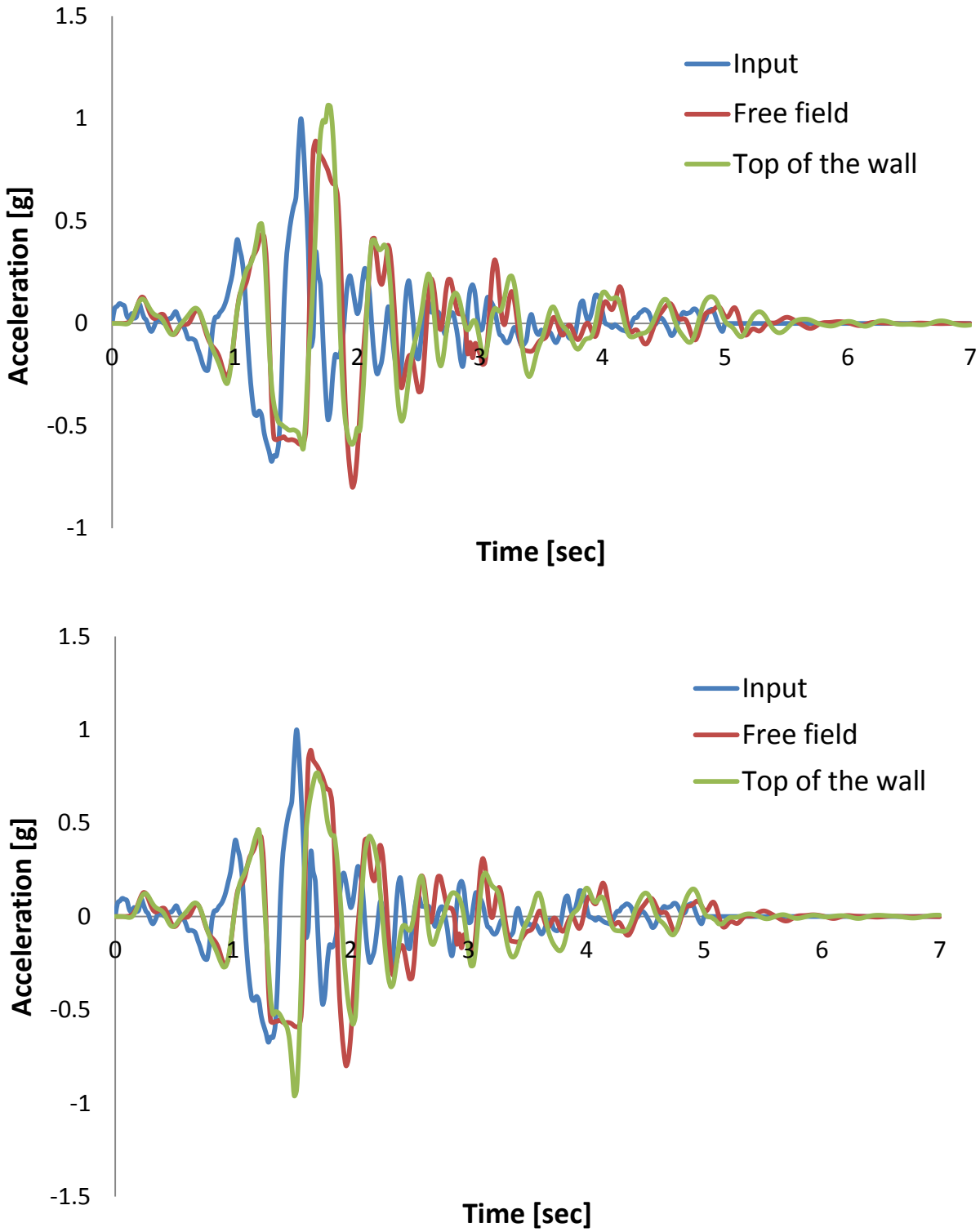

Fig. 3.16. Comparison of input acceleration and computed at the top of the a)left wall b)right wall and top of the free field when subjected to Aegion Seismic excitation with peak acceleration 1 g.

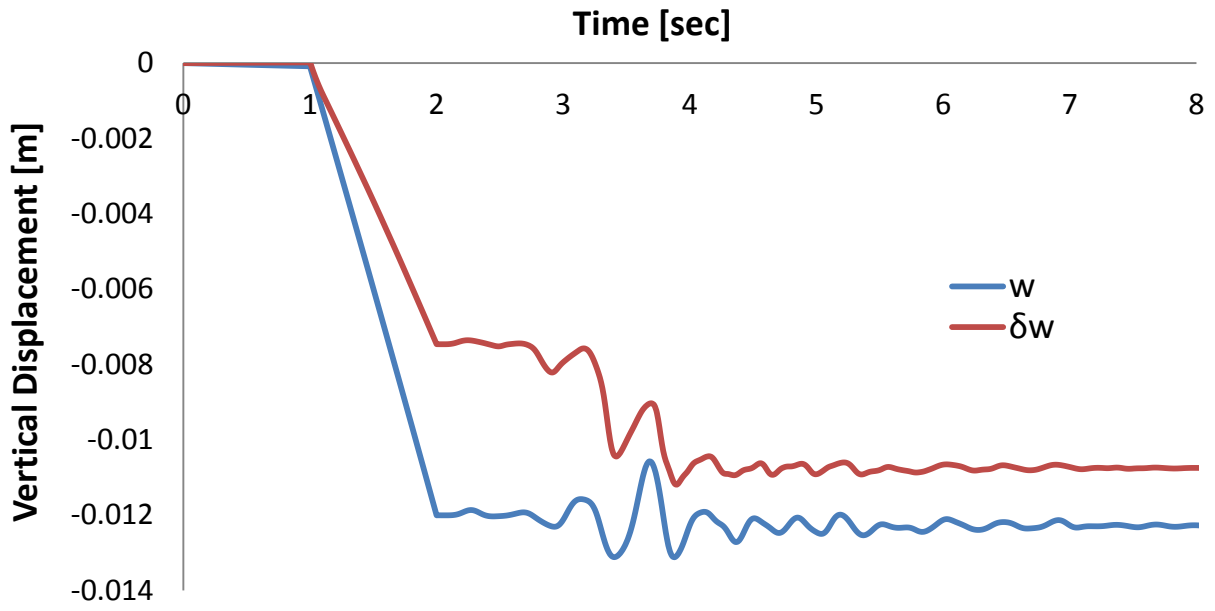

Fig. 3.17. Vertical displacement-time history of the left wall when subjected to Aegion Seismic excitation with peak acceleration 0.2g.

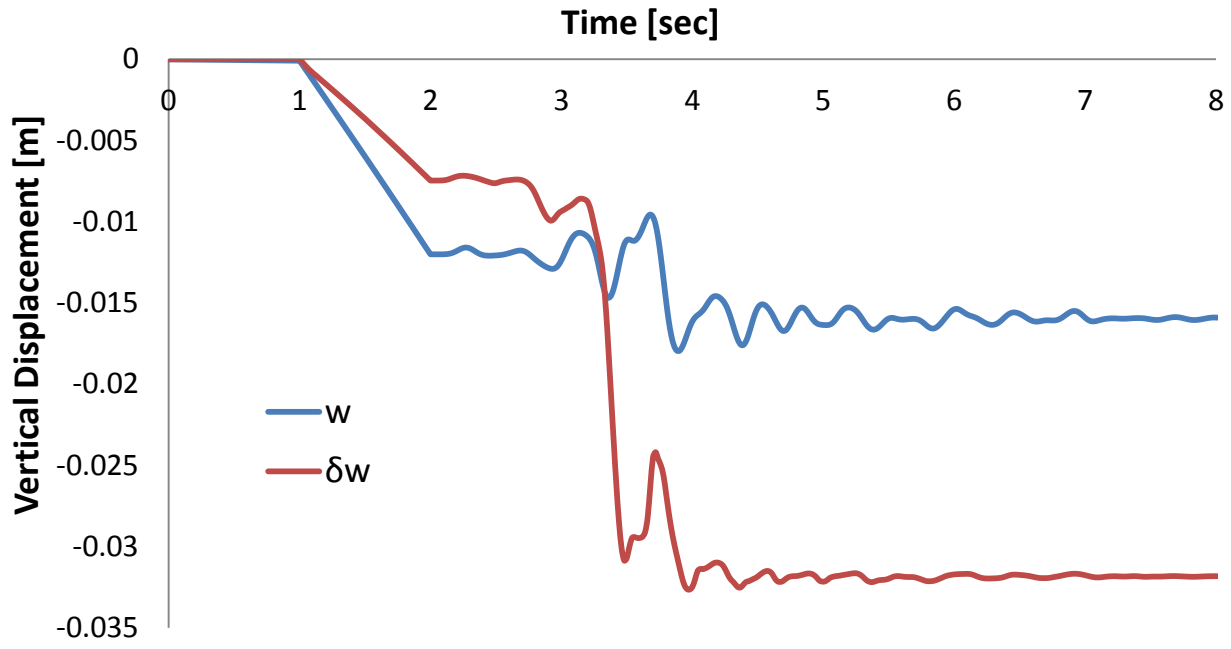

Fig. 3.18. Vertical displacement-time history of the left wall when subjected to Aegion Seismic excitation with peak acceleration 0.6g.

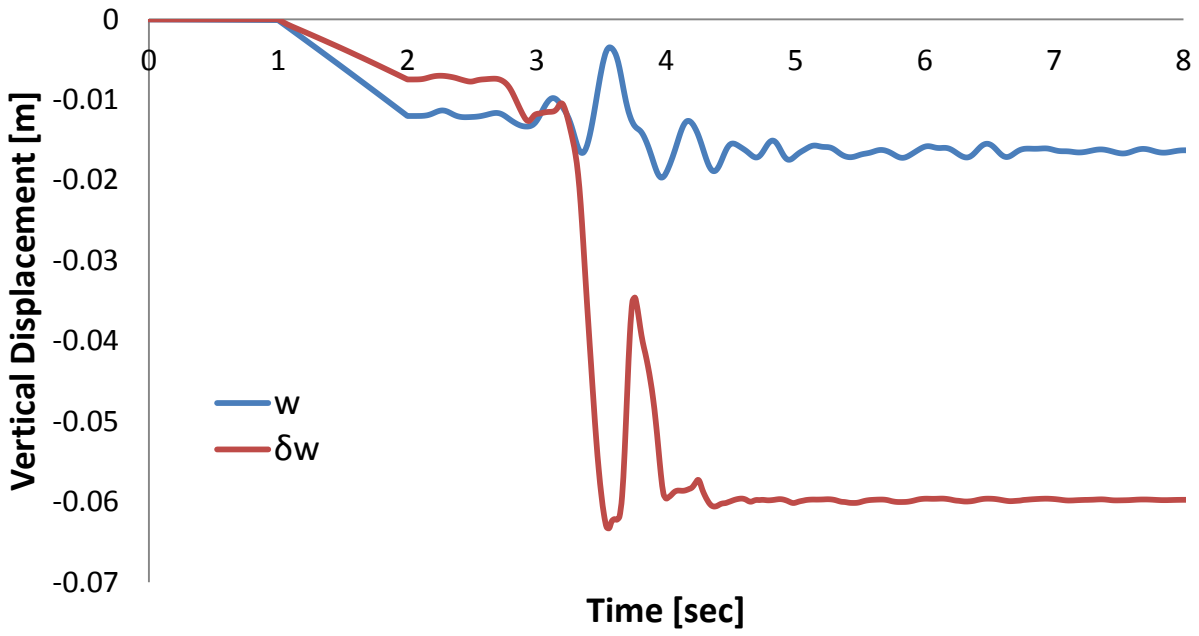

Fig. 3.19. Vertical displacement-time history of the left wall when subjected to Aegion Seismic excitation with peak acceleration 1g.

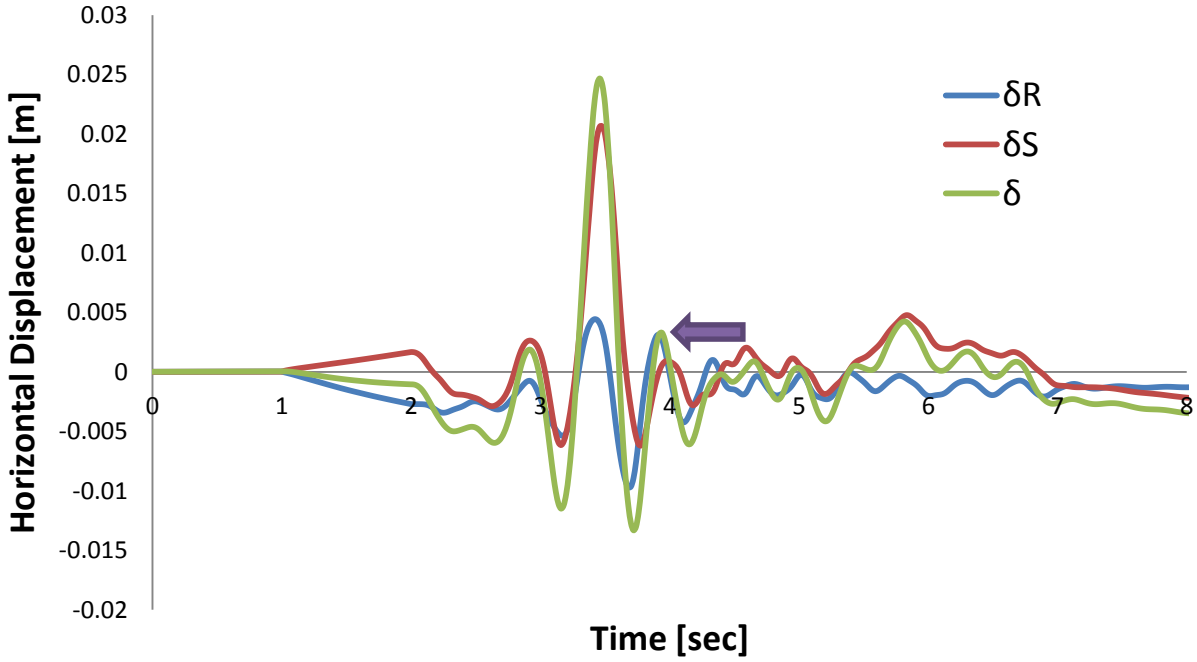

Fig. 3.20. Horizontal displacement-time history of the left wall when subjected to Aegion Seismic excitation with peak acceleration 0.2g.

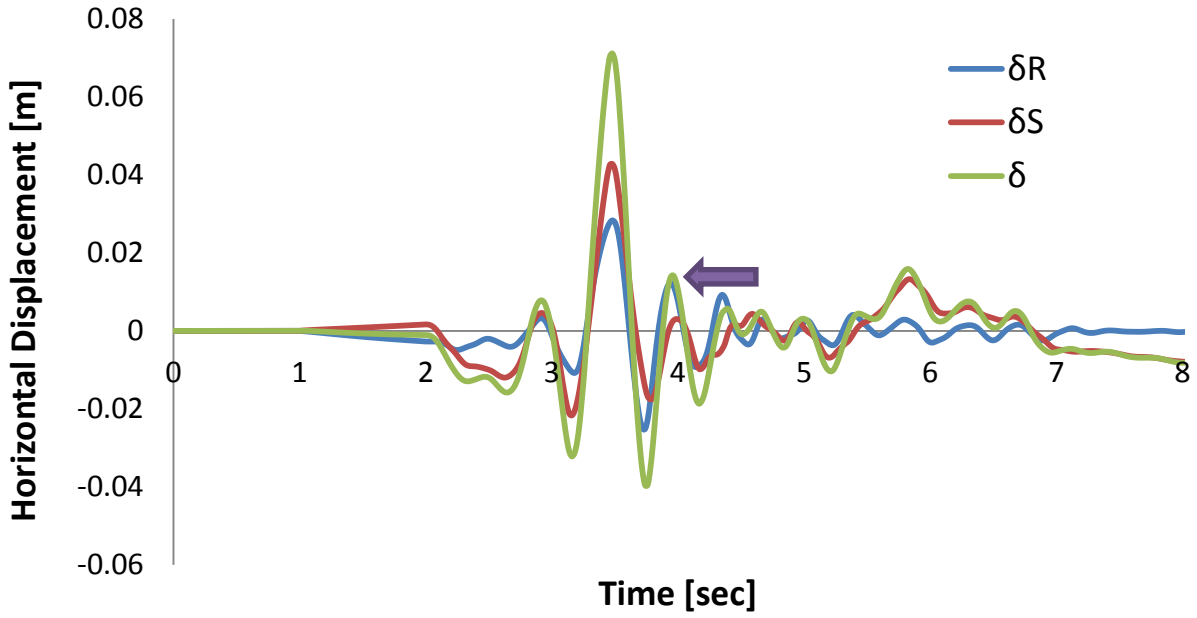

Fig. 3.21. Horizontal displacement-time history of the left wall when subjected to Aegion Seismic excitation with peak acceleration 0.6g.

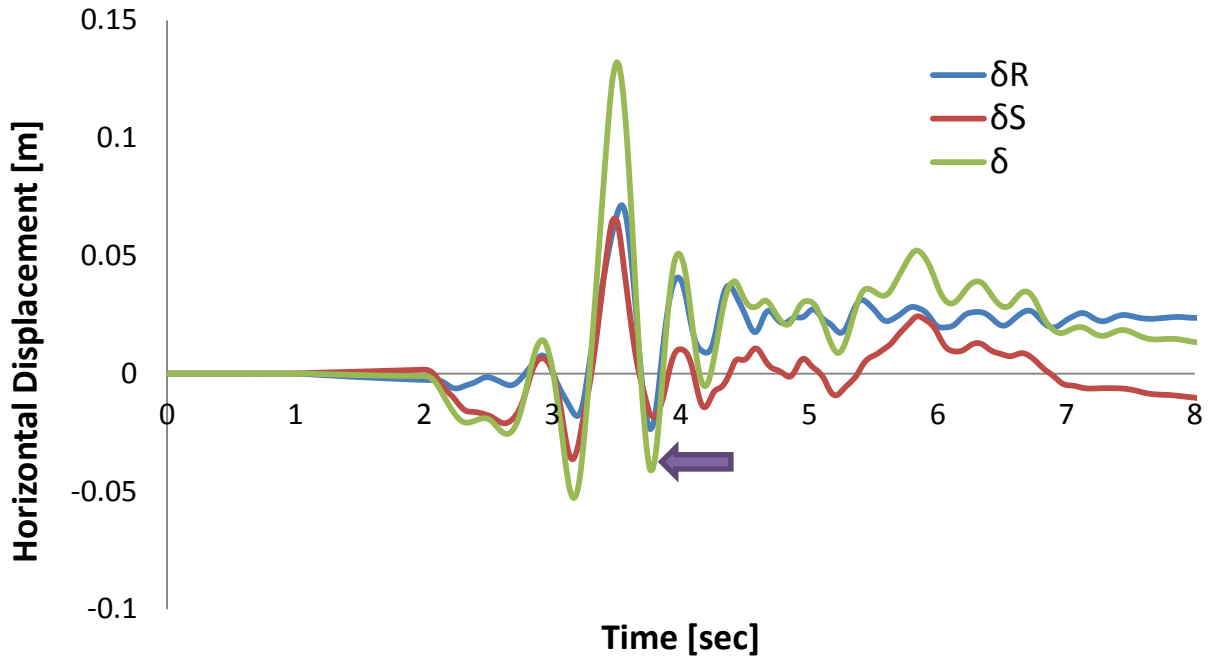

Fig. 3.22. Horizontal displacement-time history of the left wall when subjected to Aegion Seismic excitation with peak acceleration 1g.

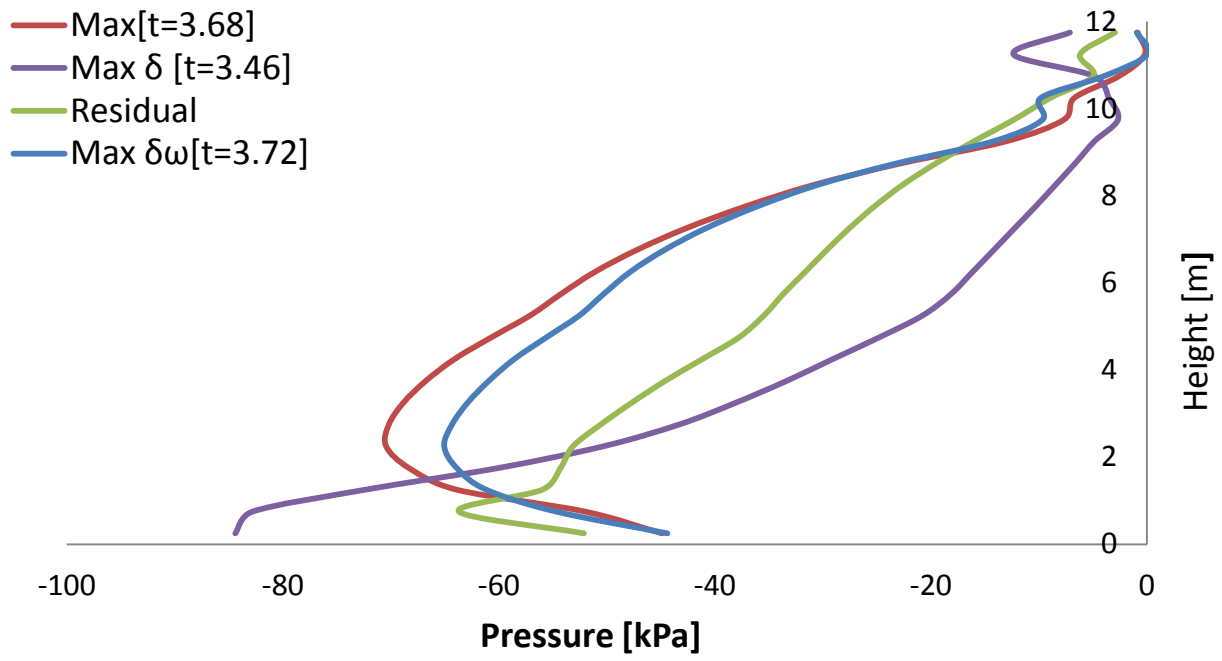

Fig. 3.23. Earth pressures profiles on the right wall at different moments when subjected to Aegion Seismic excitation with peak ground acceleration 0.2g.

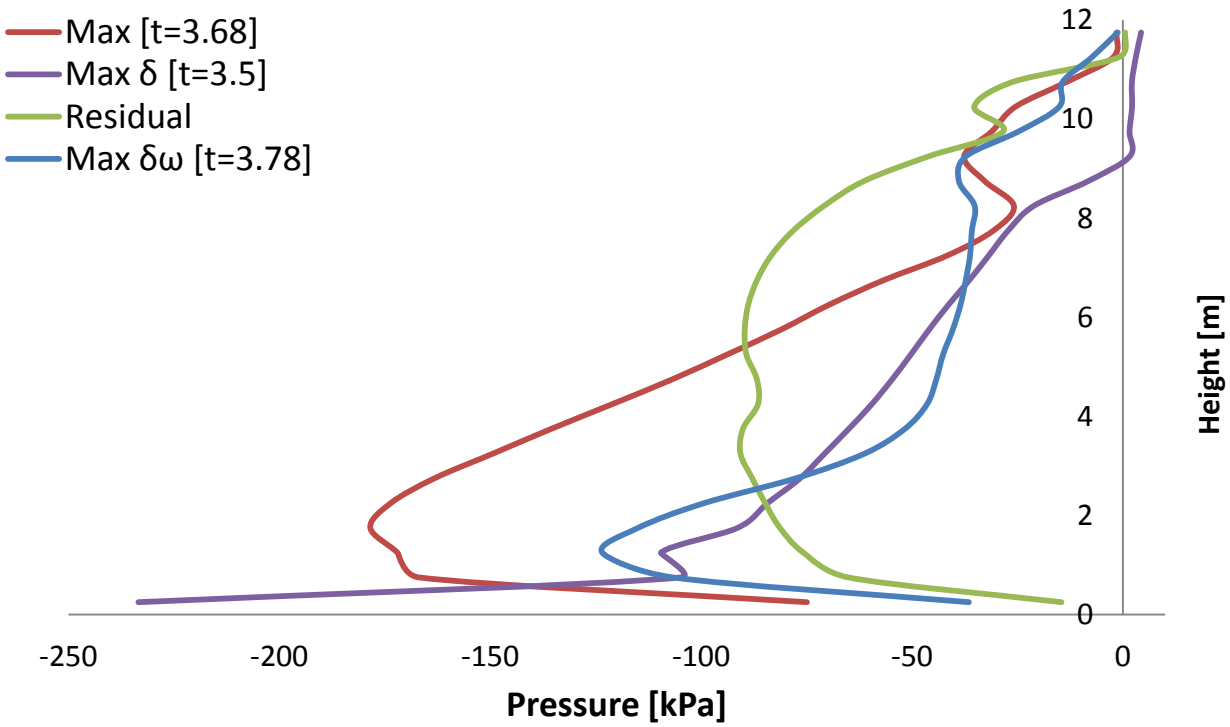

Fig. 3.24. Earth pressures profiles on the right wall at different moments when subjected to Aegion Seismic excitation with peak ground acceleration 0.6g.

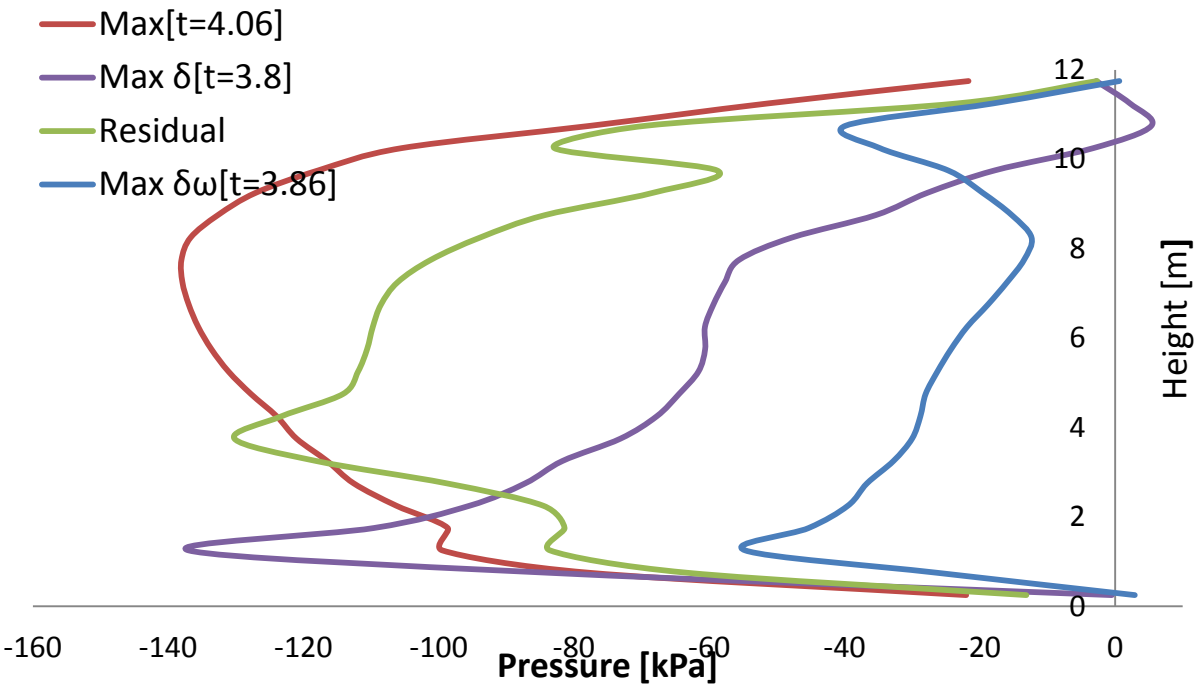

Fig. 3.25. Earth pressures profiles on the right wall at different moments when subjected to Aegion Seismic excitation with peak ground acceleration 1g.

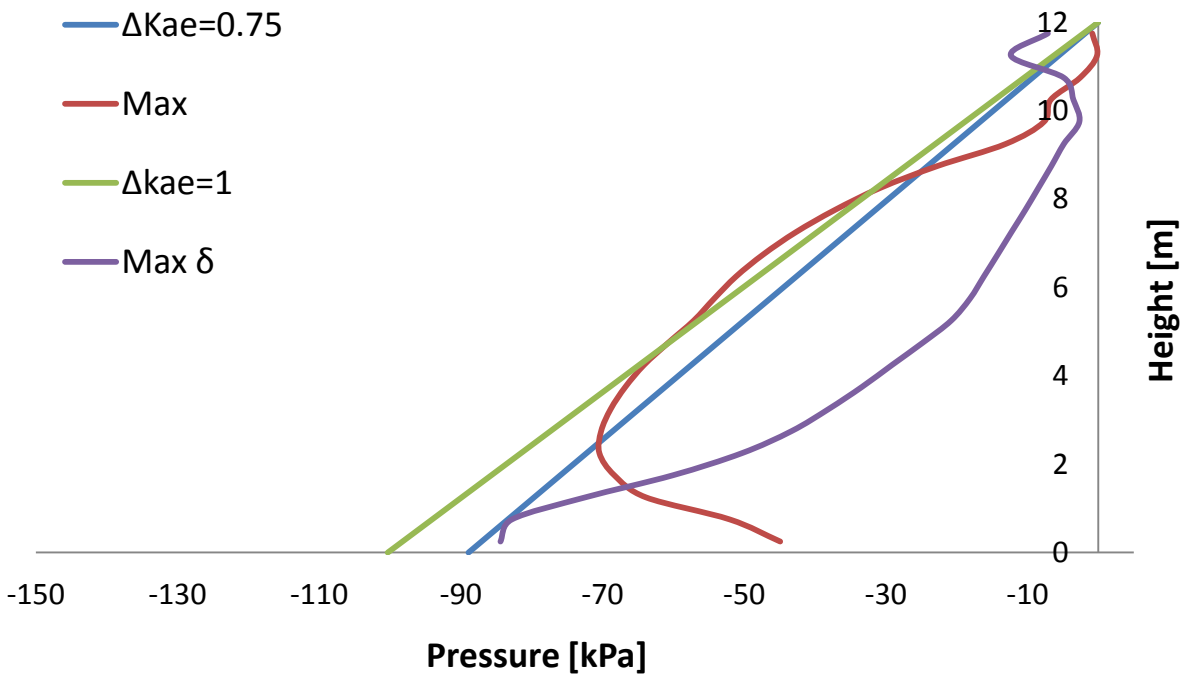

Fig. 3.26. Earth pressure profiles computed in ABAQUS and estimated using the M-O when the right wall is subjected to the Aegion Seismic excitation with peak acceleration 0.2g.

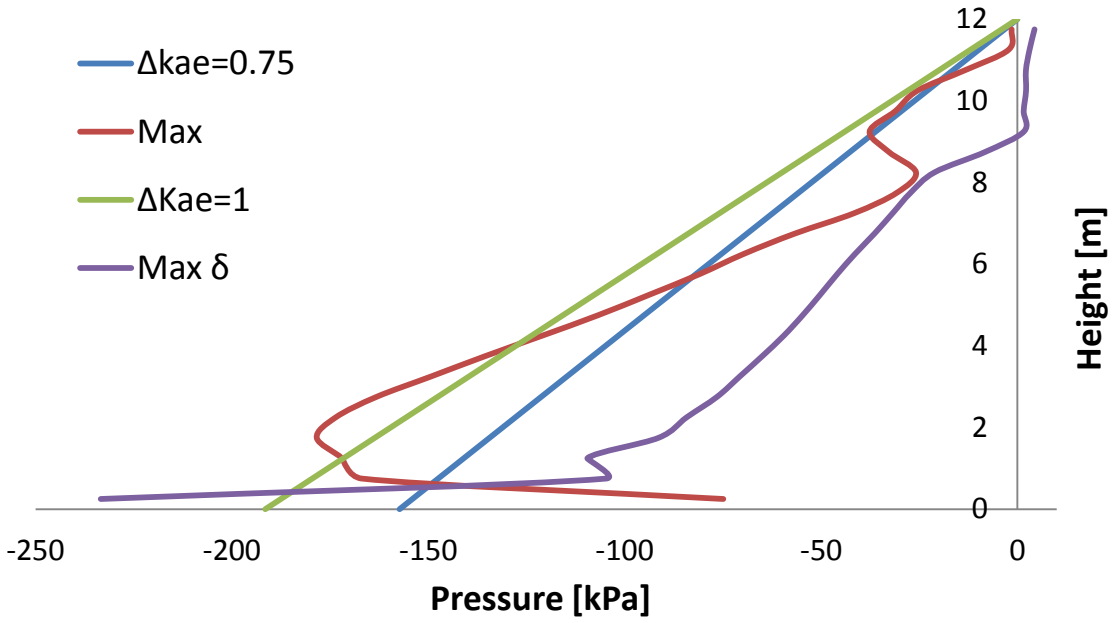

Fig. 3.27. Earth pressure profiles computed in ABAQUS and estimated using the M-O when the right wall is subjected to the Aegion Seismic excitation with peak acceleration 0.6g.

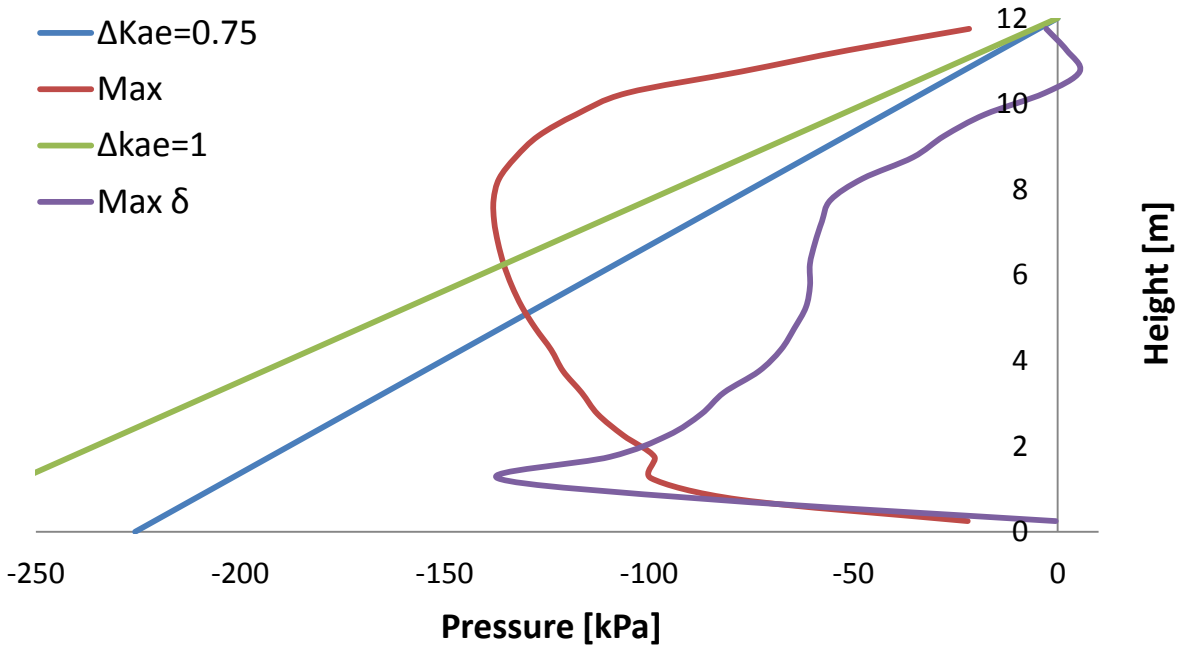

Fig. 3.28. Earth pressure profiles computed in ABAQUS and estimated using the M-O when the right wall is subjected to the Aegion Seismic excitation with peak acceleration 1g.

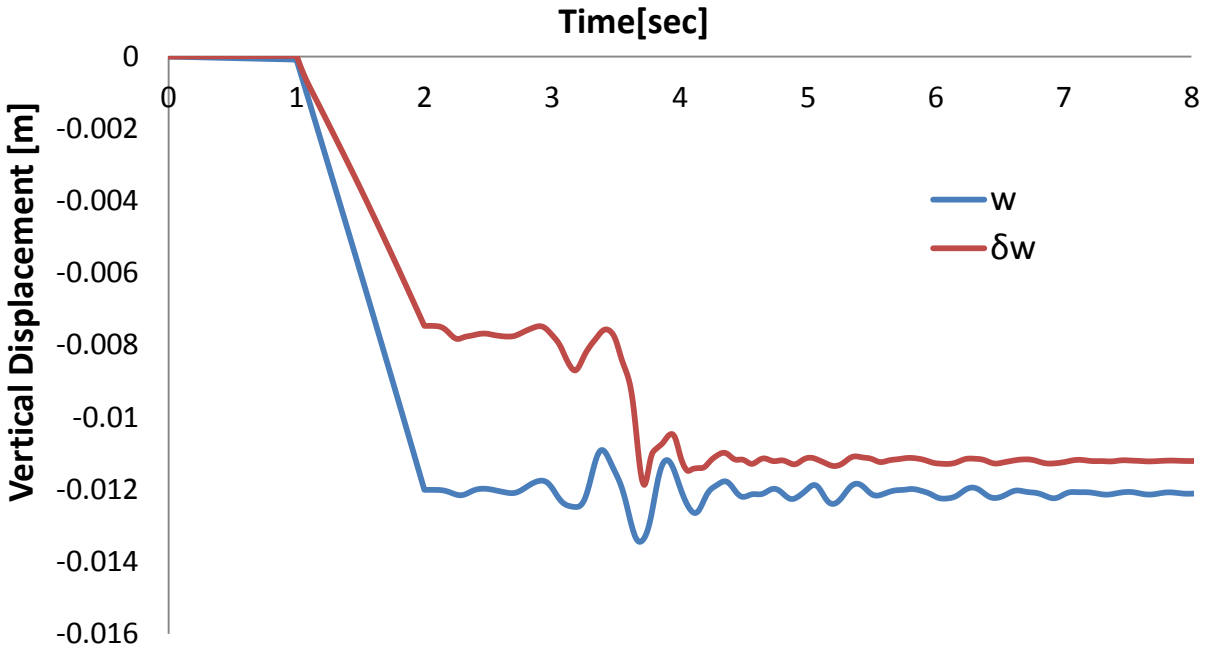

Fig. 3.29. Vertical displacement-time history of the right wall when subjected to AegionSeismic excitation with peak acceleration 0.2g.

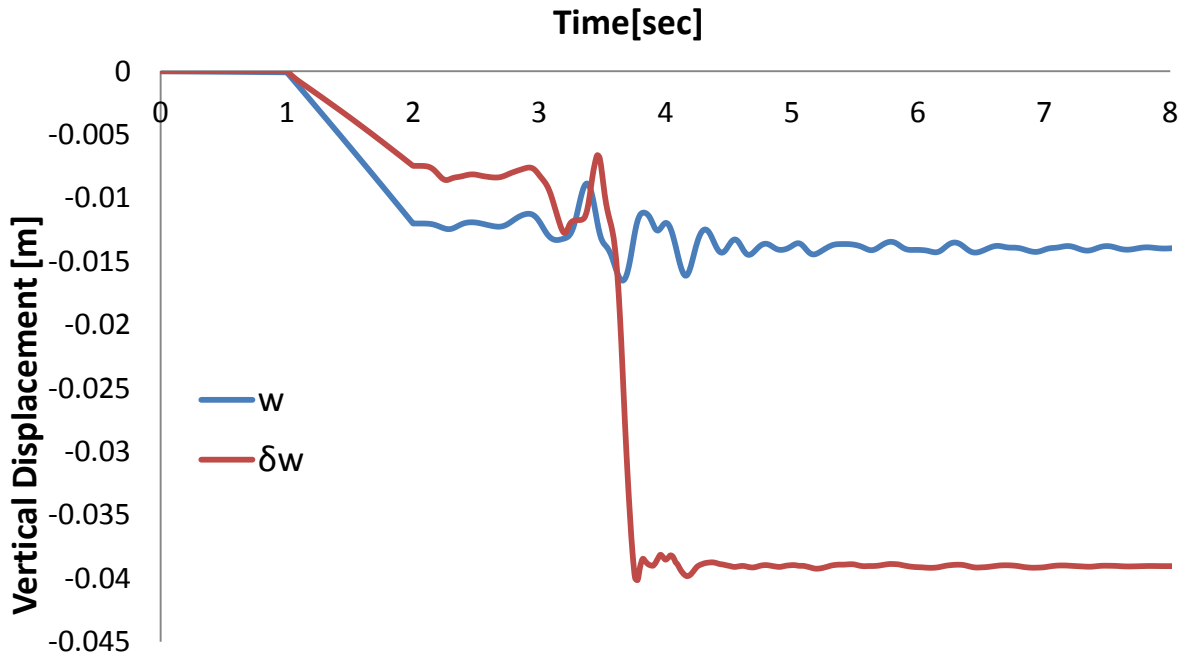

Fig. 3.30. Vertical displacement-time history of the right wall when subjected to Aegion Seismic excitation with peak acceleration 0.6g.

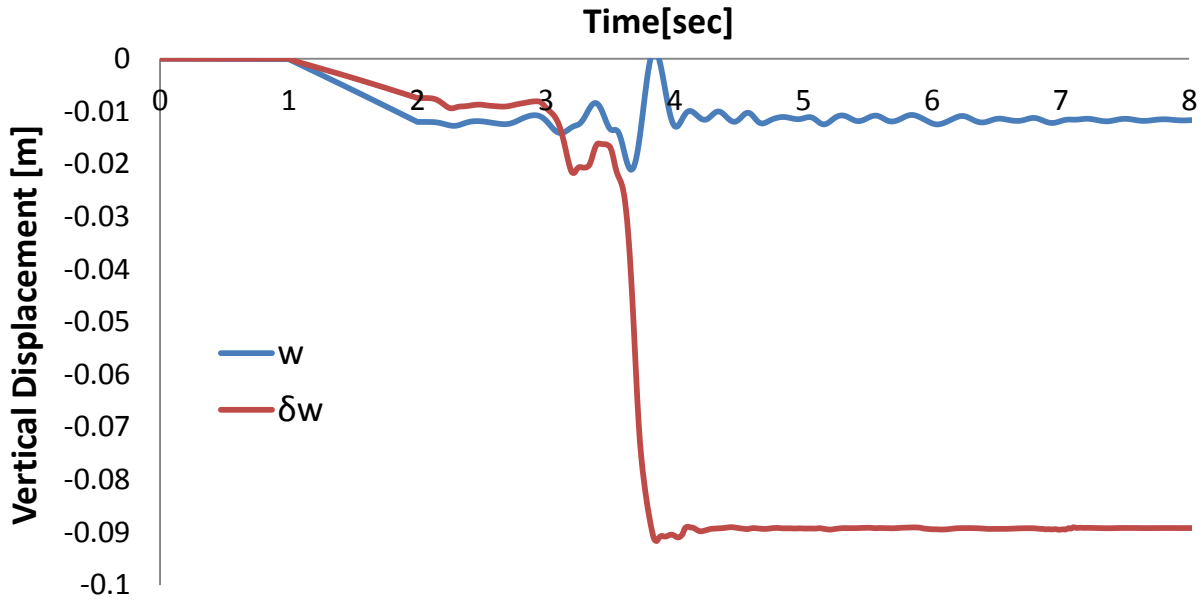

Fig. 3.31. Vertical displacement-time history of the right wall when subjected to Aegion Seismic excitation with peak acceleration 1g.

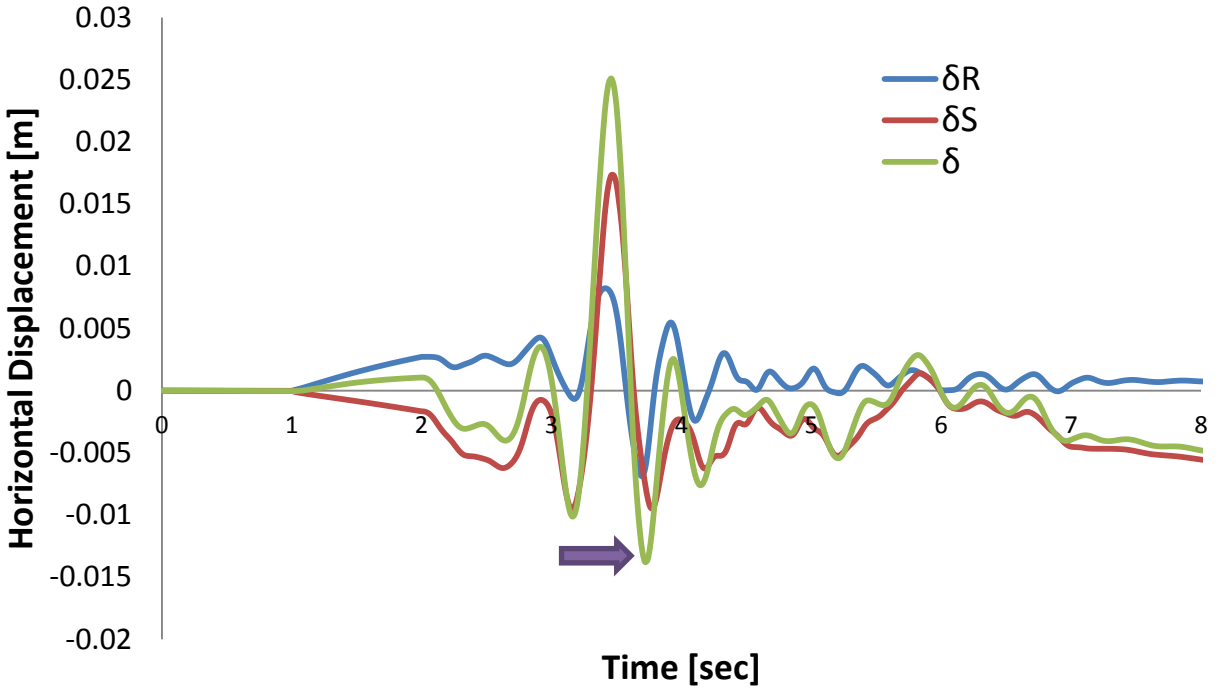

Fig. 3.32. Horizontal displacement-time history of the right wall when subjected to Aegion Seismic excitation with peak acceleration 0.2g.

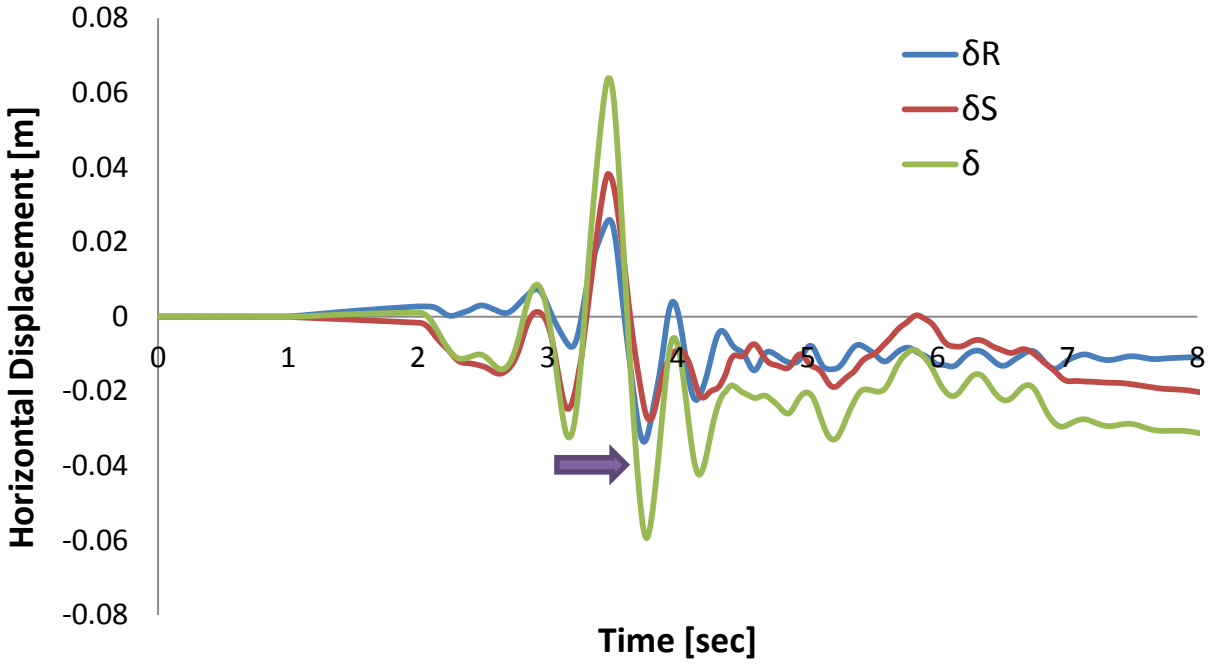

Fig. 3.33. Horizontal displacement-time history of the right wall when subjected to Aegion Seismic excitation with peak acceleration 0.6g.

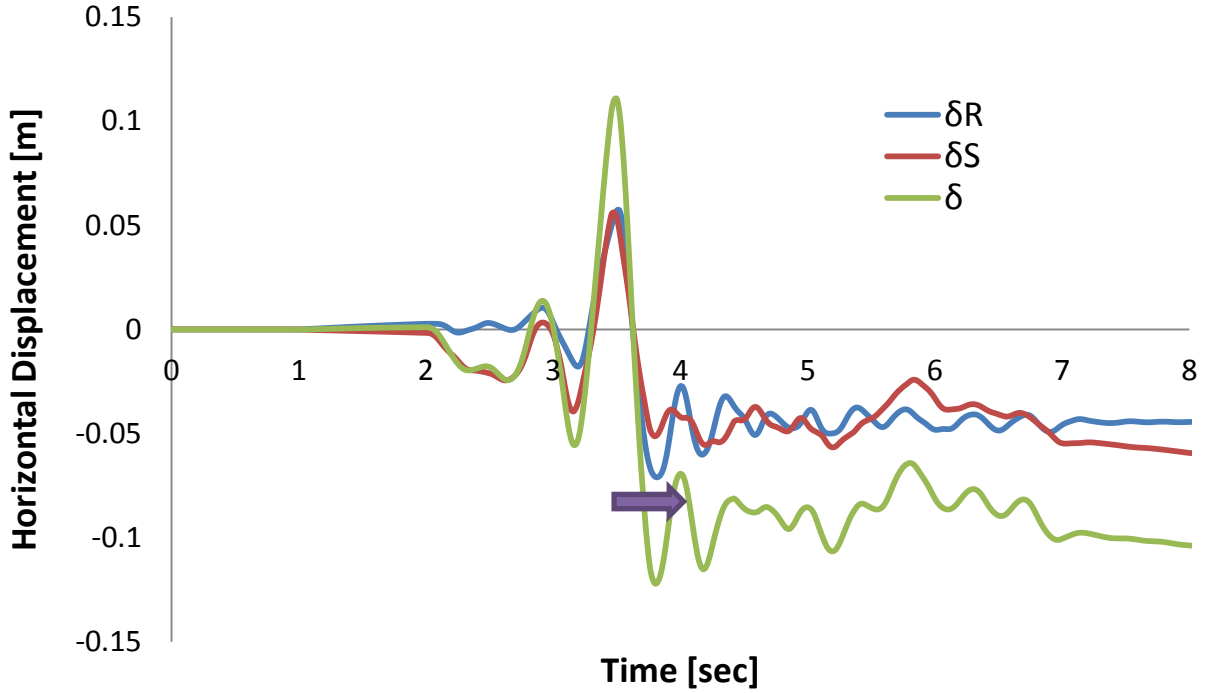

Fig. 3.34. Horizontal displacement-time history of the right wall when subjected to Aegion Seismic excitation with peak acceleration 1g.

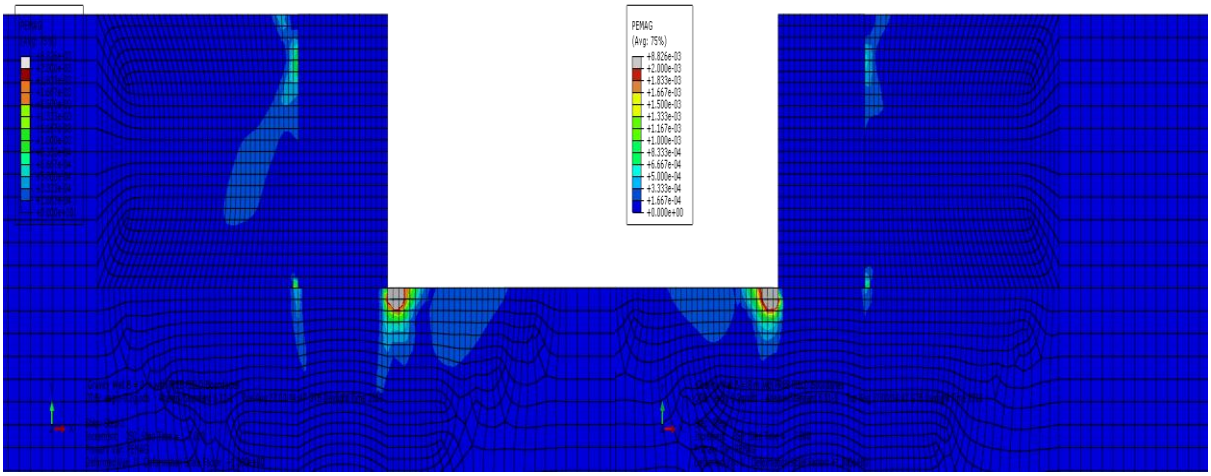

Fig. 3.35. Plastic strain contours at the end of seismic shaking (a)Left wall (b)Right wall when subjected to Aegion seismic excitation with peak acceleration 0.2g.

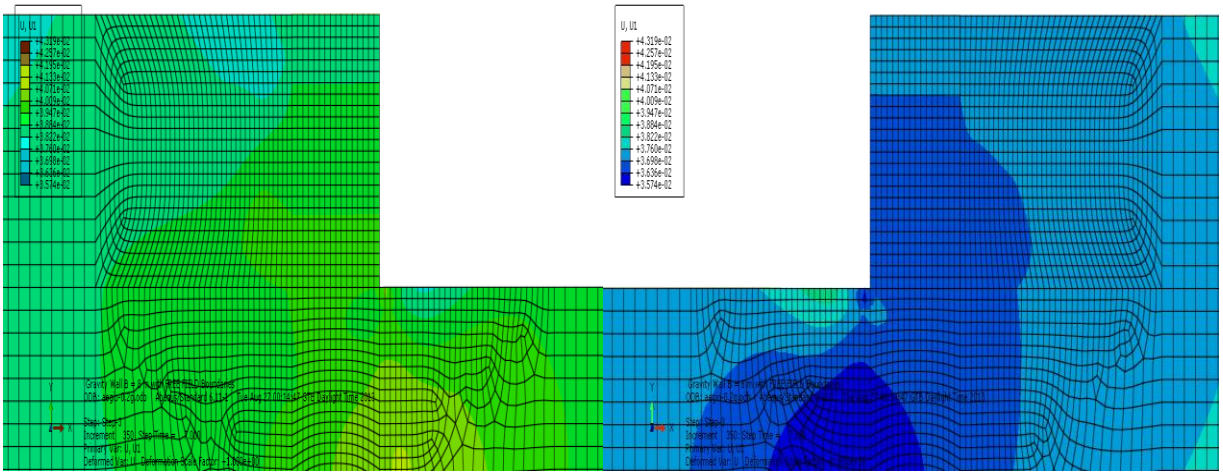

Fig. 3.36. Horizontal displacement contours at the end of the seismic excitation Aegion PGA 0.3g.

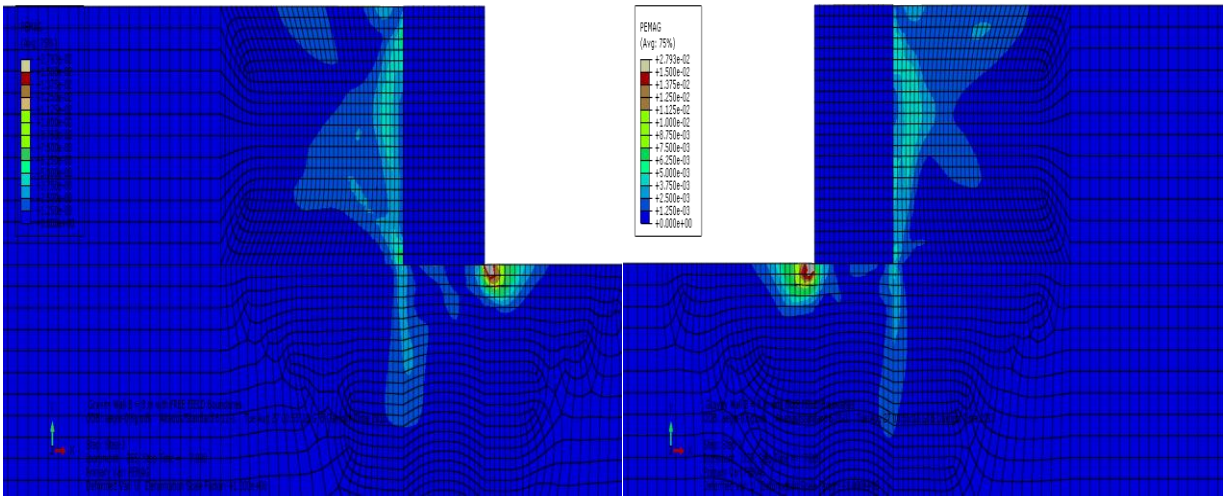

Fig. 3.37. Plastic strain contours at the end of seismic shaking (a)Left wall (b)Right wall when subjected to Aegion seismic excitation with peak acceleration 0.6g.

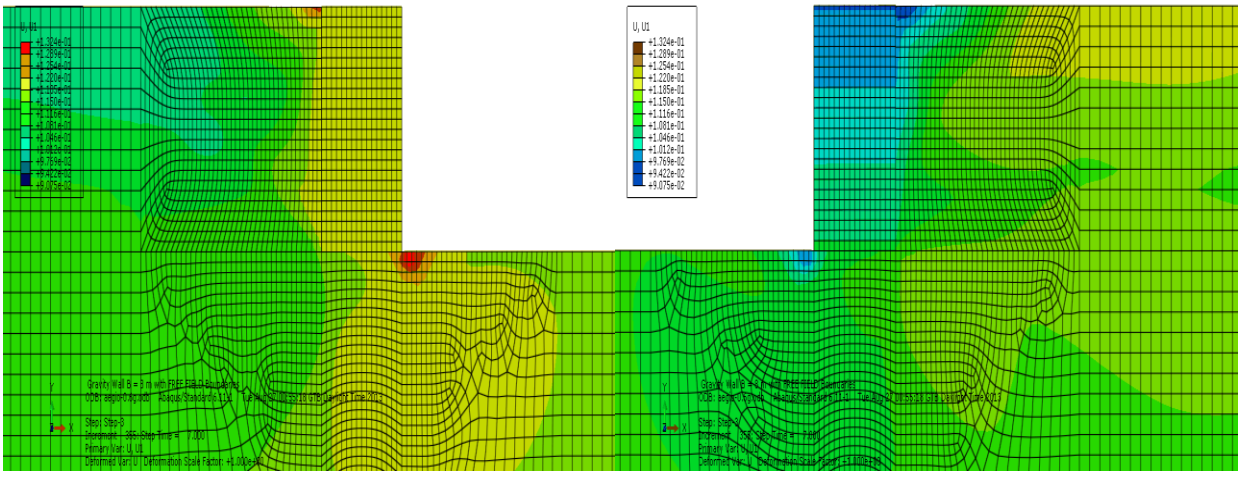

Fig. 3.38. Horizontal displacement contours at the end of the seismic excitation Aegion PGA 0.6g.

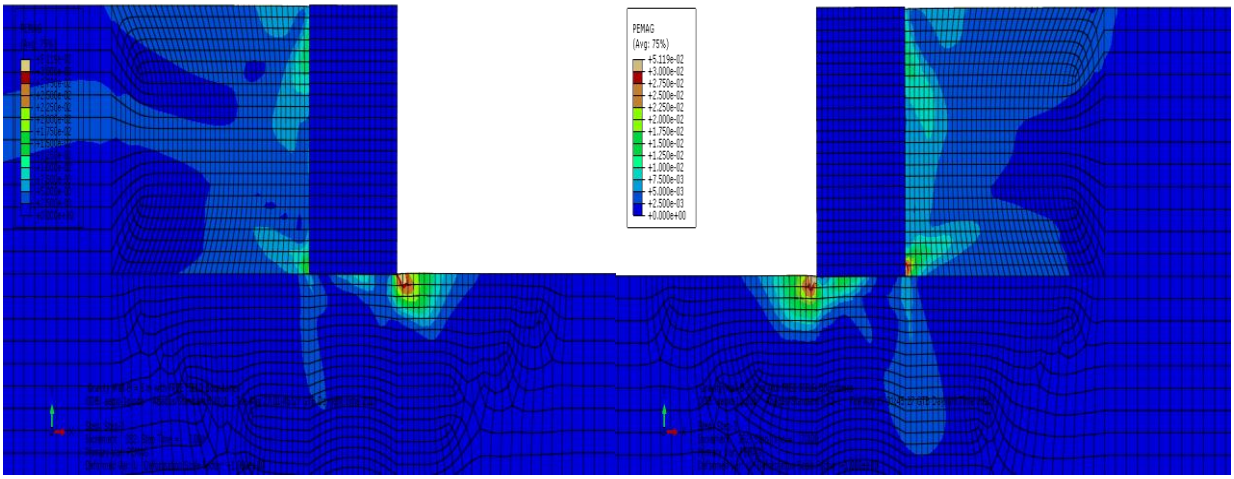

Fig. 3.39. Plastic strain contours at the end of seismic shaking (a)Left wall (b)Right wall when subjected to Aegion seismic excitation with peak acceleration 1g.

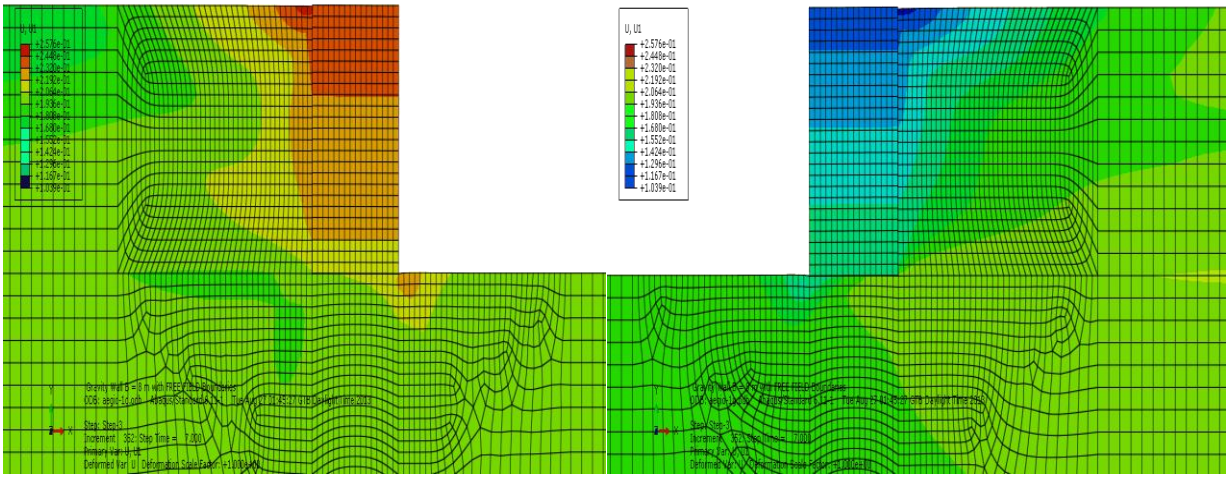

Fig. 3.40. Horizontal displacement contours at the end of the seismic excitation Aegion PGA 1g.

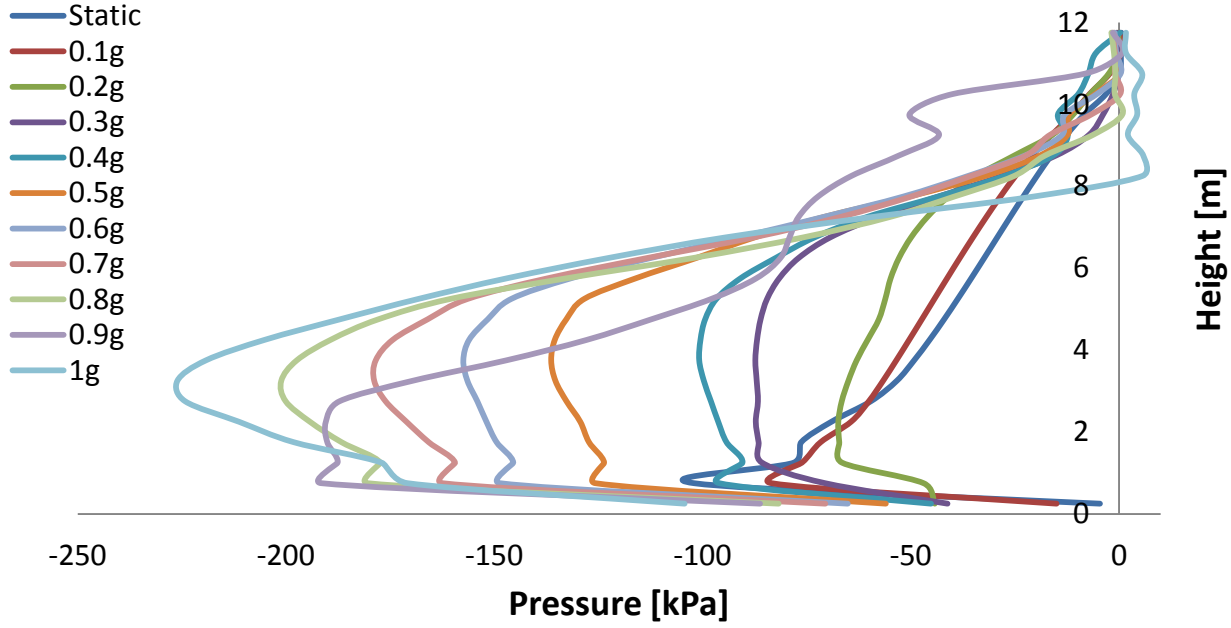

Fig. 3.41. Static and maximum earth pressure profiles for different peak accelerations on the left wall when subjected to Aegion Seismic excitation.

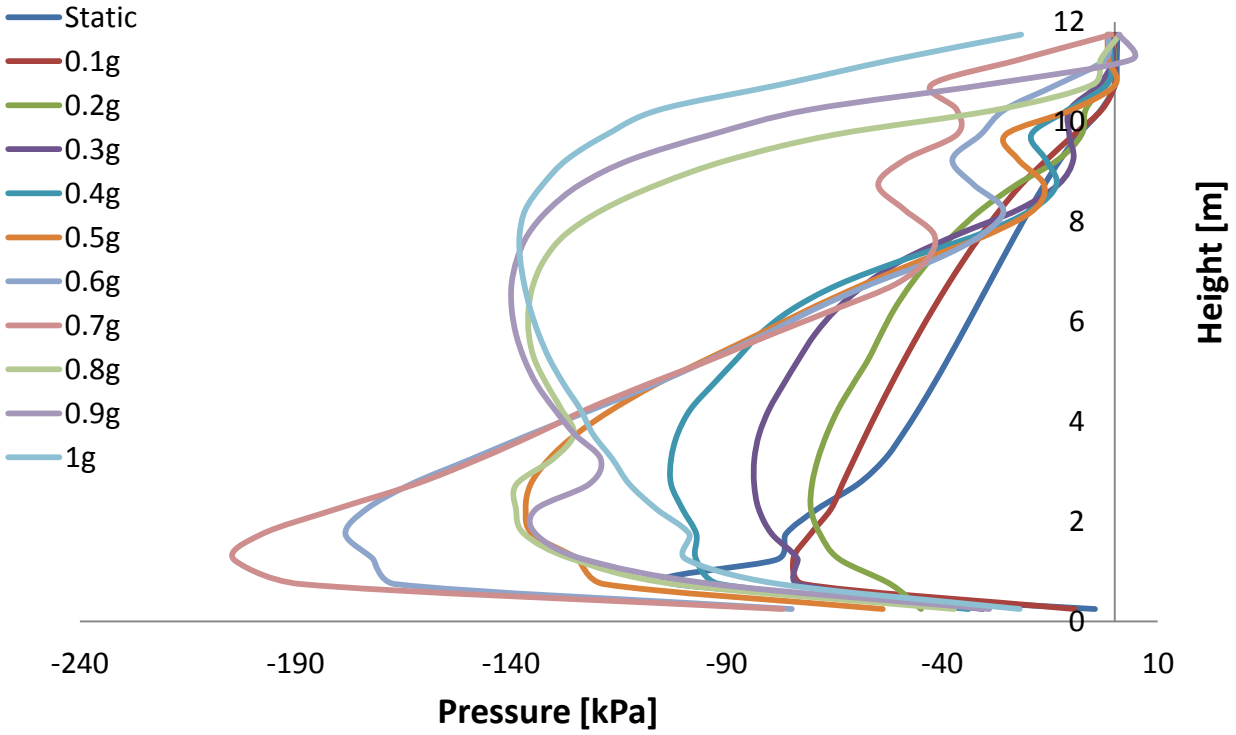

Fig. 3.42. Static and maximum earth pressure profiles for different peak accelerations on the right wall when subjected to Aegion Seismic excitation.

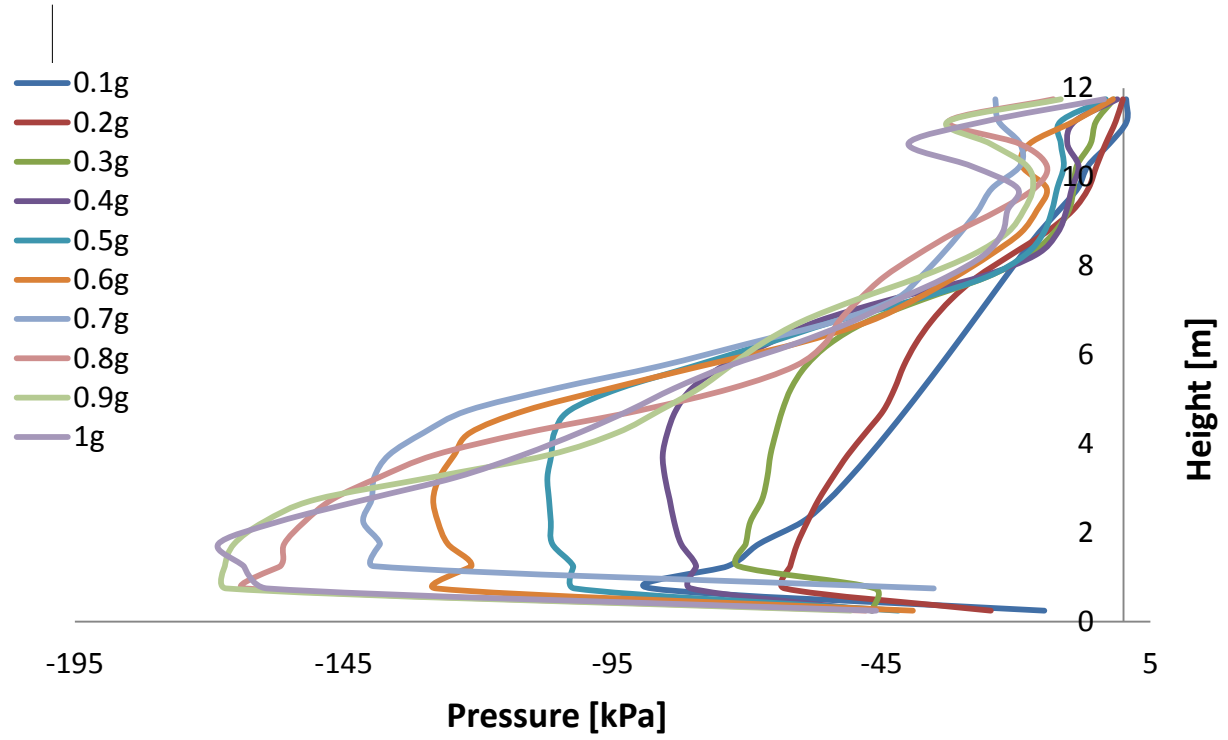

Fig. 3.43. Residual earth pressure profiles for different peak accelerations on the left wall when subjected to Ageion Seismic excitation.

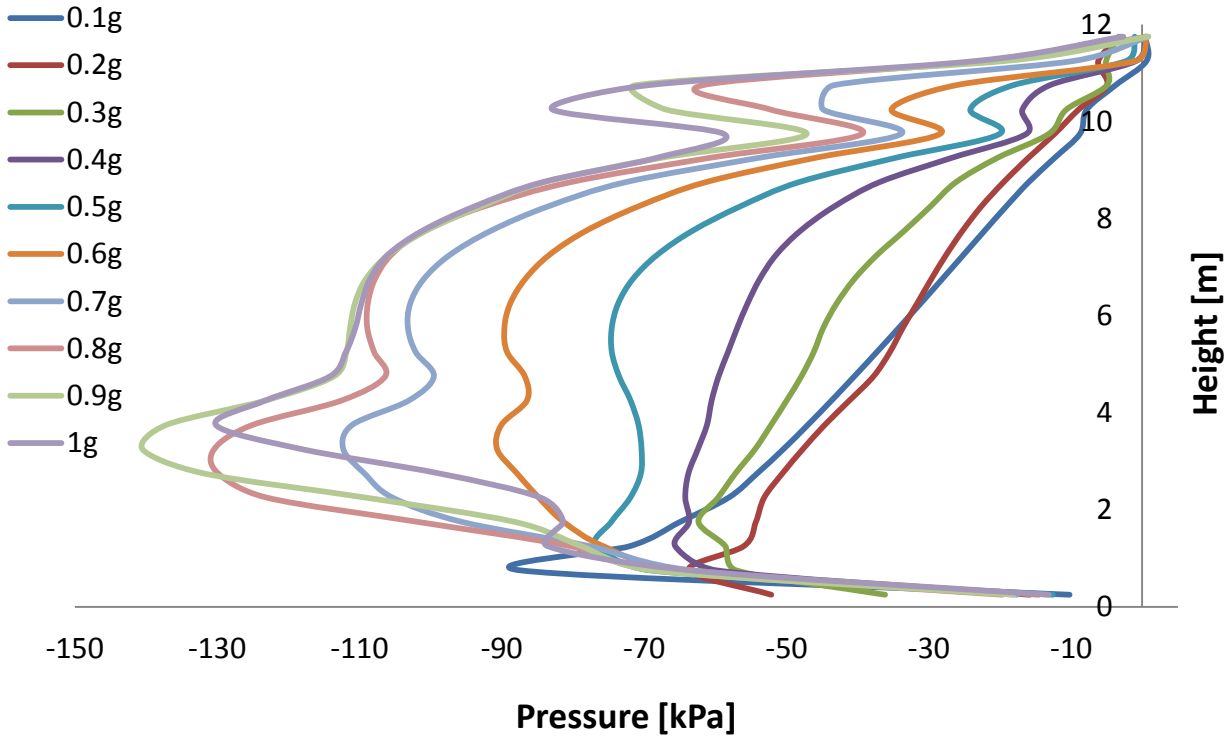

Fig. 3.44. Residual earth pressure profiles for different peak accelerations on the right wall when subjected to Ageion Seismic excitation.

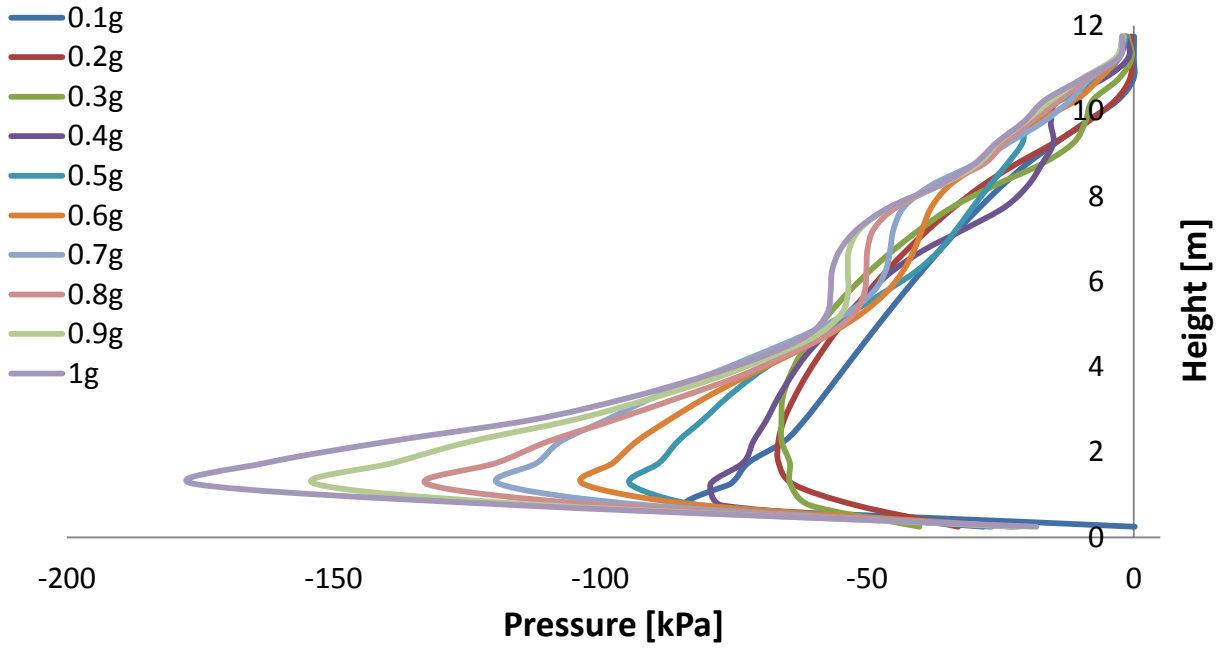

Fig. 3.45. Earth pressure profiles at maximum displacement for different peak accelerations on the left wall when subjected to Ageion Seismic excitation.

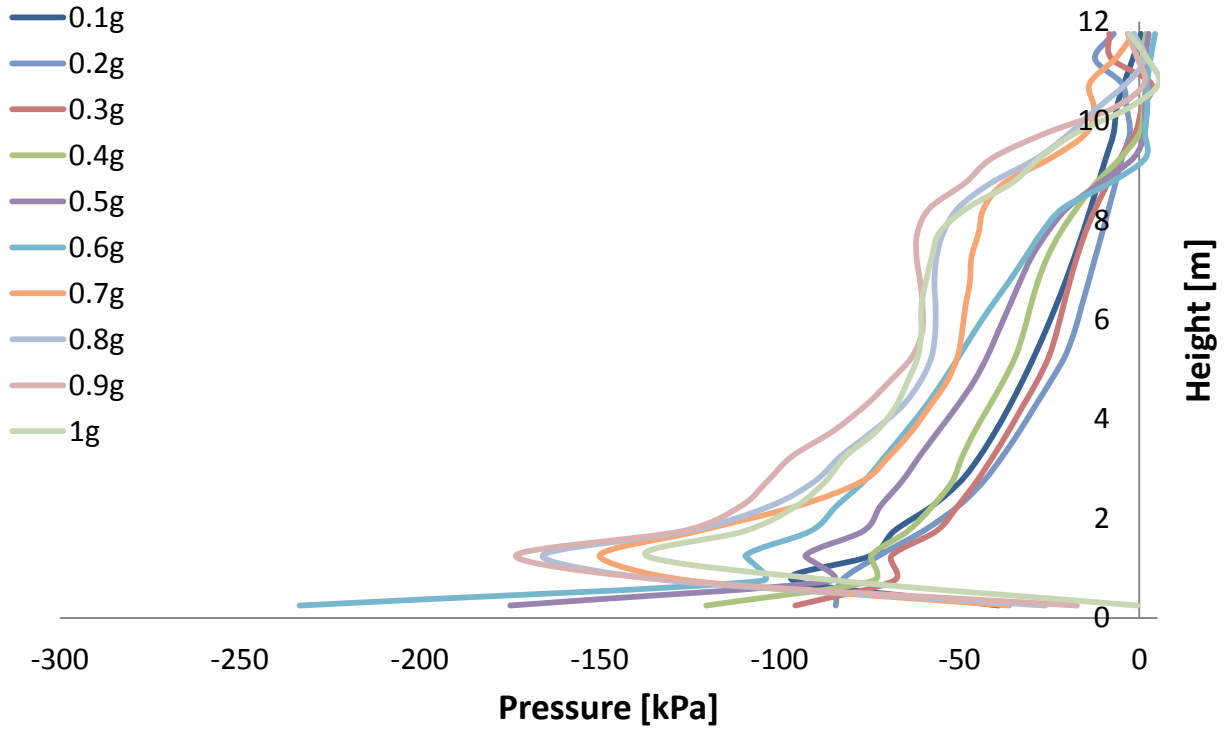

Fig. 3.46. Earth pressure profiles at maximum displacement for different peak accelerations on the right wall when subjected to Ageion Seismic excitation.

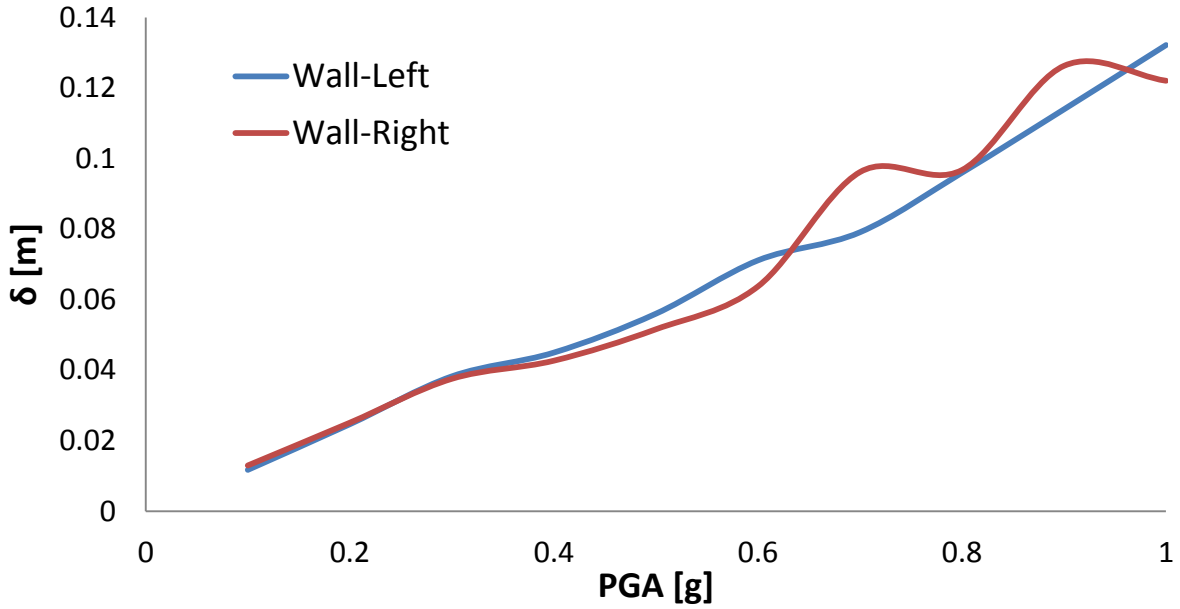

Fig. 3.47. Horizontal displacement as a function of PGA for the left and right wall when subjected to Ageion Seismic excitation.

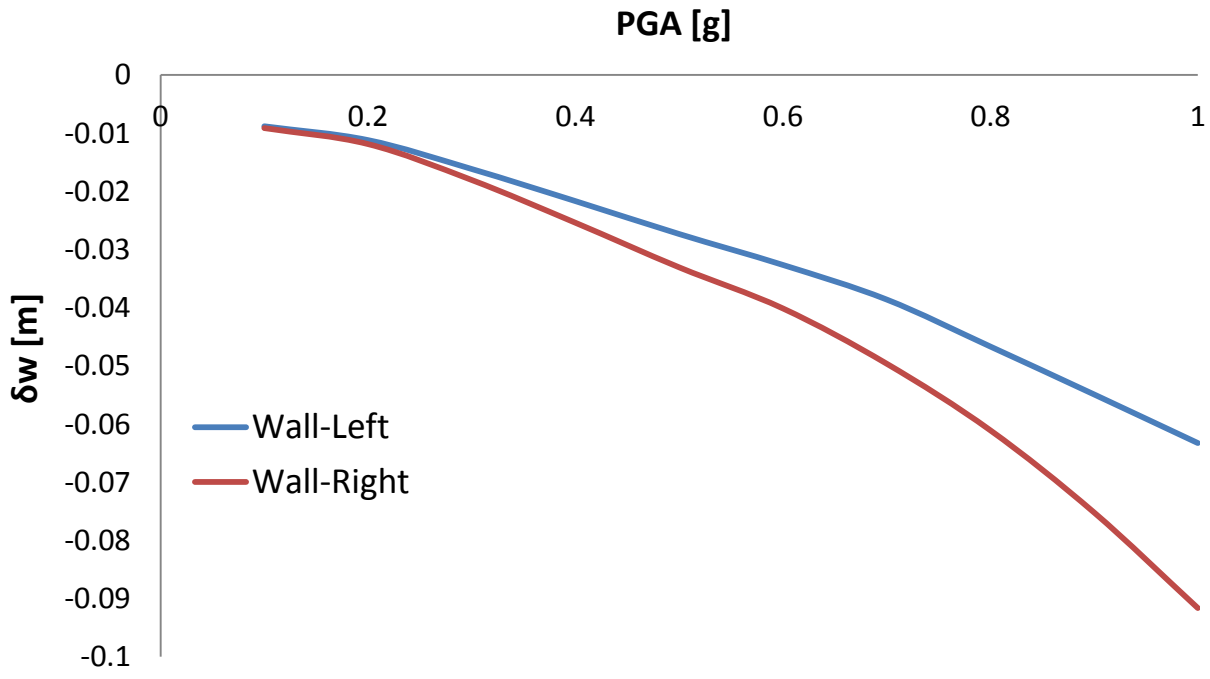

Fig. 3.48. Differential settelement as a function of PGA for the left and right wall when subjected to Ageion Seismic excitation.

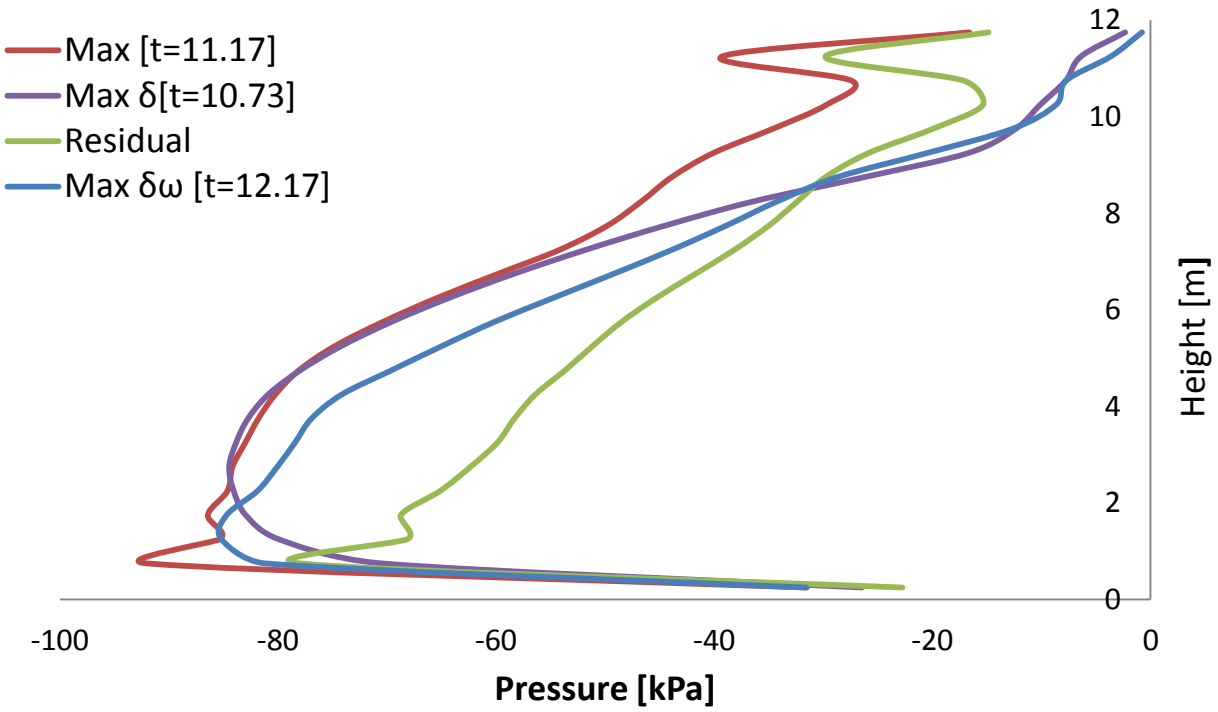

Fig. 3.49. Earth pressures profiles on the left wall at different moments when subjected to Lefkada Seismic excitation with peak ground acceleration 0.3g.

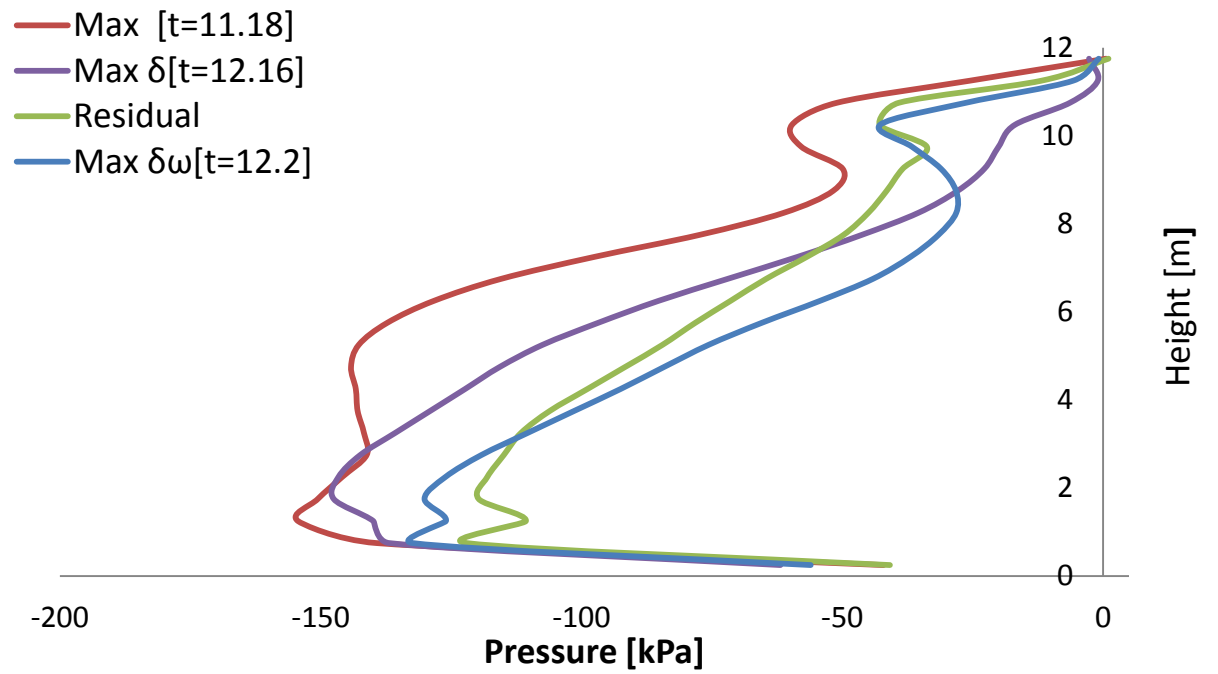

Fig. 3.50. Earth pressures profiles on the left wall at different moments when subjected to Lefkada Seismic excitation with peak ground acceleration 0.6g.

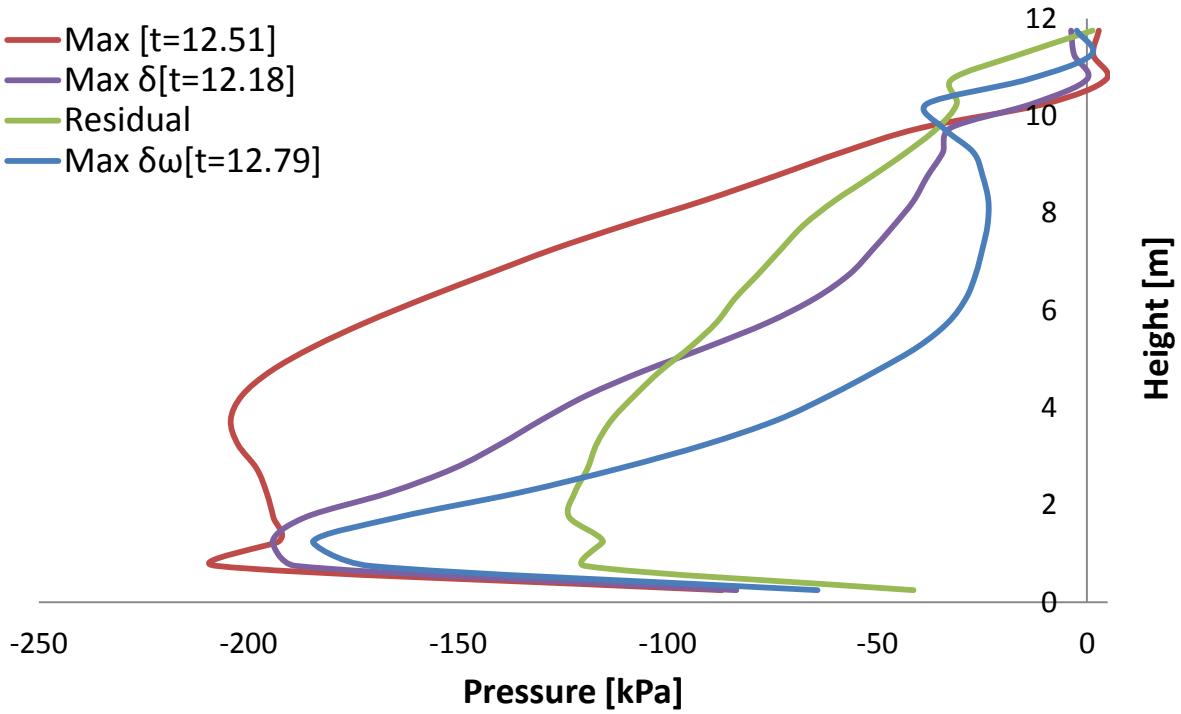

Fig. 3.51. Earth pressures profiles on the left wall at different moments when subjected to Lefkada Seismic excitation with peak ground acceleration 0.9g.

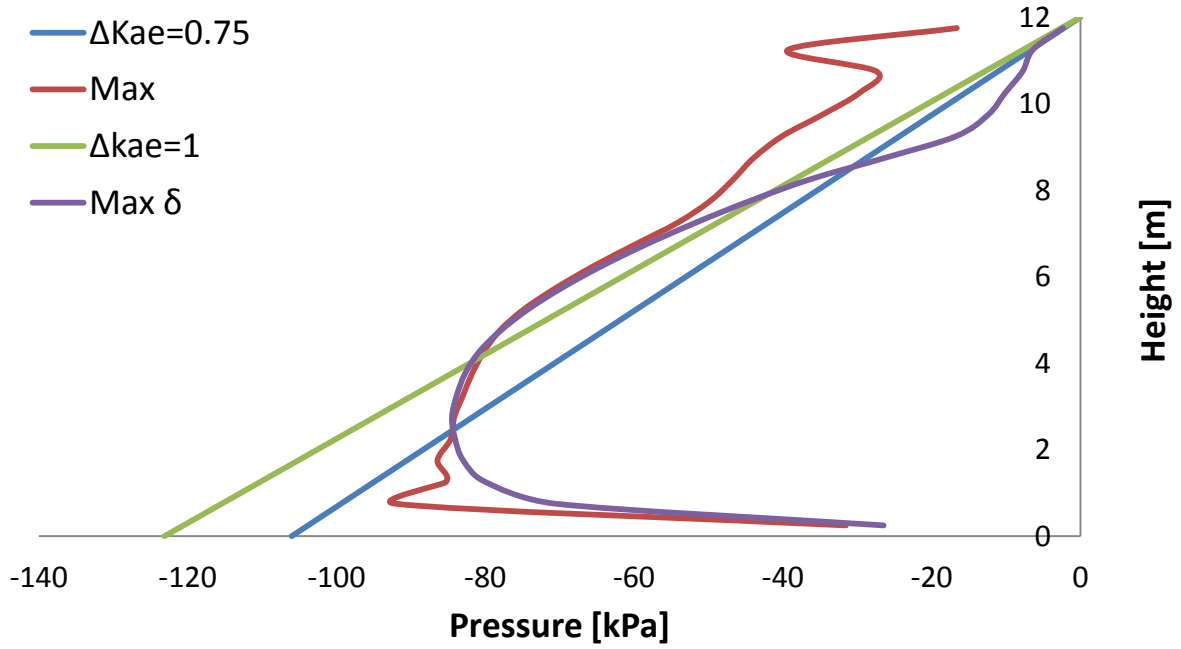

Fig. 3.52. Earth pressure profiles computed in ABAQUS and estimated using the M-O when the left wall is subjected to the Lefkada Seismic excitation with peak acceleration 0.3g.

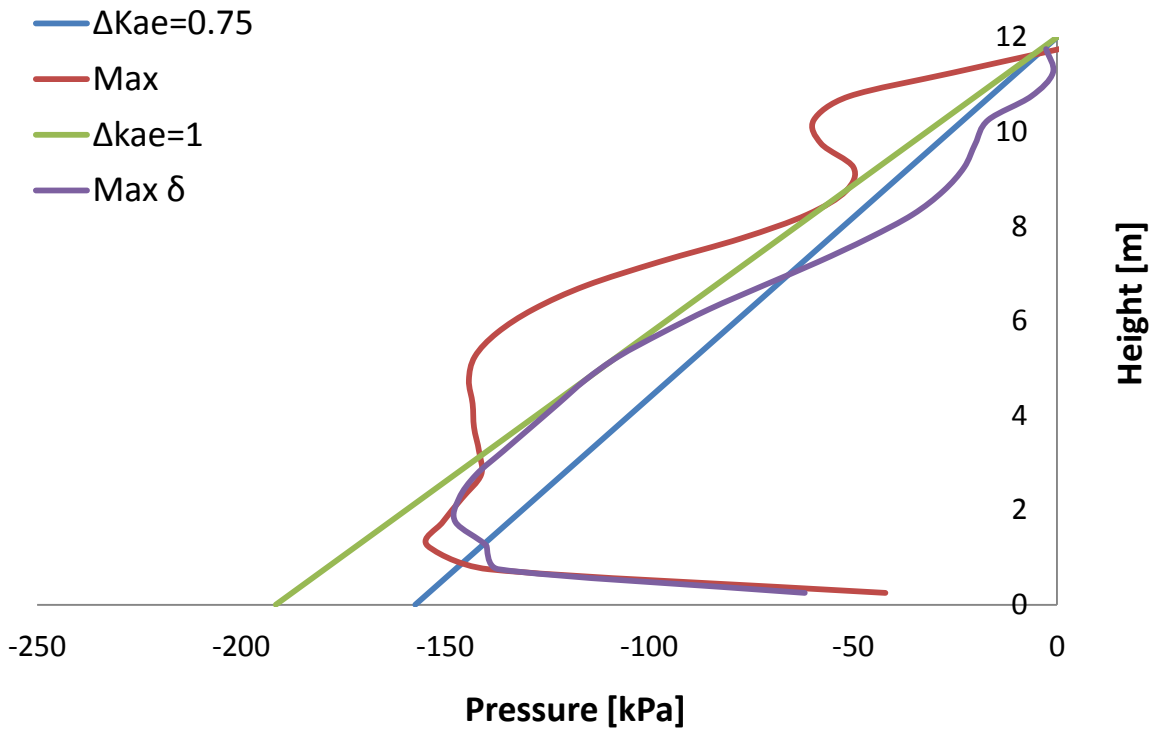

Fig. 3.53. Earth pressure profiles computed in ABAQUS and estimated using the M-O when the left wall is subjected to the Lefkada Seismic excitation with peak acceleration 0.6g.

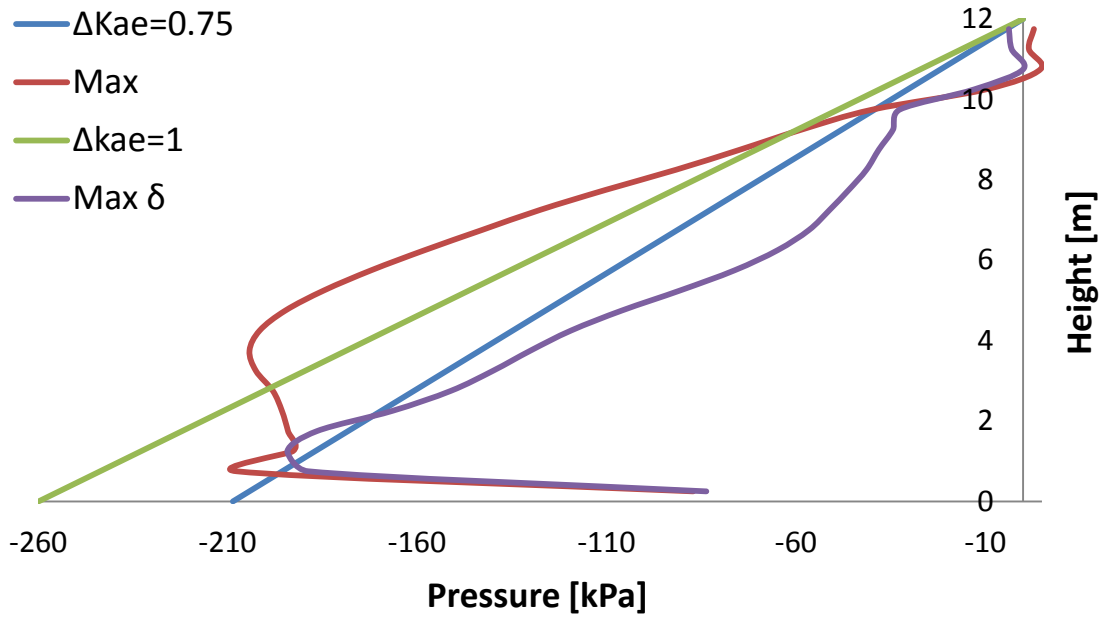

Fig. 3.54. Earth pressure profiles computed in ABAQUS and estimated using the M-O when the left wall is subjected to the Lefkada Seismic excitation with peak acceleration 0.9g.

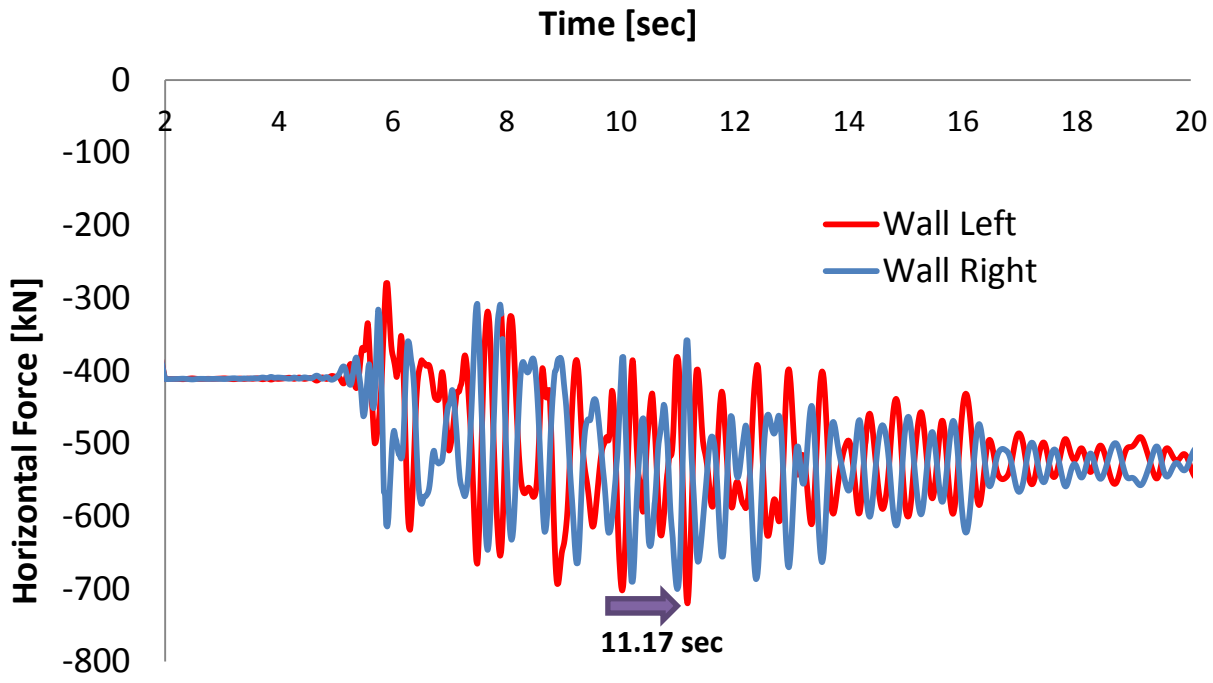

Fig. 3.55. Horizontal force-time history of the left and right wall when subjected to Lefkada Seismic excitation with peak ground acceleration 0.3g.

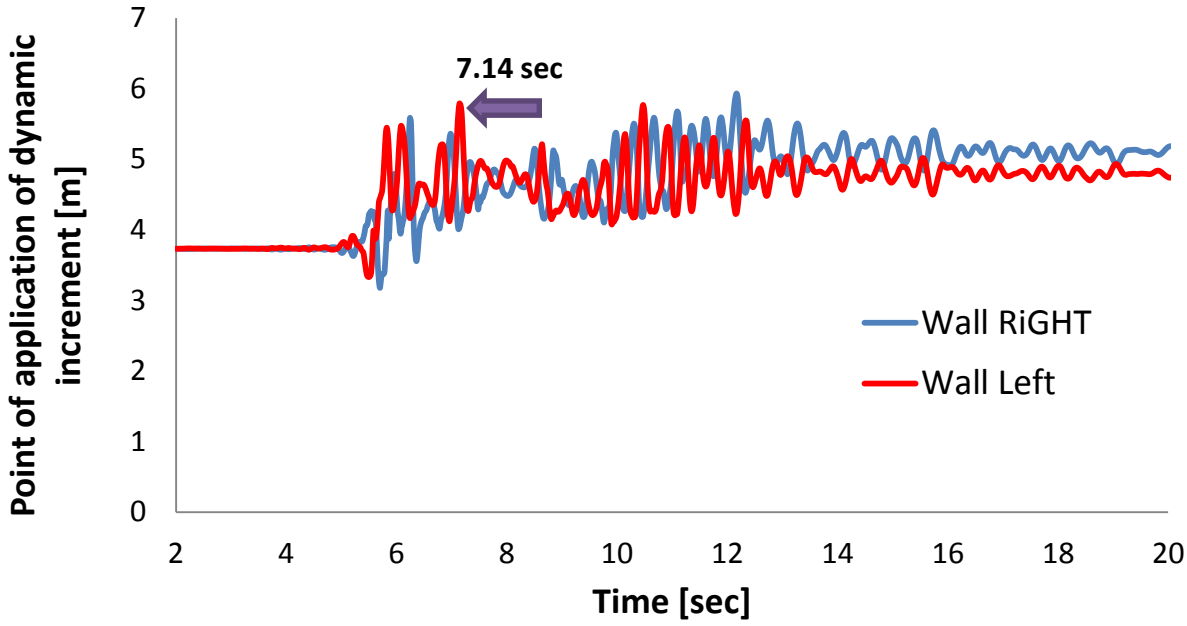

Fig. 3.56. Point of application of dynamic force on the left and right wall when subjected to Lefkada Seismic excitation with peak ground acceleration 0.3g.

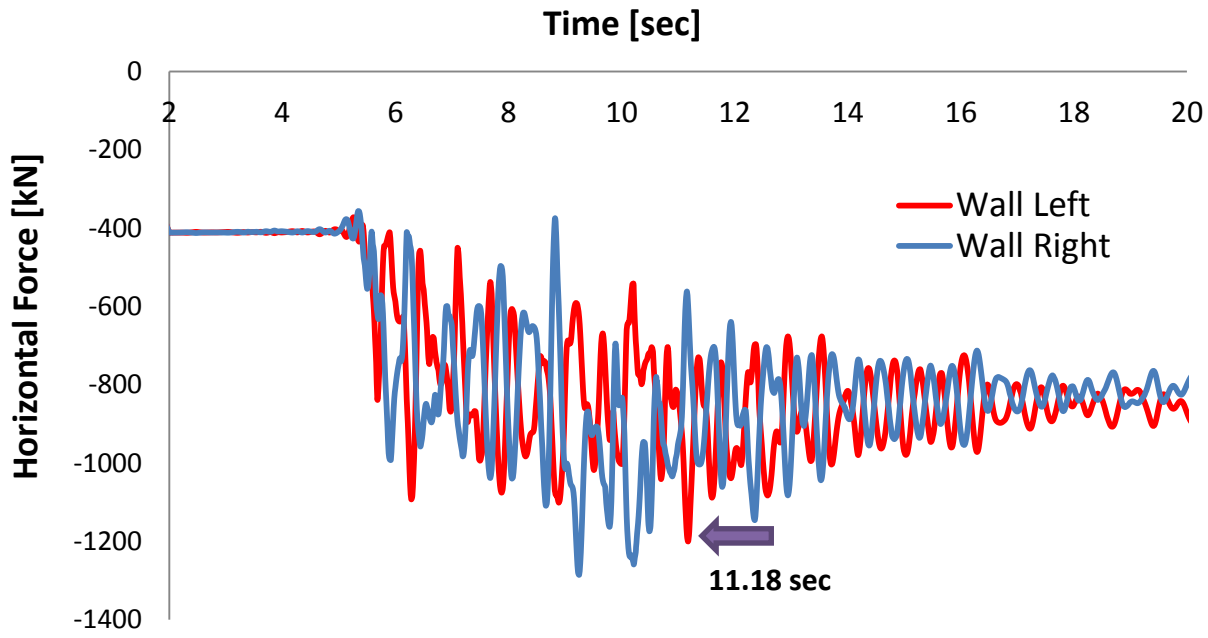

Fig. 3.57. Horizontal force-time history of the left and right wall when subjected to Lefkada Seismic excitation with peak ground acceleration 0.6g.

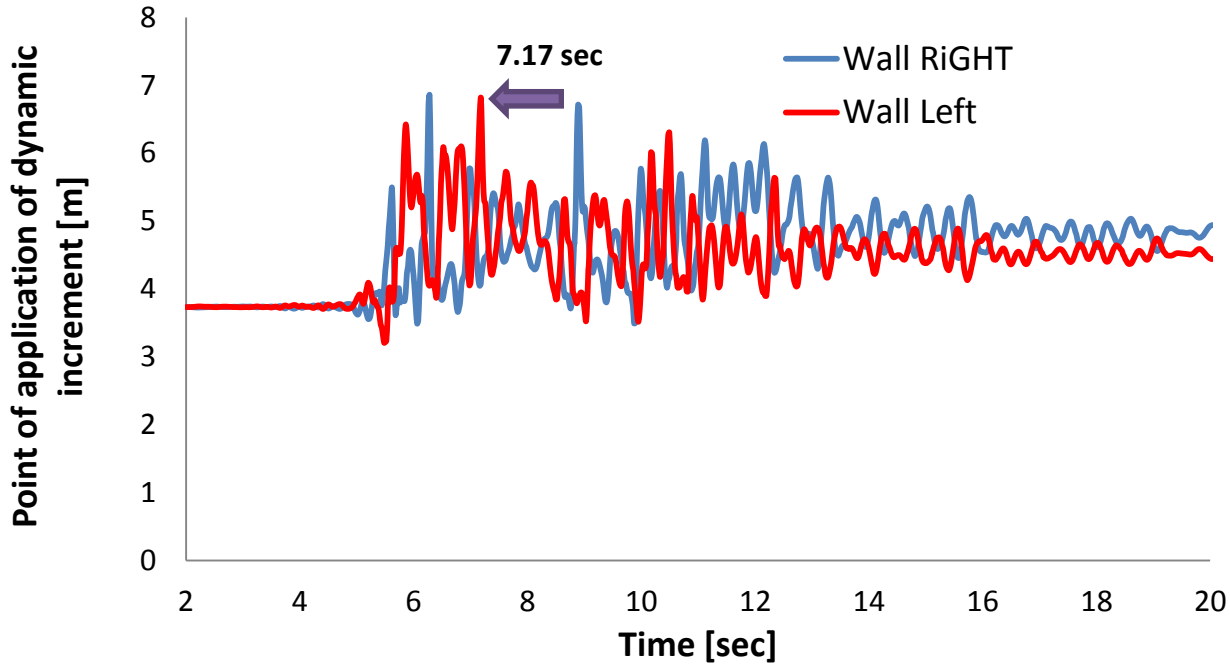

Fig. 3.58. Point of application of dynamic force on the left and right wall when subjected to Lefkada Seismic excitation with peak ground acceleration 0.6g.

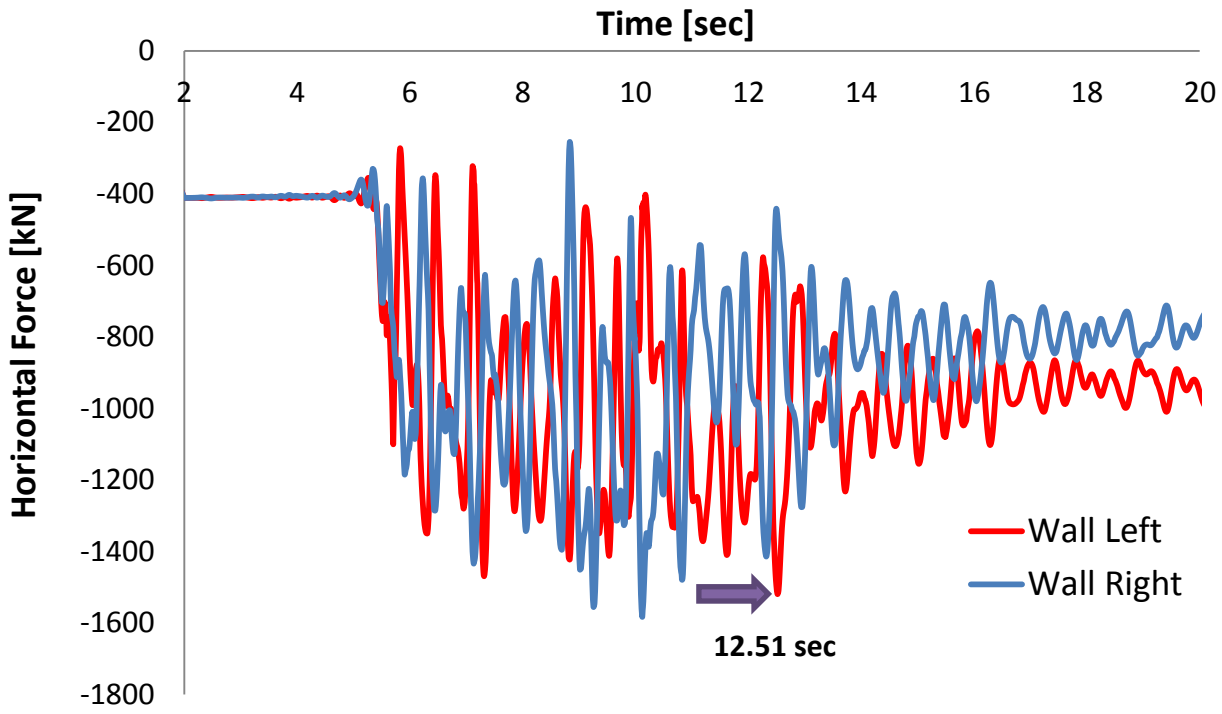

Fig. 3.59. Horizontal force-time history of the left and right wall when subjected to Lefkada Seismic excitation with peak ground acceleration 0.9g.

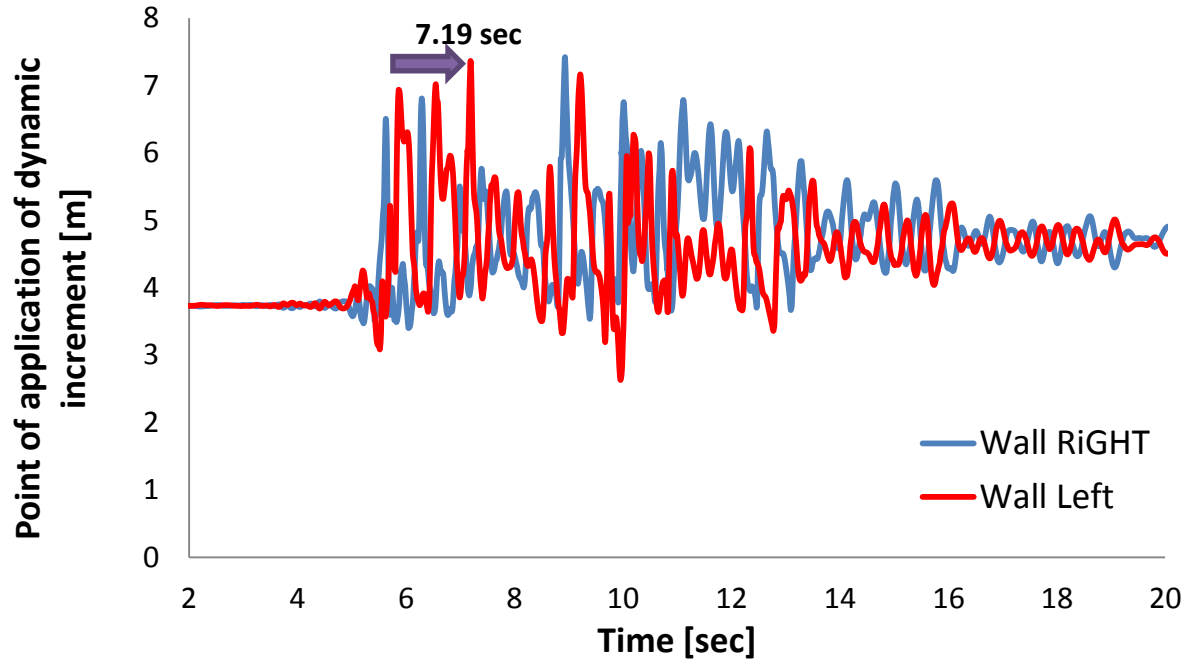

Fig. 3.60. Point of application of dynamic force on the left and right wall when subjected to Lefkada Seismic excitation with peak ground acceleration 0.9g.

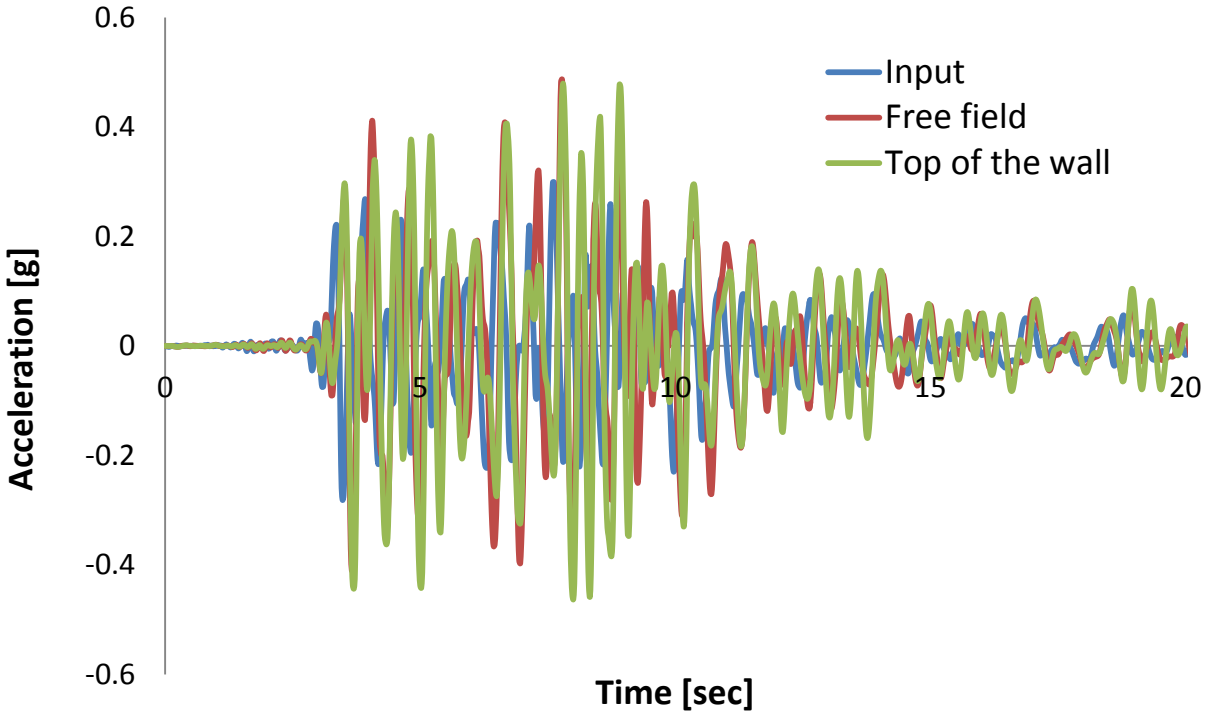

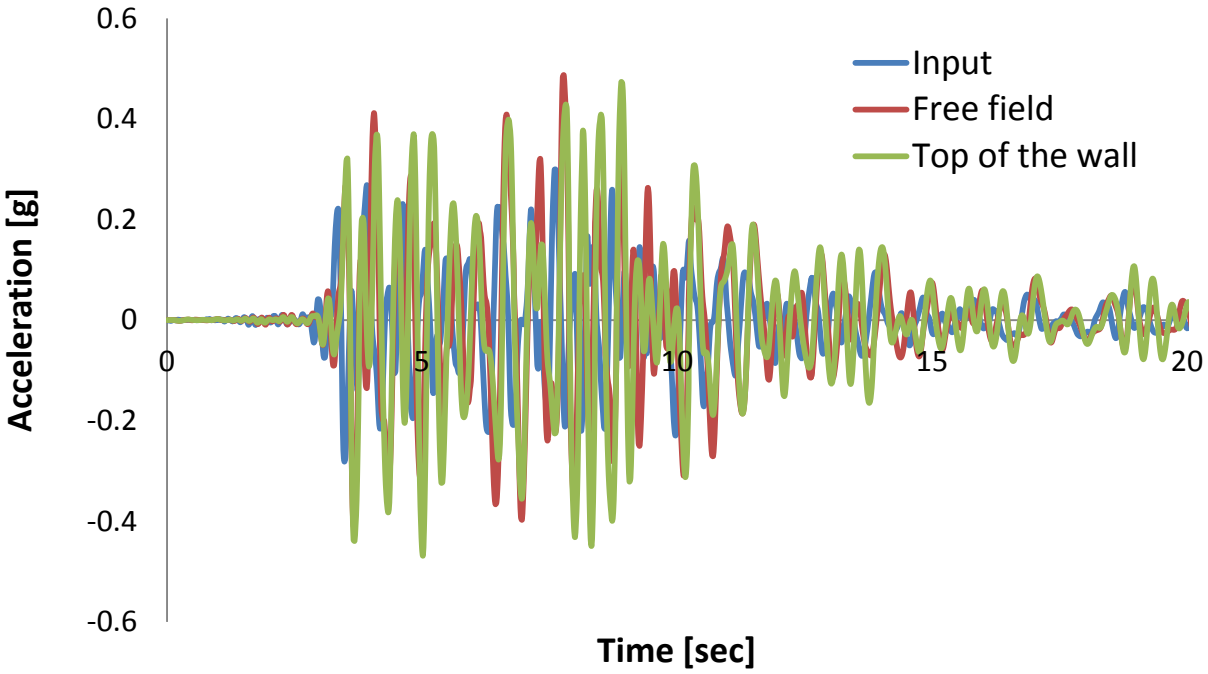

Fig. 3.61. Comparison of input acceleration and computed at the top of the a)left wall b)right wall and top of the free field when subjected to Lefkada Seismic excitation with peak acceleration 0.3g.

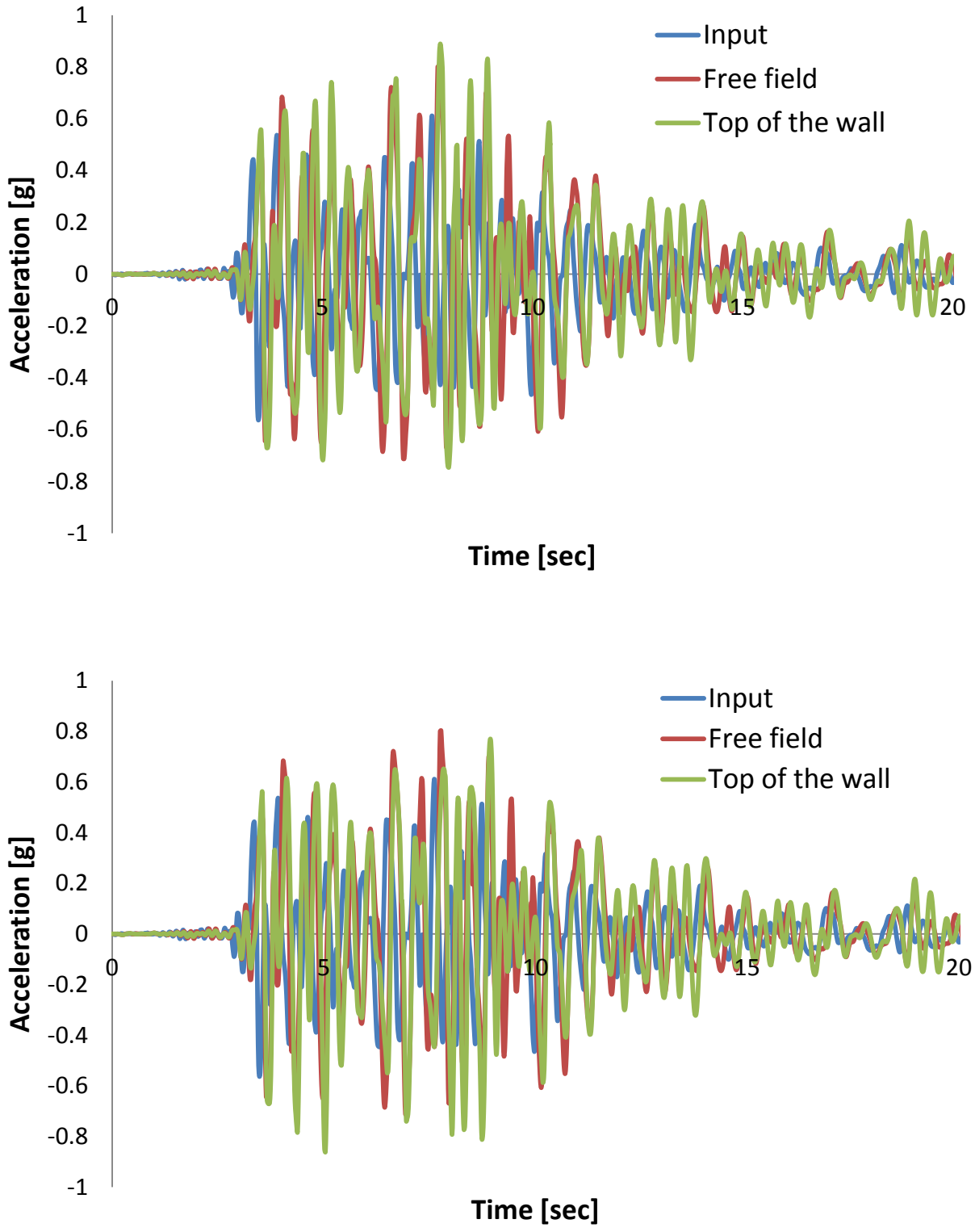

Fig. 3.62. Comparison of input acceleration and computed at the top of the a)left wall b)right wall and top of the free field when subjected to Lefkada Seismic excitation with peak acceleration 0.6g.

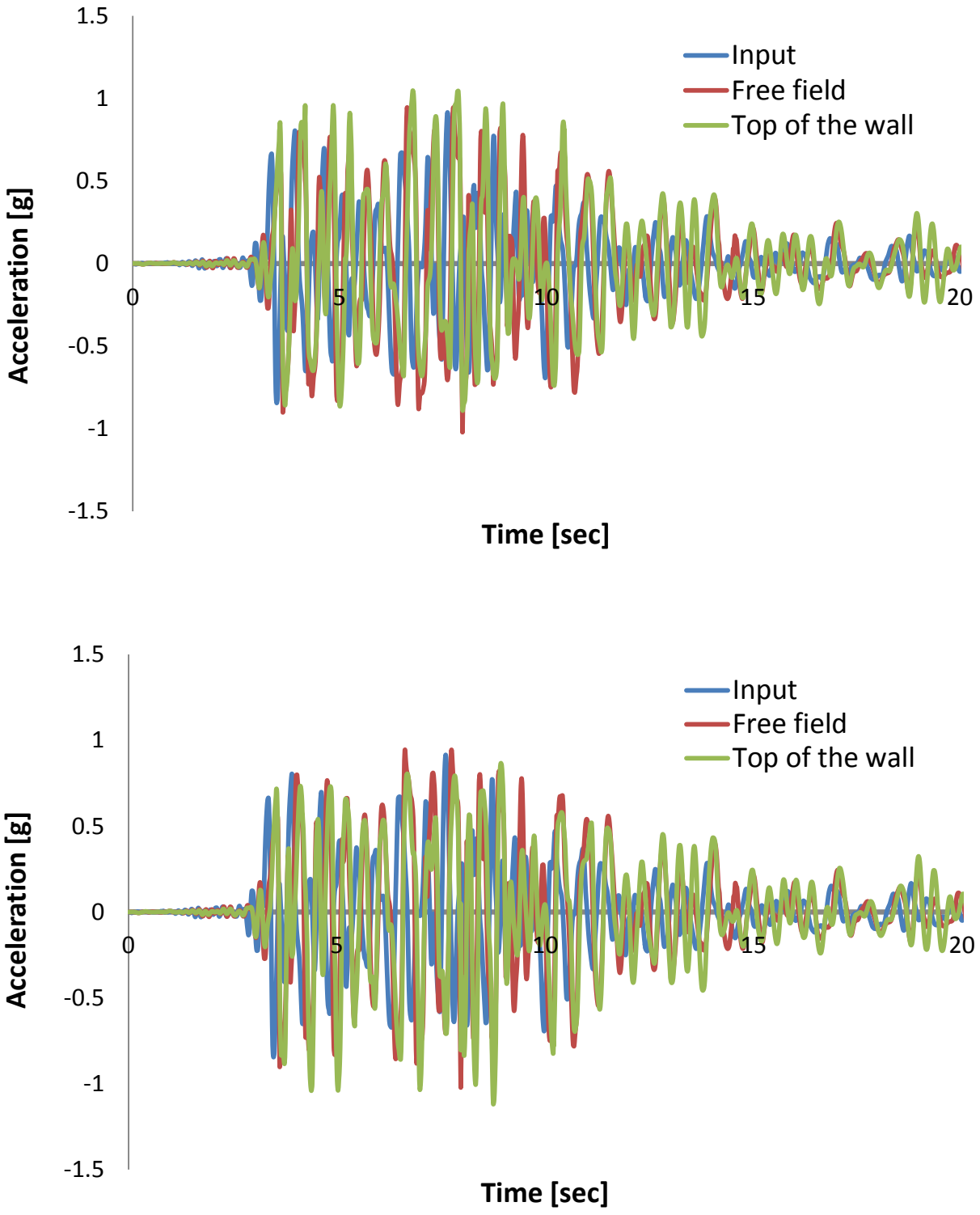

Fig. 3.63. Comparison of input acceleration and computed at the top of the a)left wall b)right wall and top of the free field when subjected to Lefkada Seismic excitation with peak acceleration 0.9g.

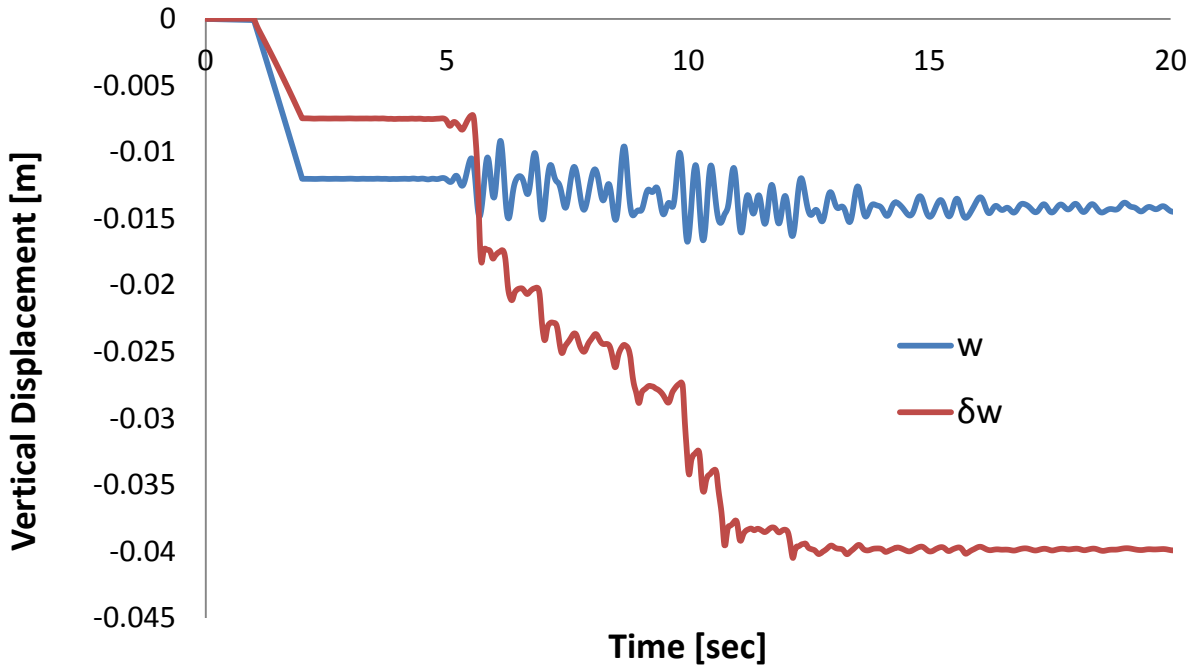

Fig. 3.64. Vertical displacement-time history of the left wall when subjected to Lefkada Seismic excitation with peak acceleration 0.3g.

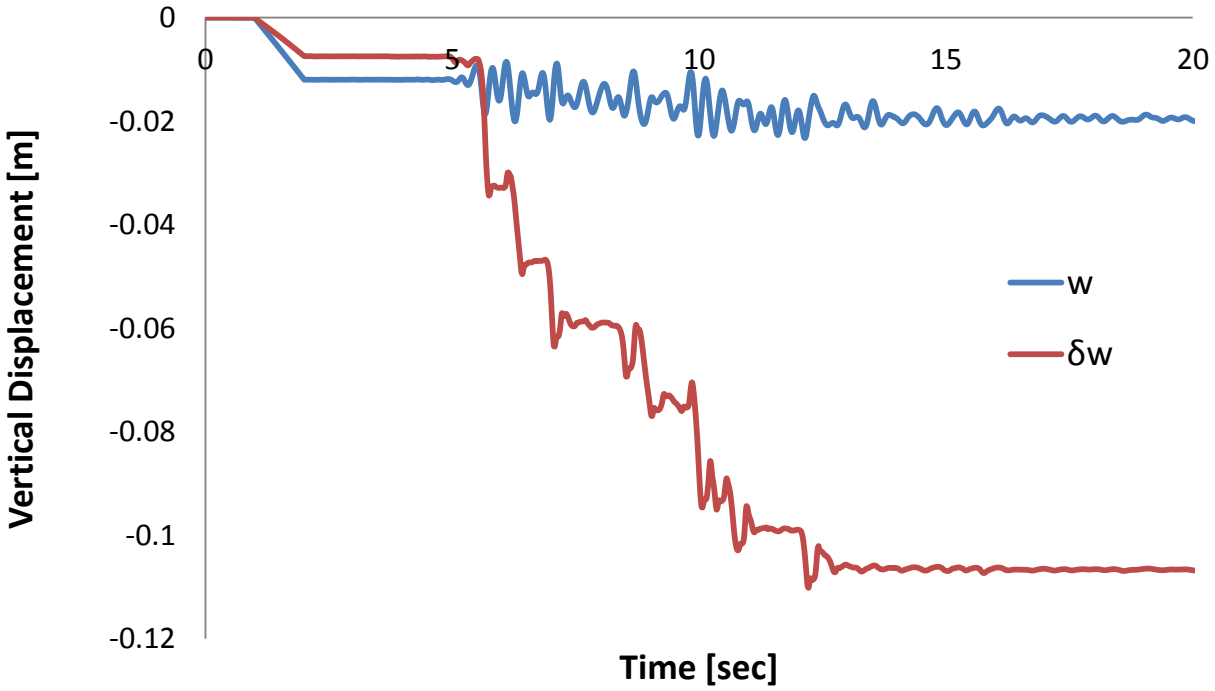

Fig. 3.65. Vertical displacement-time history of the left wall when subjected to Lefkada Seismic excitation with peak acceleration 0.6g.

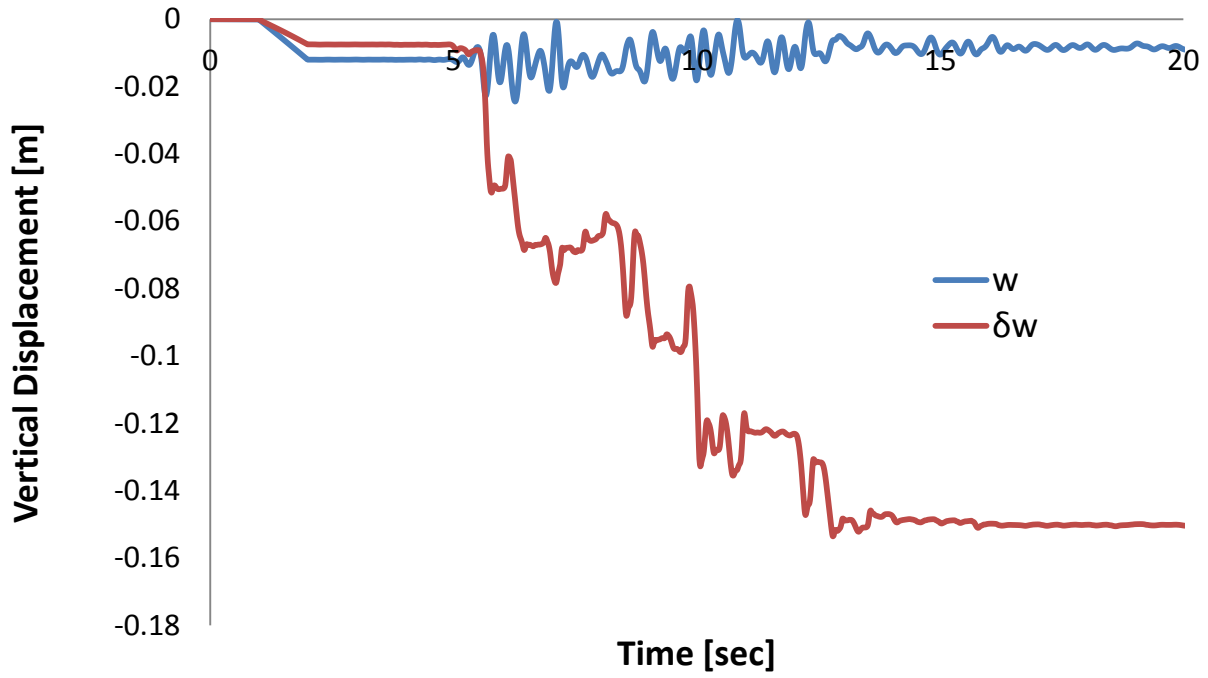

Fig. 3.66. Vertical displacement-time history of the left wall when subjected to Lefkada Seismic excitation with peak acceleration 0.9g.

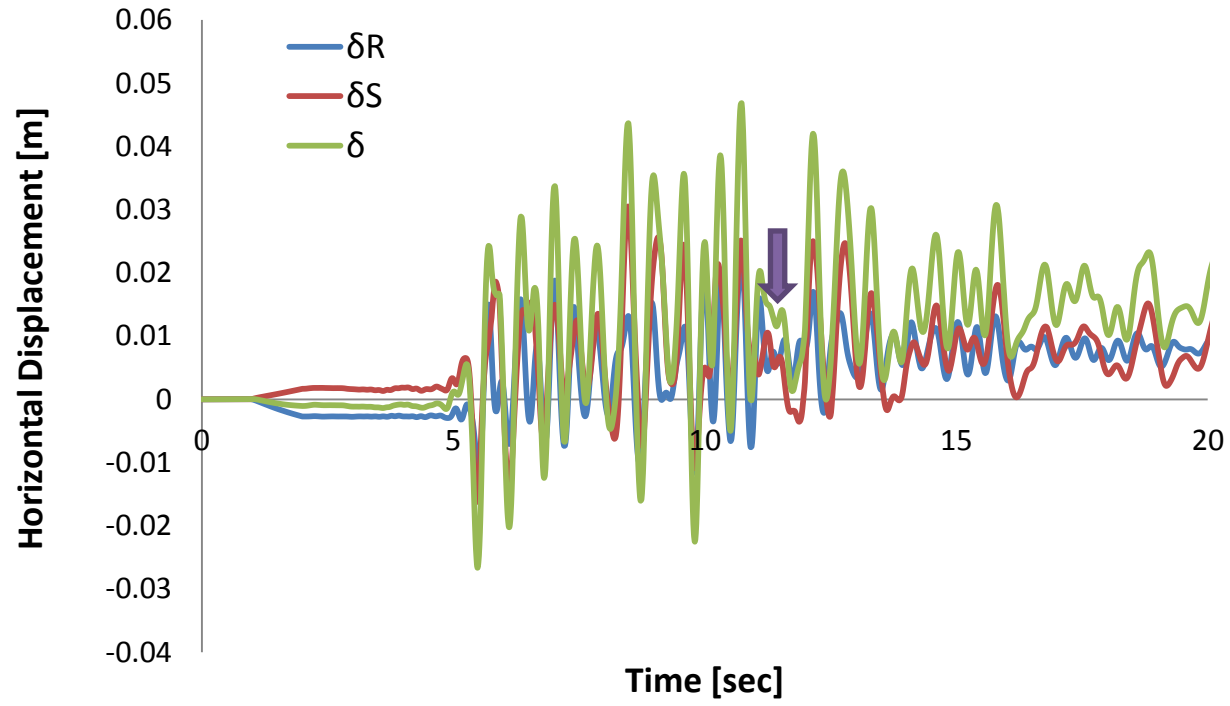

Fig. 3.67. Horizontal displacement-time history of the left wall when subjected to Lefkada Seismic excitation with peak acceleration 0.3g.

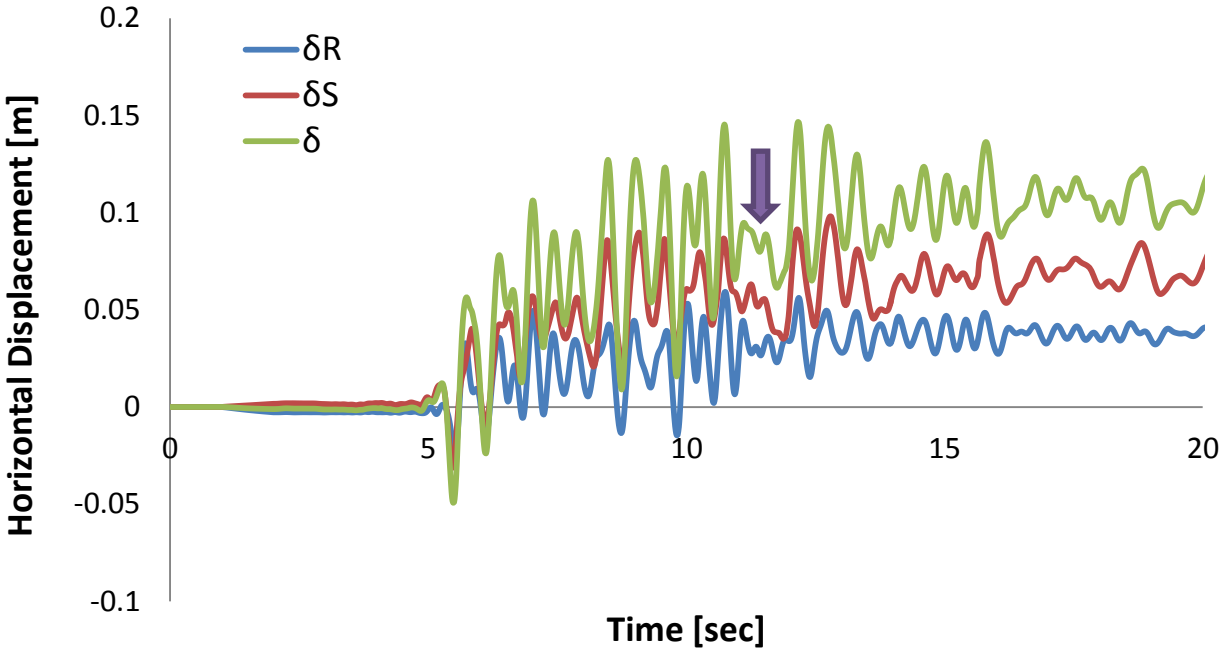

Fig. 3.68. Horizontal displacement-time history of the left wall when subjected to Lefkada Seismic excitation with peak acceleration 0.6g.

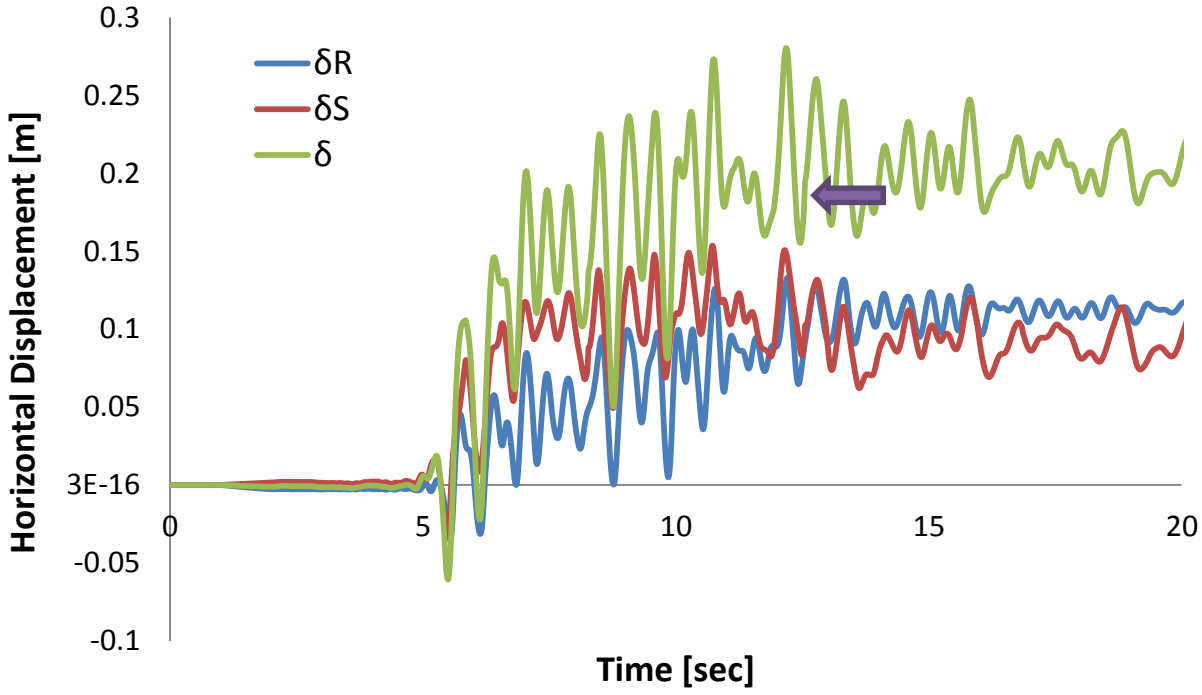

Fig. 3.69. Horizontal displacement-time history of the left wall when subjected to Lefkada Seismic excitation with peak acceleration 0.9g.

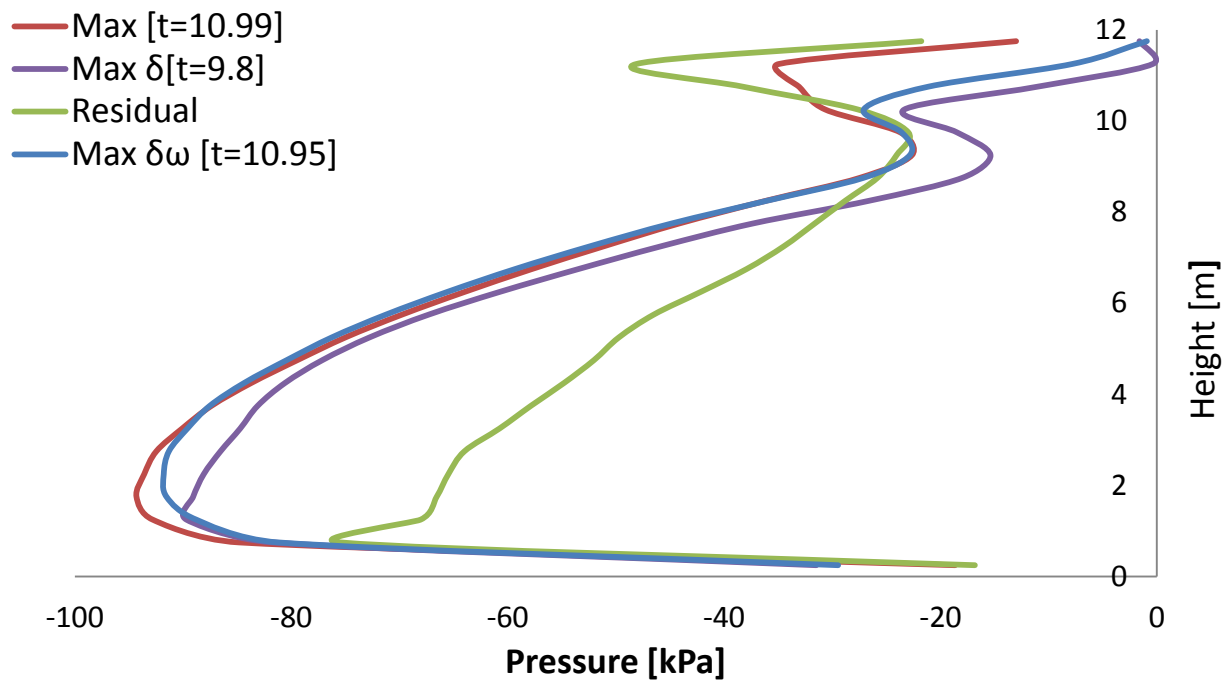

Fig. 3.70. Earth pressures profiles on the right wall at different moments when subjected to Lefkada Seismic excitation with peak ground acceleration 0.3g.

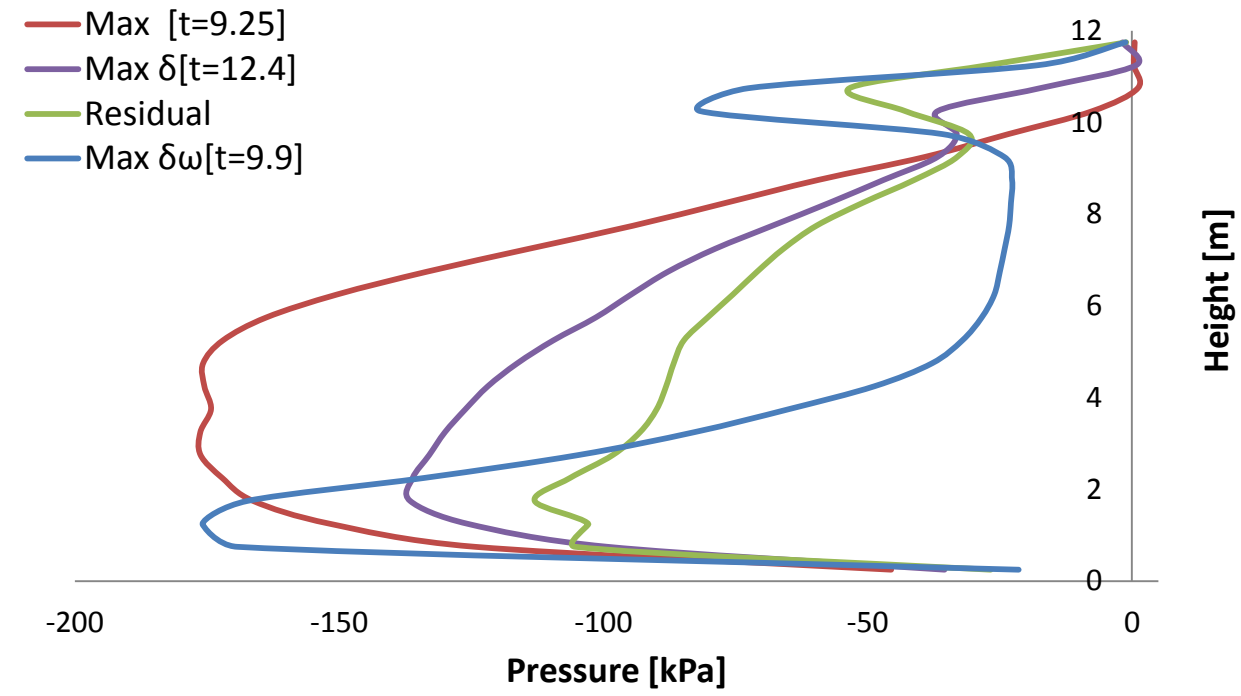

Fig. 3.71. Earth pressures profiles on the right wall at different moments when subjected to Lefkada Seismic excitation with peak ground acceleration 0.3g.

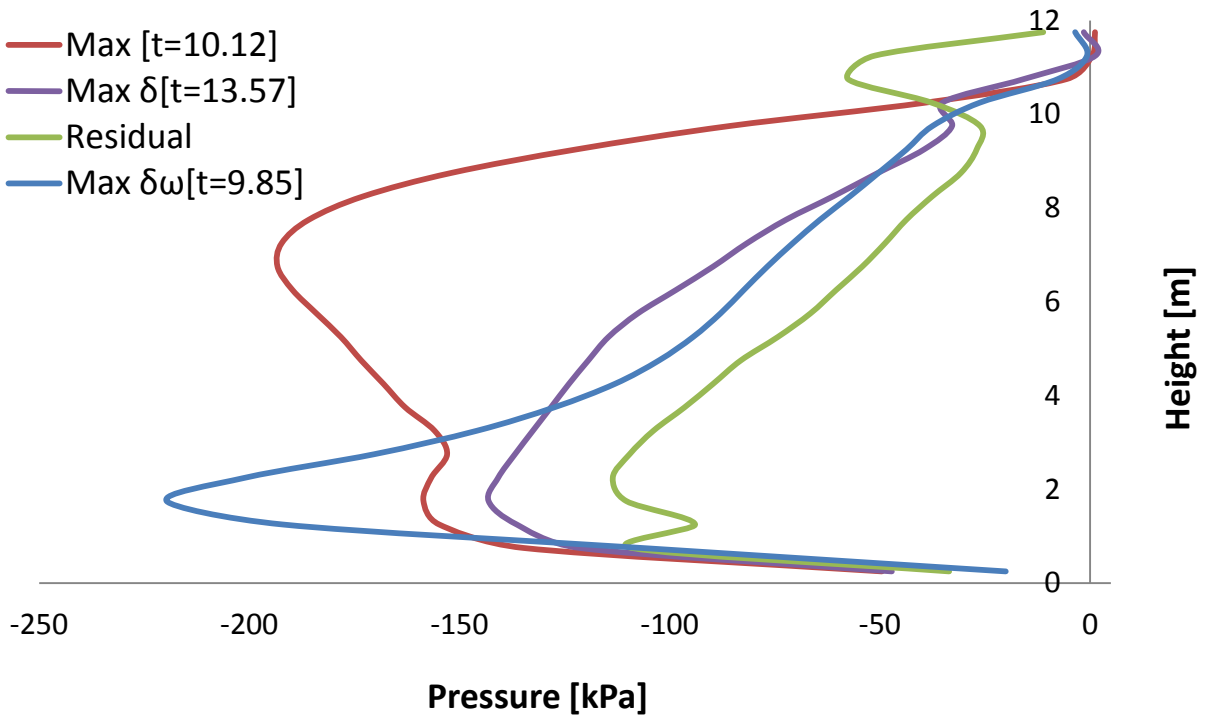

Fig. 3.72. Earth pressures profiles on the right wall at different moments when subjected to Lefkada Seismic excitation with peak ground acceleration 0.9g.

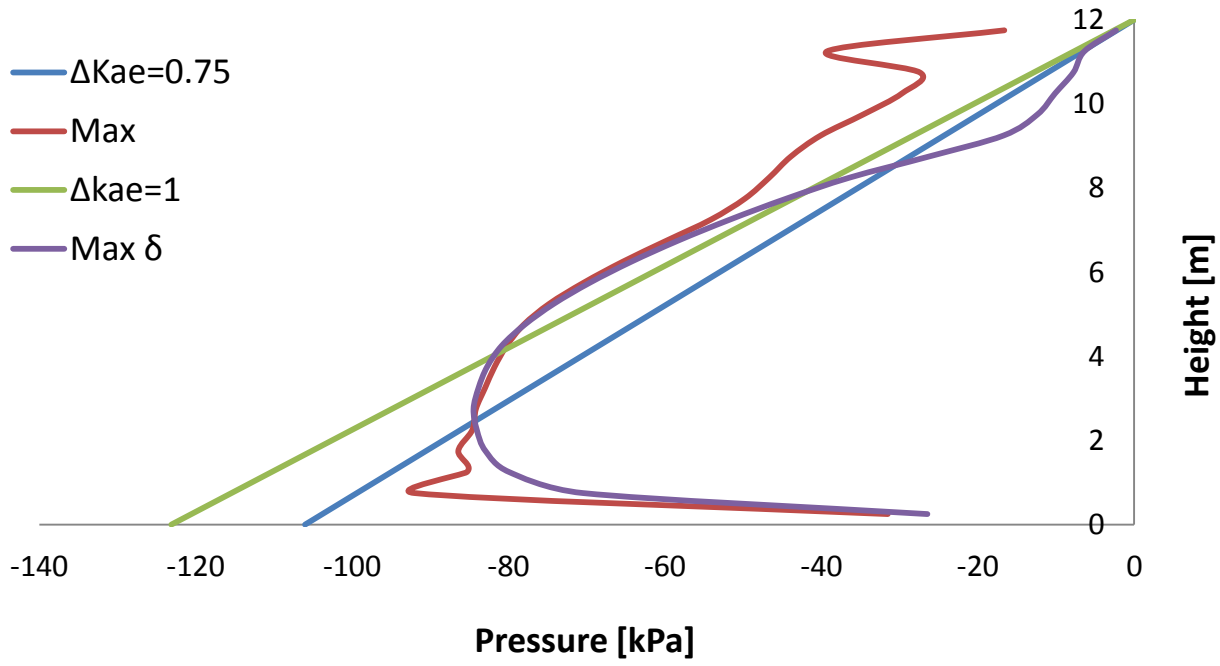

Fig. 3.73. Earth pressure profiles computed in ABAQUS and estimated using the M-O when the right wall is subjected to the Lefkada Seismic excitation with peak acceleration 0.3g.

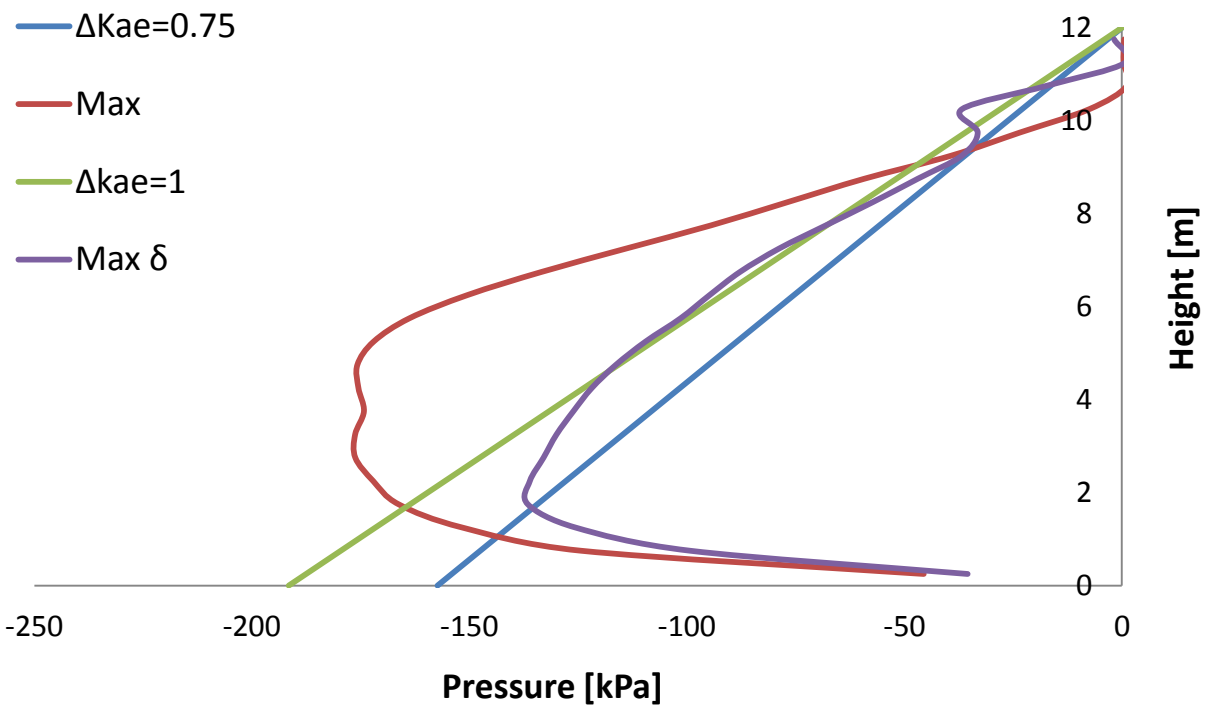

Fig. 3.74. Earth pressure profiles computed in ABAQUS and estimated using the M-O when the right wall is subjected to the Lefkada Seismic excitation with peak acceleration 0.6g.

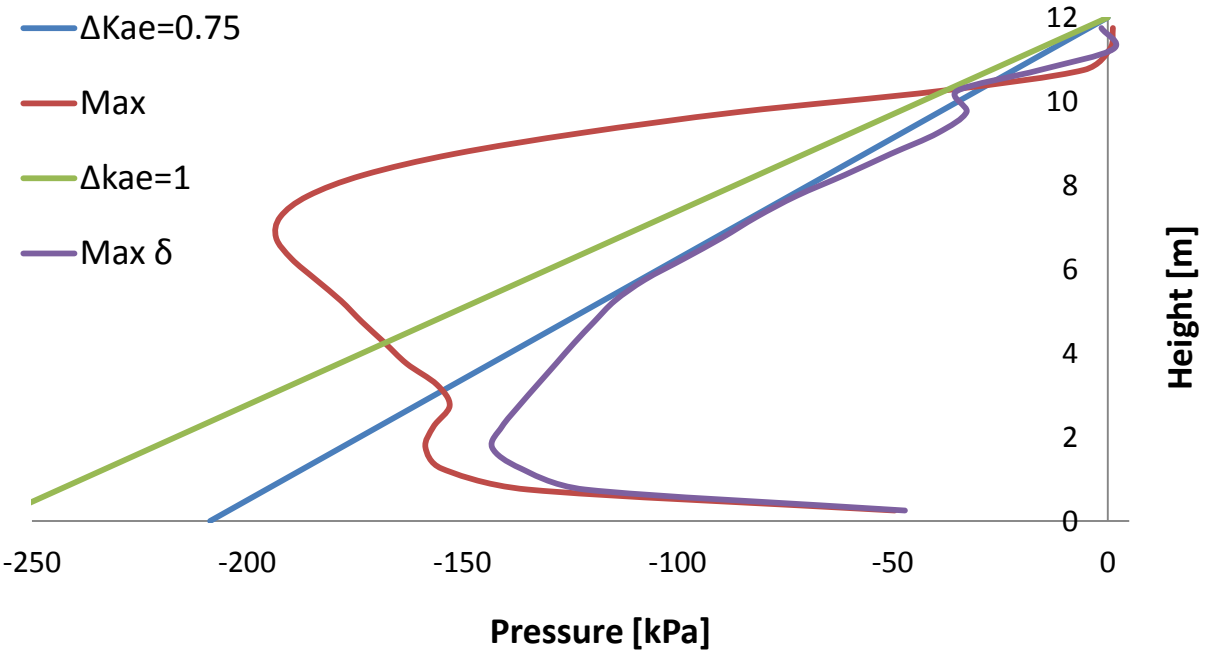

Fig. 3.75. Earth pressure profiles computed in ABAQUS and estimated using the M-O when the right wall is subjected to the Lefkada Seismic excitation with peak acceleration 0.9g.

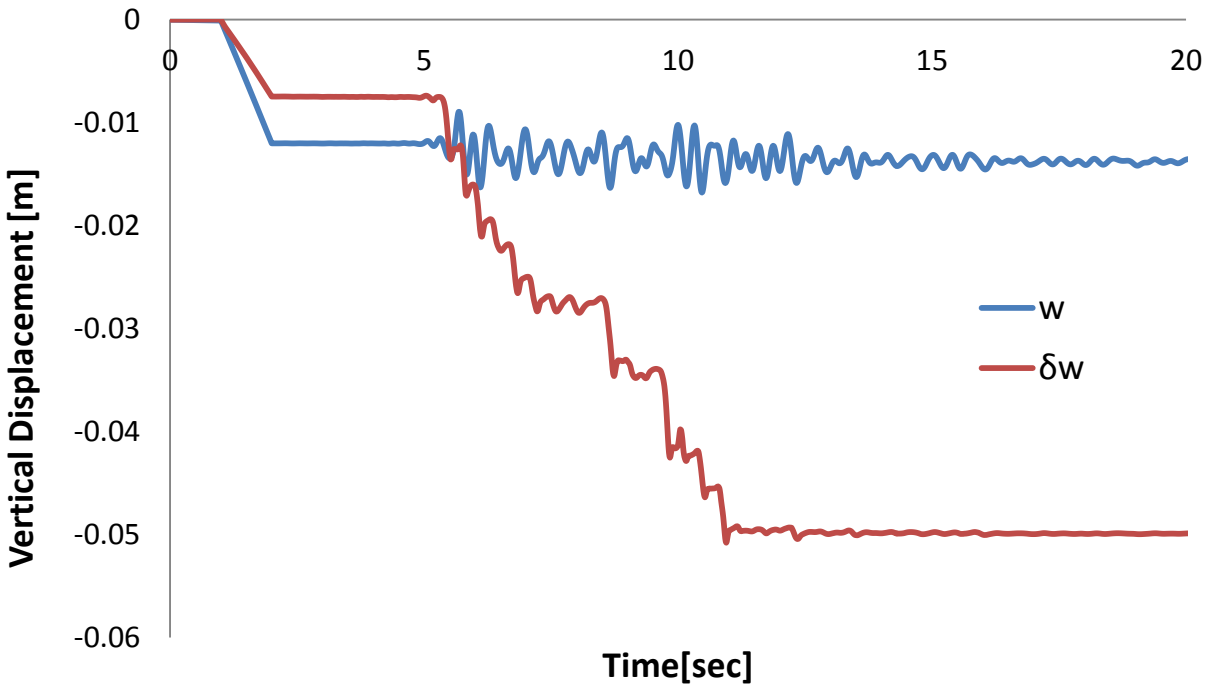

Fig. 3.76. Vertical displacement-time history of the right wall when subjected to Lefkada Seismic excitation with peak acceleration 0.3g.

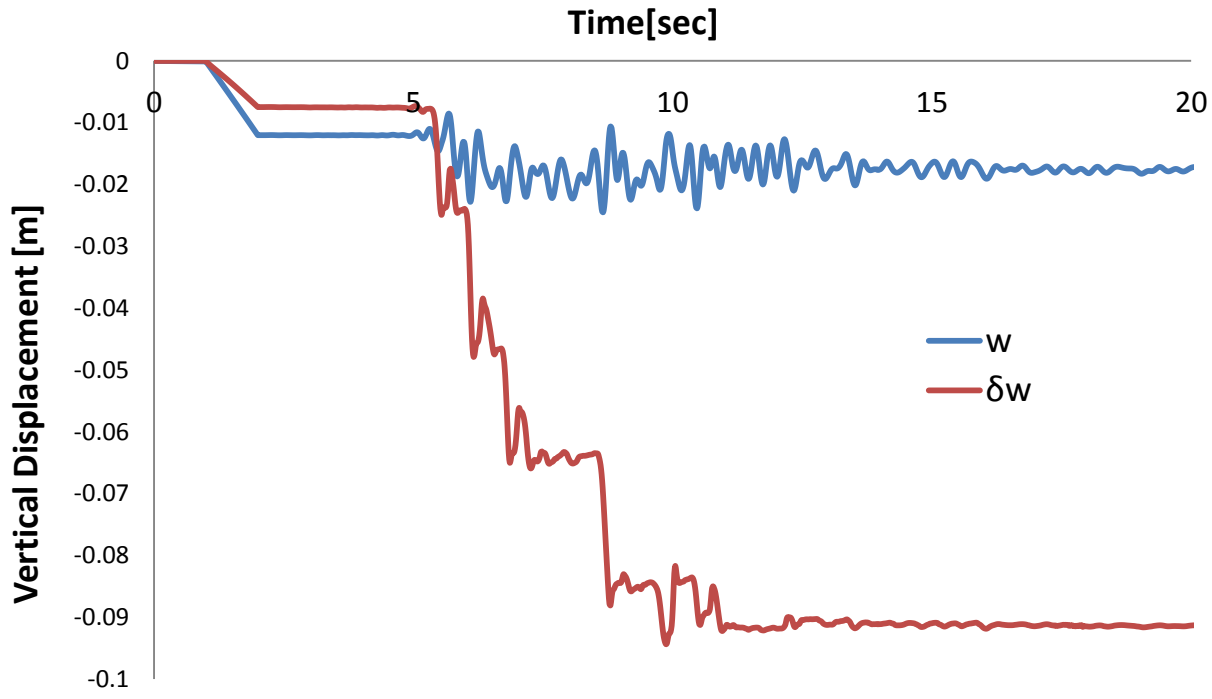

Fig. 3.77. Vertical displacement-time history of the right wall when subjected to Lefkada Seismic excitation with peak acceleration 0.6g.

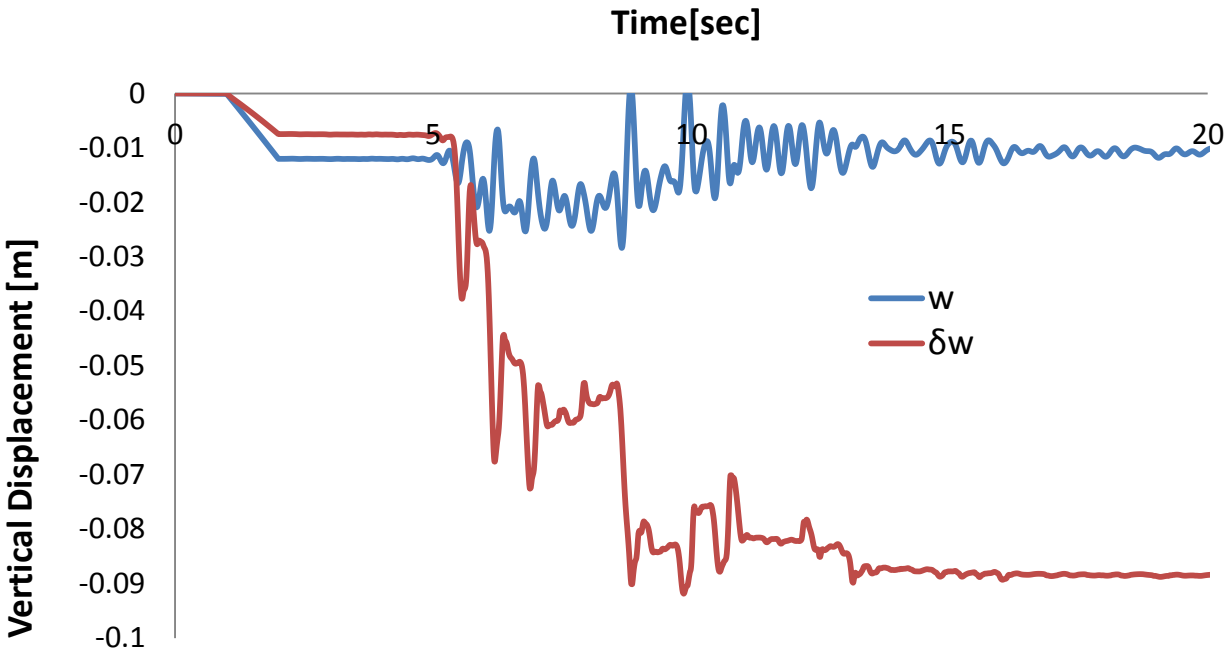

Fig. 3.78. Vertical displacement-time history of the right wall when subjected to Lefkada Seismic excitation with peak acceleration 0.9g.

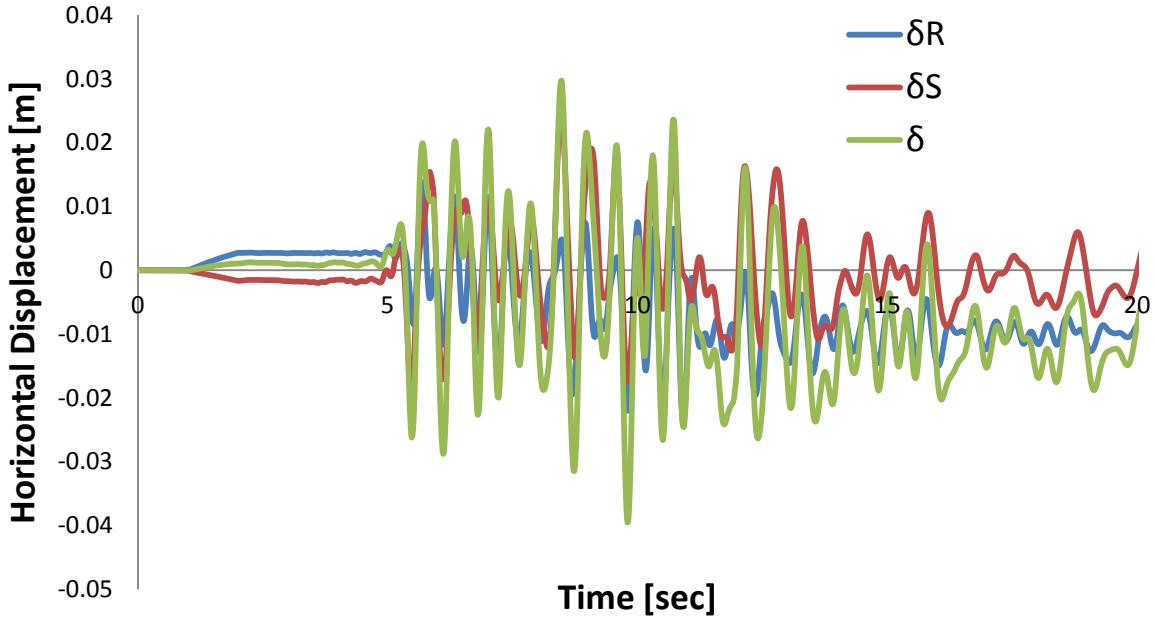

Fig. 3.79. Horizontal displacement-time history of the right wall when subjected to LefkadaSeismic excitation with peak acceleration 0.3g.

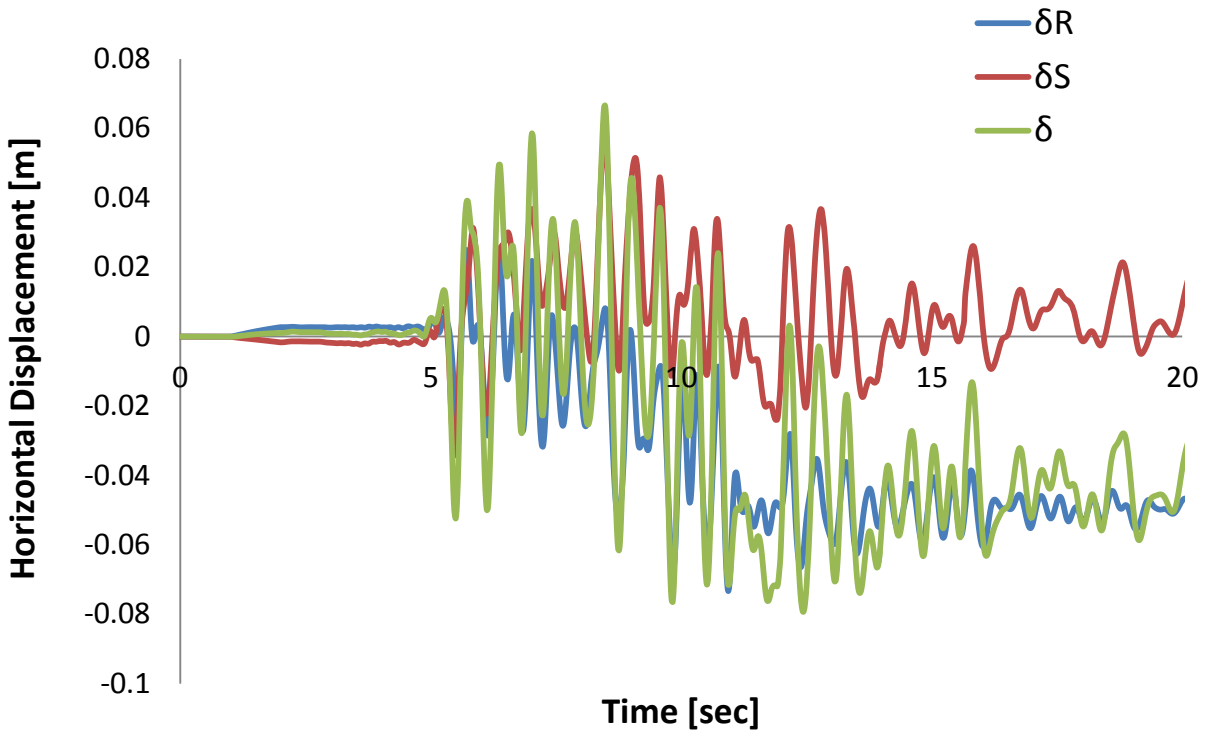

Fig. 3.80. Horizontal displacement-time history of the right wall when subjected to Lefkada Seismic excitation with peak acceleration 0.6g.

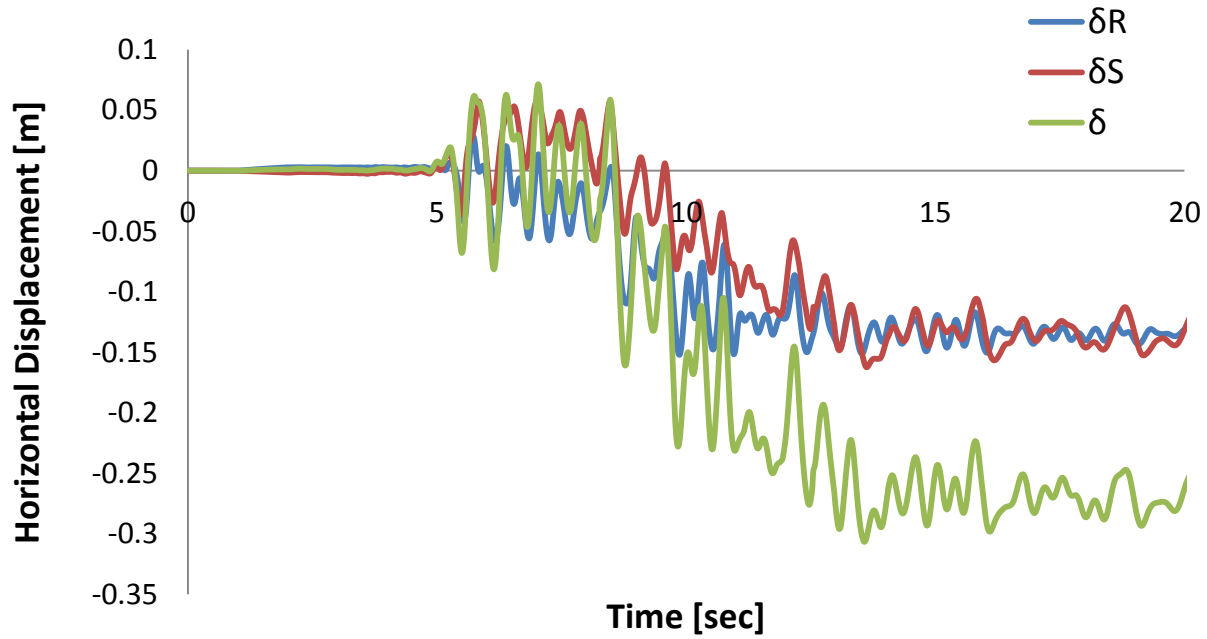

Fig. 3.81. Horizontal displacement-time history of the right wall when subjected to Lefkada Seismic excitation with peak acceleration 0.9g.

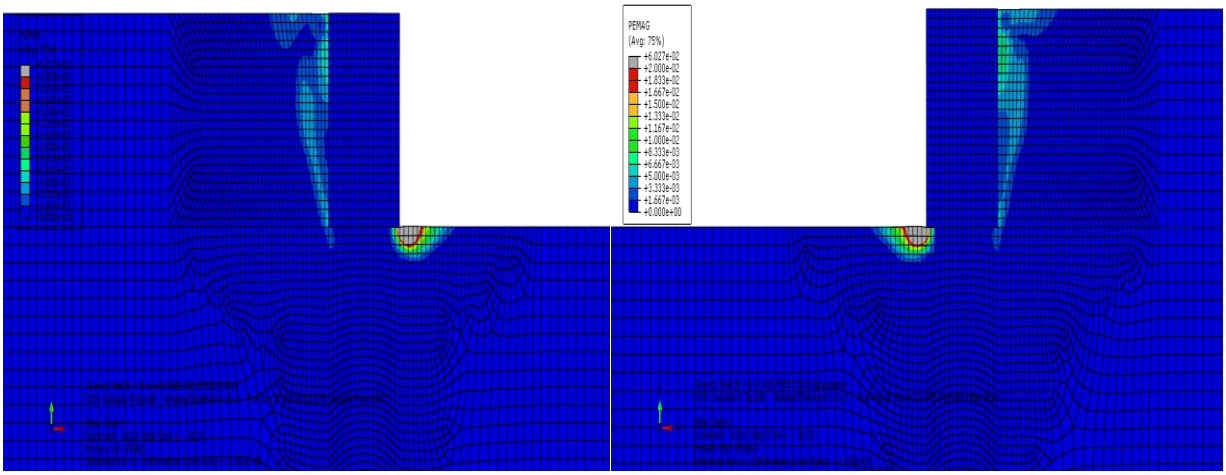

Fig. 3.82. Plastic strain contours at the end of seismic shaking (a)Left wall (b)Right wall when subjected to Lefkada seismic excitation with peak acceleration 0.3g.

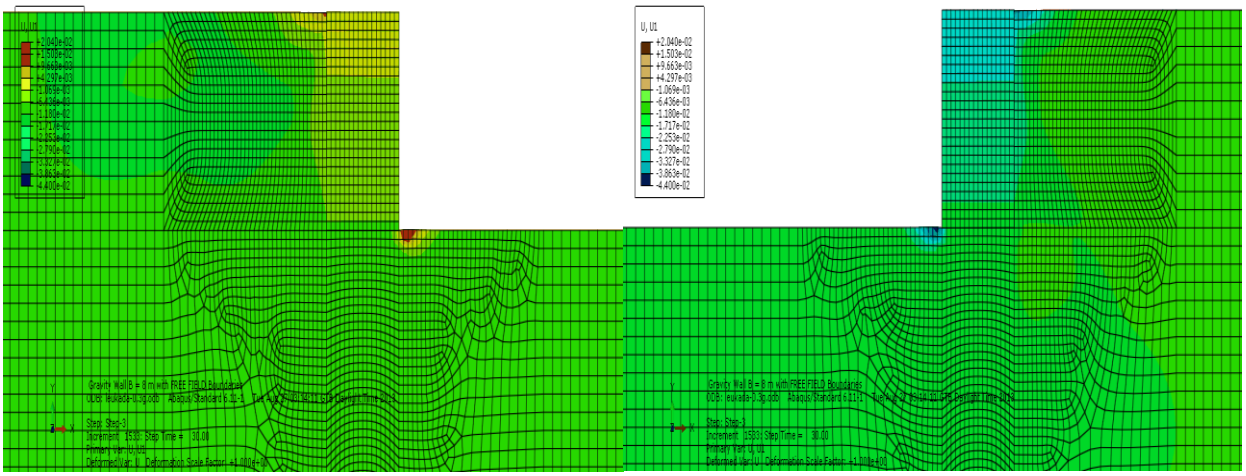

Fig. 3.83. Horizontal displacement contours at the end of the seismic excitation Lefkada PGA 0.3g.

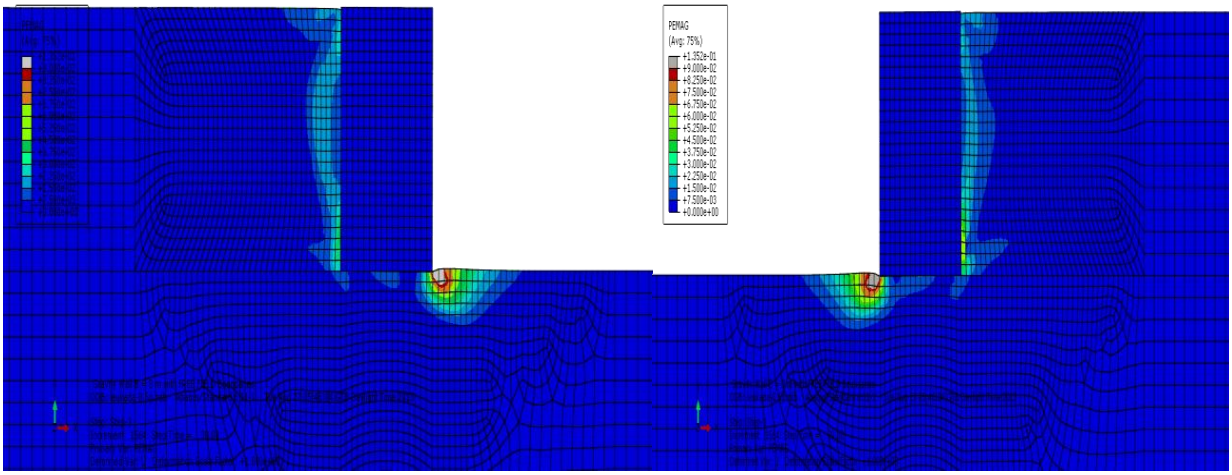

Fig. 3.84. Plastic strain contours at the end of seismic shaking (a)Left wall (b)Right wall when subjected to Lefkada seismic excitation with peak acceleration 0.6g.

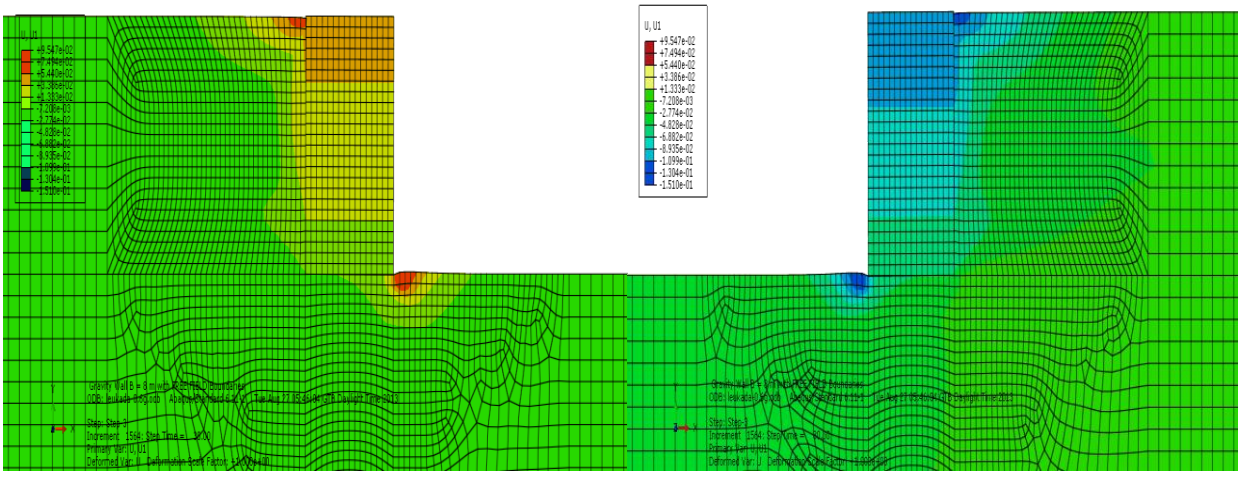

Fig. 3.85. Horizontal displacement contours at the end of the seismic excitation Lefkada PGA 0.6g.

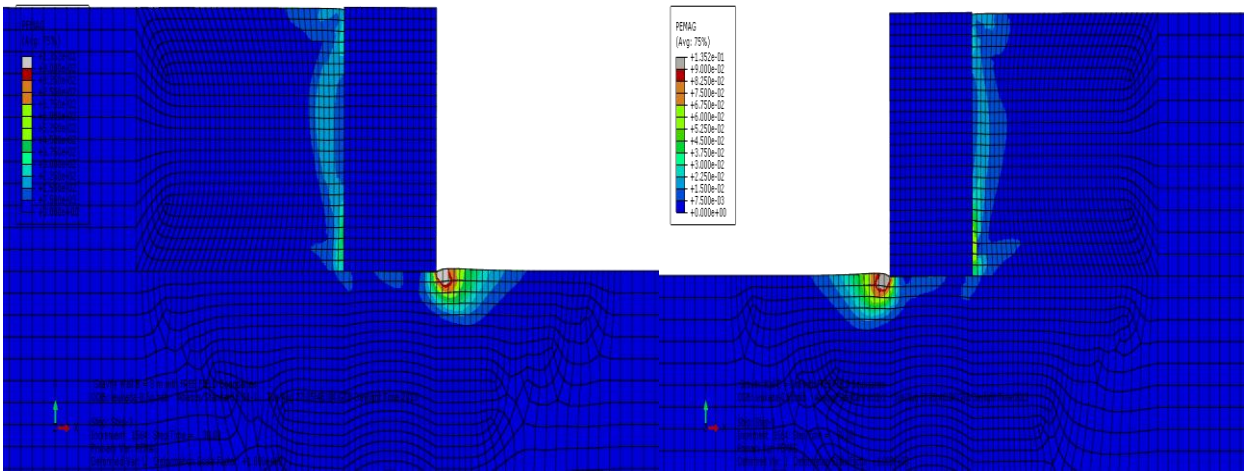

Fig. 3.86. Plastic strain contours at the end of seismic shaking (a)Left wall (b)Right wall when subjected to Lefkada seismic excitation with peak acceleration 0.9g.

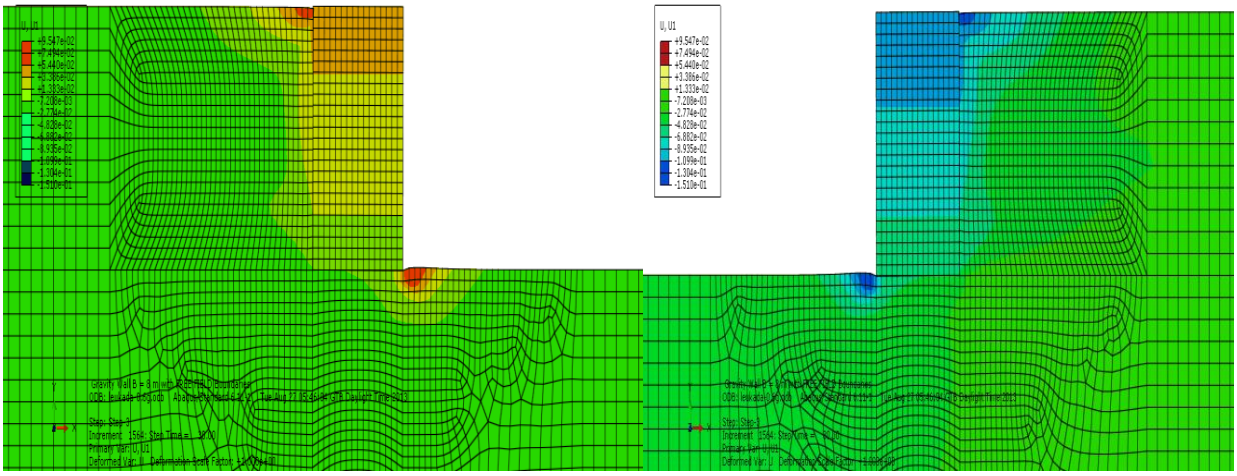

Fig. 3.87. Horizontal displacement contours at the end of the seismic excitation Lefkada PGA 0.9g.

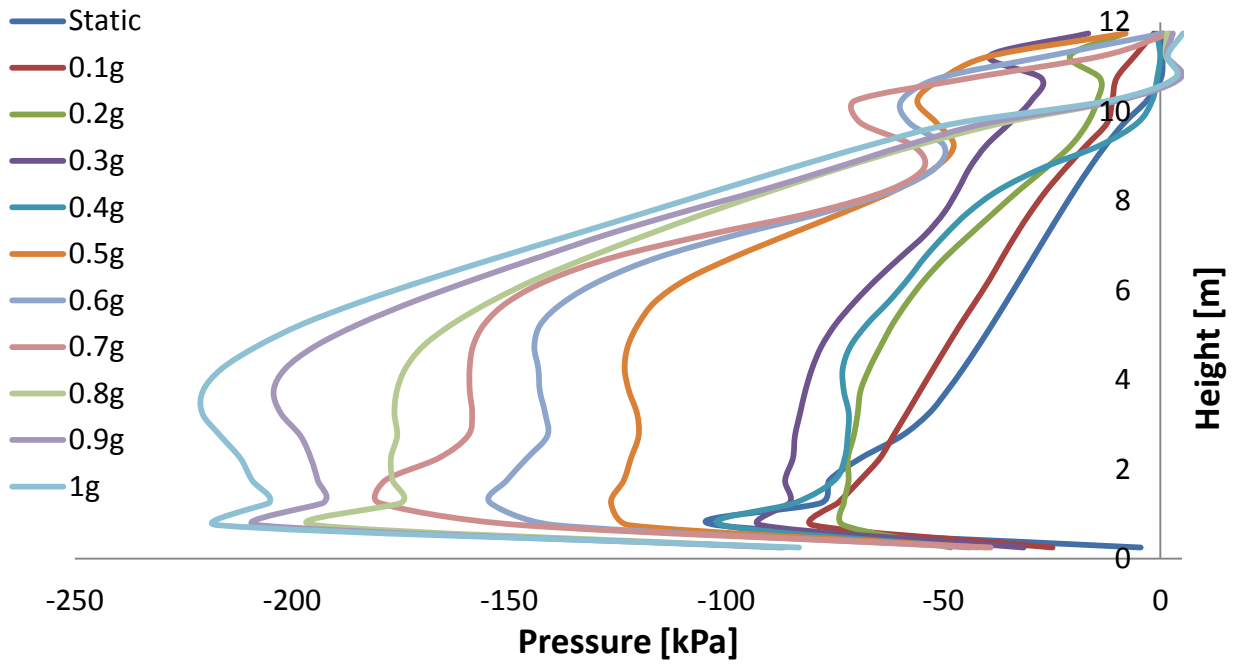

Fig. 3.88. Static and maximum earth pressure profiles for different peak accelerations on the left wall when subjected to Lefkada Seismic excitation.

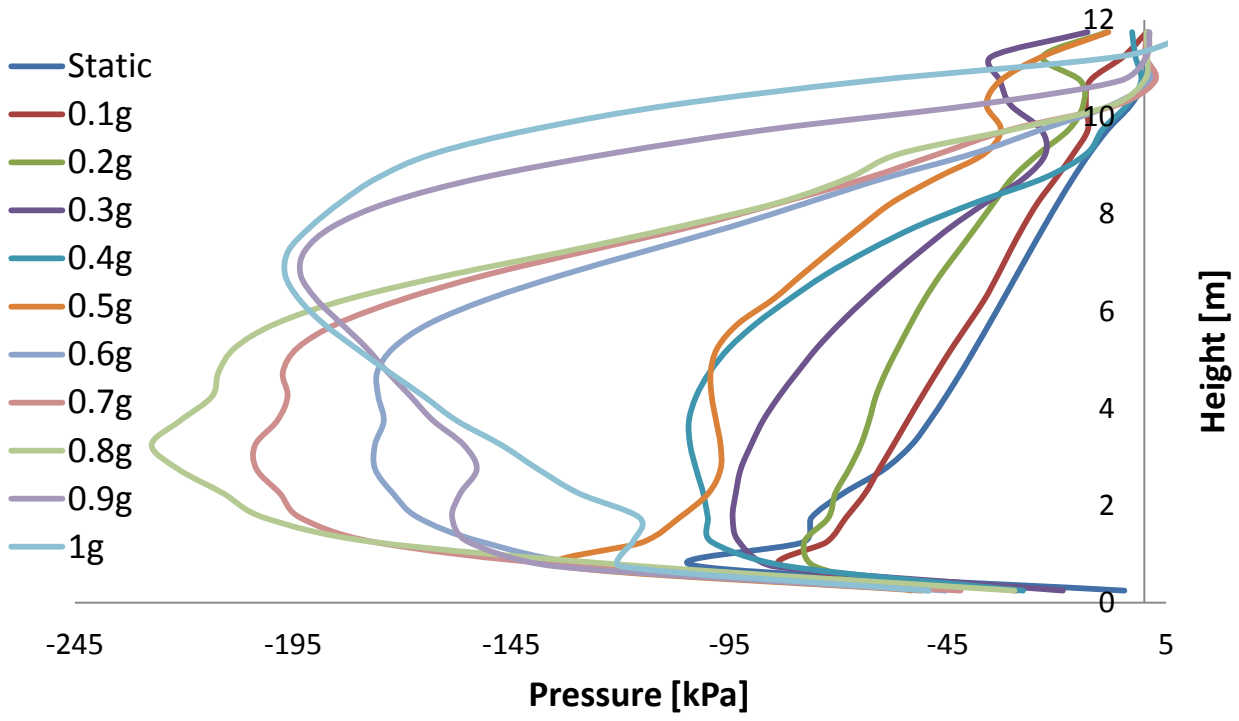

Fig. 3.89. Static and maximum earth pressure profiles for different peak accelerations on the right wall when subjected to Lefkada Seismic excitation.

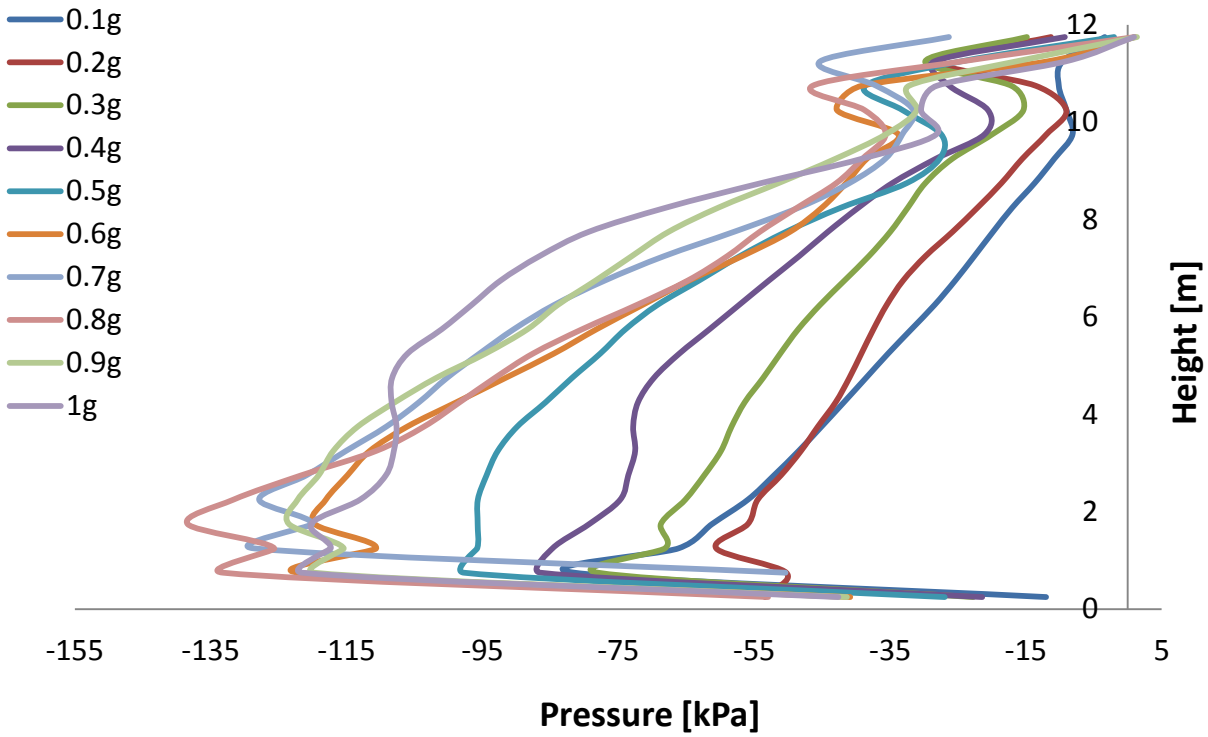

Fig. 3.90. Residual earth pressure profiles for different peak accelerations on the left wall when subjected to Lefkada Seismic excitation.

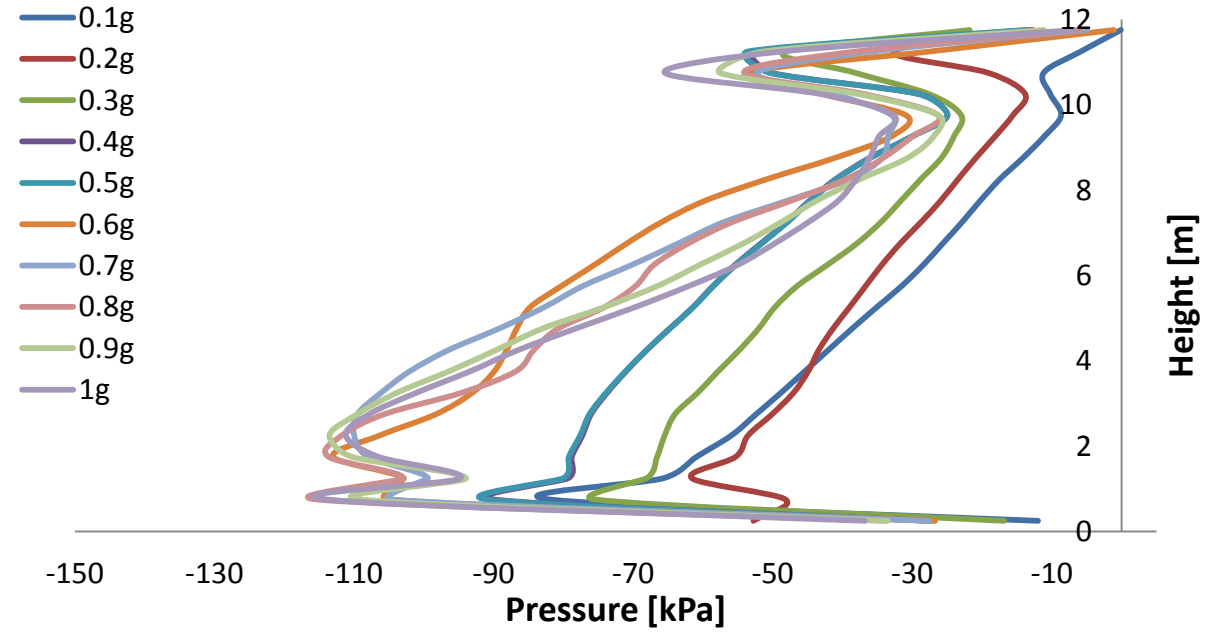

Fig. 3.91. Residual earth pressure profiles for different peak accelerations on the right wall when subjected to Lefkada Seismic excitation.

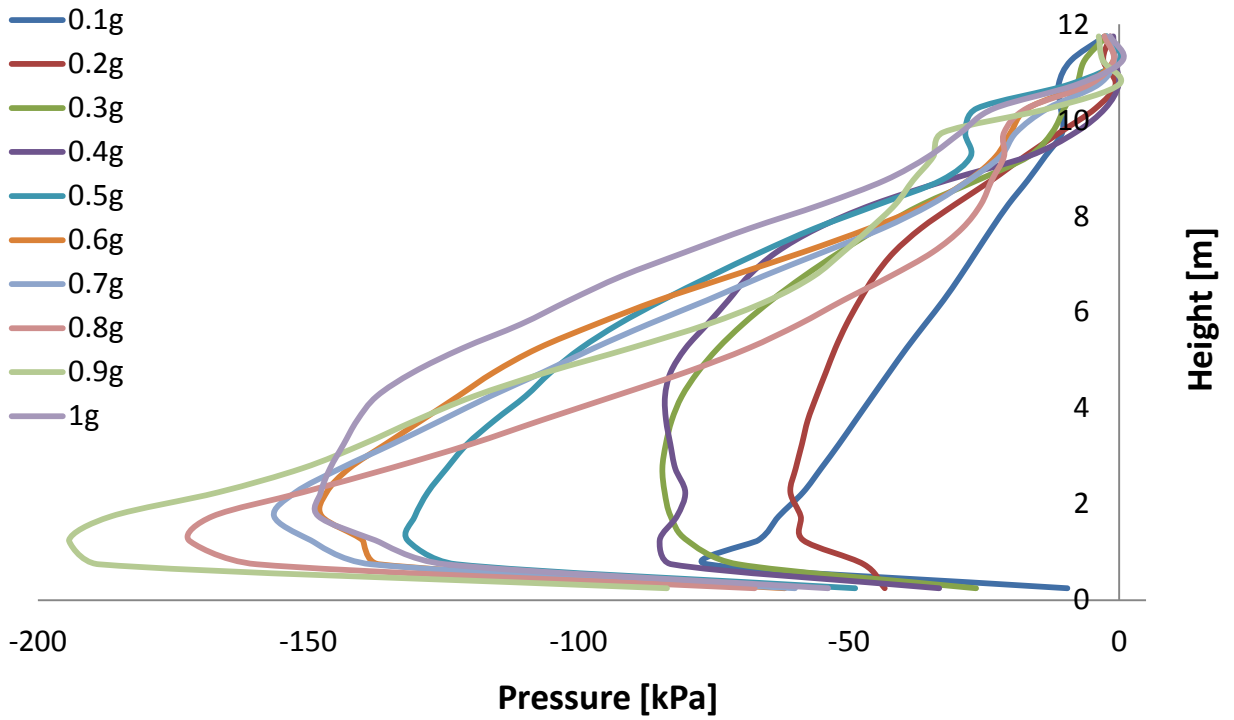

Fig. 3.92. Earth pressure profiles at maximum displacement for different peak accelerations on the left wall when subjected to Lefkada Seismic excitation.

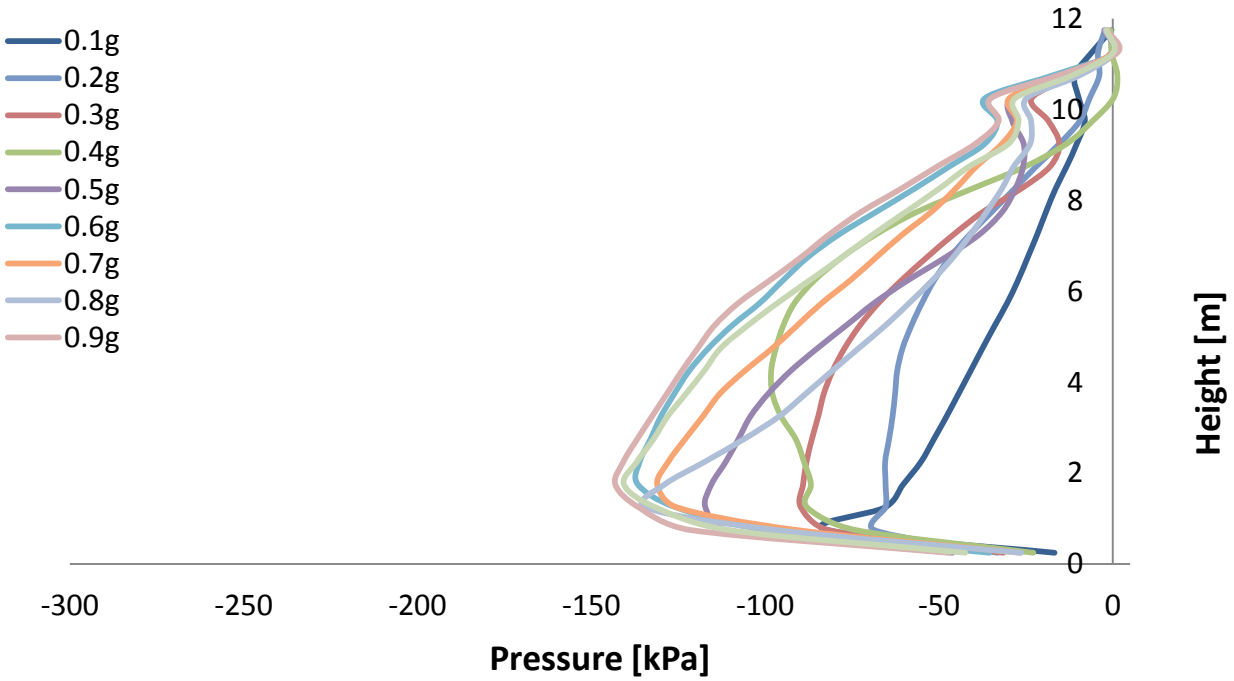

Fig. 3.93. Earth pressure profiles at maximum displacement for different peak accelerations on the right wall when subjected to Lefkada Seismic excitation.

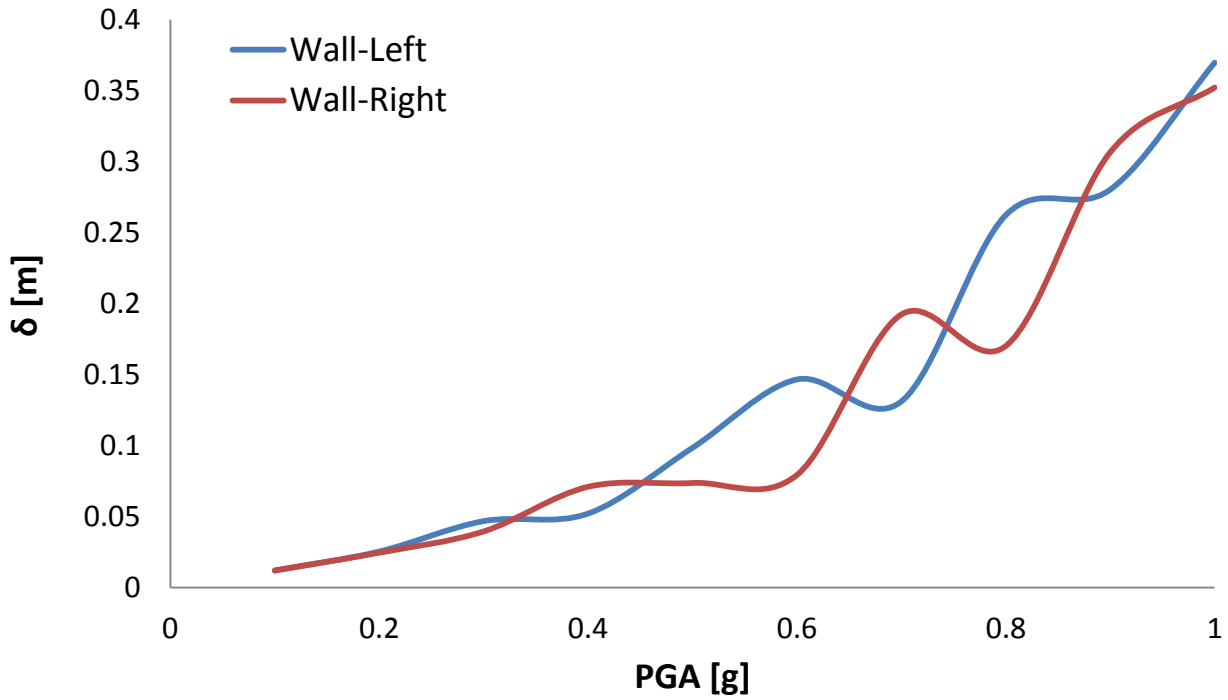

Fig. 3.94. Horizontal displacement as a function of PGA for the left and right wall when subjected to Lefkada Seismic excitation.

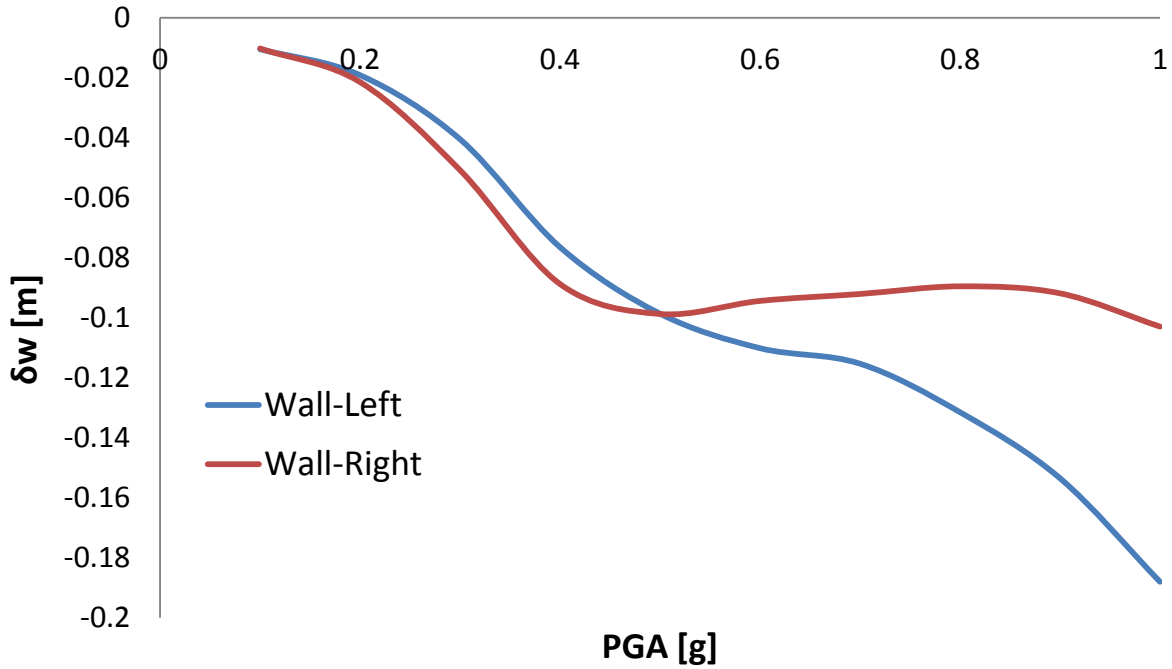

Fig. 2.95. Differential settelement as a function of PGA for the left and right wall when subjected to Lefkada Seismic excitation.

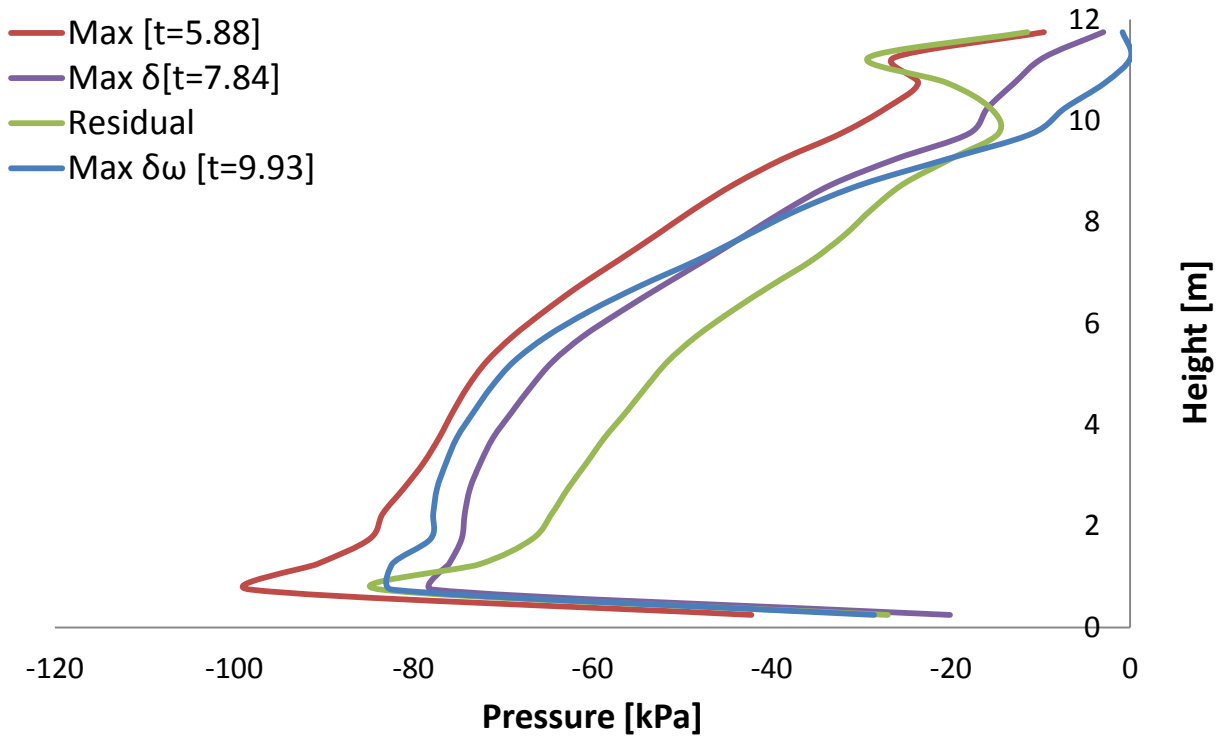

Fig. 3.96. Earth pressures profiles on the left wall at different moments when subjected to Takatori Seismic excitation with peak ground acceleration 0.3g.

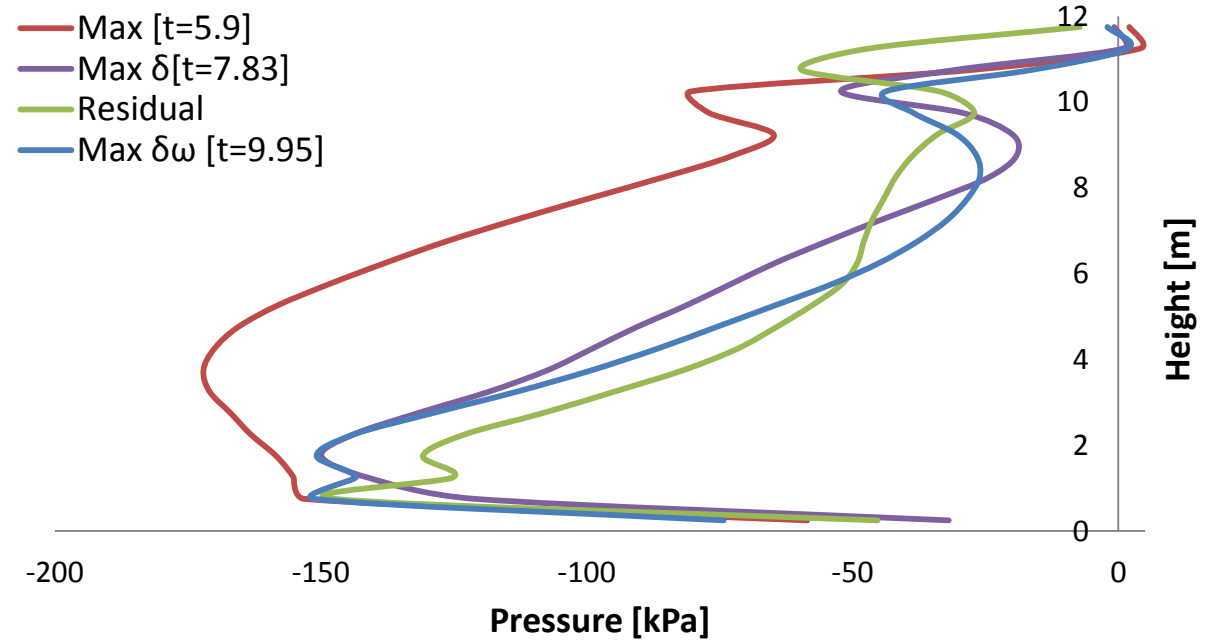

Fig. 3.97. Earth pressures profiles on the left wall at different moments when subjected to Takatori Seismic excitation with peak ground acceleration 0.6g.

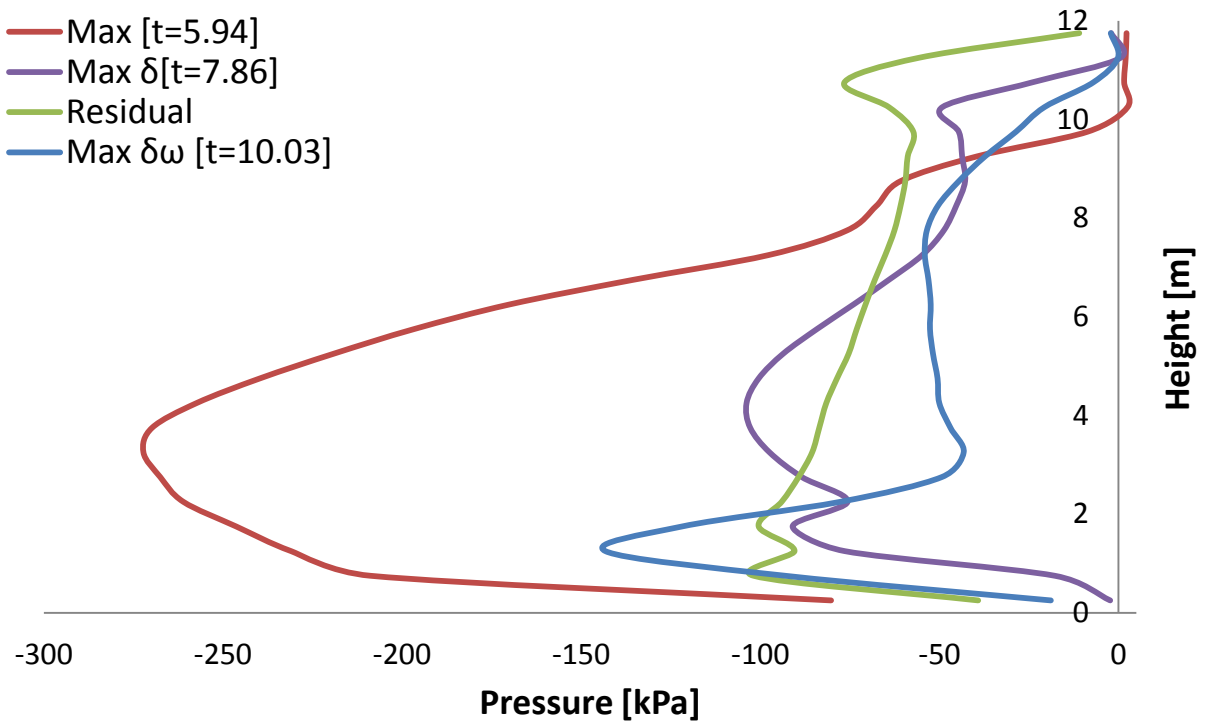

Fig. 3.98. Earth pressures profiles on the left wall at different moments when subjected to Takatori Seismic excitation with peak ground acceleration 0.9g.

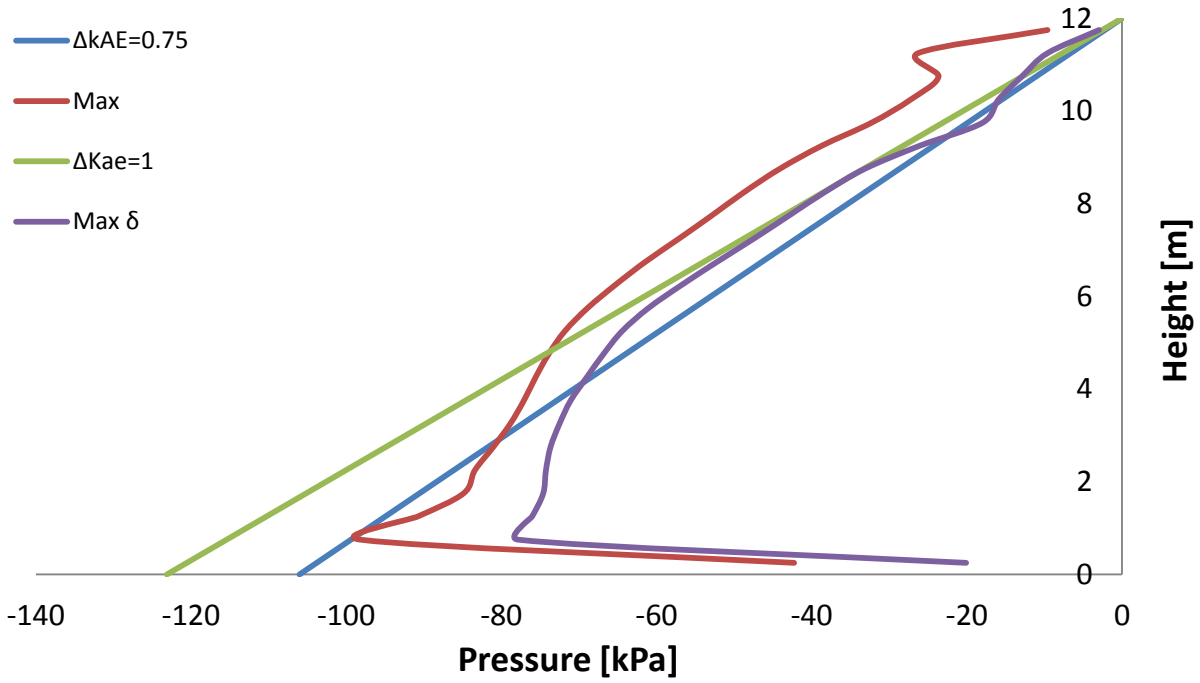

Fig. 3.99. Earth pressure profiles computed in ABAQUS and estimated using the M-O when the left wall is subjected to the Takatori Seismic excitation with peak acceleration 0.3g.

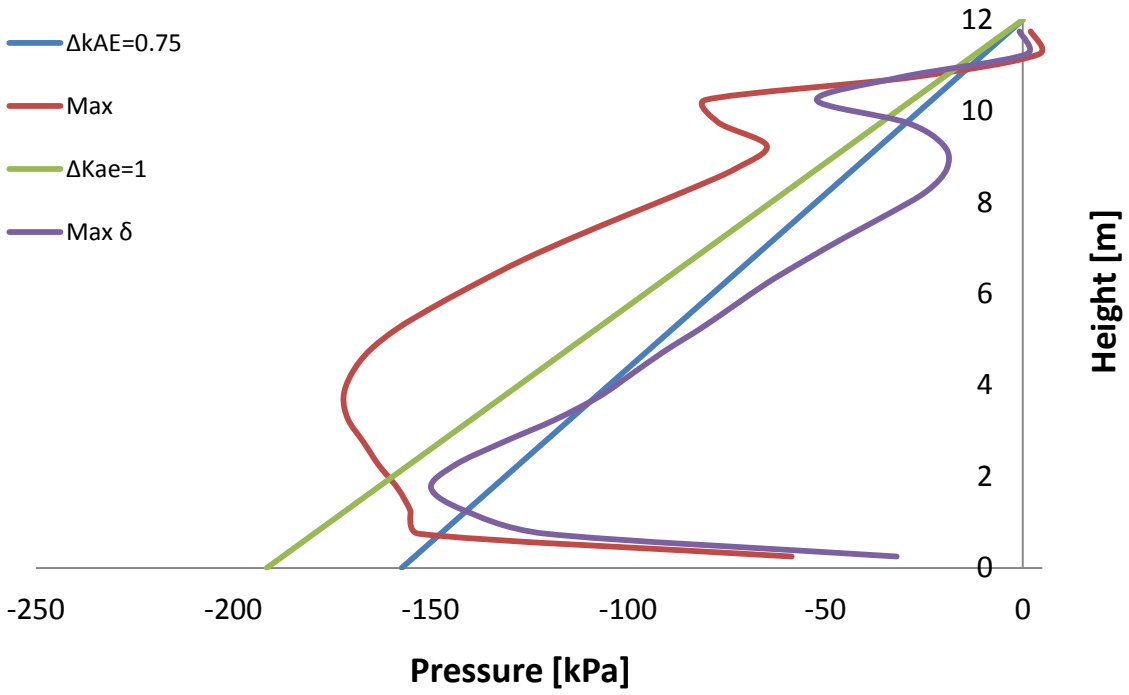

Fig. 3.100. Earth pressure profiles computed in ABAQUS and estimated using the M-O when the left wall is subjected to the Takatori Seismic excitation with peak acceleration 0.6g.

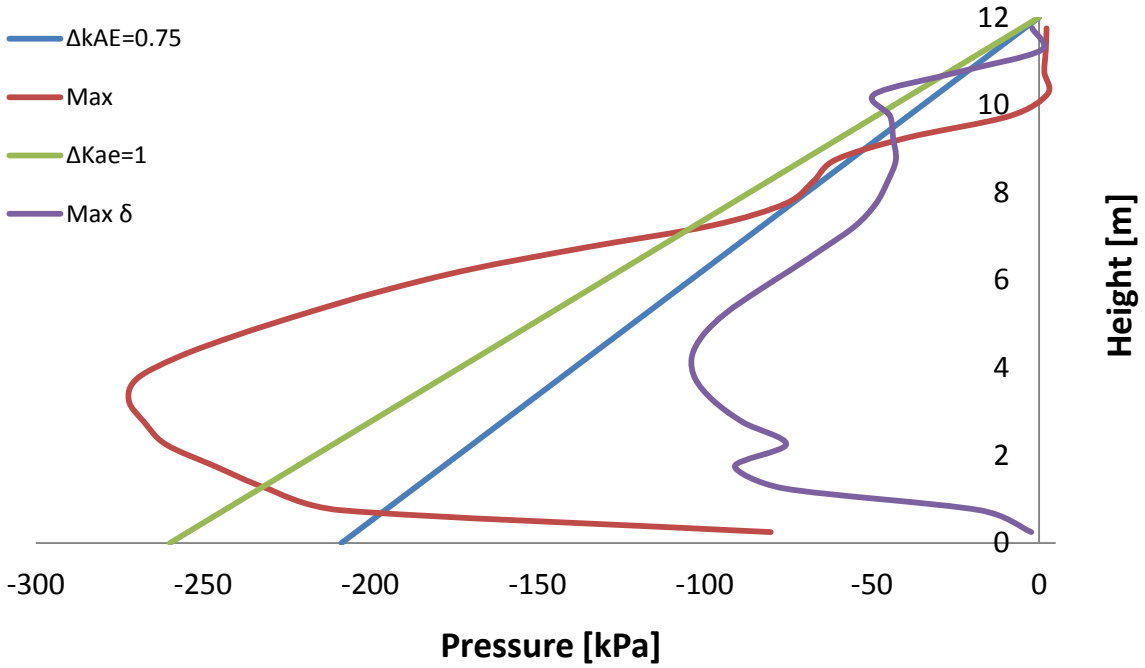

Fig. 3.101. Earth pressure profiles computed in ABAQUS and estimated using the M-O when the left wall is subjected to the Takatori Seismic excitation with peak acceleration 0.9g.

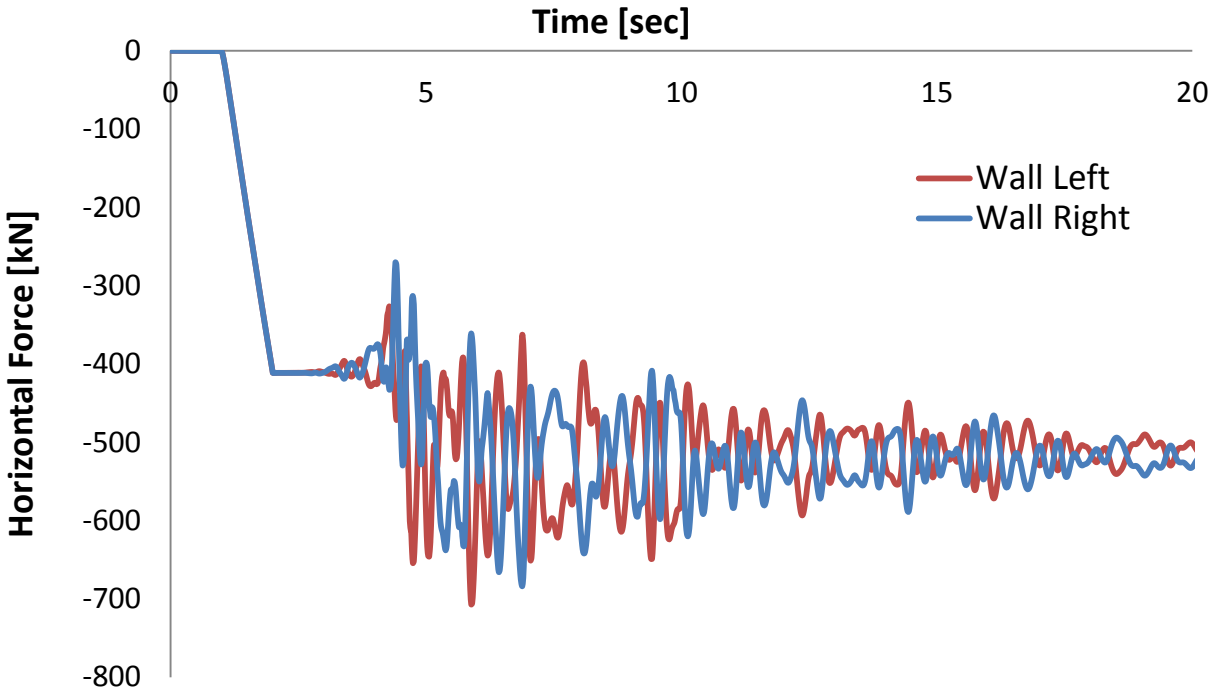

Fig. 3.102. Horizontal force-time history of the left and right wall when subjected to Takatori Seismic excitation with peak ground acceleration 0.3g.

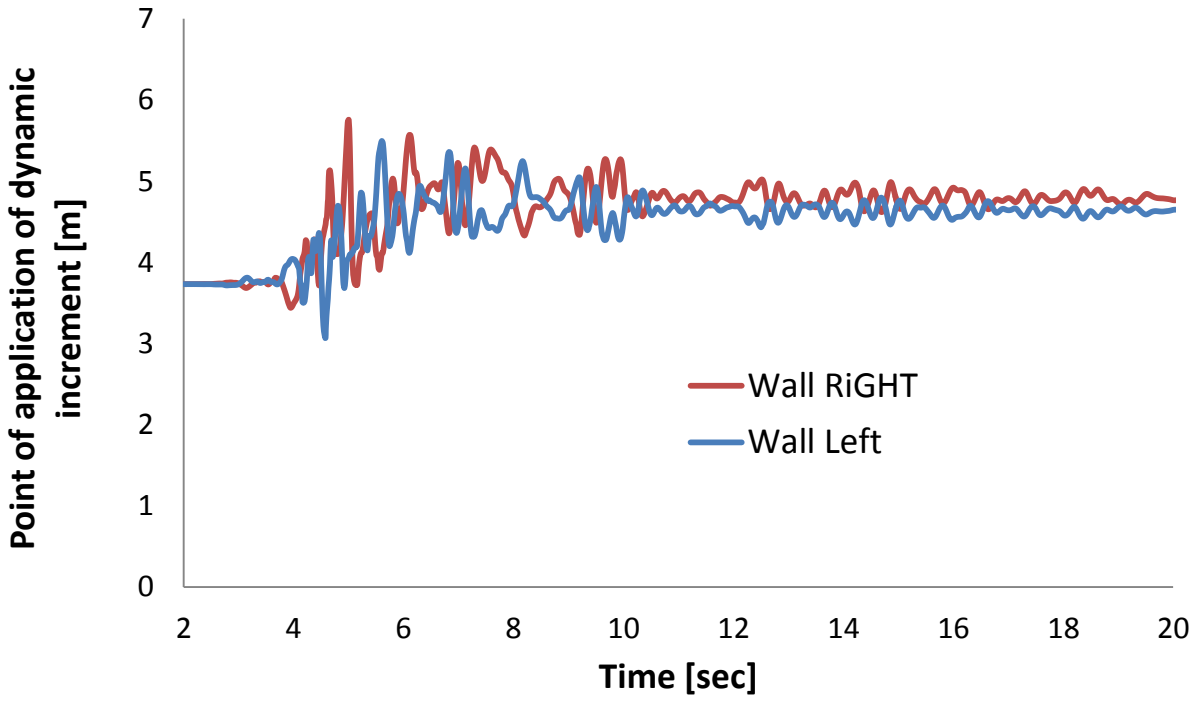

Fig. 3.103. Point of application of dynamic force on the left and right wall when subjected to Takatori Seismic excitation with peak ground acceleration 0.3g.

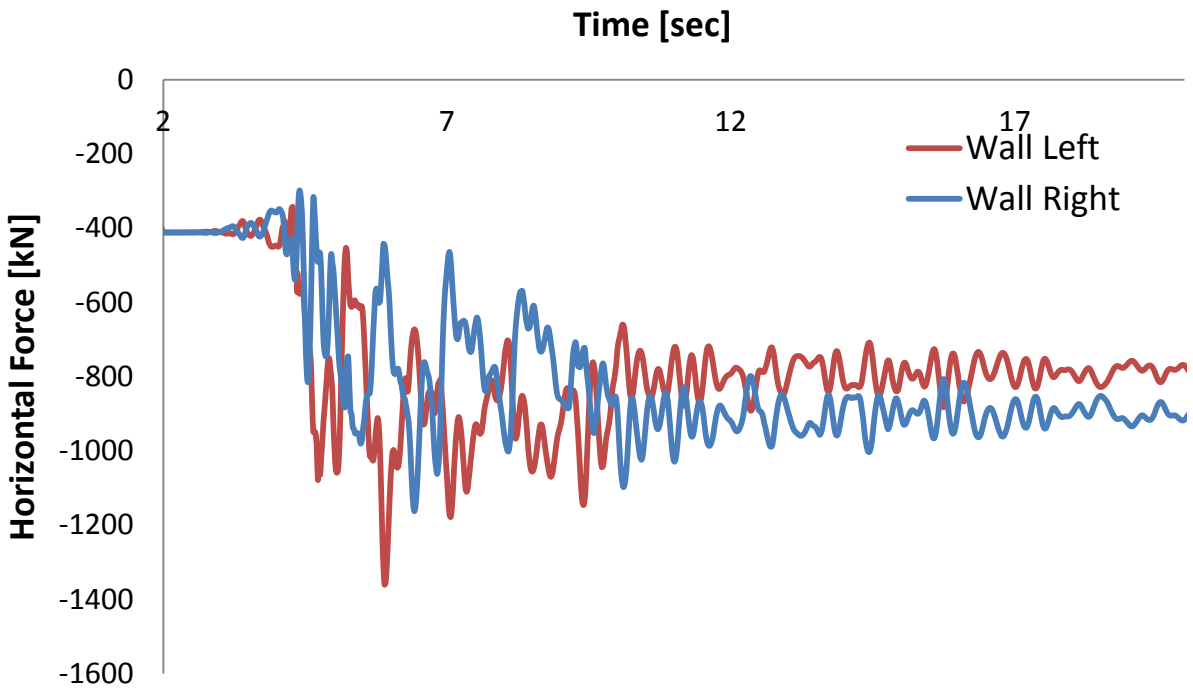

Fig. 3.104. Horizontal force-time history of the left and right wall when subjected to Takatori Seismic excitation with peak ground acceleration 0.6g.

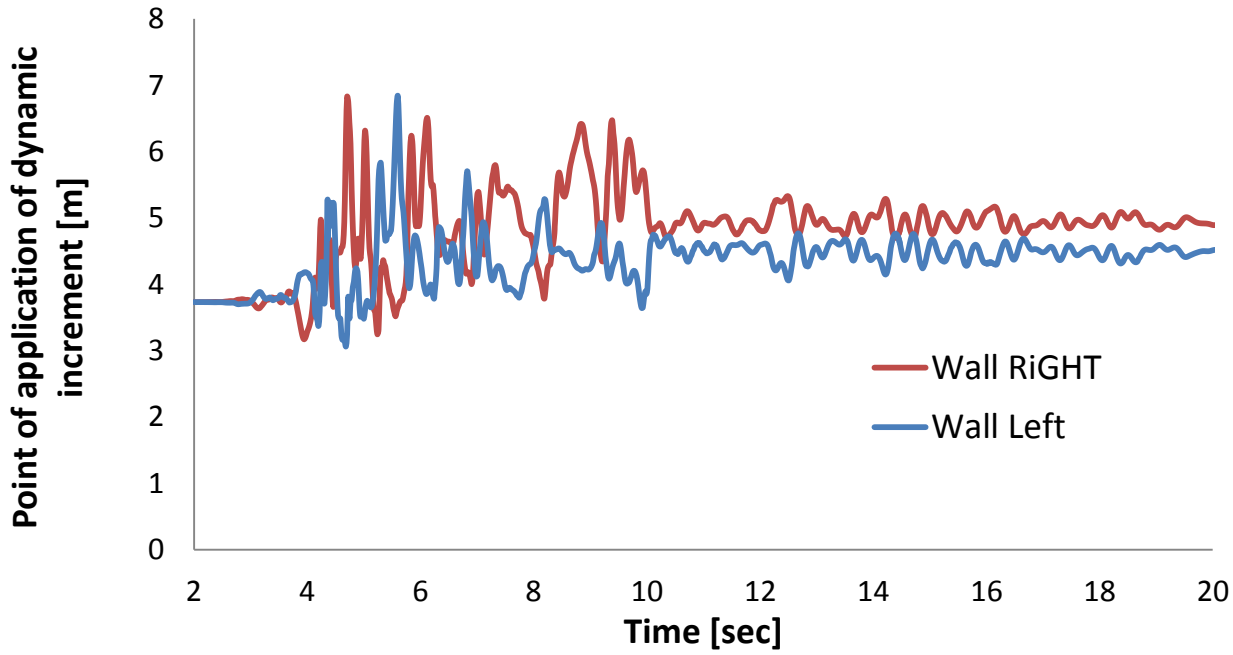

Fig. 3.105. Point of application of dynamic force on the left and right wall when subjected to Takatori Seismic excitation with peak ground acceleration 0.6g.

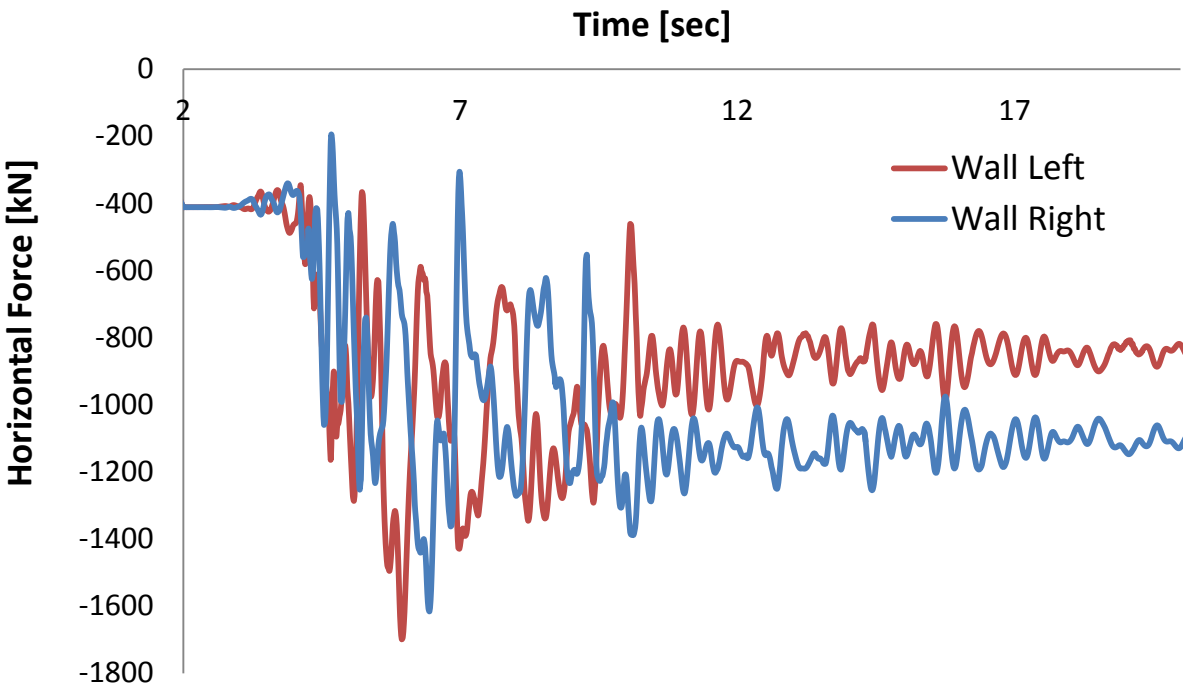

Fig. 3.106. Horizontal force-time history of the left and right wall when subjected to Takatori Seismic excitation with peak ground acceleration 0.9g.

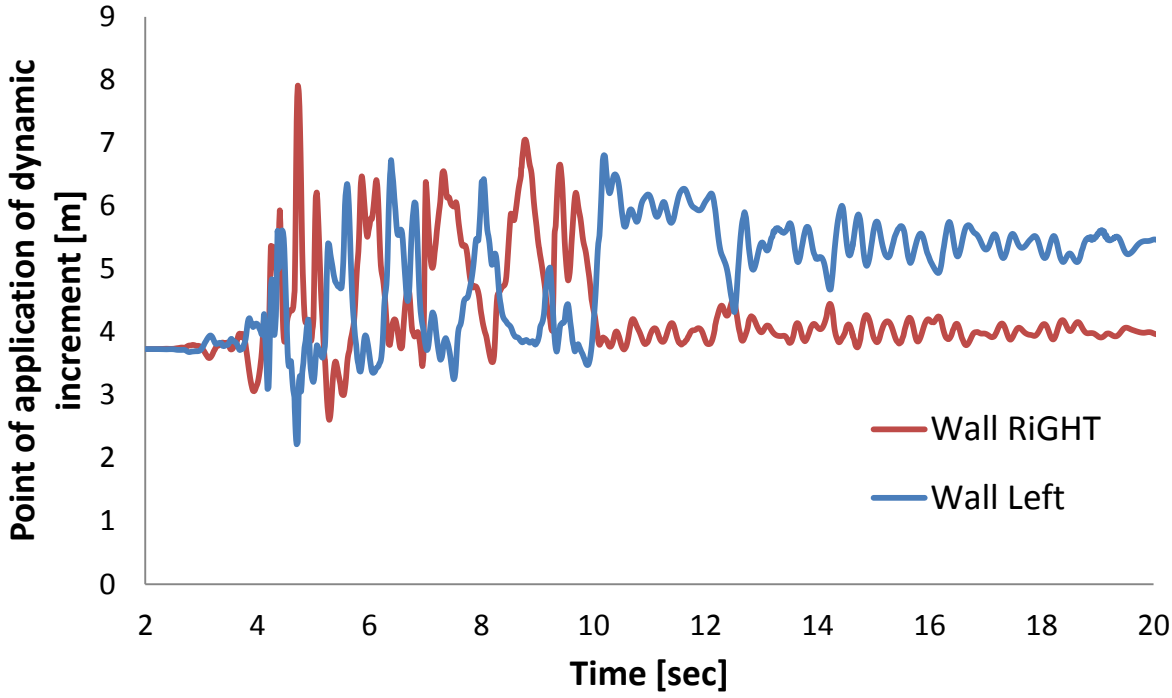

Fig. 3.107. Point of application of dynamic force on the left and right wall when subjected to Takatori Seismic excitation with peak ground acceleration 0.9g.

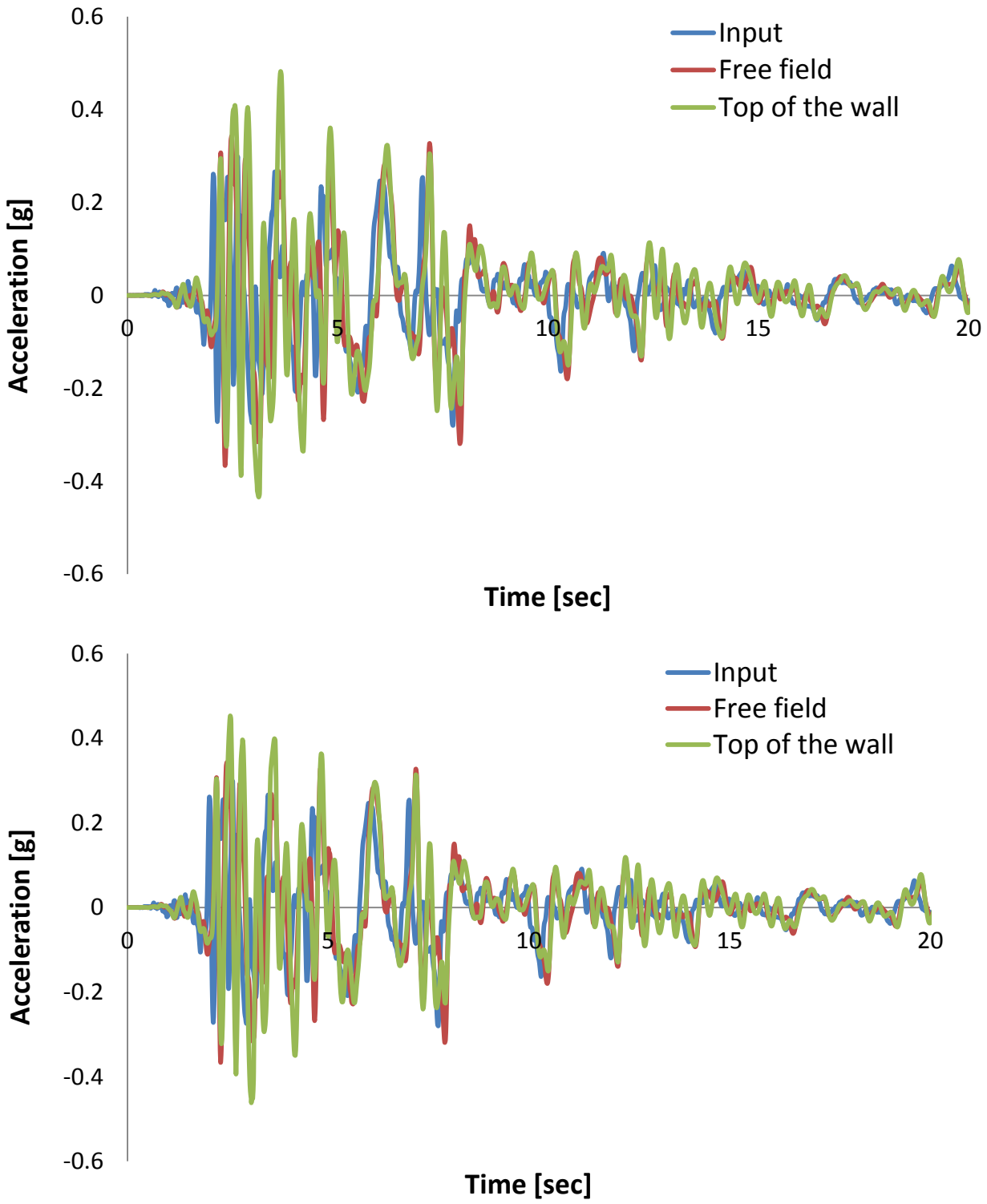

Fig. 3.108. Comparison of input acceleration and computed at the top of the a)left wall b)right wall and top of the free field when subjected to Takatori Seismic excitation with peak acceleration 0.3g.

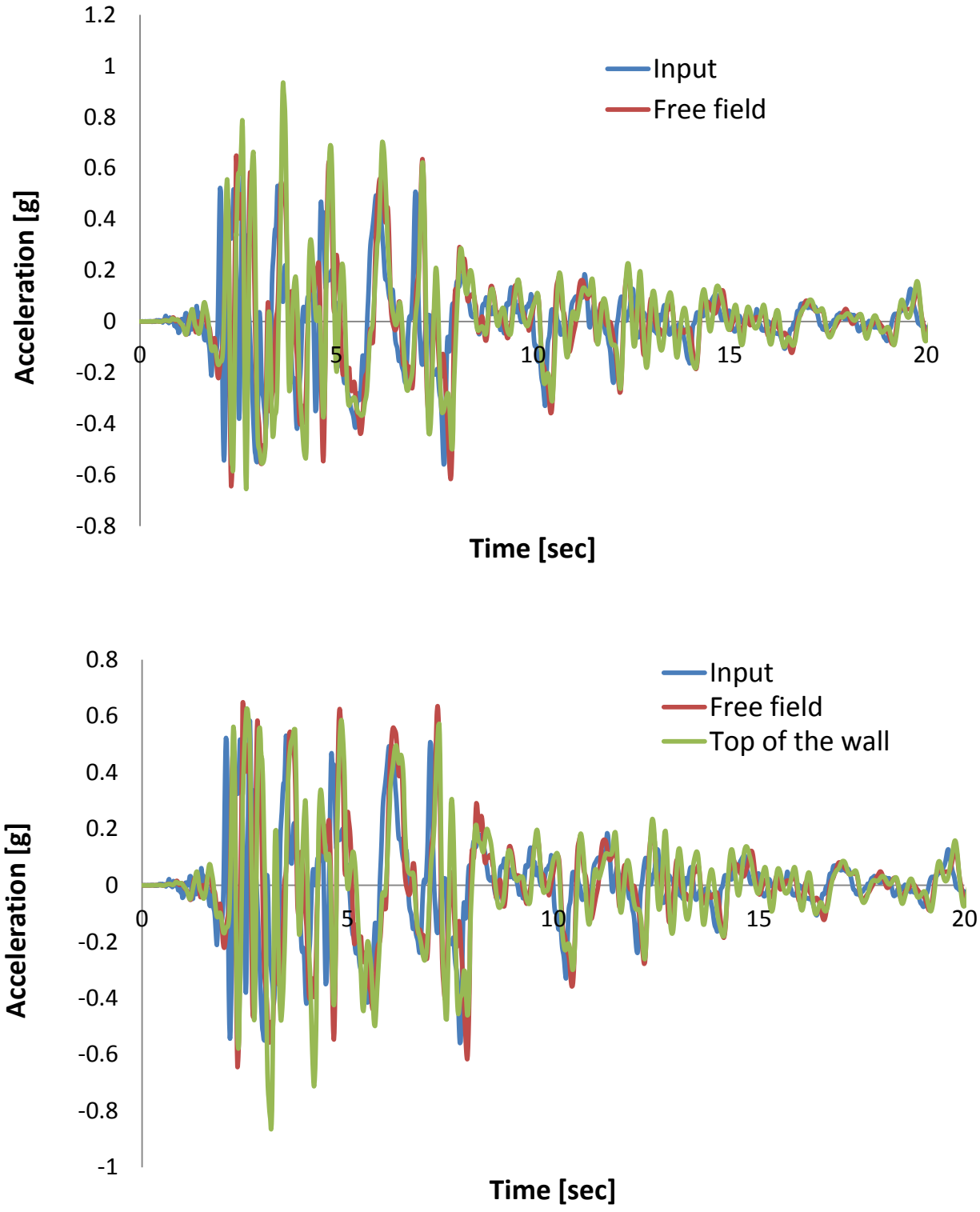

Fig. 3.109. Comparison of input acceleration and computed at the top of the a)left wall b)right wall and top of the free field when subjected to Takatori Seismic excitation with peak acceleration 0.6g.

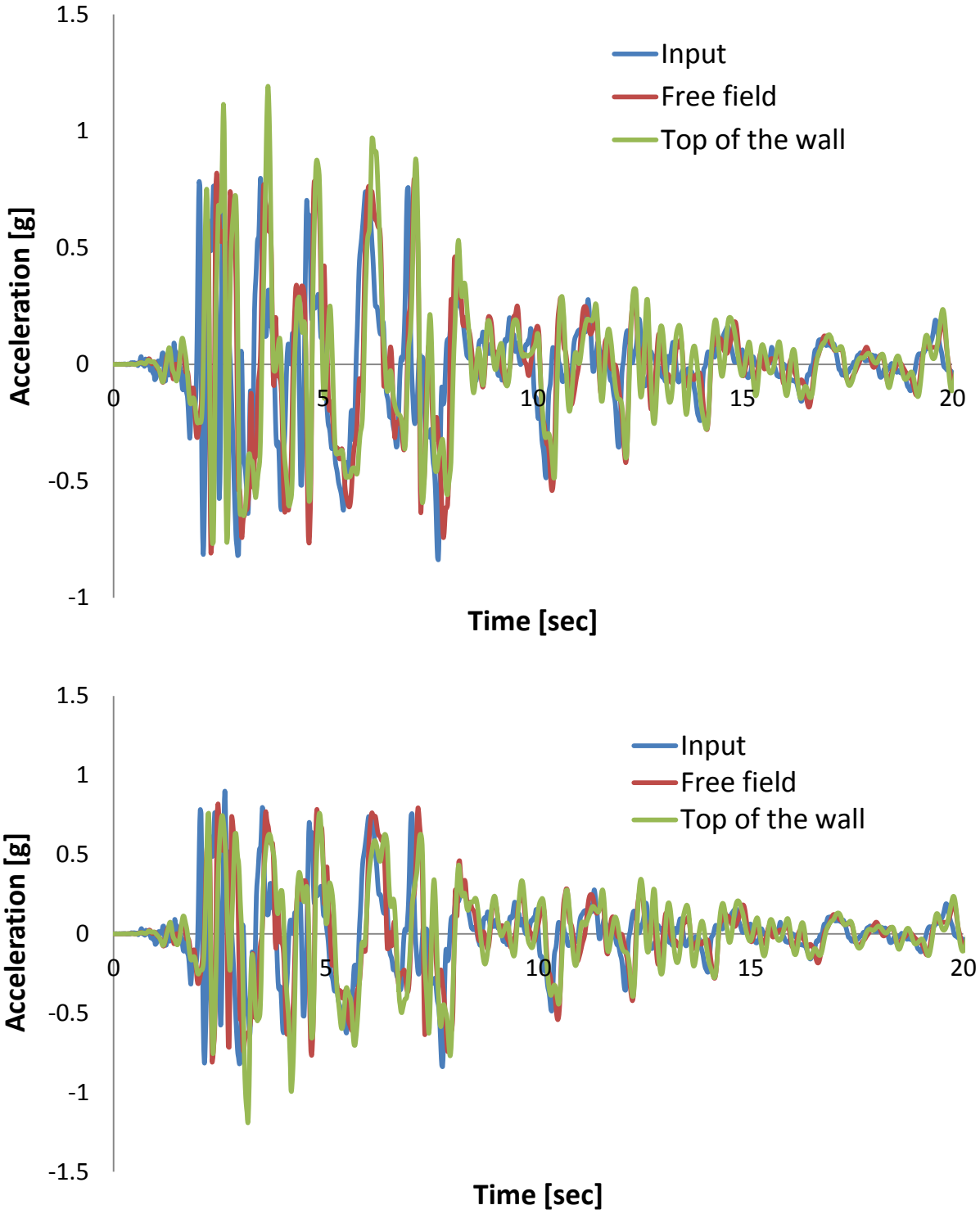

Fig. 3.110. Comparison of input acceleration and computed at the top of the a)left wall b)right wall and top of the free field when subjected to Takatori Seismic excitation with peak acceleration 0.9g.

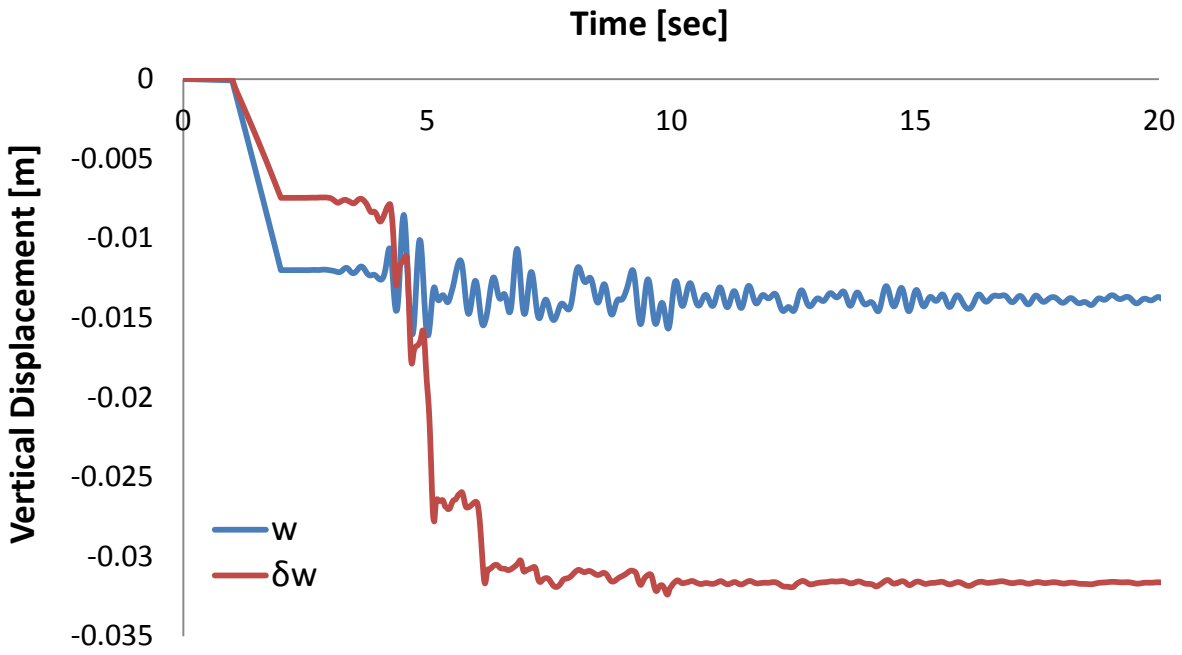

Fig. 3.111. Vertical displacement-time history of the left wall when subjected to TakatoriSeismic excitation with peak acceleration 0.3g.

.

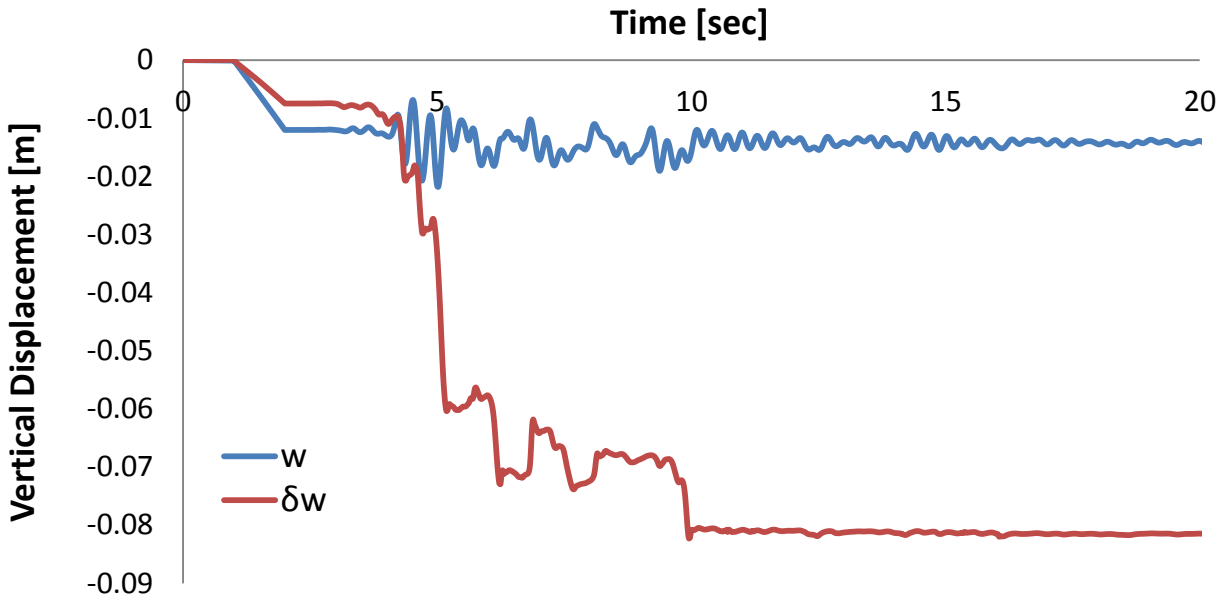

Fig. 3.112. Vertical displacement-time history of the left wall when subjected to TakatoriSeismic excitation with peak acceleration 0.6g.

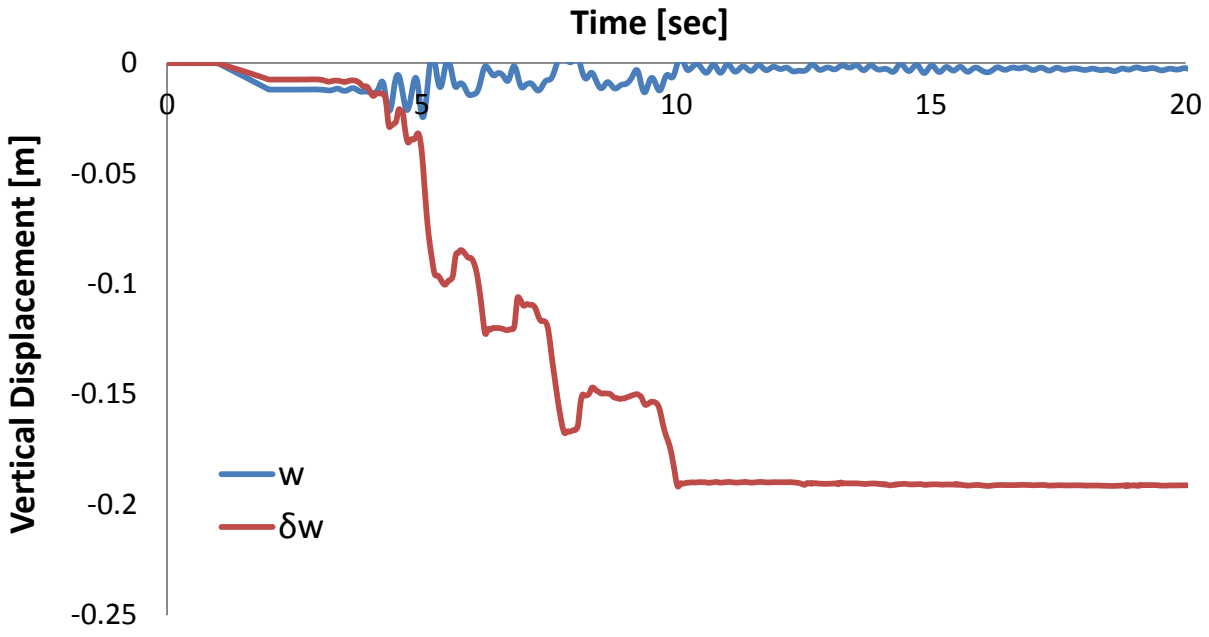

Fig. 3.113. Vertical displacement-time history of the left wall when subjected to TakatoriSeismic excitation with peak acceleration 0.6g.

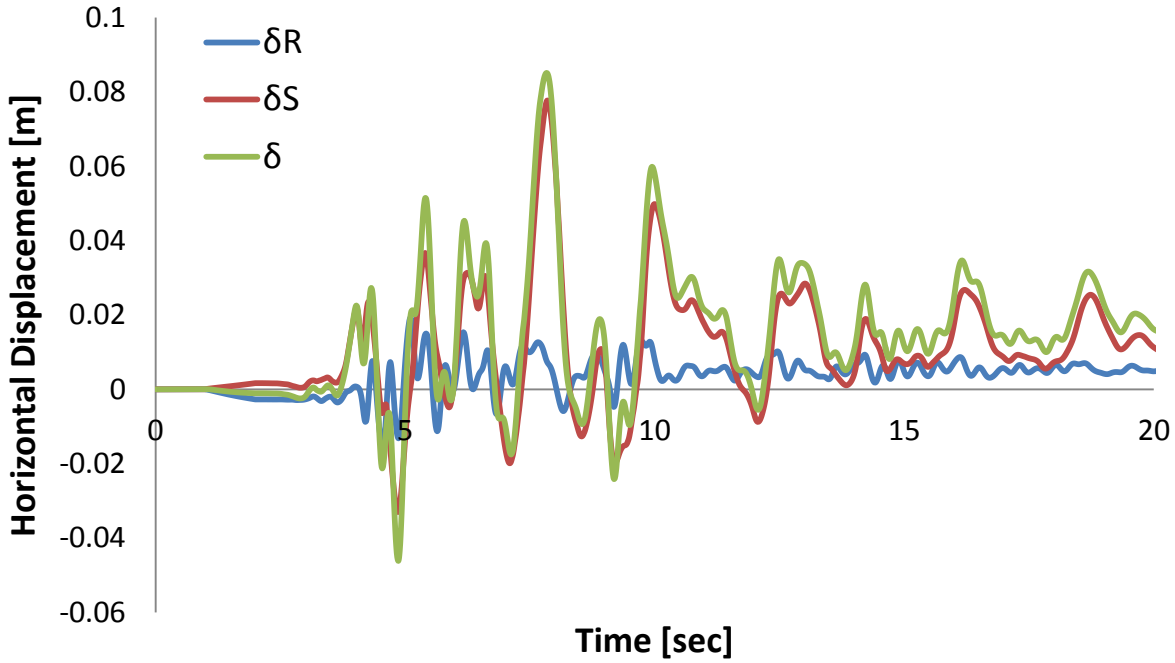

Fig. 3.114. Horizontal displacement-time history of the left wall when subjected to Takatori Seismic excitation with peak acceleration 0.3g.

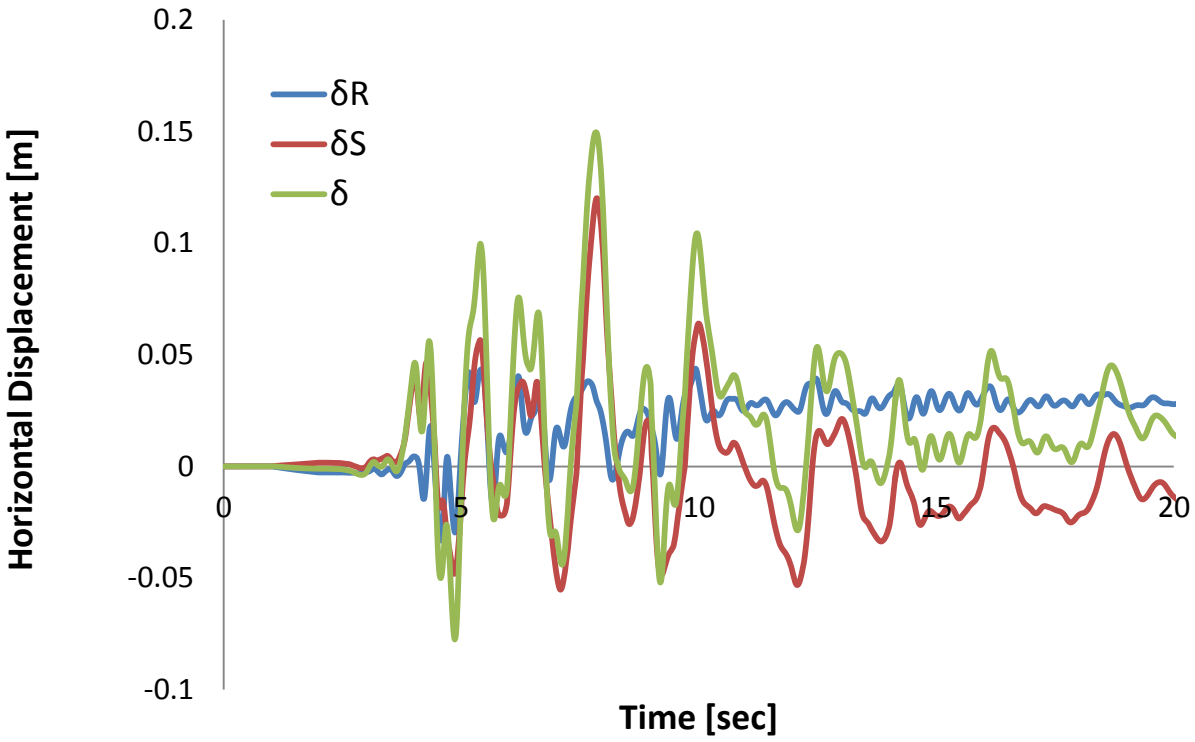

Fig. 3.115. Horizontal displacement-time history of the left wall when subjected to Takatori Seismic excitation with peak acceleration 0.6g.

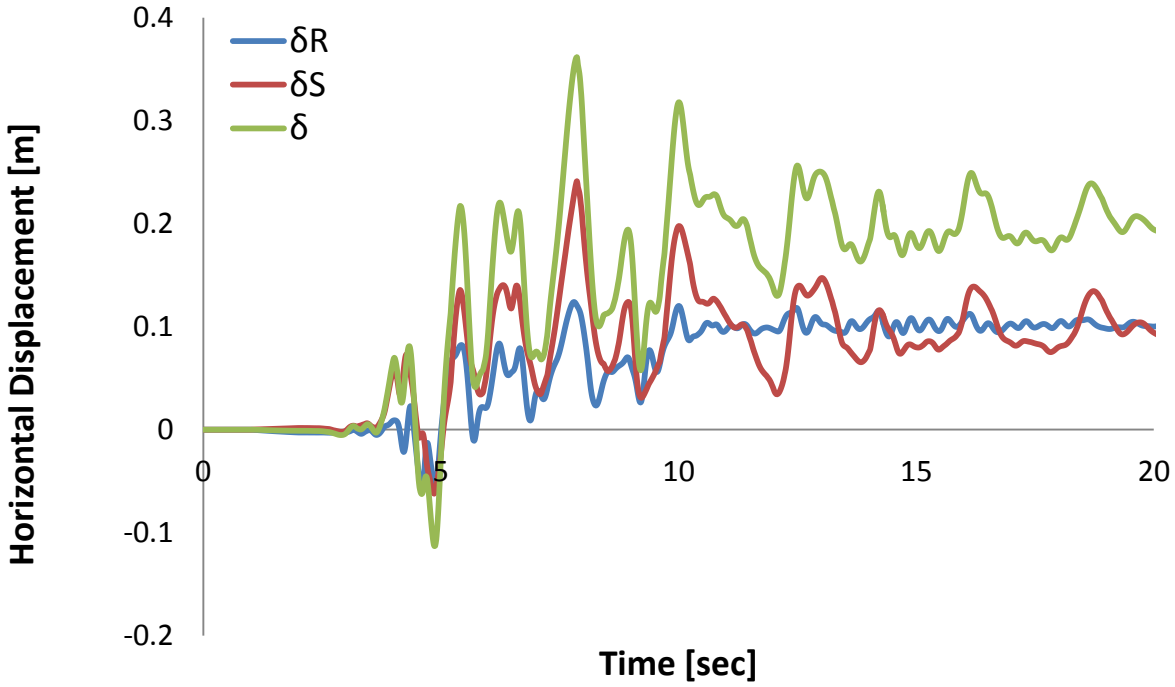

Fig. 3.116. Horizontal displacement-time history of the left wall when subjected to Takatori Seismic excitation with peak acceleration 0.9g.

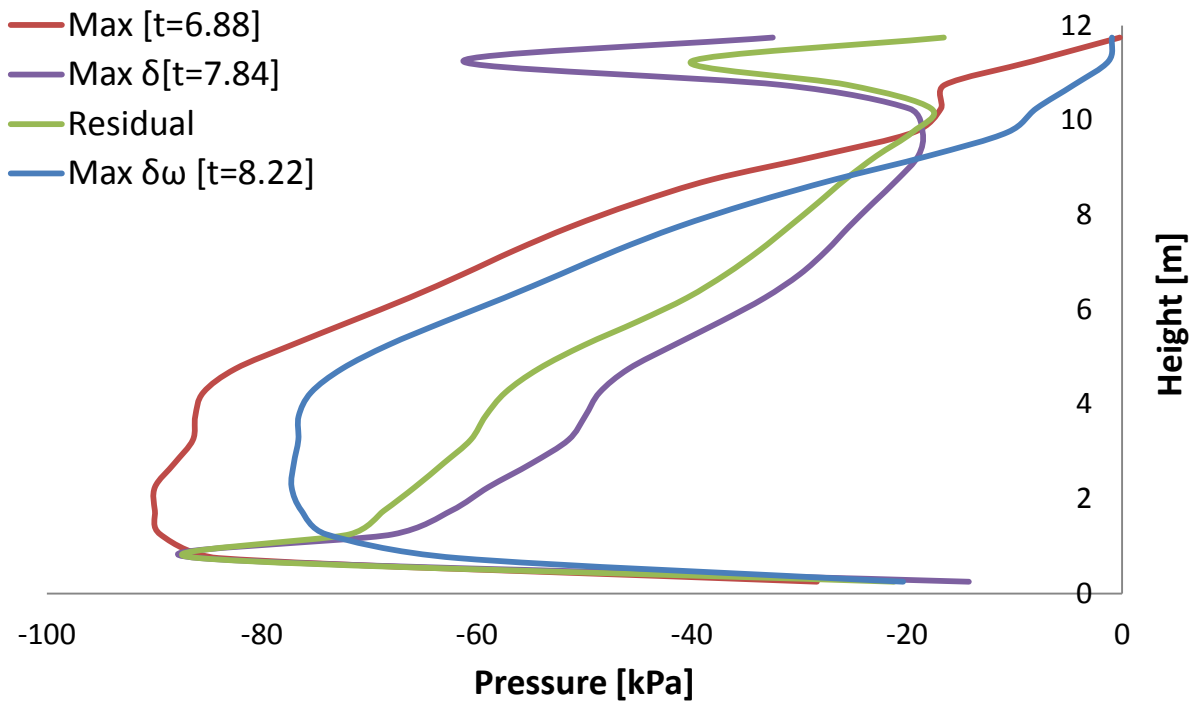

Fig. 3.117. Earth pressures profiles on the right wall at different moments when subjected to Takatori Seismic excitation with peak ground acceleration 0.3g.

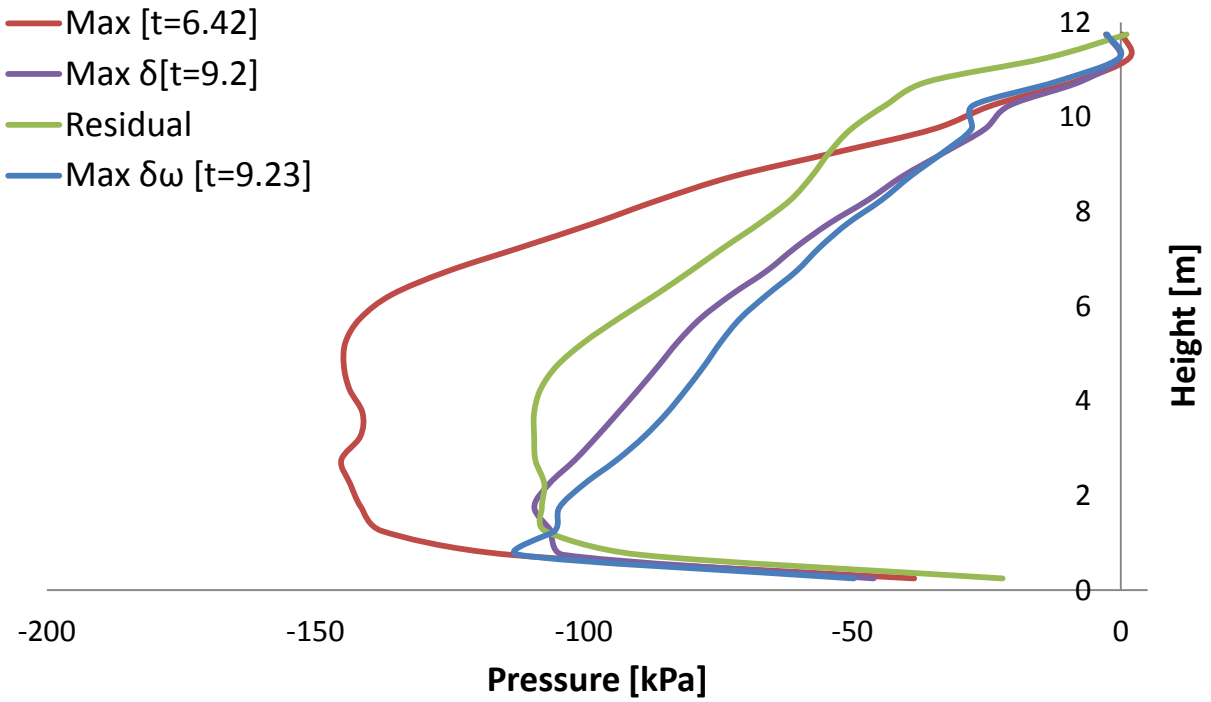

Fig. 3.118. Earth pressures profiles on the right wall at different moments when subjected to Takatori Seismic excitation with peak ground acceleration 0.6g.

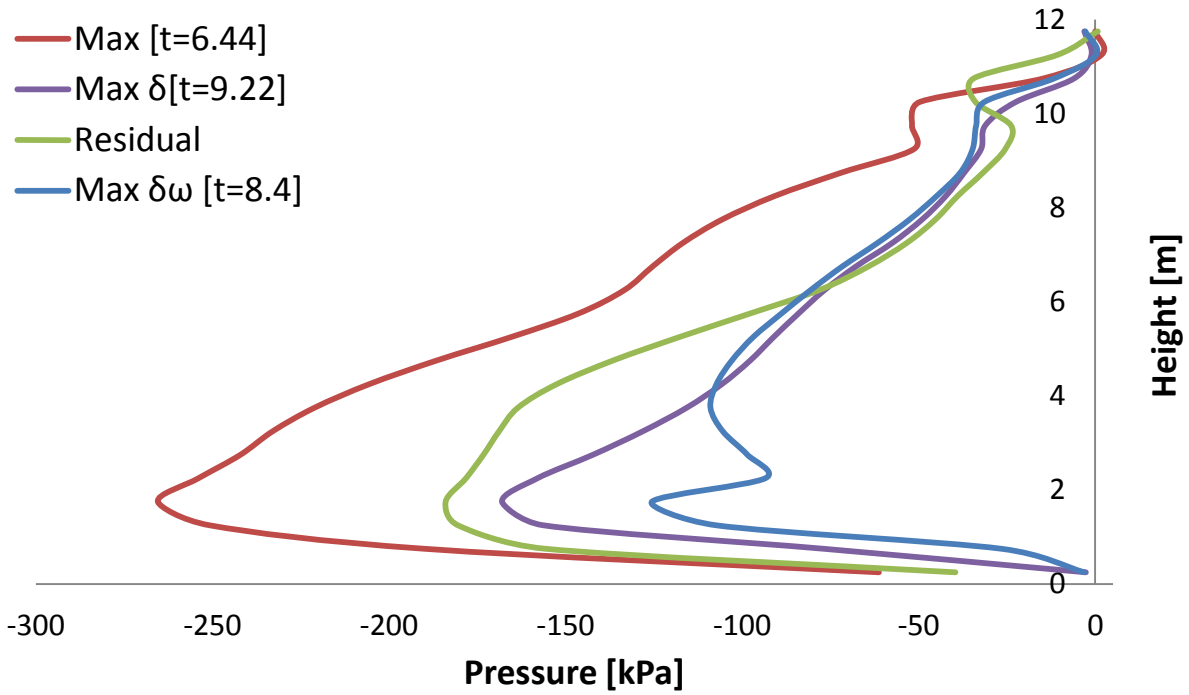

Fig. 3.119. Earth pressures profiles on the right wall at different moments when subjected to Takatori Seismic excitation with peak ground acceleration 0.9g.

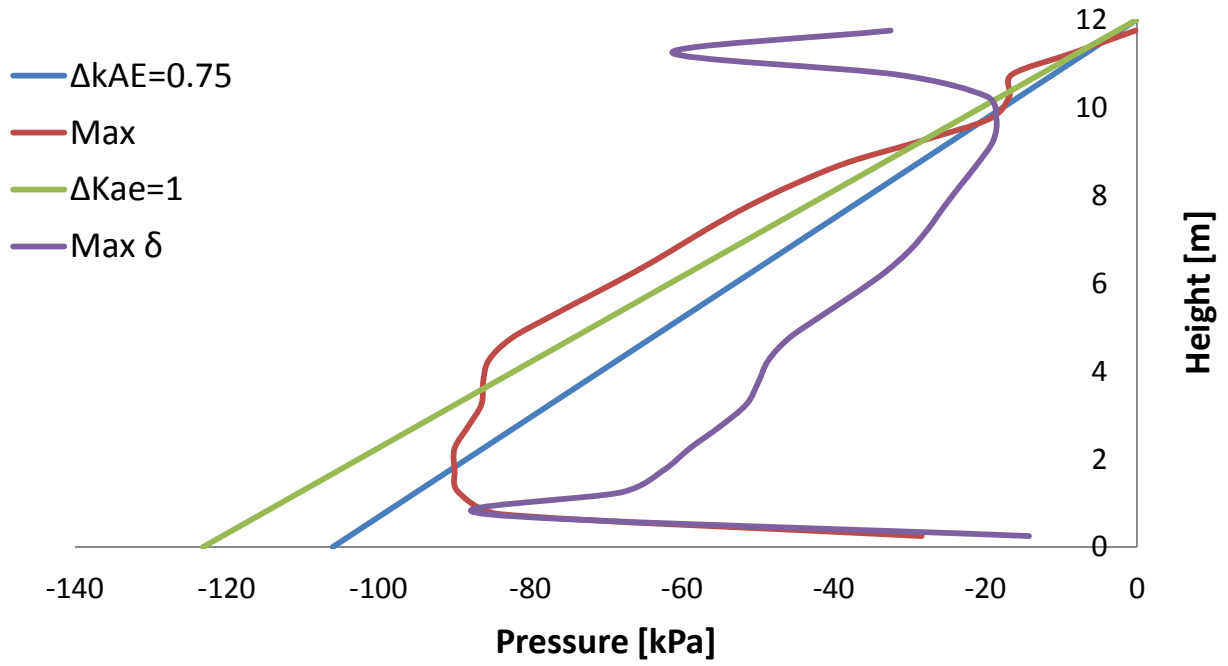

Fig. 3.120. Earth pressure profiles computed in ABAQUS and estimated using the M-O when the right wall is subjected to the Takatori Seismic excitation with peak acceleration 0.3g.

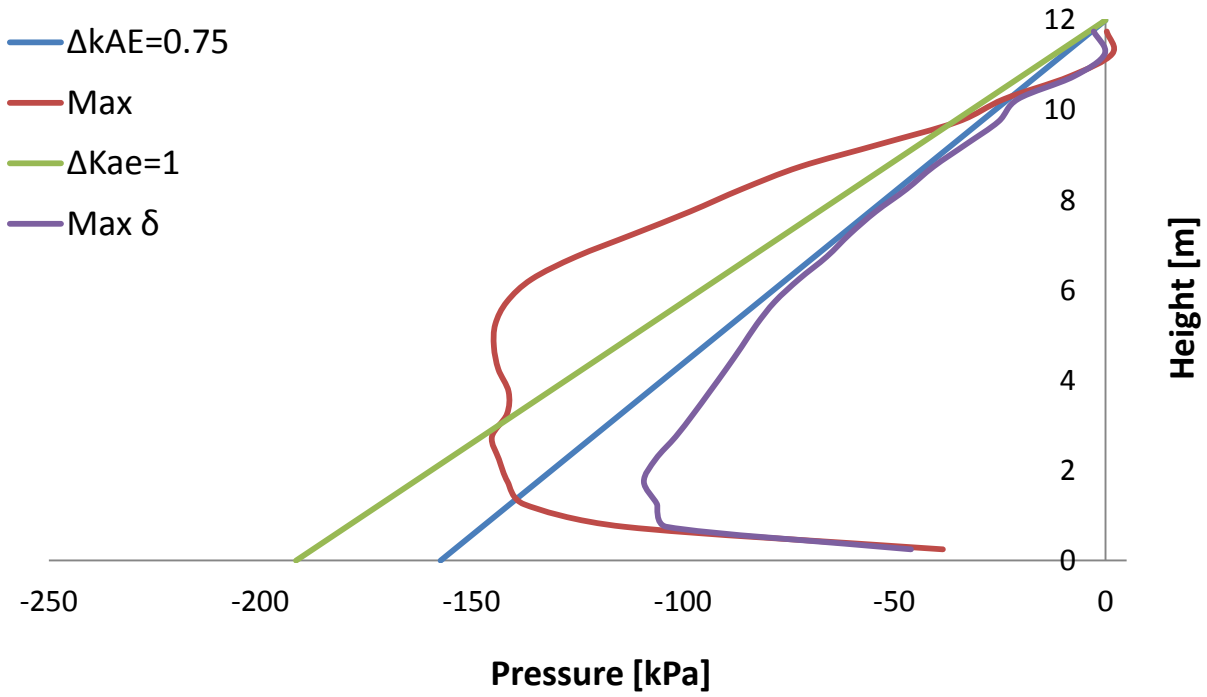

Fig. 3.121. Earth pressure profiles computed in ABAQUS and estimated using the M-O when the right wall is subjected to the Takatori Seismic excitation with peak acceleration 0.6g.

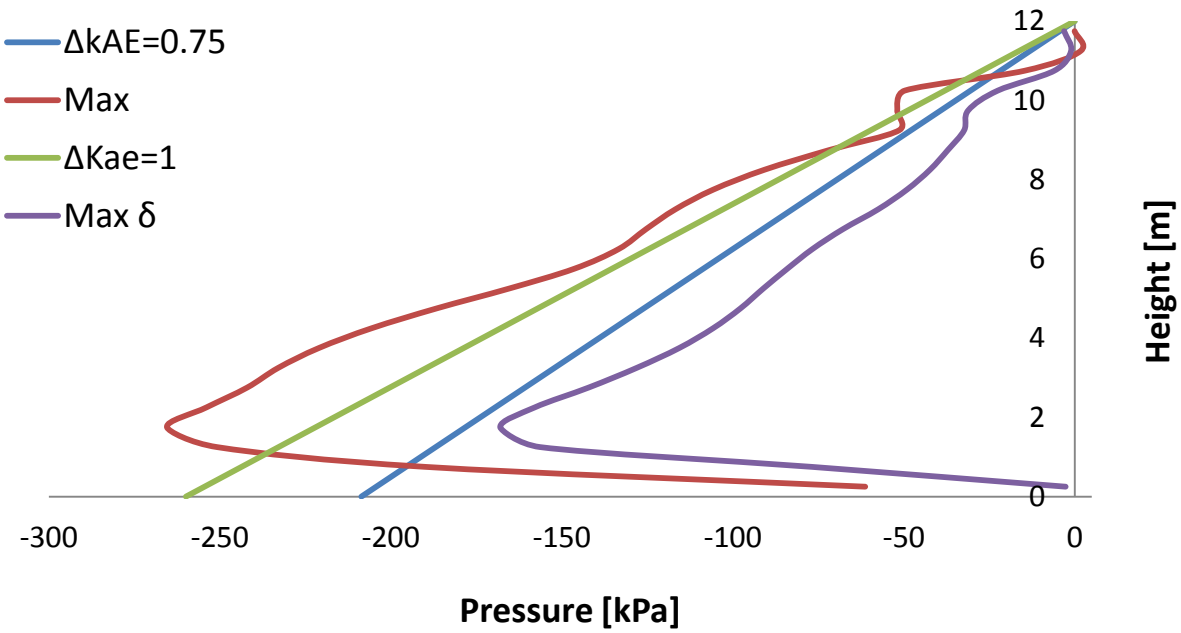

Fig. 3.122. Earth pressure profiles computed in ABAQUS and estimated using the M-O when the right wall is subjected to the Takatori Seismic excitation with peak acceleration 0.9g.

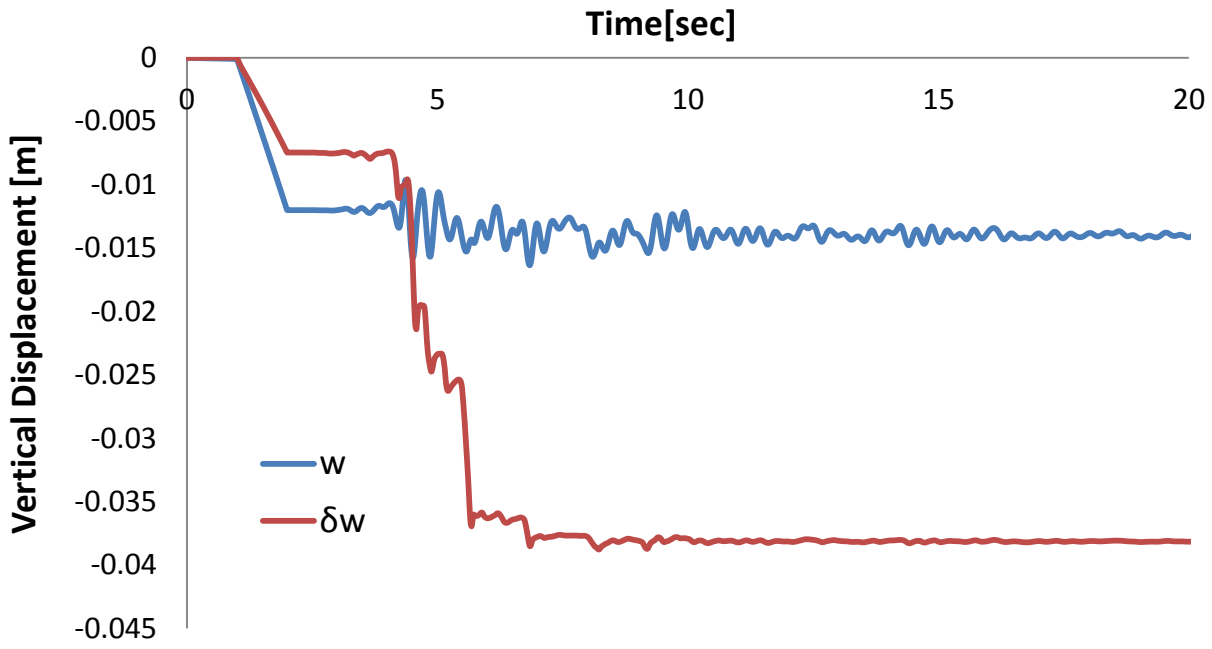

Fig. 3.123. Vertical displacement-time history of the right wall when subjected to Takatori Seismic excitation with peak acceleration 0.3g.

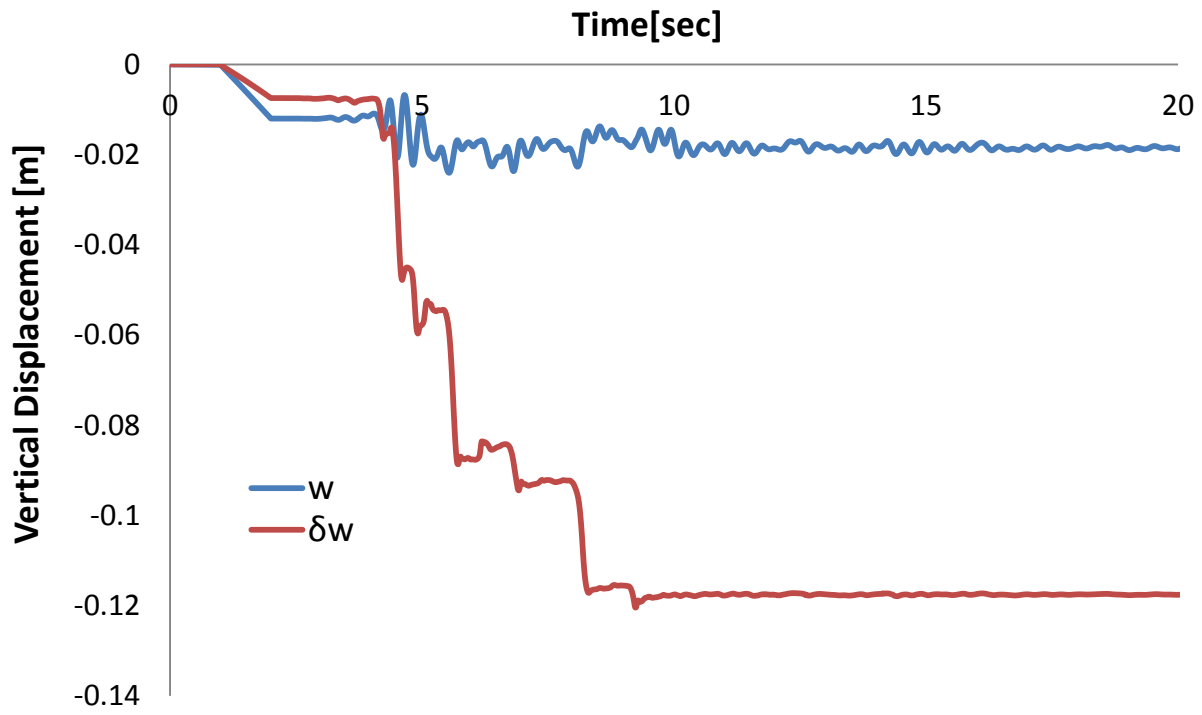

Fig. 3.124. Vertical displacement-time history of the right wall when subjected to Takatori Seismic excitation with peak acceleration 0.6g.

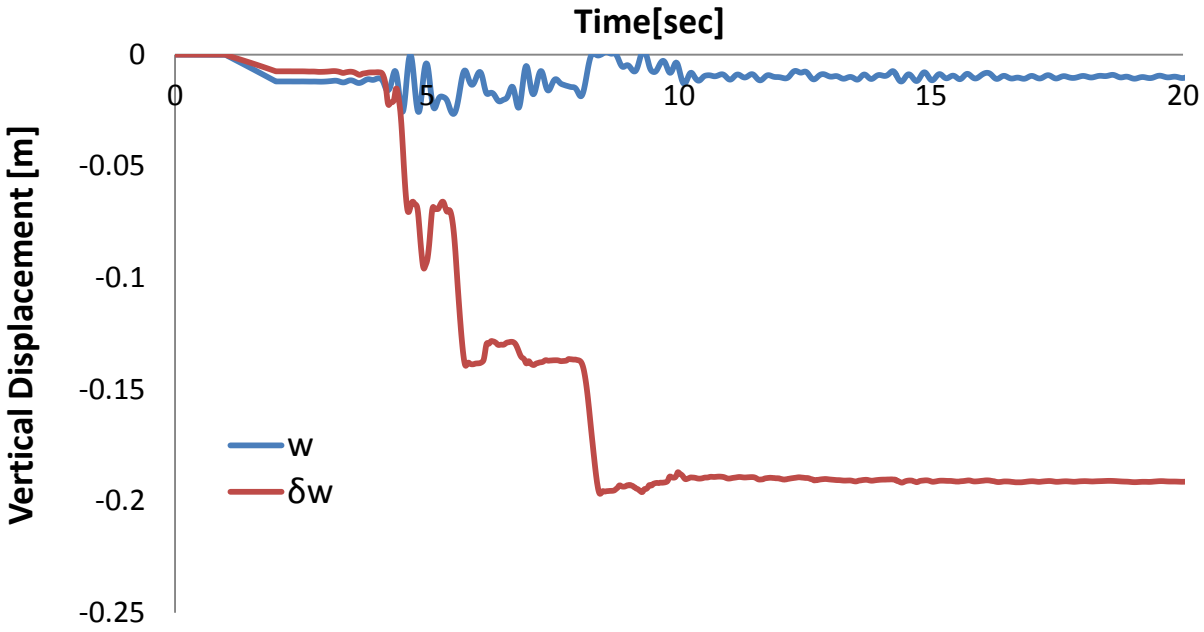

Fig. 3.125. Vertical displacement-time history of the right wall when subjected to Takatori Seismic excitation with peak acceleration 0.9g.

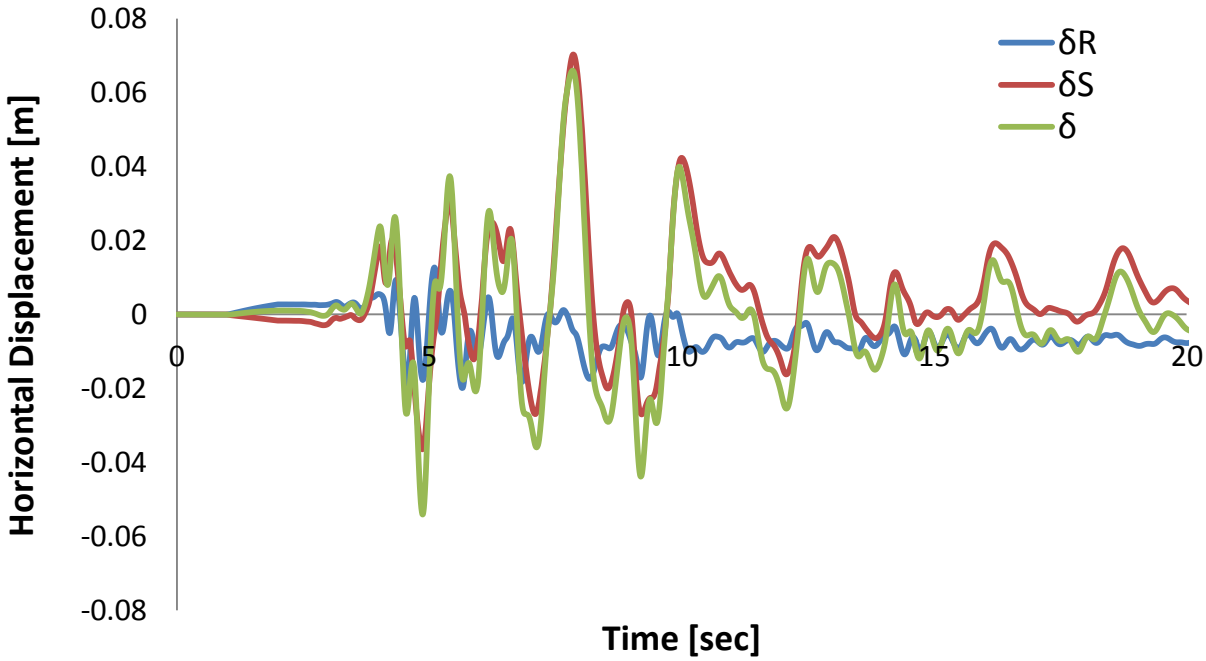

Fig. 3.126. Horizontal displacement-time history of the right wall when subjected to Takatori Seismic excitation with peak acceleration 0.3g.

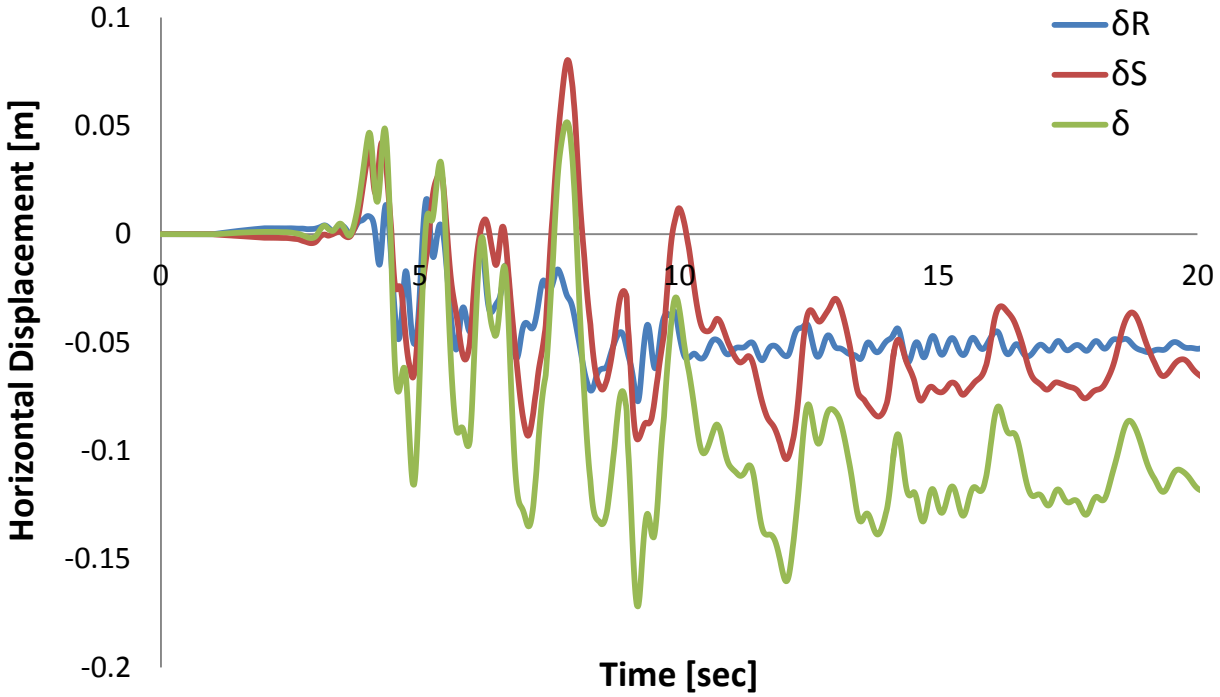

Fig. 3.127. Horizontal displacement-time history of the right wall when subjected to Takatori Seismic excitation with peak acceleration 0.6g.

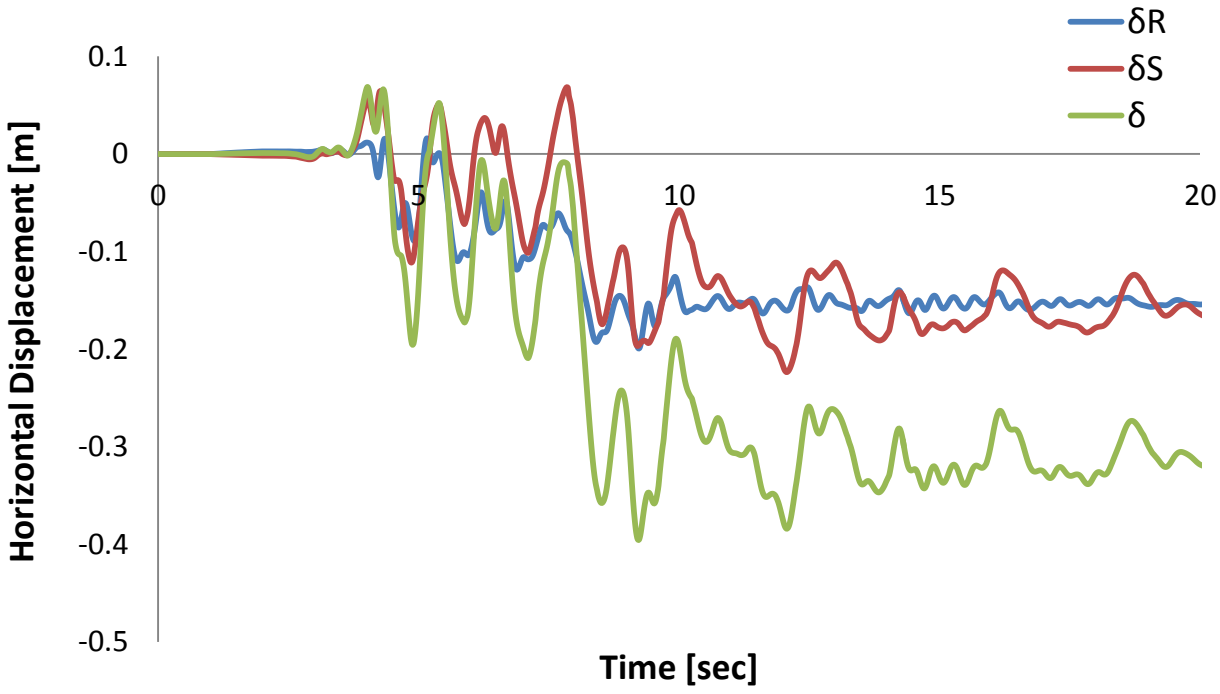

Fig. 3.128. Horizontal displacement-time history of the right wall when subjected to Takatori Seismic excitation with peak acceleration 0.9g.

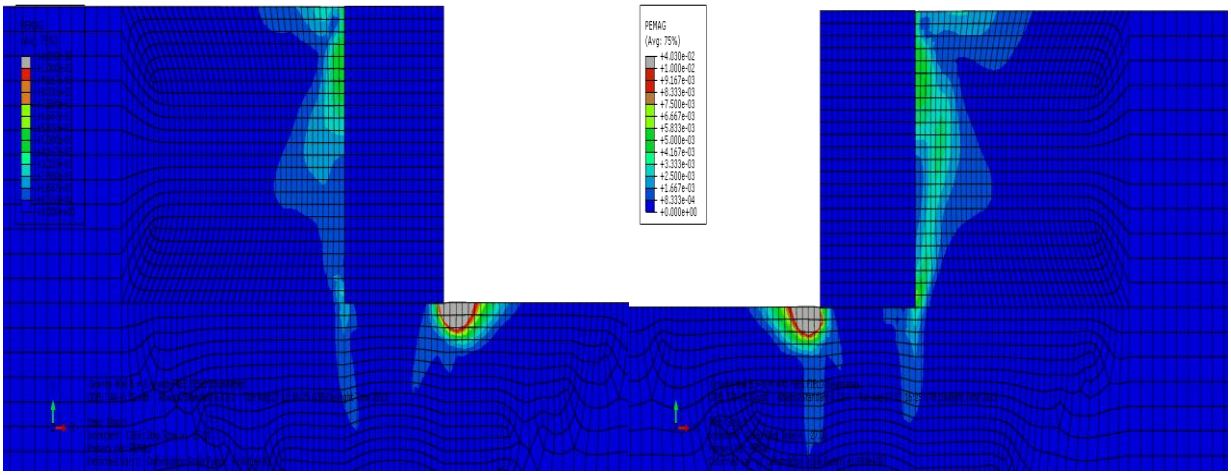

Fig. 3.129. Plastic strain contours at the end of seismic shaking (a)Left wall (b)Right wall when subjected to Takatori seismic excitation with peak acceleration 0.3g

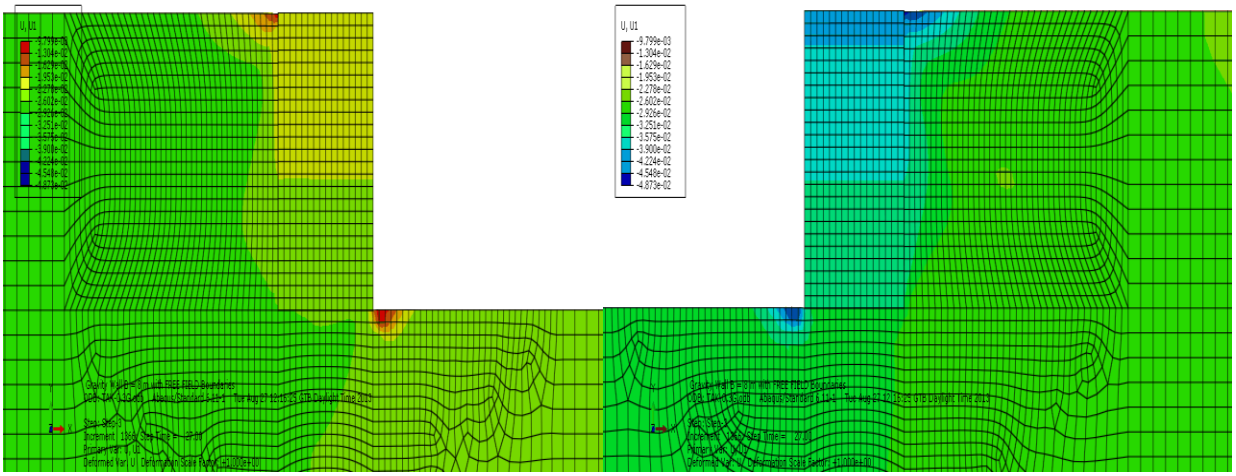

Fig. 3.130. Horizontal displacement contours at the end of the seismic excitation Takatori PGA 0.3g.

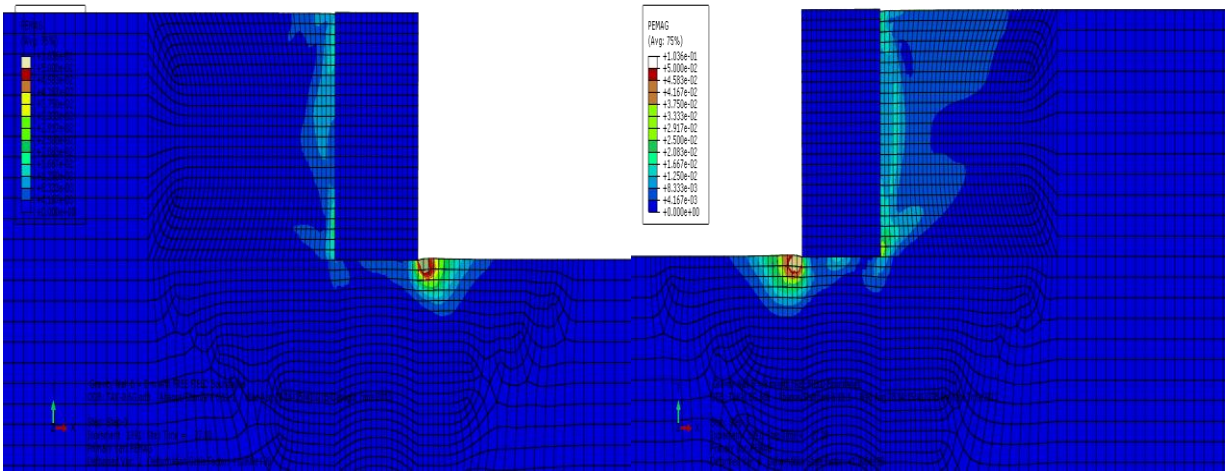

Fig. 3.131. Plastic strain contours at the end of seismic shaking (a)Left wall (b)Right wall when subjected to Takatori seismic excitation with peak acceleration 0.6g

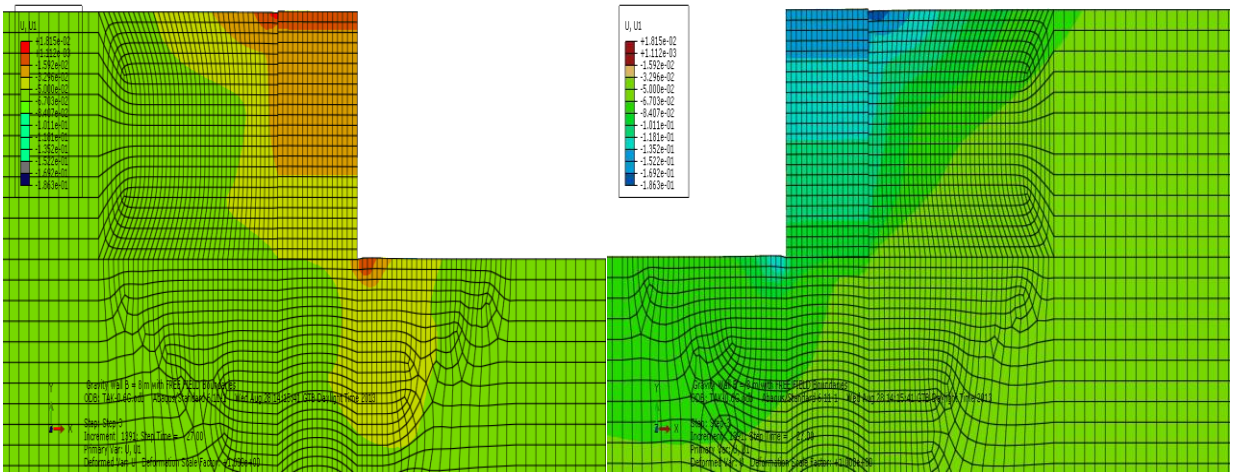

Fig. 3.132. Horizontal displacement contours at the end of the seismic excitation Takatori PGA 0.6g.

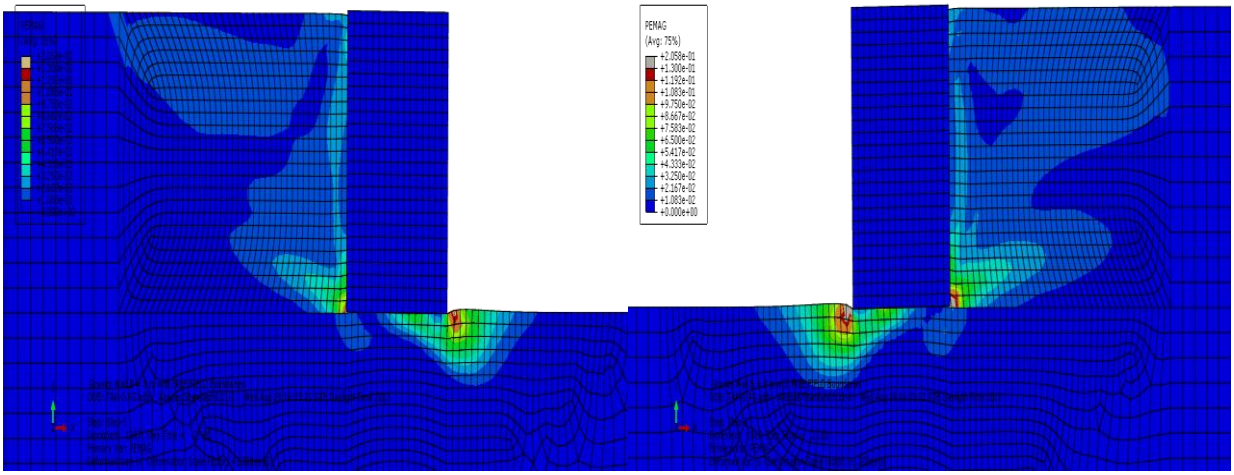

Fig. 3.133. Plastic strain contours at the end of seismic shaking (a)Left wall (b)Right wall when subjected to Takatori seismic excitation with peak acceleration 0.9g

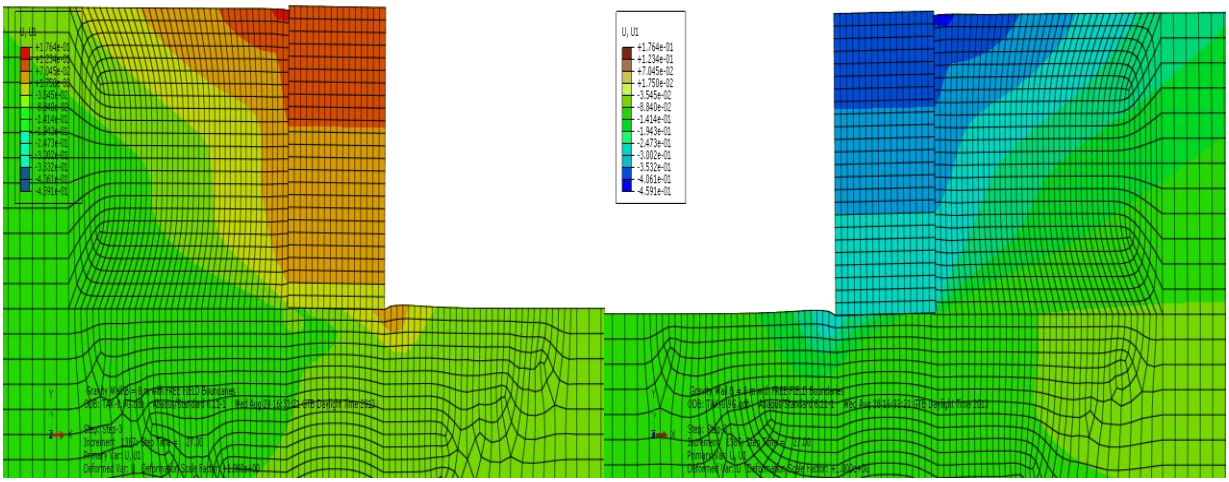

Fig. 3.134. Horizontal displacement contours at the end of the seismic excitation Takatori PGA 0.9g.

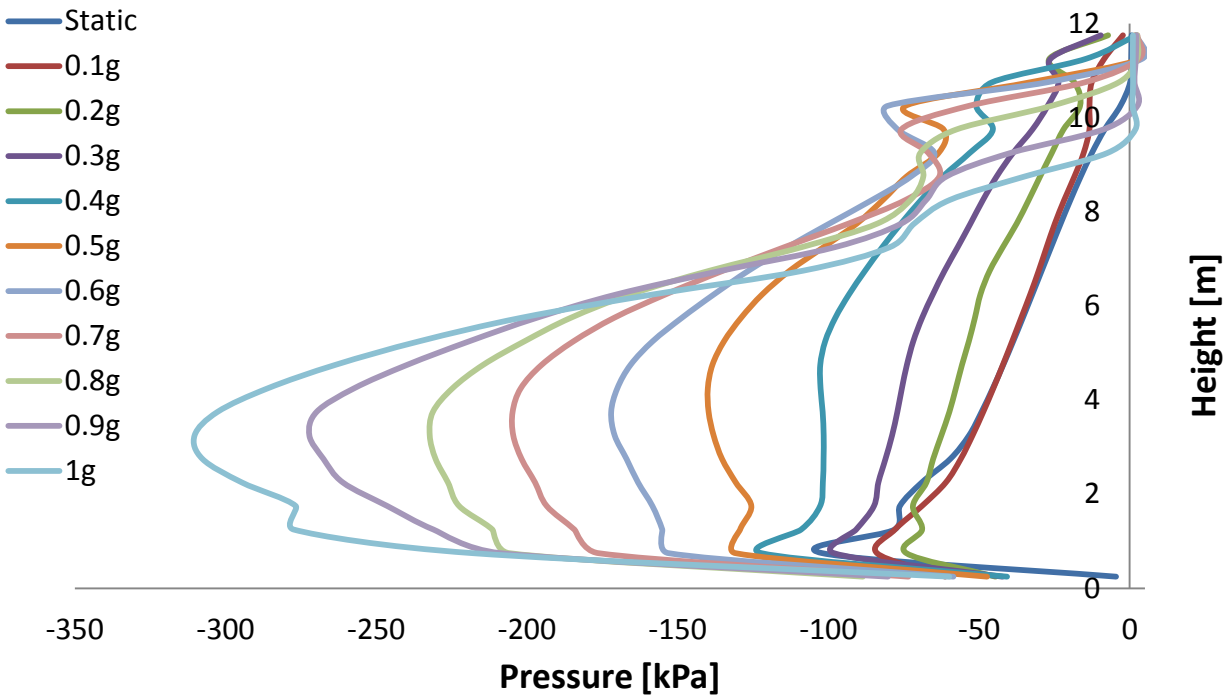

Fig. 3.135. Static and maximum earth pressure profiles for different peak accelerations on the left wall when subjected to Takatori Seismic excitation.

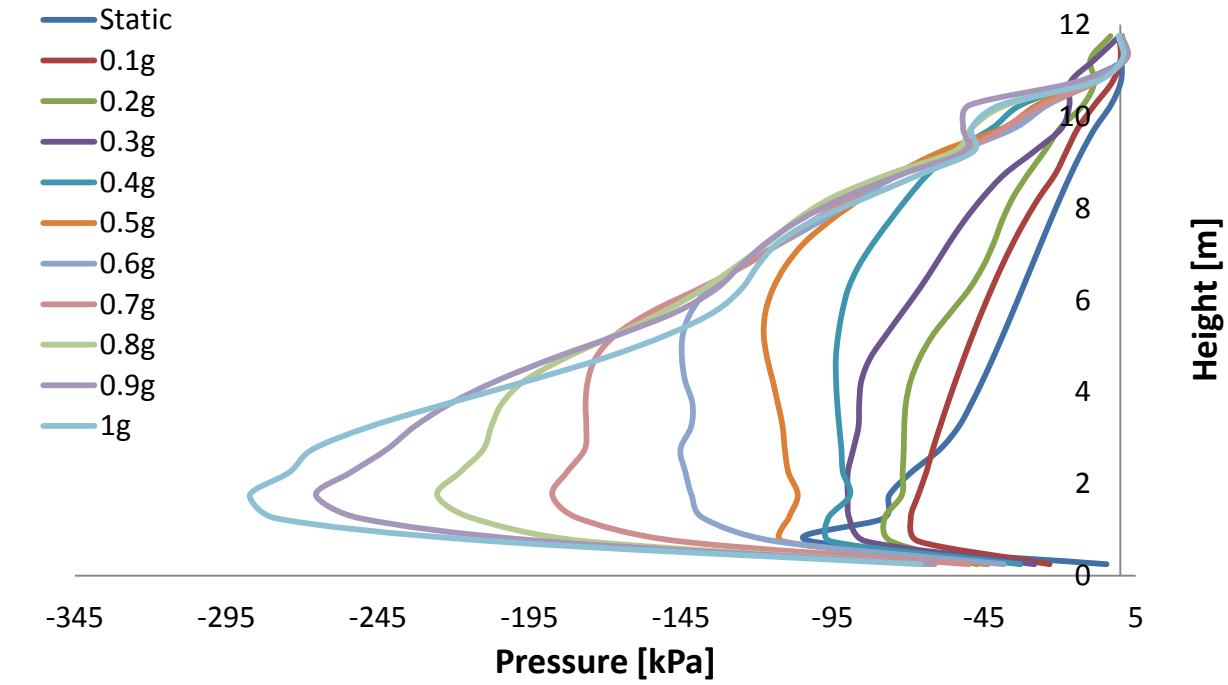

Fig. 3.136. Static and maximum earth pressure profiles for different peak accelerations on the right wall when subjected to Takatori Seismic excitation.

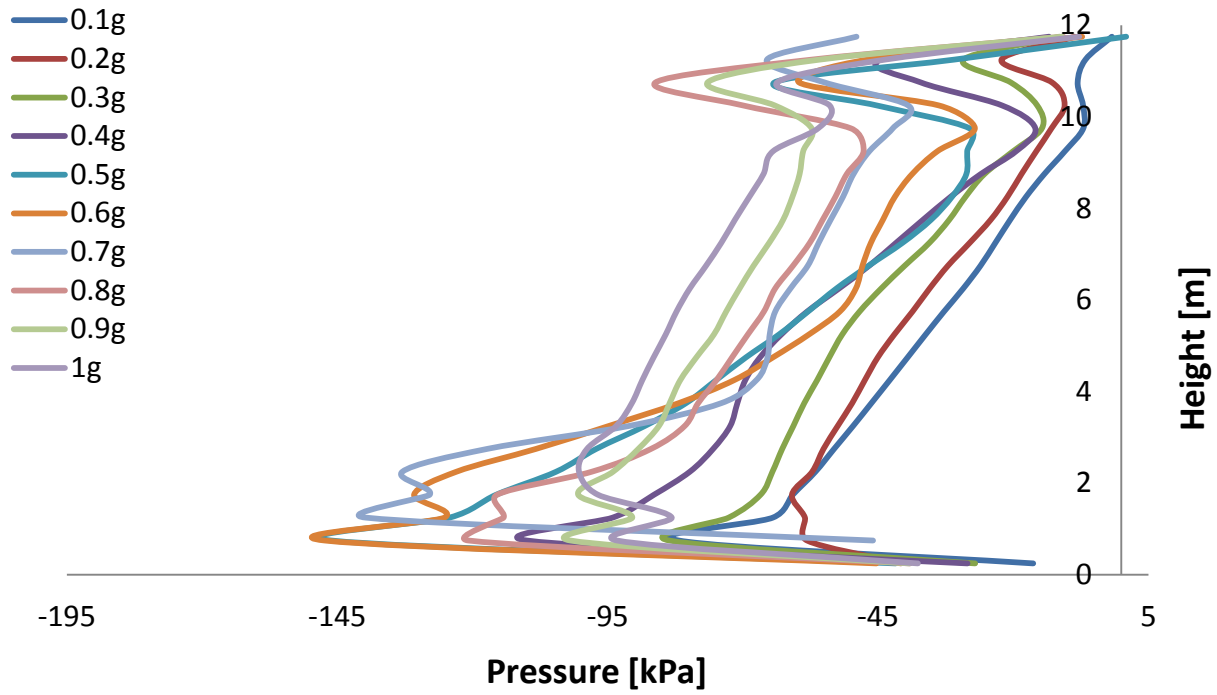

Fig. 3.137. Residual earth pressure profiles for different peak accelerations on the left wall when subjected to Takatori Seismic excitation.

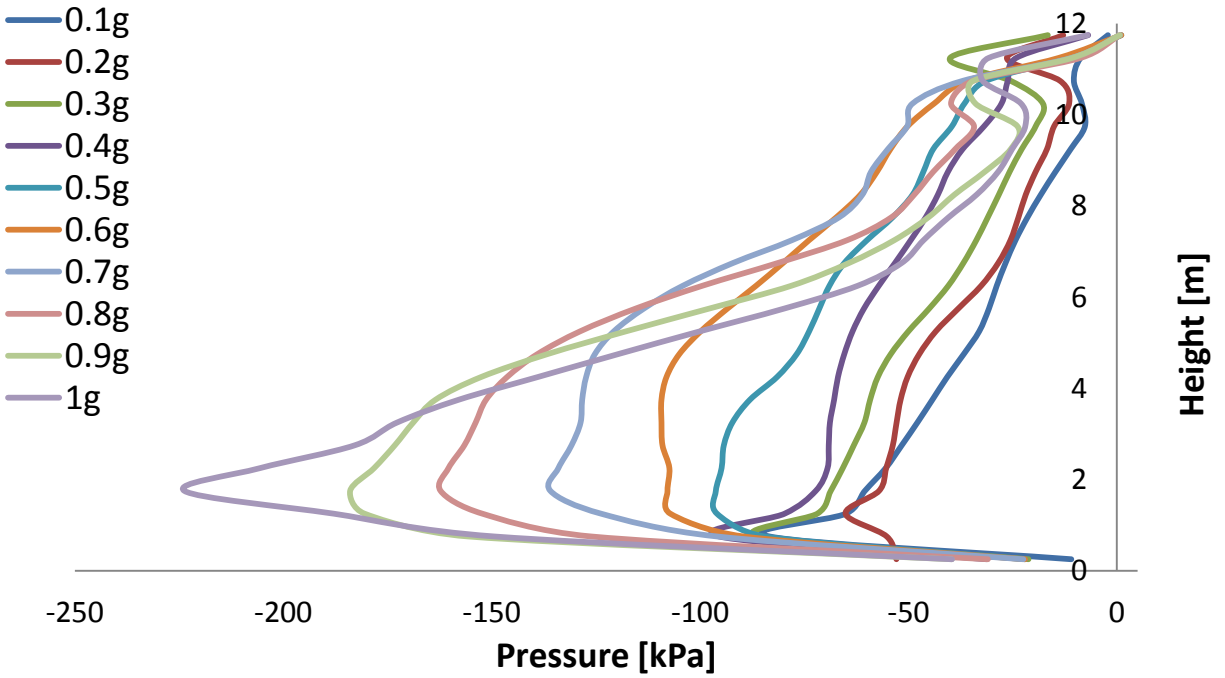

Fig. 3.138. Residual earth pressure profiles for different peak accelerations on the right wall when subjected to Takatori Seismic excitation.

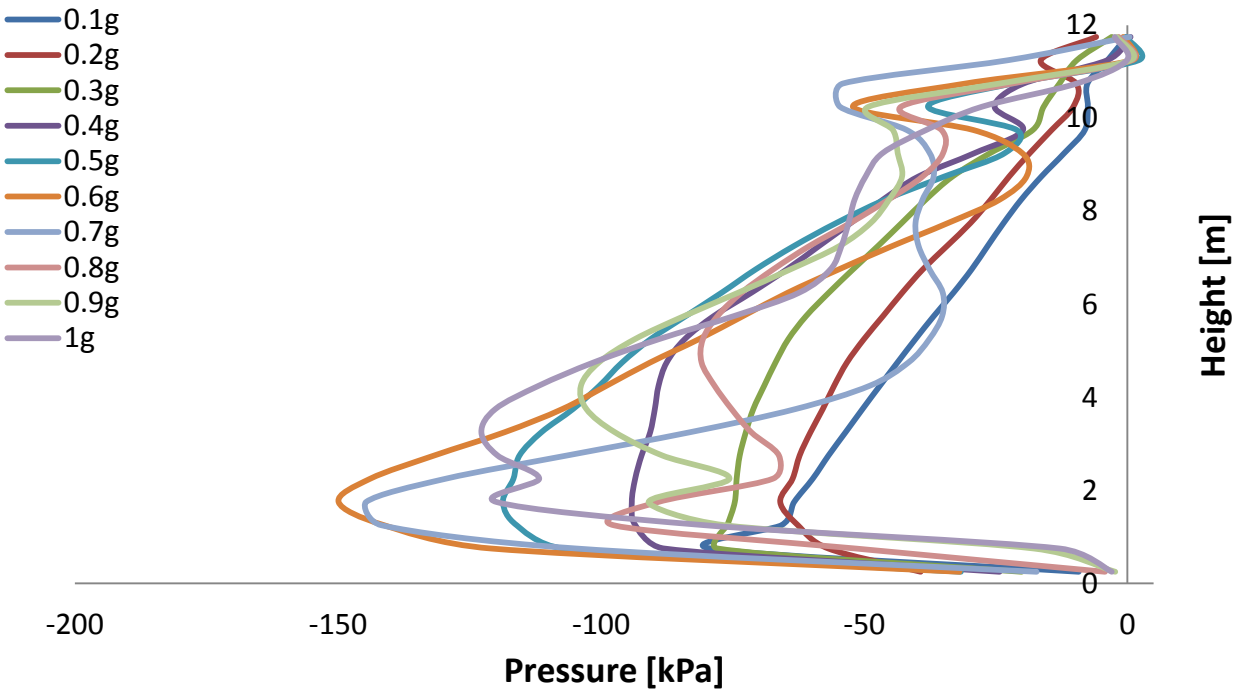

Fig. 3.139. Earth pressure profiles at maximum displacement for different peak accelerations on the left wall when subjected to Takatori Seismic excitation.

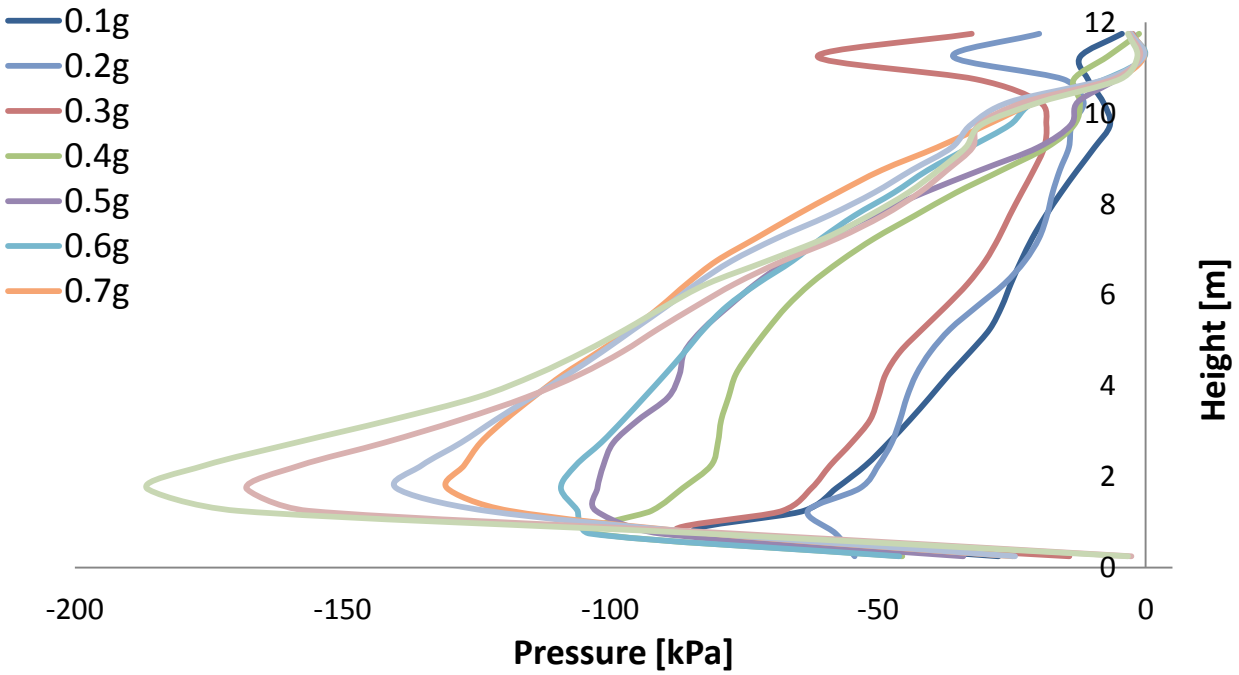

Fig. 3.140. Earth pressure profiles at maximum displacement for different peak accelerations on the right wall when subjected to Takatori Seismic excitation.

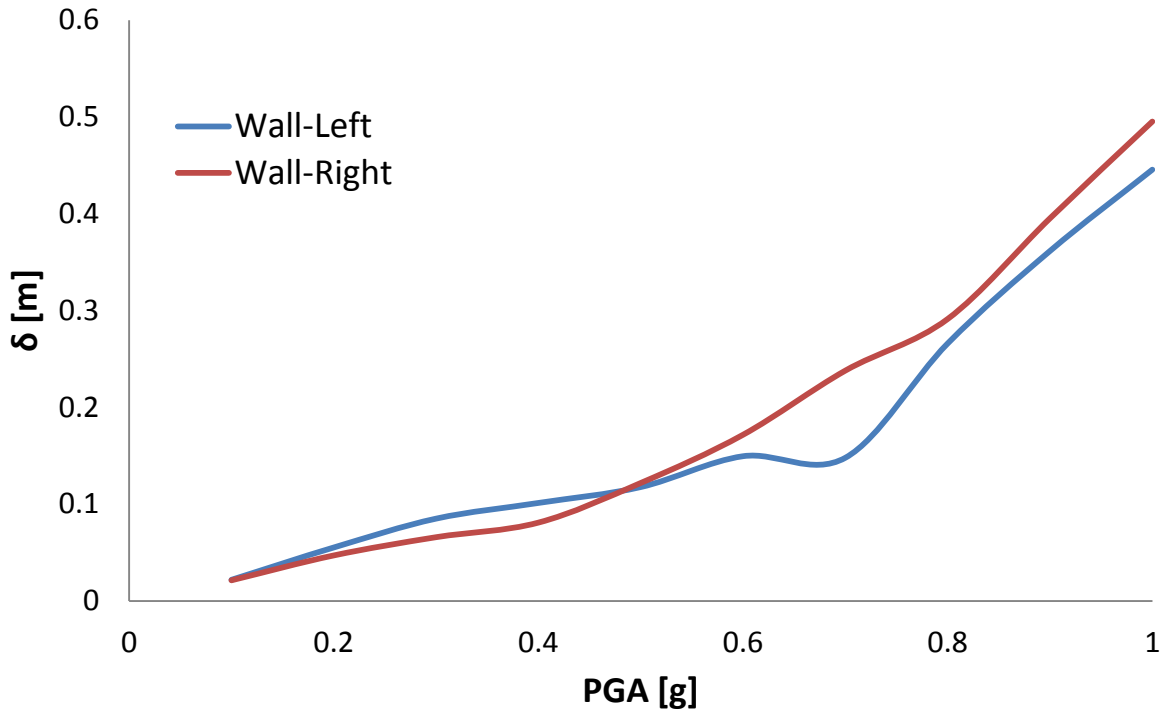

Fig. 3.141. Horizontal displacement as a function of PGA for the left and right wall when subjected to Takatori Seismic excitation.

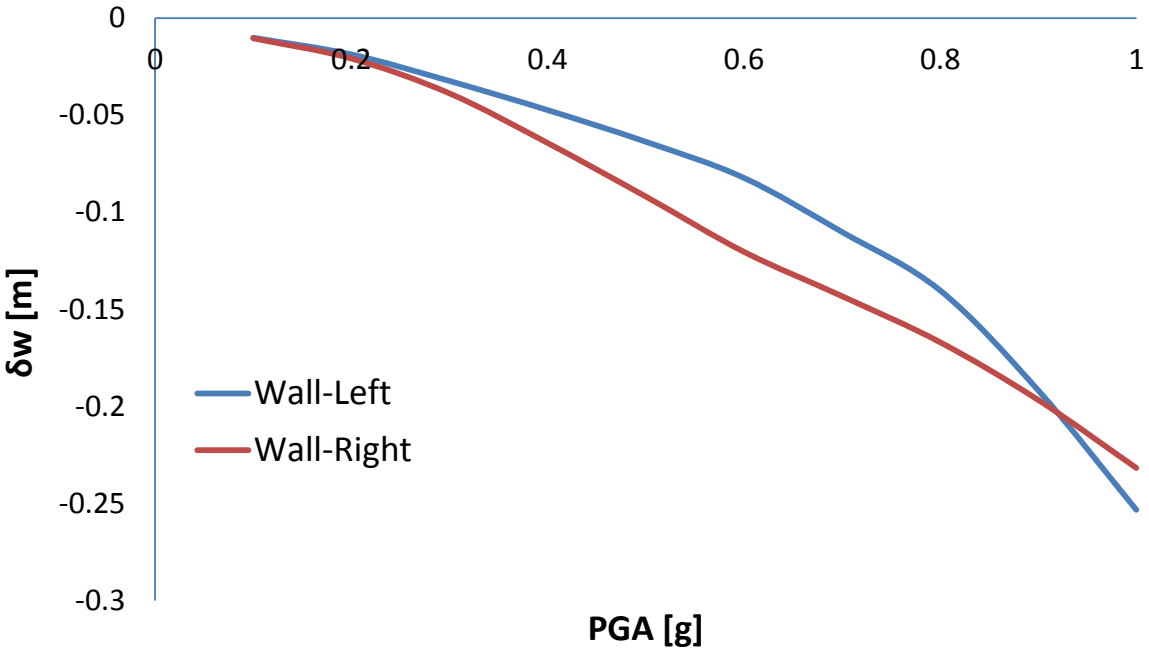

Fig. 3.142. Differential settelement as a function of PGA for the left and right wall when subjected to Takatori Seismic excitation.

Chapter 4

PARAMETRIC INVISTIGATION

4.1 Introduction

In this chapter, some parameters of the soil are changedunder a scope of understanding how they affect the behavior of the retaining wall. At first, the same numerical model as in chapter 3 was examined for different wall-foundation soil friction values. The other parameter that was examined is effect of the elasticity modulus **E**of the retained soil. In both cases,the model was subjected to two seismic excitations Aegion-0.6g and Takatori-0.6g.

4.2 The role of the friction coefficient

For a better understanding of the role of the friction coefficient **μ**, it was given different values and the same model, as in chapter 3, was subjected to two seismic excitations Takatori-0.6g and Aegion-0.6g.As seen from **Fig 4.1,**when subjected to Takatori-0.6g seismic excitation,no difference was observed when the friction coefficient is reduced to 0.6. This can be attributed to the large stiffness of the foundation soil, and to the fact that the peak ground acceleration of the input seismic excitation was equal to the friction coefficient. Meanwhile, when reduced to 0.4, the failure active wedge appears behind the retaining wall, and the plastic strains on the right of the wall disappear. This occurs because this reduction allows the sliding of the wall, which means less rotation of the wall**(Fig 4.5)**, and so the disappearance of the plastic strains on the right of the wall. One can also notice that the maximum earth pressure, residual pressure and pressure at maximum horizontal displacement are smaller for small friction coefficient, **μ=0.4 ,**while for **μ=0.6** and **μ=1** they are almost the same **(Figs 4.2-4.4)**. The reduced earth pressures can be explained by the fact that the horizontal displacements are larger for smaller **μ** (more sliding of the retaining wall). The same applies when the model is subjected to Aegion seismic **(Figs 4.7-4.9)**, but the plastic strains on the right of the wall in the case of Aegion do not disappear, this might happen because the Aegion seismic excitation is not strong enough to make the retaining wall slide **(Fig 4.6)**.

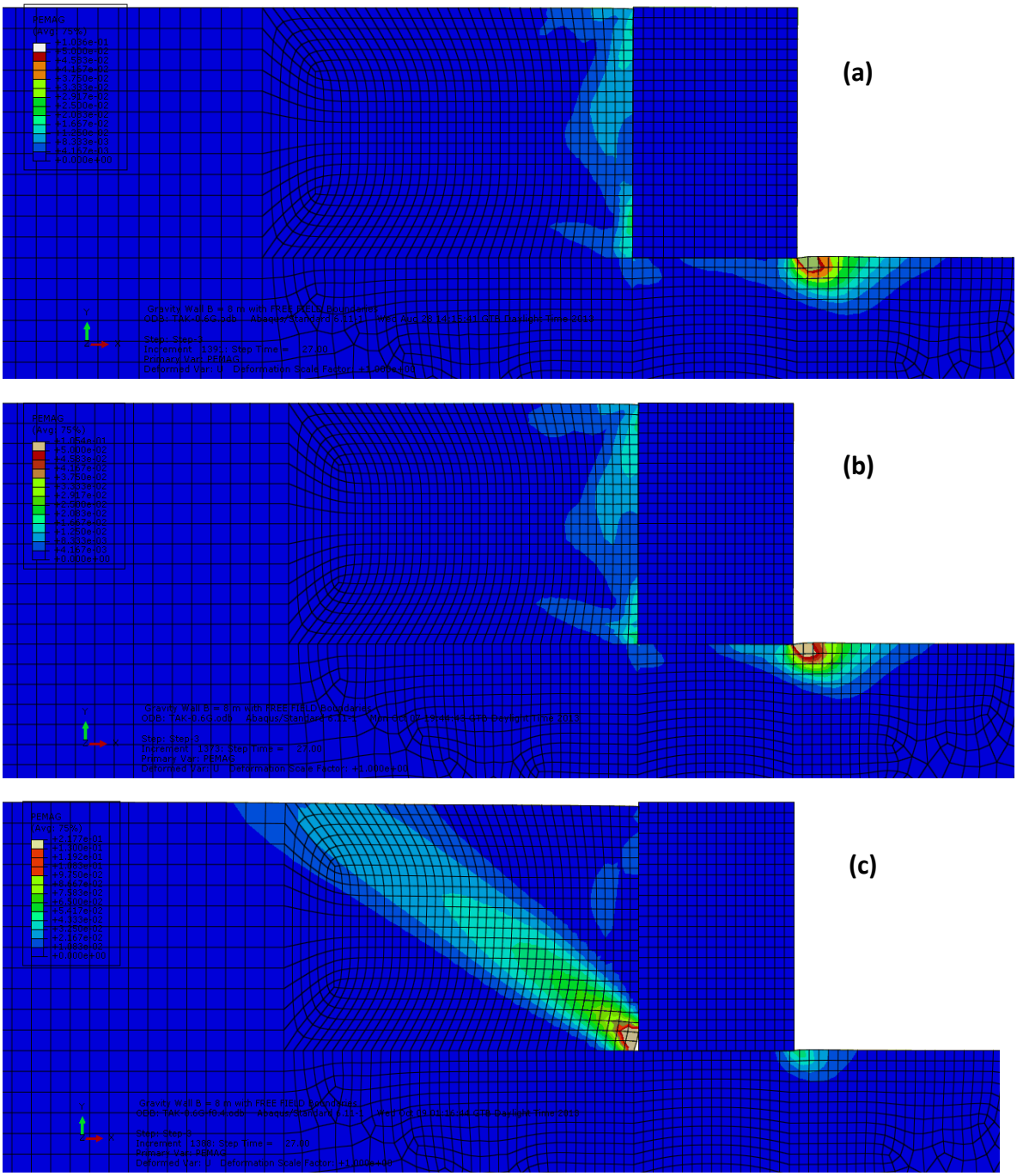

Fig. 4.1. Plastic strain contours at the end of seismic shaking (a) μ=1 (b) μ = 0.6 (c) μ = 0.4 when subjected to Takatori seismic excitation with peak acceleration 0.6g.

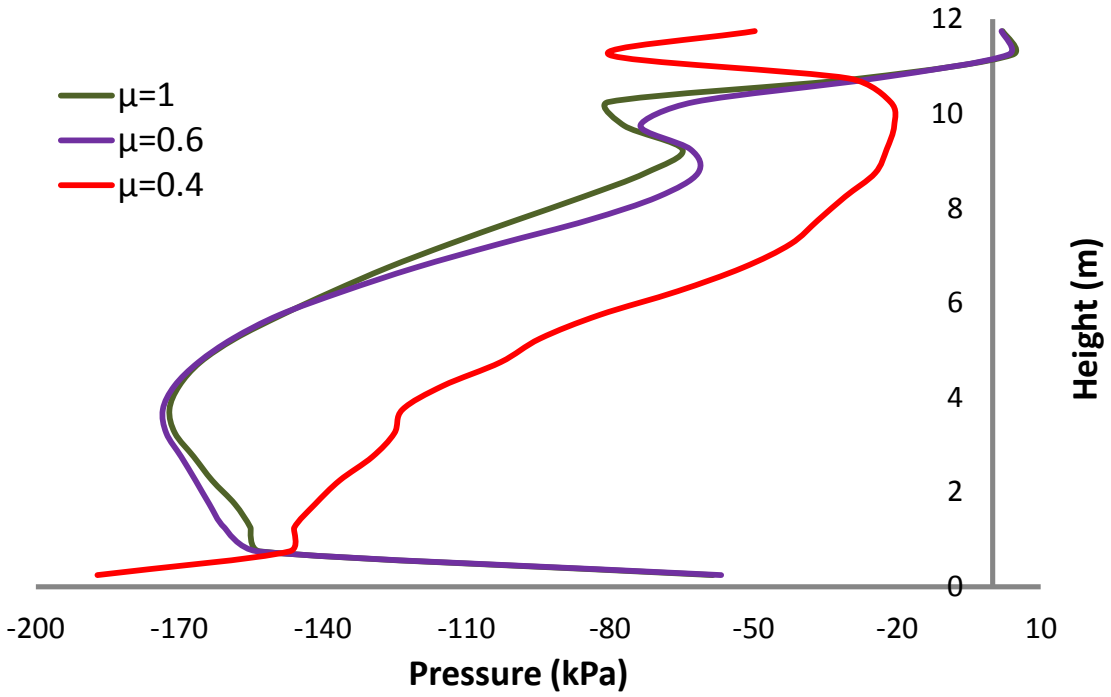

Fig. 4.2. Comparison of the maximum earth pressure on the retaining wall when subjected to Takatori seismic excitation with peak acceleration 0.6g.

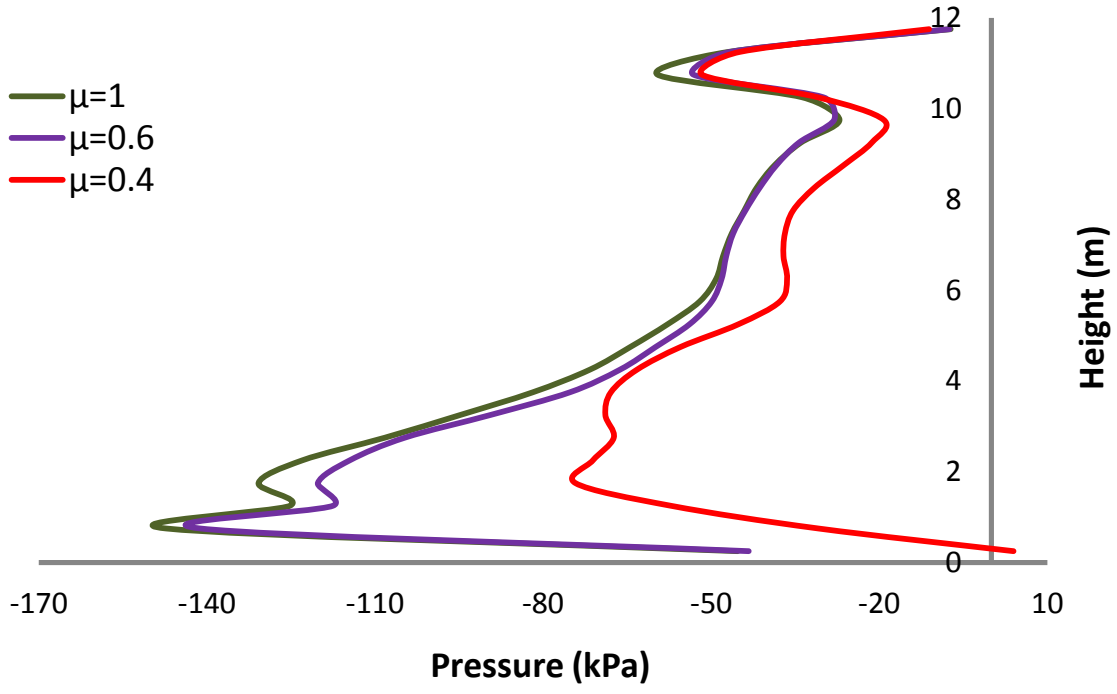

Fig. 4.3. Comparison of the residual earth pressure on the retaining wall when subjected to Takatori seismic excitation with peak acceleration 0.6g.

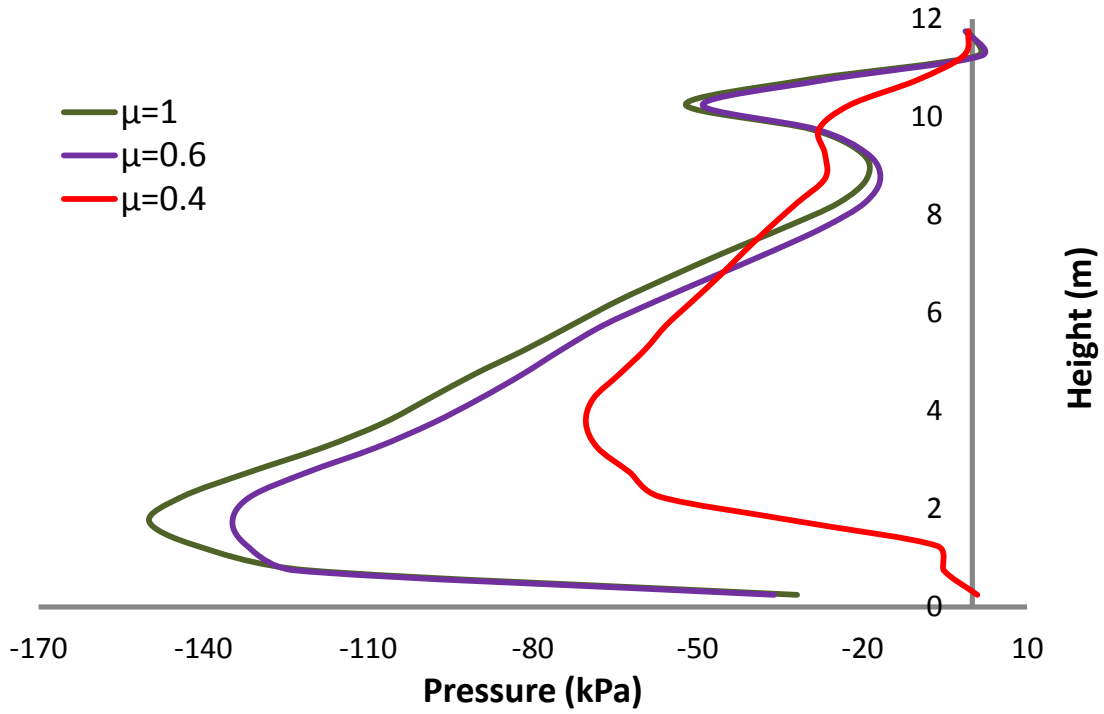

Fig. 4.4. Comparison of the earth pressure on the retaining wall at maximum horizontal displacement when subjected to Takatori seismic excitation with peak acceleration 0.6g.

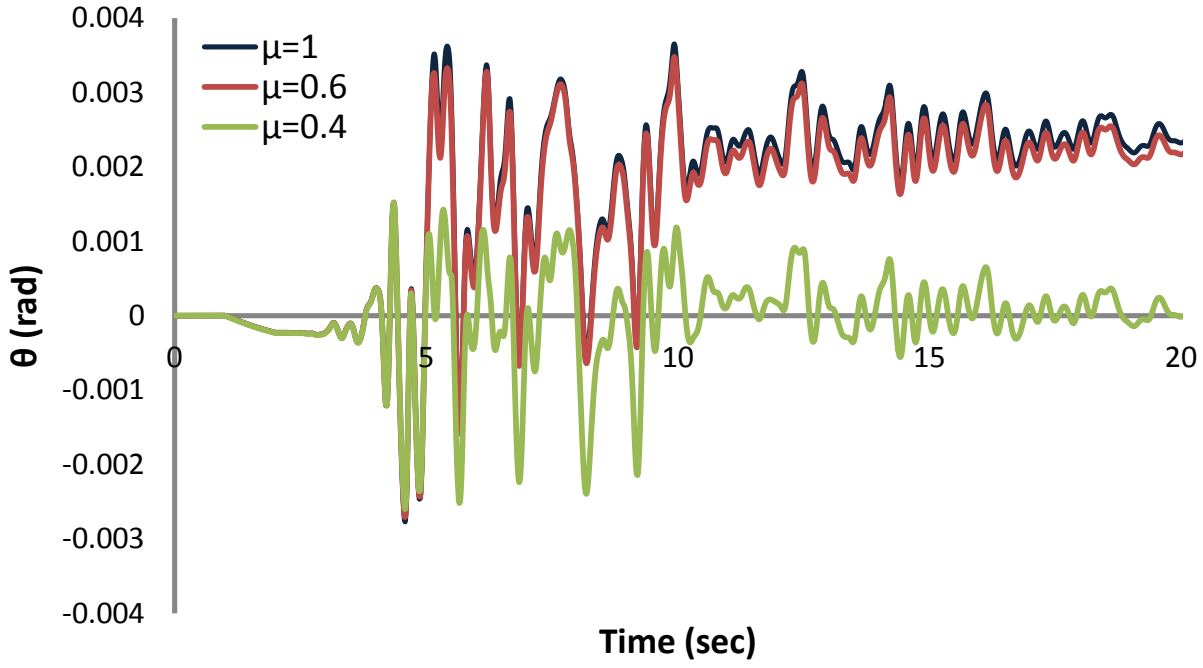

Fig. 4.5. Comparison of the rotation of the retaining wall when subjected to Takatori seismic excitation with peak acceleration 0.6g.

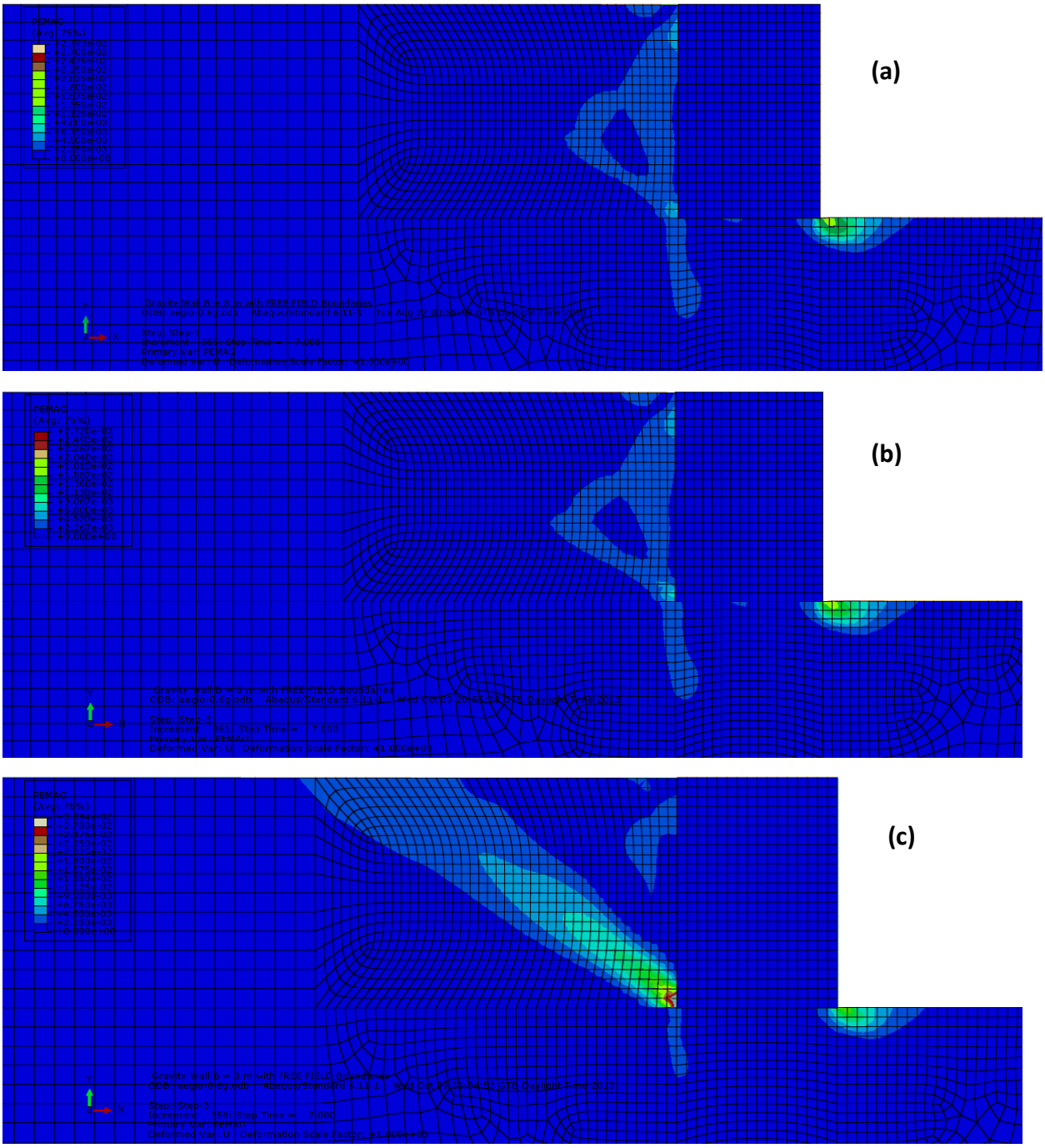

Fig. 4.6. Plastic strain contours at the end of seismic shaking (a) μ=1 (b) μ = 0.6 (c) μ = 0.4 when subjected to Aegion seismic excitation with peak acceleration 0.6g.

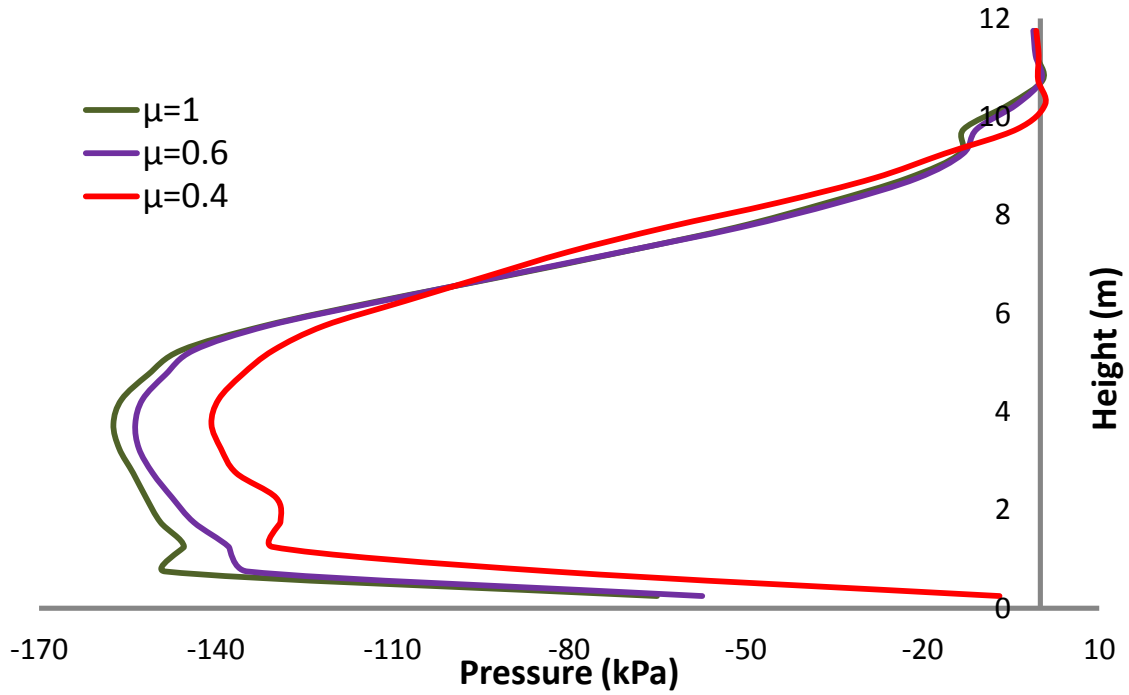

Fig. 4.7. Comparison of the maximum earth pressure on the retaining wall when subjected to Aegion seismic excitation with peak acceleration 0.6g.

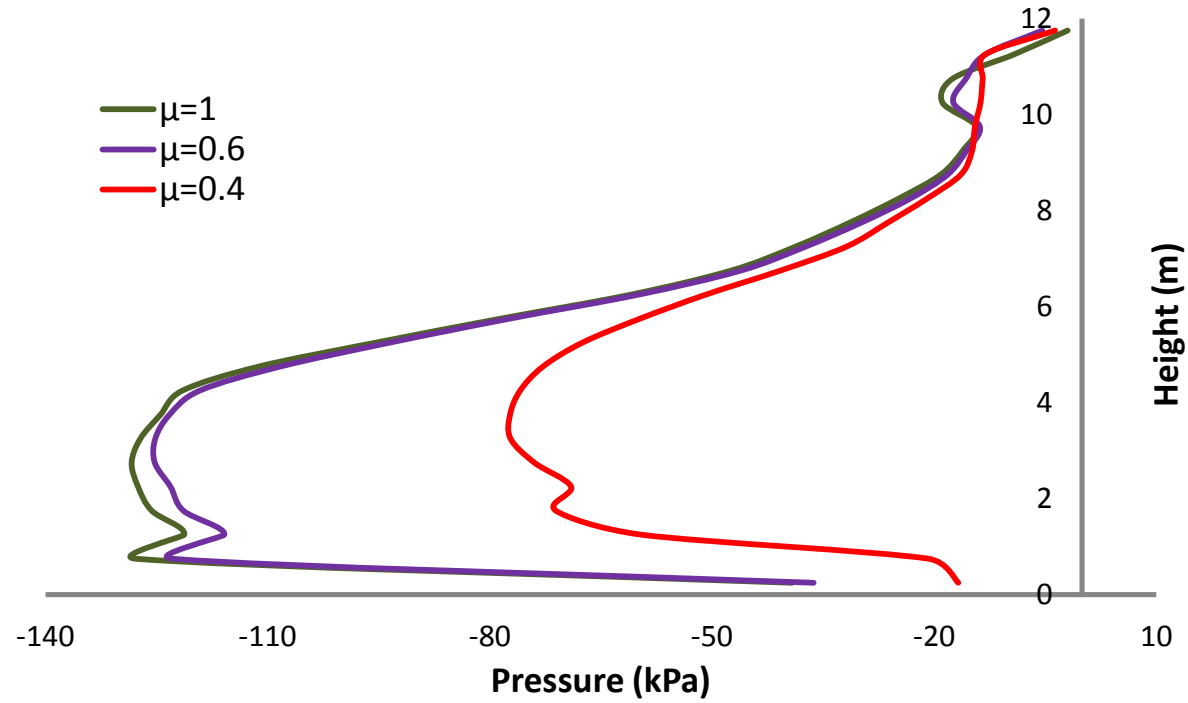

Fig. 4.8. Comparison of the residual earth pressure on the retaining wall when subjected to Aegion seismic excitation with peak acceleration 0.6g.

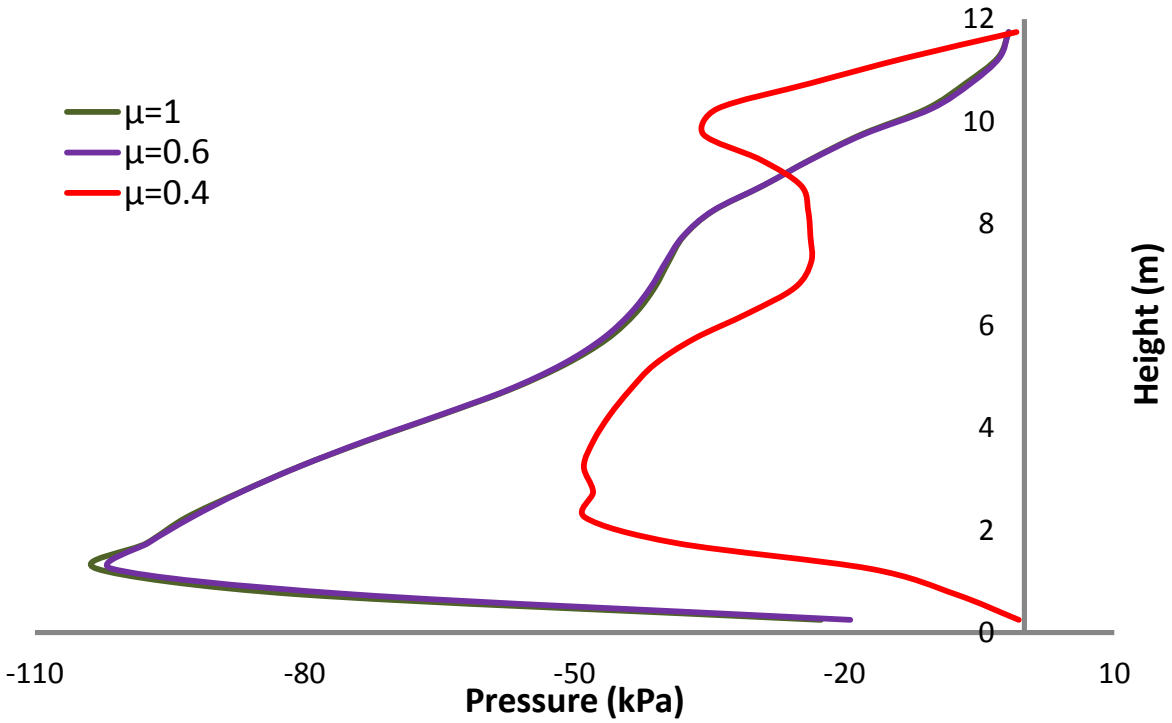

Fig. 4.9. Comparison of the earth pressure on the retaining wall at maximum horizontal displacement when subjected to Aegion seismic excitation with peak acceleration 0.6g.

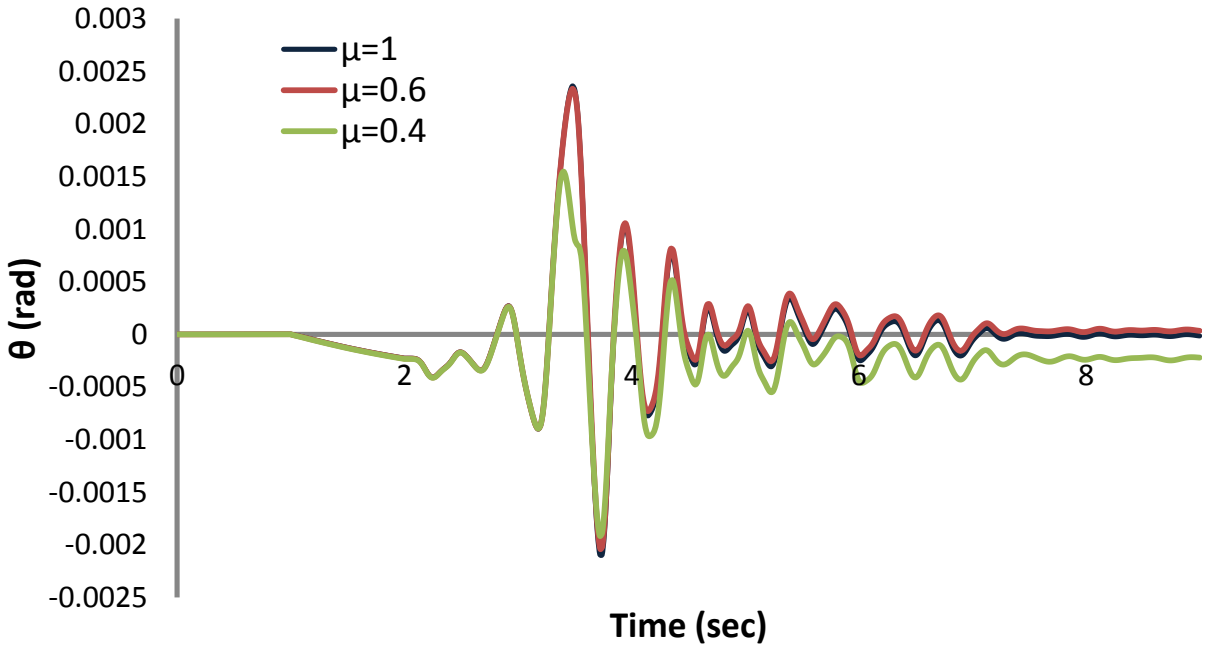

Fig. 4.10. Comparison of the rotation of the retaining wall when subjected to Aegion seismic excitation with peak acceleration 0.6g.

4.3 The role of the elasticity modulus E

Another parameter that was examined in this chapter is the role of the elasticity modulus of the retained soil. To this end, the elasticity modulus**E** of the retained soil ,in the same model as in chapter one, is reduced from 100 MPa to 25 MPaleaving the same friction angle**ϕ** (strength) of the soil.The model with its new properties is subjected to two seismic excitations Takatori-0.6g and Aegion-0.6g.

One would expect that the pressure would be greater for smaller **E** ,but as noticed from **Figs 4.7-4.9 & Figs 4.11-4.13**, the maximum pressure, residual pressure and pressure at maximum displacement are all greater when the **E** is smaller.This can be attributed to the fact that the friction angle (strength) was the same as in model 1. The same explanation applies to the smaller horizontal displacement **(Figs 4.10,4.14)**.

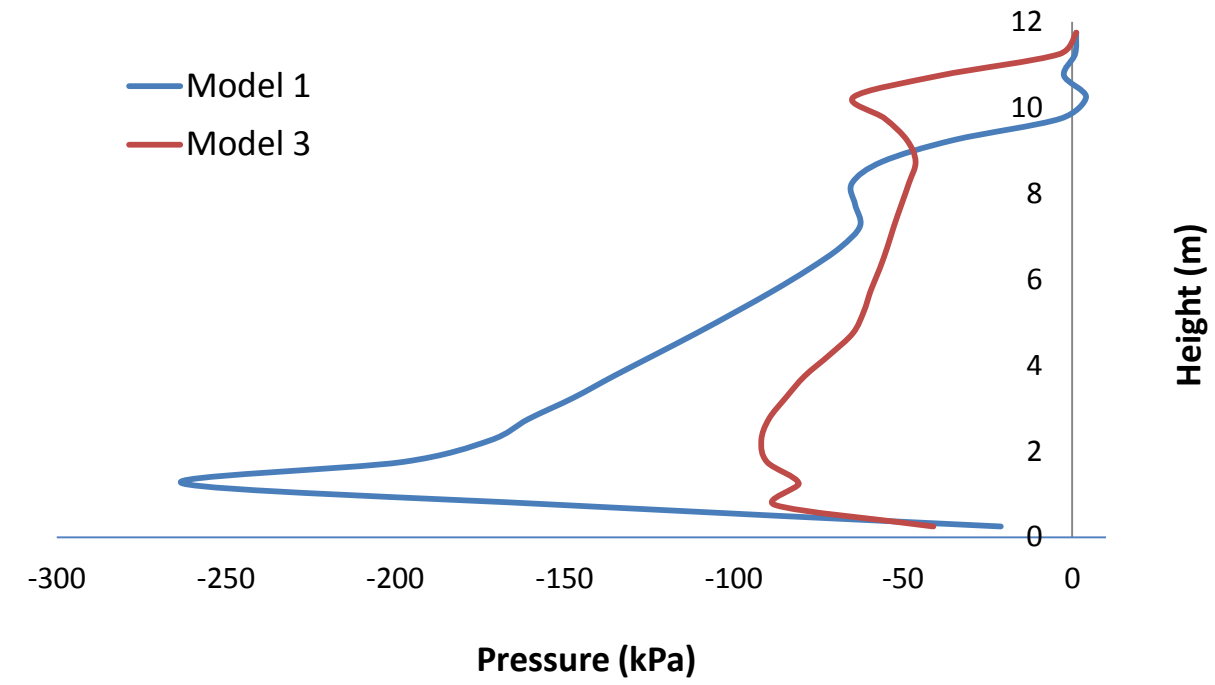

Fig. 4.7. Comparison of the maximum earth pressure on the retaining wall when subjected to Takatori seismic excitation with peak acceleration 0.6g.

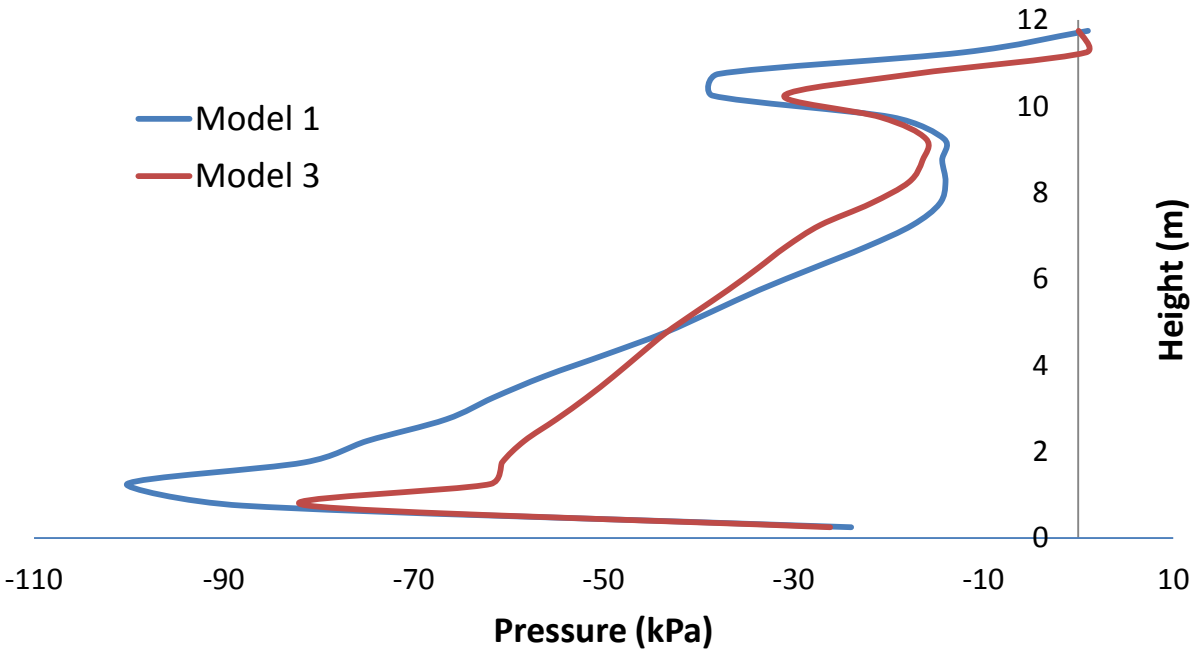

Fig. 4.8. Comparison of the residual earth pressure on the retaining wall when subjected to Takatori seismic excitation with peak acceleration 0.6g.

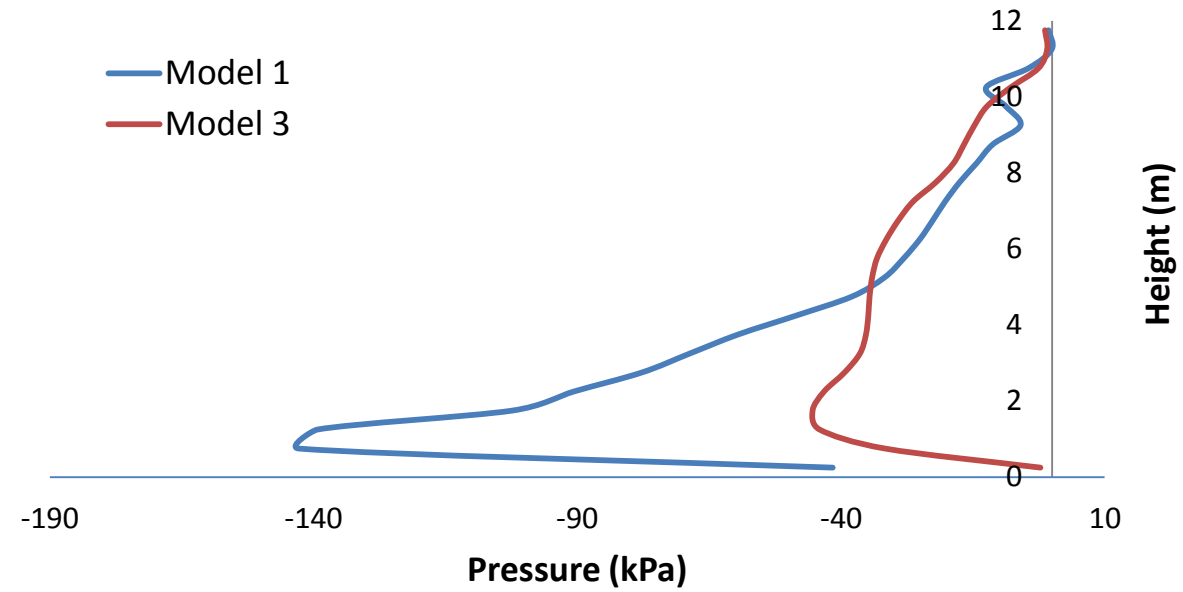

Fig. 4.9. Comparison of the earth pressure on the retaining wall at maximum horizontal displacement when subjected to Takatori seismic excitation with peak acceleration 0.6g.

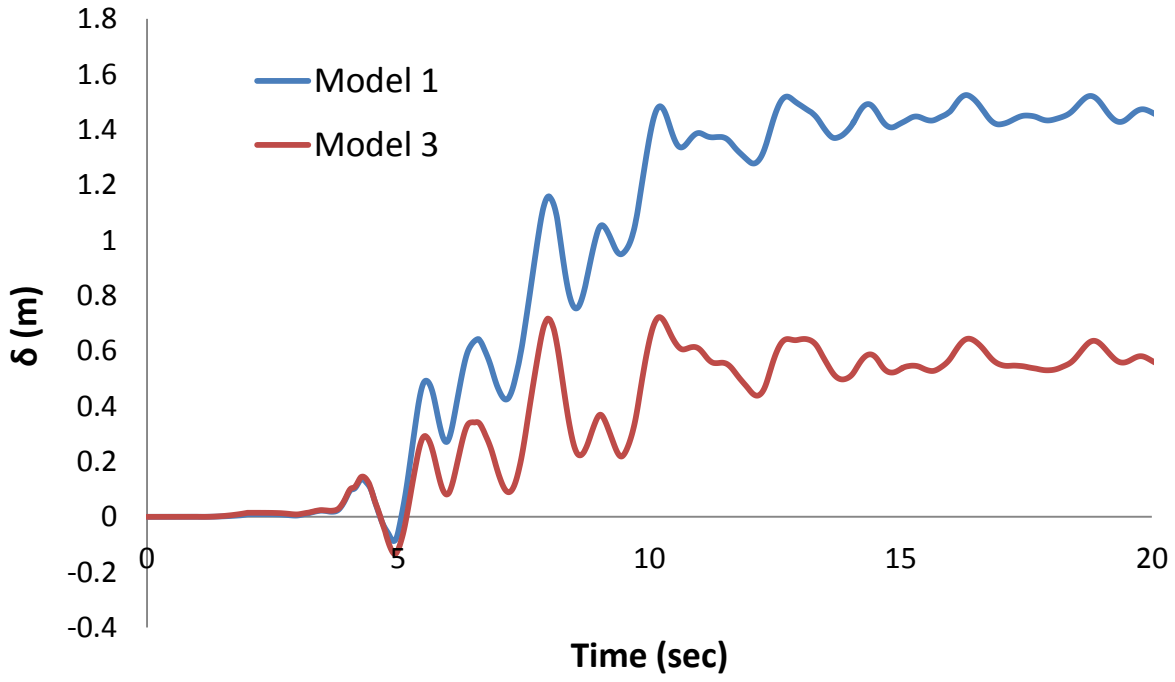

Fig. 4.10. Comparison of the horizontal displacement of the retaining wall when subjected to Takatori seismic excitation with peak acceleration 0.6g.

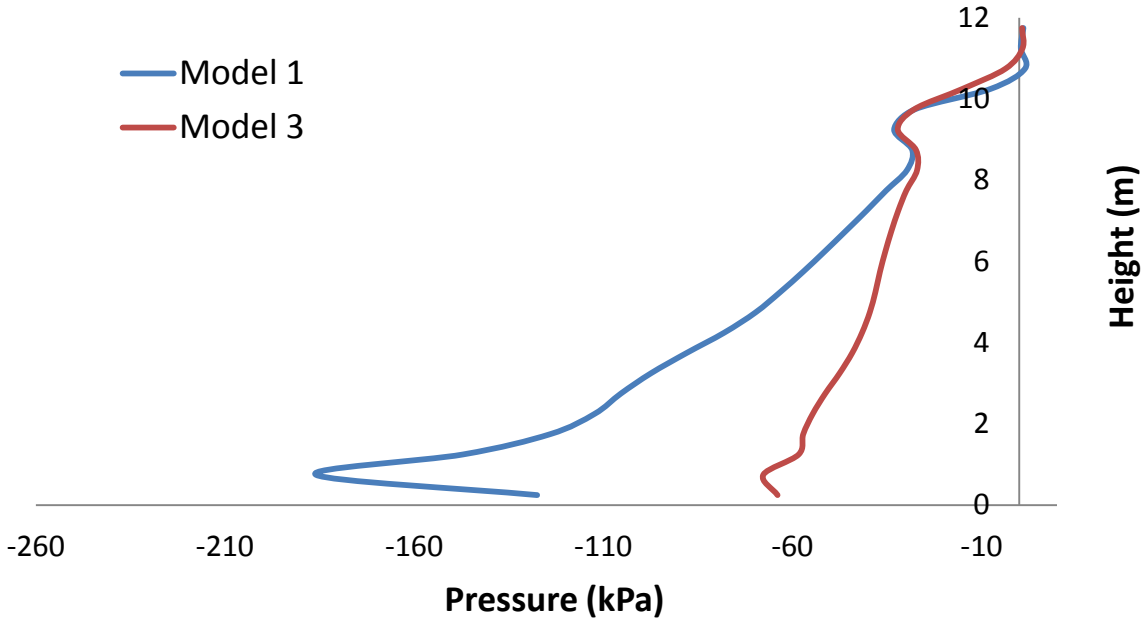

Fig. 4.11. Comparison of the maximum earth pressure on the retaining wall when subjected to Aegion seismic excitation with peak acceleration 0.6g.

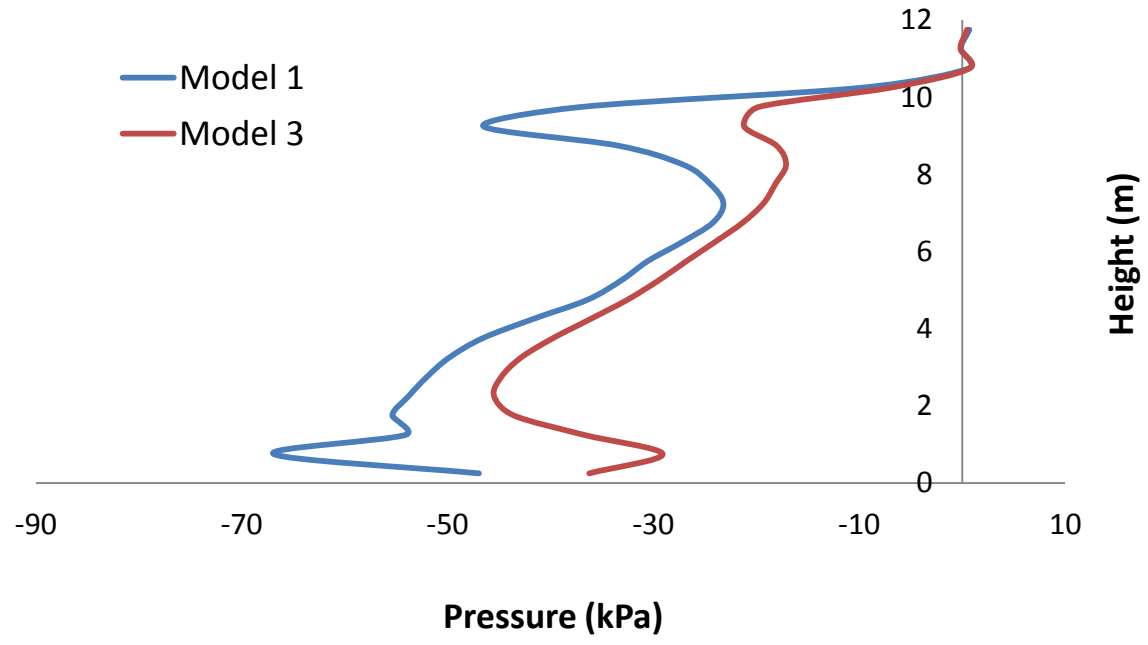

Fig. 4.12. Comparison of the residual earth pressure on the retaining wall when subjected to Aegion seismic excitation with peak acceleration 0.6g.

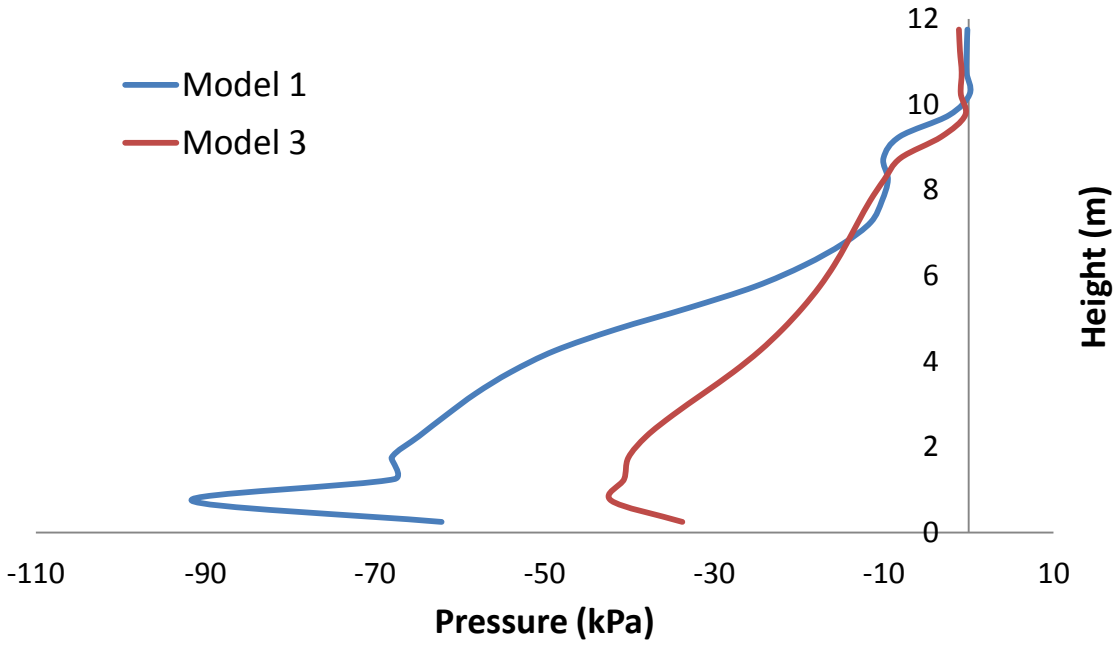

Fig. 4.13. Comparison of the earth pressure on the retaining wall at maximum horizontal displacement when subjected to Aegion seismic excitation with peak acceleration 0.6g.

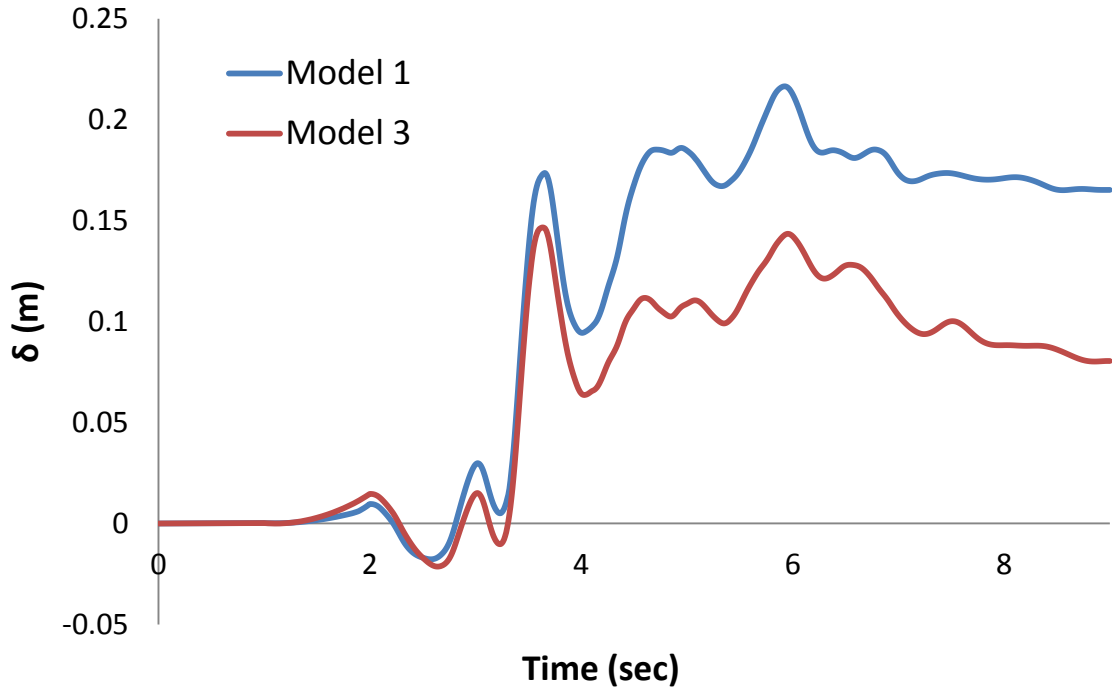

Fig. 4.14. Comparison of the horizontal displacement of the retaining wall when subjected to Aegion seismic excitation with peak acceleration 0.6g.

4.4 PEPSI

Acceleration-time histories were investigated in some characteristic points of the model, in a relation to the analysis that could have been done with pre-existing potentially sliding interface according to Gazetas and Uddin 1994.The points that were examined are shown in **Fig 4.15**.

As can be noticed from **Fig 4.16**, when the model is subjected to seismic excitation Takatori-0.9 g, the acceleration time history is symmetrical only point C ,that is 30 m away from the wall (the one that is not within the active wedge).

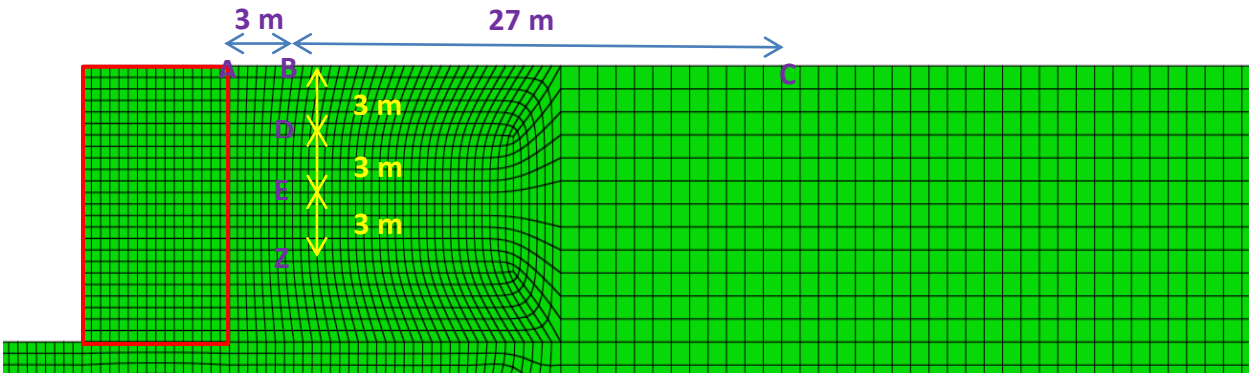

Fig. 4.15. The characheteristic points of the model that were examined.

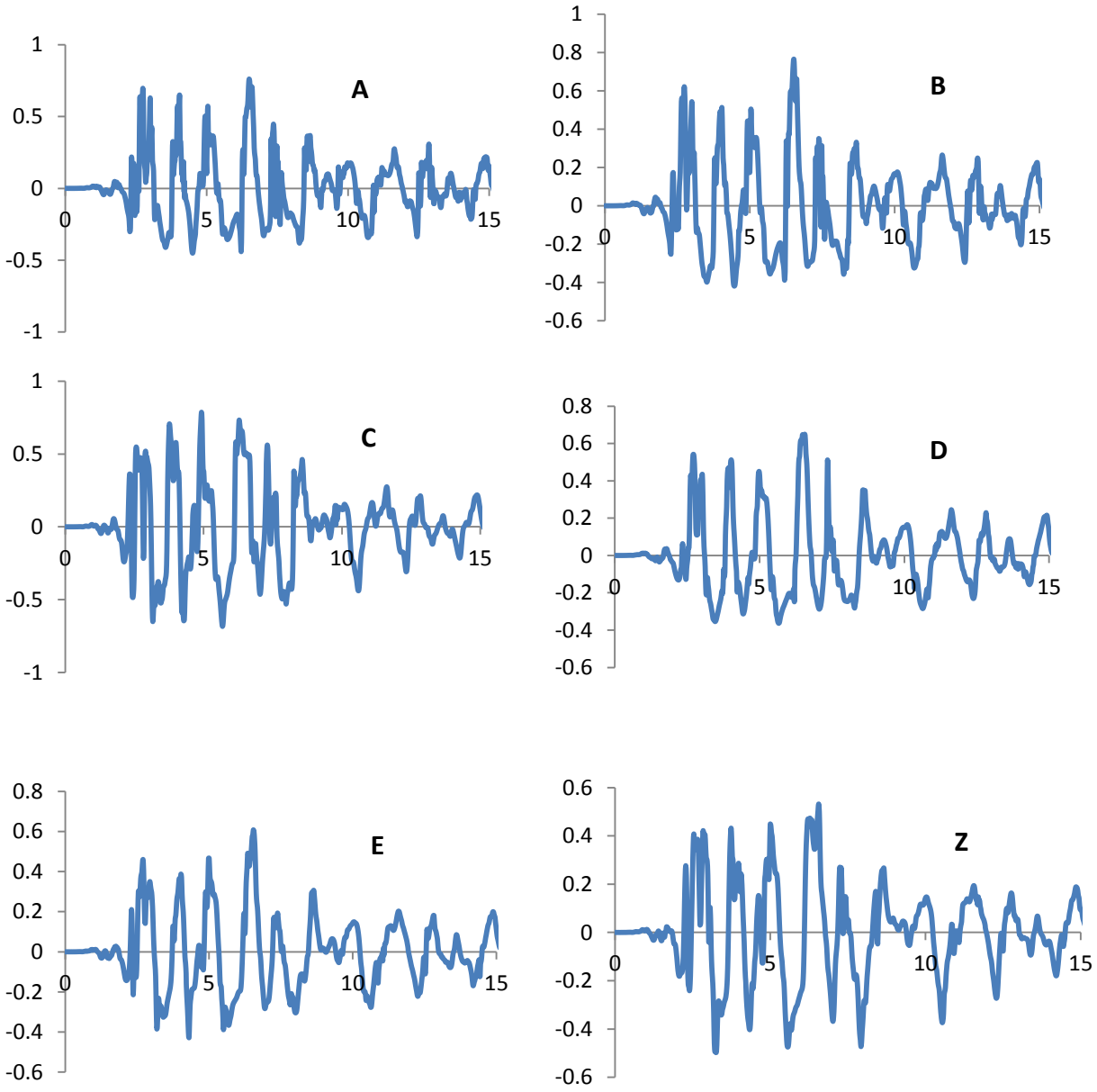

Fig. 4.16. Acceleration-time histories for different points of the model.

Chapter 5

SIMPLIFIED MODEL

5.1 Introduction

The objective of this chapter is to create a simplified model of the wall-soil system which will have the same seismic performance with the original model.To this end,a numerical model using the ABAQUS was developed in stages that are mentioned below

5.2 The First stages to construct the simplified model

According to Al-Homoud and Whitman (1999),the moment responsible for the rotation during dynamic loading is almost equal to the dynamic overturning due to wall horizontal inertia at the time of its maximum outward displacement. For this purpose, a numerical model (Fig 5.1) that consisted only of the retaining wall and the foundation soil was examined under some seismic excitations. The results are shown in **Figs 5.2-5.5**.

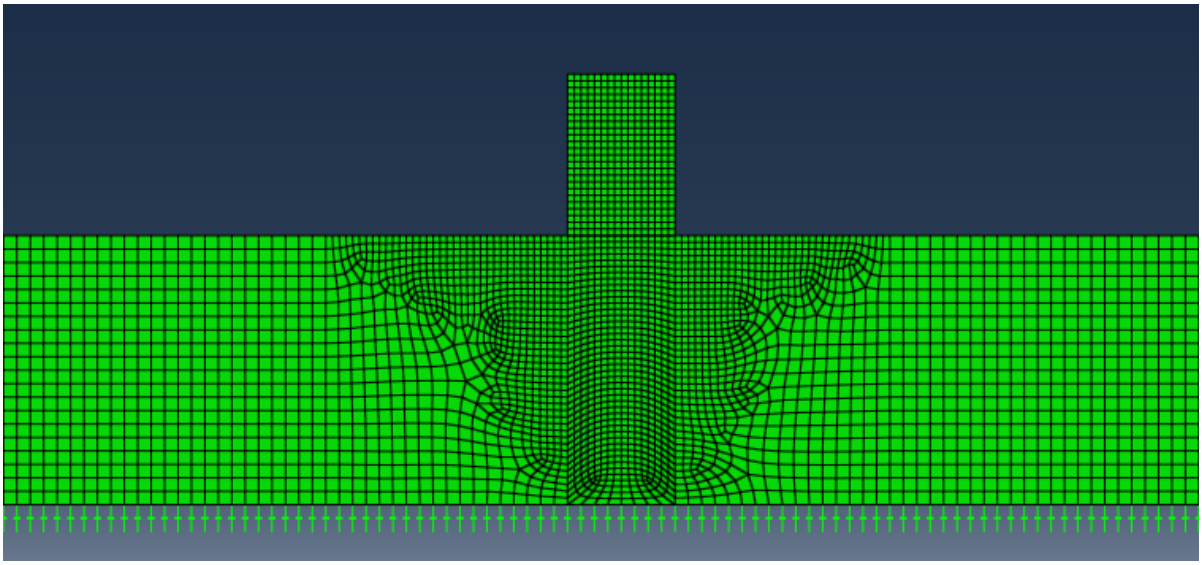

Fig. 5.1. Two-dimensional finite element mesh (ABAQUS) of the retaining wall and the foundation soil.

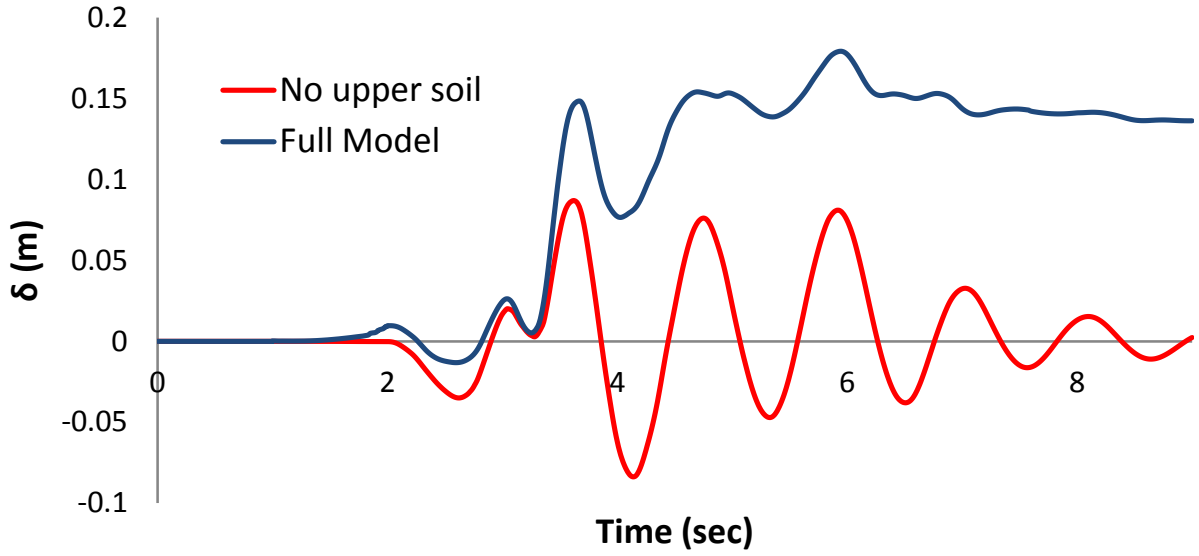

Fig. 5.2. Comparison of the horizontal displacement when subjected to seismic excitation Ageio 0.5g.

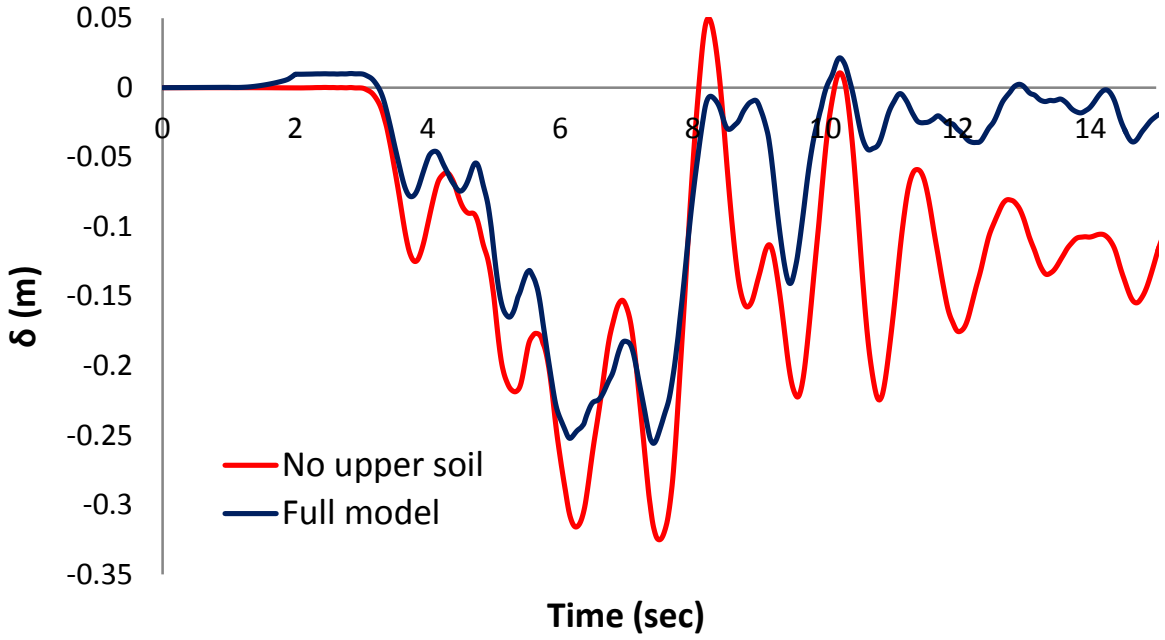

Fig. 5.3. Comparison of the horizontal displacement when subjected to seismic excitation Kodsakarya 0.4g.

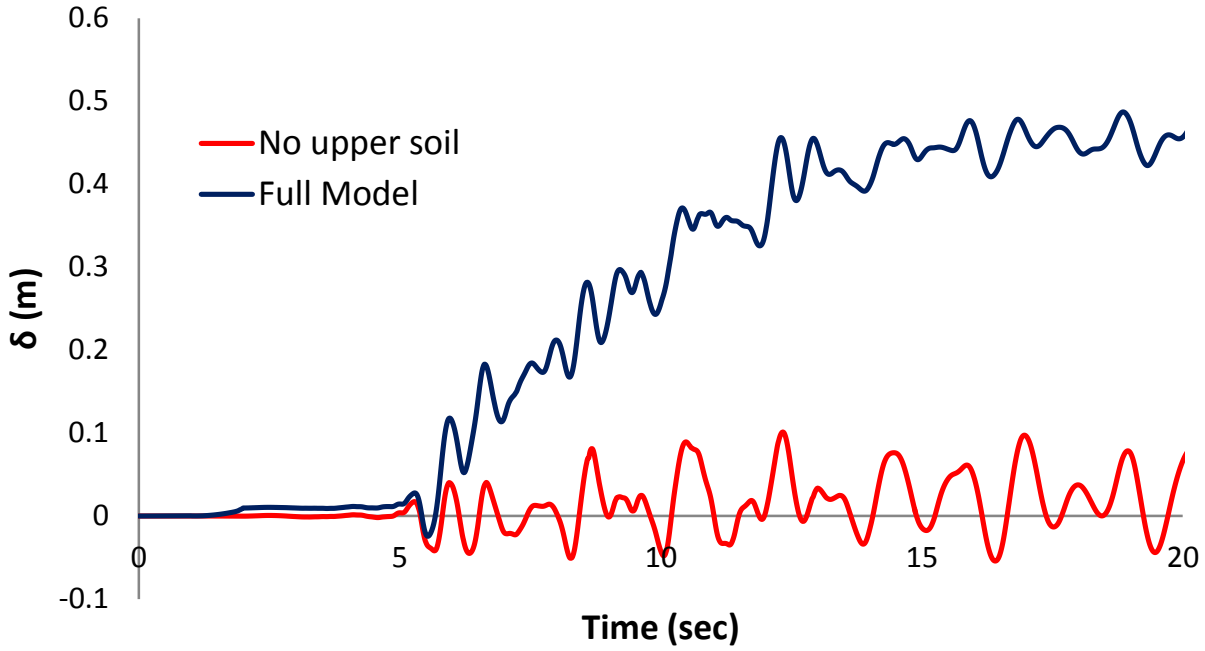

Fig. 5.4. Comparison of the horizontal displacement when subjected to seismic excitation Lefkada 0.5g.

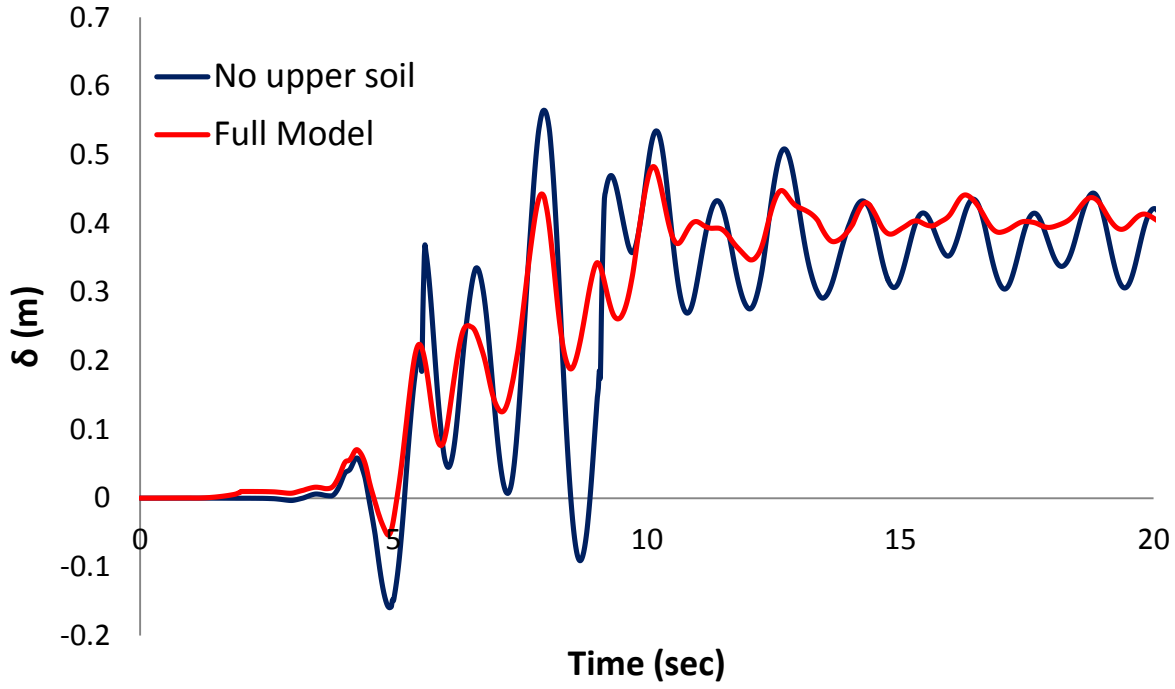

Fig. 5.5. Comparison of the horizontal displacement when subjected to seismic excitation Takatori 0.3g.

In a second stage, a constant force was added to the model ,that was equal to the static lateral force. The point of application of the load was at 3.5 m above the bottom of the wall, as found from the analyses of the full model in ABAQUS. The reduced height of the static resultant force can be attributed to the height of free cut in clay, where the soil because of its cohesion loses contact with the wall so the equivalent triangle is smaller than the computed one and so is the height of the resultant force. All the results are compared to the first model which is used as a benchmark reference (**Figs 5.5-5.9**).

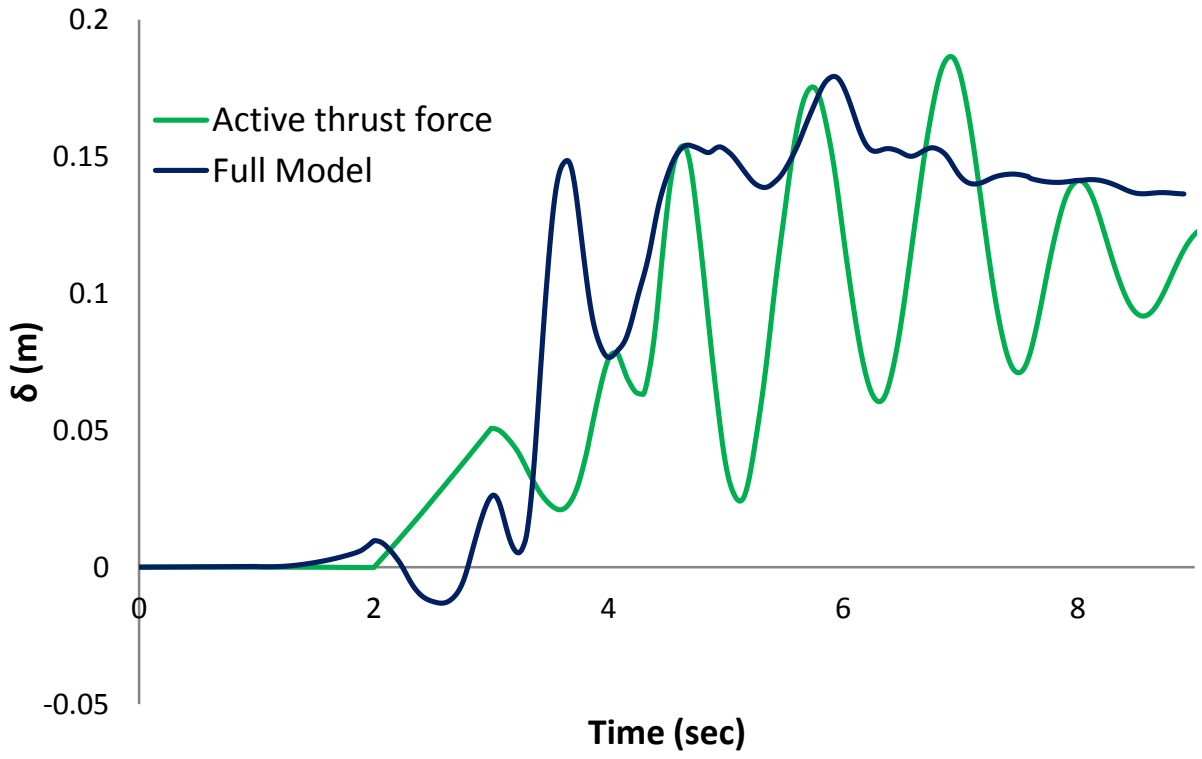

Fig. 5.6. Comparison of the horizontal displacement when subjected to seismic excitation Ageion 0.5g.

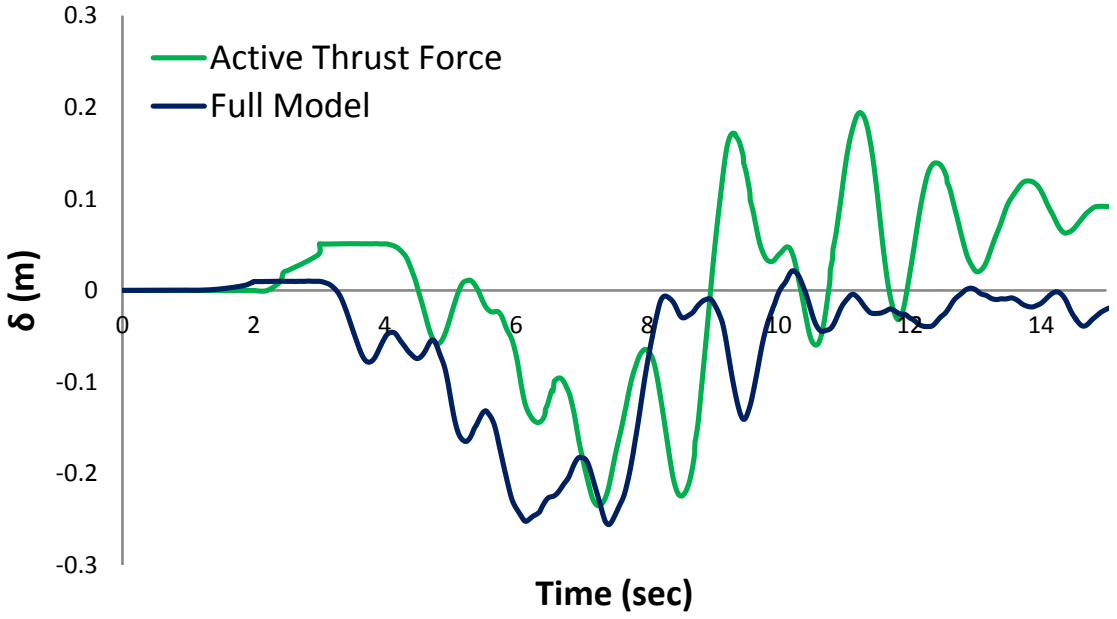

Fig. 5.7. Comparison of the horizontal displacement when subjected to seismic excitation Kodsakarya 0.4g.

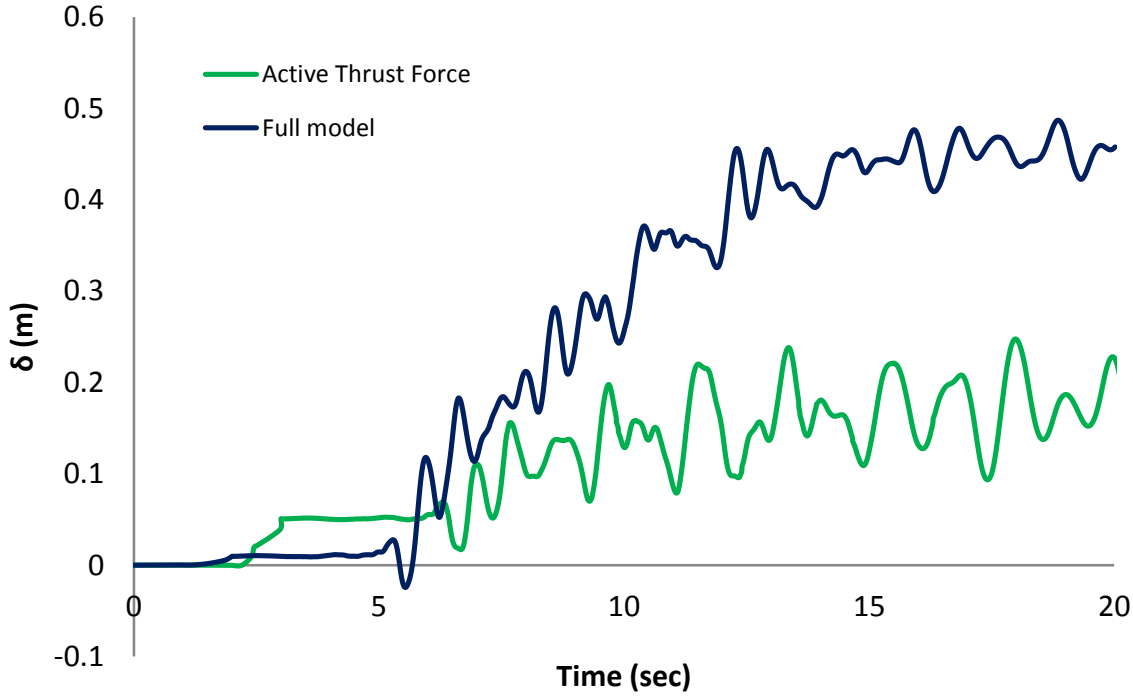

Fig. 5.8. Comparison of the horizontal displacement when subjected to seismic excitation Lefkada 0.5g.

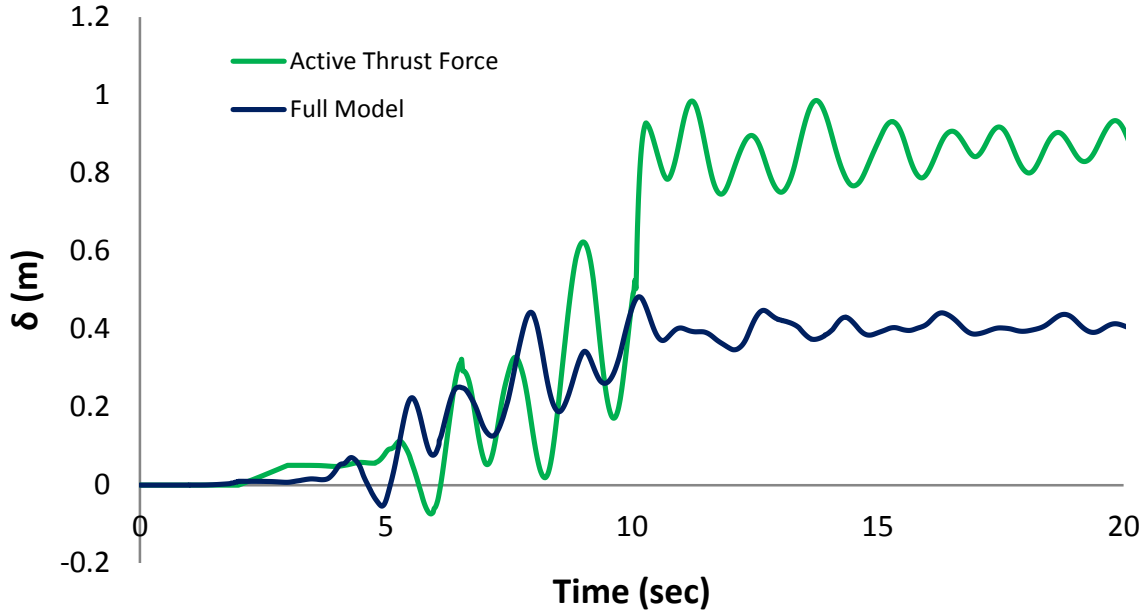

Fig. 5.9. Comparison of the horizontal displacement when subjected to seismic excitation Takatori 0.3g.

5.3 Final simplified model

The mass of the active wedge behind the wall is calculated and simulated by a concentrated mass.The sliding of the active wedge was simulated by a horizontal and a vertical slider. The sliders are placed at a height of 3.5 m above the bottom of the wall. A distributed load was also added to the model to simulate the pressure by the retained soil. In order to simulate the foundation soil, non-linear vertical and horizontal springs were added to the model.Since the active pressure is not the only force that acts upon the wall, beam and linear springs were also placed at the base of the wall to simulate the pressure by the retained soil that prevents the wall from moving only to the right and rotating.

The stiffness of the springs was estimated considering the wall and the foundation soil as a shallow foundation, static Push-over analyses were made and then calibration by comparing to

the results from the wall and foundation soil model. The stiffness of the beam was calibrated according to the initial settlement of the full model.

As shown in **Figs 5.12,5.14&5.16 ,**the horizontal displacements of the simplified and full model are in a very good agreement. A thing that doesn't apply to the horizontal force acting on the wall**(Figs 5.11, 5.13, 5.15)**. This can be explained by the two assumptions that were made for the simplified model, first that the measure of the active wedge angle is $(45^{o}+ \phi/2)$, second that the point of application of force is constant.

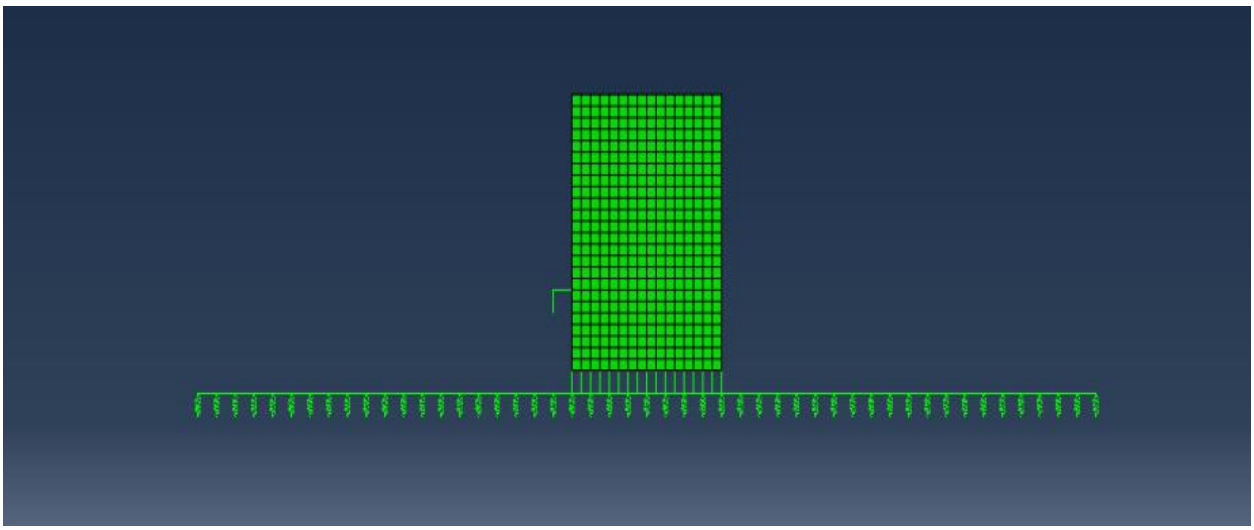

Fig. 5.10. Two-dimensional finite element mesh (ABAQUS) of the simplified model.

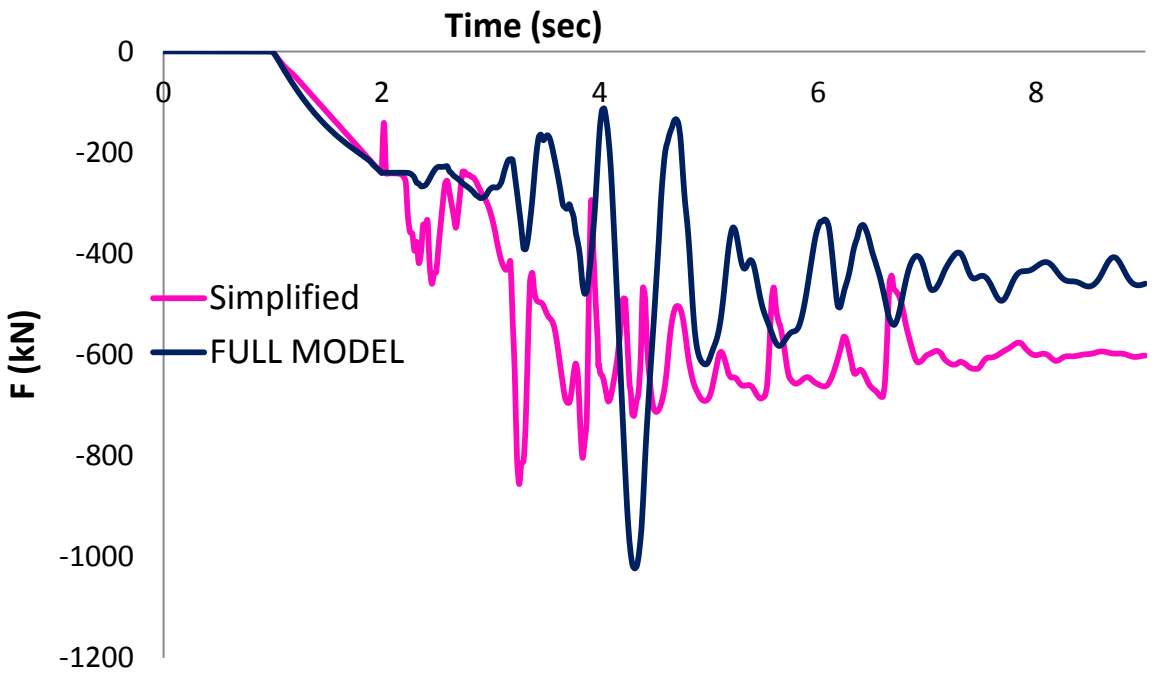

Fig. 5.11. Comparison of the horizontal force acting on the retaining wall when subjected to seismic excitation Aegion 1g.

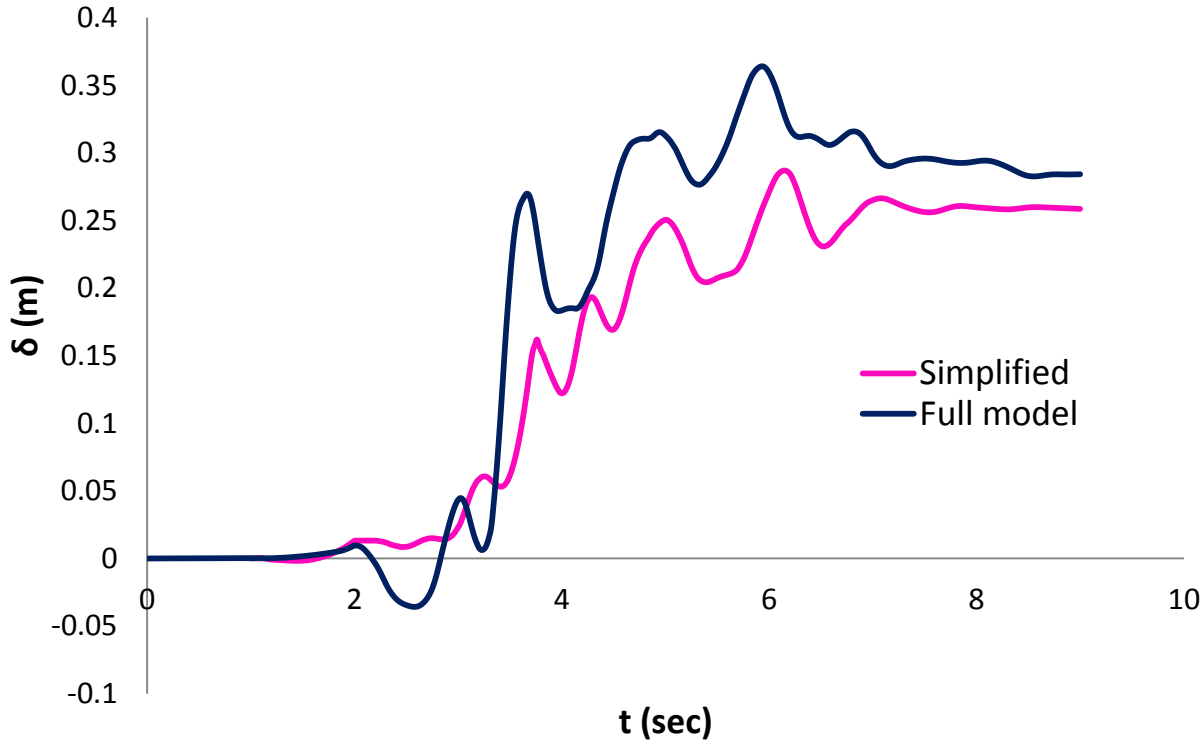

Fig. 5.12. Comparison of the horizontal displacement when subjected to seismic excitation Aegion 1g.

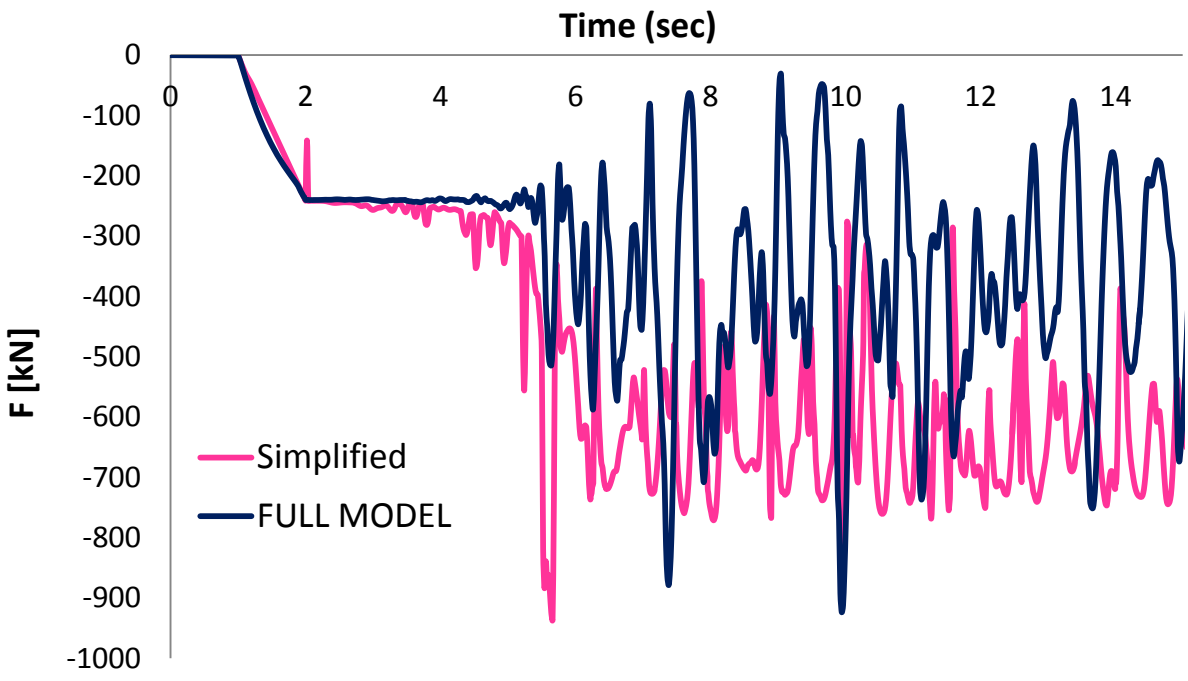

Fig. 5.13. Comparison of the horizontal force acting on the retaining wall when subjected to seismic excitation Lefkada 1g.

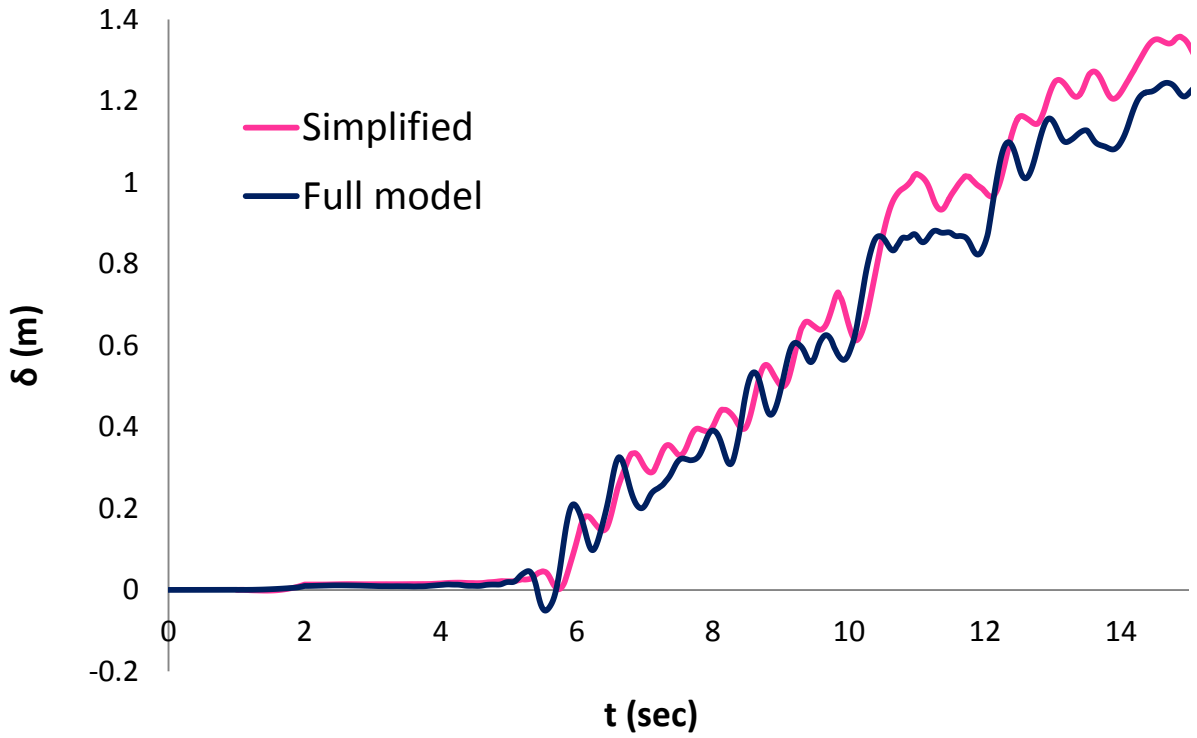

Fig. 5.14. Comparison of the horizontal displacement when subjected to seismic excitation Lefkada 1g.

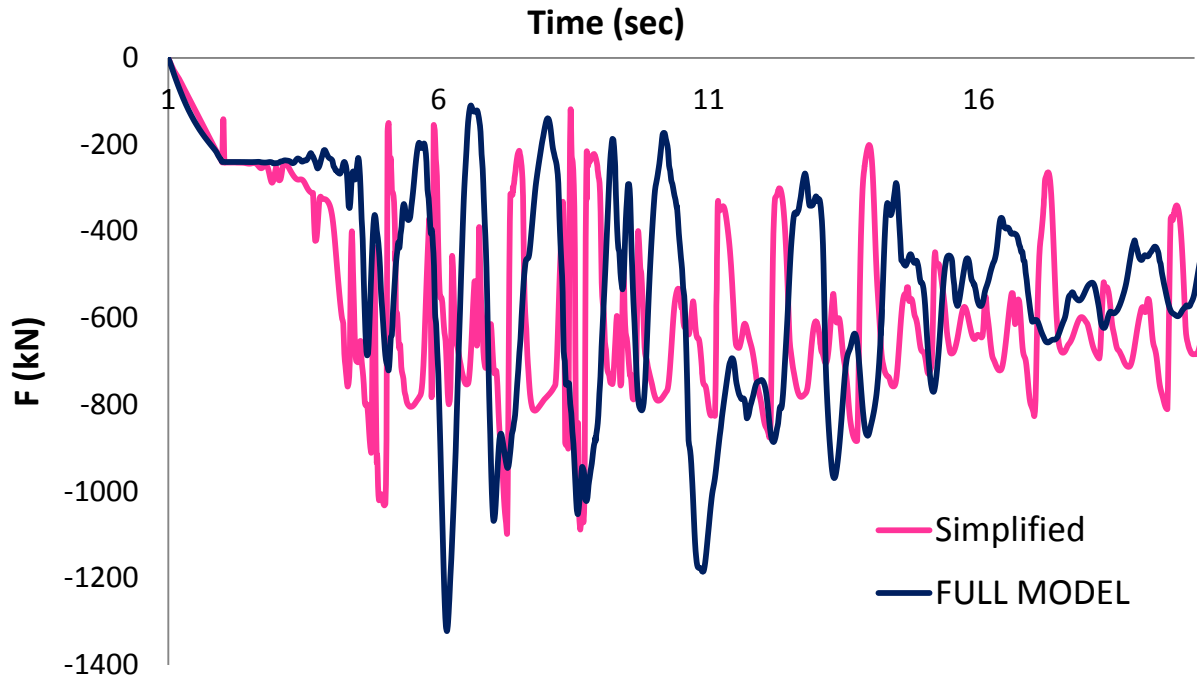

Fig. 5.15. Comparison of the horizontal force acting on the retaining wall when subjected to seismic excitation Takatori 1g.

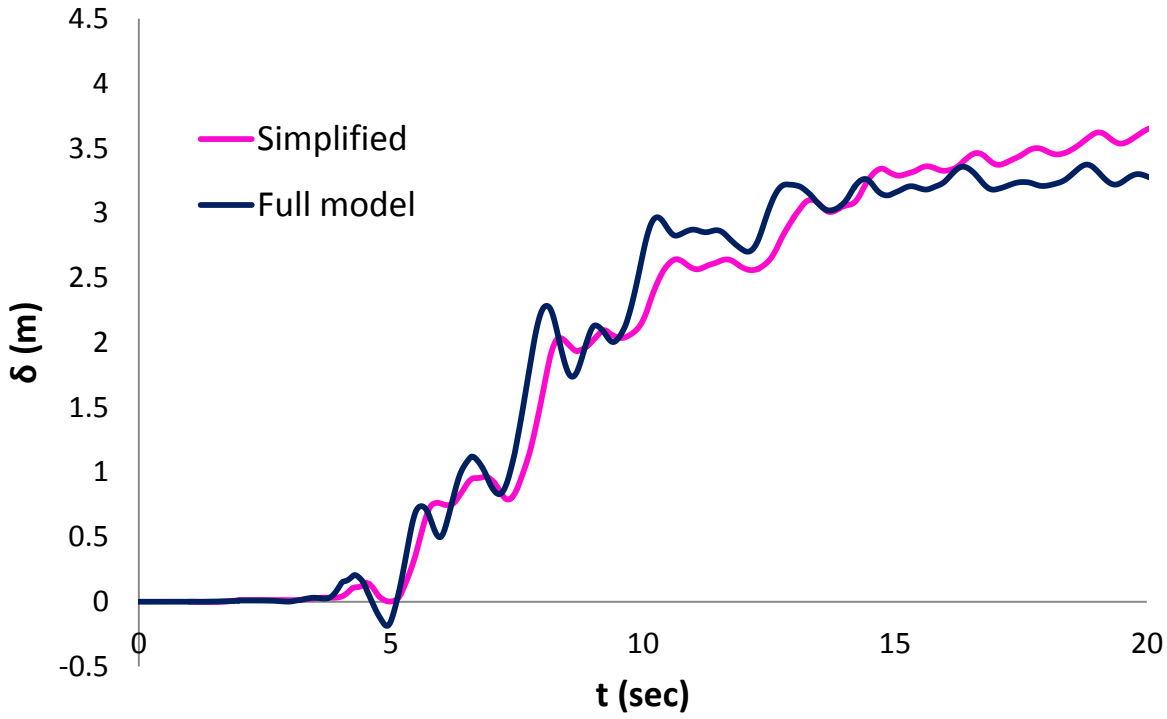

Fig. 5.16. Comparison of the horizontal displacement when subjected to seismic excitation Takatori 1g.

Chapter 6

CONCLUDING REMARKS

6.1 Concluding Remarks

The subject of the present work is the analysis of a typical gravity retaining wall.To this end 2-D analyses were conducted and the response of the retaining wall was investigated on a looser foundation soil,as well as on a stiffer foundation one for different friction coefficients **μ**= 1 , 0.6 and 0.4. Another parameter that was investigated was the elasticity modulus **E** of the retained soil. Additionaly, a first attempt to construct a numerical simplified model was made in order to reduce the computation time needed for each analysis.

The main conclusions from the above analyses are the following :

- ✓ The seismic response of a retaining wall is sensitive to the polarity of the seismic excitation (i.e. quiet different for positive and negative excitation— left and right wall, respectively).
- ✓ If the foundation soil is very stiff, the active wedge behind the retaining wall does not develop. No displacement or rotation is involved as long as the friction coefficient at the base of the wall is large and no sliding takes place.
- ✓ Reducing the compliance of the retained soil (i.e. increasing **E**), without changing its strength (i.e. friction angle **ϕ**), earth pressure and horizontal displacements decrease.
- ✓ Decreasing the friction coefficient (**μ**),leads to increased sliding of the retaining wall, hence development of the active wedge behind the wall, increased horizontal displacements and less rotation of the wall.
- ✓ The pre-existing potentially sliding interface in dams applies to the retaining walls: the acceleration time histories of the points within the active wedge are grossly asymmetrical in comparison with the accelerations of the free field.
- ✓ A simplified model comprising springs, dashpots, and masses is developed. Comparison against the finite element gave good results in terms of horizontal displacements.

BIBLIOGRAPHY

Bibliography

ABAQUS 6.10. [2010]. Standard user's manual. Dassault Systèmes Simulia Corp., Providence, RI, USA.

Al-Atik L. and Sitar N.[2009]. "Seismically induced lateral earth pressures: A new approach",17th International Conference on Soil Mechanics and Geotechnical Engineering Alexandria, Egypt

AI-Homoud and Whitman RV. [1994]."Comparison between fe prediction and results fromdynamic centrifuge tests on tilting gravity walls", Soil Dynamics and Earthquake Engineering, 14, 259–268.

Anastasopoulos I. , Loli M. , Georgarakos T.& Drosos V. [2012]. "Shaking Table Testing of Rocking—Isolated Bridge Pier on Sand",Journal of Earthquake Engineering, 17(1), 1–32.

BICA A.V.D. and CLAYTONC.R.I. [1998]. "An experimental study of the behaviour of embedded lengths of cantilever walls", Geotechnique, 48, No. 6, 731±745.

Chung-Jung Lee[2005]. "Centrifuge modeling of the behavior of caisson-type quay walls during earthquakes", Soil Dynamics and Earthquake Engineering, 25, 117–131.

Dakoulas P. &Gazetas G. [2008]."Insight into seismic earth and water pressures against caisson quay walls", Geotechnique 58, No. 2, 95–111.

Dakoulas P. and Gazetas G. [2005]. "Seismic Effective –stress of caisson quay walls: Application to kobe", Soils and foundation, 45 (4), 133–147, Japanese geotechnical society.

Dobry R., Oweis I. and Urzua A.[1976]." Simplified Procedures For Estimating The Fundamental Period Of a Soil Profile", Bulletin of the seismological society of America, 66(4), 1293–1321.

Gazetas G., Garini E., Anastasopoulos I. and GeorgarakosT. [2009]."Effects of Near-Fault Ground Shaking on Sliding Systems",Journal of Geotechnical and GeoenvironmentalEngineering", 135(12), 1906–1921.

Gazetas G., Gerolymos N.,I. Anastasopoulos I. [2005]. "Response of three Athens metro undergroundstructures in the 1999 Parnitha earthquake", Soil Dynamics and Earthquake Engineering, 25, 617–633.

Gazetas G., Psarropoulos P.N. , Anastasopoulos I., Gerolymos N. [2004]. "Seismic behaviour of flexible retaining systems subjectedto short-duration moderately strong excitation", Soil Dynamics and Earthquake Engineering, 24,537–550.

Gazetas G. and Uddin N. [1994]."Permanent Deformation Of Preexisting Sliding Surfaces In Dams", Journal of Geotechnical and GeoenvironmentalEngineering", 120(11), 2041–2061.

Giarlelis C., Mylonakis G. [2011]. "Interpretation of dynamic retaining wall model tests in light of elastic and plastic solutions", Soil Dynamics and Earthquake Engineering, 31(1), 16–24.

Houlsby G.T.and Puzrin A.M. [1998]."The bearing capacity of a strip footing on clay under combined loading."

Kotta N., Tsamis B., and Gazetas G. [1988]."Seismic failure of Kalamata harbor quay wall", 69–74.

Kourkoulis R., Anastasopoulos I., Gelagoti F., Gazetas G. [2010]."Interaction of foundationstructure systems with seismically precariousslopes: Numerical analysis with strain softening constitutive model",Soil Dynamics and Earthquake Engineering, 30, 1430–1445.

Lambe T.William and Whitman Robert V. [1979]. "Soil mechanics, SI Version", Part 3, Chapter 13 & 14, 162–226.

Loli M., Bransby M.F., Anastasopoulos I. and Gazetas G. [2012]."Interaction of caisson foundations with a seismically rupturing normalfault: centrifuge testing versus numerical simulation", . Geotechnique 62, No. 1, 29–43.

Mikola R.,Sitar N. [2013]." Seismic earth pressures on retaining structures in cohesionless soils", Department of civil and environmental engineering, University of California, Berkeley , report No. UCB/CA13-0367.

Mohamad Hisham, Soga Kenichi, Pellew Adam and Bennett Peter J.[2011]. "Performance Monitoring of a Secant-Piled Wall Using Distributed Fiber Optic Strain Sensing", Journal of Geotechnical and GeoenvironmentalEngineering, 137 (12), 1236–1243.

Panagiotidou A., Gazetas G. and Nikos Gerolymos N. [2012]."Pushover and Seismic Response of Foundations on Stiff Clay:Analysis with P-Delta Effects",Earthquake Spectra, Volume 28, No. 4, 1589–1618.

PapazafeiropoulosGeorge , Prodromos N.Psarropoulos[2010]. "Analytical evaluation of the dynamic distress of rigid fixed-base retaining systems", Soil Dynamics and Earthquake Engineering, 30(12), 1446–1461.

Pierson Matthew C., Parsons Robert L., HanJie and Brennan James J.[2011]."Laterally Loaded Shaft Group Capacities and Deflections behind an MSE Wall", Journal of Geotechnical and GeoenvironmentalEngineering, 137(10), 882–889.

Psarropoulos P.N., Klonaris G., GazetasG. [2005]. "Seismic earth pressures on rigid and flexible retaining walls", Soil Dynamics and Earthquake Engineering, 25, 795–809.

Wayne Clough G.and Tsui Yuet [1977]. "Static analysis of earth retaining structures", Numerical methods in geotechnical engineering, Chapter 15, 506–525.

Wayne C.Teng [1962]."Foundation Design", Civil engineering and engineering mechanics series,Chapter 11, 311–345.

X. Zeng [2005]. "Effect of Liquefaction on Stability of Retaining Walls", GSP 133 Earthquake Engineering and Soil Dynamics.

APPENDIX

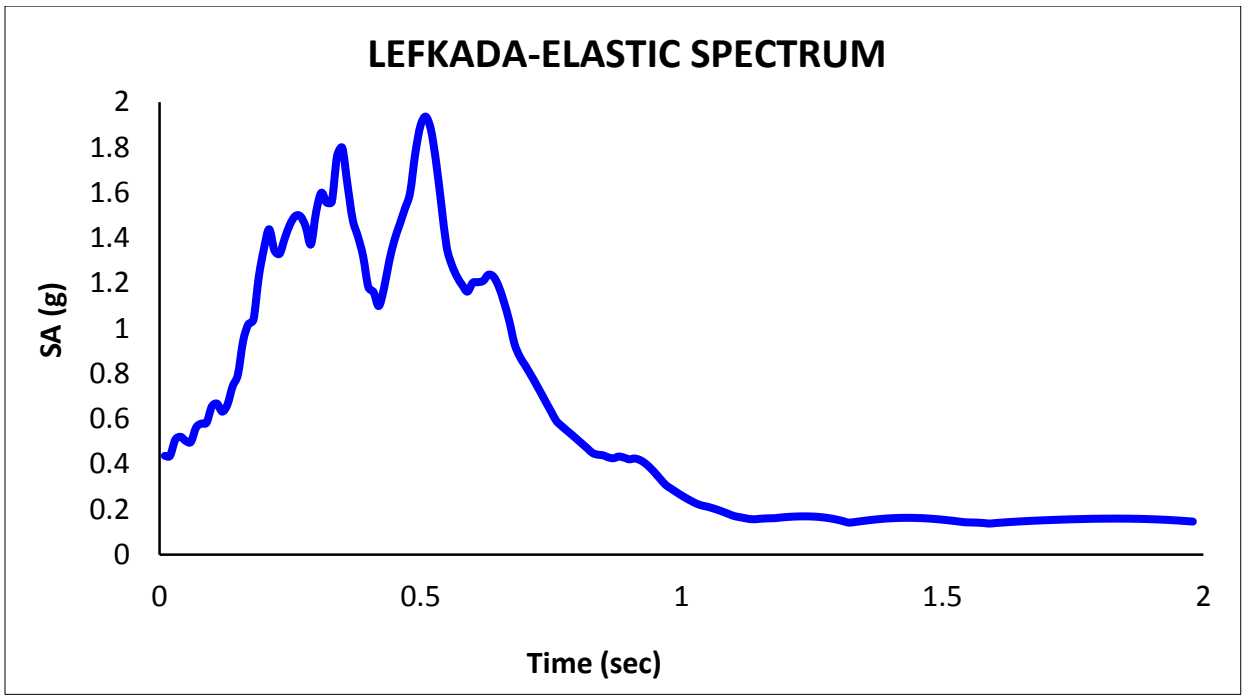
LEFKADA-ELASTIC SPECTRUM
SA (g)
2
1.8
1.6
1.4
1.2
1
0.8
0.6
0.4
0.2
0
0
0.5
1
1.5
2
Time (sec)

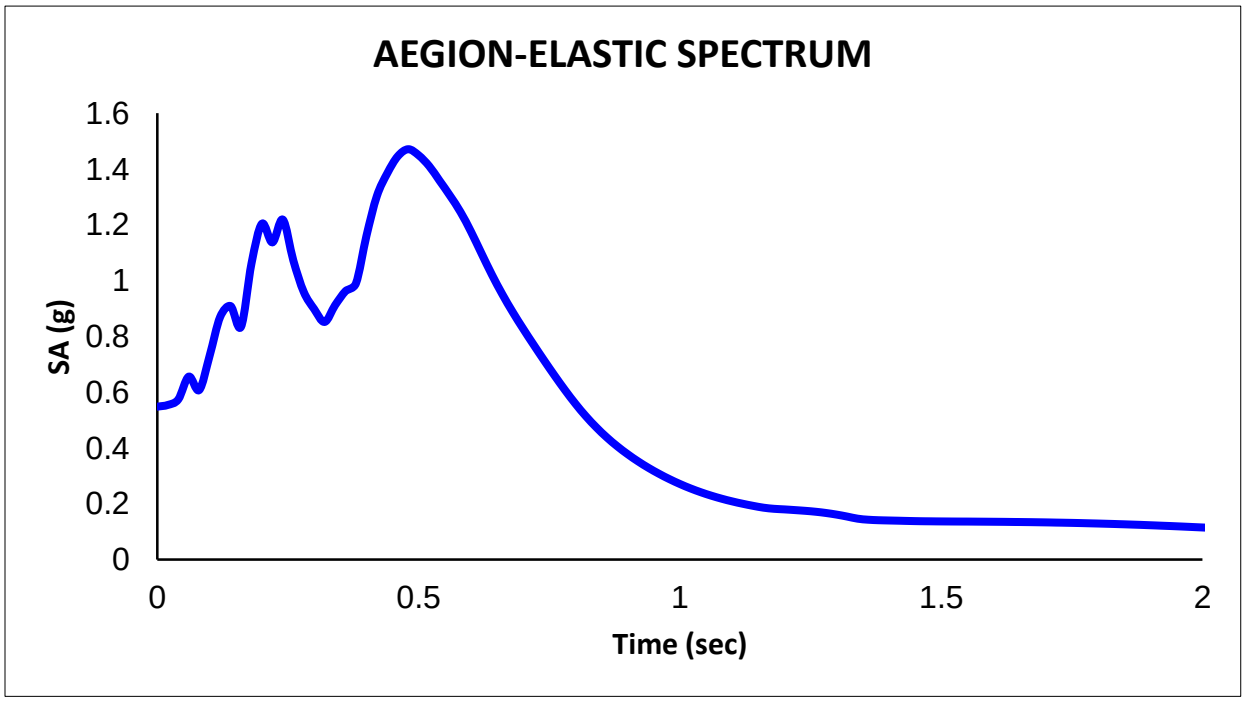
AEGION-ELASTIC SPECTRUM
SA (g)
1.6
1.4
1.2
1
0.8
0.6
0.4
0.2
0
0
0.5
1
1.5
2
Time (sec)

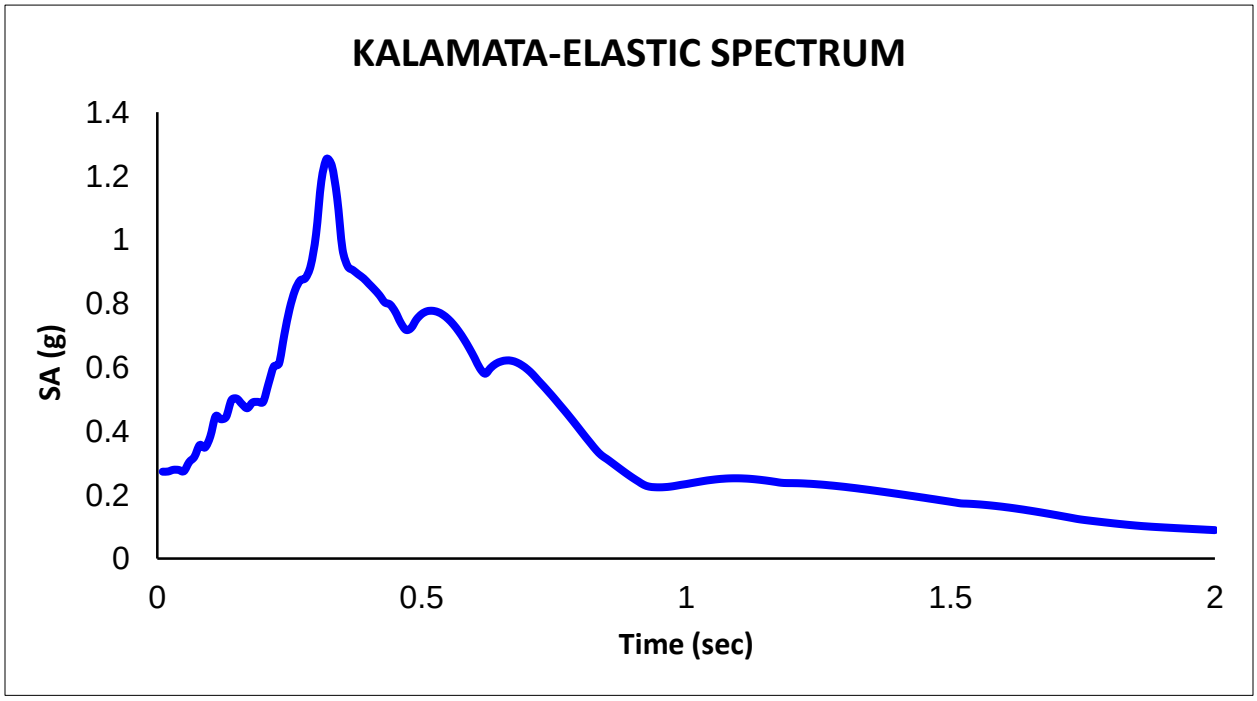
KALAMATA-ELASTIC SPECTRUM
SA (g)
1.4
1.2
1
0.8
0.6
0.4
0.2
0
0
0.5
1
1.5
2
Time (sec)

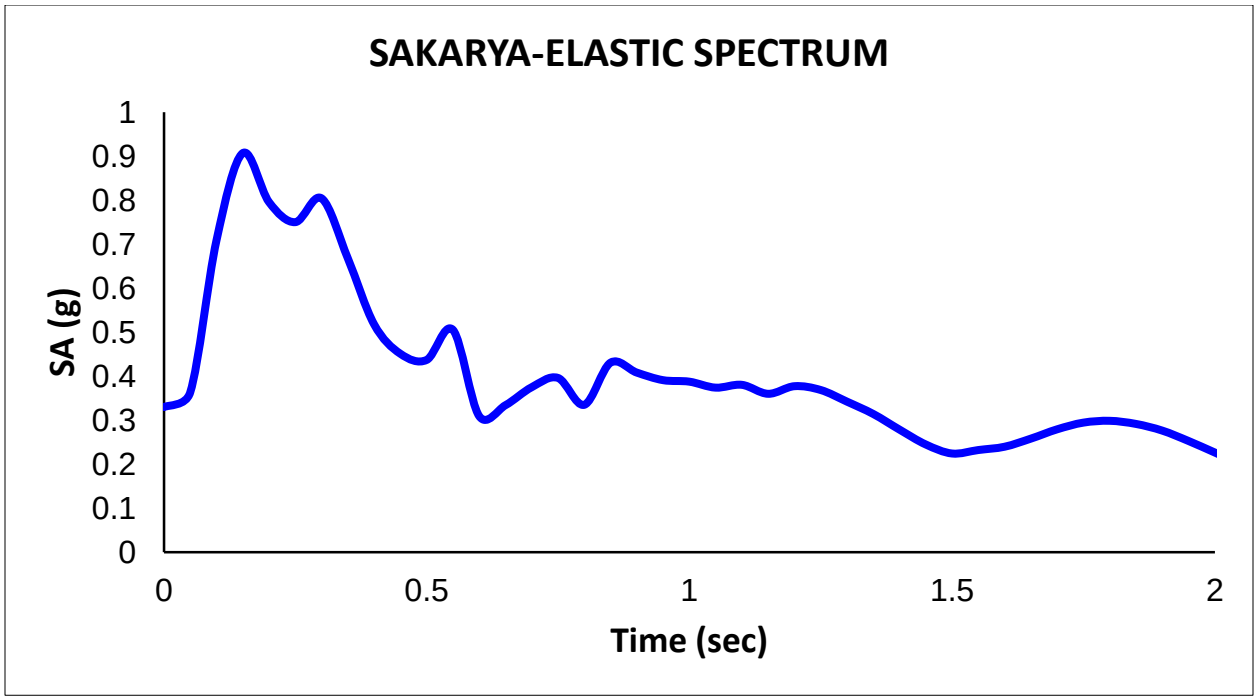
SAKARYA-ELASTIC SPECTRUM
SA (g)
1
0.9
0.8
0.7
0.6
0.5
0.4
0.3
0.2
0.1
0
0
0.5
1
1.5
2
Time (sec)

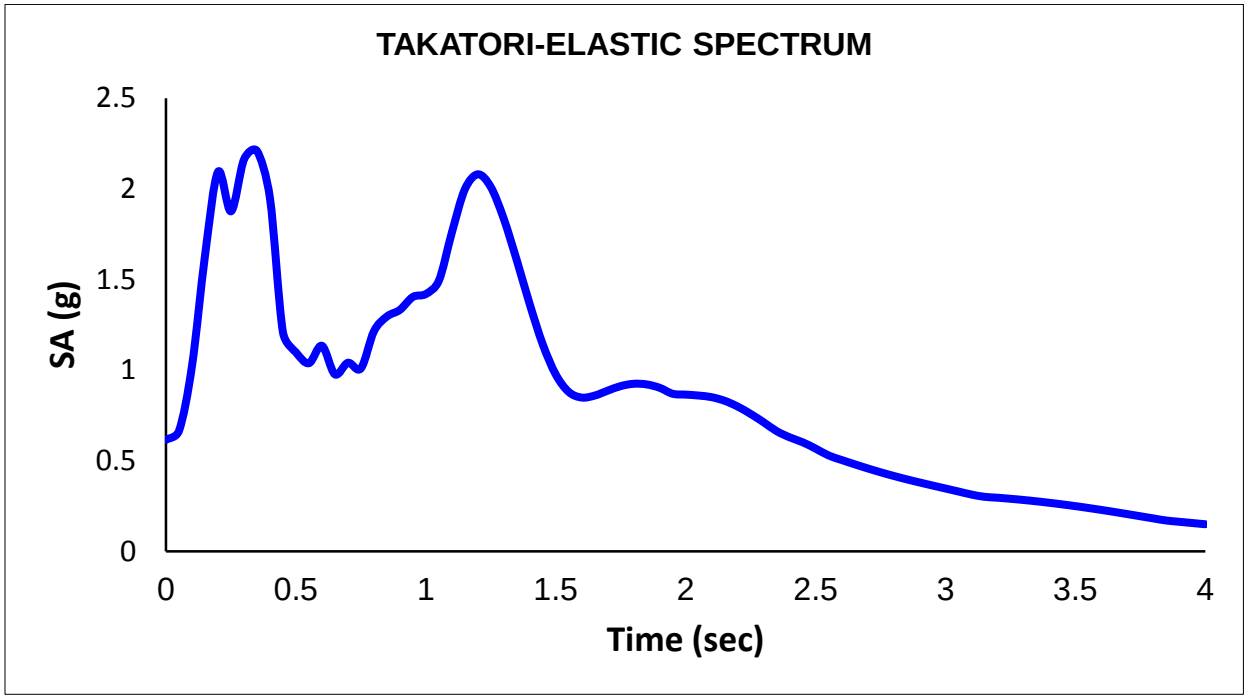
TAKATORI-ELASTIC SPECTRUM
SA (g)
2.5
2
1.5
1
0.5
0
0
0.5
1
1.5
2
2.5
3
3.5
4
Time (sec)